Standards, Applications and Quality Assurance in Medical Radiation Dosimetry (IDOS)

Proceedings of an International Symposium Vienna 9–12 November 2010

Vol. 1

ORGANIZED BY THE

International Atomic Energy Agency

IN COOPERATION WITH THE

American Association of Physicists in Medicine

Asia-Oceania Federation of Organizations for Medical Physics

Asociación Latinoamericana de Física Médica

Bureau International des Poids et Mesures

European Commission

European Federation of Organisations for Medical Physics

European Society for Therapeutic Radiology and Oncology

International Commission on Radiological Protection

International Commission on Radiation Units and Measurements

International Organization for Medical Physics

Institute of Physics and Engineering in Medicine

Society of Nuclear Medicine

United Nations Scientific Committee on the Effects of Atomic Radiation

World Federation of Nuclear Medicine and Biology

World Health Organization

STANDARDS, APPLICATIONS AND QUALITY ASSURANCE IN MEDICAL RADIATION DOSIMETRY (IDOS)

VOLUME 1

The Agency's Statute was approved on 23 October 1956 by the Conference on the Statute of the IAEA held at United Nations Headquarters, New York; it entered into force on 29 July 1957. The Headquarters of the Agency are situated in Vienna. Its principal objective is "to accelerate and enlarge the contribution of atomic energy to peace, health and prosperity throughout the world''.

PROCEEDINGS SERIES

STANDARDS, APPLICATIONS AND QUALITY ASSURANCE IN MEDICAL RADIATION DOSIMETRY (IDOS)

PROCEEDINGS OF AN INTERNATIONAL SYMPOSIUM ON STANDARDS,
APPLICATIONS AND QUALITY ASSURANCE IN
MEDICAL RADIATION DOSIMETRY (IDOS)
ORGANIZED BY THE INTERNATIONAL ATOMIC ENERGY AGENCY
IN COOPERATION WITH THE
AMERICAN ASSOCIATION OF PHYSICISTS IN MEDICINE,
ASIA–OCEANIA FEDERATION OF ORGANIZATIONS FOR MEDICAL PHYSICS,
ASOCIACIÓN LATINOAMERICANA DE FÍSICA MÉDICA,
BUREAU INTERNATIONAL DES POIDS ET MESURES,
EUROPEAN COMMISSION,
EUROPEAN FEDERATION OF ORGANISATIONS FOR MEDICAL PHYSICS,
EUROPEAN SOCIETY FOR THERAPEUTIC RADIOLOGY AND ONCOLOGY,
INTERNATIONAL COMMISSION ON RADIOLOGICAL PROTECTION,
INTERNATIONAL COMMISSION ON RADIATION UNITS AND MEASUREMENTS,
INTERNATIONAL ORGANIZATION FOR MEDICAL PHYSICS,
INSTITUTE OF PHYSICS AND ENGINEERING IN MEDICINE,
SOCIETY OF NUCLEAR MEDICINE,
UNITED NATIONS SCIENTIFIC COMMITTEE ON
THE EFFECTS OF ATOMIC RADIATION,
WORLD FEDERATION OF NUCLEAR MEDICINE AND BIOLOGY
AND THE WORLD HEALTH ORGANIZATION
AND HELD IN VIENNA, 9–12 NOVEMBER 2010

In two volumes

VOLUME 1

INTERNATIONAL ATOMIC ENERGY AGENCY
VIENNA, 2011

COPYRIGHT NOTICE

Marketing and Sales Unit, Publishing Section
International Atomic Energy Agency
Vienna International Centre
PO Box 100
1400 Vienna, Austria
fax: +43 1 2600 29302
tel.: +43 1 2600 22417
email: sales.publications@iaea.org
http://www.iaea.org/books

Printed by the IAEA in Austria
November 2011
STI/PUB/1514

IAEA Library Cataloguing in Publication Data

International Symposium on Standards, Applications and Quality Assurance in Medical Radiation Dosimetry (2010 : Vienna, Austria) Standards, applications and quality assurance in medical radiation dosimetry (IDOS) : proceedings of an international symposium, Vienna, 9–12 November 2010. — Vienna : International Atomic Energy Agency, 2011.
2 v. ; 24 cm. — (Proceedings series, ISSN 0074–1884)
STI/PUB/1514
ISBN 978–92–0–116210–6
Includes bibliographical references.

1. Radiation dosimetry — Congresses. 2. Radiation dosimetry — Standards. 3. Diagnostic imaging — Safety measures. 4. Radiation protection. I. International Atomic Energy Agency. II. Series: Proceedings series (International Atomic Energy Agency).

IAEAL 11–00712

FOREWORD

Ionizing radiation is employed in a wide variety of applications and processes in technologically advanced countries. Dosimetry is the science of measuring ionizing radiation and understanding it is essential for the safe and effective use of nuclear technology. Medical radiation dosimetry deals with those applications in which patients are irradiated.

These proceedings embody a selection of refereed papers that were presented at the International Symposium on Standards, Applications and Quality Assurance in Medical Radiation Dosimetry (IDOS) held in Vienna from 9 to 12 November 2010. More than 370 delegates representing 66 Member States, 45 observers and 12 international and professional organizations attended the meeting, at which 75 oral presentations were delivered, 4 round table discussions were held and 187 posters were presented.

Owing to its dual role in disseminating radiation measurement standards and verifying the accuracy of dosimetry applied at the hospital level, the IAEA is well positioned to convene international meetings focused on dosimetry. The previous meeting was held in Vienna in November 2002. Since then, three major developments have helped progress medical radiation dosimetry. Firstly, Member States have rapidly adopted new treatment technologies, e.g. intensity modulated radiotherapy (IMRT), and they have continued to acquire sophisticated diagnostic capabilities, e.g. computed tomography (CT) and positron emission tomography scanning. Unfortunately, the adoption of these technologies has not always been trouble-free. News stories in various countries have highlighted radiation accidents during IMRT due to dosimetric errors. In addition, overuse of CT scanning and failure to adopt clinical protocols appropriate to patient size, particularly in paediatric cases, have caused concern. Measurement of radiation dose properly necessitates adoption of new technologies and, consequently, much research has been devoted to improving dosimetry, particularly for the small fields typically used in IMRT.

Secondly, dosimetry protocols based on standards of absorbed dose to water, which simplified the translation of basic dosimetry from the standards laboratory to the hospital level, are 10 years old and need reviewing. There have been advances in dosimetry for both graphite and water calorimetry for external beam therapy and the strengthening of dosimetry for beams of protons and light ions, as their use is implemented clinically. Advances have also been made at primary laboratories to develop absorbed dose to water standards for brachytherapy sources that are inserted directly into patients. All these issues were addressed during the symposium.

Thirdly, there has been a rapid expansion in the level of diagnostic information for therapy planning, delivery and patient follow-up. New paradigms

have been created for more comprehensive quality assurance. Since auditing physical dosimetry is an integral part of quality auditing for the whole process of treating patients, one session focused on it. The ongoing need to optimize radiation doses justified a session on radiation protection dosimetry.

In addition to oral and poster presentations, four interactive, round table discussions were held, focusing on the consequences of dosimetry errors, dosimetry knowledge gaps for new technologies, the role of education and training to improve dosimetric understanding and the meaning of traceability in the dosimetric chain. A CD-ROM of the contributed papers accompanies these proceedings.

The IAEA gratefully acknowledges the contributions made by the Programme Committee, the collaborating organizations, and the session chairs, co-chairs and scientific reviewers.

EDITORIAL NOTE

CONTENTS OF VOLUME 1

SYMPOSIUM SUMMARY

BACKGROUND

The objective of the IAEA programme in human health is to enhance the capabilities in Member States to address needs related to the prevention, diagnosis and treatment of health problems through the application of nuclear techniques. The mandate arises from Article II of the IAEA's Statute: "the Agency shall accelerate and enlarge the contribution of atomic energy to health, peace and prosperity throughout the world."

Accurate measurements in radiation dosimetry are vital in a wide range of medical and industrial applications where the results are critical in reaching decisions relating to human health and safety of radiation workers and members of the public. The development of standards by primary dosimetry laboratories followed by their dissemination to secondary standards dosimetry laboratories and to end-users ensures traceability of measurements to the international system of units. Dosimetry codes of practice (or protocols) are used in conjunction with the dosimetry standards to ensure optimized use of radiation in medicine. Uniformity is equally important in dosimetry, especially for collaborative multicentre studies or clinical trials. In dosimetry for radiation protection, the uncertainty may be greater than for therapy and diagnostic X rays, but proper traceability of the measurements with a defined level of uncertainty is equally important. In recent years, new developments have occurred in dosimetry standards, audits and QA guidance, especially in the field of external radiotherapy, brachytherapy, nuclear medicine and diagnostic radiology.

The International Symposium on Standards, Applications and Quality Assurance in Medical Radiation Dosimetry (IDOS) was organized by the IAEA and held in Vienna from 9 to 12 November 2010 to foster the exchange of information along the whole dosimetry chain and highlight recent developments in this field. Three hundred and seventy two delegates representing 66 Member States, 45 observers and 12 international and professional organizations attended the meeting. Altogether, 75 oral presentations were delivered, 4 round table discussions were held and 187 posters were presented covering a broad range of topics in medical radiation dosimetry. A refereed selection of papers presented at the symposium forms the core of these Proceedings.

SYMPOSIUM OBJECTIVES

The major goal of the symposium was to provide a forum where advances in radiation dosimetry during the last decade, in radiation medicine and in radiation protection could be disseminated and scientific knowledge exchanged. It included all specialities in radiation medicine and radiation protection dosimetry, with a specific focus on those areas where the standardization of dosimetry has improved in the recent years (brachytherapy, diagnostic radiology and nuclear medicine). It summarized the present status, outlined future trends in medical radiation dosimetry and identified possible areas for improvement. Its conclusions and summaries should lead to the formulation of recommendations for the scientific community.

The Opening Session comprised two parts:

(i) Opening addresses

The opening addresses outlined the importance of traceable measurements in radiation dosimetry in a wide range of medical and industrial applications where the results of dosimetric measurements are critical to decision making in human health as well as to the safety of radiation workers and members of the public. The roles of the international organizations involved in dosimetry, the IAEA, the International Bureau of Weights and Measures and the International Commission on Radiation Units and Measurements, were also highlighted.

(ii) Keynote presentation

A key note presentation on Accuracy Requirements in Medical Radiation Dosimetry was delivered. This presentation included an overview of requirements in medical dosimetry, including radiotherapy, diagnostic radiology using X rays and nuclear medicine.

SYMPOSIUM CONCLUSIONS

These conclusions summarize information exchanged during the IDOS symposium, highlight issues of importance discussed during the meeting and identify trends and challenges for the future. They are organized into a hierarchical structure within the domain of radiation dosimetry. It begins with the international framework for metrology, which sets radiation dosimetry and other primary standards for radiation measurement into the context of the mutual recognition arrangement for national laboratories under the auspices of the International Committee for Weights and Measures (CIPM). The second step in the chain focuses on dosimetry standards, which include the primary standards developed at the National Metrology Institutes (NMIs), primary standards dosimetry laboratories (PSDLs) and the dosimetry laboratory of the International Bureau of Weights and Measures (BIPM) and their subsequent dissemination to end-users through secondary standards dosimetry laboratories (SSDLs). In general, the uncertainty associated with primary standards is lower than for the standards further along the dosimetry chain. Radiation dosimetry protocols such as the IAEA's TRS 398 and the American Association of Physicists in Medicine's (AAPM) TG-51 constitute the third step in the dosimetry chain and are implemented by end-users. This enables radiation dose to be determined under standard reference conditions, using reference quality ionization chambers calibrated by a standards dosimetry laboratory. This represents the highest level of accuracy typically available within cancer centres. Clinical dosimetry is the fourth step in the chain, which deals with determining the dose to individual patients or classes of patients undergoing diagnosis and treatment. The final step in the dosimetry chain involves dosimetry auditing, which is frequently part of a quality assurance programme. For example, external independent auditing of dosimetry at the institutional level through the use of mailed thermoluminescent dosimeters may be used to verify the accuracy of dosimetry under reference conditions and confirm a basic level of confidence in the institute's dosimetry capabilities. Dosimetry auditing may also be expanded to confirm the accuracy of calculations performed by treatment planning systems. Dosimetry verification of the treatment preparation and delivery should be systematically done within an institution for all patients, for example, using in vivo detectors or by interpreting data from electronic portal imaging devices, thereby enabling an institution to demonstrate its competence to treat patients at specific disease sites or in using specific therapeutic techniques. Frequently, matters concerning radiation protection were raised within the sessions on radiation dosimetry. The strong linkage between radiation protection and dosimetry arises during the application of the principle of optimization: minimizing the potential harm to patients and staff as a result of using ionizing radiation while at the same time acquiring the

required medical information or achieving the desired outcome of the therapy. Nevertheless, some issues in radiation protection were so specific that they comprised a separate session during the symposium and so these matters are summarized in a separate section of the Proceedings. In addition to the formal oral and poster presentations, four lively and less formal round table discussions were held during the meeting. Issues raised in those discussions and worthy of further emphasis are summarized towards the end of these conclusions.

1. INTERNATIONAL FRAMEWORK FOR RADIATION DOSIMETRY

The invited speaker took a broad perspective to establish the framework for radiation dosimetry. He pointed out that, as in most fields of science and technology, the development and improvement of standards for metrology provide the infrastructure required to enable innovations to move forward successfully. In radiation medicine, the effect on the patient (e.g. cure in the case of radiotherapy and reliability of diagnostic information in the case of nuclear medicine scans and radiology) is coupled to the radiation dose. That is, achieving the desired patient outcome safely and effectively requires knowledge of radiation dosimetry. He also pointed out that the ever increasing sophistication of diagnostic and therapeutic methods (e.g. IMRT) requires both new measurement techniques and reduced measurement uncertainties. The entry of some new technical developments, such as miniature X ray tubes for brachytherapy, demands completely new kinds of dose measurement. In principle, since medical radiation dosimetry is an applied field, the introduction of new technologies and clinical demand for better accuracy will define the topics for urgent investigation in medical radiation dosimetry.

The invited talk of Plenary Session 2, focused on dosimetry activities at the level of PSDLs within the framework of the CIPM mutual recognition arrangement. Within the last decade the results of several comparisons among PSDLs of their radiation dosimetry standards and their radioactivity measurements have been entered into the key comparison database. This enables the participating laboratories to demonstrate the degrees of equivalence of their standards and to establish the link required to the international system of units; in the case of dose, the gray, and, in the case of activity, the becquerel. Overall, the performance of PSDLs on dosimetry comparisons is consistent with the laboratories' stated uncertainties.

2. RADIATION DOSIMETRY STANDARDS

In the area of diagnostic radiology, concern has been expressed about the increase in the number of CT scans performed since the radiation dose for CT is generally larger than for routine work in diagnostic radiology. In addition, there is concern that the principle of optimization is not being applied rigorously enough, particularly in the case of paediatric cases where lower dose to the child than typically delivered to adults would still yield sufficient image quality to achieve a proper diagnosis. Frequently, kerma area product (KAP) meters are used to monitor radiation dose in diagnostic radiology. Various speakers underlined the need to improve diagnostic dosimetry standards, in particular for the calibration of KAP meters.

The BIPM and NMIs are continuing to develop and improve their dosimetry standards. The development of primary standards based on calorimetry is ongoing, specifically for high dose rate brachytherapy, protons and light ion beams, and small and non-standard radiation fields for high energy photons. The current decade has seen improvements in the direct determination of absorbed dose to water using calorimetry. Some of the work is based on graphite calorimeters and some on water calorimeters, so there is an inherent robustness that was not present in the case of air kerma standards. The NRC reported on a water calorimetry standard that applies to electron beams using Fricke dosimetry as a transfer standard for the lower energy beams. Using beams of protons and light ions to treat cancer patients would permit the creation of tighter dose distributions with lower dose in the exit beam to reduce radiation toxicity there. Although some calorimetric measurements have been performed for proton beams, there are no dosimetry standards for that modality yet.

In the case of brachytherapy sources specifically, work is under way to develop absorbed dose to water standards and to update the dosimetry protocols accordingly in order to prevent confusion at the user's level. Reclassification of brachytherapy sources in terms of low, medium and high energy has been proposed. Doing so would impact on dosimetry equipment and methodology, perhaps placing greater emphasis on the use of plastic scintillation detectors. New primary standards for ^{125}I and ^{103}Pd for reference air kerma rate have been introduced. The trend has continued for SSDLs to provide traceability for brachytherapy sources using well chambers calibrated at PSDLs.

The availability of proton and light ion beam facilities for the treatment of patients continues to increase with the expectation that approximately 50 such facilities will be operational by 2015. There was a call to develop collaborative treatment protocols that would be based on consistent and harmonized dosimetry procedures. Since calorimetry is the only technique available to determine the absorbed dose directly and since no dosimetry standards exist for proton and light

ion beams, care is required using ionization chamber dosimetry. For example, additional measurements are required to determine the W-value of carbon ion beams more accurately. Notwithstanding the need to incorporate new dosimetry data, this may have only a small effect. In general, it is believed that basic data and techniques for therapy dosimetry are sufficiently accurate for safe patient treatment. Nevertheless, treatment delivery is usually specified in terms of physical dose weighted by the relative biological effectiveness of the beams; however, these relative biological effectiveness values are not known very accurately. Clearly, dosimetry for proton and light ion facilities is an area requiring further development.

3. RADIATION DOSIMETRY PROTOCOLS

The attendees learned that the current status of dosimetry for external beams under reference conditions is in good shape. Recent data, required for use in IAEA TRS 398, do not differ significantly from the data in the original version of the code of practice (CoP). Consequently, it was recommended that no update to TRS 398 be done until revised values of key dosimetry data (I-values and stopping powers) have been agreed by the Consultative Committee for Standards of Ionizing Radiation (International Committee for Weights and Measures). Nevertheless, IAEA web pages contain values for newly designed ionization chambers that were introduced since the original publication of the protocol. The AAPM has chosen a slightly different approach for their TG-51 protocol. It will be updated to accommodate newly designed chambers used with photon beams and major changes are planned for the dosimetry of electron beams.

Radiation dosimetry is an applied science in which the research focus is frequently impacted by developments in the means of delivering radiotherapy. There has been a paradigm shift within the last decade in the way external beam radiation therapy is delivered to patients. Currently, using technologies such as IMRT, tumours are frequently irradiated using multiple small fields to create a tight distribution of radiation dose designed to spare critical targets adjacent to the tumour volume. Previously, using conformal therapy, tumours were mostly irradiated with larger, flat fields covering the whole target volume. In the latter case, routine clinical dosimetry was based on standard reference fields, typically 10 cm × 10 cm, using ionization chambers of 0.6 cm^3 volume, with the longest dimension measuring about 1.5 cm. As mentioned in the previous paragraph, reference dosimetry in such a case is in a relatively good state. Juxtaposed to this situation, dosimetry for small and non-standard fields requires considerable research and one entire session at the symposium was dedicated to this topic. Although many cancer clinics are actively treating patients with small and

non-standard beams, no dosimetry CoP currently exists. A joint task force of the IAEA and AAPM has proposed a formalism for the dosimetry of small and non-standard beam fields for which classical reference chambers are too large and the theoretically required conditions of charged particle equilibrium do not necessarily apply. In light of this formalism, substantial research and development to generate data for small and non-standard beams and suitable detectors were reported during the symposium, but more results are needed before a harmonized CoP can be created. The Institute of Physics and Engineering in Medicine has just published a comprehensive report on the clinical application of small and non-standard beams.

4. CLINICAL RADIATION DOSIMETRY

Clinical dosimetry focuses on measurements performed for individual patients, perhaps as part of a quality assurance protocol, or measurements made on a certain class of patients, for example, to confirm that calculations done by a treatment planning system for radiation treatments are consistent with the measurements. Of course, a failure to demonstrate consistency requires further investigation since it implies that patients may be misdiagnosed or treated improperly. However, the lack of consistency may also reflect a lack of care and attention applied to the measurement process or errors in the calculation. During the symposium, several sessions were held on clinical dosimetry. In the diagnostic area, three oral sessions and one poster session focused on clinical dosimetry in X ray imaging and two oral sessions focused on internal dosimetry in nuclear medicine. In the case of radiotherapy, one oral and one poster session focused explicitly on clinical dosimetry. The findings of the symposium are presented in the remainder of this section.

4.1. Clinical dosimetry in X ray imaging

Owing to the continued increase in use of computed tomography (CT) examinations, much interest was expressed in dosimetry for CT. Work from the ICRU and the AAPM is focusing on optimizing beam width and dose appropriate to patient size, particularly in the case of paediatric patients. Parameters for paediatric categorization, such as weight in the case of nuclear medicine and equivalent thickness in the case of diagnostic radiology, give better results than the use of age as a parameter for dosimetric work. Estimating CT organ dose and accurately accounting for tube current modulation are under research. In order to harmonize dosimetry practice, the medical physics community should discuss the new dosimetry methods using new instrumentation and phantoms to meet the

requirements of the new CT technology. It was reported that dosimetry for breast tomosynthesis following the European protocol agreed with the US protocol within expected uncertainties. There is an effort to identify real time dosimeters that can be used to determine trigger levels for skin dose that are procedure specific. Such dosimeters work reliably if calibrated using radiochromic film. Delegates were reminded that patient posture matters for accurate internal dosimetry in radiology and nuclear medicine studies, particularly for low energy photons. Much work was reported on the use of KAP meters. For example, there is increasing confidence in the use of KAP meters for dental examinations using panel tomography. Their use is of interest in CT dosimetry, potentially for both conventional and cone beam CT methodologies. However, delegates were warned that KAP meters need to have a traceable calibration in situ and that the assessment of their uncertainties must include effects to account for the attenuation of the table top; energy dependence, particularly with clinical beams; and humidity. Multipurpose, semi-conductor, X ray meters have been introduced to enable the measurement of several beam parameters simultaneously. The responses of such meters have been compared to laboratory standards for the quantities of dose, tube voltage, half-value layer measurement and homogeneity index. Although dose determinations agreed within 5% for 95% of these comparisons, about 20–50% of other measurement results were outside the 5% specification. Paediatric dose reference levels are being developed in a number of countries now that progress is being made in dosimetry to determine these reference levels more accurately.

4.2. Clinical dosimetry in nuclear medicine: Internal dosimetry using computational phantoms and radiobiological modelling

The measurement of radioactivity is fundamental in nuclear medicine and there is an ongoing need to standardize the measurement of activity in nuclear medicine practice. Nevertheless, knowledge of activity alone is not sufficient and so there is a need to go beyond the dissemination of traceable standards for radioactivity. To meet this need, the MIRD committee and the ICRP now have a joint formalism for nuclear medicine dosimetry, but the field still evolves. For example, there are significant differences in the derivation of dose conversion factors for stylized versus hybrid phantom anatomy. It seems possible to create more accurate hybrid models using micro-CT images. Clearly, this is an area for further work. In nuclear medicine therapy, improvements in inverse treatment planning have been attempted using NTCP and TCP formalisms. This requires better knowledge of radiobiological modelling linking effectiveness and toxicity to activity and the means to confirm that the level of activity prescribed for a particular individual was what was delivered. In order to analyse some

comparison data and to compare outcomes of multimodality treatments (e.g. external beam together with nuclear medicine therapy), the concept of isoeffective dose has been introduced but this will need to be harmonized with the radiobiological modelling used with external beam radiotherapy. It is hoped that the cross-fertilization between nuclear medicine therapy and radiotherapy will improve our overall understanding.

Delegates were reminded that using new technology such as SPECT/CT and PET/CT along with Monte Carlo calculations to determine image correction factors more accurately provides a better estimate of the activity distribution in the patient. Quantitative imaging requires the harmonization of the acquisition and interpretation of PET images. Traditional ('one size fits all') phantom based dosimetry is no longer adequate. Using realistic phantoms tailored to individual patients and data from measurements of patient specific dosimetry improves the accuracy of dosimetry overall and is needed for high dose therapy applications. Reporting the results of internal dosimetry studies must include all relevant parameters and state clearly the methodology used. In the case of patients receiving treatment with radionuclides, a proper protocol for sample analysis and image acquisition is essential. A formalism is required to address the addition of doses from nuclear medicine and radiation therapy for patients receiving both modalities. This appears to be an area for fruitful research.

4.3. Clinical dosimetry in external beam therapy

Many medical physicists working in therapy are concerned about performing accurate clinical dosimetry for modern therapy techniques such as IMRT. Some of the technical difficulties in determining the dose clinically for small and non-standard fields are discussed in the previous section on dosimetry CoPs. Furthermore, there is concern at the corporate level due to significant failure rates experienced by cancer centres undergoing external dosimetry auditing as part of credentialing tests as discussed in the next section on dosimetry auditing. Consequently, the session on clinical dosimetry in radiotherapy was headed by two invited speakers. It was pointed out that four components are needed to ensure correct dose delivery: education, verification, documentation and communication. Furthermore, many treatment planning systems perform heterogeneity corrections inadequately, as demonstrated by measurements in anthropomorphic phantoms. The session was completed with additional technical presentations. In one of these, delegates learned that large differences were demonstrated between measurements using lithium formate dosimeters and calculations done with treatment planning systems. Another paper reminded delegates that the out-of-field dose at a photon beam energy of 18 MV is dominated by the dose from neutrons.

4.4. Trends in clinical dosimetry

The availability of sophisticated technologies such as IMRT to deliver radiation therapy has stimulated interest in increasing our understanding of the role of imaging sciences to improve clinical outcomes. At the same time, quantifying image quality is moving from visual estimation of equipment parameters to mathematical estimations using image data, specific algorithms and phantoms. That is, the tools to describe image quality are improving. Advanced diagnostic capabilities have become accessible within the therapy setting. However, these diagnostic technologies were optimized primarily for the purposes of diagnosing diseases rather than for the purposes of localizing the disease anatomically. In fact, lack of knowledge of disease detection thresholds may limit the ability to define accurately the tumour volume. Consequently, cancer treatment centres are challenging their medical physics staff to learn how to use and optimize the diagnostic tools well enough to support fully the treatment delivery systems. In principle, it should be possible to exploit the diagnostic information to lower the toxicity otherwise caused by irradiating healthy regions adjacent to the tumour volume. It remains to be shown that knowing more precisely where the tumour is located will permit the beam delivery systems to confine the dose to the tumour, thereby lowering toxicity and improving patient outcomes. Alternatively, it may be possible to increase the dose to the tumour in order to achieve a greater chance for local control of the disease while maintaining the same level of complications associated with the dose delivered to the surrounding volume. If either of these scenarios plays out, it will result in a paradigm shift for dosimetry. The fact that dose, by definition, is a quantity determined at a specified location will remain. However, it is possible that the distribution of the physical dose will become a more important parameter to consider in the light of achieving clinical outcomes.

As discussed in the section above on clinical dosimetry for nuclear medicine, additional diagnostic information is being made available that may help physicians to understand better tumour biology. In particular, PET/CT systems are providing information about functionality. If it becomes possible to identify reliably regions of the tumour that are more active biologically or more resistant to therapy than other regions, this may lead to deliberately delivering more radiation dose to one region of the tumour than another, e.g. ‘dose painting’. Then, one might imagine treating patients with physical dose distributions that are deliberately not uniform in order to achieve isotoxicity throughout the tumour volume. Potentially, the incorporation of functional information into the treatment planning process will constitute the next paradigm shift. Consequently, the demand for better clinical dosimetry is expected to increase in the future.

5. RADIATION DOSIMETRY AUDITING

The session on external quality audits in radiotherapy yielded some provocative papers. It was reported that dosimetry audits using anthropomorphic phantoms failed to comply with acceptable norms for a substantial fraction of institutions. Initially, in some technologically advanced countries, about 30% of institutions preparing to participate in clinical trials using IMRT failed the dosimetry audit. Furthermore, the popular press has documented several serious accidents where patients were overexposed due to dosimetry errors. One of the round table sessions at the symposium focused on the education of medical physicists and their ongoing training and credentialing as a means of improving confidence in this aspect of delivering radiotherapy. However, concerns were expressed about the rapid pace of deployment of new treatment technologies leaving inadequate opportunities to ensure reliable dosimetry. Improvement of some quality assurance tools was reported. For example, in addition to traditional thermoluminescent dosimeters, optically stimulated luminescence and electron paramagnetic resonance based detectors, along with radiochromic film, were shown to be useful dosimetry systems for dosimetry audits. It was felt that quantification of the benefits of radiation medicine should be increasingly attempted, for example, by following up the outcomes for treated patients to ensure the effectiveness of their treatment.

Technical presentations and posters showed that external audits are clearly recognized as being valuable and having had significant impact on the quality of dosimetry practice. External auditing has identified problems in a wide range of radiotherapy centres, identifying causes, resolving problems and improving dosimetry and education in this area. All dosimetry auditing systems show improvements as the audits are repeated with time. Overall, audits raise awareness of issues in dosimetry and elevate the general level of dosimetry quality. Audits help to reduce uncertainties and increase the precision and consistency of radiotherapy dosimetry between centres. For clinical trials, audits increase compliance with trial criteria, which has been shown to be one factor in the success and cost effectiveness of clinical trials. Audits need to include checks of basic parameters, but it is also necessary to include other areas of clinical dosimetry, e.g. the performance in treatment planning and dose delivery. Experience from the reported national and international dosimetric audits indicates that IAEA support to develop the audit methodology and its scope was important for the majority of participating countries to facilitate wider implementation of audits in radiotherapy. Advanced dosimetry audits employing semi- and full anthropomorphic phantoms can be used to verify the dose distribution in realistic treatment situations, simulating the actual patient undergoing radiation treatment. Every radiotherapy centre in the world is

encouraged to participate in an external dosimetry audit. All radiation beams used clinically should be independently checked through an audit before patient treatments start and furthermore, they should be audited on a regular basis.

6. RADIATION PROTECTION ISSUES

Radiation protection is integral to the practice of radiation medicine. Nevertheless, a specific session on radiation protection was held during the symposium. In some cases, policy issues were raised. The delegates were informed that the use of BEIR VII estimates of cancer risk are more appropriate to establish patient risk than using the concept of effective dose, which was intended for the assessment of occupational risk. However, the data of BEIR VII were intended for use with populations and not individuals and since they are based on US data, they may not be fully transferable to other regions. It is important to increase the level of awareness of the management and medical staff on the risks of deterministic effects arising from the use of radiation in medical procedures and about how such risks can be minimized or better avoided. Radiation protection programmes must be in place at medical facilities for both worker and patient protection. Individual monitoring of medical staff, especially for extremity dosimetry, has been demonstrated to improve their protection. Diagnostic imaging procedures in interventional radiology and nuclear medicine should be optimized. International standards, guidance and assistance on capacity building in radiation protection remain abreast of the rapidly developing medical technology and are effectively disseminated, in particular for dosimetry. Some technical issues were also discussed. There is a proposal for double dosimetry (one badge beneath protective aprons and one above) and for eye dosimetry. One recommendation is to upgrade and/or create a dose registry at the national/State level. A radiation protection regime is needed to establish better the protection and monitoring of ‘itinerant’ medical staff. Some radiation protection issues in the medical area would be improved by greater collaboration among medical and scientific societies and organizations and the manufacturers of medical equipment. A recommendation is to monitor the ORAMED project and to participate in ISEMIR projects for improving the staff monitoring and optimization of protection. It is also recommended to implement a quality management system for monitoring and medical physics services.

7. ROUND TABLE DISCUSSIONS

During the four round table discussions, additional material was presented and several important points were highlighted. This section captures some of the discussion from those round table sessions, which may not have been emphasized sufficiently elsewhere.

7.1. When dosimetry goes wrong in therapy and imaging

Delegates were reminded that errors in therapy can be made at many different phases of the radiotherapy process. For example, errors may be made at the time of commissioning, during routine quality assurance, during treatment planning calculations, or as part of the process of selecting imaging or treatment parameters. Equipment failures can easily lead to unintended patient doses. Potentially, errors associated with imaging can harm large numbers of patients, although the doses from the imaging procedures themselves are often not large. The experience of several audit groups shows that errors in the calibration of radiotherapy equipment exist worldwide. No one can afford to be complacent. Common causes of error include inadequate education and training, insufficient staffing, lack of documented policies, poor communication, lack of a safety culture or a quality management system and obsolete, outdated or poorly functioning equipment. Proactive detection of large errors requires a more systematic approach. Errors have been related to the introduction of new techniques (see ICRU Report 112) even within clinics of high reputation. Comprehensive audit and peer review of outcomes would be helpful in decreasing the number of errors and delegates were encouraged to support this approach. Incident reporting should be encouraged. The response to an incident should include education and preventive measures to avoid future occurrences. Punishment, if required, should be appropriate.

7.2. Dosimetry challenges associated with new technology

Small field dosimetry has been associated with several patient dose delivery errors. More emphasis must be placed on ensuring the dose distribution is delivered to the intended target. Managing tumour motion from one therapy session to the next using cone beam CT and within treatment delivery using image guided radiation therapy helps by improving the therapeutic ratio but has the potential to add unwanted radiation doses in non-involved healthy tissues. Monitoring and controlling the imaging dose is a challenge but knowing it accurately will help to determine the TCP as well as reduce the risk of inducing secondary cancers. However, such new technologies bear costs in both time and

money. Patient specific dosimetry for radionuclide therapy is lacking in general and needs to be strengthened. Appropriateness criteria are needed to ensure that the widespread growth in the use of CT exams is justified. Scanning parameters must be tuned to meet the requirements of individual patients.

7.3. Education and training for radiation dosimetry

A comprehensive model for education of medical physicists should include: academic studies (education); acquisition of clinical competencies preferably following a practical, 'on the job', residency programme to define completely a medial physics 'expert'; certification and recognition by means of a credentialing process applied to both the person and the programme; and continuing education to support licensing and recertification. Better collaboration with manufacturers would be helpful for machine specific practical training and machine maintenance. The IAEA is cooperating with interregional stakeholders to develop guidelines, promote awareness and harmonize the recognition and roles and responsibilities of clinical medical physicists. Collaboration with the International Organization for Medical Physics is being pursued. Medical physicists working in radiotherapy require more training in imaging to support the implementation of new technologies. However, setting aside time for training is difficult given current workloads.

7.4. Calibration traceability: What does this mean to you?

The classical meaning is: to use dosimetry equipment whose calibration is linked through an unbroken chain of comparisons to standards that have a high degree of equivalence to the SI. In radiotherapy, a reliable basis to describe beam quality is required to support the interpolation of calibration coefficients provided by the standards laboratory to the user's beam quality. Even though some NMIs have acquired clinical linacs to be used in disseminating dosimetry standards at beam qualities appropriate to clinical use, the BIPM has yet to do so. In general, medical physics involvement in the procurement of equipment is needed in order to verify its reliability and consistency with international norms. Calibration of diagnostic beams is problematic if there is a mismatch in beam quality specifications between the standards laboratories and users.

8. SUMMARY

Delegates greatly appreciated the opportunity to attend this meeting, which was focused on medical radiation dosimetry and related QA. In general, medical

physicists are dedicated to perform all the tasks needed of them in such a way that patient diagnosis and therapy may continue to be conducted safely and effectively. Nevertheless, advances in technology for radiation therapy dose delivery require vigilance to ensure adequate quality control. In the future, advances in diagnostic capabilities may lead to better therapy planning. Certainly, the coupling between diagnostic information and therapy delivery is expected to strengthen. In this case, many challenges in dosimetry remain to be solved.

OPENING SESSION

OPENING ADDRESS

W. Burkart
R. Chhem
International Atomic Energy Agency

Presented by M. Dondi

On behalf of the Deputy Director General of Nuclear Applications at the IAEA as well as the Director of Human Health in the same Department, I am very pleased to welcome you to Vienna and to this International Symposium on Standards, Applications and Quality Assurance in Medical Radiation Dosimetry.

I am especially pleased to observe the large number of participants here today: we have more than 370 registered delegates, representing 66 Member States and 12 international and professional organizations. Clearly, this high interest by IAEA Member States reflects the importance they place on dosimetry and quality assurance in radiation medicine.

Accurate measurements in radiation dosimetry are vital in a wide range of medical and industrial applications where measurement results are critical to decision making in human health as well as to the safety of radiation workers and members of the public. The process of developing measurement standards by primary standards dosimetry laboratories followed by their dissemination to secondary standards dosimetry laboratories (SSDLs) and thence to end-users ensures traceability of measurements to the international system of units. Dosimetry codes of practice or protocols are used in hospitals in conjunction with the dosimetry standards to ensure optimal use of radiation in medicine in its myriad applications.

To the best of our knowledge, there are no international meetings dedicated exclusively to dosimetry in the terms described above. This is why the IAEA is pleased to continue the tradition of organizing this unique symposium, dedicated solely to dosimetry. It is an opportunity for hospital users and researchers to meet with scientists from standards laboratories to review the entire dosimetry chain and exchange ideas on new developments in the field.

Since the last IAEA symposium on dosimetry, held in 2002, there have been several new developments. They will be highlighted at the oral and poster sessions during the next four days.

The core of the IAEA's programme in dosimetry has two components. One is the dissemination of radiation measurement standards through the IAEA–WHO network of SSDLs. The other involves verification of the accuracy

of the dosimetry standards at the user's level in hospitals via the IAEA–WHO postal thermoluminescent dosimeter service. In the first component, the IAEA enables its Member States to measure radiation dose and in the second component, the IAEA helps its Member States to provide independent evidence of the correctness of their dosimetry measurements.

Ideally, all radiation beams used to treat cancer patients would be checked by an independent national or international body on a periodic basis, and whenever new machines are installed and commissioned. At present, the IAEA–WHO postal thermoluminescent dosimeter service checks only about 600 photon beams and none of the electron beams used to treat cancer patients. It is estimated that the reference dose in approximately half of the clinical beams and in most of the electron beams used worldwide to treat patients is not checked at all. Furthermore, only a handful of radiation beams are checked outside the conditions for reference dosimetry by specialized auditing institutions.

The IAEA is fully aware of the needs in the field and works to bridge the gap. Specifically, the IAEA intends to request extrabudgetary funding to support the growing needs of its Member States for dosimetry audits.

As you are certainly aware, within the IAEA, the mandate of the Division of Human Health is to enhance the capabilities in Member States to address needs related to the prevention, diagnosis and treatment of health problems through the application of nuclear techniques. Therefore, we have a strong focus on quality assurance to ensure the safe and effective use of radiation in medicine.

This symposium will address all areas of dosimetry, not only in radiotherapy but also in imaging, covering both diagnostic radiology and nuclear medicine, with about 30% of submitted synopses being in the field of imaging.

As acting Director of the Division of Human Health, I wish also to mention a very recent achievement. I refer to the completion of the Human Health Campus as an educational resource for professionals involved in the delivery of radiation medicine services, covering the different fields where the division is active. It required a major time commitment to prepare and we are particularly proud of the current version. This campus is available on-line at humanhealth.iaea.org.

The programme of this symposium has many other interesting sessions planned. In particular, I draw your attention to the session on dosimetry for small and non-standard radiation fields, which I hope will lead to a better understanding of the dosimetry issues for new technologies used in radiotherapy. As a nuclear medicine physician, I also note the session on internal dosimetry, which, among other topics, will address image based patient specific dosimetry and good practice for clinical dosimetry, increasingly requested for therapeutic applications of radionuclides and/or radiopharmaceuticals.

I would like to express my appreciation to the 12 organizations, including the World Health Organization, which have worked with the IAEA on organizing

this symposium. I thank all the organizations that have supported invited speakers financially so they are able to join us this week and to share their knowledge in this field. They are the International Organization for Medical Physics, the European Society for Therapeutic Radiology and Oncology, the American Association of Physicists in Medicine, the Bureau international des poids et mesures (BIPM), the European Federation of Organisations for Medical Physics, the International Commission on Radiation Units and Measurements (ICRU), the International Commission on Radiological Protection, the Institute of Physics and Engineering in Medicine and the WHO. At the international level, both the BIPM and the ICRU play a major role in radiation dosimetry and collaborate with the IAEA.

I am grateful to the 16 companies whose voluntary contributions were used to fund the participants from low and middle income countries to enable them to attend this symposium. I welcome the technical exhibitors and I am pleased by the potential interaction between industry, the IAEA and Member States. I urge delegates to visit the exhibits to learn about their new equipment in order to have a better idea of what manufacturers have to offer and also on future developments.

The Department of Technical Cooperation has provided very strong support to the symposium through the Interregional Technical Cooperation Project INT/6/054 on strengthening medical physics in radiation medicine. This is greatly appreciated. My colleague, D. Magliani, who is acting Deputy Director General for the Department of Technical Cooperation, will deliver her opening statement momentarily. The contribution from our colleagues in the Department of Nuclear Safety and Security on radiation protection dosimetry is also highly appreciated.

The collaboration of the cooperating organizations has helped to ensure that this meeting is truly international, consistent with the name and mission of the IAEA itself. You have a challenging programme ahead of you, thanks to the diligence of the symposium programme committee. The time and effort they have spent to help create this programme will, I am sure, be well rewarded.

Scientific meetings take place all too often with little proactive attempt to impact on strategic direction within the field. In the concluding session, you will have the chance to point to and influence future work in medical radiation dosimetry. Where are the gaps in our knowledge of the field of radiation dosimetry? What are the recent developments in dosimetry standards? What are the main quality assurance issues at the end-users' level? What should the priorities be, and so on? The issues identified will be used as a challenge to those in the field, including the IAEA.

During the week, you will have the opportunity to listen to 70 speakers and to visit and discuss about 200 posters. In order to create a record of all this intellectual activity, the intention is to prepare the proceedings of this symposium.

On your behalf I would like to thank the 55 reviewers, including the IAEA staff, who reviewed 326 synopses and 80 full papers. They reflect the importance and scientific quality of the symposium.

In conclusion, I trust that you will have a stimulating and interesting meeting. Vienna has a long and distinguished history in both the arts and sciences. This conference continues those traditions. Please use this opportunity to interact with each other to the fullest extent possible, to enjoy this unique environment and to exchange your experiences and ideas for the future. I wish you every success.

OPENING ADDRESS

A.M. Cetto
International Atomic Energy Agency

Presented by D. Magliani

I am very pleased to address you this morning on behalf of A.-M. Cetto, Head of the Department of Technical Cooperation, as we open this important international symposium. Interest in the symposium has been very high, with the number of registered participants greatly exceeding the number initially expected. Every region is represented in significant number, particularly Europe.

The symposium's aim, to provide a forum to discuss and exchange information on advances over the past decade in radiation dosimetry and its supportive role in radiation medicine and radiation protection, is of high importance to the technical cooperation programme, which has a long standing, well-established focus on health. Accurate measurements in radiation dosimetry are critical in decisions making related to human health and to the safety of radiation workers and the general public, and the focus of this symposium strengthens technical cooperation activities in this sector.

In each programme cycle, the IAEA receives large numbers of requests for technical cooperation support in the fields of dosimetry and medical radiation physics. Currently, we have 144 active projects that include these fields of activity. Under the scope of our interregional technical cooperation project on medical physics in radiation medicine (INT/6/054), the IAEA is working with Member States, international physics societies and the World Health Organization to promote the recognition of medical physics in radiation medicine, and to harmonize educational material in order to ensure the safe and effective diagnosis and treatment of patients. We are very pleased to support the attendance of 36 participants at the symposium under this project. Participants can expect to return home with a fresh overview of the latest developments and trends in radiation dosimetry, and a better understanding of the issues. This will contribute to standardization in the field, leading to improved diagnosis and treatment of patients using radiation medicine. The three educational courses that have been organized to take place between 8:00 and 9:00 on Wednesday, Thursday and Friday of this week, addressing current issues in radiation dosimetry of interest to clinical medical physicists working in radiotherapy, diagnostic radiology and nuclear medicine, will further strengthen participants' knowledge.

Ladies and gentlemen, symposiums such as this are an important means of sharing experiences and learning from each other. In the coming days, you will have the opportunity to participate in a range of topical sessions and round table discussions. By sharing your individual inputs and experiences, you reinforce and enrich scientific exchange, and support the definition of future potential work for the scientific community. I am certain you will experience an informative and thought provoking week, and I wish you well in your discussions.

OPENING ADDRESS

P.J. Allisy-Roberts
Bureau international des poids et mesures

The International Bureau of Weights and Measures, the BIPM, is very pleased to have collaborated with the IAEA for more than 50 years, almost since the IAEA was created in 1957. This was at about the same time that the CIPM set up an international Consultative Committee for Ionizing Radiation Metrology. This committee, on which the IAEA was represented at the start, recommended to the CIPM that an Ionizing Radiation Department be established at the BIPM. The continuing collaboration of the BIPM with the IAEA, particularly in the field of ionizing radiation dosimetry, has been very fruitful over the years, with mutual support in the dissemination of dosimetry standards to all of our Member States. Indeed, the number of countries represented at the IDOS symposium gives a good indication of how widespread the dissemination is now and the BIPM strongly supports this event, as illustrated by the fact that practically the entire BIPM dosimetry team of five is present. The BIPM looks forward to hearing how the dissemination of dosimetry and activity standards can be extended in the future to meet the growing needs for traceability to the international system of units, of which the BIPM is the guardian, and wishes every success for the 2010 IDOS symposium.

OPENING ADDRESS

D.T.L. Jones
International Commission on Radiation Units and Measurements

The International Commission on Radiation Units and Measurements (ICRU) was very pleased to have been involved with this important International Symposium on Standards, Applications and Quality Assurance in Medical Radiation Dosimetry. Its presence affirms the ICRU's strong interest in the subject matter and also cements its long standing and productive association with the IAEA in fields of mutual interest.

Since it was formed in 1925, in order to establish a unit for the measurement of radiation exposure, the ICRU has played a leading role in all aspects of medical radiation dosimetry and was responsible for defining the units for measurement of medical radiation, including the roentgen in 1928, the rad in 1953, and both the gray and the becquerel in 1974.

The ICRU has disseminated its recommendations in more than 80 published reports, many of which have been related exclusively to medical dosimetry or have had important medical dosimetry content, including very recent reports on quality assurance for radiation dosimetry, mammography, intensity modulated radiation therapy and proton therapy.

Reports currently being prepared that will include significant contributions on medical dosimetry are those on quantification of low doses, computerized tomography, brachytherapy, carbon ion therapy, small field therapy and key data for radiation dosimetry.

It was gratifying to see an attendance at the symposium that reflected the burgeoning interest of developing countries in improving standards in medical radiation dosimetry. It must always be borne in mind that the primary objective of medical dosimetry is to ensure that radiation is administered safely to the patient. These medical radiation dosimetry symposiums are important forums for learning, discussion and debate in the field and serve to bring together scientists of diverse backgrounds, knowledge and experience for their mutual benefit. The ICRU looks forward to participating in the next symposium in the series.

ACCURACY REQUIREMENTS IN MEDICAL RADIATION DOSIMETRY

P. ANDREO
Division of Medical Radiation Physics,
Stockholm University and Karolinska Institute,
Stockholm, Sweden
Email address: pedro.andreo@ki.se

Abstract

The need for adopting unambiguous terminology on 'accuracy in medical radiation dosimetry' which is consistent with international recommendations for metrology is emphasized. Uncertainties attainable, or the need for improving their estimates, are analysed for the fields of radiotherapy, diagnostic radiology and nuclear medicine dosimetry. This review centres on uncertainties related to the first step of the dosimetry chain in the three fields, which in all cases involves the use of a detector calibrated by a standards laboratory to determine absorbed dose, air kerma or activity under reference conditions in a clinical environment.

1. INTRODUCTION

Accuracy is a qualitative concept and as such it admits different interpretations. It could mean the difference between the average result of a set of measurements and a reference value, the maximum deviation between them, or a predetermined limit of the maximum deviation that can be accepted. It can also be interpreted by means of an estimated uncertainty, in which case it quantifies the 'quality' of a result after correcting for all suspected components of error.

For the term 'measurement accuracy', the Guide to the Expression of Uncertainty in Measurement (GUM) and the International Vocabulary of Metrology, recently re-issued by the JCGM [1, 2], have adopted the first of the interpretations above, that is, the closeness of the agreement between a result and a reference value. These recommendations clarify that a result can have a negligible error (be very close to a reference value) even though it may have a large uncertainty. They also emphasize that the term 'precision' should not be used for 'accuracy'; instead, precision is used to define measurement repeatability and reproducibility (Ref. [3] uses the terms 'trueness' and 'precision' to describe the accuracy of a measurement). It is stressed that, in spite of these remarks, available in ISO standards many years ago, the scientific

literature still uses incorrectly terms such as ‘precision and accuracy’, uncertainties are classified by their nature (random and systematic) rather than by their method of determination (statistical, type-A, and other means, type-B), errors are taken as uncertainties or combined with them, and differences between results are taken as uncertainties.

The purpose of this review is not to discuss differences or deviations between two clinical measurements or quantities, but rather to analyse the uncertainties required and achievable in medical radiation dosimetry. These are interpreted as the characterization of the dispersion of values that can reasonably be attributed to dosimetry quantities, using their combined standard uncertainty, u_c (or a specified multiple of it, the coverage factor k yielding the expanded uncertainty $U = k\,u_c$) [1]. The quantities are absorbed dose, air kerma or activity, determined through dosimetry measurements in a clinical environment.

In the context of uncertainty in external beam radiotherapy, ICRP 86 [4] grouped the various steps of a radiotherapy treatment according to: (i) reference dose determination or beam calibration, performed with an ionization chamber according to a dosimetry protocol; (ii) procedures involving relative beam dosimetry, performed with any type of detector suitable for measurements in a phantom; (iii) calculation of the dose distribution and dose to be delivered to the patient (monitor units or time to deliver the prescribed dose); and (iv) treatment delivery, accounting for intra- and inter-fraction variations in the patient and treatment machine instability during several weeks of treatment. Uncertainty estimates for the average target dose throughout the entire radiotherapy process were obtained from the combination of the corresponding standard uncertainties of each step, yielding around 5–6% [4].

For diagnostic radiology, for example, one could group the different steps according to: (i) reference dose determination, performed with an ionization chamber according to a dosimetry protocol; (ii) dose determination to the patient throughout the imaging system hardware for the specific clinical procedure; (iii) imaging software analysis used to produce a clinical (digital) image; and (iv) the radiologist interpretation, ideally optimized using ‘receiver operating characteristic’ analysis [5]. It is clear that steps (iii) and (iv) do not involve, per se, radiation dosimetry but they influence considerably the final dose delivered to a patient through a feedback on step (ii). Similar steps could be described for nuclear medicine procedures. Unfortunately, no detailed uncertainty estimates through the entire process exist for any of the imaging modalities.

Dealing with the uncertainties throughout all the possible steps in the various radiation medicine specialties is beyond the intended scope and extension of this work. The focus will be on uncertainties related to the first step, which involves the use of a detector calibrated by a standards laboratory to determine a given quantity in well-defined reference conditions in a clinical environment.

2. EXTERNAL BEAM RADIOTHERAPY DOSIMETRY

Uncertainty estimates in the process of clinical reference dosimetry for external beam radiotherapy have received considerable attention in the last decades (see [6, 7] and references therein) for a formalism based on an air kerma chamber calibration. These were re-estimated according to the recommendations of the GUM [1] for the absorbed dose to water formalism in the IAEA TRS 398 Code of Practice [8], and the final uncertainties became reduced considerably. For ^{60}Co gamma rays, the estimates were for the first time below 1%, whereas for megavoltage photon beams they were between 1% and 1.5%, depending on the combination of the standards laboratory beam quality used to calibrate a chamber and the beam quality correction factor k_Q for the hospital beam (see Table 1). Theestimates were rather similar for the case of electron beams except in the case

TABLE 1. ESTIMATED COMBINED STANDARD UNCERTAINTY IN D_w AT THE REFERENCE DEPTH IN WATER IN MEGAVOLTAGE PHOTON BEAMS

Physical quantity or procedure	Relative standard uncertainty (%)			
Step 1a: standards laboratory	SSDL ^{60}Co	PSDL ^{60}Co	PSDL ^{60}Co + accel.	PSDL accel.
$N_{D,w}$ calibration of the secondary standard	0.5	—	—	—
Long term stability of the secondary standard	0.1	—	—	—
$N_{D,w}$ calibration of the user dosimeter at the standards lab	0.4	0.5	0.5	0.5
Combined uncertainty of Step 1a	0.6	0.5	0.5	0.5
Step 1b: hospital				
Long term stability of user dosimeter	0.3	0.3	0.3	0.3
Establishment of reference conditions	0.4	0.4	0.4	0.4
Dosimeter reading M_Q relative to timer or beam monitor	0.6	0.6	0.6	0.6
Correction for influence quantities k_i	0.4	0.4	0.4	0.4
Beam quality correction, k_Q	1.0[a]	1.0[a]	0.7[b]	—
Combined uncertainty of Step 1b	1.3	1.3	1.1	0.9
Combined standard uncertainty in D_w (Steps 1a + 1b)	1.5	1.4	1.2	1.0

[a] Calculated values.
[b] Measured values normalized to ^{60}Co.

of plane parallel ionization chambers calibrated in a ^{60}Co beam, where the estimate was around 2%.

Even if ^{60}Co beams are used less for radiotherapy treatments in many industrialized countries, uncertainty in their dosimetry is of especial importance because ^{60}Co continues to be the reference quality for most therapeutic beams. Beam quality correction factors k_Q include data for ^{60}Co, either as a normalizing $N_{D,w,Co\text{-}60}$ in an experimental k_Q, or as the product of the water–air stopping power ratio and chamber perturbation correction factors, $(s_{w,air}\, p)_{Q=\text{Co-}60}$, in the denominator of a calculated k_Q. Even if recent data has decreased considerably the uncertainty of some perturbation factors, placing at a comparable level the use of cylindrical and plane parallel ionization chambers, new concerns have been raised. Details can be found in Ref. [9] of this volume, but briefly, for ^{60}Co and all types of charged particle that use ^{60}Co as a reference quality (electrons, protons and heavier ions), new available perturbations data would yield a change in absorbed dose of about 1.5%, representing a considerable discrepancy with current evidence, which is not likely to be in error by such large amount. In the case of megavoltage photon beams a partial cancellation of potential systematic errors occurs, yielding smaller differences.

In general, the uncertainty of calculated beam quality correction factors k_Q is estimated to be around 1% and continues to be one of the major sources of uncertainty in reference radiotherapy dosimetry with conventional beams. It is reasonable to expect that new calorimetric experimental data, for example in the case of photon beams obtained with uncertainties as low as 0.1% [10], would decrease considerably the estimated combined standard uncertainty in D_w. However, because it is unlikely that standard laboratories would decrease the statement of uncertainty provided to the user $N_{D,w}$ much below 0.5%, the final uncertainty will still be close to 1% in the most favourable case (the right hand column of Table 1, which does not rely on k_Q factors). Another argument in support of this hypothesis is the compilation of experimentally determined k_Q factors for Farmer NE-2571 chambers in megavoltage photons (Fig. 1), mostly measured at standard laboratories, which shows a rather scattered distribution. It can therefore be concluded that the standard uncertainties given in TRS 398 can still be considered valid for most users, considering perhaps, that they constitute a conservative estimate. Similar conclusions can be made for the rest of the therapeutic beams, at least until the problematic situation around ^{60}Co is clarified.

So far, the discussion has been on the dosimetry of broad reference beams used for ‘conventional’ radiotherapy. However, the number of patients treated using new therapy techniques based on narrow non-standard fields, or a combination of them, has in many instances reached levels of the order of 30% or even higher in many hospitals. This is especially the case with intensity

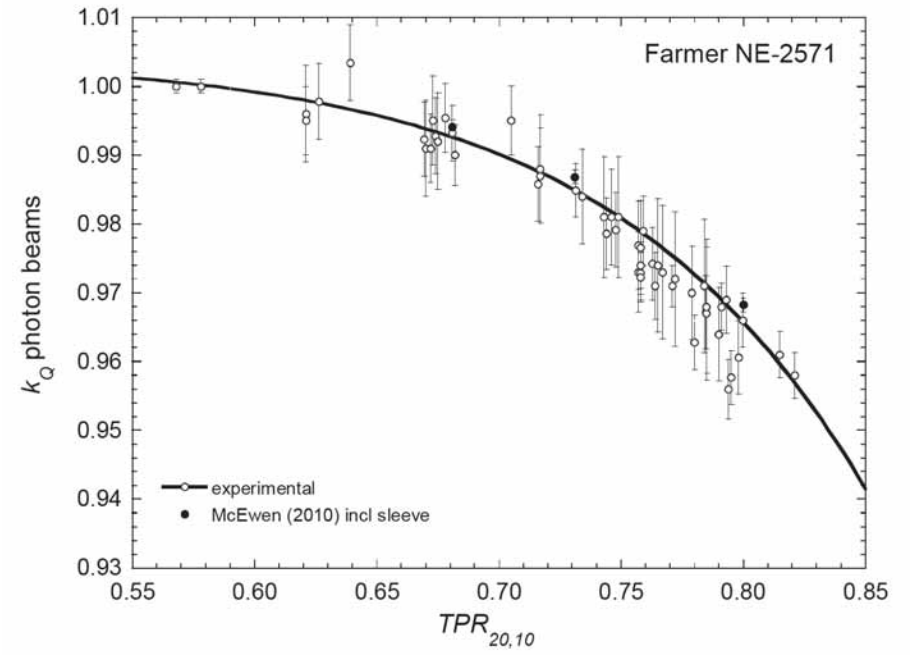

FIG. 1. Compilation of experimentally determined beam quality factors of NE-2571 Farmer chambers as a function of the quality of megavoltage photon beams, adapted from Ref. [19]. The curve is a sigmoid weighted fit of the data. Note that the most recent values (three solid circles), obtained with very low uncertainty [10], pull the curve upwards.

modulated radiotherapy (IMRT), but also with stereotactic radiotherapy and stereotactic body radiotherapy techniques, in some cases based on machines of new design. Leaving aside the non-negligible number of accidents that have occurred with the use of new technologies [11], their reference dosimetry is still far from the uncertainty levels discussed above for conventional radiotherapy. A number of studies have been published which include dosimetric aspects of IMRT [12, 13], although the topics of interest are spatial and positional uncertainties, and 'accuracy' of the treatment planning dose calculation. Yet, the latter is compared with a dose determination according to dosimetry protocols not intended for IMRT, such as TRS 398 [8]. Dosimetry errors have become considerably larger than in conventional beams mostly due to two reasons: (i) the reference conditions recommended by conventional protocols cannot be realised in some machines and (ii) the measurement of absorbed dose in small and composite fields is not standardized. On the other hand, it is known that stopping power ratios are not very sensitive to field size and position in the beam [14], but

perturbation effects and partial irradiation of the chambers may cause major dose errors [15, 16]. No recommendations exist as yet for the reference dosimetry of these non-standard fields, although progress is being made in this direction and the number of papers on the topic in this conference is a proof of evidence.

A new international formalism has been proposed [17] under the auspices of the IAEA in cooperation with the AAPM and other organizations. The formalism has been clearly summarized in Ref. [18] along with the limitations of small beam measurements. One of the key issues in applying the new dosimetry formalism to IMRT is the definition of a suitable reference field which should be as close as possible to a class of clinical plans of interest, and provide a uniform dose over a region exceeding the dimensions of a reference detector. This is a reference field for a class of dynamic or step-and-shoot delivery fields, or a class of combinations of fields in a configuration that is as close as possible to the final clinical delivery scheme, but delivers a homogenous absorbed dose to an extended and geometrically simple target volume (so-called pcsr fields). The second fundamental aspect necessary for the development and implementation of the new formalism is the determination of the necessary factors that link reference dosimetry of conventional radiotherapy to that of IMRT and small fields. This requires a considerable number of Monte Carlo simulations of the new treatment machines and their special collimation systems, as well as of the response of the detectors which can be used for the specific measurement of the reference absorbed dose. An uncertainty analysis of the dose determination under these new reference conditions and data would be needed prior to its clinical implementation.

3. BRACHYTHERAPY DOSIMETRY

The field of brachytherapy, the first medical application of radiation sources with therapy purposes, and until recently considered to have a much larger uncertainty than external beam radiotherapy, has been characterized by an enormous development in dosimetry during the latest years, both at standard laboratories and at the clinical user level. The most striking case is probably related to the calibration of high dose rate (HDR) ^{192}Ir sources, an area where primary standards did not exist a few years ago [20, 21] but several primary standards laboratories offer calibration services today. Some of the calibration procedures have also witnessed a remarkable evolution. For example, the various interpolation methods using N_K calibration coefficients at kV X rays and ^{137}Cs (or ^{60}Co) to derive that of ^{192}Ir [22–24] and obtain the reference air kerma rate (RAKR), recommended few years ago at all levels of the dosimetry chain (c.f. Ref. [20]), have now been superseded by the use of well re-entrant chambers

[25]. The need for verifying calibrations provided by source manufacturers and vendors is always stressed.

Uncertainties associated to the calibration of low dose rate (LDR) low and high energy sources have been analysed following the recommendations of the GUM and mostly considering the scenario of standard laboratories [20]. For all photon reference sources, and irrespective of the type of calibration laboratory and procedure used, the different options yield estimated combined standard uncertainties between 1.2% and 1.5% in the determination of RAKR. It is emphasized that the transfer from a primary to a secondary standards laboratory does not add more than 0.1% to these values. For non-standardized photon sources uncertainties raise up to 2% or 3%. Beta sources have on the other hand a much higher uncertainty, being of the order of 8% at primary laboratories but reaching up to 20% at the end user [20, 21]. Recent estimates for the newly developed HDR ^{192}Ir calibrations have decreased considerably the uncertainty estimates and, for example, IPEM quotes a combined standard uncertainty of 0.4% for well chambers, of which 0.35% arise from the source calibration at the NPL [25]. The most recent and comprehensive analysis of the propagation of uncertainties from the primary to the secondary laboratory and to the user has been performed by the AAPM Task Group 138 [26]. Emphasizing that the final uncertainty in dose delivery with brachytherapy techniques is similar to that of external beam radiotherapy (5% approximately), Task Group 138 details the steps associated to the determination of the RAKR (or air kerma strength, in its terminology) estimating combined standard uncertainties between 1.3% and 1.5% for different scenarios, including the clinical measurements. It is doubtful that these figures can be considered representative for most hospitals worldwide, but certainly they should be considered potential and achievable goals under careful and traceable measuring conditions.

It needs to be pointed out that, although developments have mostly been focused on air kerma standards, and at the hospital the quantity RAKR is determined using well chambers or thimble chambers measurements, some primary standards dosimetry laboratories have recently started the development of absorbed dose to water standards for brachytherapy. The practical implementation of such standards would require the development of an appropriate code of practice, or dosimetry protocol, with the expectation of reducing further the overall uncertainty in the dose delivered to patients.

4. DIAGNOSTIC RADIOLOGY DOSIMETRY

Accuracy requirements in diagnostic radiology have, in general, not been considered ‘essential’ so far. The rationale for this common argument is that risk

effects for radiation induced carcinogenesis are of stochastic nature, and therefore very difficult to estimate at low doses. This contrasts with radiotherapy treatments, where deterministic effects are of primary importance. However, radiation induced secondary cancers by low doses in tissues and organs outside radiotherapy volumes are at present an issue of great scientific interest [27–30]. This is especially critical considering today's major improvement of survival rates, and is of major concern for children and young radiotherapy patients. According to Hall [27], about 1.5% of the radiotherapy patients that survive 10 years will develop a secondary cancer as a consequence of these low doses; the percentage is expected to be doubled with the use of new radiotherapy techniques (IMRT, protons, carbon ions).

Hall [27] also emphasized that in diagnostic radiology it is clear that simple film techniques (i.e. chest X rays) involve dose deliveries far below the level at which epidemiological data show radiation induced cancer risk. If there is a risk, it must be small, even if multiplied by billions of examinations worldwide results in a large population dose. On the other hand, CT, especially advanced fast techniques using a large number of slices, and modern interventional radiology, involve the delivery of considerable dose. Quoting Hall, "they are in fact comparable with the lower end of the range of doses for which there are cancer risk estimates from the A-bomb survivors". Much has been argued on the linear no threshold model recommended by the ICRP [31], often questioned in relation with its consistency with radiobiological data (see a recent review by Tubiana [32] and references therein), but probably still remaining the most prudent risk model that can be interpreted and implemented. Figure 2, adopted from Hall [27], provides an overview of competing mechanisms at low and high dose levels which could influence cancer risks, at both ends.

The discussion above could be considered a motivation for the need of establishing a reasonably accurate dosimetry, capable of defining better low dose–effect relationships. One could say that the time is probably ripe for improving the accuracy in diagnostic radiology dosimetry under reference conditions. In addition, the wide availability of digital radiology and computerized records for enormous numbers of patients will soon yield absorbed dose data that so far no other 'experiment' has been capable of producing. At this point it is worth mentioning that the development of digital detectors yields, at least in theory, the possibility to reduce the dose delivered to patients because of their more linear dose response combined with digital post-processing. However, beam qualities should be designed to match the detector energy response, which is different from that of conventional radiographic film.

The IAEA TRS 457 Code of Practice for dosimetry in diagnostic radiology [33] provides detailed recommendations for the determination of air kerma under

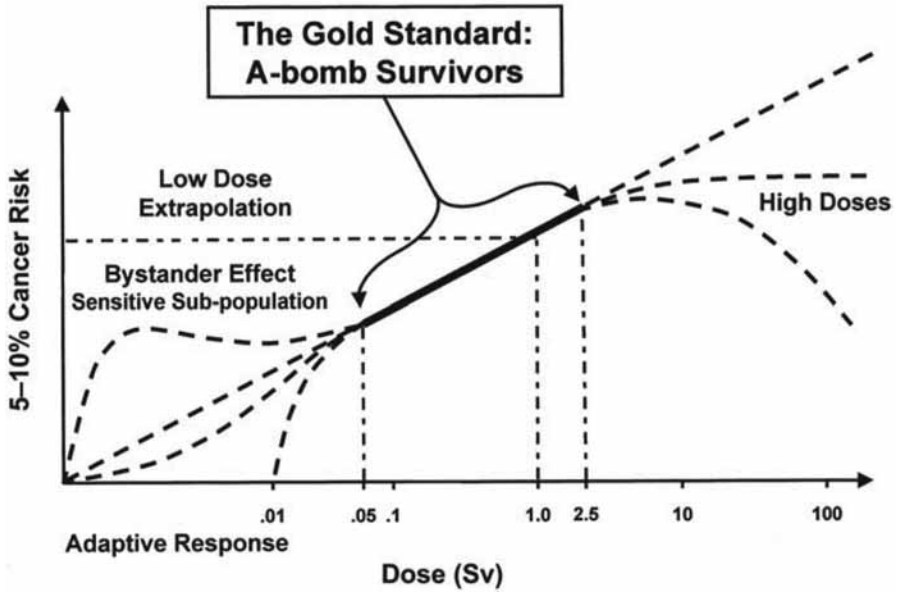

FIG. 2. Dose–response relationship for radiation induced carcinogenesis. The A-bomb data represent the 'gold standard', i.e. the best quantitative data over a dose range from about 0.1 to 2.5 Gy. Above and below this dose range, there is considerable uncertainty. At doses below this range, the ICRP [31] recommends a linear extrapolation from the high dose data; however, the bystander effect and existence of radiosensitive subpopulations would suggest this would underestimate risks, while phenomena such as the adaptive response would suggest a linear extrapolation would overestimate risks at low doses. There is equal uncertainty concerning the dose–response relationship at high doses, which is characteristic of radiation therapy. (Reproduced from Hall [27], with permission of the author).

reference conditions in clinical practice, the first step of the dosimetry chain, setting a goal of 3.5% for its relative standard uncertainty. This estimate can vary for different scenarios, ranging approximately between 2.7% and 6.3%. There are, however, a number of issues affecting the achievable uncertainty to be considered at the hospital, some of them discussed at depth in a recent IAEA report [34] on the practical implementation of TRS 457.

The strong energy dependence of the response of ionization chambers and kerma area product (KAP) meters at low photon energies is well known. For the ion chambers, Fig. 10 in TRS 398 [8] showed variations in N_K calibration coefficients of up to 7% for a given chamber type (PTW M23342) as a function of the kV, and up to 2% for a given HVL with different kVs. For KAP meters, similar results were found by Toroi [35], 5% and 2% respectively, which in addition included detailed information on beam filtration. These results

confirmed what has long been known [36]: (a) that one single parameter is not enough to specify appropriately the quality of the beam, (b) that at least two parameters are needed, and (c) that the interpolation of calibration coefficients is an additional source of uncertainty. In this respect, it is worth quoting ICRU 74 [37]: "In most cases, the quality of an X-ray beam can be adequately specified by means of the combined information on tube voltage, HVL_1, and HVL_2, or the tube voltage, HVL_1, and total filtration." The need for additionally specifying the HVL_2, or information on the total filtration, suggests using the 'homogeneity coefficient' defined as the ratio $h = HVL_1/HVL_2$ [36], which is unity for monoenergetic rays. Thus, the triplet (kV, HVL_1, h) could be used for the beam quality specification of kV X rays.

A second issue of importance, closely related to the discussion above, is the difference between the beam qualities at the standard laboratories and those used for clinical practice at hospitals. A decade ago this topic generated vigorous debates in radiotherapy dosimetry [38], leading to the worldwide preferred option for using medical accelerators at standard laboratories; the IAEA then acquired a clinical mammography unit for chamber calibrations at its standards laboratory. Excluding mammography, radiodiagnostic beam qualities at most standards laboratories usually rely on the so-called RQR, RQA and RQT specifications of IEC-61267 [39]. However, manufacturer trends in recent years have produced a much broader range of qualities which are widely used at hospitals. Fig. 3 illustrates this point, showing the differences in beam quality at laboratories and large hospitals, and the zones where users are not able to get detector calibrations and must rely on inaccurate interpolations and sometimes extrapolations.

Interesting enough, the situation is reversed in the case of mammography X ray beams. For example the PTB catalogue shows 140 different beam qualities for this diagnostic modality, generated by seven tube voltages between 20 kV and 50 kV, three targets (Mo, Rh, W) and five filter materials (Al, Mo, Rh, Pd, Ag; sometimes the filtration includes two materials). Only eight of these qualities have a correspondence with the RQR-M and RQA-M specifications of IEC-61267 [39]. On the other hand, four modern mammography units (from three manufacturers) in two large hospitals in Sweden routinely perform examinations with 33 beam qualities, all generated with W targets and using Rh and Ag filtrations, covering a rather small fraction of the qualities available at PTB. The situation is not too different in the United Kingdom according to the beam quality recommendations of its NHS Breast Screening Programme (NHSBSP) [40], even if advanced new machines evaluated by the NHSBSP are considered [41], and recently published data for the UK, European and IAEA breast dosimetry protocols [42], which include a broad periphery of qualities, are restricted to an interval of 25–40 kV (0.36–0.82 mm Al HVL). The scenario is illustrated in

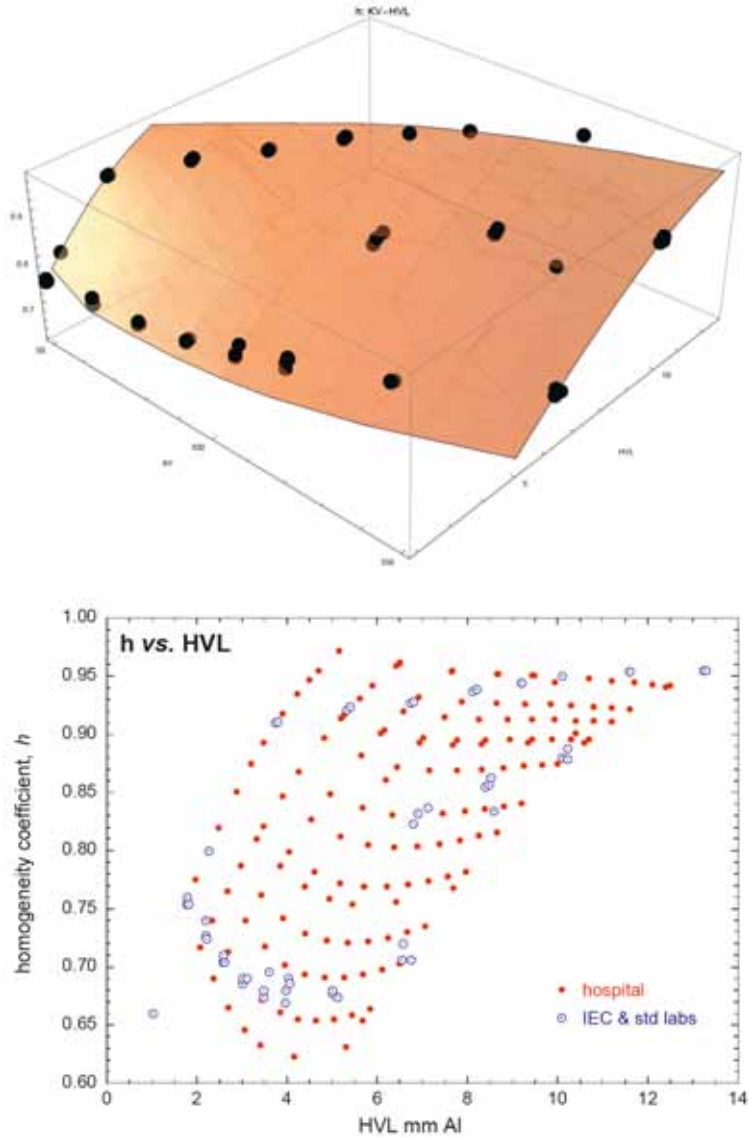

FIG. 3. The upper panel illustrates beam qualities for diagnostic X rays generally available at standards laboratories (dots) for general radiography, fluoroscopy and computed tomography, and at a large hospital (transparent surface), showing the reduced zones where users can get detector calibrations. The lower panel shows the differences in beam filtration (through the homogeneity coefficient, h) as a function of the HVL.

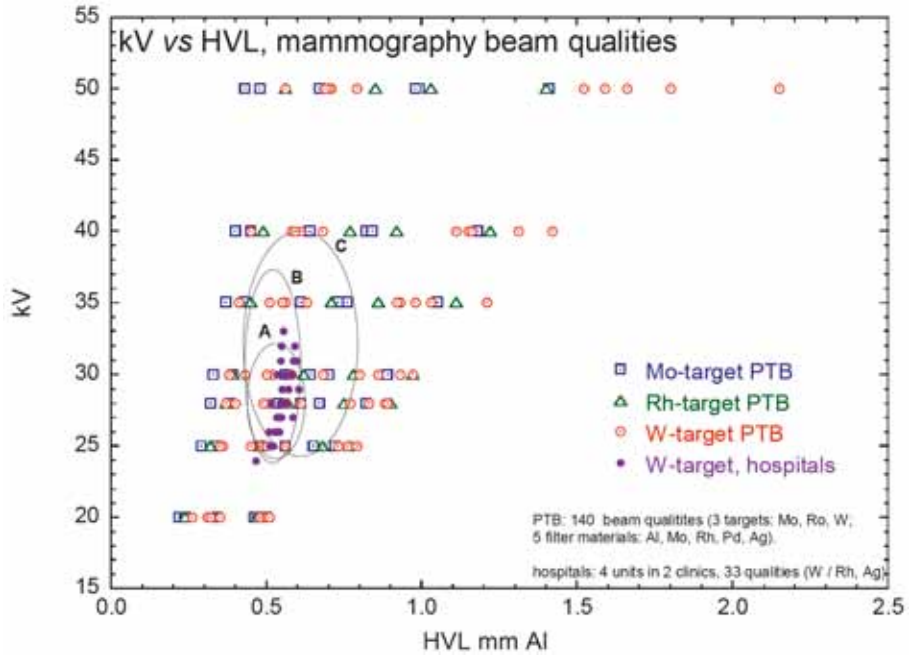

FIG. 4. Range of beam qualities for mammography X rays available at a primary standards dosimetry laboratory (PTB, Germany) and qualities used for clinical routine examinations at two large hospitals in Sweden (from three manufacturers), open and filled symbols. The ellipses A, B and C correspond, respectively, to the beam quality recommendations of the UK's NHSBSP [40], to the qualities of an advanced new machine evaluated by the NHSBSP [41], and to recent data for the UK, European and IAEA breast dosimetry protocols [42], which include a broad periphery of qualities.

Fig. 4. It is not known if the clinical use of mammography X ray beams in other countries and regions is very different from the cases mentioned.

The same type of constraints with regard to beam quality applies to the availability of dosimetric data, for instance the backscatter factors included in TRS 457. These are given for a reduced quality range compared with that at the clinic (see Fig. 5) and, interesting enough, the qualities do not match IEC specifications either. Again, it is the user who must develop a mechanism for interpolating or acquiring the necessary data. An aspect which aggravates the situation is the availability of advanced interventional radiology units capable of modifying the quality of the beam dynamically during a clinical exploration. Kilovoltage and filtration, as well as beam intensity, are varied according to a pre-established protocol in order to improve the image registered in digital detectors (as feedback), yielding what, in parallel with IMRT, could be termed

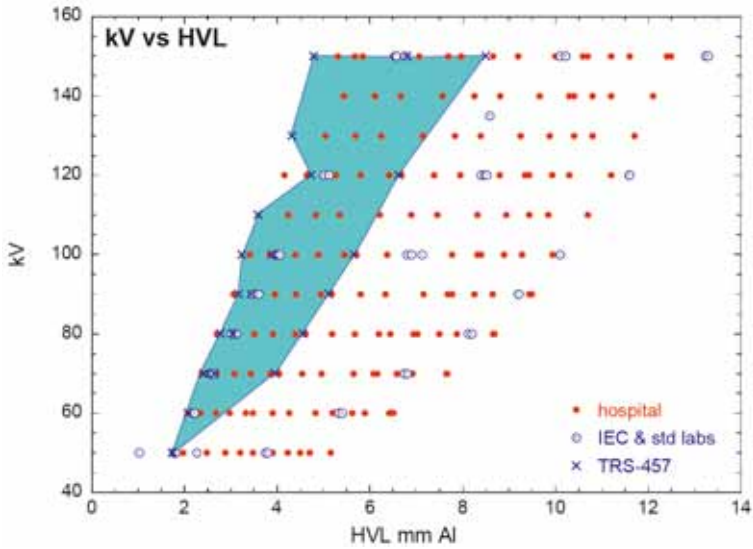

FIG. 5. Beam qualities (kV, HVL) for which backscatter factors (B) are given in IAEA TRS 457 (surface) and those where data are needed at large hospitals (dots). Open circles correspond to IEC qualities and those generally available at standards laboratories.

intensity modulated diagnostic radiology or beam modulated diagnostic radiology.

Last, but not least, the configuration used at some standard laboratories for the calibration of KAP meters deserves being mentioned. Although TRS 457 provides detailed protocols for calibrations both in terms of transmitted and of incident radiation, the latter is unfortunately still in common use. This leaves the user with the responsibility of 'correcting' the value of the calibration coefficient for the attenuation (absorption and scattering) in the chamber walls which, even if done in an approximate manner, requires knowledge of specific constructional details at a level not readily available to many users.

5. NUCLEAR MEDICINE DOSIMETRY

Dosimetry in nuclear medicine is still dominated by a large uncertainty in dose delivery, both in diagnostic and in therapeutic procedures. In the first case, stochastic effects are of importance, and the general arguments given under diagnostic radiology would apply. In therapeutic procedures, however, deterministic effects are the primary goal. The criticality of a ±5% tolerance

interval, demonstrated clinically in radiotherapy, raises concern with regard to the lack of ‘accuracy requirements’ in nuclear medicine and its therapeutic efficiency. Should not high accuracy in absorbed dose determination be a requirement for clinical application in radionuclide therapy, just as it is in external beam radiotherapy? Dose delivery in therapeutic nuclear medicine is often governed by a conservative approach; there are, for example, no widely accepted protocols to implement dose escalation, which in turn prevents obtaining clearly differentiated results for various dose delivery schemes, yielding a ‘chicken and egg’ situation. Comprehensive reviews of dosimetry in nuclear medicine [43] describe advanced trends and techniques, as well as issues like patient specific dose calculations, but uncertainty estimates are not even mentioned.

The first step in the dosimetry chain of nuclear medicine is the determination of the activity of a radioactive sample, using a ‘radionuclide activity calibrator’ or re-entrant (well type) ionization chamber. A primary standard laboratory may provide a chamber calibration with a standard uncertainty better than 1.5%, which so far has been thought to reach levels up to ten times higher at the clinic. Recent investigations, however, seem to provide grounds to expect the situation to be slightly better in general. Comparisons among laboratories using test samples of ^{131}I [44] and ^{57}Co (as a surrogate of ^{99m}Tc) [45] have shown ‘degrees of equivalence’[1] to within 4% in both cases, even for laboratories using instrument calibrations by manufacturers. Standard uncertainties estimated by the laboratories for their measurements were up to 5% in the worst case. This means that, hypothetically, using careful methodology a hospital could also achieve this level of accuracy (trueness and uncertainty) for standard volumes and geometries. Unfortunately, it is unrealistic to think that for routine procedures in a hospital such levels can be reached, as shown in some recent comparisons where a considerable number of outliers by more than 10% have been found [46, 47].

6. CONCLUDING REMARKS

A thorough discussion on terms related to ‘accuracy’ emphasizes the need for adopting an unambiguous terminology consistent with international

[1] As defined by the Mutual Recognition Agreement of the Comité International des Poids et Mesures. In measurement comparisons, a reference value is established from the results by standards laboratories (comparison reference value (CRV)). This is compared with the value obtained by a given participant, establishing the degree of equivalence as the difference between this value and the CRV.

recommendations. The concept of tolerance intervals and their relation to the uncertainty of the quantity under consideration are highlighted (see the appendix). Focusing on the first step of the dosimetric chain, the determination of absorbed dose, air kerma or activity under reference conditions, the following remarks can be made in relation with their attainable uncertainty:

- Radiotherapy dosimetry for external beams using conventional treatments appears to be at the level of 1–1.5% in most cases, and in general it seems improbable to lower this level. The current status for the common reference quality ^{60}Co creates unexpected unknowns which need to be resolved urgently. Advanced radiotherapy with narrow non-standard fields (radiosurgery), or a combination of them (IMRT), needs standardization in its dosimetry which will allow reliable uncertainty estimates, non-existent at present.
- Brachytherapy dosimetry has made big advances in recent years, notably with the development of primary standards at various laboratories. As a result, the use of well-chambers has been encouraged. In general, for all LDR and HDR photon sources, uncertainties are estimated to be within a 1%–1.5% interval, even if for ^{192}Ir HDR sources, estimated uncertainties have become even lower in the UK (0.4%). Ongoing developments of absorbed dose to water primary standards point at the convenience of developing a dosimetry protocol for brachytherapy in the near future.
- Current developments in radiobiology and radiation protection motivate the need for establishing a reasonably accurate dosimetry in radiodiagnostic procedures. Although the IAEA TRS 457 protocol has provided a mechanism for achieving this goal, issues mostly left to the user's responsibility jeopardize accuracy at the clinic. Differences in beam quality between standards laboratories and hospitals, and lack of data relevant to clinical use, have been emphasized.
- Nuclear medicine dosimetry continues requiring attention, especially for radionuclide therapy, where requirements similar to those in external beam radiotherapy would need to be developed. These requirements would promote the improvement of activity measurements whose potentiality has been demonstrated through careful studies.

Appendix

ON ACCURACY, UNCERTAINTY AND TOLERANCE

Paraphrasing J. Müller [48], some ruminations on accuracy, uncertainty and tolerance are presented in this appendix. The discussion takes radiotherapy as the main example because this is the only radiation medicine specialty where dosimetry accuracy requirements have been discussed at length. The concepts can be extended to any other specialty as long as a clinical requirement can be made for dosimetry accuracy, which in radiotherapy could be interpreted, for instance, as the maximum deviation between the prescribed and the delivered dose.

In its Report 24 on patient dose determination in radiotherapy procedures, the ICRU [49] concluded in 1976 a "need for an accuracy of ±5% in the delivery of an absorbed dose to a target volume if the eradication of the primary tumour is sought". According to some authors [50, 51] this requirement was based on the clinical evidence that deviations of ±10% in the dose delivered can significantly change the probability of tumour control or normal tissue complication, so that "the accuracy needed had to be smaller". Wambersie [51] clarified that the ±5% accuracy requirement was selected as a "reasonable compromise" between what should be ideal and what could be reached in practice. More recent and specific analysis based on clinical data [52] have complemented these references, confirming estimates already made 40 years ago [53]; it has also been indicated that the accuracy requirement limits vary for different tumour types. Thus, there appears to be a wide consensus to conclude that, in general, a dose delivery outside the ±10% limits has immediate clinical relevance.

The terms 'tolerance limit' and 'tolerance interval' are widely used in engineering and industry. The limits of the variation allowed for the values of a given parameter are known as the tolerance limits of the parameter and define the tolerance interval[2]. It seems therefore reasonable to use the ±10% difference between prescribed and delivered dose as a 'tolerance interval' $\pm T$ outside which most fractionated curative treatments would be considered unacceptable. However, the quantity absorbed dose, as with any other parameter, has an uncertainty $\pm U$ associated with its value that reflects the lack of 'exact knowledge' of the quantity. To take into account the influence of the uncertainty

[2] The ISO standard 3534 on statistical quality control [54] defines tolerance interval as the variate values of the characteristic between and including the tolerance limits (1.4.5). These are the upper and lower bounds of the permissible values (1.4.3).

U, and establish unequivocally that a result is within tolerance, the tolerance interval *T* has to be reduced to what could be termed 'corrected tolerance interval' $T_c = \pm(T\text{-}U)$; otherwise, some results may fall outside the required interval. The illustration of this concept is shown in Fig. 6 where the shaded areas correspond to the estimated standard uncertainty of a hypothetical parameter determination.

There are no details on the clinical data available, or in the references mentioned above, to ascertain if the range of dose deviations within ±10% (or any other limits) should be interpreted as a tolerance interval, or if the limits stated already took into account dosimetry uncertainties, in which case they would correspond to the bounds of a corrected tolerance interval. In the first case, using a commonly estimated dosimetry uncertainty for the entire radiotherapy process (around 5% or 6%, see Ref. [4]), would make the corrected tolerance interval around the 'optimal dose' to be approximately ±5%, which incidentally coincides with the accuracy requirement of ICRU 24 [49]. The corrected tolerance interval would be wider if the uncertainties in dose delivery were smaller, as the shaded areas in Fig. 7 would become narrower.

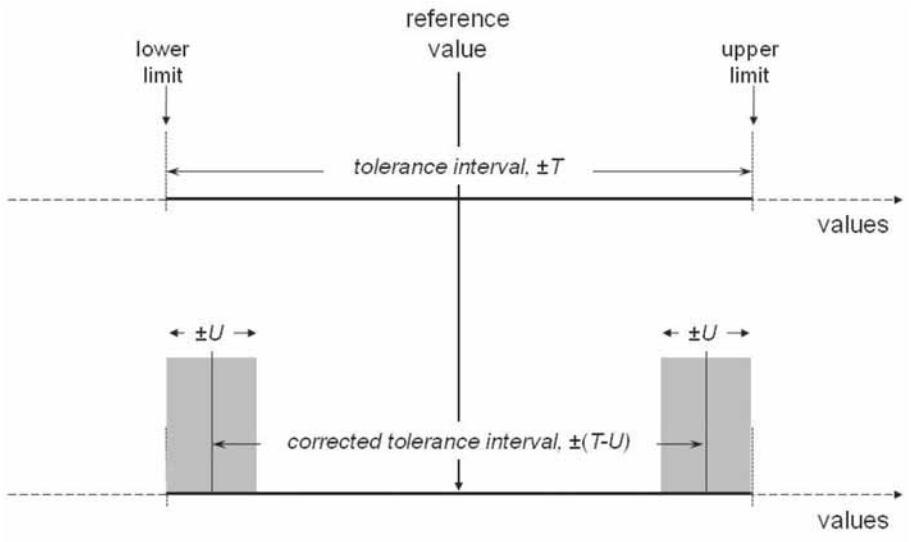

FIG. 6. Illustration of the concepts 'tolerance interval' and 'corrected tolerance interval' for a hypothetical process. The upper panel represents the range of acceptable values along the axis (dashed) between two limiting bounds around a reference value, which corresponds to the tolerance interval, ±T. The lower panel shows the effect of the uncertainty ±U of the values (shaded areas) decreasing the width of the tolerance interval; the constricted range corresponds to the corrected tolerance interval, $T_c = \pm(T\text{-}U)$. The height of the shaded areas are shown for clarification purposes and do not correspond to amplitudes.

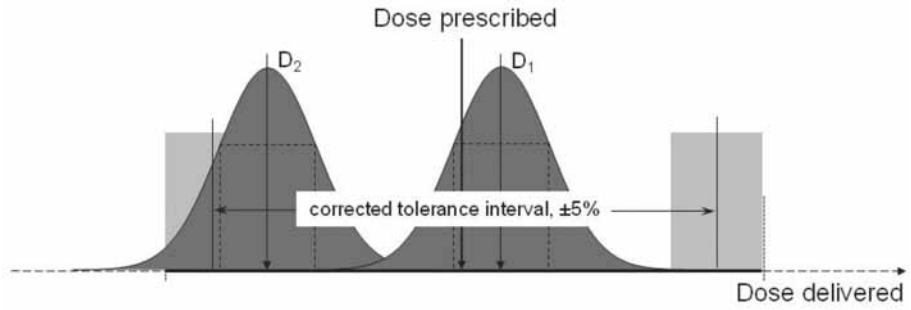

FIG. 7. Two hypothetical radiotherapy dose deliveries, D_1 and D_2, including their uncertainties, are illustrated as Gaussian distributions with mean values within the ±5% range of acceptable values around the prescribed dose. The distributions should fit as much as possible within the corrected tolerance interval, which is not the case for D_2 even if its mean value falls within the corrected tolerance interval. The height of the shaded areas and Gaussians are shown for clarification purposes and do not correspond to amplitudes.

It is unfortunate that the numerical values of the corrected tolerance interval and the uncertainty that can be achieved in radiotherapy are so close, making radiotherapy a very special process with little parallelism in other branches of science, where uncertainties are usually only a fraction of the tolerance. However, radiotherapy is not the only field in which the limits are about the same magnitude as the measurement uncertainty. It also occurs in monitoring the environmental dose rates around the perimeters of nuclear reactors, where international dose limits are comparable with the level of natural background radiation.

To conclude, the model presented here leads to postulating that the recommended 'accuracy of ±5%' in dose delivery (or any accuracy requirement in another speciality) does not correspond to an uncertainty estimate but to an interval of 'acceptable' dose deviations, which has been determined empirically. It is the dose delivery itself which has an uncertainty, and the corresponding dose distribution must fit as much as possible within the required corrected tolerance interval (see Fig. 7). This represents a difference from the interpretations of other authors [52, 55, 56] with regard to the ICRU 24 'need for accuracy' being at one, one and a half, or two standard deviations.

ACKNOWLEDGEMENTS

The author is indebted to A. Fransson for her generous contribution to the section on diagnostic radiology, and to S. Palm on nuclear medicine. Fruitful discussions over the years on accuracy, uncertainty and tolerance in radiotherapy with A. Brosed, J.E. Burns and P. Ortiz are gratefully acknowledged.

REFERENCES

[1] JOINT COMMITTEE FOR GUIDES IN METROLOGY, Evaluation of measurement data — Guide to the expression of uncertainty in measurement (GUM), JCGM/WG 1 Rep. 100:2008, BIPM, Sévres (2008).

[2] JOINT COMMITTEE FOR GUIDES IN METROLOGY, International vocabulary of metrology — Basic and general concepts and associated terms (VIM), JCGM/WG 2 Rep. 200:2008, BIPM, Sévres (2008).

[3] INTERNATIONAL ORGANIZATION FOR STANDARDIZATION, Accuracy (trueness and precision) of measurement methods and results, ISO Rep. 5725, Geneva (1994).

[4] INTERNATIONAL COMMISSION ON RADIOLOGICAL PROTECTION, Prevention of Accidental Exposures to Patients Undergoing Radiation Therapy, ICRP Publication 86, Annals of the ICRP **30** (2000).

[5] INTERNATIONAL COMMISSION ON RADIATION UNITS AND MEASUREMENTS, Receiver Operating Characteristic Analysis in Medical Imaging, ICRU Rep. 79, Bethesda, MD (2008).

[6] ANDREO, P., Uncertainties in dosimetric data and beam calibration, Int. J. Radiation Oncology Biol. Phys. **19** (1990) 1223-1247.

[7] THWAITES, D.I., "Uncertainties at the end point of the basic dosimetry chain", Measurement Assurance in Dosimetry (Proc. Symp. Vienna, 1993), IAEA, Vienna (1994) 239–255.

[8] INTERNATIONAL ATOMIC ENERGY AGENCY, Absorbed Dose Determination in External Beam Radiotherapy: An International Code of Practice for Dosimetry Based on Standards of Absorbed Dose to Water, Technical Reports Series No. 398, IAEA, Vienna (2000).

[9] BENMAKHLOUF, H., ANDREO, P., "Ten years after: Impact of recent research in photon and electron beam dosimetry on the IAEA TRS-398 Code of Practice", these Proceedings, Vol. 1 .

[10] McEWEN, M.R., Measurement of ionization chamber absorbed dose k_Q factors in megavoltage photon beams, Med. Phys. **37** (2010) 2179-2193.

[11] INTERNATIONAL COMMISSION ON RADIOLOGICAL PROTECTION, Preventing Accidental Exposures from New External Beam Radiation Therapy Technologies, ICRP Publication 112, Annals of the ICRP **39** (2009).

[12] JIN, H., PALTA, J., SUH, T.S., KIM, S., A generalized a priori dose uncertainty model of IMRT delivery, Med. Phys. **35** (2008) 982-996.

[13] ZEFKILI, S., et al., Recommandations pour un protocole d'assurance de qualité de la radiothérapie conformationnelle avec modulation d'intensité des cancers de la tête et du cou. [Recommendations for a head and neck IMRT quality assurance protocol], Cancer/Radiothérapie **8** (2004) 364–379.

[14] SÁNCHEZ-DOBLADO, F., ANDREO, P., CAPOTE, R., LEAL, A., PERUCHA, M., et al., Ionization chamber dosimetry of small photon fields: A Monte Carlo study on stopping-power ratios for radiosurgery and IMRT beams, Phys. Med. Biol. **48** (2003) 2081–2099.

[15] BOUCHARD, H., SEUNTJENS, J., Ionization chamber-based reference dosimetry of intensity modulated radiation beams, Med. Phys. **31** (2004) 2453–2464.

[16] CAPOTE, R., et al., An EGSnrc Monte Carlo study of the microionization chamber for reference dosimetry of narrow irregular IMRT beamlets, Med. Phys. **31** (2004) 2416–2422.

[17] ALFONSO, R., et al., A new formalism for reference dosimetry of small and nonstandard fields, Med. Phys. **35** (2008) 5179–5186.

[18] MACKIE, T.R., "Dosimetry for IMRT", Clinical Dosimetry Measurements in Radiotherapy, (Rogers, D.W.O.and Cygler, J.E., Eds), Medical Physics Publishing, Madison, WI, (2009) 605–635.

[19] ANDREO, P., A comparison between calculated and experimental k_Q photon beam quality correction factors, Phys Med Biol **45** (2000) L25-38.

[20] INTERNATIONAL ATOMIC ENERGY AGENCY, Calibration of Photon and Beta Ray Sources Used in Brachytherapy, IAEA-TECDOC-1274, IAEA, Vienna (2002).

[21] SOARES, C.G., DOUYSSET, G., MITCH, M.G., Primary standards and dosimetry protocols for brachytherapy sources, Metrologia **46** (2009) S80-S98.

[22] BUERMANN, L., KRAMER, H.M., SCHRADER, H., SELBACH, H.J., Activity determination of ^{192}Ir solid sources by ionization chamber measurements using calculated corrections for self-absorption, Nucl. Instr. Meth. A. **339** (1994) 369–376.

[23] VERHAEGEN, F., VAN DIJK, E., THIERENS, H., AALBERS, A., SEUNTJENS, J., Calibration of low activity ^{192}Ir brachytherapy sources in terms of air kerma rate with large volume spherical ionization chambers, Phys. Med. Biol. **37** (1992) 2071–2082.

[24] GOETSCH, S.J., ATTIX, F.H., PEARSON, D.W., THOMADSEN, B.R., Calibration of ^{192}Ir high-dose-rate afterloading systems, Med. Phys. **18** (1991) 462–467.

[25] BIDMEAD, A.M., et al., The IPEM code of practice dor determination of the reference air kerma rate for HDR ^{192}Ir brachytherapy sources based on the NPL air kerma standard, Phys. Med. Biol. **55** (2010) 3145–3159.

[26] DEWERD, L.A., et al., A dosimetric uncertainty analysis for photon-emitting brachytherapy sources: Report of AAPM Task Group No. 138 and GEC-ESTRO, Med. Phys. **38** (2011) in press.

[27] HALL, E.J., Henry S. Kaplan Distinguished Scientist Award 2003. The crooked shall be straight; dose-response relationships for carcinogenesis, Int. J. Radiat. Biol. **80** (2004) 327–337.

[28] HALL, E.J., The inaugural Frank Ellis Lecture-latrogenic cancer: the impact of intensity-modulated radiotherapy, Clin Oncol (R Coll Radiol) **18** (2006) 277–282.

[29] HALL, E.J., Intensity-modulated radiation therapy, protons, and the risk of second cancers, Int. J. Radiat. Oncol. Biol. Phys. **65** (2006) 1–7.

[30] TUBIANA, M., Can we reduce the incidence of second primary malignancies occurring radiotherapy? A critical review, Radiother. Oncol. **91** (2009) 4–15.
[31] INTERNATIONAL COMMISSION ON RADIOLOGICAL PROTECTION, Low-dose extrapolation of radiation-related cancer risk, ICRP Publication 99, Annals of the ICRP **35** (2005).
[32] TUBIANA, M., FEINENDEGEN, L.E., YANG, C., KAMINSKI, J.M., The linear no-threshold relationship is inconsistent with radiation experimental data, Radiology **251** (2009) 13–22.
[33] INTERNATIONAL ATOMIC ENERGY AGENCY, Dosimetry in Diagnostic Radiology: An International Code of Practice, Technical Reports Series No. 457, IAEA, Vienna (2007).
[34] INTERNATIONAL ATOMIC ENERGY AGENCY, Implementation of the International Code of Practice on Dosimetry in Radiotherapy (TRS 398): Review of Testing Results, IAEA-TECDOC-1455, IAEA, Vienna (2005).
[35] TOROI, P., KOMPPA, T., KOSUNEN, A., TAPIOVAARA, M., Effects of radiation quality on the calibration of kerma-area product x-ray beams, Phys. Med. Biol. **53** (2008) 5207-21.
[36] INTERNATIONAL COMMISSION ON RADIATION UNITS AND MEASUREMENTS, Physical aspects of irradiation, ICRU Rep. 10b, Bethesda, MD (1962).
[37] INTERNATIONAL COMMISSION ON RADIATION UNITS AND MEASUREMENTS, Patient Dosimetry for X Rays Used in Medical Imaging, ICRU Rep. 74, Bethesda, MD (2006).
[38] ANDREO, P., On the beam quality specification of high-energy photons for radiotherapy dosimetry, Med Phys **27** (2000) 434-40.
[39] INTERNATIONAL ELECTROTECHNICAL COMMISSION, Medical diagnostic X-ray equipment — Radiation conditions for use in the determination of characteristics, IEC Rep. 61267 2nd ed, Geneva (2005).
[40] NHS CANCER SCREENING PROGRAMMES, Guidance on beam quality selection in the NHS Breast Screening Programme, NHSBSP Rep. 0704, Sheffield, UK (2007).
[41] NHS CANCER SCREENING PROGRAMMES, Technical evaluation of the Sectra MDM-L30 full field digital mammography system, NHSBSP Rep. 0805, Sheffield, UK (2007).
[42] DANCE, D.R., YOUNG, K.C., VAN ENGEN, R.E., Further factors for the estimation of mean glandular dose using the United Kingdom, European and IAEA breast dosimetry protocols, Phys. Med. Biol. **54** (2009) 4361–4372.
[43] STABIN, M.G., TAGESSON, M., THOMAS, S.R., LJUNGBERG, M., STRAND, S.E., Radiation dosimetry in nuclear medicine, Appl. Radiat. Isot. **50** (1999) 73–87.
[44] ZIMMERMAN, B.E., MEGHZIFENE, A., SHORTT, K.R., Establishing measurement traceability for national laboratories: Results IAEA comparison of ^{131}I, Appl. Radiat. Isot. **66** (2008) 954-9.
[45] ZIMMERMAN, B.E., PALM, S., Results of an international comparison of ^{57}Co, Appl. Radiat. Isot. **68** (2010) 1217-20.
[46] DOS SANTOS, J.A., et al., National intercomparison program for radiopharmaceutical activity measurements, Appl. Radiat. Isot. **60** (2004) 523–527.

[47] SMART, R., Australian Radionuclide Dose Calibrator Survey 2007/08, ANZ Nucl. Med. **39** (2008) 14–17.
[48] MÜLLER, J.W., "Ruminations on uncertainties — Question and answers, invited review paper", International Symposium on Metrology INSYMET '86 (Proc. Conf. CTVSV, Bratislava, 1986).
[49] INTERNATIONAL COMMISSION ON RADIATION UNITS AND MEASUREMENTS, Determination of absorbed dose in a patient irradiated by beams of X or gamma rays in radiotherapy procedures, ICRU Rep. 24, Bethesda, MD (1976).
[50] DUTREIX, A., When and how can we improve precision in radiotherapy?, Radioth. Oncol. **2** (1984) 275–292.
[51] WAMBERSIE, A., VAN DAM, J., HANKS, G., MIJNHEER, B.J., BATTERMANN, J.J., "What accuracy is needed in dosimetry", Radiation Dose in Radiotherapy from Prescription to Delivery, IAEA-TECDOC-734, IAEA, Vienna, (1994) 11–35.
[52] MIJNHEER, B.J., The clinical basis for dosimetric accuracy in radiotherapy, Brit. J. Radiol. Suppl "Radiation Incidents" (1996) 16–20.
[53] HERRING, D.F., COMPTON, D.M.J., "The clinical basis for dosimetric accuracy in radiotherapy", Computers in Radiotherapy, Special Report Series No. 5, Brit. Inst. Radiol., London, (1971) 51–58.
[54] INTERNATIONAL ORGANIZATION FOR STANDARDIZATION, Statistics — Vocabulary and symbols — Part 2: Statistical quality control, ISO Rep. 5725, Geneva (1993).
[55] MIJNHEER, B.J., BATTERMANN, J.J., WAMBERSIE, A., What degree of accuracy is required and can be achieved in photon and neutron therapy?, Radioth. Oncol. **8** (1987) 237–252.
[56] GOITEIN, M., Nonstandard deviations, Med. Phys. 10 (1983) 709–711.

RADIATION MEASUREMENT STANDARDS FOR IMAGING AND THERAPY

(Session 1)

Chairpersons

P.J. ALLISY-ROBERTS
Bureau international des poids et mesures

H.M. KRAMER
Germany

P. ANDREO
Sweden

Co-Chairpersons

A. MEGHZIFENE
IAEA

K. ROSSER
United Kingdom

J. SEUNTJENS
American Association of Physicists in Medicine

THE BIPM GRAPHITE CALORIMETER STANDARD FOR ABSORBED DOSE TO WATER

S. PICARD, D.T. BURNS, P. ROGER
Bureau international des poids et mesures,
Sevres Cedex, France
Email: spicard@bipm.org

Abstract

The BIPM has constructed a graphite calorimeter for use as a primary standard for absorbed dose. It is employed to measure absorbed dose to water in the BIPM ^{60}Co reference beam and in accelerator photon beams. It is currently in use for a series of international comparisons of absorbed dose to water in the accelerator photon beams of national metrology institutes. The paper describes the BIPM calorimeter and presents some recent results.

1. INTRODUCTION

National metrology institutes use graphite and water calorimeters as primary standards for absorbed dose to water. Each of these methods has its own advantages and disadvantages. A review on the state of the art has recently been given by Seuntjens and Duane [1].

The BIPM chose to construct a graphite calorimeter to be used in a series of international comparisons of absorbed dose to water in accelerator photon beams [2]. When designing the BIPM calorimeter, one guiding criterion was to enable the radiation measurements and the electrical calibrations to be made under optimum conditions. This places conflicting requirements on the calorimeter design, and consequently the calorimeter has no in-built electrical calibration, but is based on the specific heat capacity determined for the graphite core.

Another design criterion was to reduce the associated systematic uncertainties by arranging pairs of complementary measurements with either geometrical or electrical parameters in common. The uncertainties are reduced when the ratio of two such measurements is taken. In particular, this approach has a significant impact on the uncertainty of the Monte Carlo calculations used for determining absorbed dose to water from the measured graphite absorbed dose.

This paper describes the graphite calorimeter. The details of the Monte Carlo dose conversion are presented in a separate paper [7], and are outlined in the comparison protocol [3].

2. REALIZATION

2.1. Measurement principle

The absorbed dose to graphite measured with the BIPM calorimeter, D_c, is determined by measuring the temperature rise ΔT at the temperature T of the irradiated graphite sample when the specific heat capacity, c_p, is known:

$$D_c = c_p(T)\Delta T \tag{1}$$

2.2. Specific heat capacity

The specific heat capacity, c_p, of the graphite from which the calorimeter core was fabricated has previously been determined in a separate experiment [4]. These measurements spanned a period over nearly two years, using an arrangement for which the mechanical and thermal conditions were optimized and which are not the same as those required for radiation calorimetry.

The sample for which the c_p is determined is equipped with two thermistors to measure temperature, each one in opposite arms of a d.c. Wheatstone bridge. An arrangement to calibrate the measured temperature dependent voltage output of the bridge against a known temperature reference was developed. In this arrangement, the cylindrical sample is in thermal contact with a heat sink of well-known temperature that can be varied. The same voltmeter was used during this calibration procedure as for the subsequent measurements of c_p.

As energy must be injected into the sample, a third thermistor is attached for this purpose. A temperature rise is generated by passing a current through this thermistor. It was observed that if the heat leaving the sample by conduction in the connecting wires of the heater is not re-absorbed, systematic errors of several percent can result. For this reason, these wires are wound around the sample several times.

The c_p was measured for a group of samples, machined from the same graphite block as three calorimeter cores, by determining the temperature rise when injecting energy over a temperature range covering realistic laboratory temperatures. The data were analysed using an empirical physical model developed for this purpose. A further measurement series was made for one sample using a novel differential method [4]. The results are shown in Fig. 1. Based on these results, the specific heat capacity of the calorimetric samples is taken to be

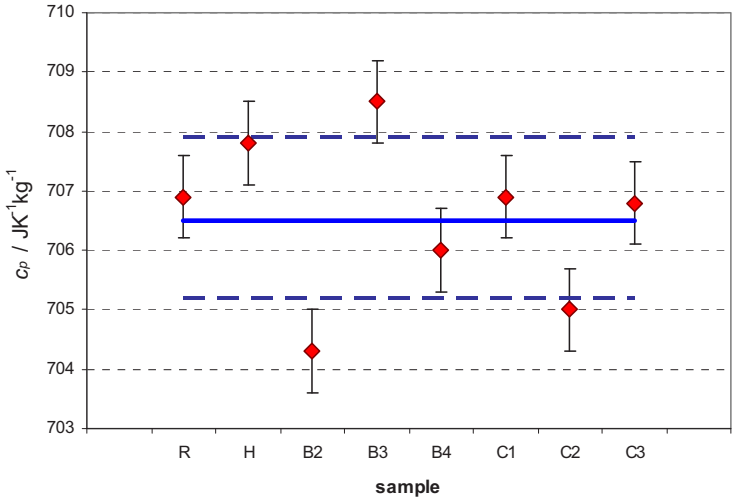

FIG. 1. The measured specific heat capacity of eight separate samples machined from the same graphite block. The sample 'R' was measured using a differential method. The mean value and the combined standard uncertainty of the distribution are indicated by the solid and dashed blue lines, respectively (combined uncertainty of 1 × 10^{-3}).

$$c_p(T) = 706.9 + 2.9(295.15 - T)\,\mathrm{J \cdot kg^{-1} \cdot K^{-1}} \qquad (2)$$

with a combined standard uncertainty of 9 parts in 10^4.

2.3. Design of the graphite calorimeter

The calorimeter consists of a cylindrical graphite core 45 mm in diameter and 6.7 mm thick. It is placed in a cylindrical graphite jacket with an outer diameter of 60 mm and an outer thickness of 32 mm. supported by four rigid thin metal needles. The hollow space in which the core is mounted, 51 mm in diameter and 11.2 mm wide, is of the same dimensions as the BIPM parallel-plate ionization chamber; this type of chamber replaces the core (and vacuum gap) in the complementary ionometric measurements that form part of the determination of absorbed dose to water. For this reason, the mass thickness of the core was chosen to be the same as the total mass thickness of the parallel-plate ionization chamber.

Three thermistor pairs mounted around the periphery of the core are connected to three independent d.c. bridges. This improves the statistical uncertainty of each dose determination and also provides information on the statistical uncertainty associated with the analysis of each temperature–time

curve. The sample mass and the mass of the added thermistor beads and epoxy are determined when preparing the sample; the amount of added non-graphite material is kept as low as practicable. A factor k_{imp} is applied to correct for differences in the heat capacity and electron stopping power of these added materials from those for graphite:

$$D_{\text{c}} = c_p(T)\Delta T k_{\text{imp}} \tag{3}$$

The jacket is also equipped with thermistors to track the temperature difference between the core and the jacket. The signals for the core and jacket thermistors are calibrated in temperature, as described in Section 2.4.

A critical design criterion is to obtain the same temperature rise in the core and jacket during an irradiation so that heat flow between the core and jacket is minimized. To this end, the jacket is not machined as a front component and a rear component, but is composed of two hollow semi-cylindrical pieces, as shown in Fig. 2. This allows a much more rapid distribution of heat between front and back so that the temperature distribution in the core rapidly becomes homogeneous.

Although the plan initially was for a demountable calorimeter in which the core could be separated from the jacket, this proved to be impractical as the thermistors' connections are very fragile. Therefore, once the core is mounted in the jacket, it is deemed an ensemble. In addition, the components of the complete calorimeter (described below) are successively assembled each time it is positioned in the beam.

FIG. 2. The jacket consists of two hollow semi-cylindrical components to improve the conduction of heat generated by the irradiation. In the centre, the graphite core is shown and the thermistor leads can be seen.

The core and jacket ensemble is supported by an adjustable aluminized PMMA holder placed in an evacuated cubic PMMA vacuum phantom with side length 300 mm, as shown in Fig. 3. The phantom has the same outer dimensions as the BIPM reference water phantom, again to reduce uncertainties when combining the complementary measurements and calculations.

The reference depth in the ^{60}Co beam (5 g/cm^2) is achieved by adding a graphite entrance plate. The graphite plate also acts to mechanically support the 4 mm thick PMMA entrance window (the same thickness as the window of the BIPM reference water phantom), which would otherwise be unable to support the vacuum under which the calorimeter operates. To obtain a depth of 10 g/cm^2 for accelerator photon beams, an additional 5 g/cm^2 graphite block is placed between the graphite entrance plate and the calorimeter. This configuration is shown schematically in Fig. 4.

Heat transfer by convection is negligible due to the vacuum in the phantom ($<2 \times 10^{-4}$ hPa), as is heat conduction in air. Other conduction paths are kept as

FIG. 3. The calorimeter, housed in an evacuated PMMA phantom. The dimension of the outer side of the PMMA container is 30 cm. The yellow block is the concave aluminized PMMA block placed downstream of the jacket to prevent radiative heat loss, seen from the back, as indicated in Figure 4. The external collimator of the BIPM ^{60}Co reference source is seen to the right of the photograph. The thermal shielding for the calorimeter phantom is not shown.

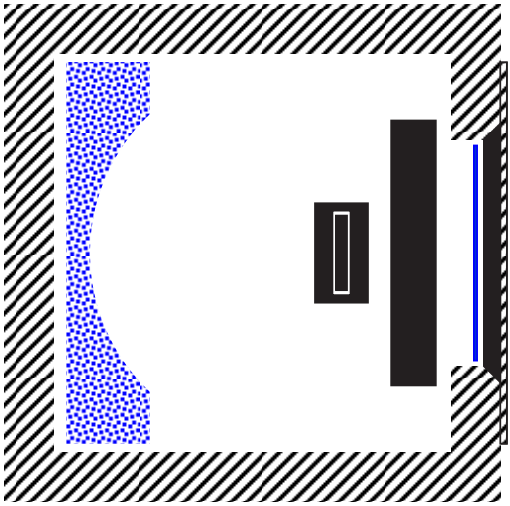

FIG. 4. Schematic diagram of the calorimeter configuration. Here, the beam is incident from the right. Graphite is represented in solid black; PMMA is indicated by dashed lines and aluminized PMMA by blue speckle. The beam then traverses a PMMA window, a graphite entrance plate, an aluminized PMMA reflector, a graphite block (to obtain 10 g/cm^2 in accelerator photon beams) and the front half of the jacket before reaching the core.

small as possible by reducing all contact surfaces. Radiative heat transfer from the jacket to its surroundings is reduced by employing reflecting surfaces: the inner surface of the PMMA jacket holder is aluminized and an aluminized PMMA reflector 2.5 mm thick is placed in front of the jacket, included in the mass thickness. Further, a concave aluminized PMMA mirror positioned downstream of the jacket reflects heat radiation back to the jacket. Unique to the BIPM calorimeter, this reflector is used not only in the corresponding ionization chamber measurements, but also in the Monte Carlo calculations for these geometries. In this way, its influence on the water absorbed-dose determination is taken fully into account. The evacuated PMMA phantom is surrounded by a double-layered housing that acts both as thermal insulation and as a Faraday cage.

The three thermistor pairs of the core are connected to three nanovoltmeters. To reduce noise on each bridge signal, the path length between the bridge output and the nanovoltmeter input has been minimized by incorporating the bridge into the nanovoltmeter housing. The bridges are powered by a d.c. power supply of low noise and good long term stability. The thermistors monitoring the jacket temperature are connected to ohm-meters. All

electronic equipment is mounted in a transportable electronic rack. The measurements and data collection are computer controlled via an IEEE card.

2.4. Temperature calibration

Before assembling the calorimeter core in its jacket, the output voltage for each bridge is calibrated against a reference thermometer in a stable water-bath arrangement. For these measurements, the core is placed in thermal contact with a temperature regulated heat sink. In this way, the self-heating of the thermistors is absorbed by the core and transported to the heat sink, provided that there is good thermal contact between the thermistors and the core. The bridge signals therefore represent the temperature of the core, which is taken to be that of the water bath. However, when the core is mounted in its jacket, the aim is to have as little thermal contact as possible with other materials. Under these conditions self-heating is no longer removed, and the core temperature will rise relative to its surroundings. Nevertheless, if good thermal contact between thermistors and core is maintained, the thermistors will continue to measure the true temperature of the core.

Materials irradiated over a long period can show accumulated changes in their characteristics. A particular concern is the possibility that thermistors can change sensitivity. Another possibility is degradation of the epoxy that assures thermal contact between core and thermistors. For these reasons the temperature calibration of the bridges is repeated at regular intervals for the assembled core and jacket. In addition, the repeat measurements of the absorbed dose rate in the BIPM ^{60}Co reference beam represent an overall test of the stability of the calorimeter.

3. RESULTS

As noted in Section 2.3, a critical design criterion was to obtain the same radiation-induced temperature rise in the core and jacket. When the bridge voltage is switched on, the core and jacket heat up as a result of self-heating in the thermistors. After some time (typically within 24 h), their temperatures reach a quasi-stable state, and irradiations can begin. The temperatures of the core and jacket before, during and after a typical irradiation are shown in Fig. 5, where it can be observed that the temperature difference between the core and the jacket remains constant. This reduces the likelihood of radiative heat transfer between the core and jacket, and the calorimeter can be considered to be operating in a quasi-adiabatic mode.

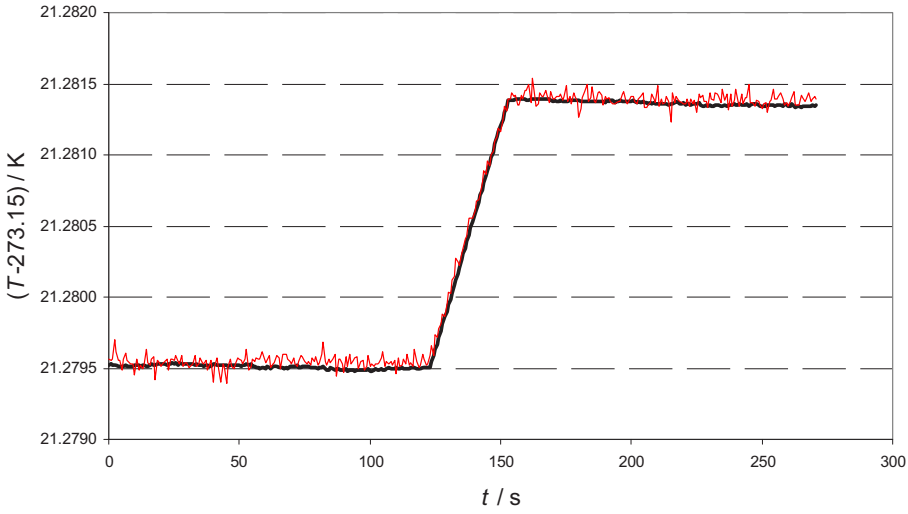

FIG. 5. Temperatures measured before, during and after irradiation of the calorimeter in an accelerator beam at 6 MV, demonstrating quasi-adiabatic behaviour. The black curve represents the temperature of the calorimeter core using two thermistors in opposite arms of a d.c. Wheatstone bridge, while the noisier red curve shows the temperature of the jacket. The jacket is measured using a single thermistor and an ohm-meter and is therefore noisier than the core signal.

The sensitivity of the calorimeter is such that the temperature rise is less than 1 mK after 120 s of irradiation in the present BIPM ^{60}Co reference beam (around 0.4 Gy/min), but can reach a few mK in accelerator photon beams after 30 s. As radiative heat transfer is likely to be negligible, only heat loss via conduction is considered, which behaves linearly with temperature difference. The analysis of the heat curve is made by extrapolating the pre- and post-irradiation curves to the time corresponding to the mid-temperature. By studying the influence of the noise on the uncertainty of the extrapolation, a minimum is identified when the pre- and post-heat time is about 120 s.

Owing to the relatively poor signal-to-noise ratio inherent in absorbed-dose calorimetry for radiotherapy, a large number of irradiations is generally needed to improve the statistical uncertainty. In the BIPM ^{60}Co reference beam, irradiations are made repeatedly over a period of 72 h to achieve a single mean value. The standard uncertainty of the mean of each such series is about two parts in 10^3 (120 s irradiation; 500 data points). Data accumulated between January 2009 and June 2010 are shown in Fig. 6 for the three different resistance bridges.

During the comparisons in accelerator beams, although the dose rate is generally higher, time constraints do not allow data to be accumulated over such long periods. For a single radiation quality, a standard uncertainty of the mean of

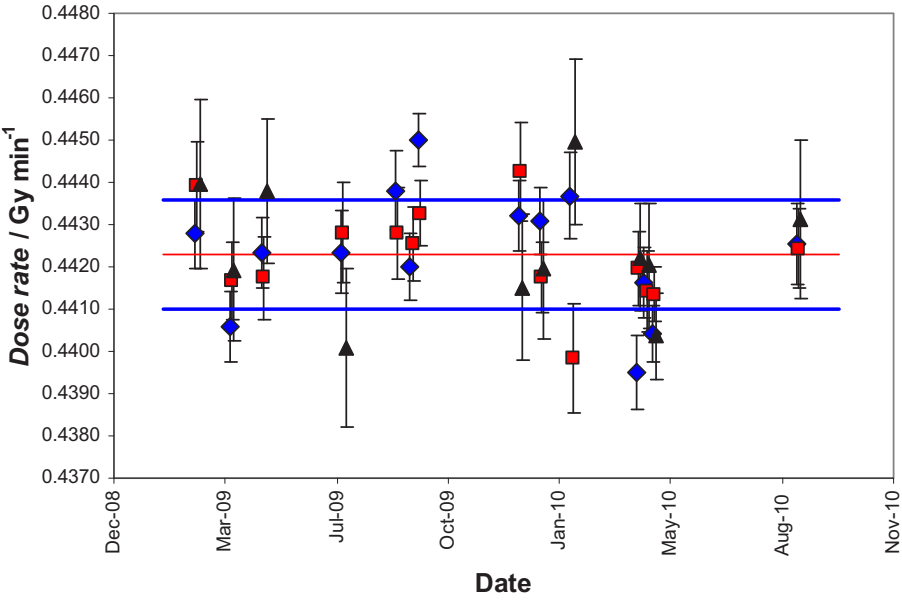

FIG. 6. Decay corrected data of the absorbed dose rate to graphite in the BIPM ^{60}Co reference beam from January 2009 until June 2010. The red squares and the blue diamonds represent two of the three resistance bridges, each with two thermistors. The black triangles represent the third resistance bridge containing only one thermistor. The red and blue lines represent the mean value and the standard uncertainty (3×10^{-3}) of the distribution, respectively.

two parts in 10^3 can be obtained after a day at dose rates of about 4 Gy/min (30 s irradiations; 60 data points).

The main contributions to the uncertainty of the graphite absorbed dose determination in accelerator photon beams are given in Table 1. As the output from accelerator beams can show variations of several per cent, it is necessary to monitor the relative dose rate during the measurements. The standard uncertainty of the mean is therefore dependent on the quality of the accelerator and the monitoring. The beam profile is dependent on each accelerator and beam quality. A correction factor k_{rn} is applied to correct for the deviation of the beam profile from a 'flat' profile across the diameter of the calorimeter core. Note that the uncertainty of the dose conversion from graphite to water is addressed in a separate paper [3].

TABLE 1. UNCERTAINTY COMPONENTS FOR THE BIPM GRAPHITE CALORIMETER IN AN ACCELERATOR PHOTON BEAM

Type A relative standard uncertainty component	$u_A(y)/y/10^{-3}$
standard uncertainty of the mean absorbed dose to graphite including uncertainties linked to monitoring	1.0–2.0[a]
Type B relative standard uncertainty component	$u_B(y)/y/10^{-3}$
specific heat capacity of graphite [4]	0.9
impurity correction	0.2
k_m for BIPM calorimeter in accelerator beam	0.5–1.5[a]
temperature calibration	0.5
linear model for temperature extrapolation	0.7
axial position of calorimeter	0.5

[a] A range of numerical estimates is given for the beam monitoring and for k_m as these depend on the specific accelerator facilities.

4. CONCLUSION

A graphite calorimeter has been constructed at the BIPM as a primary standard for absorbed dose to water. It is used on a regular basis to determine the absorbed dose rate in the BIPM ^{60}Co reference beam, where the existing standard is a cavity ionization chamber. A statistical uncertainty of around 2 parts in 10^3 is currently achievable for a single 72 h series of measurements and data accumulated to date show a standard uncertainty of the mean of around six parts in 10^4.

The calorimeter is transportable and is also being used in an ongoing comparison of absorbed dose to water in accelerator photon beams [2]. Three comparisons in this series have already been carried out, with the National Research Council (Canada) in June 2009 [5], the Physikalish-Technische Bundesanstalt (Germany) in March 2010, and the National Institute of Standards and Technology (USA) in October 2010. Arrangements have been initiated for the next comparison in the series, at the METAS (Switzerland) in March 2011.

REFERENCES

[1] SEUNTJENS, J., DUANE, S., Photon absorbed dose standards *Metrologia* **46** (2009) S39–S58.

[2] Calorimetric Comparison of Absorbed Dose to Water at High Energies 2009 BIPM Key Comparison BIPM.RI(I)-K6, *Protocol 1.3; CCRI(I)* http://kcdb.bipm.org/AppendixB/appbresults/bipm.ri(i)-K6/BIPM.RI(I)-K6_Technical_Protocol.pdf

[3] BURNS, D.T., The dose conversion procedure for the BIPM graphite calorimeter standard for absorbed dose to water (in preparation).

[4] PICARD, S., BURNS, D.T., ROGER, P., Determination of the Specific Heat Capacity of a Graphite Sample Using Absolute and Differential Methods, *Metrologia* (2007) **44** 294–302.

[5] PICARD, S., et al., Comparison of the standards for absorbed dose to water of the NRC and the BIPM for accelerator beams (this Proceedings).

THE LNE-LNHB WATER CALORIMETER: MEASUREMENTS IN A ^{60}Co BEAM

B. RAPP, A. OSTROWSKY, J. DAURES
Commissariat à l'Énergie Atomique,
Laboratoire National Henri Becquerel (LNE-LNHB),
Gif-Sur-Yvette, France
Email: benjamin.rapp@cea.fr

Abstract

Graphite and water calorimeters are used to establish absorbed dose standards in most of the national metrology laboratories involved in ionizing radiation dosimetry. To date, a graphite calorimeter is the reference dosimeter for radiotherapy photon beams at Laboratoire National Henri Becquerel (LNE-LNHB). A new water calorimeter has been developed in order to compare different ways to establish the absorbed dose to water. This paper describes this new calorimeter and the results obtained in the laboratory ^{60}Co beam. The LNE-LNHB can now operate both graphite and water calorimetry, and thus has two independent methods to measure the absorbed dose to water.

1. INTRODUCTION

Calorimetry is the best technique available to perform absolute measurement of absorbed dose [1]. The energy imparted by ionizing radiations to matter per unit mass is directly measured, matching the definition of the absorbed dose quantity. Graphite or water calorimeters are mainly used as references for absorbed dose to water in most of the national metrology laboratories involved in ionizing radiation dosimetry. The Laboratoire National Henri Becquerel (LNE-LNHB) has long experience with graphite and tissue equivalent calorimeters [2], so graphite calorimeter is still today the reference for photon beam dosimetry. Using a transfer procedure from graphite to water, it leads to the reference of absorbed dose to water, which is the reference quantity for radiotherapy. It was decided a few years ago to develop water calorimetry at LNE-LNHB, not to replace the graphite calorimeter but to carry out parallel measurements on the same radiation beams as often as possible. A comparison of the results of these two primary methods should provide much useful information. The first section describes the design of the water calorimeter; the second section shows the measurement principles, performance and main correction factors involved in the uncertainty budget. A discussion of the results

achieved in a ^{60}Co beam with respect to the previous graphite calorimeter measurements is given in the third section.

2. THE LNE-LNHB WATER CALORIMETER

The water calorimeter of the LNE-LNHB laboratory was built taking into consideration the experiences of other metrology laboratories using this primary method [4]. Thus, the calorimeter was built to operate at 4°C, the maximum density of water, to minimize convection currents inside the water phantom. The temperature rise is measured by a thermistor probe, placed inside a vessel containing high purity water with a zero or known heat defect.

The inner part of the thermal enclosure of the water calorimeter (Fig. 1) consists of a radiotherapy water phantom cube of side 30 cm. A second PMMA container is built around this phantom to form a double wall, in which a cooling fluid regulated at 4°C circulates, except in front of the entrance window facing the beam. A thick layer (8 cm) of polystyrene foam around the container is used for insulating against ambient atmosphere.

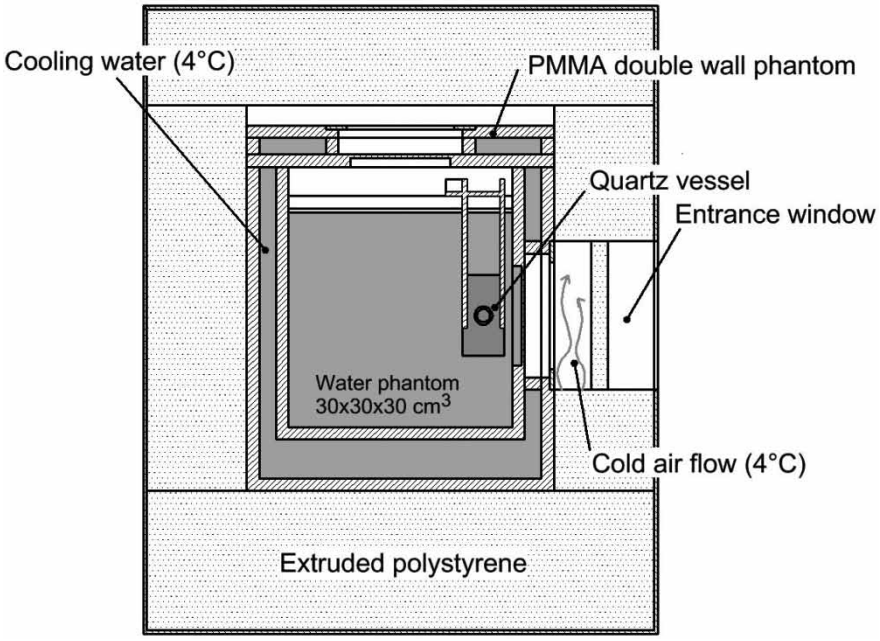

FIG. 1. Schematic view of the LNE-LNHB water calorimeter.

Heat transfers inside the calorimeter were simulated with the finite element software COMSOL [5] in order to improve the design of the different elements ensuring the thermal control of the water phantom. A hot zone appears behind the entrance window due to the lack of water regulation and insulation at the level of the window. A temperature map of the thermal enclosure, made with thermistors confirms the calculations. Taking into account this observation, a special system was built to cool the region of the thermal enclosure in front of the beam. It consists of a cooling system producing a flow of cold air at 4°C between two Mylar foils through the window.

This flow of cold air is generated by a commercial vortex tube fed with compressed air and connected to a pressure regulator. The regulator is part of a PID control loop, programmed under the LabView environment, in which the process variable is the temperature measured in the calorimeter window by a Pt100 probe. This system allows the creation of an air layer stable in temperature (±0.01°C) with a minimum of material in front of the beam. A 2 cm thick slab of polystyrene is all that is needed to avoid the condensation of water vapour from ambient air on the calorimeter window. This additional cooling system has significantly improved the temperature gradients. A second generation calorimeter has been built, relying only on this principle in which the regulating fluid circulating around the water phantom is replaced by a flow of cold air generated by vortex tubes. This allows a more compact and transportable design. This calorimeter is presently under test.

The temperature probe consists of a sealed quartz capillary of 0.6 mm outer diameter with a negative temperature coefficient (NTC) thermistor inside. The thermistor beads are glass encapsulated, and their diameter is 0.28 mm. The thermistor is connected to a cable through Pt/Ir wires (Ø = 0.05 mm), insulated with Kapton^{Ò} tubes. Each is sealed with epoxy resin, and the capillary is filled under vacuum. Quartz material was chosen to avoid contamination of high purity water inside the vessel. The resistance of the thermistor probe is measured by a DC Wheatstone bridge built with high precision resistors of 8000 Ω, connected to a precision voltmeter. The bridge is used near equilibrium without rebalancing after each irradiation; instead the bridge equation was applied to calculate the resistance of the thermistor. Each temperature probe is calibrated with its bridge and voltmeter, so the parameters of the bridge need not be known accurately. A DC Wheatstone bridge was chosen deliberately instead of an AC bridge; the DC bridges can be noisier than the AC ones, but their calibration is easier and more stable. Moreover, no further calibration is needed during the measurement process.

The temperature probe is positioned inside a quartz vessel of cylindrical shape of 10 cm in radius and 5 cm in length. The front and back walls of the vessel consist of thin foils of quartz, 0.8 mm in thickness. The quartz vessel is

filled with high purity water saturated with N_2 gas, and is fixed inside the water phantom of the calorimeter.

3. MEASUREMENT PRINCIPLE AND CORRECTION FACTORS

The absorbed dose is calculated from the temperature rise by:

$$D_W = C_p \Delta T \left(1 - h\right)^{-1} k_c k_p k_\rho \tag{1}$$

where h is the water heat defect, C_p the specific heat of water, k_c the thermal conduction correction factor, k_p the radiation field perturbation correction factor and k_ρ the density of water correction factor.

The low thermal diffusivity of water allows the measurement of a local temperature rise and thus the absorbed dose at the reference point in the water phantom. A balance between irradiation time — to obtain a good signal to noise ratio — and the time scale of thermal diffusivity has to be chosen. Consequently, some sequences of four irradiations of 4 min, followed by a pause time of 1.5 hs were made, to allow the cone of heat produced by irradiation in the water phantom to vanish. The noise of the temperature probe is around 30 μK, and the thermal stability is lower than 20 μK/min. To determine the temperature rise, the method of extrapolation to mid-irradiation is used, based on the linear fits of the temperature evolution before and after irradiation.

To evaluate the correction factor due to thermal conduction (k_c), the Monte Carlo simulation of the heat deposition in water by radiation was combined with the calculation of heat transfer in the calorimeter. The absorbed dose distribution simulation is obtained with MCNPX [6] Monte Carlo code using a simplified geometry of the water phantom and the quartz vessel. The generated 3D distribution of dose is then used as a heat source for time dependent finite element calculations, made with COMSOL [5] software, with the same geometry used for the Monte Carlo calculation.

The perturbation factor of the radiation field (k_p) caused by the calorimeter materials has been determined both by ionization chamber measurements and Monte Carlo calculations. It is the direct comparison of the calorimeter enclosure with its quartz vessel, to a simple radiotherapy water phantom.

In water, depending on the contents of gases and impurities, all the energy deposited by radiation is not converted into thermal heat (heat defect of water h). In order to obtain a zero heat defect, high purity water saturated with N_2 gas is used to fill the quartz vessel. A pre-irradiation of the water vessel of several hundred grays is needed to stabilize the heat defect before measurements are made. Simulations of the water radiolysis, based on real measurements of the

dissolved oxygen concentration and organic carbon impurities, have been used to estimate the uncertainty on the heat defect, which is the major term of the uncertainty budget. The uncertainty obtained of 0.3% is in agreement with those used by other metrology laboratories [1].

4. ABSORBED DOSE TO WATER MEASURED IN A ^{60}CO BEAM

The water calorimeter has been used in the LNE-LNHB ^{60}Co beam [7]. The measurements were carried out under the following conditions: a source–detector distance of 1 m and a depth in the water phantom of 5 cm (4.6 cm of water + 0.4 cm of PMMA — thickness of the phantom window). The water absorbed dose rate of the source during measurements is about 0.4 Gy/min. The water absorbed dose rate is corrected for the ^{60}Co decay for comparison with previous reference values established at a fixed reference date. The absorbed dose to water measured by the water calorimeter (Fig. 2) presents a dispersion between 1 and 2%, but the automation of measurements enables a reduction in the uncertainty on the mean value to 0.07% by carrying out a large number of irradiations (N = 420). The absorbed dose rate to water measured by water calorimetry is about 56.75 Gy/h, and the final combined relative standard uncertainty is 0.49% (Table 1).

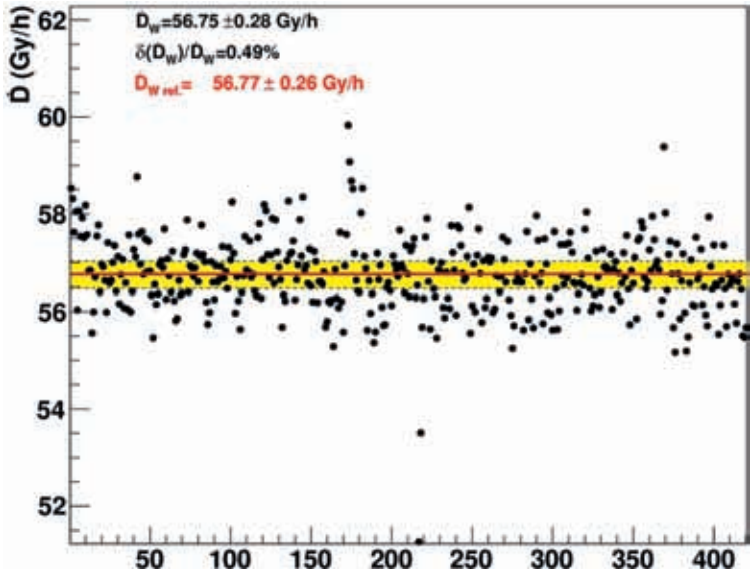

FIG. 2. Absorbed dose to water measured by the water calorimeter (black dots), the mean value of the absorbed dose and the combined relative standard uncertainty at 1 σ is represented by the band delimited by dashed lines. The present reference value in the ^{60}Co reference beam of the laboratory, based on graphite calorimetry, is drawn on the same figure (bold line).

TABLE 1. UNCERTAINTY BUDGET

Source of uncertainty	Value	Relative uncertainty	
		100 s_i	100 u_i
Temperature probe calibration		0.1	
Temperature probe positioning			0.3
Specific heat of water ($J \cdot kg^{-1} \cdot K^{-1}$)	4204.8		0.1
Thermal conduction correction factor k_c	[a]		0.1
Radiation field perturbation correction factor k_p	1.0032	0.15	
Heat defect of water h	0		0.3
Density of water correction factor k_ρ	1.00032	0.01	
ΔT measurement reproducibility ($N = 420$)		0.07	
Quadratic summation		0.19	0.45
Combined relative standard uncertainty on D_w			**0.49**

[a] Thermal conduction correction factor (t_{irr} = 240 s) applied to each of the four consecutive irradiations of 4 min of one acquisition sequence:
k_c = 1.0043, 1.0012, 1.0004, 0.9997

The water calorimetry results are in good agreement with the present reference value based on graphite calorimetry [8] of 56.77 Gy/h (0.46%). The relative difference between the two values is about 0.04%.

The absorbed dose rate to graphite using the graphite calorimeter is given by:

$$\dot{D}_g = \frac{L_c}{m} F_{el} \prod k_i \tag{2}$$

where L_c is the rate of change of resistance as measured by the bridge, F_{el} the electrical calibration coefficient, m the mass of the core of calorimeter and Πk_i the product of correction factors.

The original measurement with the graphite calorimeter in a graphite phantom at 1 m from the source and a depth in graphite of 5 g/cm^2 is 45.66 Gy/h (0.24%). To obtain this value, two series of measurements have been combined: a first series of 20 measurements and ten electrical calibrations, and a second of 14 measurements and ten calibrations. The statistical uncertainty (Type A) is taken as the standard deviation on the mean, and is about 0.021% on the L_c factor and about 0.026% on the F_{el} calibration factor. Graphite calorimetry is able to give a result with a lower dispersion compare to water calorimeter. Only 34 measurements gives a lower uncertainty compared to the result with 420 measurements using water calorimetry (0.07%). The reason is mainly due to the difference in sensitivity between the graphite and water calorimeters resulting

from the different specific heat capacities for the two materials (about 700 $J \cdot kg^{-1} \cdot K^{-1}$ for graphite and 4200 $J \cdot kg^{-1} \cdot K^{-1}$ for water).

In graphite calorimetry, the main sources of uncertainty are correction factors such as the vacuum gap correction (0.15%) or graphite impurities correction (0.1%); whereas in water calorimetry it is mainly the heat defect of water (0.3%).

However, even if the overall uncertainty on the absorbed dose to graphite (0.24%) is about two times lower than the uncertainty on the absorbed dose to water obtained by the water calorimeter (0.49%), a transfer coefficient has to be applied to obtain the dose in water from the dose obtained by graphite calorimetry. This coefficient can be determined by three methods: (i) ionometry, (ii) Monte Carlo calculation and (iii) Fricke dosimetry. The reference value for ^{60}Co of LNE-LNHB is obtained today with a transfer coefficient from graphite to water determined both by ionometry and Fricke dosimetry combined with Monte Carlo simulations [9]. The mean value for the transfer coefficient calculated from these methods is 1.0558 with an uncertainty of 0.26%, which is similar to the overall uncertainty of the absorbed dose to graphite. The combined uncertainty is 0.35%, but an ionometric transfer coefficient must also be applied, because the ^{60}Co source of the irradiator has been replaced between the graphite and water calorimetry measurements, leading to a final standard uncertainty of 0.46% for the absorbed dose to water using the graphite calorimeter.

The graphite calorimeter alone gives a more precise measurement than the water calorimeter, without the need to make several hundred irradiations. However, the transfer from graphite to water is needed, water being the medium of interest for dosimetry in radiotherapy. Finally, the application of both methods gives a similar uncertainty, and in addition to any decision on which method to use, it is of metrological interest to compare two independent primary measurements of the absorbed dose to water. By choosing to maintain and develop the two types of calorimeter at the LNE-LNHB, confidence is gained in the value of the transfer coefficient of graphite to water by comparison of both methods. The joint use of both calorimetry methods will be useful in the exploration of new radiation fields such as hadron therapy or the study of small radiation fields for IMRT.

5. CONCLUSION

The new water calorimeter allows the measurement of absorbed dose to water with a relative standard uncertainty lower than 0.5% and is complementary to the existing references based on graphite calorimetry. This new instrument permits the consistency of the laboratory dosimetric references to be verified by

two independent methods. It is highly valuable to operate both graphite and water calorimetry at LNE-LNHB to have a different approach in photon and electron beams for radiotherapy purposes. It will now be used to contribute to the references for accelerator high energy X ray and electron beams, and to establish new references for medium X ray and proton/ion beams.

REFERENCES

[1] SEUNTJENS, J., DUANE, S., Photon absorbed dose standards, Metrologia **46** (2009) S39–S58.

[2] DAURES, J., OSTROWSKY, A., Test of the new GR9 graphite calorimeter. Comparison with GR8, Absorbed Dose and Air Kerma Primary Standard Workshop (9–11 May 2007, Paris).

[3] DAURES, J., OSTROWSKY, A., New constant-temperature operating mode for graphite calorimeter at LNE-LNHB, Phys. Med. Biol. **50** (2005) 4035.

[4] ROSS, C.K., KLASSEN N.V., Water calorimetry for radiation dosimetry, Phys. Med. Biol. **41** (1996) 1–29

[5] COMSOL 3.5 Multiphysics, http://www.comsol.com/

[6] LOS ALAMOS NATIONAL LABORATORY, MCNPX — Monte Carlo N-Particle Transport Code System for Multiparticle and High Energy Applications, http://mcnpx.lanl.gov/

[7] RAPP, B., OSTROWSKY, A., DAURES, J., Development of water calorimetry at LNE-LNHB, 14th International Congress of Metrology, 22–25 June 2009, Paris, France.

[8] Report of the 19th meeting of the Consultative Committee for Ionizing Radiation (CCRI), CCRI(I): 19th meeting (May 2009), BIPM, France.

[9] CHAUVENET, B., BALTÈS, D., DELAUNAY, F., Comparison of graphite-to-water absorbed-dose transfers for ^{60}Co photon beams using ionometry and Fricke dosimetry, Phys. Med. Biol. **42** (1997) 2053–2063.

DESIGN AND PRINCIPLES OF A GRAPHITE CALORIMETER FOR BRACHYTHERAPY

T. SANDER, P. OWEN, M. BAILEY, S. DUANE, H. PALMANS
National Physical Laboratory,
Teddington, Middlesex, United Kingdom
Email: thorsten.sander@npl.co.uk

Abstract

A graphite calorimeter for the measurement of absorbed dose of HDR ^{192}Ir brachytherapy sources was designed and built at the National Physical Laboratory (NPL) and will be commissioned as an absorbed dose standard. Calorimetry is regarded as the most direct method of measuring absorbed dose, which is based on the assumption that all or a known fraction of the absorbed radiation energy appears as heat, so that the measurement of absorbed dose reduces to a measurement of a temperature change. Both water and graphite calorimeters are currently in use at national standards laboratories for the reference dosimetry of external radiation fields used in radiotherapy. Compared to existing external beam calorimeters, where the distance from the radiation source to the measurement point in the medium is relatively large and the core receives a uniform absorbed dose rate, the design of the brachytherapy calorimeter had to be optimized in order to deal with the self-heating of the radioactive source, large dose gradients close to the source, as well as the need for measuring absorbed dose at distances of a few centimetres from the source and for making the geometry as homogeneous and water-equivalent as possible. Monte Carlo (MC) simulations and heat transfer simulations based on the finite element method were used to derive a suitable design of the calorimeter. Graphite was chosen as the absorber medium for NPL's new brachytherapy calorimeter. The initial heat transfer simulations showed that due to the high thermal diffusivity of graphite, the core of the calorimeter had to be isolated from the surrounding graphite phantom by introducing several vacuum gaps. Perturbation correction factors and the graphite-to-water conversion factor for the final design of the calorimeter were calculated using refined MC simulations. The design and principles of the new HDR ^{192}Ir calorimeter are discussed in this report.

1. INTRODUCTION

Over recent years, the use of high dose rate (HDR) brachytherapy has increased worldwide with ^{192}Ir now being the most commonly used radionuclide [1]. Brachytherapy dosimetry for gamma ray sources is currently based on source calibrations in terms of reference air kerma rate (RAKR) or air kerma strength (AKS) [2]. However, the quantity of interest is the absorbed dose rate to water at a distance of 1 cm from the source centre, $\dot{D}_w$, which is currently calculated from

RAKR or AKS by applying the formalism described in the AAPM Task Group 43 protocol [3] and update TG-43U1 [4]. Determining the quantity of interest via an air kerma measurement is rather complex, and many correction factors have to be applied, leading to relatively large overall measurement uncertainties. As for external beam radiotherapy dosimetry, there is now a growing need for accurate brachytherapy source dosimetry traceable to national absorbed dose primary standards, and some national standards laboratories have recently developed absorbed dose standards for HDR ^{192}Ir based on water calorimetry [5]. Using this more direct method may reduce the uncertainty in $\dot{D}_w$.

2. DESIGN OF THE BRACHYTHERAPY CALORIMETER

2.1. Initial heat transfer simulations

Initially, heat transfer simulations (COMSOL Multiphysics version 3.3a) [8] were performed at the design stage of NPL's new calorimeter in order to investigate the effects of the source self-heating and radiation heating on the measurement of absorbed dose in both homogeneous water and graphite phantoms at distances between 1 cm and 5 cm from the centre of an HDR ^{192}Ir brachytherapy source.

Conduction was the only mode of heat transfer considered here. Figure 1 shows the temperature change in graphite due to a Nucletron microSelectron classic HDR ^{192}Ir source with a typical activity of 370 GBq.

Figure 1 shows that an accurate measurement of the temperature change at a point in a large homogeneous graphite phantom would not be possible because of the high diffusivity of graphite, unless the measurement point is isolated from the surrounding phantom by introducing either air or vacuum gaps. The numerical solution of the heat conduction equation was compared with the analytically calculated ideal temperature change, assuming no heat transfer in the absorber and an initial source temperature of 10 K above the equilibrium temperature of '0 K'. The excess heat energy is transferred to the surrounding graphite phantom within fractions of a second, as shown by the temperature peak at the beginning of the simulation. After removing the source from the phantom, the post-drift curve shows a steep negative gradient due to the high diffusivity of graphite. Simulations in water showed that an absorbed dose measurement in water would also be affected by a 'heat wave' reaching the point of interest close to the brachytherapy source. Graphite was identified as a suitable absorber medium for the new brachytherapy calorimeter. Graphite offers various

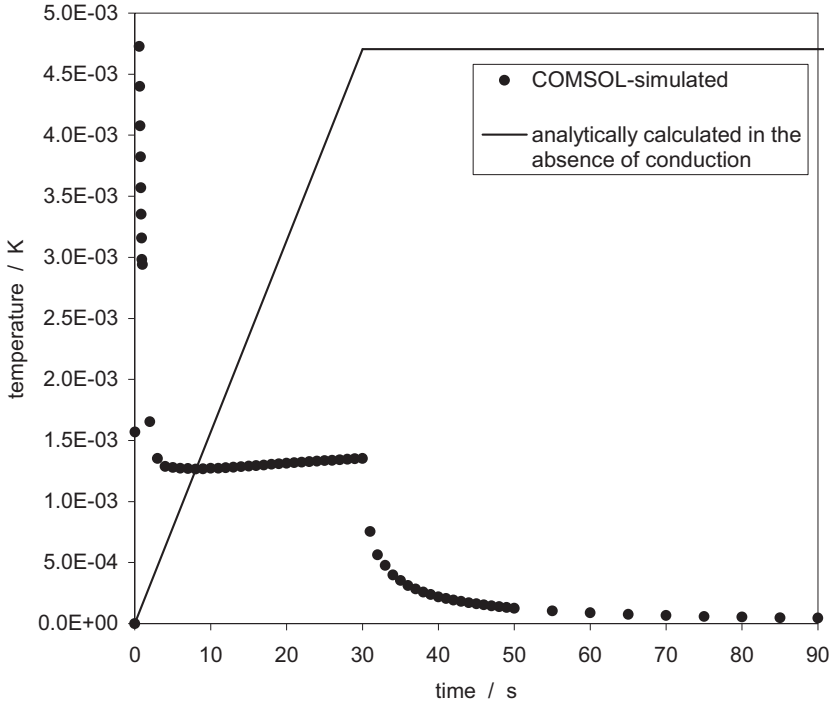

FIG. 1. Time-dependent solution of the heat conduction equation, T(1 cm, t), in graphite. The 370 GBq ^{192}Ir source was simulated at the centre of a large, homogeneous, spherical graphite phantom with radius r = 1 m for 30 s. The initial temperature of all media was set to T(r, 0) = '0 K' (relative temperature). An initial source temperature of 10 K above the equilibrium temperature of '0 K' was assumed. The source was then removed and T(1 cm, t) was simulated for another 60 s. The solid line represents the analytically calculated (ideal) temperature increase in graphite at a distance of 1 cm from the centre of the source, assuming no heat conduction in the medium. The black circles show COMSOL-simulated values for T(1 cm, t) in graphite at discrete times, with heat conduction enabled. Both distributed radiation heating and self-heating of the source contribute to the temperature change at the point of interest.

advantages over water when used for building calorimeters [9]. The graphite-to-water conversion factor was determined by Monte Carlo (MC) simulations.

2.2. Initial MC simulations

MC simulations using the EGSnrc user code DOSRZnrc (version V4-r2-2-5) [10] were then made in order to obtain suitable dimensions of the different parts of the new calorimeter. The results are summarized in Table 1.

TABLE 1. SUMMARY OF THE INITIAL MC SIMULATIONS OF A NUCLETRON MICROSELECTRON CLASSIC ^{192}Ir SOURCE PLACED AT THE CENTRE OF AN UNBOUNDED, HOMOGENEOUS GRAPHITE PHANTOM WITH DENSITY ρ = 1.7 g/cm^3, HEIGHT OF CYLINDER: 60 cm, RADIUS: 30 cm

Centre-to-centre source-to-core distance in graphite (cm)	Min. radius of graphite phantom (cm)	Min. height of graphite phantom (cm)	Max. height of graphite core (cm)	Variation of dose rate along the transverse axis over ±1 mm (%)	Dose rate from 370 GBq ^{192}Ir source (Gy/s)	ΔT in 120 s (K)
1	4.0	5.4	0.25	34.2	9.99E-02	1.68E-02
2	8.1	10.9	0.48	18.3	2.52E-02	4.24E-03
2.5	10.1	13.6	0.60	14.9	1.60E-02	2.69E-03
3	12.1	16.3	0.72	12.7	1.12E-02	1.88E-03
4	16.2	21.7	0.95	9.8	6.21E-03	1.04E-03
5	20.2	27.1	1.20	8.0	3.94E-03	6.61E-04

Note: The minimum and maximum dimensions of the phantom and the core are those to give 99.5% full scatter conditions at the relevant measurement distances.

Following the MC ○simulations, a centre-to-centre source-to-core distance of 2.5 cm was identified as suitable. This offered the optimum balance between keeping the overall dimensions of the calorimeter at a manageable size while ensuring full-scatter conditions and maintaining the sensitivity in terms of rate of temperature change at the point of measurement. The dimensions of the core were chosen so that the volume averaging correction would be kept within a few tenths of a percent and the total mass of thermistors embedded in the core would be approximately 0.1% of the mass of the core, therefore minimizing the inhomogeneity correction. The final design of the calorimeter is presented in the next section.

3. SECTIONAL VIEW OF THE NEW CALORIMETER

Figure 2 shows a sectional view of the new HDR ^{192}Ir calorimeter in RZ-geometry. The symmetry axis, r = 0, is indicated by the dash-dotted line.

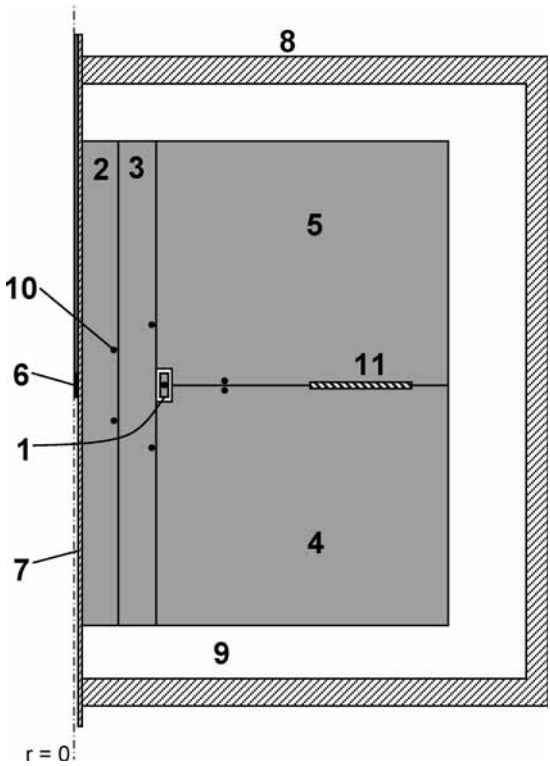

FIG. 2. Sectional view (RZ-geometry) of the new calorimeter showing the main components (not to scale): 1 = graphite core surrounded by 1 mm wide vacuum gap, 2 = inner graphite tube assembly, 3 = outer graphite tube assembly, 4 = lower graphite ring assembly, 5 = upper graphite ring assembly, 6 = HDR ^{192}Ir brachytherapy source 7 = central aluminium tube, 8 = vacuum housing, 9 = vacuum gap, 10 = heating or sensing thermistors embedded in the graphite parts (four heaters and four sensors each in parts 1 to 5), 11 = annular printed circuit boards.

The graphite calorimeter comprises a ring-shaped core (minimum radius = 24 mm, maximum radius = 26 mm, height = 5 mm) and four graphite cylinders providing buildup and full scatter conditions at the point of measurement. By using a ring-shaped core, the calorimeter is not sensitive to small variations in the source position relative to the geometric centre of the core. The absorbed dose is integrated over the total length of the graphite ring, and the average dose rate is measured. The annular core is surrounded by a 1 mm vacuum gap in order to reduce the heat transfer from the point of measurement to the outer graphite phantom, and together with three further 0.25 mm wide vacuum gaps between the central aluminium tube and the inner and outer graphite tube

assemblies, this shields the core from the self-heating of the source. Each of the five graphite pieces contains four sensing thermistors and four heating thermistors, allowing the operation in adiabatic or thermostatic mode [9]. Various types of HDR brachytherapy source can be located at the geometric centre of the cylindrical graphite phantom (radius = 10 cm, height = 14 cm) and the sources can be inserted through an aluminium tube connected to a vacuum housing, which fully encloses the graphite calorimeter. Two 250 μm thick annular printed circuit boards are located in the outer graphite phantom for cable management of the thermistors leads.

4. MEASUREMENT EQUATION FOR THE ^{192}Ir ABSORBED DOSE STANDARD

The quantity of interest is the absorbed dose rate to water at a distance of 1 cm from the centre of the HDR ^{192}Ir source along its transverse bisector axis. In thermostatic mode, the measured radiation power absorbed in the ring-shaped core of the calorimeter described in this report can be converted to the dose rate to water at the reference time, $\dot{D}_w$, via the following equation:

$$\dot{D}_w = \frac{P_{rad}}{m_{core}} \cdot k_h \cdot k_{dec} \cdot k_{graph/water} \cdot k_{imp} \cdot k_{volavg} \cdot k_{gap} \cdot k_{inh} \cdot k_{full\ scat} \quad (1)$$

where

P_{rad} is the radiation power absorbed in the graphite core;
P_{rad} is obtained from a measurement by substitution, with radiation heating power replaced by electrical heating power in a null measurement [9];
m_{core} is the mass of the core;
k_h is the heat transfer correction factor, resulting from heat transfer to and from the core;
k_{dec} is the decay correction factor which corrects to the reference time;
$k_{graph/water}$ is the graphite-to-water conversion factor;
k_{imp} is the impurity correction factor (correcting for the effects of impurities in graphite only);
k_{volavg} is the volume averaging correction factor;
k_{gap} is the vacuum gap correction factor;
k_{inh} is the inhomogeneity correction factor (correcting for the effects of all non-graphite materials between the ^{192}Ir source and the outside of the large graphite phantom); and

$k_{\text{full scat}}$ is the correction factor to correct the measurement to full scatter conditions.

5. CORRECTION FACTORS DETERMINED BY MC SIMULATIONS

Both the gamma spectrum and the beta spectrum of the ^{192}Ir source were considered in the refined MC simulations. The average dose rate to the graphite core at 2.5 cm distance from a Nucletron microSelectron classic ^{192}Ir source with an activity of 370 GBq was calculated as 1.61×10^{-2} Gy/s. The beta spectrum contributes only 0.1% to the total dose absorbed in the core.

In this work, correction and conversion factors were determined by MC simulations based on the final design. These factors include the graphite-to-water conversion factor, and perturbation correction factors shown in Table 2 and used in Eq. (1).

The graphite-to-water conversion factor, $k_{\text{graph/water}}$, was calculated as the ratio of the absorbed dose to a point in water at a distance of 1 cm, and the absorbed dose to a point in pure graphite at the measurement distance of 2.5 cm. $k_{\text{graph/water}}$ can be factorized as follows:

$$k_{\text{graph/water}} = 2.5^2 \cdot k_{\text{att+scat}} \cdot k_{\varphi} \cdot \left(\frac{\bar{\mu}_{\text{en}}}{\rho} \right)_{\text{graphite}}^{\text{water}} \tag{2}$$

where $k_{\text{att+scat}}$ = 0.9864 ± 0.0024 is the combined attenuation and scatter correction factor, k_{φ} = 1.0006 ± 0.0010 is a correction factor accounting for the difference in the photon spectra at 2.5 cm in graphite and at the water equivalent distance of 4.137 cm in water. The water equivalent distance was calculated by

TABLE 2. MC CALCULATED CORRECTION FACTORS AND STATISTICAL (TYPE-A) UNCERTAINTIES

Symbol	Description	Value	Standard uncertainty
k_{imp}	Impurity correction factor	0.9997	0.0003
k_{volavg}	Volume averaging correction factor	1.0024	0.0008
k_{gap}	Vacuum gap correction factor	0.9992	0.0004
k_{inh}	Inhomogeneity correction factor	1.0008	0.0004
$k_{\text{full scat}}$	Full scatter correction factor	1.0060	0.0005

applying the electron density scaling factor [11], which is based on the assumption that all photon interactions in the medium are due to Compton scattering

$$\left(\bar{\mu}_{\text{en}}/\rho\right)^{\text{water}}_{\text{graphite}} = 1.1190 \pm 0.0017 \tag{3}$$

is the mass energy absorption coefficient ratio water-to-graphite. The standard uncertainties quoted on the MC results are only the statistical (type-A) uncertainties. The accuracy of the MC calculated correction factors depends on the cross- section data used and their uncertainties , which are typically 1% or more [12]. A sensitivity study needs to be carried out in order to investigate the effect of the uncertainties on the ratios of cross sections and to estimate the systematic (type-B) uncertainties of the MC calculated correction factors.

6. REFINED HEAT TRANSFER SIMULATIONS

An MC calculated dose map of the final design of the calorimeter due to a Nucletron microSelectron classic HDR ^{192}Ir source was used in a refined heat transfer model, where both the heat flow due to the source self-heating and the distributed radiation heating were investigated. Both conductive heat transfer and radiative heat transfer across all vacuum gaps were simulated using COMSOL Multiphysics [8]. Figure 3 shows the temperature evolution in all five graphite parts of the brachytherapy calorimeter due to a 370 GBq HDR ^{192}Ir source. The simulated core temperature was compared to the analytically calculated ideal temperature increase in the absence of conduction. From Fig. 3 it can be seen that following the introduction of vacuum gaps between the ^{192}Ir source and the point of measurement, both curves representing the core temperature are now almost identical, as opposed to the curves shown in Fig. 1. The curve showing the simulated core temperature is below the analytically calculated curve (assuming no conduction) because of the lower temperature of the parts surrounding the core.

7. FUTURE WORK

It is planned to validate the refined heat transfer model by measuring the response of the calorimeter using a dummy heat source. A dummy heat source was built by embedding a small thermistor into the steel capsule of a Nucletron microSelectron classic dummy source. The source self-heating of the radioactive ^{192}Ir source can be simulated by electrical heating of the thermistor. The

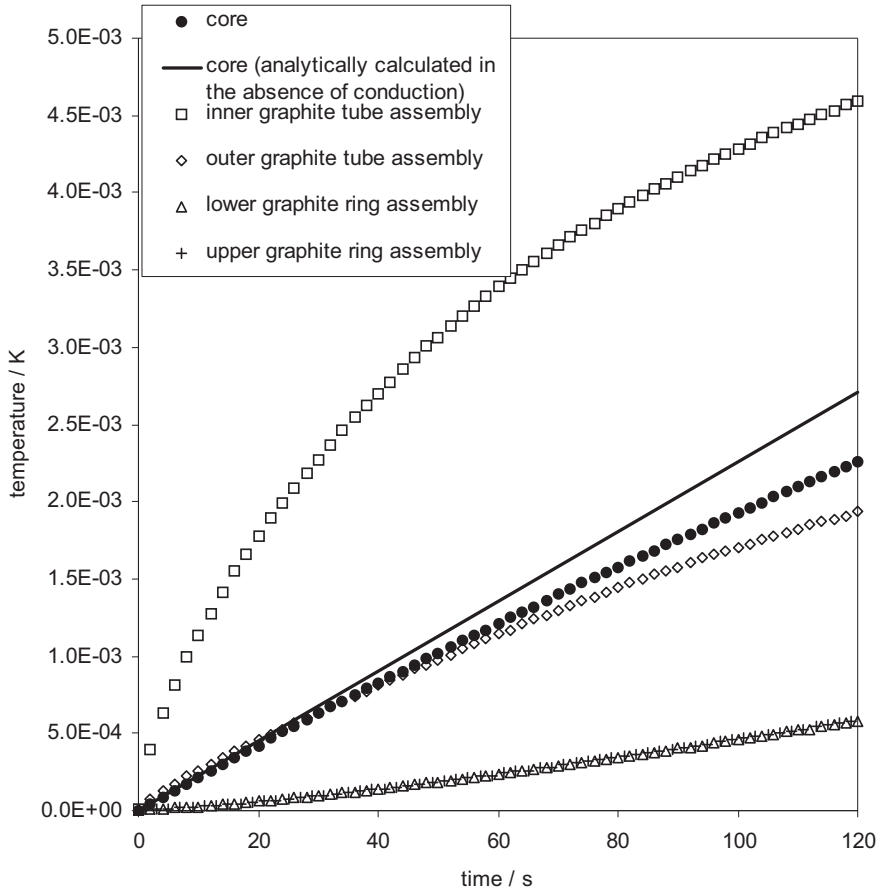

FIG. 3. Time-dependent solution of the heat equation for conductive and radiative heat transfer in the five graphite parts of the brachytherapy calorimeter. The 370 GBq ^{192}Ir source was simulated at the centre of the calorimeter for 120 s. The initial temperature of all media was set to T(r, 0) = '0 K' (relative temperature). The solid line represents the analytically calculated (ideal) temperature increase averaged over the graphite core in the absence of heat conduction. The COMSOL-simulated values of the temperature in the five graphite parts are indicated by the symbols shown in the legend.

self-heating power of a 370 GBq ^{192}Ir source due to a radiation dose delivered to the ^{192}Ir cylinder and the stainless steel encapsulation was estimated with MC simulations as 18.35 mW.

Together with existing air kerma primary standards for HDR ^{192}Ir, the new calorimeter offers the possibility of experimentally determining dose rate constants, L, of commercially available HDR brachytherapy sources.

8. CONCLUSIONS

A novel absorbed dose calorimeter for the measurement of HDR ^{192}Ir brachytherapy sources has been designed and built at NPL. This will allow for more accurate determinations of the absorbed dose rate to water at the reference distance of 1 cm, compared to the present air kerma based approach, with a potential reduction in the overall uncertainty associated with brachytherapy dosimetry.

ACKNOWLEDGEMENT

This work was supported by the UK National Measurement Office.

REFERENCES

[1] THOMADSEN, B.R., RIVARD, M.J., BUTLER, W.M., (Eds), Brachytherapy Physics, AAPM Medical Physics Monograph **31** (2005) 59–74.
[2] SANDER, T., NUTBROWN, R.F., The NPL air kerma primary standard TH100C for high dose rate 192Ir brachytherapy sources, (2006).
[3] NATH, R., et al., Dosimetry of interstitial brachytherapy sources: Recommendations of the AAPM Radiation Therapy Committee Task Group No. 43. Med. Phys. **22** (1995), 209–234.
[4] RIVARD, M.J., et al., Update of AAPM Task Group No. 43 Report: A revised AAPM protocol for brachytherapy dose calculations, Med. Phys. **31** (2004), 633–674.
[5] SARFEHNIA, A., et al., An absorbed dose to water standard for HDR ^{192}Ir brachytherapy sources based on water calorimetry: Numerical and experimental proof-of-principle Med. Phys. **34** (2007) 4957–4961.
[6] SARFEHNIA, A., SEUNTJENS, J., Development of a water calorimetry-based standard for absorbed dose to water in HDR ^{192}Ir brachytherapy Med. Phys. **37** (2010) 1914–1923.
[7] BAMBYNEK, M., et al., Calorimetric determination of absorbed dose to water for a ^{192}Ir HDR brachytherapy source in near-field geometry, World Congress on Medical Physics and Biomedical Engineering, Munich, Germany, IFMBE Proc. Vol. 25, Springer (2009).
[8] COMSOL Multiphysics^{TM} Reference Manual Version 3.3a, Stockholm: Comsol AB (2007).
[9] SEUNTJENS, J., DUANE, S., Photon absorbed dose standards, Metrologia, **46** (2009) S39–S58.
[10] KAWRAKOW, I., ROGERS, D.W.O., The EGSnrc code system: Monte Carlo simulation of Electron and Photon Transport, NRCC Report PIRS-701 (2006).

[11] ATTIX, F.H., Introduction to radiological physics and radiation dosimetry, A Wiley-Interscience Publication, John Wiley & Sons, New York, Chichester, Brisbane, Toronto, Singapore (1986).
[12] ROGERS, D.W.O., Fifty years of Monte Carlo simulations for medical physics, Phys. Med. Biol., **51** (2006), R287–R301.

PRIMARY WATER CALORIMETRY FOR CLINICAL ELECTRON BEAMS, SCANNED PROTON BEAMS AND ^{192}Ir BRACHYTHERAPY

A. SARFEHNIA*, K. STEWART*, C.K. ROSS**, M.R. McEWEN**,
B. CLASIE***, E. CHUNG*, H.M. LU***, J. FLANZ***,
E. CASCIO***, M. ENGELSMAN***, H. PAGANETTI***,
J. SEUNTJENS*

* Medical Physics Unit, McGill University, Montreal,
Quebec
Email: asarfehnia@medphys.mcgill.ca

** National Research Council of Canada, Ottawa,
Ontario

Canada

*** Massachusetts General Hospital and Harvard Medical School, Boston,
Massachusetts, United States of America

Abstract

The aim of this manuscript is to present an overview of a unified set of water-calorimetry-based measurements performed using a single water calorimeter for three clinically relevant modalities: clinical high energy electron beams, scanned proton beams and ^{192}Ir brachytherapy. Water calorimetry allows for the direct measurement of absolute absorbed dose to water D_w by determination of the temperature rise in water, and through dissemination, enables primary standards laboratories to calibrate user detectors directly in the beam type and for the beam quality of interest. In this work, an in-house built transportable water calorimeter was used to measure D_w directly for the three different beam types and beam energies. The physics of operating the calorimeter in these three modalities lies in the accurate determination of the correction factors together with the uncertainty budget. Based on detailed comparison work with dosimetry using other detectors, this work demonstrates that a primary absorbed dose standard based on water calorimetry is feasible in brachytherapy, scattered and scanned proton beams, as well as in high energy clinical electron beams, down to 6 MeV.

1. INTRODUCTION

Water calorimetry is one of the most direct techniques to establish absorbed dose to water D_w in a beam or near a source of ionizing radiation. Since in radiation therapy the quantity of interest is dose to water, development of water calorimetry based primary standards for the different modalities would not only allow for the direct measurement of the quantity of interest, but could potentially improve the uncertainty on D_w by eliminating the various conversion and correction factors that would otherwise be necessary to account for such effects as intrinsic and/or extrinsic energy dependence of the detector.

In water calorimetry, the absorbed dose to water D_w at a point $\vec{r}$ is determined by [1, 2]

$$D_w(\vec{r}) = c_{w,p} \cdot \Delta T(\vec{r}) \cdot \prod_i k_i = c_{w,p} \cdot \Delta T(\vec{r}) \cdot k_{dd} k_\rho k_p k_{hd} k_{ht} \quad (1)$$

where $c_{w,p}$ is the specific heat capacity of water at constant pressure and ΔT is the radiation-induced local temperature rise at the measurement point $\vec{r}$.

The temperature rises of interest in water calorimetry are often of the order of hundreds of microkelvin or at best a few millikelvin. Moreover, there are several correction factors k_i that need to be carefully determined for a successful measurement of absorbed dose. These include:

k_{dd} corrects for the dose profile, and accounts for the dose measured at the thermistor detectors relative to dose at the reference point (on the central axis of the beam).

k_ρ corrects for water density differences if the calorimeter is operated at temperatures other than room-temperature under which dosimetry measurements are often performed. The small density difference manifests itself as a small change in the effective point of measurement.

k_{hd} is the heat defect correction factor and accounts for potential heat loss or gain from endothermic or exothermic chemical reactions that may occur in water as a result of impurities and unknown dissolved gases. This factor is minimized through embedding the detectors inside a glass vessel and controlling the purity of the water that is sealed inside the vessel. The factor k_{hd} has been experimentally measured and/or numerically calculated for several systems and beams of various LET [3].

k_p is a dose perturbation correction factor which corrects for any perturbation of the dose distribution due to the presence of non-water materials. This

factor is often calculated using Monte Carlo techniques for the specific beam quality and measurement setup.

k_{ht} is the heat transfer correction factor and accounts for the effects of conduction and convection on the temperature distribution inside the water calorimeter. It is defined as the ratio of the ideal temperature rise (a temperature rise solely due to locally deposited absorbed dose in the absence of heat transfer) to the actual temperature rise (with the effects of heat transfer taken into account) at a given point. The factor k_{ht} is calculated by solving the heat transport partial differential equations, often using finite element method.

Currently, water calorimetry is only fully established at standards laboratories as a primary standard for high energy photon beams. This paper discusses both numerically and experimentally, the feasibility of using water calorimetry as a primary standard in clinical high energy electron beams, HDR ^{192}Ir brachytherapy, and scattered and scanned proton therapy beams. Currently, an absorbed dose to water standard based on water calorimetry is unavailable for all of these therapeutic modalities. The complexity of extracting accurate values for absorbed dose to water lies in the handling of the correction factors and these, together with measurement reproducibility, determine the overall uncertainty on the D_w measurement. The main effects determining the correction factors are heat loss (or gain) due to non-uniform temperature distribution in the calorimeter and the heat defect of water. In this paper, briefly discuss the challenges in developing a water calorimetry based primary standard are briefly discussed for each of the described modalities, and the water calorimetry based results are compared to present protocols that measure dose to water indirectly for each of the modalities.

2. MATERIALS AND METHODS

2.1. Measurements

A transportable stagnant 4°C Domen-type water calorimeter has been developed in-house at McGill University [4]. The calorimeter consists of a 30 cm × 30 cm × 20 cm Lucite water tank that is surrounded by a sophisticated system of temperature cooling and temperature control [4]. All measurements are made with the calorimeter maintained in a narrow 0.06°C temperature range around the nominal 3.98°C mean water temperature. A Pyrex parallel plate calorimeter vessel was used to house two glass-coated bead thermistors (nominal resistance of 10 kΩ at 4°C), which were positioned with a nominal 2.4 mm separation centered on the central axis of the beam, and at a nominal separation of

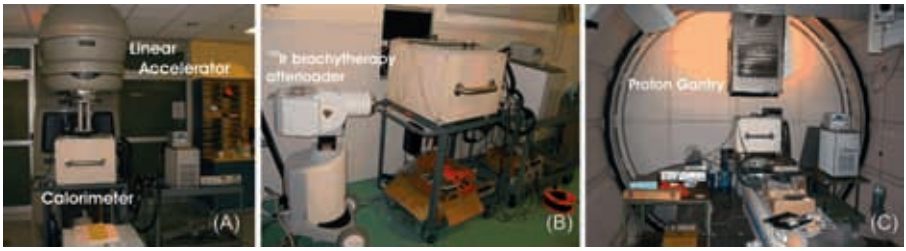

FIG. 1. Water calorimeter setup under a clinical linear accelerator (A), for ^{192}Ir brachytherapy (B), and under a proton nozzle (C).

11 mm from the top surface of the glass vessel. The thermistors act as accurate point temperature detectors. The calorimeter was validated in high energy photon beams against Canada's national standard at the National Research Council of Canada (NRC).

Figure 1 shows the calorimeter in the three modes of operation described. The overall calorimeter setup was similar for all external beams (i.e. high energy photon and electron beams, as well as proton beams). The external beam was incident on the calorimeter from the top (Fig. 1(A) and (C)). In the case of brachytherapy, the setup deviated slightly from conventional calorimeter measurement setup, as the calorimeter was modified such that the iridium source could enter the water tank through a Nucletron 4 French nylon-12 'breast-comfort' catheter [4] (Fig. 1(B)).

Both nitrogen and hydrogen saturated systems were used for photon and electron measurements. The heat defect for such systems when brought to steady state is well studied and is generally taken to be zero [3]. A hydrogen saturated system was used in the proton study for which the heat defect has also been numerically evaluated to be zero for LET values up to 25 eV/nm [5]. Hydrogen saturated systems show a large transient exothermic behavior in the presence of small concentrations of oxygen [6, 7]. Past this transient oxygen consumption peak, the system reaches a steady state with zero heat defect [1]. In this work, only the calorimetric runs past the oxygen consumption peak have been used in the data analysis.

2.2. Beam set-up

2.2.1. Electron beam water calorimetry

The water calorimetric measurements were performed under 6, 9, 12, 16, and 20 MeV electron beams of a clinical Varian Clinac 21EX machine. The small penetration of the 6 MeV beam requires a very shallow measurement depth. The

thermistors were positioned 13.4 mm below the water surface, with the top window of the glass vessel at a mere 2 mm below the water surface. The sharp dose fall-off of the beam that occurs inside the vessel makes the calculation of k_{ht} challenging, while the uncertainty introduced by minute positioning differences also affects the overall dose uncertainty significantly. The nominal depths of thermistors with respect to the water surface were 13.4 mm, 20.2 mm, 28.6 mm, 38.8 mm, and 48.6 mm for 6 MeV, 9 MeV, 12 MeV, 16 MeV, 20 MeV beams, respectively.

2.2.2. Proton beam water calorimetry

The measurements were performed both for a double-scattered and scanned proton beams. The measurements were performed at the Massachusetts General Hospital's Francis H. Burr Proton Therapy Center [8, 9]. In double scattering, the thermistors were positioned at a water-equivalent depth of 126.10 mm (R_{res} = 5.48 g/cm^2) of a spread out proton Bragg peak with a 90% distal dose fall-off of 175 mm. The scanned beam was produced by superposition of 15 Bragg curve layers with energies ranging between 128 MeV and 151 MeV. The thermistors were positioned at a water equivalent depth of 131.15 mm (R_{res} = 3.75 g/cm^2). The variation of dose in a ±1 cm range around the thermistor detectors was measured to be less than 0.4% and 0.2% in scattered and scanned beams, respectively.

2.2.3. Brachytherapy water calorimetry

The measurements were performed with a ^{192}Ir HDR brachytherapy source. Transfer tubes were used to connect the catheter to the Nucletron afterloader, which was programmed to remotely insert the source through the transfer tube and catheter into the calorimeter. The absolute absorbed dose to water measurements were made for several different Nucletron microSelectron ^{192}Ir sources of air kerma strength ranging between 21000 and 38000 U, and for source-to-detector separations ranging between 25 mm and 70 mm. While the range of source activities cover the clinical useful source activity range, the source-to-detector separation $d_{src\text{-}det}$ was selected based on an optimization solution that weighed the signal to noise ratio (improves at small $d_{src\text{-}det}$) against the effects of $d_{src\text{-}det}$ uncertainty on measured dose uncertainty (improves at larger $d_{src\text{-}det}$). The large dose gradient around the source, as well as the large inherent temperature of the source (due to the self-attenuation of the photons produced by the source itself, termed 'source self-heating') add up to make a very sharp temperature gradient.

2.3. Heat transport calculations

Assuming the chemical heat defect to be well under control, the most significant correction factor in water calorimetry in the modalities studied here, is the heat transfer correction factor k_{ht} in Eq. 1. This correction factor is often calculated using software that solves the heat transport problem (the conduction and convection problem) based on finite element or finite difference method. The COMSOL MULTIPHYSICS™ software (referred to hereon as COMSOL) was one such program that was used in this work.

It is a common and accepted practice to ignore convection in the heat transport simulation when performing external beam high energy photon 4°C water calorimetry heat transfer calculations. This is because by operating the calorimeter in a narrow temperature band around 3.98°C, the volumetric thermal expansion coefficient α for water remains very close to zero thereby eliminating the driving force of convection. Under these conditions, the temperature gradients formed in water during external high energy photon water calorimetry are too small for the onset of convective effects. Although this is a good approximation for all external radiotherapy beams, it was identified that in HDR ^{192}Ir brachytherapy calorimetry, the effects of convection are non-negligible due to the high temperature gradients as a result of source self-heating. As such, the 'conduction and convection' module of COMSOL was combined with the 'Navier-Stokes incompressible fluid' module, to perform the full convection calculation.

3. RESULTS AND DISCUSSION

3.1. Electron beam water calorimetry

Absorbed dose measurements were performed in 4–12 independent sets of 10–20 runs for each energy value at a dose rate of approximately 6 Gy/min. Heat transport calculations depended mostly on the separation of vessel flat walls and on beam energy but were otherwise rather insensitive (at the 0.1% level) to many of the experimental parameters. Table 1 shows a summary of the calorimeter correction factors and uncertainties as a function of R_{50} in electron beam calorimetry. The standard uncertainty on k_{ht} varied from 0.58% at 6 MeV to 0.13% at 20 MeV and is dominated by the uncertainties on the vessel perturbation and the heat loss corrections at 6 MeV. Correction factors are also largest at 6 MeV due to the thickness of the front wall and the proximity of the back wall.

The water calorimeter was used to calibrate an Exradin A12 and a PTW Roos chamber. To this end, the calorimeter was brought to room temperature and

TABLE 1. SUMMARY OF THE VALUES OF THE k_{ht} COEFFICIENT FOR ALL THE THERAPEUTIC MODALITIES STUDIED IN THIS WORK

Energy	k_{ht}	$u_{k_{ht}}$ (%)	u_{k_p} (%)	$u_{k_{hd}}$ (%)	$u_{k_{dd}}$ (%)	u_{k_ρ} (%)	u_{D_w} (%)
6 MeV (R_{50} = 2.25 cm)	**1.022**	0.58	0.63	0.3	0.05	0.05	**1.03**
9 MeV (R_{50} = 3.54 cm)	**1.011**	0.16	0.24	0.3	0.05	0.05	**0.52**
12 MeV (R_{50} = 4.94 cm)	**1.010**	0.10	0.26	0.3	0.05	0.05	**0.49**
16 MeV (R_{50} = 6.64 cm)	**1.010**	0.14	0.26	0.3	0.05	0.05	**0.51**
20 MeV (R_{50} = 8.26 cm)	**1.012**	0.13	0.27	0.3	0.05	0.05	**0.52**
6 MV	**1.01**	0.13	0.13	0.3	0.01	0.04	**0.46**
Scattered proton (250 MeV)	**0.996**	0.10		0.3	0.002	0.03	**0.38**
Scanned proton (128–150) MeV	**0.953**	0.42		0.3	0.01	0.05	**0.64**
^{192}Ir brachytherapy	**0.963**	0.35	0.1	0.3	0.45	0.05	**1.90**

Note: The exact value of the k_{ht} is dependent on the exact details of the modeled setup. The contributions to the most significant portions of the uncertainty budgets from the various correction factors have also been included. The total uncertainty on D_w as determined with water calorimetry is noted in the last column.

the chambers were positioned with their effective point of measurement at the position of the centre of the thermistor probes. Ion recombination and polarity effects were accounted for, and the measurement was performed with the lid in place so as to minimize differences in setup between calorimetry and ionization chamber dosimetry. Figure 2 shows preliminary k'_{R50} factors obtained by direct calibration in the water calorimeter, normalized at R_{50} of 7.5 cm relative with results from the AAPM TG-51 [10] and the IAEA TRS-398 [11] 'Codes of Practice'.

The results show a good agreement between the calorimeter PTW Roos k'_{R50} values and the protocol values down to 6 MeV. This result is surprising to a certain extent since, from recent Monte Carlo calculations by Zink and Wulff [12], one would expect the k'_{R50} to be higher by about 0.6 to 1% than the protocol-predicted value at lower R_{50} values (corresponding to the 6–9 MeV range). However, based on the present combined uncertainty (~1%), this conclusion cannot be ruled out. For the Exradin A12 chamber (k'_{R50}), the calorimeter

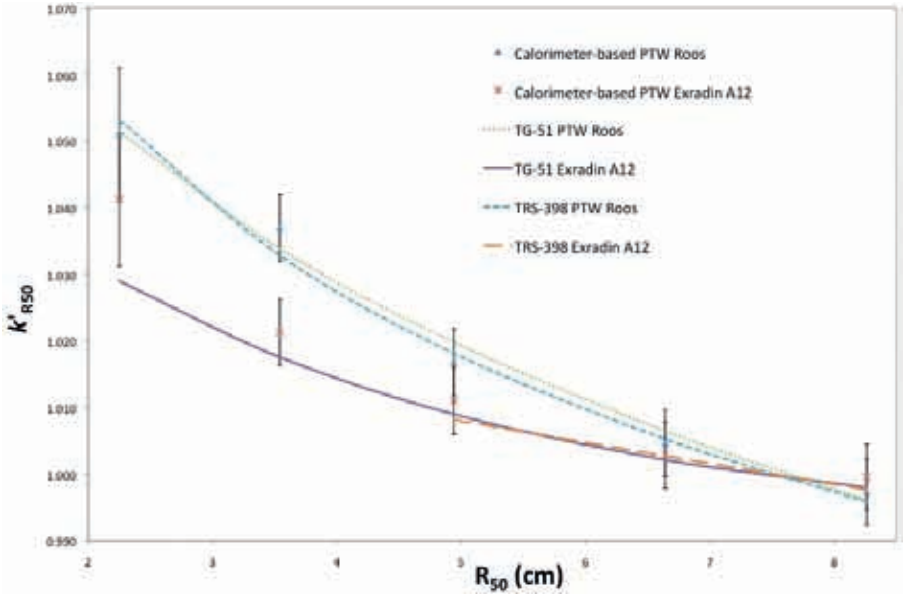

FIG. 2. Water calorimetry-based k'_{R50} for Exradin A12 and PTW Roos chambers as a function of R_{50}. Results are compared against the AAPM TG-51 and IAEA TRS-398 calculated results.

expected value is 1.1% higher relative to the protocol value at 6 MeV, but less than 0.2% different at 12 MeV and higher energies. The relative difference in absorbed dose response of the Exradin A12 and PTW Roos chambers is in agreement with the literature [13]. By reducing the thickness of the vessel's front wall and moving the downstream wall further away, the calorimeter vessel design could be optimized especially for water calorimetry at low electron energies (6 MeV, 9 MeV) and for scanned proton beams.

3.2. Proton beam water calorimetry

A typical calorimeter run in scattered and scanned proton beam is shown in Fig. 3. A demonstration of the feasibility of the direct measurement of absorbed dose to water in scanned beams depends on the treatment of the heat loss problem associated with the sequential painting of the layers spread out over the entire irradiation time. In the case of scanned beam delivery, this heat loss problem for a calorimeter operated at 4°C, is determined by irradiation time per layer, switch time between different layers, and to a significant extent, the vessel–thermistor configuration. A complete description of the heat loss correction factors in scattered and scanned beam delivery is given in Ref. [9]. Table 1 shows an

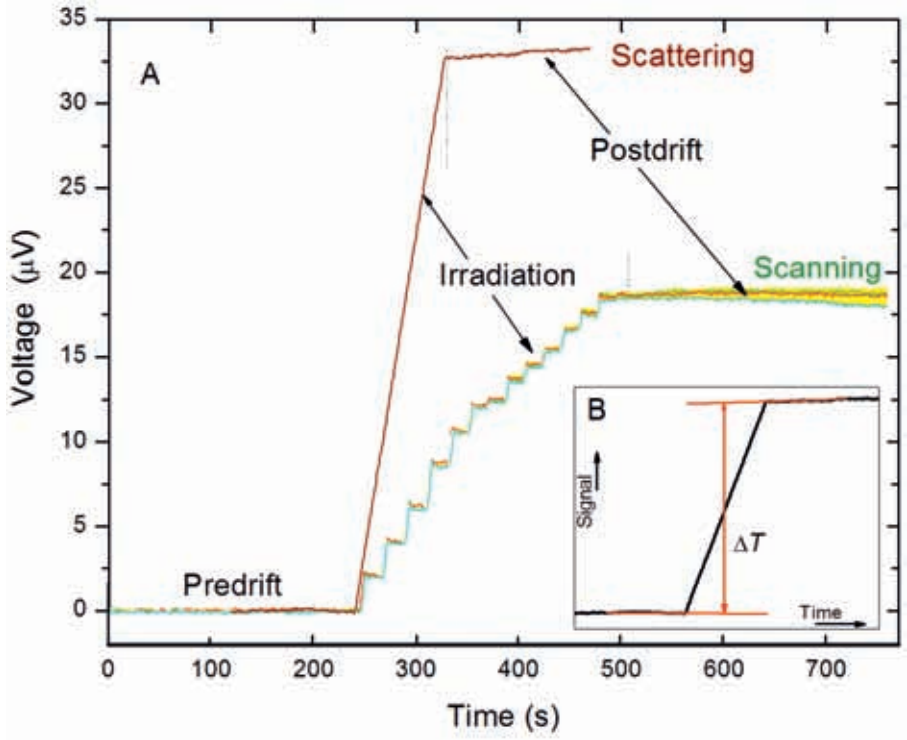

FIG. 3. Calorimeter trace, expressed as calorimeter bridge output voltage as a function of time, during a typical scattered beam and a set of scanned beam runs. Whereas only a single measurement run is shown for the scattered beam, in the case of scanned proton beam drift curve, the 1-sigma range of the measurements along with a few calorimetric runs are shown. Inset: example of typical calorimeter run analysis. (Courtesy of the American Association of Physicists in Medicine (see Ref. [9]).)

overview of the calorimeter correction factors and uncertainties for scanned and scattered beam deliveries used in this work. The overall standard uncertainty on the absorbed dose to water measured using the calorimeter was 0.4% and 0.6% in scattered and scanned beam delivery, respectively.

3.3. Brachytherapy water calorimetry

The inherent nature of ^{192}Ir brachytherapy measurements with the hot, active source inserted inside the water phantom resulted, even at 4°C, in the formation of non-negligible convective currents inside the phantom and especially close to the source. Although the calorimeter vessel acts as a

convective barrier and virtually eliminates the effects of convection inside the vessel, relatively large non-linear drifts, caused by conduction of the large convective effects outside the vessel, were found to still form inside the calorimeter following every calorimetric run. The drifts can be minimized either by increasing the waiting time in between each run to allow for the system to reach a new thermal equilibrium, or by decreasing the source-to-detector separation $d_{\text{src-det}}$ to achieve higher dose rate and, by reducing the drift extrapolation times, an adequate signal to noise ratio could be achieved. At such small $d_{\text{src-det}}$, the positioning accuracy becomes vital, and small positioning differences can drastically affect D_{w}. Owing to time constraints and equipment limitations, neither of the two options was feasible in this work. Hence, the measurements were performed generally at $d_{\text{src-det}}$ = 5 cm to 7 cm separation. The resulting non-linear drifts affecting the drift curve were corrected to a large extent through a characterization of the thermal evolution inside the calorimeter and non-linear fitting [4]. Such a drift-corrected run together with a modeled COMSOL drift curve are shown in Fig. 4. The estimated standard uncertainty on D_{w} using this method was 1.9%, which can potentially be further reduced if longer wait times (>1.5 h used in this work) in between consecutive calorimetric runs are allowed. As shown in Table 2, the dose rates measured agreed well to within 0.83% with currently accepted AAPM TG-43 results as well as with in-water Gafchromic and film measurements [14].

4. CONCLUSIONS

This paper summarizes a decade of calorimetry work at McGill University. The goal was the demonstration of feasibility, both numerically and experimentally, of the use of water calorimetry as a direct, primary method of absolute dosimetry in clinical electron beams, scanned proton beams and HDR brachytherapy source dose measurements. Provided the calorimeter was brought to a chemical steady state corresponding to zero heat defect, in each of these modalities, the dominating remaining effect leading to a correction was the heat transfer. Using detailed numerical modeling, however, it is possible to accurately calculate and validate the correction factor leading to an overall standard uncertainty from 0.4 to 1.9% depending on the modality. This work should lead to better thermally optimized, second generation primary standards that will form the basis of new absorbed dose standards for these modalities.

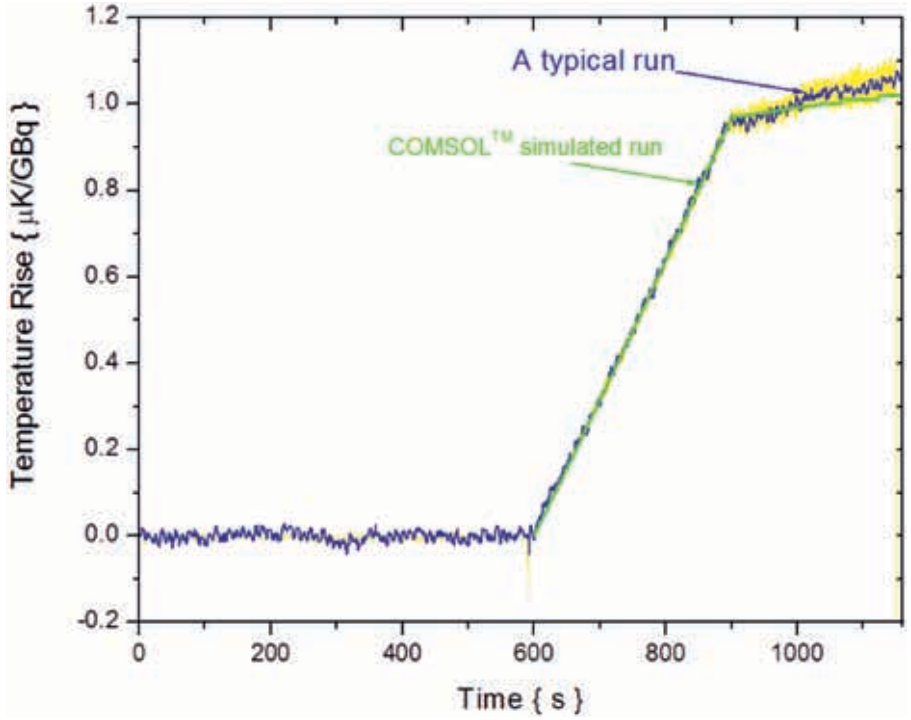

FIG. 4. A typical brachytherapy experimental run corrected for the non-linear drift, superimposed on a COMSOL calculated drift curve. The highlighted region displays the maximum range of all measurement runs collected. The results are shown in air kerma strength-normalized temperature rise at the point of measurement.

TABLE 2. OVERALL DIFFERENCE BETWEEN DIFFERENT DOSIMETRY TECHNIQUES AND CALORIMETRY FOR DIRECT DOSE TO WATER MEASUREMENTS IN AN HDR ^{192}Ir SET-UP

Method	Relative difference from water calorimetry
Ionization chamber	–0.83%
Radiochromic film	0.83%
TG-43	0.55%

Note: See Ref. [14] for more detail.

REFERENCES

[1] SEUNTJENS, J., DUSAUTOY, A.R., " Review of calorimeter based absorbed dose to water standards", Standards and Codes of Practice in Medical Radiation Dosimetry (Proc. Int. Symp. Vienna, 2002), IAEA Vienna (2003) 37–66.

[2] SEUNTJENS, J.P., DUANE, S., Metrologia **46** (2009) S39–S58.

[3] KLASSEN, N.V., ROSS, C.K., J Res Natl Inst Stand Technol **102**, (1997) 63–74.

[4] SARFEHNIA, A., SEUNTJENS, J., Med Phys **37** (4), (2010) 1914–1923.

[5] SASSOWSKY, M., PEDRONI, E., Phys Med Biol **50** (22) (2005) 5381–5400.

[6] KRAUSS, A., ROOS, M., Thermochimica Acta **310** (1998) 53–60.

[7] PALMANS, H., KACPEREK, A., AEKEL, O., Clinical Dosimetry Measurements in Radiotherapy, Rogers, D.W.O., Cygler, J.E. (Eds.) (Medical Physics Publishing, Madison, Wisconsin (2009).

[8] FLANZ, J., DURLACHER, S., GOITEIN, M., LEVINE, A., REARDON, P., SMITH, A., NIM-B **99** (1995) 830–834.

[9] SARFEHNIA, A., CLASIE, B., CHUNG, E., LU, H.M., FLANZ, J. CASCIO, E., ENGELSMAN, M., PAGANETTI, H.. SEUNTJENS, J., Med Phys **37** (2010) 3541–3551.

[10] ALMOND, P.R., BIGGS, P.J., COURSEY, B.M., HANSON, W.F., HUQ, M.S., NATH, R., ROGERS ,D.W., Med Phys **26** (9) (1999). 1847–1870.

[11] [11] INTERNATIONAL ATOMIC ENERGY AGENCY, Absorbed Dose Determination in External Beam Radiotherapy: An International Code of Practice for Dosimetry Based on Standards of Absorbed Dose to Water, Technical Reports Series No. 398, IAEA, Vienna (2000).

[12] ZINK, K., WULFF, J., Phys Med Biol **53** (2008) 1595–1607.

[13] STEWART, K., SEUNTJENS, J. Med Phys **29** (284) (2002) 284–289.

[14] SARFEHNIA, A., KAWRAKOW, I., SEUNTJENS, J., Med Phys **37** (4) (2010). 1924–1932.

DETERMINATION OF ABSORBED DOSE TO WATER IN MEGAVOLTAGE ELECTRON BEAMS USING A CALORIMETER–FRICKE HYBRID SYSTEM

C.D. COJOCARU, G. STUCKI, M.R. McEWEN, C.K. ROSS
Ionizing Radiation Standards,
Institute for National Measurement Standards,
National Research Council Canada,
Ottawa, Ontario, Canada
Email: Claudiu.Cojocaru@nrc-cnrc.gc.ca

Abstract

A water calorimeter–Fricke solution hybrid dosimetry system was developed at the National Research Council of Canada to be used for reference dosimetry for high energy electron beams in the energy range produced by medical linear accelerators. The system uses water calorimetry for higher energy beams of 18 MeV and 22 MeV, while Fricke dosimetry is used for the lower energies of 4 MeV, 8 MeV and 12 MeV. Fricke solution dosimetry was also used for 18 MeV and 22 MeV to determine the Fricke solution's $\varepsilon \cdot G(Fe^{3+})$ coefficient needed for calculations at lower energies. The deviation from linearity of the system in the dose range from 6 to 52 Gy was typically 0.2–0.3% for all energies, while the average repeatability for a single dosimeter was about 1%. As a practical application, the energy dependence of the response of a parallel-plate ionization chamber was investigated. It was found that at higher energies, the predictions were similar to those calculated by TG-51 and TRS 398, while for lower energies, differences were observed of up to 1%, consistent with new Monte Carlo and experimental investigations of chamber perturbation corrections,

1. INTRODUCTION AND THEORY

Water calorimetry is a well-established procedure for measuring absolute absorbed dose to water in photon and electron beams. For the lower energy electron beams, due to the short range of the electrons, it becomes increasingly difficult (due to the geometrical size of the containing glass vessel) to fit a water calorimeter vessel in the water tank at the reference depths. In order to be able to extend the measurement of absorbed doses to lower energy electron beams, an alternative solution is to use a system based on Fricke solution [1]. Fricke dosimetry constitutes an attractive approach due to its water equivalency. In addition, Fricke dosimetry has an extensive history at the National Research Council (NRC) of Canada [2].

Fricke dosimetry has been used for almost a century and it has been extensively studied and is well understood. Its applications for radiation dosimetry in medical physics are still an open field of exploration. The Fricke dosimeter solution is a dilute aqueous system formed by adding ferrous ammonium sulphate and sulphuric acid to aerated, high-purity water. When radiation passes through the solution, molecules of water are changed into reactive species, e.g. electrons (e^-), hydrogen atoms and ions (H and H^+), hydroxyl radicals (OH and OH^-), or molecules, e.g. hydrogen (H_2) and hydrogen peroxide (H_2O_2). Some of these initial products (OH, H_2O_2 and HO_2) chemically interact with the ferrous ions, Fe^{2+}, in the Fricke solution, creating ferric ions, Fe^{3+}. The concentration of created Fe^{3+} ions is proportional to the absorbed dose deposited in the solution and can be measured using UV absorption spectrophotometry.

The absorbed dose to Fricke solution, D_F, is given by:

$$D_F = \Delta OD/(\varepsilon \cdot G(Fe^{3+}) \cdot \rho \cdot l) \quad (1)$$

where

ΔOD is the change in the absorption between the irradiated and un-irradiated solution;
ε is the extinction coefficient;
$G(Fe^{3+})$ is the chemical yield of Fe^{3+};
ρ is the density; and
l is optical path length of the cuvettes used for readout in the UV spectrophotometer at a given wavelength.

Contaminants can significantly affect performance and therefore great care must be taken during preparation and readout. Traditionally, Fricke solution has been irradiated in solid vials usually made of quartz or glass, but this leads to significant correction factors needed for the presence of the container. The innovative approach taken here is to irradiate the Fricke solution in sealed thin polyethylene bags. This minimizes any wall correction and allows one to custom design the dosimeter shape to the application.

2. MATERIALS AND METHODS

2.1. Preparation of the Fricke solution

The success in using the Fricke solution is highly influenced by the quality of the products used and the careful manipulation during the preparation and operating process. At the NRC, high purity aerated water produced by a Millipore water system [2] is used. The sulphuric acid is a high purity 99.999%, Ultrex II grade. The ferrous ammonium sulphate hexahydrate has a purity of 99.997%. The sodium chloride has a purity of 99.999%, Ultrex grade. The water–acid mixture is pre-irradiated to a dose of 10 Gy, using ^{60}Co gamma rays. This should eliminate effects resulting from any organic impurities in the acid at low doses. The final molar concentrations for each component is: 0.4 mol/L H_2SO_4; 0.001 mol/L $(NH_4)_2Fe(SO_4)_2{\cdot}6H_2O$; and 0.001 mol/L NaCl. Two litres of solution are created at a time and stored for future use.

2.2. The sensitivity coefficient ($\varepsilon{\cdot}G(Fe^{3+})$)

An important aspect of using Fricke dosimetry is to determine an accurate value of $\varepsilon{\cdot}G(Fe^{3+})$. This is determined using the NRC primary standard water calorimeter in a high energy electron beam (≥18 MeV). The energy independence of the Fricke dosimeter is subsequently used to determine the dose in lower energy electron beams (≤12 MeV). Results presented by the Swiss Institute for Metrology (METAS) show evidence that the value of $G(Fe^{3+})$ is independent of the electron beam energy for the range relevant for radiation therapy [3, 4]. As Fig. 1 shows, there is no compelling evidence that a systematic deviation from a constant value occurs for electron beams above 4 MeV. It is expected that for softer electron spectra, the $G(Fe^{3+})$ value decreases, as demonstrated by Klassen et al. [5]. For the purpose of this work it is assumed that the sensitivity coefficient is energy independent in the radiation therapy range of high energy electron beams.

This hybrid approach provides a system that can determine the absolute absorbed dose over the complete range of electron beam energies available from clinical linear accelerators. The dose measured using this system is traceable to the NRC primary standard water calorimeter, and the Fricke dosimeter is used to transfer the dose from high to low energies.

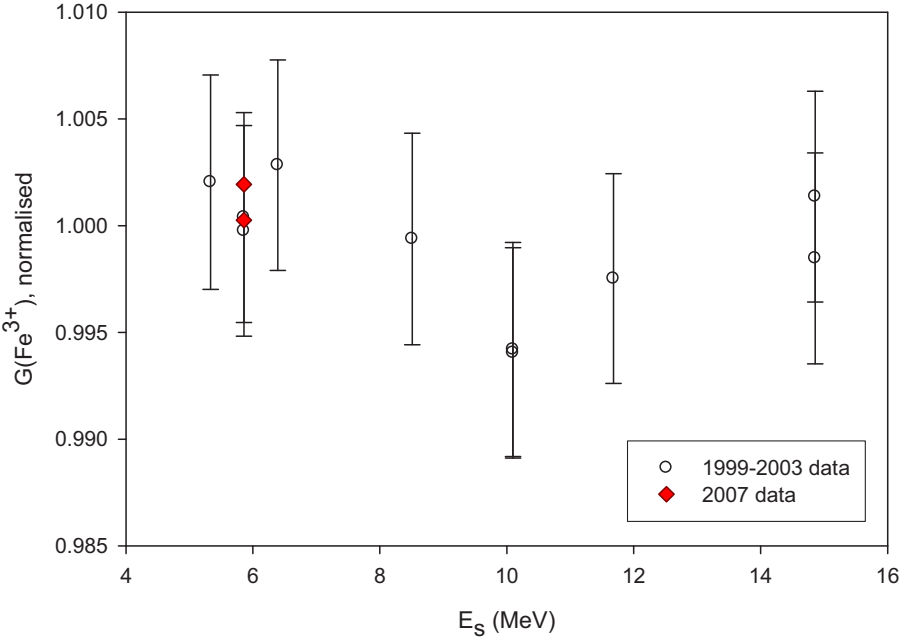

FIG. 1. The G value as a function of the electron beam energy measured by the Swiss Institute for Metrology (METAS) [4]. The E_s is the effective energy of the electrons entering the Fricke solution. There is no compelling evidence that a systematic deviation from a constant value occurs for electron beams above 4 MeV. An uncertainty of 0.25% was calculated for a linear fit through the points with a null slope.

2.3. Readout using a UV spectrophotometer

After irradiations, the sealed bags were opened and the irradiated Fricke solution was pipetted into a clean quartz cuvette for its absorbance reading with a Cary 400 UV-Vis spectrophotometer. The cuvettes had transparent lateral surfaces, were covered with Teflon cuvette covers and had a 2 cm path length. The absorption spectrum of ferric ions has two broad maxima at 224 nm and 303 nm, at a temperature of 25°C. The readings were performed at the 303 nm wavelength and the sample compartment was heated to a temperature of 25.00 ± 0.05°C in order to minimize any temperature correction. Four readings were performed simultaneously for the four available slots in the UV spectrophotometer: two cuvettes with irradiated solution (from two independent irradiations at the same dose), one metal-on-quartz standard absorption filter for monitoring the sensitivity of the spectrophotometer, and one empty slot for measuring the background.

In order to assess the cleanliness of the cuvettes and the stability of the solution in time, control measurements were performed with the two cuvettes filled with high purity water and with samples of un-irradiated Fricke solution from the bulk storage. Furthermore, in order to correct for the effect of storing the solution in the polyethylene bags, control samples of solution that spent various amounts of time in bags were measured each day of the experiment. The storage time varied from 45 to 180 min covering the usual time interval between the filling of the bags and the readout in the actual procedure. These corrections were applied when calculating the change in the optical density between the irradiated and un-irradiated samples, needed to calculate the absolute absorbed dose in the Fricke solution.

2.4. Irradiations of the Fricke dosimeters

Irradiations were carried out using the Elekta Precise medical linac at the NRC, which produces electron beams with nominal energies of 4 MeV, 8 MeV, 12 MeV, 18 MeV and 22 MeV. The dosimeters were placed with their centre at z_{ref} in a 30 × 30 × 30 cm^3 water phantom, and doses in the range 6–52 Gy were delivered to investigate signal-to-noise and any dose dependence by studying the sensitivity (the slope of the absorbance dependence on dose). The irradiations were carried out over a period of five months to evaluate the long term repeatability of the system.

The Fricke solution was put into heat-sealed polyethylene bags for the irradiations. For the measurements in electron beams, the bag size was approximately 40 × 40 × 3 mm^3, with a Fricke solution volume of 4 cm^3. The bags were supported in a PMMA holder to constrain their shape and for positioning at the reference depths in the water phantom.

Owing to the variation in the yield of ferric ions with the temperature of the Fricke solution during irradiation, a temperature dependent correction had to be applied [2]. The reference irradiation temperature was chosen to be 25°C, but typically the irradiations were performed at about 19°C.

2.5. 2.5. Conversion from dose to the Fricke solution to dose to water

There are a few aspects that need to be considered when going from the absorbed dose in the Fricke solution, D_F, to the absorbed dose in water, D_w. The formula used for conversion is:

$$D_w = D_F \cdot f_{w,F} \cdot P_{wall} \cdot k_{dd} \quad (2)$$

A correction to consider comes from the difference in the radiation absorption properties of the two liquids, $f_{w,F}$. The Monte Carlo based calculations were used to accurately determine a value of 1.003 for this correction factor, independent of beam energy. It was found that the contaminating effect of the polyethylene bag on the absorbance signal was small and could be accurately corrected for using un-irradiated controls and carefully measuring the time from filling each bag to readout.

The polyethylene bag wall and the PMMA holder introduce differences that are accounted for by a correction factor, P_{wall}. Again, MC calculations provided a good estimation of the correction factor needed to be applied. The value of this correction is 0.1 to 0.4%, increasing with decreasing beam energy. Monte Carlo calculations also showed that the effect of an air bubble (present in the bag after sealing) was below 0.1% for all energies and is included in P_{wall}.

Overall, the correction factor, $f_{w,F} \cdot P_{wall}$, due to the dosimeter itself when going from Fricke dose to water dose is about 0.5 to 0.8%, increasing with decreasing beam energy [6].

In addition, the irradiation fields for various radiation beams are not perfectly uniform over the irradiated volume, so a correction factor, k_{dd}, needs to be applied for non-uniformities over the volume of the irradiated solution. Direct measurements of the 3-D dose distribution can give an estimation of this correction. For various energies, the correction factor ranges from 1.003 to 1.028, increasing with decreasing electron beam energy. The large value of this correction at low energies is due to the use of a non-standard applicator, which was specifically designed for the water calorimeter, producing a large radial non-uniformity. Axial averaging, due to the thickness of the dosimeter bag, is small for all energies.

2.6. Uncertainties

The uncertainty in the water calorimetry measurement at the NRC is mostly due to reproducibility and calorimeter corrections. The overall uncertainty (k = 1) in the measurement of absorbed dose to water in a high energy electron beam is estimated to be 0.35% [7].

As noted above, an important assumption in this system is the energy independence of the G value. Based on the METAS data of measurements of $G(Fe^{3+})$ in the 4 to 20 MeV energy range, an uncertainty of 0.25% was calculated for a linear fit through the points with a null slope (see Figure 1).

The process of measuring the absorbance with the UV spectrometer and the linac stability add small contributions to the overall uncertainty. The estimated value is 0.02% for the former and 0.05% for the latter.

A full uncertainty budget is not presented here because there are continued investigations of a number of the significant components (e.g. energy dependence of $G(Fe^{3+})$, performance of the water calorimeter at high energies correction for radial beam uniformity).

3. RESULTS AND DISCUSSION

The method described in the previous section was first applied to irradiations performed at a beam energy of 18 MeV. A set of irradiations at various doses was performed. The average repeatability on a single dosimeter was 1.1%. Figure 2 shows the variation in absorbance with the dose delivered for the 18 MeV beam. In this case, the reference (that gives the values on the *x*-axis) is the primary standard water calorimeter [7–9]. The relationship is linear, and the standard uncertainty in the gradient is estimated to be 0.2%. Figure 2 also shows

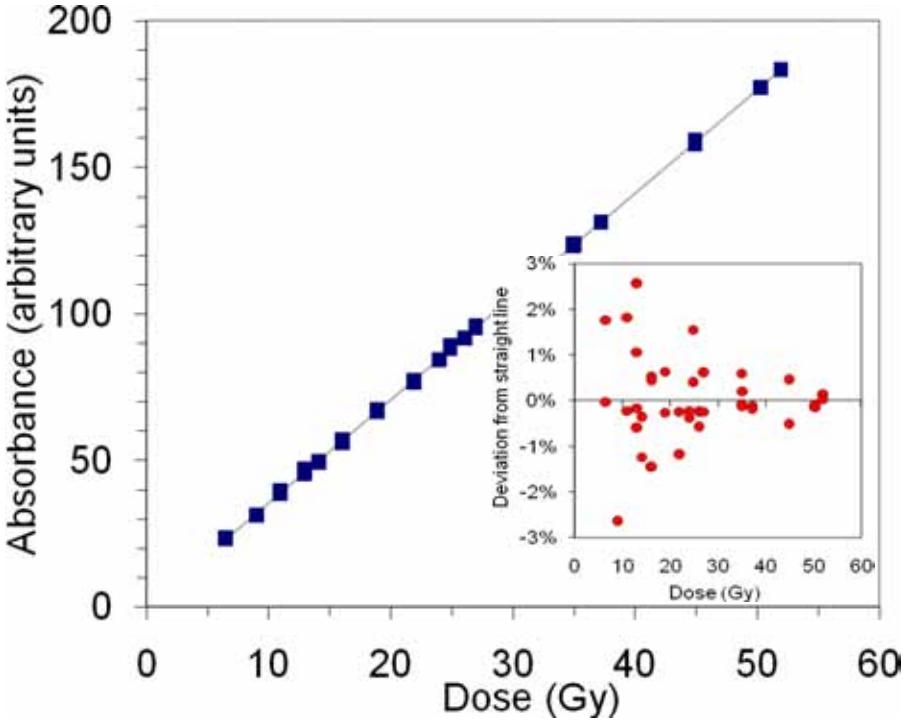

FIG. 2. Response of the system for the 18 MeV electron beam in the 6–52 Gy dose range. The error on the slope is estimated at 0.2%. In the inset, the deviation from a straight line of individual data points (the residuals from the linear fit) is shown.

the deviation of the measured points from a straight line fit (the residuals from the linear fit). The $\varepsilon \cdot G(Fe^{3+})$ value of 3.524 cm^2 /J obtained from the 18 MeV measurements, which agrees with the high energy X ray values of Klassen et al. [5], 3.532 ± 0.012 cm^2 /J at 20 MV and 3.523 ± 0.013 cm^2 /J at 30 MV, was used for the calculation of Fricke doses for all five energies. The overall uncertainty (k = 1) in the measurement of absorbed dose to water for the lower electron beam energies is estimated to be below 0.5%.

As a first practical application of the developed system, the energy dependence of the response of a PTW Roos parallel-plate ion chamber was investigated and compared to the TG-51 [10] and TRS 398 [11] protocols. The PTW Roos parallel-plate chamber was placed in the same water phantom with its effective point of measurement at the same reference depths as for the Fricke system for all five energies. Figure 3 shows the results for the PTW Roos parallel-plate ionization chamber, comparing measurements with TG-51 and TRS 398 calculations. The data are normalized at the 18 MeV beam point (R_{50} = 7 cm). The standard uncertainty in the experimental determination of the energy dependence was estimated to be 0.2–0.5%, increasing with decreasing energy.

No differences between the measured and predicted factors were seen at higher energies of 22 MeV, 18 MeV and 12 MeV. At lower energies of 8 MeV and 4 MeV, the experimental energy dependence deviates from that predicted by calculations and is in good agreement with recent Monte Carlo and experimental investigations of chamber perturbation corrections [12–16].

4. CONCLUSION

The well-established technique of water calorimetry was successfully combined with Fricke dosimetry to establish a hybrid system for the measurement of absorbed dose to water in electron beams. The uncertainty on the linearity of the system was typically 0.2–0.3% for all energies investigated. As an application, the experimental energy dependence was determined for a PTW Roos parallel-plate ionization chamber. The results were similar to the TG-51 and TRS 398 predictions for higher energies of 22 MeV, 18 MeV and 12 MeV, but differ by up to 1% for 4 MeV electron beams. These findings are in good agreement with recent Monte Carlo and experimental investigations of chamber perturbation corrections.

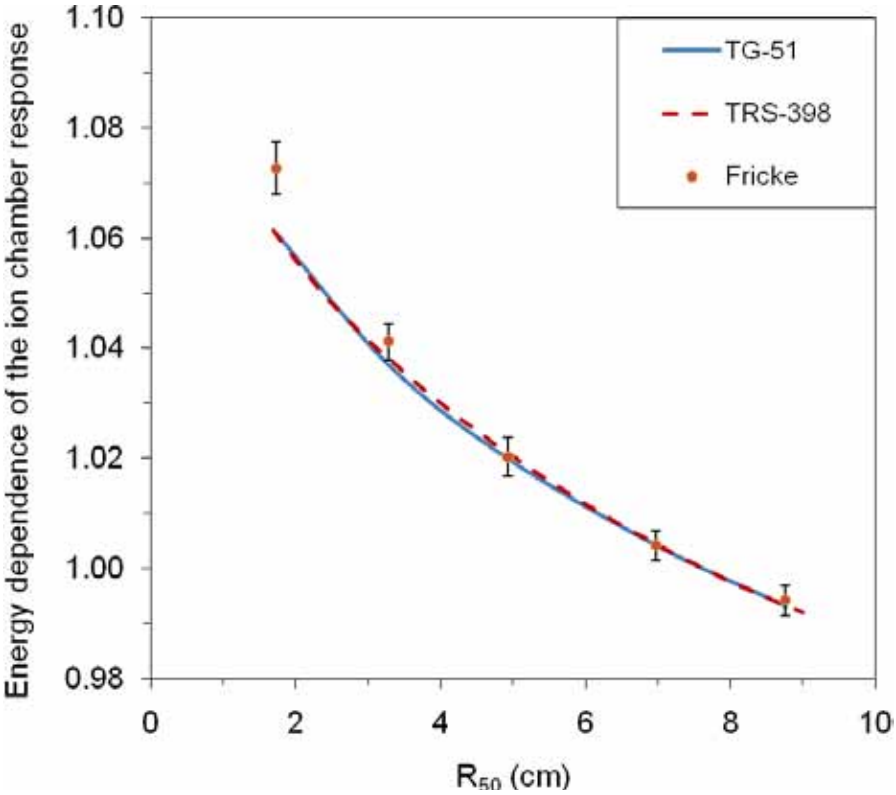

FIG. 3. The variation of the PTW Roos parallel-plate ionization chamber response with beam energy. The standard uncertainty in the experimental determination of the energy dependence was estimated to be 0.2–0.5%. The measured and calculated values are overlapped at the 18 MeV data point. No differences between the measured and calculated factors are seen at higher energies of 22 MeV, 18 MeV and 12 MeV, but the experimental energy dependence deviates from that predicted by calculations at low energies of 8 MeV and 4 MeV, and is in good agreement with recent Monte Carlo investigations of chamber perturbation corrections.

ACKNOWLEDGEMENT

The authors would like to thank D. Marchington, who provided technical support and built the PMMA Fricke solution bag holder used for irradiations.

REFERENCES

[1] FRICKE, H., MORSE, S., The actions of x-rays on ferrous sulfate solutions, Phil. Mag. (1929) 7–129.

[2] OLSZANSKI, A., KLASSEN, N.V., ROSS, C.K., SHORTT, K.R., The IRS Fricke dosimetry system (2002), PIRS-0815, http://irs.inms.nrc.ca/publications/reports

[3] STUCKI, G., MUENCH, W., QUINTEL, H., "The METAS absorbed dose to water calibration service for high energy photon and electron beam radiotherapy", Standards and Codes of Practice in Medical Radiation Dosimetry, (Proc. Int. Symp. Vienna, 2002), IAEA, Vienna (2003) 103–113.

[4] STUCKI, G., VÖRÖS, S., "Experimental $k_{Q,Q0}$ electron beam quality correction factors for the types NACP02 and PTW34001 plane-parallel chambers" (Proc. Absorbed Dose and Air Kerma Primary Standards Workshop, Paris, France 2007) (Saclay: LNE-LNHB) (2007).

[5] KLASSEN, N.V., SHORTT, K.R., SEUNTJENS, J., ROSS, C.K., Fricke dosimetry: the difference between $G(Fe^{3+})$ for ^{60}Co γ-rays and high-energy x-rays, Phys. Med. Biol. **44** (1999) 1609–1624.

[6] VÖRÖS, S., STUCKI, G., Simulation Monte Carlo pour la realization d'un etalon primaire de la dose absorbee dans l'eau pour des faisceaux d'electrons, Radioprotection **42** (2007) 565–75.

[7] McEWEN, M.R., ROSS, C.K., "Direct calibration of ion chambers in linac electron beams" (Workshop on Absorbed Dose and Air Kerma Primary Standards, Paris, France) (Saclay: LNE-LNHB) (2007).

[8] SEUNTJENS, J.P., ROSS. C.K., KLASSEN, N.V., SHORTT, K.R., A status report on the NRC sealed water calorimeter (1999), PIRS-0584, http://irs.inms.nrc.ca/publications/reports

[9] McEWEN, M.R., DUSAUTOY, A.R., Primary standards of absorbed dose for electron beams, Metrologia **46** (2009) S59–S79.

[10] ALMOND, P.R., et al. AAPM's TG-51 protocol for clinical reference dosimetry of high-energy photon and electron beams, Med. Phys. **26** (1999) 1847–1870.

[11] INTERNATIONAL ATOMIC ENERGY AGENCY, Absorbed Dose Determination in External Beam Radiotherapy: An International Code of Practice for Dosimetry Based on Standards of Absorbed Dose to Water, Technical Reports Series No. 398, IAEA, Vienna (2000).

[12] BUCKLEY, L.A., ROGERS, D.W.O., Wall correction factors, P_{wall}, for parallel-plate ionization chambers, Med. Phys. **33** (2006) 1788–1796.

[13] ARAKI, F., Monte Carlo calculations of correction factors for plane-parallel ionization chambers in clinical electron dosimetry, Med. Phys. **35** (2008) 4033–4040.

[14] CHIN, E., PALMANS, H., SHIPLEY, D., BAILEY, M., VERHAEGEN, F., Analysis of dose perturbation factors of a NACP-02 ionization chamber in clinical electron beams", Phys. Med. Biol. **54** (2009) 307–326.

[15] ZINK, K., WULFF, J., Monte Carlo calculations of beam quality correction factors k(Q) for electron dosimetry with a parallel-plate Roos chamber, Phys. Med. Biol. **53** (2008). 1595–1607.

[16] LACROIX, F., et al., Extraction of depth-dependent perturbation factors for parallel-plate chambers in electron beams using a plastic scintillation detector, Med. Phys. **37** (2010) 4331–4342.

DETERMINATION OF THE FRICKE G VALUE FOR HDR ^{192}Ir SOURCES USING IONOMETRIC MEASUREMENTS

L. FRANCO*,**, S. GAVAZZI**, M. COELHO*, C.E. DE ALMEIDA*

* Laboratorio de Ciencias Radiologicas (LCR)–UERJ
Email: cea71@yahoo.com.br

** Instituto Militar de Engenharia (IME)

Rio de Janeiro, Brazil

Abstract

High dose rate (HDR) brachytherapy using ^{192}Ir is widely accepted as an important treatment option, and thus requires an accurate dosimetry standard. However, a dosimetry standard for the direct measurement of absolute dose to water is currently not available. The dose to water conversion is calculated via the dose rate constant Λ and several correction factors accounting for the scatter, attenuation, and anisotropy of the dose distribution, among other effects. Two potentially useful procedures have been reported, including one by Sarfehnia et al., which used a water-based calorimeter with an uncertainty of 1.9% for k = 1, and a second by Austerlitz et al. and de Almeida et al., which used Fricke dosimetry with estimated uncertainties of 3.9% for k = 1 and 1.4% for k = 1, respectively. Chemical dosimetry using a standard $FeSO_4$ solution has shown potential to be a reliable standard of absorbed dose for the HDR ^{192}Ir source. A major uncertainty is associated with the G values reported by Fregene, which had a numerical value of 1.1%. However, that reference provided very little detail of the experimental procedures for the ^{192}Ir source. The *G* value may be obtained by using a calorimeter or ionometric measurements. In the absence of calorimetric data, this paper aims to measure the *G* value for the HDR ^{192}Ir sources using ionometric measurements and recommendations from dosimetry protocols.

1. INTRODUCTION

High dose rate (HDR) brachytherapy using ^{192}Ir is widely accepted as an important treatment option, and thus requires an accurate dosimetry standard. A dosimetry standard for the direct determination of absolute dose to water for this particular type of source is currently not available. The AAPM TG-43 Report [1] and its update [2] constitute the accepted protocol for determining the dose to water based on an air-kerma strength ($S_{k,air)}$) measurement. The dose to water

conversion is calculated via the dose rate constant Λ, which converts the air-kerma strength to the dose to water, and several relative correction factors accounting for the scatter, attenuation, and anisotropy of the dose distribution, among other effects [2–7].

The dosimetry methods in common use [8–11] were proposed by Goetsch et al. [12] and Marechal et al. [13, 14], the latter of which is one of the methods recommended by the IAEA to the Secondary Standards Dosimetry Laboratory network [15].

In clinical practice, the measurement of the quantity absorbed dose to water is highly desirable because it is the quantity used as reference for dose delivery for patient treatment.

Fricke dosimetry is one of the methods that have been explored to measure this quantity directly. Nevertheless, using Fricke requires a much lower experimental uncertainty than the ones reported to date. The G value is the radiation chemical yield of ferric ions at the irradiation temperature of 25ºC., which is proportional to the absorbed dose.

This paper presents the results of measurements made to determine the G value for HDR ^{192}Ir sources using an ionometric method and recommendations from dosimetry protocols.

2. MATERIALS AND METHODS

2.1. The Fricke system

As described by de Almeida [6], the Fricke solution was composed of the following chemicals of high purity as indicated: ammonium iron (II) sulphate hexahydrate [$(NH_4)_2$ Fe $(SO_4)_2.6H_2O$] (99%), sodium chloride [NaCl] (99.5%), and sulphuric acid [H_2SO_4] (95.0–99.0%). All chemicals were obtained from MERCK-KGaA.

The Fricke solution was prepared following the protocol outlined by Olszanski et al. [16]. The ammonium sulphate and sodium chloride were weighed using an analytical Ainsworth model AA-200 balance calibrated with 0.0100, 0.020, 0.0500, 0.1000, 0.2000 and 0.500 g weights with an accuracy of 0.0005 g. The Fricke solution contained 10^{-3} M ferrous ammonium sulphate, 10^{-3}M sodium chloride and 0.4M sulphuric acid. The sodium chloride is added to protect the solution from harmful effects of organic contaminants.

2.2. Spectrophotometer measurements

The optical density (OD) of the Fricke dosimeter solutions was measured using a B-52 Micronal spectrophotometer with a digital LCD display at a wavelength of 304 nm, a resolution of 1 nm, and a photometric accuracy of 0.010 Abs, which was tested with a set of traceable filters in the operational range of 190–1100 nm. The cuvette holder had four compartments for 1.0 cm cuvettes. Because a thermal bath was unavailable, the temperature inside the solution during reading was measured by a thermal probe previously calibrated against a mercury thermometer traceable to NIST with a 0.1°C resolution. The nominal dimensions of the three cuvettes were 1.0 cm × 1.0 cm × 4.5 cm, and the optical path lengths were measured to be 0.9995, 1.0005 and 0.9975 cm with an uncertainty of 0.0005 cm. Each one was used consistently to measure the absorbance of water samples as well as non-irradiated and irradiated solutions.

2.2.1. Ionometric measurements

The measurements were conducted with the microSelectron HDR ^{192}Ir Alpha Omega source, which consisted of an iridium metal (density of 22.42 g cm^{-3}) cylinder 0.60 mm in diameter and 3.50 mm in length. The iridium core was encapsulated in 316 L of stainless steel and had a density of 7.99 g/cm^3. The outer diameter of the source was 1.10 mm, and the wall thickness was 0.19 mm. The cable was stainless steel with a 1.10 mm diameter and an effective density of 4.81 g/cm^3. Because several irradiations and measurements were conducted on different occasions, the source activities are not specified.

The quantity S_K for the ^{192}Ir source was determined using a calibrated Farmer type PTW model TN 30011 cylindrical chamber calibrated by the Brazilian SSDL and by using the method proposed by Marechal et al. [14] and recommended by the IAEA [15]

Following the recommendations of Rivard et al. [2], the quantity S_K (with cGy·cm^2·h^{-1} = U) was then converted to dose to water, *Dw*, by Eq. (1):

$$Dw = \Lambda S_K \Delta t \quad (1)$$

where Λ is presently the most accurate dose rate constant value, 1.108 (0.13%) cGy·h^{-1}/U, which is specific for this type of source as reported by Daskalov et al. [17], and Δt is the time necessary to deliver the desired dose to the reference point. A dose of 20 Gy was consistently used throughout the experiments.

A positioning gadget was made with a special design, as shown in Fig. 1, to allow both the centre of the source and the ion chamber to be aligned with the Fricke solution containers. The containers were made of PMMA with a wall

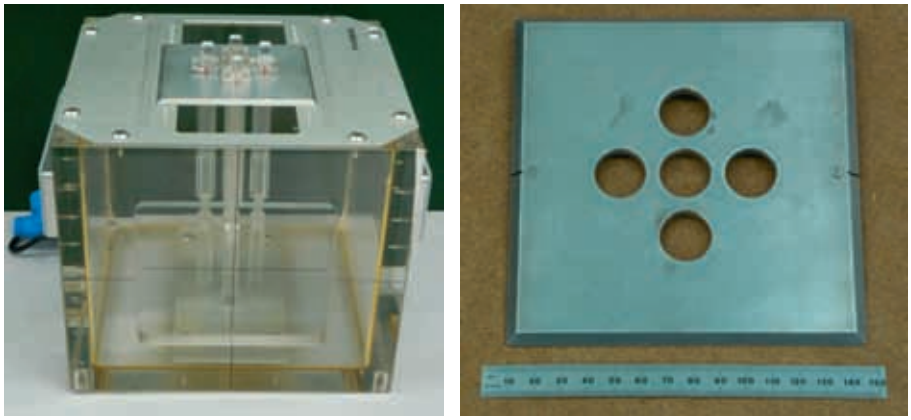

FIG. 1. The set-up geometry for simultaneous irradiation around the HDR ^{192}Ir source of a Farmer chamber and the Fricke solution inside an acrylic (PMMA) sheath in a water phantom.

thickness of 1.0 mm, the same volume, geometry and internal dimensions as for the 0.6 cm^3 ion chamber. The vertical position was mechanically stable because the base of the PTW holder was placed into a hole located at the bottom of the phantom. The measurements were taken with the ion chamber inserted into one of the holders and with the Fricke solutions in the other three holders. The chamber and the Fricke container were rotated around the source four times to minimize the position uncertainties, and the average values were taken at the end. The entire system was immersed in water at the central position of a 30 cm × 30 cm × 30 cm PTW water phantom to fulfil the conditions for electronic equilibrium.

A similar gadget was made for the measurements with the 6.0 MV photon beam and ^{60}Co gamma rays using the same holders to maintain the lateral alignment between the ion chamber and the center of the Fricke solution, as shown in Fig. 2. Two Farmer type PTW model TN 30011 cylindrical chambers calibrated by the Brazilian SSDL were used.

The vertical position was fixed using the same principle as previously described. The measurements were taken with the Fricke solution initially placed in the middle position (of a 10 cm × 10 cm field size at 100 cm of SSD) and the ion chambers on each side. The positions of the chamber and the Fricke containers were exchanged several times to minimize the positional uncertainties and any differences associated with beam flattening, and the average values were taken at the end. Measurements were conducted at two depths in water (5.0 and 10.0 cm), and the data were verified for any inconsistencies.

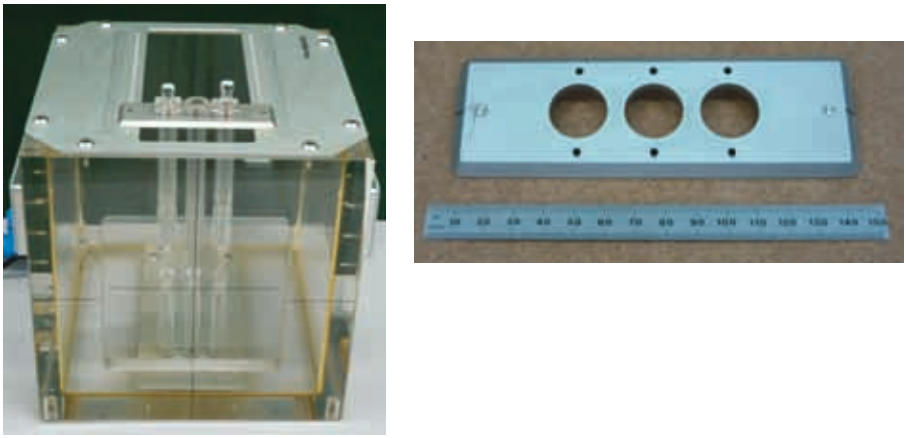

FIG. 2. The set-up geometry for simultaneous irradiation side by side in the 6.0 MV photon beam of a Farmer chamber and Fricke dosimeter solutions inside an acrylic (PMMA) sheath in a water phantom. Radiation beams are directed through the Mylar sidewall.

The radiation chemical yield of the ferric ions, the *G* value, was determined using the following equation proposed by ICRU [19] and Klassen et al. [20]:

$$G(F_e^{3+}) = \frac{\Delta OD}{Dw\, d\, \rho\, \varepsilon} \tag{2}$$

where ΔOD is defined as the OD increase at 304 nm, taking into account the temperature effect, Dw is the absorbed dose to water determined by ionometric means following the protocol TRS 398 [18], d is the optical path length of the cuvette, ρ is the density of the Fricke solution (1.023 g cm^{-3}) at 25°C, and ε is the value for the molar linear absorption coefficient for ferric ions (equal to 2174 M^{-1}·cm^{-1} at 304 nm, where M is the solution concentration), which is numerically equal to the value used by Klassen et al. [20].

By convention, the values of G and ε are for a solution irradiated at the temperature (T_i) and spectrophotometer measurement temperature (T_r) of 25°C.

The temperatures during the spectrophotometer readings and during irradiation were measured and used to correct the dose-induced change in OD using a reference temperature of 25°C. This relationship, initially described by Fregene [7] and modified by Olszanski et al.,[16] is given in Eq. (2):

$$\Delta OD = (OD_i - OD_c) \cdot [1 + 0.0012\,(25 - T_i)] \cdot [1 + 0.0069\,(25 - T_r)] \tag{3}$$

Where, OD_i and OD_c are the optical densities of the irradiated and control solutions, respectively, T_i is the temperature in °C of the Fricke solution during irradiation, and T_r is the temperature in °C of the Fricke solution during the spectrophotometer reading.

In order to verify the need for correction factors due to the possible differences between the holders, mechanical measurements of the wall thickness were made using a calibrated caliper. This was followed by measurements in a HDR ^{192}Ir unit with the same chamber inserted alternatively in all holders in the same position, and the differences were found to be negligible.

2.3. Results

The results presented for the ionometric method were consistent, although 0.4% lower than those reported by Klassen [20] for the ^{60}Co gamma rays and slightly higher than the ones reported for 6 MV. For the HDR ^{192}Ir source, the results were 1.1% higher than those reported by Fregene [7] and 1.4% higher than those reported by de Almeida et al. [6], the latter using an energy-weighted method for the HDR ^{192}Ir source.

The measured *G* values at the 5.0 and 10.0.cm depths were similar. Table 1 shows that despite some inconsistencies in the way the data have been reported in the past, the results are close and quite encouraging. However, it is believed that more accurate values of *G* for ^{192}Ir will only be possible with the use of a water calorimeter currently under development.

The uncertainties involved in the experimental procedure were, in general, conservative and corresponded to k = 1.

TABLE 1. COMPARISON OF THE RESULTS OBTAINED IN THE PRESENT STUDY WITH THE PUBLISHED VALUES (MOLE/J)

Energy (MV)	Present study	Fregene [7]	Klassen [20]	de Almeida et al. [6]
0.397[a]	1.578 (1.0%) k = 1	NR[b]	NR	1.555 (1.1%) k = 1
0.382[c]	NR	1.56 (1.1%) k = 1	NR	NR
1.25	1.592 (0.9%) k = 1	NR	1.598 (+/–0.010)	NR
6 .0	1.613 (0.9%) k = 1	NR	NR	NR

[a] Mean energy of ^{192}Ir as reported by de Almeida et al. [6].
[b] NR: not reported.
[c] Mean energy of ^{192}Ir as reported by Fregene [7].

3. CONCLUSIONS

Chemical dosimetry using a standard $FeSO_4$ solution has been shown by Austerlitz et al. [5] and de Almeida et al. [6] to be a potentially good standard of absorbed dose for HDR ^{192}Ir sources. The uncertainties due to the vessel dimensions, wall thicknesses, dose calculation, wall attenuation, UV light band, source anisotropy and source transit time were determined to represent a small fraction of the uncertainty budget, as shown in Table 2.

TABLE 2. UNCERTAINTY BUDGET RELATED TO THE DETERMINATION OF THE *G* VALUE FOR ^{192}Ir SOURCES

	Uncertainty type A%	Uncertainty type B%	Reference
Fricke irradiation process:			
Solution container position	0.07		
Solution temperature		0.1	Calibration certificate
Solution specification			
Extinction coefficient		0.1	19
Density		0.14	6
Reading process			
Cuvette dimensions	0.06	0.05	Manufacturer
Instrument repeatability	0.01		6
Wavelength band		0.01	21
Solution fading		0.01	21
Effect of PMMA on solution		0.001	6 and 22
D_w determination	0.77	0.6	SSDL certificate
Combined Uncertainty (k = 1)	1.0		
Combined Uncertainty (k = 2)	2.0		

Since the transit time and the source anisotropy are common factors for the ion chamber and the Fricke solution, their associated uncertainties may be neglected. In addition, the wall thicknesses of the holders were not sufficiently different to produce a measurable difference in the ionization chamber readings.

The results presented here using an ionometric method are consistent with the published values and have smaller uncertainties. However, it is anticipated that the use of a water calorimeter to determine the dose directly will most likely provide more accurate values with even lower uncertainties than the ones presented here.

ACKNOWLEDGMENT

The authors would like to thank the CNPq for the research grant.

REFERENCES

[1] NATH, R., et al., Dosimetry of interstitial brachytherapy sources: Recommendations of the AAPM Radiation Therapy Committee Task Group No. 43. American Association of Physicists in Medicine, Med. Phys. 22, (1995) 209–234.

[2] RIVARD, M.J., et al., Update of AAPM Task Group No. 43 Report: A revised AAPM protocol for brachytherapy dose calculations, Med. Phys. 31 (2004) 633–674.

[3] SARFEHNIA, A., SEUNTJENS, J., Development of a water calorimetry-based standard for absorbed dose to water in HDR ^{192}Ir brachytherapy, Med. Phys. 37 (2010) 1914–1923.

[4] SARFEHNIA, A., KAWRAKOW, I., SEUNTJENS, J., Direct measurements of absorbed dose to water in HDR ^{192}Ir brachytherapy: Water calorimetry, ionization chamber, Gafchromic film and TG 43, Med. Phys. 37, (2010) 1924–1932.

[5] AUSTERLITZ, C., et al., Determination of absorbed dose in water at the reference point $D(r_0,\theta_0)$ for an ^{192}Ir HDR brachytherapy source using a Fricke System, Med. Phys. 35 (2008) 5360–5365.

[6] DE ALMEIDA, C.E., et al., A Fricke based absorbed dose to water standard for ^{192}Ir HDR brachytherapy sources (2010).

[7] FREGENE, O., Calibration of ferrous sulphate dosimeter by ionometric and calorimetric methods for radiations of a wide range of energy, Rad. Res. 31 (1967) 256–272.

[8] DOUYSSET, G., et al., Comparison of dosimetric standards of USA and France for HDR brachytherapy, Phys. Med. Biol. 50 (2005) 1961–1978.

[9] DE ALMEIDA, C.E., PEREIRA, A.J., MARECHAL, M.H., CRUZ, J.C., FERRAZ, , GIORDANI, A.J., KHALIL, C.M., MARTINS, E.H., MENEGUSSI, G., MOREIRA, D., ROCHA, J.R., PINTO, M.A., Intercomparison of calibration procedures for ^{192}Ir HDR sources in Brazil, Phys. Med. Biol. 44 (1999) 31–38.

[10] DOUYSSET, G., SANDER, T., GOURIOU, J., NUTBROWN, R., Comparison of air kerma standards of LNE-LNHB and NPL for ^{192}Ir sources: EUROMET project 814, Phys. Med. Biol. 53 (2008) 85–97.

[11] DI PRINZIO, R., DE ALMEIDA, C.E., Air kerma standard for calibration of well type chambers in Brazil using ^{192}Ir HDR sources and its traceability, Med. Phys. 36 (2009) 953–960.

[12] GOETSCH, S.J., ATTIX, F.H., PEARSON, D.W., THOMADSEN, B.R., Calibration of ^{192}Ir high-dose-rate afterloading systems, Med. Phys. 18 (1991) 462–467.

[13] MARECHAL, M.H., DE ALMEIDA, C.E., SIBATA, C.H., Calibration of ^{192}Ir high dose rate brachytherapy sources, IAEA Report No. TECDOC- 896 (1996) 203–206.

[14] MARECHA, M.H., FERREIRA, I.H., PEIXOTO, J.G., SIBATA, C.H., DE ALMEIDA, C.E., A Method to Determine the Air Kerma Calibration Factor for Thimble Ionization Chambers Used for Ir-192 HDR Source Calibration, Physica Medica, XIX (2003) 131–135.

[15] INTERNATIONAL ATOMIC ENERGY AGENCY, Calibration of Photon and Beta Ray Sources Used in Brachytherapy**,** IAEA-TECDOC-1274, IAEA, Vienna (2002).

[16] OLSZANSKI, A., KLASSEN, N.V., ROSS, C.K., SHORTT, K.R., The IRS Fricke Dosimetry System., INMS, National Research Council, Ottawa, Ontario (2002).

[17] DASKALOV, G.M., LOFFLER, E., WILLIAMSON, J.F., Monte Carlo-aided dosimetry of a new high dose-rate brachytherapy source, Med. Phys. 25 (1998) 2200–2208.

[18] INTERNATIONAL ATOMIC ENERGY AGENCY, Absorbed Dose Determination in External Beam Radiotherapy: An International Code of Practice for Dosimetry Based on Standards of Absorbed Dose to Water, Technical Reports Series No. 398, IAEA, Vienna (2000).

[19] INTERNATIONAL COMMISSION ON RADIATION UNITS AND MEASUREMENTS (ICRU) , Radiation Dosimetry: Electron Beams with energies between 1 and 50 MeV, Report 35 (1984).

[20] KLASSEN, N.V., SHORTT, K.R., J. SEUNTJENS, J., ROSS, C.K., Fricke dosimetry: the difference between $G(Fe^{3+})$ for ^{60}Co γ rays and high-energy x rays, Phys. Med. Biol. 44, (1999) 1609–1624.

[21] SHALEK, R., SMITH, C., Chemical dosimetry for the measurement of high energy photons and electrons, Annals of the NY Academy of Sciences 161 (1969) 44–62.

[22] MORRISON, R., BOYD, R., Organic chemistry. Prentice Hall, New Jersey, 6th edn (1992).

ESTABLISHMENT OF REFERENCE RADIATION QUALITIES FOR MAMMOGRAPHY AT THE BIPM

C. KESSLER, D.T. BURNS, P. ROGER, P.J. ALLISY-ROBERTS
Bureau international des poids et mesures,
Sèvres Cedex, France
Email: ckessler@bipm.org

Abstract

An X ray tube with a molybdenum anode was installed at the BIPM. Four radiation qualities were established as international reference beams for mammography comparisons and calibrations. A new primary standard was constructed at the BIPM to be used for the dosimetry of these beams.

1. INTRODUCTION

Low energy X ray key comparisons and calibrations have been carried out at the BIPM since the early 1960s in the range from 10 kV to 50 kV, using a tungsten-anode X ray tube with aluminium filters. In 2001, the CCRI requested that the BIPM extend these activities to mammography in order to meet the needs of the National Metrology Institutes (NMIs) for comparisons in this domain and to provide calibrations for national standards traceable to the International System of Units (SI). The BIPM began this work by establishing a set of nine radiation qualities using the existing tungsten-anode X ray tube with molybdenum and rhodium as filters to simulate the radiation beams used in clinical mammography [1]. In 2009, after the installation of a molybdenum-anode X ray tube, a set of four radiation qualities was established as reference beams for mammography comparisons and calibrations, following the recommendations made by the Consultative Committee for Ionizing Radiation, Section I (CCRI(I)) during the 19th meeting (May 2009) held at the BIPM. In addition, a new free-air chamber primary standard for air kerma was constructed at the BIPM to be used for the dosimetry of these beams. The suitability of the simulated mammography X ray qualities for the calibration of two ionization chambers of the type currently used by NMIs for mammography dosimetry was carried out by comparing their responses to both tungsten/molybdenum and molybdenum/molybdenum sets of radiation qualities.

2. IRRADIATION FACILITY AND NEW RADIATION BEAMS

The Mo-anode X ray tube was installed in the low energy X ray laboratory at the BIPM, sharing the facilities with the W-anode tube (high-voltage generator, voltage stabilization and anode current measuring system). The stationary Mo-anode tube, target angle 40°, is operated in continuous mode with anode currents in the range of 6–17 mA; its inherent filtration is 0.8 mm beryllium.

The reference plane is 600 mm from the tube centre. Radiographic films were used for the study of the radiation field (size, shape and beam axis). Horizontal and vertical radial profiles were measured using a thimble ionization chamber. Using the data from the radial profiles and the radiographic images, a system of two lead collimators was designed and machined to produce a circular field 10 cm in diameter at the reference plane.

Four radiation qualities were set up as reference beams for comparisons and calibrations, in the range from 25–35 kV. The beam quality, expressed in terms of the aluminium half-value layer (HVL), was determined for each beam using the new primary standard. The anode current for each quality was chosen to give an air-kerma rate of 2 mGy/s in the reference plane. A molybdenum filter 30 μm in thickness is used for all the qualities. The characteristics of the beams are given in Table 1.

3. MEASUREMENT AND SIMULATION OF ENERGY SPECTRA

The photon energy spectra were measured using the Compton scattering method, described in Ref. [1]. The scattered photons were detected at 90° with a low energy pure germanium detector. The primary X ray spectra were reconstructed from the resulting pulse-height distribution using commercial software [3].

TABLE 1. CHARACTERISTICS OF THE CCRI RADIATION QUALITIES[a] FOR MAMMOGRAPHY

Beam parameter	Radiation quality			
	Mo25	Mo28	Mo30	Mo35
Generating potential (kV)	25	28	30	35
Additional filtration	30 μm Mo			
Al HVL (mm)	0.277	0.310	0.329	0.365

[a] Similar but not identical to the IEC RQR-M series [2].

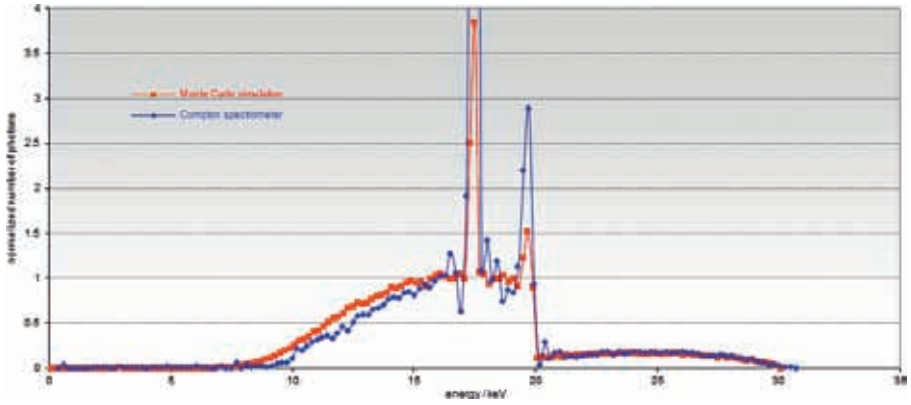

FIG. 1. Comparison of the simulated and measured spectra for the Mo30 quality.

The mammography spectra corresponding to the qualities Mo25 and Mo30 were also obtained by simulation with Monte Carlo techniques using the code PENELOPE [4]. The X ray tube configuration (Mo target, Mo filter and collimation) was simulated using the PENELOPE geometry code PENGEOM. Details of the simulation of the spectra can be found in Ref. [1].

The spectra corresponding to the Mo30 quality are shown in Fig. 1, where the detail is illustrated and the complete spectra are shown (inset).

4. PRIMARY STANDARD

4.1. Design and construction

The new standard is a parallel-plate, free-air chamber designed to be used up to 50 kV and to minimize the correction factors involved in the air-kerma determination.

The separation between the high-voltage plate and the collector is 70 mm, just sufficient to reduce electron loss to a negligible amount for the most energetic of the W-anode beam qualities (allowing the new standard to be used as a replacement for the existing standard if the need arises).

The collector support was designed to allow the co-planarity of the collector and the guard plate to be adjusted with a tolerance of around 5 µm.

The collector and the guard plate are of aluminium with a thin graphite coating; the collector is placed in the centre of the guard plate surrounded by an air gap of 0.5 mm; and the collector length, including half of the upstream and downstream gaps between collector and guard plate, is 15.537 mm.

A system of 17 guard strips, uniformly spaced between the ground and high voltage plates and parallel to them, surrounds the air cavity to produce a uniform electric field in the collecting region.

A tungsten alloy diaphragm 13.04 mm thick with an aperture 9.998(1) mm in diameter defines the reference plane at 100.2 mm from the centre of the collecting region. To reduce photon transmission through the downstream edge, the innermost 2.9 mm forms a conical section that increases in diameter to 15.8 mm. The effective aperture length is therefore 10.1 mm.

The collecting volume defined by the aperture diameter and the collector length is 1219.8(4) mm^3.

The air temperature inside the chamber is measured using a thermistor, placed just above the high-voltage plate, the position being optimized to best represent the mean air temperature within the collecting region.

A 3 mm thick lead plate (with an aperture exposing the entrance diaphragm) was added to the front of the chamber to minimize photon transmission through the aluminium wall.

4.2. Correction factors

The correction factors for the standard involved in the determination of K_{air} were obtained either by calculation using Monte Carlo techniques or experimentally by ionometric measurements. The Monte Carlo code PENELOPE [4] was used for the determination of the correction factors for electron loss k_e, photon scatter k_{sc}, fluorescence k_{fl}, photon transmission through the diaphragm edge and photon scatter from its surface k_{dia} and photon transmission through the front wall of the chamber. The corrections were calculated for mono-energetic photons from 2 to 50 keV in steps of 2 keV. For these calculations, a detailed simulation of the BIPM standard was performed using the PENELOPE geometry package PENGEOM. The results for mono-energetic photons were folded with the spectra measured with the BIPM Compton spectrometer.

The correction factor for the lack of saturation due to ion recombination and diffusion k_s was determined following the method proposed by De Almeida and Niatel [5], as detailed by Boutillon [6]. The correction factor for air attenuation k_a within the chamber was measured using the same method (reduced air pressure pipe) employed in the existing standard for the tungsten-anode qualities [7]. The beam profiles were used to calculate the correction due to the non-uniformity of the beam k_{rn} across the chamber aperture. The correction factors corresponding to the Mo28 quality are presented in Table 2.

TABLE 2. ESTIMATED RELATIVE UNCERTAINTIES IN THE DETERMINATION OF THE AIR-KERMA RATE

Symbol	Parameter/unit		Relative standard uncertainty[a]	
			s_i	u_i
Physical constants				
ρ_a	dry air density (0°C, 101.325 kPa)/(kg/m^3)			0.01
W/e	mean energy per charge/(J/C)			0.15
g	fraction of energy lost in radiative processes			0.01
Correction factors		*Values for Mo28*		
k_{sc}	scattered radiation	0.9977		0.03
k_{fl}	fluorescence	0.9976		0.05
k_e	electron loss	1.0000		0.01
k_s	saturation	1.0015	0.01	0.01
k_{pol}	polarity	1.0000	0.01	—
k_a	air attenuation [b]	1.0244	0.02	0.01
k_d	field distortion	1.0000		0.07
k_{dia}	diaphragm	0.9995		0.03
k_p	wall transmission	1.0000	0.01	
k_h	humidity			0.03
Measurement of I/υ				
I	ionization current (T, P, air compressibility)		0.02	0.02
υ	volume		0.03	0.05
	positioning of standard		0.01	0.01
Combined uncertainty of the BIPM determination of air-kerma rate				
quadratic summation			0.05	0.19
combined relative standard uncertainty			0.20	

[a] s_i represents the relative standard Type A uncertainty, estimated by statistical methods; u_i represents the relative standard Type B uncertainty, estimated by other means.

[b] Values at 293.15 K and 101.325 kPa for an attenuation length of 10.0 cm.

4.3. Uncertainties in the determination of air kerma

For a free-air ionization chamber standard with measuring volume *V*, the air-kerma rate is determined by the relation

$$\dot{K} = \frac{I}{\rho_{\text{air}} V} \frac{W_{\text{air}}}{e} \frac{1}{1 - g_{\text{air}}} \prod_i k_i \qquad (1)$$

where ρ_{air} is the density of air under reference conditions, I is the ionization current under the same conditions, W_{air} is the mean energy expended by an electron of charge e to produce an ion pair in air, g_{air} is the fraction of the initial electron energy lost by radiative processes in air, and $\Pi\, k_{\text{i}}$ is the product of the correction factors to be applied to the standard.

The uncertainties in the determination of the air-kerma rate estimated in accordance with [8] are listed in Table II.

5. CHAMBER RESPONSE TO THE SIMULATED MAMMOGRAPHY BEAMS

A set of simulated mammography beams was set up at the BIPM by using a combination of a W-anode X ray tube with a Mo filter 60 μm in thickness [1]. A study of the suitability of these beams for the calibration of ionization chambers was carried out for two types of ionization chamber commonly used for mammography dosimetry. A Radcal RC6M and an Exradin A11TW ionization chamber were calibrated in the BIPM W/Mo beams and the responses compared with those obtained through calibration in Mo/Mo mammography beams. The calibration coefficients measured in the simulated mammography beams are in agreement with those obtained in the Mo-anode beams at the level of two parts in 10^3. Consequently, national standards laboratories not equipped with Mo-anode X ray tubes can, at this level of uncertainty, implement W/Mo beams to calibrate these types of chamber for subsequent use in Mo-anode beams. This method, however, should not be extended to other chamber types without similar verification in W/Mo and Mo/Mo beams.

6. INTERNATIONAL COMPARISONS

Comparisons with the NMIJ (Japan), NIST (USA) and the PTB (Germany) have been carried out in the BIPM mammography radiation qualities and a

comparison with the NRC (Canada) was made in the simulated mammography beams; all the comparisons were carried out using transfer chambers belonging to the NMIs. The NMIs and the BIPM compare favourably and the corresponding comparison reports are awaiting publication; the results will be available in the BIPM key comparison database of the CIPM MRA [9] with reference BIPM.RI(I)-K7.

7. CONCLUSION

A new reference facility, consisting of a specially constructed primary standard (free-air chamber) and radiation beams defined by the CCRI, has been established for mammography dosimetry at the BIPM. This facility addresses the need for international comparisons with national metrology institutes (NMIs) having primary standards and provides SI traceable characterizations of national standards for those NMIs not having primary standards. The facility became available in 2009 and four NMIs have already participated.

REFERENCES

[1] KESSLER, C., 2006, Establishment of simulated mammography radiation qualities at the BIPM (Rapport BIPM-2006/08) 8 pp.

[2] INTERNATIONAL ELECTROTECHNICAL COMMISSION, Rep. IEC 61267 Medical diagnostic X-ray equipment — Radiation conditions for use in the determination of characteristics, IEC 2005.

[3] MATSCHEKO, G., RIBBERFORS, R., 1989, A generalised algorithm for spectral reconstruction in Compton spectroscopy with corrections for coherent scattering, Phys. Med. Biol. **34** (1989) 835–841.

[4] SALVAT, F., FERNANDEZ-VAREA, J.M., SEMPAU, J., 2003, PENELOPE — A Code System for Monte Carlo Simulation of Electron and Photon Transport, Workshop Proc. (Issy-les-Moulineaux, France, 7–10 July 2003, OECD 2003).

[5] DE ALMEIDA, C.E., NIATEL, M.T., 1986, Comparison between IRD and BIPM exposure and air kerma standards for cobalt gamma rays. Rapport BIPM-1986/12 (Bureau International des Poids et Mesures, Sèvres).

[6] BOUTILLON, M., 1998, Volume recombination parameter in ionization chambers, Phys. Med. Biol., **43** (1998) 2061–2072.

[7] BURNS, D.T., BÜERMANN, L., 2009, Free-air ionization chambers, *Metrologia*, 46(2) (2009) S9–S23.

[8] Evaluation of measurement data — Guide to the expression of uncertainty in measurement, JCGM 100 (2008).

[9] CIPM MRA: Mutual recognition of national measurement standards and of calibration and measurement certificates issued by national metrology institutes, International Committee for Weights and Measures, 1999, 45 pp., http://www.bipm.org/pdf/mra.pdf

ANALYSIS OF THE TANDEM CALIBRATION METHOD FOR KERMA AREA PRODUCT METERS VIA MONTE CARLO SIMULATIONS

A. MALUSEK, G. ALM CARLSSON
Division of Radiological Sciences,
Department of Medical and Health Sciences, Linköping University,
Linköping
Sweden
Email: alexandr.malusek@liu.se

Abstract

The IAEA recommends that uncertainties of dosimetric measurements in diagnostic radiology for risk assessment and quality assurance should be less than 7% on the confidence level of 95%. This accuracy is difficult to achieve with kerma area product (KAP) meters currently used in clinics. The reasons range from the high energy dependence of KAP meters to the wide variety of configurations in which KAP meters are used and calibrated. The tandem calibration method introduced by Pöyry, Komppa and Kosunen in 2005 has the potential to make the calibration procedure simpler and more accurate compared to the traditional beam-area method. In this method, two positions of the reference KAP meter are of interest: (a) a position close to the field KAP meter and (b) a position 20 cm above the couch. In the close position, the distance between the two KAP meters should be at least 30 cm to reduce the effect of back scatter. For the other position, which is recommended for the beam-area calibration method, the distance of 70 cm between the KAP meters was used in this study. The aim of this work was to complement existing experimental data comparing the two configurations with Monte Carlo (MC) simulations. In a geometry consisting of a simplified model of the VacuTec 70157 type KAP meter, the MCNP code was used to simulate the kerma area product, P_{KA}, for the two (close and distant) reference planes. It was found that P_{KA} values for the tube voltage of 40 kV were about 2.5% lower for the distant plane than for the close one. For higher tube voltages, the difference was smaller. The difference was mainly caused by attenuation of the X ray beam in air. Since the problem with high uncertainties in P_{KA} measurements is also caused by the current design of X ray machines, possible solutions are discussed.

1. INTRODUCTION

The IAEA recommends that uncertainties of dosimetric measurements in diagnostic radiology for risk assessment and quality assurance should be less than 7% on the confidence level of 95% (coverage factor k = 2) [1]. While this accuracy can easily be achieved in measurements of air kerma using ionization chambers with walls made of air equivalent materials, uncertainties of measurements with kerma area product (KAP meters — plane-parallel ionization chambers measuring the kerma area product — are noticeably higher. For instance relative differences between calibration coefficients of KAP meters derived by different practitioners at selected clinics deviated as much as ±15% [2]. To make KAP meters light transparent, conductive coating containing high atomic number elements is used. It breaks charged particle equilibrium in the air cavity and results in high dependence of KAP meters' response on the radiation quality of the beam. For these reasons, the international standard IEC 60580 [12] recommends that a combined uncertainty of 25% (k = 2) should not be exceeded in KAP measurements within the range of specified conditions. Although this requirement is typically achieved, there is an aim to increase the accuracy of KAP measurements so that the uncertainty does not exceed 7%. This accuracy can only be achieved if radiation quality correction factors are used [3].

The kerma area product, P_{KA}, is defined as

$$P_{KA} = \int_A K_{air} \tag{1}$$

where K_{air} is the air kerma in a reference plane perpendicular to the beam axis and A is the integration area in that plane [4].

The P_{KA} values are used to estimate the amount of radiation incident on the patient during a diagnostic X ray examination. In idealized conditions with no absorption and scatter of photons, P_{KA} is independent of the position of the reference plane and the integration area that must be large enough to cover the entire beam, including the penumbra region. Real KAP meters and the surrounding air scatter and absorb photons, and thus the calibration coefficient of a KAP meter depends on both the integration area and the position of the reference plane [5]. A widely used calibration method using an ionization chamber to measure K_{air} in the centre of a 10 cm × 10 cm field and a film to measure the nominal beam area in a plane close to the patient was published by NRPB [6]; the integral in Eq. (1) was approximated by a product of the two measured quantities. The IAEA Code of Practice [1] extends the NRPB method by allowing the usage of either a film or a digital detector for the determination of

the nominal beam area. It also specifies that the measurement should be performed 20 cm above the couch; this position approximately corresponds to the entrance patient plane. These methods are known as beam-area calibration methods [7]. An alternative approach was proposed by Pöyry, Komppa and Kosunen in 2005 [13]. Their tandem calibration method estimates the kerma area product for the reference plane via a second KAP meter. The method is simpler to perform because it avoids the determination of the nominal area. It can also be more accurate as it avoids the calculation of the integral in Eq. (1) from a single value of K_{air} measured at the beam axis. From all possible positions of the reference KAP meter, only two positions are of interest for over-couch in situ calibrations: (i) a position close to the field KAP meter, and (ii) a position 20 cm above the couch. In the first position, the distance between the two KAP meters should be at least 30 cm to reduce the effect of back scatter from the reference KAP meter on the field KAP meter [7]. In the second position, which is recommended for the beam-area calibration method and corresponds to the entrance patient plane, the distance between the two KAP meters depends on the distance of the field KAP meter from the couch. Measurements showed that the relative differences between P_{KA} values measured at the two different positions were relatively small, less than about 2.5% for the tube voltage of 80 kV and the distance of 70 cm between the two chambers [7]. The aim of this work was to complement these experimental data with Monte Carlo (MC) simulations.

2. METHODS

The MCNP5 [8] code was used to calculate the kerma area product for two different reference planes: the ‘close’ plane positioned 30 cm from the field KAP meter and the 'distant' plane positioned 70 cm from the field KAP meter (see Fig. 1a). Corresponding values are denoted P_{KAr} and P_{KAp}, respectively. Values of P_{KAp} were calculated as a function of the radius of the integration area in the distant (patient) plane.

The geometry consisted of a point isotropic source and a simplified model of the VacuTec’s type 70157 KAP meter. Both were positioned in a large cylinder (height of 1 m and radius of 5 m) containing the surrounding medium (air or vacuum). The source emitted photons into a cylindrical cone beam with the aperture of 3º; radii of beam sectional areas in the close and distant reference planes were 3.14 cm and 5.24 cm, respectively. Unfiltered X ray spectra for tube voltages of 40 kV, 80 kV and 140 kV were taken from the catalogue of X ray spectra [9] and filtered with 5 mm of Al. The voltages of 40 kV and 140 kV delimited a typical range of values used in diagnostic X ray radiology (except mammography, which uses lower tube voltages). The KAP meter was modelled

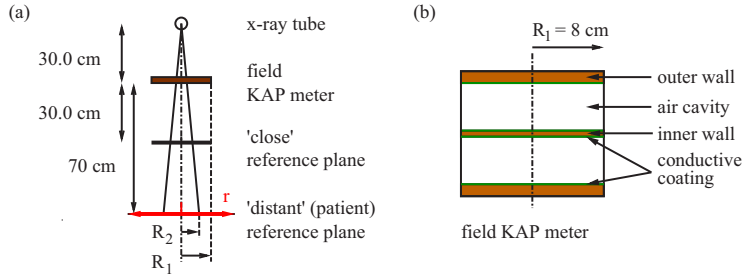

FIG. 1. (a) Schematic view of the simulation geometry. Reference planes were positioned 30 cm and 70 cm from the field KAP meter. Radius of the beam in the distant plane was R_2 = 5.24 cm. Radius of the integration area in the close plane was R_1 = 8cm, corresponding radius in the distant plane varied. (b) The cylindrical field KAP meter consisted of air cavities, and inner and outer walls covered with conductive coating. The figures are not to scale.

via a set of cylinders with radii of 8 cm, see Fig. 1(b). Thicknesses of PMMA walls were 1.5 mm and 1.0 mm for the outer and inner electrodes, respectively. Thickness of each of the air cavities was 5.9 mm. Thickness of the conductive coating covering the walls was provided under a non-disclosure agreement from the manufacturer. In practice, In_2O_3 doped with Sn is used, but in these simulations, the dopant was omitted. Air kerma in the two reference planes was scored using 9 and 11 ring detector tallies, respectively, centered at the beam axis. Radii of these rings were set to optimally cover the integration area in Eq. (1) and ranged from 0.02 cm to 8 cm for the 'close' reference plane, and from 0.02 cm to 32 cm for the 'distant' reference plane.

The dose scoring function of the tally was defined as $E\mu_{tr}/\rho$, where E is the photon energy and μ_{tr}/ρ is the energy dependent mass energy transfer coefficient for air. The latter was obtained by interpolation of mass energy transfer coefficients μ_{en}/ρ taken from [10]; it was assumed that $\mu_{tr}/\rho = \mu_{en}/\rho$ for low energy photons. The detailed physics treatment mode of MCNP was used to transport photons and electrons. Simulations were performed for three tube voltages (40 kV, 80 kV, and 140 kV) and two surrounding media (air, vacuum), for a total of six configurations. Finally, the integration of Eq. (1) was performed numerically in polar coordinates and ratios $P_{KAp}(r)/P_{KAr}$ as functions of the radius r of area A at the distant (patient) plane were calculated.

3. RESULTS

The $P_{KAp}(r)/P_{KAr}$ ratio, where $P_{KAp}(r)$ and P_{KAr} are the kerma area products for the distant and close reference planes, respectively, is plotted in Fig. 2 as a

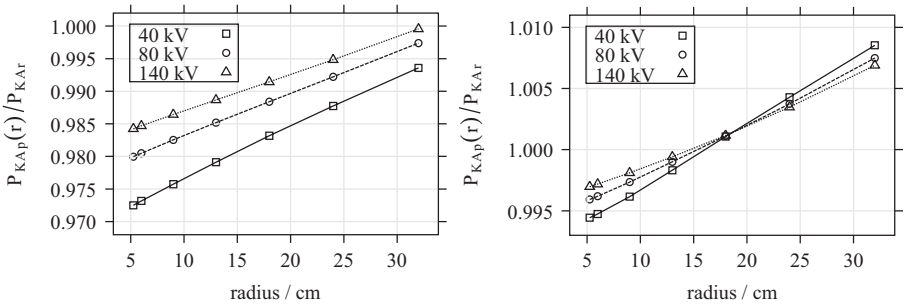

FIG. 2. The ratio $P_{KAp}(r)/P_{KAr}$ as a function of the integration area radius in the patient plane. Left: The field KAP meter was placed in air. Right: The field KAP meter was placed in vacuum.

function of the radius r of the integration area in the distant reference plane (r = 8 cm in the close reference plane) for air and vacuum as the surrounding media.

Values of P_{KA} for the tube voltage of 40 kV were about 2.5% lower for the distant plane (for r = 8 cm) than the close plane. For higher tube voltages, the difference was smaller, about 1.4% for 140 kV. This means that the field KAP meter calibrated using the close reference plane will measure higher values than the field KAP meter calibrated using the distant reference plane. A larger integration area (r > 8 cm) at the distant (patient) plane resulted in a smaller relative difference, about 1.5% for the radius of 20 cm and 40 kV. Variations between results for different X ray tube voltages were mostly caused by attenuation of the beam in air; this follows from a comparison of Fig. 2 (left) with Fig. 2 (right). The latter contains results calculated for a geometry where air surrounding the field KAP meter was replaced by vacuum. (The fact that KAP meters are vented ionization chambers was neglected in this case; air pressure in the air cavity was the same as in the configuration with surrounding air.) Also note that although the relative difference in Fig. 2 is less than 1% for the radius of 32 cm, the function $P_{KAp}(r)/ P_{KAt}$ is known to diverge to infinity for large r in vacuum [2].

4. DISCUSSION

The aim of this article is to compare two configurations of the tandem calibration method using = MC simulations. Nevertheless, it is worth discussing the topic from a broader perspective. Problems with the KAP meter calibration have two aspects. The first is related to current clinical practice. KAP meters are used in different configurations, and a simple calibration method that fits all

apparently does not exist. Accurate calibration of each possible setup would be too laborious and time consuming. The tandem calibration cannot completely solve this problem, but it has the potential to simplify the procedure. If (i) a reference KAP meter with a low energy dependence (e.g. like the Radcal calibrator [11]) is used, (ii) a KAP meter holder can easily be attached to the X ray tube for the purpose of a calibration, and (iii) the resulting calibration coefficients can easily be transferred to the X ray machine software, then the tandem calibration can be performed quickly, easily and with sufficient accuracy. The second aspect is related to the definition of the measured kerma area product. For the tandem calibration method, the quantity is relatively well defined (the integration area can be defined as the sensitive area of the reference KAP meter), and the definition can be used for machines with C-arms. As showed in Ref. [7] and in this paper, differences between P_{KA} values measured by KAP meters calibrated using the two studied configurations are relatively small for over-couch geometries. In this respect, the tandem calibration method (with field–reference KAP meter distance of ~30 cm) can be used as a replacement of the traditional beam-area method for the over-couch setup. In the under-coach setup, the reference KAP meter can be placed above the patient couch as suggested in Ref. [7].

For currently used machines, the problem with accurate KAP meter calibration cannot be solved easily. New machines, however, may be designed so that the tandem calibration can be performed quickly and easily for several different configurations of tube voltage and filter settings. The usage of a reference KAP meter with low energy dependence will then lower uncertainties of the calibration coefficient [11].

5. CONCLUSION

Relative differences between P_{KA} values calculated for the distances of 30 cm and 70 cm from the field KAP meter were less than 2.5% for all considered tube voltages; attenuation of the beam in air was the main contributing factor. These results indicate that the tandem calibration method using the distance of 30 cm between KAP meters can be used as a replacement of the beam-area calibration method. P_{KA} values measured with KAP meters calibrated using the tandem calibration method will not significantly differ from P_{KA} values measured with KAP meters calibrated using the beam-area calibration method unless the X ray tube has a strong heel effect or extra focal radiation. In that case, the tandem calibration method has the potential to produce more accurate results. To achieve this, however, the reference KAP meter should have low dependence of the calibration factor on the beam quality.

ACKNOWLEDGEMENTS

The authors would like to thank Dr. E. Helmrot and Dr. M. Sandborg (Linköping University Hospital) for information on KAP meter calibration procedures at their Department, and Dr. P. Larsson (Linköping University Hospital) for help with MC calculations.

REFERENCES

[1] INTERNATIONAL ATOMIC ENERGY AGENCY, Dosimetry in Diagnostic Radiology: An International Code of Practice, Technical Reports Series No. 457, IAEA, Vienna (2007).

[2] LARSSON, J., PERSLIDEN, J., SANDBORG, M., ALM CARLSSON, G., Transmission ionization chambers for measurements of air collision kerma integrated over beam area. Factors limiting the accuracy of calibration, Phys. Med. Biol. **41** (1996) 2381–98.

[3] TOROI, P., Patient exposure monitoring and radiation qualities in two-dimensional digital x-ray imaging. Academic dissertation, Radiation and Nuclear Safety Authority, STUK-A239 (2009).

[4] INTERNATIONAL COMMISSION ON RADIATION UNITS AND MEASUREMENTS, Patient dosimetry for x rays used in medical imaging, ICRU Report No. 74, J. ICRU 5(2) (2005) 1–113.

[5] MALUSEK, A., LARSSON, J.P., ALM CARLSSON, G., Monte Carlo study of the dependence of the KAP-meter calibration coefficient on beam aperture, x-ray tube voltage and reference plane, Phys. Med. Biol. **52** (2007) 1157–70.

[6] NATIONAL RADIOLOGICAL PROTECTION BOARD, National protocol for patient dose measurements in diagnostic radiology, Technical Report (Chilton: NRPB)

[7] TOROI, P., KOMPPA, T., KOSUNEN, A., A tandem calibration method for kerma-area product meters, Phys. Med. Biol. **53** (2008) 4941–4958.

[8] LOS ALAMOS NATIONAL LABORATORY, X5 Monte Carlo Team, MCNP — Ageneral Monte Carlo N-particle transport code, version 5 Technical Report LA-UR-03-1987 (Los Alamos, NM: Los Alamos National Laboratory) (2004).

[9] CRANLEY, K., GILMORE, B.J., FOGARTY, G.W.A., DESPONDS, L., IPEM Report 78: Catalogue of diagnostic x-ray spectra and other data (Electronic version prepared by D. Sutton), York, The Institute of Physics and Engineering in Medicine (IPEM) (1997) CD-ROM.

[10] HUBBELL, J.H., SELTZER, S.M., Tables of x-ray mass attenuation coefficients and mass energy absorption coefficients version 1.4 (Gaithersburg, MD: National Institute of Standards and technology) (2006) http://physics.nist.gov/xaamdi

[11] TOROI, P., KOSUNEN, A., The energy dependence of the response of a patient dose calibrator, Phys. Med. Biol., **54** (2009) N151–6.

[12] INTERNATIONAL ELECTROTECHNICAL COMMISSION (IEC), Medical electrical equipment – dose area product meters IEC 68580, 2nd edn, Geneva (2000).

[13] PÖYRY, P., KOMPPA, T., KOSUNEN, A., Calibration of dose-area product meters for diagnostic x-ray beams (Proc. XXXIX Ann. Conf. Finnish Phys. Soc., Report Series, Helsinki University of Technology Laboratory, Espoo, Finland) (2005)247.

REFERENCE DOSIMETRY AND COMPARISONS IN EXTERNAL BEAM RADIOTHERARY

(Session 2)

Chairpersons

S. HUQ
American Association of Physicists in Medicine

J. MEDIN
Sweden

Co-Chairpersons

H. PALMANS
United Kingdom

D.T.L. JONES
International Commission on Radiation Units and Measurements

TEN YEARS AFTER: IMPACT OF RECENT RESEARCH IN PHOTON AND ELECTRON BEAM DOSIMETRY ON THE IAEA TRS-398 CODE OF PRACTICE

H. BENMAKHLOUF, P. ANDREO
Division of Medical Radiation Physics,
Stockholm University and Karolinska Institute,
Stockholm, Sweden
Email: pedro.andreo@ki.se

Abstract

Developments in the field of reference radiotherapy dosimetry have been analysed during the last decade, notably with the use of Monte Carlo simulations to derive perturbation correction factors of ionization chambers in high energy photon and electron beams. Complemented with comparisons to experimental data available for beam quality correction factors, the potential impact has been evaluated of the new calculations on the data included in the IAEA TRS-398 Code of Practice. For megavoltage photon beam data, there is good agreement in general for many ionization chambers, but less so for the NE-2571 Farmer type chamber. Differences with experimental data at the highest energies are still of the same order, although with a reverse sign as those ten years ago for TRS-398, which is around 0.5%. Considering the small differences between the new Monte Carlo data for some chamber types and TRS-398, the lack of experimental and calculated data for most commercial chambers, and the additional uncertainty caused by the need for adopting new *I*-values and stopping powers, it can be concluded that the time has not yet come for recommending changes to the data in TRS-398. For electron beams substantial differences between new Monte Carlo data and the perturbation correction factors used in TRS-398 have been found for plane-parallel chambers, particularly at low energies. However, the often large range of variation of the new calculations precludes a trustworthy analysis on their adequacy. Comparison with experimental data shows better agreement for TRS-398 than for the new Monte Carlo results, pointing to an apparent overestimation of the overall perturbation factor, which can probably be related to the assumption of independent perturbation effects and/or an inadequate description of chamber geometry. For ^{60}Co γ rays, new Monte Carlo data would yield a change in absorbed dose of about 1.5%, representing a considerable discrepancy with the current evidence for this beam quality, and for other beams using ^{60}Co as a reference quality, which is not likely to be in error by such large amount. The need for finding a solution that provides consistent dose determination in the entire electron and photon radiotherapy energy range, irrespective of the procedure used for deriving the necessary data, remains a major priority.

1. INTRODUCTION

Ten years after the publication in 2000 of the IAEA TRS-398 Code of Practice for reference radiotherapy dosimetry [1] is a reasonable period over which to analyse the impact of the research conducted in this field, mostly with the use of Monte Carlo (MC) simulations to derive perturbation correction factors of ionization chambers in high energy photon and electron beams. The use of experimentally determined $N_{D,w,Q}$ calibration coefficients and k_{Q,Q_0} beam quality factors for the user chamber at primary standards dosimetry laboratories (PSDLs), the preferred option in TRS-398, is an increasingly common practice, following the increased availability of absorbed dose to water national primary standards [2]. It is also the most suitable procedure to verify the calculated k_{Q,Q_0} values in TRS-398, using perturbation correction factors derived between 15 and 30 years ago, and those that would result from the adoption of recent MC calculations. Although at the time of the publication of TRS-398, a comparison with experimental k_{Q,Q_0} data for photon beams was carried out [3] concurrently with a parallel comparison for the AAPM TG-51 protocol values [4, 5], new experimental values have become available both for photons and for electrons.

This work reviews perturbation correction factors for ionization chambers calculated by different authors and whenever possible present them as a fit of the data using linear and non-linear 'robust techniques' in MatLab™ that minimize the influence of outliers. The fits are compared to the corresponding factors in TRS-398. The individual corrections are then combined to derive beam quality correction factors, which are compared to the k_{Q,Q_0} values given in TRS-398. Both datasets are compared to experimental k_{Q,Q_0}, mostly determined at PSDLs and to a few values determined with MC calculations, which do not assume independent perturbation effects nor stopping-power ratios for 'ideal' Bragg–Gray cavities [6]. From the onset, it is emphasized that the new MC results available are restricted to a few cylindrical and plane-parallel chamber types. Most have been calculated with the same MC code system, EGSnrc [7] and the PENELOPE system [8] has been used in a few occasions only. Most results are still based on the classical approach of assuming independent perturbation correction factors due to different chamber components, rather than simulating in detail real ionization chambers and deriving an overall correction factor.

2. PHOTON BEAMS

2.1. ^{60}Co γ ray beams

Displacement perturbation correction factors, p_{dis}, for NE-2571 Farmer type cylindrical ionization chambers in ^{60}Co beams were calculated in Refs [9, 10], both using EGSnrc, and values 0.8–0.9% higher than in the classical experiment of Johansson in 1977 [11], included in TRS-398, obtained. The reason for the increase is explained in Ref. [12] in terms of an incorrect assumption by Johansson, considering that the mass ionization at the depth of the maximum absorbed dose for ionization chambers of different radii was identical. Wall perturbation correction factors, p_{wall}, have been calculated in Refs. [9, 13], also using EGSnrc, and values 0.6% higher than the values from the semi-empirical expression by Almond-Svensson [14], included in TRS-398, obtained. It is not surprising that two groups of authors using the same tool obtained almost the same value. The new product of these two perturbation factors, p_{dis} and p_{wall}, would raise the absorbed dose to water (D_w) at ^{60}Co by approximately 1.5%, which, considering the wide dissemination of standards at this quality, raises major concerns because such a large change would have extraordinary implications in dosimetry. This increase, however, is not consistent with the improved ratio of D_w determined using $N_{D,w}$ and N_K, which as a consequence of the raise in the BIPM K_{air} standard, is approximately 1.005 at present (it was 1.010 at the time TRS-398 was developed). Furthermore, although in the case of megavoltage photon beams, a ratio MV/^{60}Co of p_Q would partially cancel out any systematic error in the simulations, a change in the overall perturbation correction factor for ^{60}Co would be transmitted to electron beam dosimetry and all other charged particles (protons and heavier ions), including when plane-parallel ionization chambers cross-calibrated against cylindrical ionization chambers are used. As discussed below, an increase in p_Q would lower the absorbed dose to water by the same amount. for electron beams, and for all types of radiotherapy beams that use ^{60}Co as a reference quality.

For the wall perturbation correction factor, p_{wall}, of plane-parallel ionization chambers in ^{60}Co beams, the values published for NACP chambers [15–17] show very small differences with the values used in TRS-398 (see Fig. 1). For the Roos chamber, it can be observed that, whereas excellent agreement has been found with one MC calculated value [16], there are considerable differences with some of the experimental values [18–20]. It is important to emphasize, however, that these experimental determinations are based on the cross-calibration of the chambers, a procedure that depends strongly on the data set used at the various steps; cases discussed in Refs [19] and [20] are based on the German dosimetry protocol [21], which differs from TRS-398. Weighted mean values of p_{wall} have

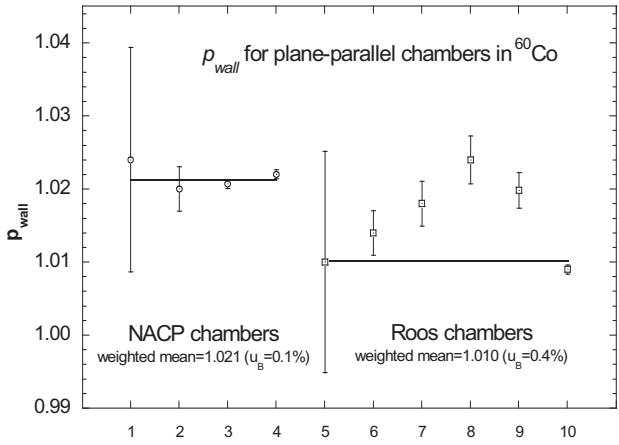

FIG. 1. New experimental and MC data on the p_{wall} correction factor for NACP (circles) and Roos (squares) plane-parallel ionization chambers in ^{60}Co beams, plotted along the TRS-398 values (#1 and 5). Data points Nos 2–4 are from Refs [15–17] and Nos 6–10 from Refs [15, 16, 18–20]; the MC results can be identified by their reduced uncertainty. The horizontal lines correspond to the weighted mean value for each chamber.

been obtained for all the data available, yielding 1.021 and 1.010 for the NACP and Roos chambers, respectively, their type-B standard uncertainties being 0.1% and 0.4%. While the agreement of these values with TRS-398 is remarkable, emphasis is given to the fact that their uncertainty has decreased considerably, reaching similar levels as for Farmer type ionization chambers due to the use of MC calculations. It is interesting to note that the value of p_{wall} for NACP chambers determined by EGSnrc [16] and PENELOPE [17] agree well, considering their very low uncertainties, which is the only case where two different MC systems have been used to determine the same correction.

2.2. Megavoltage photon beams

There is in general good agreement between new MC calculated data of beam quality correction factors of ionization chambers and the data in TRS-398. The NE-2571 Farmer type cylindrical ionization chamber is, however, an exception already observed ten years ago in Ref. [3].

Displacement perturbation correction factors, p_{dis}, for the NE-2571 in high energy photon beams have been calculated in Refs. [9, 10, 12] using EGSnrc (see Fig. 2, left panel). As in the case of ^{60}Co beams, both sets of results yield displacement perturbation correction factors that differ substantially (between 0.5–0.8%) from the values in TRS-398, except at the highest energies. The reason for the discrepancy is also based on the assumptions made in the experiments of

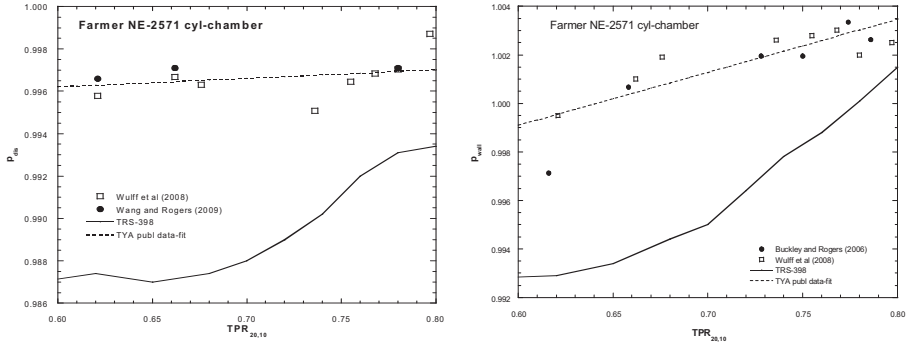

FIG. 2. Data for the displacement (left) and wall (right) perturbation correction factors of the NE-2571 Farmer type chamber as a function of the photon beam quality. The solid lines are TRS-398 data and the dashed lines represent the robust fits of the present analysis.

Johansson. Using data from these references, a robust linear fit was obtained for p_{dis} as a function of the photon beam quality, which is included in Fig. 2; it yields a mean deviation from the published values of 3.7×10^{-5}.

Wall perturbation correction factors, p_{wall}, for NE-2571 Farmer type cylindrical ionization chambers in high energy photon beams have been calculated in Refs. [9, 13] using EGSnrc (see Fig. 2, right panel). The discrepancy between the new p_{wall} values and those in TRS-398, based on the empirical approximation of Ref. [14], is greater than 0.2% in the whole energy range, being significant (>0.5%) only for photon beam qualities below $TPR_{20,10} = 0.70$. Using data from these references, a robust linear fit of p_{wall} as a function of the photon beam quality was obtained; the mean deviation from the published values was 5.8×10^{-4}.

Central electrode perturbation correction factors, p_{cel}, for NE-2571 Farmer type cylindrical ionization chambers in high energy photon beams have been calculated in Refs [9, 22, 23] using EGSnrc (see Fig. 3). The difference between the values in TRS-398 and those from the references is below 0.2%. The three set of values were combined into a robust linear fit with a mean deviation from the published values of 2.9×10^{-4}. The difference between the TRS-398 values and the new values may be due to the different versions of the MC code used, since the values in TRS-398 were calculated with the former EGS4/PRESTA.

Experimentally determined beam quality correction factors k_Q for Farmer type NE-2571 chambers as a function of beam quality are shown in Fig. 4, where data compiled in Ref. [3], mostly from PSDLs, have been updated and complemented according to new publications. A sigmoid weighted fit is included in the figure, which is used in the following comparison. Fitted values for the new p_{dis}, p_{wall} and p_{cel} were used to calculate beam quality correction factors, k_Q, and

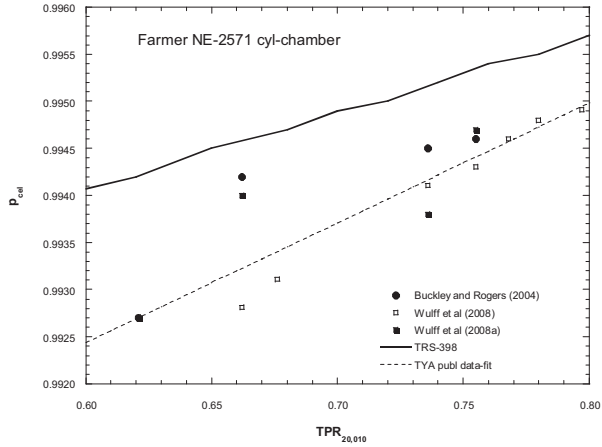

FIG. 3. The central electrode perturbation correction factor of the NE-2571 Farmer type chamber as a function of the photon beam quality; the solid line are TRS-398 data and the dashed line is the robust fit of the present analysis.

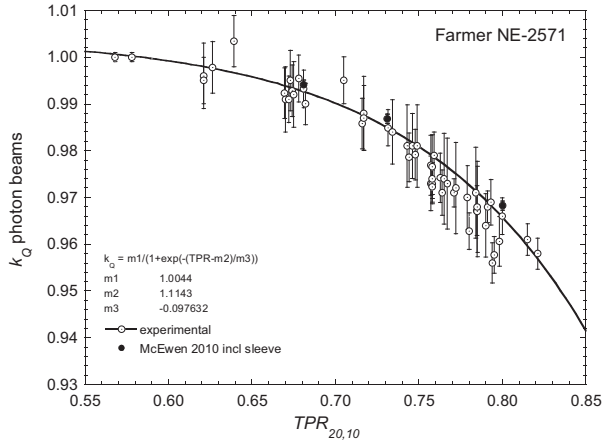

FIG. 4. Experimentally determined beam quality correction factors k_Q of NE-2571 Farmer type chambers for high energy photon beams, as a function of $TPR_{20,10}$. The curve is a sigmoid weighted fit of the published data, which includes the most recent experimental values (three solid circles), obtained with very low uncertainty [25], which pull the curve upwards.

compared with the k_Q data in TRS-398 in Fig. 5, together with the fit to experimental data. It can be seen that the difference between the two theoretical k_Q datasets is smaller than 0.2% for beam qualities below $TPR_{20,10} \approx 0.70$ (approx. 8 MV) but becomes rather pronounced at high energies, the difference being larger than 0.5% for qualities beyond 0.73 (approx. 10 MV) and reaching

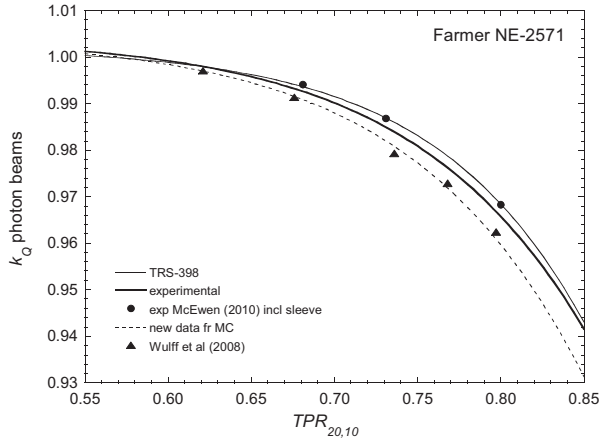

FIG. 5. Comparison of theoretical and experimentally determined k_Q factors for the NE-2571 Farmer type chamber for high energy photon beams, as a function of $TPR_{20,10}$. The most recent experimental values [25] (three solid circles) show excellent agreement with the data given in TRS-398. The triangles correspond to detailed MC simulations of the overall chamber response [9].

up to 1.2%. It is emphasized that the main reason for this large difference rests on the discrepancy of p_Q values for ^{60}Co, which appears in the denominator of k_Q. It can also be observed that the calculated data for this chamber agree rather well with the experimental results except at the highest energies, where the experimental curve lies practically between TRS-398 and the new MC data, with a fortuitous slightly better agreement for TRS-398. For completeness, MC results where the NE-2571 chamber was fully simulated in detail [9] have also been included in Fig. 5, showing consistency with the values resulting from assuming independent perturbations.

Data for other chambers are scarce, but Ref. [3] showed good agreement between k_Q values derived from experiments and those recommended in TRS-398 for other graphite (NE-2561/2611) and plastic walled (PTW-30001 and PR-06C) chambers. Refs [9, 24] confirmed good agreement between their MC calculations and TRS-398 for a variety of graphite and plastic-walled chambers from various manufacturers (PTW, Wellhöfer, Exradin) fully simulated in detail. New calorimetric experimental k_Q data, having very low uncertainty, have recently become available for a variety of chambers and beam qualities [25] where for the majority of chambers, the agreement with TRS-398 is within 0.5%. Thus, there appears to be a lack of consistency in the agreement or disagreement between the new MC data and TRS-398 that most likely can only be resolved by carrying out systematic fully detailed simulations for the exact geometry of

commercially available chambers, preferably using more than just one MC system to avoid potential bias.

To complicate the situation even further, Ref. [9] has also shown a clear dependence of k_Q (for the NE-2571) with the mean excitation energy of graphite, the *I*-value entering into the stopping power formula, which results in differences of about 0.5% in k_Q for *I*-values currently under discussion; k_Q increases with $I_{graphite}$. At present, there is an ICRU working group on key data for dosimetry, which will most likely issue a recommendation for new $I_{graphite}$ and I_{water} values, both currently under scrutiny. Of special interest for the present discussion is the analysis of Burns [26], which raises $I_{graphite}$ from 78 eV to 82.5 eV.

3. ELECTRON BEAMS

For electron beams TRS-398 assumed p_{cav} to be unity for 'well-guarded' plane-parallel chambers. Despite evidence that wall effects introduce a non-negligible p_{wall}, the lack of reliable data also led to recommend this factor to be unity.

Using MC calculations, mostly simulating NACP plane-parallel chambers with EGSnrc, several publications [27–31] have concluded that wall perturbation correction factors differ from unity. The evidence for p_{wall}, including its energy dependence, appears to be consolidated, varying approximately between 1–2% for R_{50} between 8 cm and 1 cm, respectively (see Fig. 6, left panel). The values were described by an exponential fit with a mean deviation of the published values of 1.4×10^{-3}.

On the other hand, for the cavity perturbation p_{cav}, there is a considerable spread in the MC data [10, 27, 30, 31] showing discrepancies larger than 1% at some energies despite having used the same MC system. The spread shown in Fig. 6 (right panel) thus precludes a trustworthy analysis. It is stressed that some conclusions in the references quoted regarding the variation of MC transport cut-offs, as well as chamber dimensions claimed to be rather different from manufacturer specifications, are contradictory or cannot be confirmed. Notwithstanding these constraints, robust fits have been performed on the available theoretical datasets and values of $k_{Q,Qint}$ calculated using the present fits of p_{wall} and p_{cav}.

The set of experimentally determined $k_{Q,Qint}$ for NACP plane-parallel chambers at PSDLs [32] have been included in our analysis and a robust fit obtained on the data. Results are compared in Fig. 7, which shows better agreement between TRS-398 and the experimental data than the results obtained with the new available MC data. Significant discrepancies with the experimental

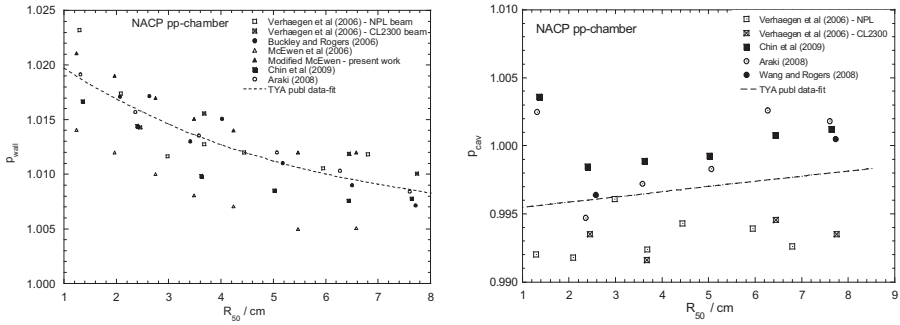

FIG. 6. Compilation of MC calculated perturbation correction factors p_{wall} (left) and p_{cav} (right) for the NACP plane-parallel chamber in electron beams by different authors. The p_{wall} values labelled 'Modified McEwen' are from Ref. [29] corrected by the contribution of the side walls (not taken into account in Ref. [29]) using data from Ref. [27]. The dashed lines are robust fits of the data. (TYA: 'Ten years after TRS-398').

data can be observed only at the lowest energies (0.5% for the TRS-398 data versus 1.3% for the new MC data), whereas there is remarkable agreement at the high energy end, especially for the TRS-398 data. Fig. 7 also includes results of detailed simulations of the overall response of a NACP chamber performed with Penelope [6], which, while deviating at low energy, in general are closer to the TRS-398 values than the independent perturbations based MC determinations analysed above. The comparison points at an apparent overestimation of the overall perturbation factor p_Q with the new MC data, probably related to the assumption of independent perturbation effects. The influence of the chamber geometry being simulated cannot be underestimated either.

The data for ^{60}Co γ ray beams play a fundamental role in electron beam dosimetry, both using cylindrical and plane-parallel chambers, as they enter into k_Q calculations and whenever plane-parallel chambers are cross-calibrated against cylindrical chambers. An important achievement for the p_{wall} of NACP plane-parallel chambers is that the value recommended in TRS-398 has practically been confirmed with independent MC calculations using both EGSnrc and Penelope at a very low uncertainty. It is then remarkable that the uncertainty in k_Q becomes considerably reduced, eliminating the major constraint for the use of ^{60}Co-calibrated NACP chambers, and thus its k_Q factors, for electron beam dosimetry as well as for other charged particle beams (protons and carbon ions).The use of a cylindrical chamber in electron beams with energies higher than about 10 MeV, either for a direct D_w determination or for plane-parallel chamber cross-calibration, acquires particular relevance if the new MC calculated values of perturbation correction factors for Farmer type chambers at ^{60}Co are

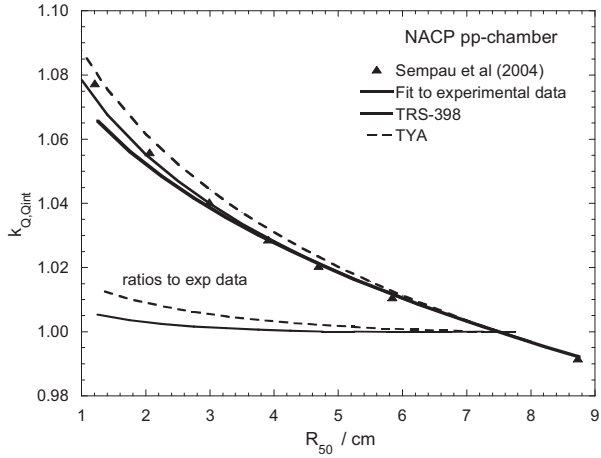

FIG. 7. Comparison of theoretical and experimentally determined $k_{Q,Qint}$ factors for the NACP plane-parallel chamber for electron beams, as a function of R_{50}. The triangles correspond to detailed MC simulations of the overall chamber response [6]. The lower solid and dashed lines show respectively ratios of TRS-398 and of the new MC data (TYA: 'Ten years after TRS-398') to the experimental $k_{Q,Q_{int}}$ factors.

taken into account. It is emphasized that the resulting overall increase of 1.5% in p_Q, compared with TRS-398, would appear in the denominator and therefore decrease k_Q (of electrons) by the same amount. As a result, the D_w used for a cross-calibration and all relevant k_Q factors for plane-parallel chambers would also decrease by approximately the same amount, as the new electron perturbation factors discussed above do not compensate for such large increase. Only for very low electron energies where the p_Q correction approximates 1% would there be a partial balance, but the large difference would persist at medium and high energies. In addition, excellent experimental agreement (at the level of 0.2–0.5%) has been shown between electron dosimetry based on NACP chambers that have been either cross-calibrated or calibrated directly in ^{60}Co and in electron beams at a primary standards laboratory [33]. The decrease in absorbed dose of about 1.5% discussed here would yield a considerable discrepancy with such current evidence, which is not likely to be in error by such a large amount. Similar changes would appear in the k_Q factors of protons and heavier ions using ^{60}Co γ rays as reference quality.

4. CONCLUDING REMARKS

Data for the reference dosimetry of external beam radiotherapy published since the IAEA TRS-398 Code of Practice was issued in 2000 have been analysed. The analysis focuses on MC derived perturbation correction factors of ionization chambers in photon and electron beams, which are compared with those used in TRS-398, mostly obtained decades ago. Their combinations into beam quality correction factors, k_Q, have also been compared with TRS-398 and with experimental determinations.

It is emphasized that new data are available for a reduced set of chambers, notably the NE-2571 Farmer type and the NACP plane-parallel chamber, and that most of the MC data have been obtained using the EGSnrc system under the assumption of independent perturbation effects. It is expected that results obtained with the same tools and approximations yield similar results. On the other hand, and despite using the same MC system but probably different user codes, remarkable discrepancies have also been found, especially for the NACP chamber in electron beams, pointing at questionable simulation geometries and/or transport parameters. Fully detailed simulations of ionization chambers would be preferred to the use of independent perturbation correction factors, as well as data for a larger set of commercial chambers. To avoid potential bias, other MC systems should also be used, as is currently done at PSDLs.

For megavoltage photon beams, new MC data agree quite well with the values in TRS-398 with the exception of the NE-2571 Farmer type chamber. Perturbation correction values for this chamber differ significantly (>0.5%) from TRS-398 data at low energies, as they do in ^{60}Co beams, whereas at the highest energies the differences are approximately within 0.2%. The ratio MV/^{60}Co of p_Q-values causes differences in k_Q factors that increase with energy up to 1.2% due to the influence of the ^{60}Co values in the denominator. On the other hand, comparing the new MC-based k_Q values with experimental data at the highest energies shows similar differences, although with reverse sign, as for TRS-398 which is around 0.5%. It is therefore questionable that new MC data for the NE-2571 would represent an improvement on the entire TRS-398 dataset. In addition, overall uncertainties in calculated k_Q would not decrease by more than 0.1–0.2% either, as both $s_{w,air}$ and W_{air} dominate the overall uncertainty with their estimates of 0.5% [1]. Considering the small differences between the new MC data for some chambers and TRS-398, the lack of experimental and calculated data for most commercial chambers, and the additional uncertainty caused by the need of adopting new I-values and stopping powers, it can be concluded that time has not yet come for recommending changes to the data in TRS-398.

For electron beams substantial differences with the perturbation factors in TRS-398 have been found for plane-parallel chambers, particularly NACP at low

energies. However, the large range of variation of the new data for p_{cav} precludes trustworthy conclusions and estimating low uncertainties. It also results in a situation, which, unfortunately, resembles the lack of reliable data already existing at the time of developing TRS-398. In addition, the comparison with experimental k_Q data shows better agreement for TRS-398 than for the new MC-based k_Q results, pointing at an apparently overestimated overall perturbation factor which can probably be related to the assumption of independent perturbation effects and/or inadequate description of chamber geometry. These findings, together with the constraints on *I*-values and stopping powers, point again at the convenience of a reasonable waiting time before changes in TRS-398 can be recommended.

Finally, and as a problem dominating most therapeutic beam types, the new MC data for ^{60}Co would yield a change in absorbed dose of about 1.5%, representing a considerable discrepancy with the current evidence for this reference beam quality, which is not likely to be in error by such large amount. The increase affects all type of beams that use ^{60}Co as a reference quality, particularly charged particles (electrons, protons and heavier ions). The major priority is still on finding data that provides consistent dose determination in the entire electron and photon radiotherapy energy range, as well as for all type of charged particles, irrespective of the procedure used for deriving the necessary data.

In all cases, comparisons with high quality experimental data are the final evidence for any calculation. It is stressed that the MC technique is not a magic black box. Quoting an old statement by Bielajew (pers. comm.), *"Be sceptical of the Monte Carlo results of anybody else. Be especially sceptical of your own Monte Carlo results; no matter how you word your disclaimer, you will still carry the can filled with your own bugs"*.

REFERENCES

[1] INTERNATIONAL ATOMIC ENERGY AGENCY, Absorbed Dose Determination in External Beam Radiotherapy: An International Code of Practice for Dosimetry Based on Standards of Absorbed Dose to Water, Technical Reports Series No. 398, IAEA, Vienna (2000).

[2] ALLISY, P.J., BURNS, D.T., ANDREO, P., International framework of traceability for radiation dosimetry quantities, Metrologia **46** (2009) S1–S8.

[3] ANDREO, P., A comparison between calculated and experimental k_Q photon beam quality correction factors, Phys. Med. Biol. **45** (2000) L25-L38.

[4] SEUNTJENS, J.P., ROSS, C.K., SHORTT, K.R., ROGERS, D.W.O., Absorbed-dose beam quality conversion factors for cylindrical chambers in high energy photon beams, Med Phys, **27** (2000) 2763–2779.

[5] ALMOND, P.R., BIGGS, P.J., COURSEY, B.M., HANSON, W.F., HUQ, M.S., NATH, R., ROGERS, D.W.O., AAPMs TG-51 protocol for clinical reference dosimetry of high-energy photon and electron beams, Med Phys. **26** (1999) 1847–1870.

[6] SEMPAU, J., ANDREO, P., ALDANA, J., MAZURIER, J., SALVAT, F., Electron beam quality correction factors for plane-parallel ionization chambers: Monte Carlo calculations using the PENELOPE system. Phys Med Biol, **49** (2004) 4427–4444.

[7] KAWRAKOW, I., MAINEGRA-HING, E., ROGERS, D.W.O., TESSIER, F., WALTERS. B.R.B., The EGSnrc Code System: Monte Carlo Simulation of Electron and Photon Transport, NRCC (2009) Report PIRS-701.

[8] SALVAT, F., FERNÀNDEZ-VAREA, J.M., SEMPAU, J., PENELOPE-2008: A Code System for Monte Carlo Simulation of Electron and Photon Transport (Issy-les-Moulineaux, France: OECD Nuclear Energy Agency) (2009).

[9] WULFF, J., HEVERHAGEN, J.T., ZINK, K., Monte-Carlo-based perturbation and beam quality correction factors for thimble ionization chambers in high-energy photon beams, Phys Med Biol, **53** (2008) 2823–2836.

[10] WANG, L.L.W., ROGERS, D.W.O., Calculation of the replacement correction factors for ion chambers in megavoltage beams by Monte Carlo simulation, Med Phys, **35** (2008) 1747–1755.

[11] JOHANSSON, K.-A., MATTSON, L.O., LINDBORG, L., SVENSSON, H., "Absorbed-dose determination with ionization chambers in electron and photon beams having energies between 1 and 50 MeV", National and International Standardization of Radiation Dosimetry (Proc. Int. Symp. Atlanta, 1977), Vol. 2, IAEA, Vienna (1978) 243–270.

[12] WANG, L.L.W., ROGERS, D.W.O., The replacement correction factors for cylindrical chambers in high-energy photon beams, Phys. Med. Biol. **54** (2009) 1609–1620.

[13] BUCKLEY, L.A., ROGERS, D.W.O., Wall correction factors, p_{wall}, for thimble ionization chambers. Med. Phys. **33** (2006) 455–464.

[14] ALMOND, P.R., SVENSSON, H., Ionization chamber dosimetry for photon and electron beams. Acta Radiol. **16** (1977) 177–186.

[15] PALM, A., MATTSON, O., ANDREO, A., Calibration of plane-parallel chambers and determination of p_{wall} for the NACP and Roos chambers for ^{60}Co gamma-ray beams, Phys. Med. Biol. **45** (2000) 971–981.

[16] MAINEGRA-HING, E., KAWRAKOW, I., ROGERS, D.W.O., Calculations for plane-parallel ion chambers in ^{60}Co beams using the EGSnrc Monte Carlo code, Med. Phys. **30** (2003) 179–189.

[17] PANETTIERI, V., SEMPAU, J., ANDREO, P., Chamber-quality factors in ^{60}Co for three plane-parallel chambers for the dosimetry of electrons, protons and heavier charged particles: PENELOPE Monte Carlo simulations, Phys. Med. Biol. **53** (2008) 5917–5926.

[18] PALM, A., CZAP, L., ANDREO, P., MATTSON, P., Performance analysis and determination of the p_{wall} correction factor for ^{60}Co gamma-ray beams for Wellhöfer Roos-type plane-parallel chambers, Phys. Med. Biol. **47** (2002) 631–640.

[19] CHRIST, G., DOHM, S., BRUGGMOSER, G., SCHÜLE, E., The use of plane-parallel chambers in electron dosimetry without any cross-calibration, Phys Med Biol. **47** (2002) N121–N126.

[20] KAPSCH, R.P., BRUGGMOSER, G., CHRIST, G., DOHM, O.S., HARTMANN, G.H., SCHÜLE, E., Experimental determination of p_{Co} perturbation factors for plane-parallel chambers. Phys Med Biol, **52** (2007) 7167–7181.

[21] DEUTSCHES INSTITUT FÜR NORMUNG, Dosismessverfahren nach der Sondenmethode für Photonen- und Elektronenstrahlung, DIN 6800-2 (2006).

[22] BUCKLEY, L.A., KAWRAKOW, I., ROGERS, D.W.O., CSnrc: correlated sampling Monte Carlo calculations using EGSnrc, Med. Phys. **31** (2004) 3425–3435.

[23] WULFF, J., ZINK, K., KAWRAKOW. I., Efficiency improvements for ion chamber calculations in high energy photon beams, Med Phys, **35** (2008) 1328–1336.

[24] GONZALEZ-CASTAÑO, D.M., HARTMANN, G.H., SANCHEZ-DOBLADO, F., GOMEZ, F., KAPSCH, R.-P., PENA, J., CAPOTE, R., The determination of beam quality correction factors: Monte Carlo simulations and measurements, Phys. Med. Biol. **54** (2009) 4723–4741

[25] McEWEN, M.R., Measurement of ionization chamber absorbed dose k_Q factors in megavoltage photon beams, Med. Phys. **37** (2010) 2179-2193.

[26] BURNS, D.T., A re-evaluation of the I-value for graphite based on an analysis of recent work on W, $s_{c,a}$ and cavity perturbation corrections, Metrologia **46** (2009) 585–590.

[27] VERHAEGEN, F., ZAKIKHANI, R., DUSAUTOY, A., PALMANS, H., BOSTOCK, G., SHIPLEY, D., SEUNTJENS, J., Perturbation correction factors for the NACP-02 plane-parallel ionization chamber in water in high-energy electron beams, Phys. Med. Biol. **51** (2006) 1221–1235.

[28] BUCKLEY, L.A., ROGERS, D.W.O., Wall correction factors, p_{wall}, for parallel-plate ionization chambers, Med. Phys. **33** (2006) 1788–1796.

[29] McEWEN, M., PALMANS, H., WILLIAMS, A., An empirical method for the determination of wall perturbation factors for parallel-plate chambers in high-energy electron beams, Phys Med Biol, **51** (2006) 5167–5181.

[30] CHIN, E., PALMANS, H., SHIPLEY, D., BAILEY, M., VERHAEGEN, F., Analysis of dose perturbation factors of a NACP-02 ionization chamber in clinical electron beams, Phys. Med. Biol. **54** (2009) 307–326.

[31] ARAKI, F., Monte Carlo calculations of correction factors for plane-parallel ionization chambers in clinical electron dosimetry, Med. Phys. **35** (2008) 4033–4040.

[32] McEWEN, M.R., DUSAUTOY, A.R., Primary standards of absorbed dose for electron beams, Metrologia **46** (2009) S59–S79.

[33] ANDREO, P., WESTERMARK, M., McEWEN, M., DUSAUTOY, R., THOMAS, R., "Electron beam dosimetry in TRS-398: theoretical *vs* experimental $k_{Q,Qo}$ values. Influence on D_w of the various plane-parallel chamber calibration modalities", Proc. Int. Symp. on Standards and Codes of Practice in Medical Radiation Dosimetry, Vienna, 2002 (extended synopsis) .

APPLICATION OF A NEW DOSIMETRY FORMULISM TO IMRT HEAD AND NECK RADIOTHERAPY

K.E. ROSSER
The London Clinic, London
Email: K.Rosser@thelondonclinic.co.uk

E.M. FERNANDEZ
Joint Department of Physics,
The Institute of Cancer Research
and The Royal Marsden NHS Foundation Trust,
Sutton, Surrey

United Kingdom

Abstract

The aim of this paper is to investigate the use of a new dosimetry formulism for head and neck IMRT radiotherapy. Two plan class specific reference (PCSR) fields were devised, both using seven fields at different gantry angles; one was based on clinical plans and inverse planned while the other was forward planned and simpler, consisting of three segments per beam. Factors were then measured to convert the dose from the 10 cm × 10 cm reference field to the PCSR field and then from the PCSR field to the treatment plan. The dose was measured in the reference field, two PSCR fields and two clinical plans using NE2571 and cc13 ionization chambers and alanine dosimeters. These doses were also compared with the dose calculated using a Pinnacle^3 planning system. It was found that the dose measured using the alanine agrees with that planned using Pinnacle^3 planning system; the maximum difference being 2.7% for the simple PCSR. The factors

$$k_{Q_{pcsr},Q}^{f_{pcsr},f_{ref}} \text{ and } \Omega_{Q_{clin},Q_{pcsr}}^{f_{clin},f_{pcsr}}$$

are higher for the IBA cc13 than for the NE2571 by 1.6%.

1. INTRODUCTION

Modern radiotherapy has become complex as various techniques such as IMRT, VMAT, RapidArc Tomotherapy and Cyberknife are becoming routine practice. These techniques use a composite of small fields so that the dose conforms to the planning target volume, whilst minimizing the dose to surrounding tissue.

Traditional dosimetry recommended in Codes of Practice [1–3] uses a standard 10 cm × 10 cm static field as the starting block. However, as this bears no resemblance to modern dose distributions, Alfonso et al. [4] proposed a dosimetry method that has an interim step between the standard field and the treatment field (clin) and called it the plan class specific reference (PCSR) field. The PCSR field is a reference field, which is as close as possible to the final clinical delivery scheme but delivers a homogeneous absorbed dose to a simple target volume where the detector will be placed. It is expected that PCSR fields will be dependent on the treatment modality and the treatment site.

The purpose of this study is to investigate the application of the dosimetry formalism proposed by Alfonso et al. [4] to head and neck (H&N) IMRT in the clinic. The aim is to design a representative f_{pcsr} for H&N treatments using IMRT, and evaluate the corresponding correction factors

$$k_{Q_{pcsr},Q}^{f_{pcsr},f_{ref}} \text{ and } \Omega_{Q_{clin},Q_{pcsr}}^{f_{clin},f_{pcsr}}$$

for a NE2571 and IBA cc13 chamber used in the clinic. This is similar to work done by Rosser and Bedford [5] for VMAT dosimetry and Chung et al. [6] for H&N IMRT.

2. FORMULISM

The formulism suggested by Alfonso et al. [4] introduced a PCSR where the absorbed dose to water

$$\left[D_{w,Q_{pcsr}}^{f_{pcsr}} \right]$$

is determined using:

$$D_{w,Q_{pcsr}}^{f_{pcsr}} = M_{Q_{pcsr}}^{f_{pcsr}} \cdot N_{D,W,Q_0} \cdot k_{Q,Q_0} \cdot k_{Q_{pcsr},Q}^{f_{pcsr},f_{ref}} \tag{1}$$

where

$M_{Q_{pcsr}}^{f_{pcsr}}$ is the reading on the dosimeter in the PCSR corrected for influence quantities;

N_{D,w,Q_0} is the calibration coefficient in terms of absorbed dose to water for an ionization chamber at a reference beam quality Q_0; and

k_{Q,Q_0} is the beam quality correction factor, which corrects for the differences between the reference beam quality Q_0 at the standards laboratory and the beam quality Q of the conventional field f_{ref}.

The factor

$$k_{Q_{pcsr},Q}^{f_{pcsr},f_{ref}}$$

is a factor that corrects for the difference between the reference field (f_{ref}) and the PCSR and is defined as:

$$k_{Q_{pcsr}Q}^{f_{pcsr},f_{ref}} = \frac{D_{w,Q_{pcsr}}^{f_{pcsr}} / M_{Q_{msr}}^{f_{pcsr}}}{D_{w,Q}^{f_{ref}} / M_{Q}^{f_{ref}}} \quad (2)$$

From this, the absorbed dose to water in a clinical beam is obtained from:

$$D_{w,Q_{clin}}^{f_{clin}} = D_{w,Q_{pcsr}}^{f_{pcsr}} . \Omega_{Q_{clin},Q_{pcsr}}^{f_{clin},f_{pcsr}} \quad (3)$$

where Q_{clin} is the beam quality of the clinical beam f_{clin}, and

$$\Omega_{Q_{clin},Q_{pcsr}}^{f_{clin},f_{pcsr}}$$

is a field factor which converts the absorbed dose to water for the PCSR field to the absorbed dose to water for the clinical field.

3. MATERIALS AND METHOD

The measurements were taken using an Elekta Synergy MLCi Linac at 6 MV (TPR_{2010} = 0.684) to irradiate alanine, NE2571and cc13 chambers. For all of the measurements, a cuboid phantom (30 cm × 30 cm × 20 cm) made of slabs of solid water (Gammex $RMI_{(R)}$ Middleton, WI, USA) was used. Each detector had its own slab: the NE2571 chamber's was made of solid water, the cc13, of CIRS, while that for alanine, of Perspex.

Each detector was irradiated on separate occasions with the measurement of dose using a NE2571 chamber under reference conditions linking the sessions. Each session consisted of three main sections: first, the dose was measured for the chosen detector in the reference field; second, to determine

$$k_{Q_{pcsr},Q}^{f_{pcsr},f_{ref}}$$

the detectors were irradiated using the inverse planned PCSR field and the simple PCSR field separately; and finally, to determine

$$\Omega_{Q_{clin},Q_{pcsr}}^{f_{clin},f_{pcsr}}$$

each detector was irradiated using the two clinical plans.

The alanine [7] was used as an absolute measurement of dose in the reference, PCSR and clinical fields. To minimize the uncertainty on the dose measurement using alanine, 10 Gy was given for the reference field. Each of the PCSR and clinical plans was delivered four times giving approximately 8 Gy to the alanine.

3.1. PCSR fields

To establish a representative PCSR field, ten clinical H&N plans were investigated. It was found that the most commonly used treatment adopted seven beams and collimator angle close to zero. An inverse plan was produced according to normal clinical protocol using this beam arrangement on typical primary and nodal PTVs defined on an anthropomorphic phantom. (see Fig. 1).

This plan was recalculated on the solid water cuboid phantom with the high dose PTV located around the measurement volume so that the dose was uniform within 1% across the chamber. In addition it was thought that this approach was not practical for routine use, so a second simpler PCSR field was also produced. This PCSR field was forward planned with seven fields at the typical clinical gantry angles, each with a 5^{o} collimator angle. For each field the same 3 rectangular segments were used, making a wedge effect and giving a uniform dose over the chamber. Figure 2 shows the segments for one gantry angle.

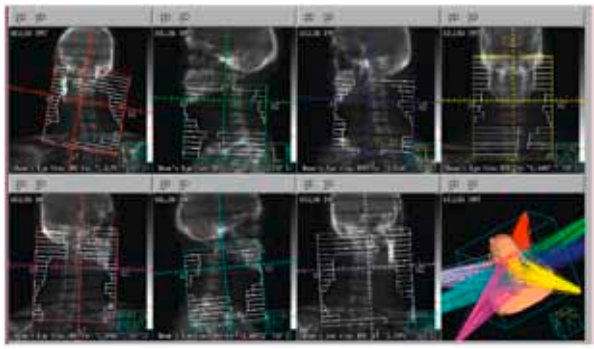

FIG. 1. Inverse planned PCSR field.

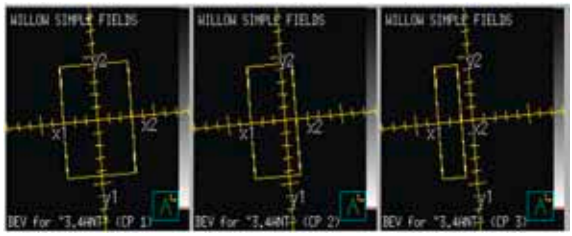

FIG. 2. Simplified PCSR field.

3.2. Clinical plans

Two clinical plans that had recently been used to treat H&N patients were recalculated on the cuboid solid water phantom using Pinnacle[3]. Each plan had seven fields at similar gantry angles and collimator angles to the PCSR fields, but Plan 1 consisted of 58 segments and Plan 2 had 66 segments. Each plan was positioned on the phantom such that the detector was in a region of uniform dose.

4. RESULTS

The doses predicted by Pinnacle[3] for the PCSR and clinical plans are compared with those measured using alanine in Table 1. The alanine was irradiated to a dose of approximately 8 Gy i.e. given four fractions. For this comparison the dose was scaled to a single fraction. The Pinnacle[3] plans were corrected for couch transmission at gantry angle 150° and 210° (as is done

TABLE 1. COMPARISON OF DOSE MEASURED BY ALANINE AND DOSE CALCULATED BY Pinnacle[3]

Plan	Dose measured using alanine (cGy)	Dose calculated using Pinnacle[3] (cGy)	Difference (%)
Inverse planned PCSR	199.1	198.2	0.5
Simple PCSR	203.6	198.1	2.7
Clinical plan 1	197.9	198.6	0.3
Clinical plan 2	201.4	198.6	1.4

routinely for clinical plans) [8] and also for the density of the perspex slab in which the alanine was situated. The values of

$$k_{Q_{pcsr},Q_0}^{f_{pcsr},f_{ref}} \text{ and } \Omega_{Q_{clin},Q_{pcsr}}^{f_{clin},f_{pcsr}}$$

for NE2571 and cc13 chamber for the two PCSR fields are shown in Table 2.

5. DISCUSSION

The use of the Alfonso formulism has been investigated for H&N MRT using two different PCSR fields, one simple and one inverse planned. It was found that the two PCSR fields gave very similar values of

$$k_{Q_{pcsr},Q}^{f_{pcsr},f_{ref}} \text{ and } \Omega_{Q_{clin},Q_{pcsr}}^{f_{clin},f_{pcsr}}$$

The advantage of the simple PCSR is that it is easy to plan and quick to deliver.

It is also interesting to note that the dose measured using the alanine agrees with that planned using the Pinnacle[3] planning system, the maximum difference being 2.7% for the simple PCSR. This may be due to the problem of positioning the alanine in a region that is not homogeneous outside the measurement area.

The factors

$$k_{Q_{pcsr},Q}^{f_{pcsr},f_{ref}} \text{ and } \Omega_{Q_{clin},Q_{pcsr}}^{f_{clin},f_{pcsr}}$$

are higher for the IBA cc13 than for the NE2571. This difference was not foreseen as one would expect the IBA cc13 to give factors closer to unity since it

TABLE 2. COMPARISON OF $k_{Q_{pcsr},Q}^{f_{pcsr},f_{ref}}$ AND $\Omega_{Q_{clin},Q_{pcsr}}^{f_{clin},f_{pcsr}}$

Detector	$k_{Q_{pcsr},Q}^{f_{pcsr},f_{ref}}$		$\Omega_{Q_{clin},Q_{pcsr}}^{f_{clin},f_{pcsr}}$			
			Plan 1		Plan 2	
	Inverse planned PCSR field	Simple PCSR field	Inverse planned PCSR field	Simple PCSR field	Inverse planned PCSR field	Simple CSR field
NE2571	1.005	1.001	0.993	0.996	0.999	0.997
IBA cc13	1.021	1.021	1.033	1.032	1.033	1.034

TABLE 3. COMPARISON OF RECENTLY PUBLISHED $k_{Q_{pcsr},Q}^{f_{pcsr},f_{ref}}$ FACTORS FOR NE2571 CHAMBER

$k_{Q_{pcsr},Q}^{f_{pcsr},f_{ref}}$						
This publication		Rosser and Bedford [5]			Chung et al. [6]	
Inverse planned PCSR field	Simple PCSR field	PCSR 1	PCSR 2	PCSR 3	Fully rotated	Collapsed delivery
1.005	1.001	1.005	0.997	1.014	0.997	0.993

is a smaller chamber. The reason for this difference requires further investigation, but may be due to the rotational characteristics of the IBA cc13 chamber.

From Table 3 it is interesting to note that the values of

$$k_{Q_{pcsr},Q}^{f_{pcsr},f_{ref}}$$

for a NE2571 chamber are similar for very different PCSR fields, providing that the dose is homogeneous over the detector but this requires further investigation.

ACKNOWLEDGEMENT

The author would like to thank J. Warrington from The Royal Marsden Hospital for his help and inspiration throughout this project.

REFERENCES

[1] LILLCRAP, S.C., OWEN, B., WILLIAMS, J.R., WILLIAMS, P.C., Code of Practice for high-energy photon therapy dosimetry based on the NPL absorbed dose calibration service, Phys. Med. Biol. 35 (1990) 1355–1360.

[2] INTERNATIONAL ATOMIC ENERGY AGENCY, Absorbed Dose Determination in External Beam Radiotherapy: An International Code of Practice for Dosimetry Based on Standards of Absorbed Dose to Water, Technical Reports Series No. 398, IAEA, Vienna (2000).

[3] ALMOND, P.R., BIGGS, P.J., COURSEY, B.M., HANSON, W.F., HUQ, M.S., NATH, R., ROGERS, D.W., AAPM TG5,'protocol for clinical reference dosimetry of high-energy photon and electron beams, Med. Phys. **26** (1999) 1847–1870.

[4] ALFONSO, R., ANDREO, P., CAPOTE, R., SAIFUL HUQ, M., KILBY, W., KJÄLL, P., MACKIE, T.R., PALMANS, H., ROSSER, K., SEUNTJENS, J., ULLRICH, W., VATNITSKY, S., A new formalism for reference dosimetry of small and nonstandard fields, Med. Phys. **35**(2008) 5179–5186.

[5] ROSSER, K.E., BEDFORD, J.L., Application of a new dosimetry formalism to vulmetric modulated arc therapy (VMAT), Phys. Med. Biol. 54 (2009) 7045–7061.

[6] CHUNG, E., BOUCHARD, H., SEUNTJENS, J., Investigation of three radiation detectors for accurate measurement of absorbed dose in nonstandard fields, Med. Phys. **37** (2010) 2404–2413.

[7] SHARPE, P., SEPHTON, J., "Therapy level alanine dosimetry at the NPL" (Proc. of the 216th PTB Sem. 'Alanine Dosimetry for Clinical Application' PTB, Braunschweig), PTB-Dos-51 (2006).

[8] BLASIAK-WAL, I., private communication 2010.

SMALL AND COMPOSITE FIELD DOSIMETRY: THE PROBLEMS AND RECENT PROGRESS

H. PALMANS
National Physical Laboratory, Teddington,
United Kingdom
Email: hugo.palmans@npl.co.uk

Abstract

The increased use of small fields in intensity modulated and stereotactic treatments has created the demand for more standardization of dosimetry procedures for these non-reference fields. In addition, treatment units such as GammaKnife, CyberKnife and TomoTherapy cannot establish broad beam reference conditions prescribed in conventional dosimetry. For dynamic, modulated deliveries, the step between dosimetry in the conventional static broad beam reference field and the actual treatment delivery is large and it has been suggested that performing reference dosimetry for an intermediate field may substantially reduce the uncertainty. This paper reviews the problems associated with introducing standard dosimetry procedures for these non-standard fields, proposed solution and a status of data and information needed for providing recommendations for reference dosimetry.

1. INTRODUCTION

While reference dosimetry for broad external beams has been well established [1], the increased use of small fields in intensity modulated radiotherapy (IMRT) and stereotactic radiosurgery (SRS) has revealed many questions about the accuracy of their dosimetry and what constitutes best practice and numerous problems with small and composite field dosimetry have been reviewed [3] Various incidents reported recently involved the miscalibration of small fields and demonstrate the need for clear guidelines and recommendations for small field dosimetry.

National and international working groups have been established to provide literature review, guidelines and recommendations for small and composite field dosimetry (IPEM, DIN, NCS, IAEA/AAPM, etc.). The Institute of Physics and Engineering in Medicine (IPEM) has recently published a report providing an extensive review of small field dosimetry and recommendations derived from existing experience that are not, however, at the level of a code of practice [3]. An international working group on small and composite field dosimetry formed by the IAEA in collaboration with the AAPM, published a formalism extending the recommendations from IAEA TRS-398 to fields that cannot establish

conventional reference conditions as well as to composite fields [4]. This formalism introduces the concepts of machine specific or intermediate reference fields for static small fields, and plan-class specific reference (PCSR) fields for composite fields, which both deviate from conventional reference fields and bridge the gap with smaller fields and clinical composite fields, respectively.

This paper reviews the problems associated with small and composite field dosimetry for high energy photon beams and various recent solutions that have been proposed.

2. PROBLEMS AND PROPOSED SOLUTIONS: SMALL FIELDS

2.1. Small field conditions

Two or three aspects that are usually considered to contribute to small field conditions are as follows [5]:

(i) If the field size is smaller than the lateral electron equilibrium (LEE) length, the penumbrae of the field overlap, resulting in a characteristic sharp drop of output when the field size decreases further. This effect is energy dependent; the LEE length in water is about 0.6 cm for a ^{60}Co gamma ray beam and 1.3 cm for a 6 MV high energy X ray beam [6].

(ii) If the primary photon source at the exit plane of the target is partially occluded by the collimators, as viewed from the measurement point, the direct photon penumbrae overlap leading to a reduced output as well. For modern accelerators where the spot size is not larger than 5 mm this usually occurs at field sizes smaller than those where lateral electron disequilibrium starts.

(iii) Sometimes the size of a detector is mentioned as a determining factor. Although this is not an unambiguous criterion (a large detector could make any field look small), it is relevant to consider since volume averaging, an important source of detector perturbations in small fields, is indeed very dependent on detector size. A useful proposal could be that small field conditions exist when any lateral edge of the detector is less than the LEE length away from the field edge.

For practical reasons, it may be preferable to use a generic fixed field size below which fields are defined as small; e.g. the IPEM has defined small fields as having at least one dimension smaller than 3 cm [3]. On the other hand, it could be advisable to use an energy dependent criterion, which could be helpful for the GammaKnife by considering the largest available field size (1.8 cm or 1.6 cm)

that would still to be suitable for broad beam reference dosimetry with a sufficiently small ionization chamber. Based on the assumption that collision kerma equals absorbed dose in charged particle equilibrium (CPE) conditions, the minimal circular beam radius for achieving LEE as a function of the photon beam quality index $TPR_{20,10}$ was determined as [6]:

$$r_{LEE} = 5.973 \cdot TPR_{20,10} - 2.688 \text{ (g/cm}^2\text{)} \quad (1)$$

2.2. Small field size

Conventionally, the field size is defined by the collimator setting, either by a linear relation for straight edged focused collimators, or by a quadratic relation for cylindrically curved collimators. In broad beams, the field size defined by the collimator setting corresponds well with the full width at half maximum (FWHM) of the lateral dose profile at isocentric depth, and thus the latter is often used as a verification of the field size setting. In small fields, however, due to the overlap of penumbrae and the resulting reduction in beam output, the FWHM would be measured at a different dose level, and the functional relation between field width based on collimator setting and FWHM breaks down [5]. It is ofimportance, therefore, to know unambiguously how the field size is defined in a planning system or in scientific publications. Preference is given to collimator setting since the FWHM usually has a non-zero limiting value as the collimator field size setting goes to zero [3].

2.3. Energy spectrum and beam quality

Various effects contribute to the change of in-phantom spectra in the centre of small photon fields as compared to conventional broad beam reference fields:

- The amount of scattered photons from primary collimator and flattening filter (head scatter) is reduced, resulting in a hardening of the photon spectrum. (For off-axis fields, however, there may be an increased relative contribution of scattered photons.).
- The phantom scatter contribution on the central axis is reduced since photons scattering out of the small field will not be compensated by inscattering photons. (For most depths, this is a larger effect than the reduced head scatter.)
- When the field is too small for lateral CPE, there will be a deficit of low energy electrons reaching the central axis resulting in an increase of the mean electron energy.

On the beam axis, the average photon energy and consequently the average electron energy will increase with decreasing field size [3]. Off-axis it is not a priori clear what the net effect will be. The deficit of low energy electrons due to a lack of CPE will also affect the electron spectrum and dose. Due to this complexity, it is very difficult to establish simple generic models for energy spectra and for energy dependent detector perturbation correction factors [8].

In conventional broad field based reference dosimetry, a simple beam quality specifier is measured which is sufficiently representative and characteristic for the energy spectrum. For heavily filtered beams, $TPR_{20,10}$ is well correlated with the water to air mass collision stopping power ratio, $s_{w,air}$ [1]. For flattening filter free photon beams (such as CyberKnife and TomoTherapy), the relation between $s_{w,air}$ and $TPR_{20,10}$ may be different [9]. For small fields, it is not a priori clear if $TPR_{20,10}$ is sufficiently representative, but evidence from Monte Carlo simulations indicates that the influence of field size on $s_{w,air}$ is limited to 0.3–0.5% at the reference depth of 5 cm in a 6 MV photon beam from 10 cm × 10 cm reference fields down to 0.3 cm × 0.3 cm square fields and 0.3 cm diameter circular fields [7] .

A second concern is that in some units, the conventional 10 cm × 10 cm reference field cannot be established, making it impossible to measure $TPR_{20,10}$ according to its definition. One proposed approach [13] is to measure the dose ratio at 20 cm and 10 cm depth (with constant SDD of 100 cm) in a small field, SF, denoted $TPR_{20,10}$(SF), and correct it for the field size dependence based on generic data from BJR Supplement 25 [15]. For flattening filter free beams, equivalent field sizes must be used accounting for the different amount of phantom scatter given the conical lateral beam profile [14]. In addition, for units such as CyberKnife and TomoTherapy, where the isocentric distance is less than 100 cm, a correction to account for this non-reference distance is required.

2.4. Suitable dosimeters

The ideal detector is point-like, water equivalent and has a linear dose response which is energy and dose-rate independent. Unfortunately, no single detector that performs well on all these criteria yet exists.

Water calorimeters, the most water equivalent dosimeters, have no known energy dependent or dose rate dependent response, but the diffusion of heat away from the measurement point limits the field size down to which it can be used with acceptable accuracy. Water calorimetry has reportedly been successful down to a field size of 5 cm × 5 cm [16]. Graphite calorimeters have less problems with these heat losses since the core (over which the average dose is measured) is thermally isolated from the environment by vacuum gaps. Successful application

of graphite calorimetry in a 3 cm diameter circular field has been demonstrated, albeit in a proton beam [17].

Ionization chambers have a fairly energy independent dose response and can in principle be made very tiny. In practice, however, their lower size is limited by the signal to noise ratio. In addition, for very small chambers, radiation induced stem and cable currents become unacceptably large compared with the signal.

Alanine is close to water equivalent, but due to its rather low sensitivity, the pellets with which acceptable radiotherapy level dosimetry is achieved are usually quite large (typically, 5 mm diameter and 2.5 mm thick) and thus prone to substantial volume averaging. A study in a CyberKnife unit demonstrated that it is possible to obtain accurate values of the volume perturbation correction factors from detailed dose distributions obtained with gel dosimetry [18].

Solid state dosimeters offer better qualities from the viewpoint of size but often exhibit a dose rate or energy dependent dose response. Diamond detectors can be close to water-equivalent but exhibit substantial dose rate dependent recombination effects. A disadvantage of diodes is their energy dependence. At large fields, unshielded diodes over-respond due to the low energy photon component while the perturbations in shielded diodes caused by high-Z sleeves used to filter out these low energy photons are undesirable and difficult to quantify in small fields. Other solid state dosimeters of interest are scintillators, thermoluminescent dosimeters, radioluminescent glass rods and optically stimulated aluminium oxide devices. Radiochromic film has high intrinsic resolution; however, it requires elaborate protocols and commissioning to achieve acceptably accurate reference dosimetry. Liquid ion chambers are close to water-equivalent and small, but also require detailed investigation of substantial recombination corrections. A more extensive overview and discussion of detectors for small field dosimetry is given in Ref. [3].

2.5. Detector size and perturbations

Volume averaging makes many detectors unsuitable for small field dosimetry. The extent to which other perturbations are important depends on the mass density difference of the detector compared to water and the presence of high-Z materials close to the sensitive volume.

Ionization chambers of sufficient sensitivity are in general too voluminous for small fields, and due to the large difference in mass density between air and water, the perturbation of the charged particle fluence due to the presence of the ionization chamber in the absence of CPE can be substantial. Depending on the alignment of the chamber with the central axis of the small field, the perturbation due to changing the mass density in the cavity from that of water to air is of

similar magnitude to the correction for volume averaging, as demonstrated in a Monte Carlo study for PTW 31006 and PTW 31016 PinPoint chambers [19], while other corrections are much smaller in comparison.

Also, solid state detectors exhibit some level of volume averaging, which, given their size, shows up only at the smallest therapeutic fields. Other perturbations may play a role as well, e.g. those due to backscatter at metallic electrodes. For unshielded silicon diodes, Monte Carlo simulations indicate negative corrections of 2–3% for a square field size of 0.5 cm × 0.5 cm [8] and of about 5% for a circular field of 0.5 cm diameter [21].

2.6. Detector energy dependence

The change of the photon spectrum as a function of field size means that detectors exhibiting energy dependent absorbed dose sensitivity will exhibit a field size dependent dose response. For ionization chambers, this is assumed to be minimal, as discussed above [7].

For silicon diodes, the variation of the response with field size is considerable and easily explained since the ratio of mass energy absorption coefficients of silicon over water for photons with energies around 50 keV is a factor eight higher than for 1 MeV photons. In broad photon beams, this results in a dose response linearly increasing with field size due to the increasing low energy photon component from head and phantom scatter. It has been suggested that this linear variation can be extrapolated to smaller field sizes [22] to establish corrections for silicon devices at field sizes below the smallest, where an ionization chamber can be used allowing for the definition of a suitable intermediate calibration field. This model was confirmed by Monte Carlo simulations [20], which also showed, however, the influence of other corrections at the level of 2–3% for field sizes smaller than 1 cm.

For dosimeters such as diamond, radiochromic film, organic scintillators, lithium fluoride thermoluminescent dosimeter and liquid ionization chambers, the energy dependence is assumed to be negligible given the near water equivalence of the materials constituting the sensitive detector volume.

For dosimeters that contain higher-Z elements such as aluminium oxide detectors, glass rods, but also PinPoint chambers with a steel electrode, and to a lesser extent, those with an aluminium electrode, considerations similar to those for silicon diodes apply.

2.7. Intermediate reference field

The possibility of cross-calibrating a suitable dosimeter for small field dosimetry against a reference ionization chamber in an intermediate field was

hinted at in the previous section. The idea is to establish output factors between a conventional reference field and this intermediate field using reference ionization chambers, while for lower field sizes, the cross-calibrated instrument would be used. For some treatment modalities that cannot establish conventional reference conditions, this intermediate field may be the largest achievable at the unit.

The question then arises as to what criteria define a suitable intermediate reference field. One obvious criterion is that the field is not small, i.e. that lateral CPE exists. For all units including CyberKnife, TomoTherapy and even GammaKnife (despite the maximum field diameter of 1.8 cm or 1.6 cm as discussed before), this appears to be feasible. It is then a matter of having a sufficiently small ionization chamber that can serve as a reference instrument. It has been shown that some sufficiently small ionization chambers fulfil this condition [23].

A contradicting criterion is that the size of the intermediate field should be as small as possible so that the variation of the perturbation factor of the cross-calibrated instrument towards smaller field sizes is minimized. The lower limit of the field size is then determined by ensuring that the perturbation corrections for the reference ionization chamber are sufficiently small, which in practice means that it should be well encompassed by a region of lateral CPE.

Evidence that conventional reference ionization chambers can be used in smaller fields without additional corrections comes from a water calorimeter study in which no significant variation of the k_Q for Farmer type chambers down to a field size of 5 cm × 5 cm was observed within the uncertainty on k_Q of 0.3% [16]. This can probably be extrapolated to somewhat smaller fields and even more probably so, for shorter chambers such as the NE2611.

3. PROBLEMS AND PROPOSED SOLUTIONS: COMPOSITE FIELDS

3.1. Dose verification

Verification of IMRT plans is often performed by applying the delivery sequence of the clinical plan to a reference phantom, recalculating the dose distribution of this sequence for the reference phantom and performing absolute and relative dose measurements for comparison with the recalculated dose distribution. This can be field by field for ‘a step and shoot’ or dynamic delivery with fixed beam angles, as a full delivery to a cylindrical or anthropomorphic phantom, or as a collapsed delivery in which the entire sequence is delivered at a single fixed beam angle.

An IMRT dose distribution is by definition inhomogeneous, making accurate dosimetry very difficult, and its in-phantom verification requires a

judicious choice of possible measurement locations and reference detectors. This is exemplary of the huge leap between the static fields used for reference and relative dosimetry, on the one hand, and the way a clinical IMRT treatment is actually delivered, on the other hand. Comparisons are often limited to two dimensional analyses involving a quantitative measure of the differences. It would be desirable to have a possible intermediate reference dosimetry step for a field that at the same time fulfils criteria for a reference field and has a close resemblance to the clinical delivery sequence.

3.2. Concept of dose at a point

Due to the inhomogeneity of IMRT verification plans, the concept of dose at a point becomes difficult to handle, since this quantity will be extremely dependent on the exact location of that point with respect to local gradients. Small detectors lose their suitability for the calibration or dosimetric verification of these fields since the high gradients require them to be positioned with a clinically unreasonable accuracy. In contrast to this, the response of a relatively large detector is much less sensitive to the exact positioning in heterogeneous fields [24].

A Monte Carlo study similar to the one mentioned for small fields [19] demonstrated that volume averaging makes up about half of the perturbation for ionization chambers in IMRT fields [25] and thus contributes substantially to the uncertainty, suggesting that if a mean dose would be specified over the volume of water displaced by the chamber, a gain in accuracy would result. Since the main goal of IMRT is to conform a certain dose level around the planning target volume, it is more relevant and completely natural to specify dose and to calibrate instruments in terms of an average dose over a volume, rather than attempting to quantify an absorbed dose at any individual point. The recommendations in ICRU Report 83 [26] are entirely consistent with this approach.

3.3. Reference field

The need for an intermediate reference dosimetry step for a field that has a close resemblance to the clinical delivery sequence has led to the concept of a PCSR field. It is not possible to define a single reference field that would be relevant for all possible plans. The PCSR field will be machine specific and will depend on the treatment site. The choice of multiple reference conditions for accelerator beams is not new; in fact. it is current practice for electron and light ion beams. The phantom used for calibration should have relevant characteristics for the site, with respect to size and anatomical structure, or other features that have a substantial influence on dose distributions.

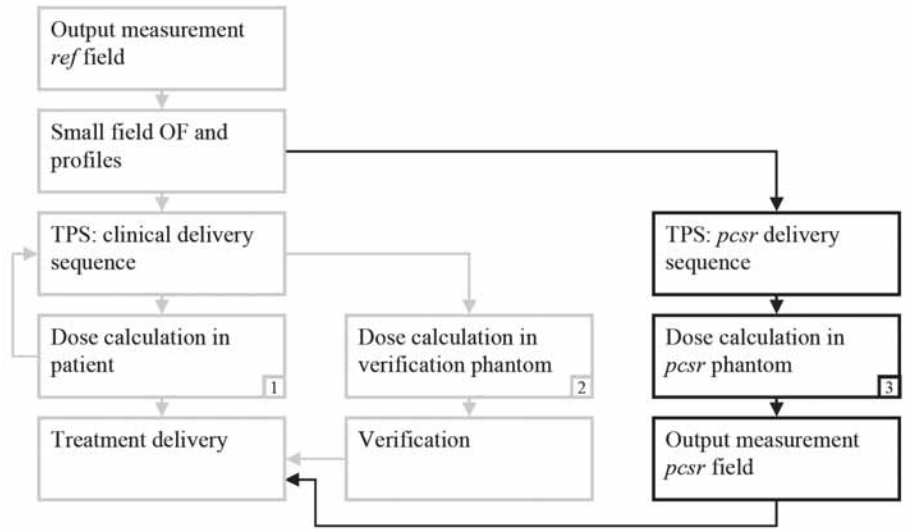

FIG. 1. Schematic diagram of the additional route (shown in black) involving reference dosimetry in a PCSR field. The numbers in the 'dose calculation' boxes are referred to in the text.

The method to obtain a relevant reference plan for a class of clinical deliveries has not been well established and is under active investigation. One criterion proposed is that the PCSR field should have a region with a homogeneous dose distribution well encompassing the volume of the reference ionization chamber. The concept of performing reference dosimetry with a composite delivery as the reference field is not new; it has been used clinically in the TomoTherapy system for a decade, and has, to some extent, obviated the conventional static field calibration [27]. A schematic diagram of the additional route (shown in black) involving reference dosimetry in a PCSR field is shown in Fig. 1.

There is a correlation between what is calculated in route 1 and 3, and thus some aspect of the treatment planning system (TPS) will be calibrated with the PCSR output measurement. An advantage of route 3 is that the dose distribution is homogeneous, contrary to the verification plan in route 2. The challenge of the new route lies in ensuring that the PCSR sequence is representative for the clinical delivery at hand, but at the same time, observing the requirement of dose homogeneity over the detector volume so as to simplify the determination of correction factors for the reference detectors used, as will be discussed in the next section.

3.4. Ionization chamber corrections

A Monte Carlo study [25] showed that the gradient component of the replacement effect is the major contribution to the overall perturbation factor and on average composed of equal contributions from volume averaging and change of density. It was also demonstrated that, since beam quality plays no role in the energy dependence of the correction factors and since an idealized delivery that reconstitutes CPE in a time-averaged sense only differs from the reference field by the gradient effect, the perfect PCSR field should have a correction factor equal to:

$$k_{Q_{pcsr},Q}^{f_{pcsr},f_{ref}} = \frac{1}{P_{gr}^{f_{ref}}} \tag{2}$$

This consideration is only valid under the assumption that the composite fields realize full CPE in a time-averaged sense, and the question remains if this can be established.

Another paper [24] investigated different detectors (diamond detector, liquid ionization chamber, EBT Gafchromic film) to determine PCSR correction factors in an IMRT field for five air-filled chambers, and demonstrated that the correction factor was not different from unity by more than 0.8% for both fully rotated and collapsed deliveries. In general, Farmer type chambers appeared to yield PCSR correction factors in a narrower range than small-volume chambers, and the PCSR correction factor predicted by Eq. (2) was generally higher than the one measured. This was attributed to: (a) the dose distribution of the PCSR field over the region of measurement, not being perfectly uniform, (b) perturbation effects due to MLC, and (c) positioning uncertainties that would more affect small-volume chambers than Farmer type chambers.

It may be surprising that a well-understood effect such as recombination poses problems for composite field dosimetry. A comprehensive study in a TomoTherapy unit [28] considered the spatial and temporal distribution of energy deposition within the cavity by integrating the recombination effects over the length of the ion chamber and over time. It was shown both experimentally and theoretically that the volume recombination in a 1 cm slice helical field is only 55% of that in a 2.5 cm slice helical field for the same accumulated dose in that TomoTherapy unit.

4. FORMALISM

The appropriate formalism for non-standard field dosimetry has been described at length in Ref. [4] and details can be found therein. Essential for its application is the availability of correction factors for the used detectors, both for reference dosimetry and for the determination of field output factors.

For static small fields, correction factors

$$k_{Q_{msr},Q}^{f_{msr},f_{ref}}$$

are needed that correct for the difference between the ion chamber's dose response in an intermediate or machine specific reference field (MSR) and a conventional reference field (as defined in Refs [1]). These can be obtained as ratios of calibration factors in the MSR field and the conventional reference field:

$$k_{Q_{msr},Q}^{f_{msr},f_{ref}} = \frac{N_{D,w,Q_{msr}}}{N_{D,w,Q}} = \frac{D_{w,Q_{msr}}^{f_{msr}}}{D_{w,Q}^{f_{ref}}} \cdot \frac{M_{Q}^{f_{ref}}}{M_{Q_{msr}}^{f_{msr}}} \tag{3}$$

This requires dose to water to be measured by either a primary standard or by a dosimeter that can measure absolute dose with a sufficiently low uncertainty (alanine, radiochromic film, diamond, liquid ion chambers, ferrous sulphate dosimetry, etc.). Alternatively, the correction factor could be calculated by Monte Carlo simulations.

Field output factors are defined as a ratio of doses and can be expressed in terms of a ratio of detector readings as follows:

$$\Omega_{Q_{clin},Q_{msr}}^{f_{clin},f_{msr}} = \frac{D_{w,Q_{clin}}^{f_{clin}}}{D_{w,Q_{msr}}^{f_{msr}}} = \frac{M_{Q_{clin}}^{f_{clin}}}{M_{Q_{msr}}^{f_{msr}}} \cdot \left[\frac{D_{w,Q_{clin}}^{f_{clin}} \Big/ M_{Q_{clin}}^{f_{clin}}}{D_{w,Q_{msr}}^{f_{msr}} \Big/ M_{Q_{msr}}^{f_{msr}}} \right] = \frac{M_{Q_{clin}}^{f_{clin}}}{M_{Q_{msr}}^{f_{msr}}} \cdot k_{Q_{clin},Q_{msr}}^{f_{clin},f_{msr}} \tag{4}$$

Note that a field output factor will require a correction factor and it is thus incorrect to report ratios of readings as output factors. $k_{Q_{clin},Q_{msr}}^{f_{clin},f_{msr}}$ can be determined in exactly the same way as $k_{Q_{msr},Q}^{f_{msr},f_{ref}}$:

$$k_{Q_{clin},Q_{msr}}^{f_{clin},f_{msr}} = \frac{D_{w,Q_{clin}}^{f_{clin}}}{D_{w,Q_{msr}}^{f_{msr}}} \cdot \frac{M_{Q_{msr}}^{f_{msr}}}{M_{Q_{clin}}^{f_{clin}}} \tag{5}$$

Often, only ratios of readings or relative readings (normalized at an MSR field) are reported in which case only relative correction factors can be derived:

$$\frac{k_{Q_{msr},Q}^{f_{msr},f_{ref}}(1)}{k_{Q_{msr},Q}^{f_{msr},f_{ref}}(2)} = \frac{M_{Q}^{f_{ref}}(1)}{M_{Q_{msr}}^{f_{msr}}(1)} \cdot \frac{M_{Q_{msr}}^{f_{msr}}(2)}{M_{Q}^{f_{ref}}(2)} = \frac{M_{rel,Q_{clin}}^{f_{clin}}(2)}{M_{rel,Q_{clin}}^{f_{clin}}(1)} \tag{6}$$

For PCSR fields, the same considerations apply and correction factors can be related with reference to either a conventional reference field or an MSR field:

$$k_{Q_{pcsr},Q}^{f_{pcsr},f_{ref}} = \frac{D_{w,Q_{pcsr}}^{f_{pcsr}}}{D_{w,Q}^{f_{ref}}} \cdot \frac{M_{Q}^{f_{ref}}}{M_{Q_{pcsr}}^{f_{pcsr}}} \text{ or } k_{Q_{pcsr},Q_{msr}}^{f_{pcsr},f_{msr}} = \frac{D_{w,Q_{pcsr}}^{f_{pcsr}}}{D_{w,Q_{msr}}^{f_{msr}}} \cdot \frac{M_{Q_{msr}}^{f_{msr}}}{M_{Q_{pcsr}}^{f_{pcsr}}} \tag{7}$$

Data from the literature analysed according to these equations are reviewed in the next section.

5. DATA FOR SMALL FIELDS

5.1. Machine specific reference fields

Table 1 compiles

$$k_{Q_{msr},Q}^{f_{msr},f_{ref}}$$

values from published data either obtained by direct comparison of ionization chambers against a water calorimeter [16] or by comparison with alanine [18] or radiochromic film [31]. For the results of Refs [18] and [30] the reference field should be regarded as a hypothetical conventional field while for the result from Ref. [31] the assumption that both detectors were consistent in the reference ^{60}Co beam had to be made.

The general observation is that

$$k_{Q_{msr},Q}^{f_{msr},f_{ref}}$$

values are unity within the uncertainties. Concerning the CyberKnife results, it should be noted that a theoretical value of

$$k_{Q_{msr},Q}^{f_{msr},f_{ref}} = 1.01$$

TABLE 1. $k_{Q_{msr},Q}^{f_{msr},f_{ref}}$ VALUES DERIVED FROM PUBLISHED DATA

Ref.	Unit	MSR field	Ref. dosimeter	Chamber(s)	$k_{Q_{msr},Q}^{f_{msr},f_{ref}}$
[16]	Philips SL 75-20	5 cm × 5 cm ($TPR_{20,10}$ = 0.716)	water calorimeter	NE2561 NE2571	0.999 (3) 0.999 (3)
		5 cm × 5 cm ($TPR_{20,10}$ = 0.762)	water calorimeter	NE2561 NE2571	1.000 (3) 1.001 (3)
[18]	CyberKnife	6 cm diameter	alanine	NE2571	0.999 (16)
[29]	TomoTherapy HiArt	5 cm × 10 cm	alanine	NE2611 Exradin A1SL	1.000 (8) 0.996 (8)
[30]	TomoTherapy HiArt	5 cm × 10 cm	alanine	NE2611 NE2571 Exradin A1SL	0.996 (12) 1.013 (14) 0.984 (11)
[31]	GammaKnife	1.8 cm helmet	MD-55 (radiochromic film)	PTW 233642	0.997 (19)

Note: The numbers in brackets represent standard (1SD) uncertainties on the final digit(s).

would be predicted due to volume averaging in the unflattened beam profile [18]. In the data from Ref. [30], the lower value of the Exradin A1SL chamber is consistent with an overestimation of recombination [28], while the value of the NE2571 is consistent with the theoretical prediction mentioned above. For the GammaKnife data from Ref. [31], the 1.8 cm diameter helmet field was considered sufficiently large to serve as an MSR field, making the conventional ^{60}Co calibration coefficient valid with a small additional uncertainty [32]. Other studies have assumed that the

$$k_{Q_{msr},Q}^{f_{msr},f_{ref}}$$

correction factor for the GammaKnife is unity [33].

Monte Carlo calculated results have been reported for TomoTherapy MSR fields using MCNP4C3 [35] and BEAMnrc [36] to calculate k_Q values for a generic graphite-walled Farmer type chamber and for an Exradin A1SL chamber, respectively. For an MSR field of 5 cm × 10 cm at 85 cm SSD with reference to a hypothetical 10 cm × 10 cm reference field with the same beam quality, both studies found correction factors within 0.3% of unity. An EGSnrc Monte Carlo study [37] for full ionization chamber geometries in the same field, reported preliminary results of

$$k_{Q_{msr},Q}^{f_{msr},f_{ref}} = 0.997\ (1),\ 1.000\ (3) \text{ and } 0.996\ (3)$$

for the Exradin A1SL, Exradin A12 and PTW-30013, respectively and those obtained with PENELOPE were consistent with them.

5.2. Field output factors

Out of many examples from the literature, only one is used here as an illustration [18]. This study reported measured ratios of output readings and derived corrected field output factors for circular CyberKnife fields with diameters of 5 mm, 7.5 mm and 10 mm at an SDD of 80 cm. The uncertainties were taken as reported without considering any possible correlations.

Figure 2 shows relative output readings with respect to the 6 cm diameter *msr* field, derived ratios of correction factors with reference to the unshielded diode obtained with Eq. (6), and correction factors obtained using the method in Ref. [38] for ionization chambers and diodes, and using 3-D gel dosimetry to derive volume averaging corrections for the alanine dosimeters. A comparison of the measured and calculated ratios of correction factors indicates that the mutual corrections are adequate. The last pane in Fig. 2 shows, for the smallest field,

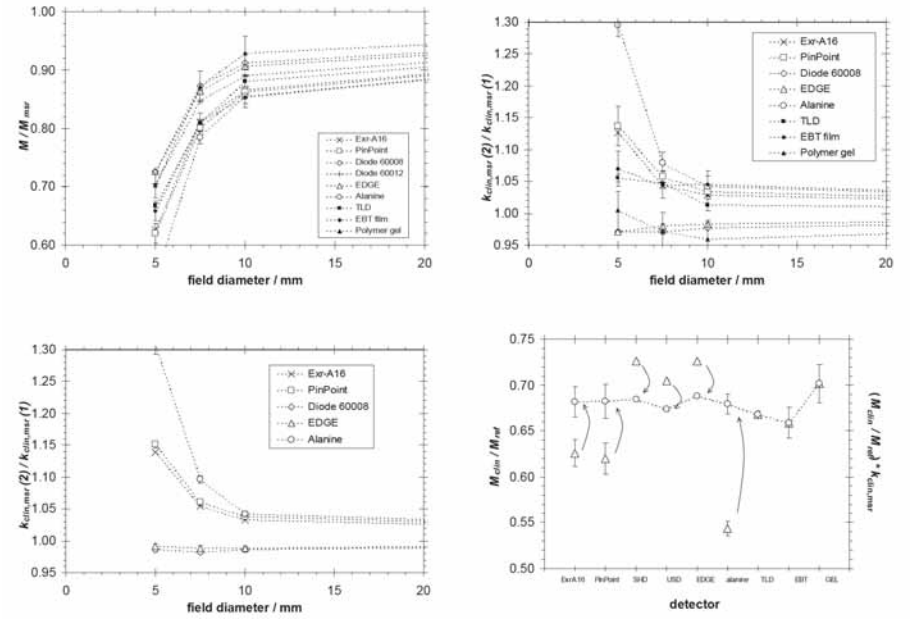

FIG. 2. Data for CyberKnife from Ref. [18]. Upper left: relative output readings (ratio of detector readings in the small field and the 6 cm diameter msr field). Upper right: ratios of relative output readings with respect to the unshielded diode. Lower left: ratios of correction factors as obtained by the method from Ref. [38] or from 3-D gel dosimetry data. Lower right: relative output readings for the 5 mm diameter field (triangles) and derived field output factors (circles).

relative output readings as well as field output factors (obtained by multiplying the relative output readings with the calculated correction factors). The improved consistency between the data after correction is visually obvious, but can also be quantitatively expressed by a statistical chi-square consistency test [39] showing that the set of corrected values form a consistent set.

6. DATA FOR COMPOSITE FIELDS

6.1. Plan class specific reference fields

A limited number of studies on dosimetry for PCSR fields are available. A comparison of NPL's alanine dosimetry with ionization chamber dosimetry in three helical fields delivered to a cylindrical polystyrene phantom by a TomoTherapy unit has been reported [30]. Another reference [24] described a comparison of ionization chambers with diamond, liquid ionization chamber and

radiochromic film as reference instruments for head and neck dynamic IMRT plans at a Varian 6EX unit delivered to a PMMA head and neck phantom. The plans were delivered in both a fully rotated and a collapsed mode. Another study [40] concerned a comparison of ionization chamber dosimetry with NPL's alanine dosimetry for three PCSR fields in a 6 MV Elekta VMAT unit.

Data for the NE2571 were taken as an example since all three studies included this chamber type. All fields were characterized by delivering a homogeneous target dose over a region well encompassing the dimensions of the Farmer. Correlated uncertainties due to the calibration of the batch of alanine pellets were taken out the overall uncertainty for two of the studies [30]. For the former, the reference field was the 10 cm × 5 cm MSR field, since no data in a conventional reference field were reported.

As can be seen from Fig. 3, the data are consistent and indicate a value of

$$k_{Q_{pcsr},Q}^{f_{pcsr},f_{ref}}$$

which is unity within the uncertainties, suggesting that the criterion of sufficiently encompassing the ionization chamber with a homogeneous dose region are

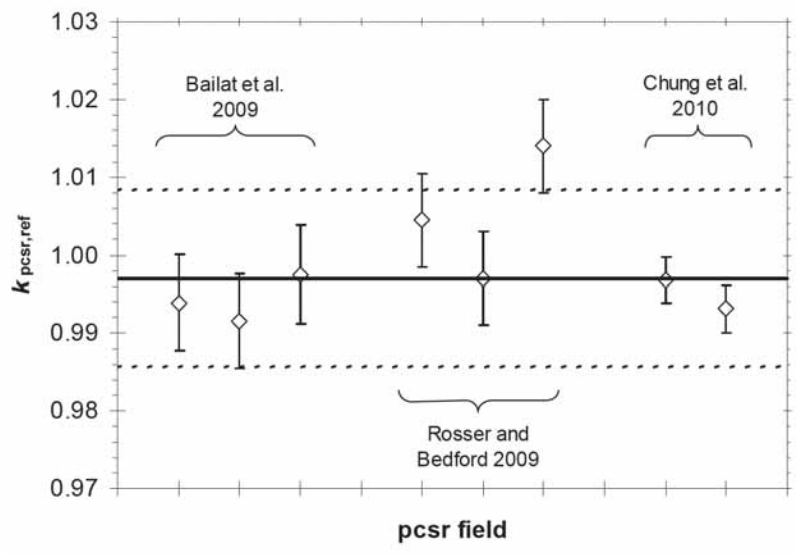

FIG. 3. $k_{Q_{pcsr},Q}^{f_{pcsr},f_{ref}}$ *correction factors measured for the NE2571 chamber in eight PCSR fields at different units and by different methods. The full line represents the weighted mean and the dashed lines define the expanded uncertainty interval (k = 2) based on the weighted variance of the data.*

sufficient for the corrections in the PCSR field to be consistent and negligible, as well as that the conditions for the validity of Eq. (2) are not fulfilled.

ACKNOWLEDGEMENTS

The author acknowledges substantial input and advice on this manuscript from Maria Mania Aspradakis (Cantonal Hospital of Lucerne, Switzerland), and in particular on the sections on composite field dosimetry, from Jan Seuntjens (McGill University, Montreal, Canada) as well as input and discussions over many years with the other members of the IAEA/AAPM Working Group (Rodolfo Alfonso, Pedro Andreo, Roberto Capote, Saiful Huq, Joanna Izewska, Jonas Johansson, Per Kjäll, Warren Kilby, Rock Mackie, Ahmed Meghzifene, Karen Rosser, Ken Shortt and Wolfgang Ullrich), members of the IPEM working party (John Byrne, John Conway, Simon Duane and Jim Warrington) and members of the DIN Small Field Working Group (Gregor Bruggmoser, Dietrich Harder, Harald Feist, Simon Foschepoth, Ralph-Peter Kapsch, Martin Janich, Edmund Schüle, Oliver Dohm, Kai Henkel, Otto Sauer, Björn Poppe, Harald Treuer and Bernhard Rhein) and many others.

REFERENCES

[1] INTERNATIONAL ATOMIC ENERGY AGENCY, Absorbed Dose Determination in External Beam Radiotherapy: An International Code of Practice for Dosimetry Based on Standards of Absorbed Dose to Water, Technical Reports Series No. 398, IAEA, Vienna (2000).

[2] ALMOND, P.R., BIGGS, P.J., COURSEY, B.M., HANSON, W.F., SAIFUL HUQ, M., NATH, R., ROGERS, D.W.O., AAPM's TG-51 protocol for clinical reference dosimetry of high-energy photon and electron beams, Med. Phys. **26** (1999) 1847–70.

[3] ASPRADAKIS, M.M., BYRNE, J.P., PALMANS, H., CONWAY, J., ROSSER, K., WARRINGTON, A.P., DUANE, S., Small field MV photon dosimetry, IPEM Report 103, IPEM, York, UK (2010).

[4] ALFONSO, R., ANDREO, P., CAPOTE, R., SAIFUL HUQ, M., KILBY, W., KJÄLL, P., MACKIE, T.R., PALMANS, H., ROSSER., K., SEUNTJENS, J., ULLRICH, W., VATNITSKY, S., A new formalism for reference dosimetry of small and non-standard fields, Med. Phys. **35** (2008) 5179–5186.

[5] DAS, I.J., DING, G.X., AHNESJÖ, A., Small fields: nonequilibrium radiation dosimetry, Med. Phys. **35** (2008) 206–215.

[6] LI, X.A., SOUBRA, M., SZANTO, J., GERIG, L.H., Lateral electron equilibrium and electron contamination in measurements of head-scatter factors using miniphantoms and brass caps, Med. Phys. **22** (1995) 1167–1170.

[7] EKLUND, K., AHNESJÖ, A., Fast modelling of spectra and stopping-power ratios using differentiated fluence pencil kernels, Phys. Med. Biol. **53** (2008) 4231–4247.
[8] SCOTT, A.J., NAHUM, A.E., FENWICK, J.D., Monte Carlo modeling of small photon fields: quantifying the impact of focal spot size on source occlusion and output factors, and exploring miniphantom design for small-field measurements, Med. Phys. **36** (2009) 3132–3144.
[9] XIONG, G., ROGERS, D.W.O., Relationship between $\%dd(10)_x$ and stopping-power ratios for flattening filter free accelerators: a Monte Carlo study, Med. Phys. **35** (2008) 2104–2109.
[10] SANCHEZ-DOBLADO, F., ANDREO, P., CAPOTE, R., LEAL, A., PERUCHA, M., ARRANS, R., NUNEZ, L., MAINEGRA, E., LAGARES, J.I.,CARRASCO, E., Ionization chamber dosimetry of small photon fields: a Monte Carlo study on stopping-power ratios for radiosurgery and IMRT beams, Phys. Med. Biol. **48** (2003) 2081–2099.
[11] ARAKI, F., Monte Carlo study of a Cyberknife stereotactic radiosurgery system, Med. Phys. **33** (2006) 2955–2963.
[12] KAWACHI, T., SAITOH, H., INOUE, M., KATAYOSE, T., MYOJOYAMA, A., HATANO, K., Reference dosimetry condition and beam quality correction factor for CyberKnife beam, Med. Phys. **35** (2008) 4591–4598.
[13] SHARMA, S.C., OTT, J.T., WILLIAMS, J.B., DICKOW, D., Commissioning and acceptance testing of a CyberKnife linear accelerator, J. Appl. Clin. Med. Phys. **8** (2007) 119–125.
[14] SAUER, O., Determination of the quality index (Q) for photon beams at arbitrary field sizes, Med. Phys. **36** (2009) 4168–4172.
[15] BRITISH JOURNAL OF RADIOLOGY, Central Axis Depth Dose Data for Use in Radiotherapy, Br. J. Radiol. Suppl. **25** (1996).
[16] KRAUSS, A., KAPSCH, R.-P., Calorimetric determination of k_Q factors for NE 2561 and NE 2571 ionization chambers in 5 cm × 5 cm and 10 cm × 10 cm radiotherapy beams of 8 MV and 16 MV photons, Phys. Med. Biol. **52** (2007) 6243–59.
[17] PALMANS, H., THOMAS, R., SIMON, M., DUANE, S., KACPEREK, A., DUSAUTOY, A.,VERHAEGEN, F., A small-body portable graphite calorimeter for dosimetry in low-energy clinical proton beams, Phys. Med. Biol. **49** (2004) 3737–3749.
[18] PANTELIS, E., MOUTSATSOS, A., ZOURARI, K., KILBY, W., ANTYPAS, C., PAPAGIANNIS, P., KARAISKOS, P., GEORGIOU, E., SAKELLIOU, L., On the implementation of a recently proposed dosimetric formalism to a robotic radiosurgery system, Med. Phys. **37** (2010) 2369–79.
[19] CROP, F., REYNAERT, N., PITTOMVILS, G., PAELINCK, L., DE WAGTER, C., VAKAET, L.,THIERENS, H., The influence of small field sizes, penumbra, spot size and measurement depth on perturbation factors for microionization chambers, Phys. Med. Biol. **54** (2009) 2951–2969.
[20] EKLUND, K., Modeling silicon diode dose response in radiotherapy fields using fluence pencil kernels, PhD Thesis, Uppsala University, Sweden (2010).
[21] FRANCESCON, P., CORA, S., CAVEDON, C. Total scatter factors of small beams: a multidetector and Monte Carlo study, Med. Phys. **35** (2008) 504–513.
[22] SAUER, O.A.,WILBERT, J., Measurement of output factors for small photon beams, Med. Phys. **34** (2007)1983–1988.

[23] McEWEN, M. R., Measurement of ionization chamber absorbed dose kQ factors in megavoltage photon beams, Med. Phys. **37** (2010) 2179–2193.
[24] CHUNG, E., BOUCHARD, H., SEUNTJENS, J., Investigation of three radiation detectors for accurate 2404-2413 measurement of absorbed dose in nonstandard fields, Med. Phys. **37** (2010).
[25] BOUCHARD, H., SEUNTJENS, J., CARRIER, J.-F., KAWRAKOW, I., Ionization chamber gradient effects in nonstandard beam configurations, Med. Phys. **36** (2009) 4654–4663.
[26] ICRU, Report 83: Prescribing, Recording, and Reporting Photon-Beam Intensity-Modulated Radiation Therapy (IMRT), Journal of the ICRU **10** (2010).
[27] LANGEN, K.M., PAPANIKOLAOU, N., BALOG, J., FOLLOWILL, D., GODDU, S.M., GRANT III, W., OLIVERA, G., RAMSEY, C.R., SHI, C., QA for helical tomotherapy: Report of the AAPM Task Group 148, Med. Phys. **37** (2010) 4817–4853.
[28] PALMANS, H., THOMAS, R.A.S., DUANE, S., STERPIN, E., VYNCKIER, S., Ion recombination for ionisation chamber dosimetry in a tomotherapy unit, Med. Phys. **37**: (2010) 2876–2889.
[29] DUANE, S., NICHOLAS, D., PALMANS, H., SCHAEKEN, B., SEPHTON, J., SHARPE, P., THOMAS, R., TOMSEJ, M., VERELLEN, D., VYNCKIER, S., Dosimetry audit for Tomotherapy using alanine/EPR, Med. Phys. **33** (2006) 2093–2094.
[30] BAILAT, C.J., BUCHILLIER, T., PACHOUD, M., MOECKLI, R., BOCHUD, F.O., An absolute dose determination of helical tomotherapy accelerator, TomoTherapy High-Art II, Med. Phys. **36** (2009) 3891–3896.
[31] SOMIGLIANA, A., CATTANEO, G.M., FIORINO, C., BORELLI, S., DEL VECCHIO, A., ZONCA, G., PIGNOLI, E., LOI, G., CALANDRINO, R., MARCHESINI, R., Dosimetry of Gamma Knife and linac-based radiosurgery using radiochromic and diode detectors, Phys. Med. Biol. **44**: (1999) 887–897.
[32] MELTSNER, S.G., DEWERD, L.A., Air kerma based dosimetry calibration for the Leksell Gamma Knife, Med Phys. **36** (2009) 339–350.
[33] DRZYMALA, R.E., WOOD, R.C., LEVY, J., Calibration of the Gamma Knife using a new phantom following the AAPM TG51 and TG21 protocols, Med. Phys. **35** (2008) 514–521.
[34] PERKS, J., GAO, M., SMITH, V., SKUBIC, S., GOETSCH, S., Glass rod detectors for small field, stereotactic radiosurgery dosimetric audit, Med. Phys. **32** (2005)726–732.
[35] JERAJ, R., MACKIE, T.R., BALOG, J., OLIVERA, G., Dose calibration of non-conventional treatment systems applied to helical tomotherapy, Med. Phys. 32: (2005) 570–577.
[36] THOMAS, S.D., MACKENZIE, M., ROGERS, D.W.O., FALLONE, B.G., A Monte Carlo derived TG-51 equivalent calibration for helical tomotherapy, Med. Phys. **32** (2005) 1346–1353.
[37] STERPIN, E., MACKIE, T., LU, W., OLIVERA, G., VYNCKIER, S., Full Monte Carlo computation of K correction factors calculated in tomotherapy static and helical deliveries for future ion chamber reference dosimetry protocols of non standard beams, Med. Phys. **36** (2009) 2615–2616.
[38] FRANCESCON, P., CORA, S., CAVEDON, C., Total scatter factors of small beams: A multidetector and Monte Carlo study, Med. Phys. 35 (2008) 504–513.

[39] COX, M.G., The evaluation of key comparison data: determining the largest consistent subset, Metrologia **44** (2007) 187–200.

[40] ROSSER, K.E., BEDFORD, J.L., Application of a new dosimetry formalism to volumetric modulated arc therapy (VMAT), Phys. Med. Biol. **54**: (2009) 7045–7061.

MEASUREMENT CORRECTIONS FOR OUTPUT FACTOR MEASUREMENTS OF SMALL ROBOTIC RADIOSURGERY BEAMS FORMED BY A VARIABLE APERTURE COLLIMATOR

P. FRANCESCON*, W. KILBY**, N. SATARIANO*, S. CORA*

* Medical Physics Department, Vicenza Hosiptal,
Vicenza, Italy
Email: paolo.francescon@ulssvicenza.it

** Accuray Incorporated, Sunnyvale, California,
United States of America

Abstract

Monte Carlo (MC) detector simulations and measurements have been used to investigate the corrections needed for small field output factor measurements with the IRIS collimator on a CyberKnife System for a range of detectors. These corrections are found to be larger than 2.5% for all detectors at the smallest (5 mm) field size and to follow similar trends as those observed previously for fixed collimators on this treatment device. The correction factors for microchambers (Exradin A16 and PTW PinPoint 31014) ranged from 1.102 at 5 mm to 1.006 at 12.5 mm field sizes. The correction factors for diode detectors (PTW 60012 and Sun Nuclear Edge Detector) varied between 0.958 and 0.991 over the same field size range, and for a liquid filled ionization chamber (PTW microLion), the correction factor variation was 1.027–0.993. Before correction, measured output factors differed by up to 15% at 5 mm field size, which reduced to a maximum inter-detector variation of 3% after corrections were applied. The agreement of measured output factors to those calculated directly by MC simulation of dose to water was also improved after corrections were applied. In conclusion, these results support the use of measurement correction factors for small field output factor commissioning and QA. The correction factor dataset presented here can be used to apply this method to the IRIS Collimator on the CyberKnife System.

1. INTRODUCTION

The Alfonso et al. proposed dosimetry formalism for small and non-standard fields includes the application of a correction factor to measured output factors to remove the influence of detector size and composition on the measurement result [1]. The CyberKnife® Robotic Radiosurgey System (Accuray Incorporated, Sunnyvale, USA) uses a 6 MV X ray beam and a set of

12 cylindrical secondary collimators to produce circular treatment fields ranging from 5 mm to 60 mm diameter at a nominal 800 mm treatment distance from the X ray focus [2]. Francescon et al. have previously investigated the corrections that should be applied to output factor measurements for the smallest of these collimators [3–5]. Their correction method is consistent with the Alfonso et al. formalism [1]. Specifically, when the machine specific reference (MSR) field is defined by the 60 mm collimator then the correction factors F_{corr} presented by Francescon et al. are equivalent to the

$$k_{Q_{clin},Q_{msr}}^{f_{clin},f_{msr}}$$

factors in the Alfonso et al. formalism. The results show that corrections of approximately 10% are required for small volume (0.007−0.015 cm^3) ionization chambers, and 4−10% for solid state (diode, diamond, and MOSFET) detectors with the 5 mm collimator. The correction factors approach unity with increasing field size but remain up to 3% for the 10 mm collimator. These factors have been independently verified by comparison with output factors measured using alanine dosimeters corrected for volume averaging [6].

Subsequent changes made to the CyberKnife System may alter these corrections. Most significantly, the IRIS™ Variable Aperture Collimator (Accuray Inc.) was introduced. This achieves the same set of field sizes as fixed collimators, but uses a very different mechanical design (e.g. it has a total collimator thickness of 120 mm in comparison to 70–87 mm for fixed collimators, and forms a 12-sided polygonal beam shape rather than a true circle) [7]. Changes have also been made to the linac target and beam filtration. In addition, new detectors have become commercially available that might be better optimized for small field dosimetry. The microLion liquid filled ionization chamber (PTW-Freiburg, Germany) provides a higher spatial resolution than air-filled chambers, without the disadvantage of high atomic number materials associated with small diode detectors. The purpose of this work was to investigate the

$$k_{Q_{clin},Q_{msr}}^{f_{clin},f_{msr}}$$

factors for small fields produced by the IRIS Collimator on the latest CyberKnife System using small volume ionization chambers, diode detectors and a liquid filled ionization chamber. These correction factors were verified by inter-comparison of measured output factors before and after correction, and by comparison with Monte Carlo (MC) calculated output factors.

2. METHODS AND MATERIALS

2.1. MC simulation

The CyberKnife treatment head including the IRIS collimator has been simulated according to manufacturer specifications using BEAMnrc as a particle source for the EGS_chamber (Fig. 1). Directional Bremsstrahlung Splitting and range rejection variance reduction methods were used. The splitting field was equal to the radiation with a margin of 5 cm to take into account possible scattering from this margin toward the field axis. Range rejection was applied to electrons with energy less than 1MeV.

In order to optimize the electron beam model parameters, the EGS_chamber code was used to simulate dose profiles obtained with the PTW 60012 diode, and both output factors and tissue-phantom ratios (TPR) obtained with the PTW 31014 PinPoint microchamber, PTW 60012, PTW microLion chamber and Sun Nuclear Edge detector. Each dosimeter was simulated according to manufacturer specifications using EGS4 with cut-off energies AE = 521 keV and AP = 1 keV. These simulations took advantage of the Intermediate Phase Space Storage (IPSS) volume, a user-defined volume containing the positions of the detector along the profile or, in the case of output

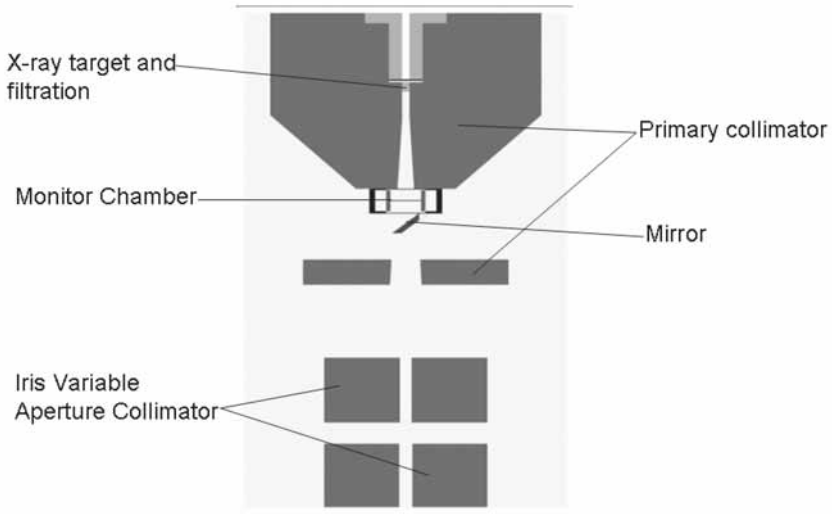

FIG. 1. MC simulation model of the CyberKnife treatment head. The IRIS collimator was modelled as two hexagonal blocks, rotated by 30° with respect to each other, with variable face-to-face aperture size for the upper and lower banks to mimic the divergent opening of the actual collimator [7].

factors, a volume that contains the detector on the beam axis. The simulation starts in the geometry outside the IPSS and stops at its surface where the particle phase space is stored. Then, this phase space is used to start the simulation for each position of the detector inside the IPSS. As the state of the number generator is also stored in the IPSS, there is maximum correlation between the calculated doses. An XCSE volume surrounding the IPSS was also defined, inside which the photon cross-section enhancement variance reduction technique was applied. In these simulations, the margin between XCSE and IPSS was approximately 10 mm on the upper side, 5 mm laterally and zero below. The enhancement factor was 512. The energy and the width of the electron beam source were determined in a trial-and-error procedure until the simulated profiles, output factors and TPR matched measured data obtained using the same detectors as those simulated.

The correction factors

$$k^{f_{clin},f_{msr}}_{Q_{clin},Q_{msr}}$$

were determined with IRIS collimator fields 5, 7.5, 10, 12.5, 15, 25 and 60 mm diameter using the relationship [1];

$$k^{f_{clin},f_{msr}}_{Q_{clin},Q_{msr}} = \frac{\left(\frac{D^{f_{clin}}_{w,Q_{clin}}}{M^{f_{clin}}_{Q_{clin}}} \right)}{\left(\frac{D^{f_{msr}}_{w,Q_{msr}}}{M^{f_{msr}}_{Q_{msr}}} \right)} \quad (1)$$

MC simulations generated the four terms on the right hand side of equation (1). The dose to water terms, D_w, were calculated as the absorbed dose in a small volume of water (0.5 cm^3) on the beam central axis, and the measurement terms, M, as the absorbed dose to water deposited within each detector geometry. The machine specific references (MSR) field was the 60 mm fixed collimator. Correction factors were calculated for electron energies 6.5, 7.0 and 7.5 MeV and for electron beam FWHM 1.6, 1.9, 2.2 and 2.5 mm, at 15 mm depth and 800 mm source–detector distance (SDD). Calculations were performed for all of the detectors listed previously, plus the Exradin A16 microchamber.

2.2. Experimental Measurements

Output factors were measured for the 5, 7.5, 10, 12.5, 15, 20 and 60 mm diameter IRIS collimator fields using all of the detectors listed previously except

the Exradin A16. All measurements were performed with the effective point of measurement placed at 15 mm or 100 mm depth and 800 mm SDD, using a scanning water phantom. Orthogonal beam profiles were acquired to align each detector with the beam central axis. Measurements were performed using both bias voltage polarities for each microchamber and averaged. The power supply for the PTW MicroLion chamber was found to be faulty during this experiment. Measurements with this detector were performed using a bias voltage of ±400 V (the maximum possible) rather than the vendor recommended ±800 V.

Uncorrected output factors were defined by the ratio of detector reading at each field size to the 60 mm IRIS collimator field. Strictly, each of these measured output factors should be multiplied by the ratio of detector reading with the 60 mm IRIS collimator field to the 60 mm fixed collimator field in order to be correctly normalized to the MSR field. Review of site commissioning data obtained with 24 CyberKnife systems installed with IRIS collimators between November 2008 and March 2010 shows that this ratio is 0.998 ± 0.002 (measurements mostly using PTW 60012 diode or Sun Nuclear Edge detector), which is consistent with the observation that, for field sizes larger than 7.5 mm, the IRIS collimator output factors are not substantially different from fixed collimator output factors [7]. Therefore, this correction ratio was assumed to be unity.

The components of measurement uncertainty were estimated as follows:

(a) Measurement reproducibility due to detector and monitor chamber sensitivity variations was assessed by repeating a measurement five times, without adjusting the collimator aperture or detector position.
(b) The effect of aperture reproducibility was assessed by repeating a measurement ten times, opening and then closing the collimator aperture to the desired nominal setting between each measurement. The detector was not moved. Each of these ten aperture specific measurements was taken as the mean of five repeated measurements, as described in (a) above.
(c) The effect of detector positioning accuracy was assessed by MC simulation, assuming a rectangular probability distribution for positioning error of ±0.5 mm about the central axis in both x and y.

All of these uncertainty estimates were performed using the 60012 diode.

3. RESULTS

Figures 2 and 3 compare measured and MC simulated beam profiles. Together with a comparison between uncorrected measured output factors and

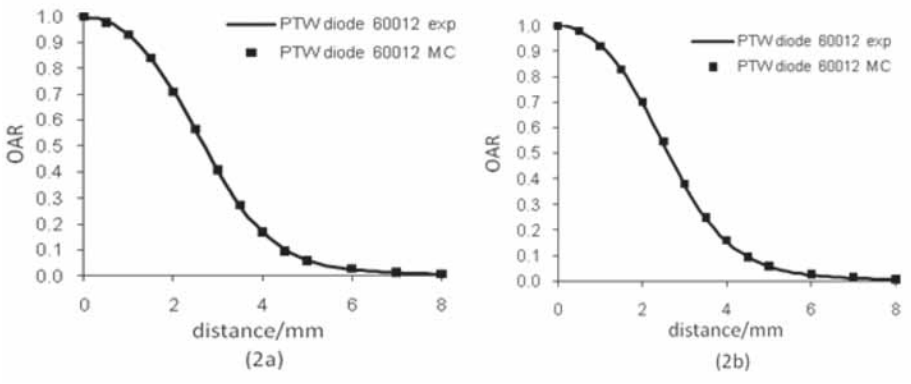

FIG. 2. Comparison of MC simulated and measured off-axis ratio (OAR) beam profiles, using a 60012 diode for the 5 mm diameter IRIS collimator field at 800 mm SDD. Profiles are shown in orthogonal X (a) and Y (b) directions. The MC results were generated using the optimized model parameters E = 7.0 MeV and FWHM = 2.2 mm (X) and 2.0 mm (Y).

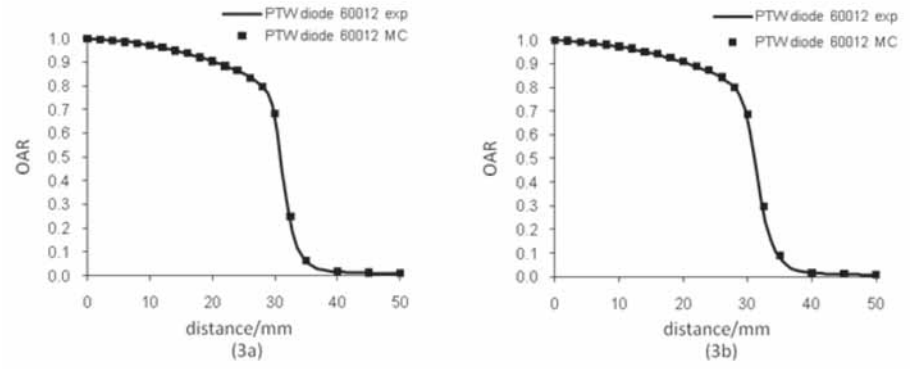

FIG. 3. Comparison of MC simulated and measured off-axis ratio beam profiles, using a 60012 diode for the 60mm diameter IRIS collimator field at 800 mm SDD. Profiles are shown in orthogonal X (a) and Y (b) directions. The MC results were generated using the optimized model parameters E = 7.0 MeV and FWHM = 2.2 mm (X) and 2.0 mm (Y).

MC simulations of the same measurements, these results were used to optimize the MC treatment head model. Parameters giving optimal agreement between calculation and measurement were E = 7.0 MeV and FWHM = 2.1 mm (2.2 mm in X, 2.0 mm in Y), which is consistent with simulations of the previous CyberKnife linac design [3]. With these parameters, the output factor comparisons at depths 15 mm and 100 mm gave a mean agreement of

0.7% ± 1.3%, and the TPR (d = 100 mm) comparisons gave a mean agreement of –0.6% ± 1.1%, expressed relative to local dose.

Table 1 shows the calculated

$$k_{Q_{clin},Q_{msr}}^{f_{clin},f_{msr}}$$

factors at 15 mm depth as a function of nominal IRIS collimator field size and electron beam FWHM. The random uncertainty in each value is ±0.2−0.3%. An average correction factor is stated for all FWHM when the maximum variation between correction factors is not statistically significant. It can be seen that the correction factors are independent of FWHM at all field sizes for diode detectors, and at larger field sizes for microchambers. At small field sizes (≤10–15 mm), the microchamber results exhibit significant variation with FWHM but this variation is without any clear pattern. The correction factor variation with electron beam energy in the range 6.5–7.5 MeV was typically ±0.2–0.3% of the mean correction factor. This was not considered to be significant, and therefore only the results at E = 7.0 MeV are presented. Table 2 shows the

$$k_{Q_{clin},Q_{msr}}^{f_{clin},f_{msr}}$$

correction factors at 15 mm depth calculated at optimum E = 7.0 MeV and FWHM = 2.1 mm (obtained by linear interpolation of the results at 1.9 mm and 2.2 mm FWHM when these are shown separately in Table 1), including the 20 mm field size, which is calculated by linear interpolation of the results for 15 mm and 25 mm fields.

Figure 4(A) shows uncorrected measured output factors at 15 mm depth. The maximum inter-detector variation was 15% for the 5 mm field size. Figure 4(B) shows the same data after correction using the

$$k_{Q_{clin},Q_{msr}}^{f_{clin},f_{msr}}$$

factors in Table 2. The maximum inter-detector variation was reduced to 3% at the 5 mm field size. The figures also include output factors directly calculated by MC simulation of the dose delivered to a small water volume on the central axis with the optimum model parameters (E = 7.0 MeV, FWHM = 2.1 mm. The estimated measurement uncertainties are reported in Table 3.

TABLE 1. $k_{Q_{clin},Q_{msr}}^{f_{clin},f_{msr}}$ FACTORS AT D = 15 mm AS A FUNCTION OF NOMINAL IRIS COLLIMATOR FIELD SIZE AND ELECTRON BEAM FWHM, CALCULATED AT E = 7.0 MEV

	$k_{Q_{clin},Q_{msr}}^{f_{clin},f_{msr}}$						
FWHM (mm)	5 mm	7.5 mm	10 mm	12.5 mm	15 mm	25mm	60 mm
			Edge				
1.6−2.5	0.958	0.969	0.977	0.985	0.993	1.003	1.001
			60012				
1.6−2.5	0.958	0.970	0.982	0.991	0.995	1.000	1.000
			microLion				
1.6	1.024	0.992	0.993	0.993	0.996	0.998	0.999
1.9	1.029	0.998	0.993				
2.2	1.026	1.003	0.999				
2.5	1.020	1.006	0.993				
			31014				
1.6	1.103	1.031	1.014	1.002	1.003	0.999	0.998
1.9	1.106	1.038	1.015	1.009			
2.2	1.100	1.047	1.007	1.004			
2.5	1.093	1.050	1.017	1.010			
			A16				
1.6	1.097	1.027	1.014	1.005	1.004	1.005	1.000
1.9	1.100	1.034	1.013	1.009	1.001		
2.2	1.093	1.042	1.007	1.005	1.004		
2.5	1.090	1.051	1.020	1.012	1.011		

TABLE 2. $k_{Q_{clin},Q_{msr}}^{f_{clin},f_{msr}}$ FACTORS AT D = 15 mm FOR THE SIX SMALLEST IRIS COLLIMATOR FIELD SIZES, CALCULATED AT THE OPTIMUM E = 7.0 MeV and FWHM = 2.1 mm

	$k_{Q_{clin},Q_{msr}}^{f_{clin},f_{msr}}$					
	5 mm	7.5 mm	10 mm	12.5 mm mm	15 mm	20 mm
Edge	0.958	0.969	0.977	0.985	0.993	0.998
60012	0.958	0.970	0.982	0.991	0.995	0.998
microLion	1.027	1.001	0.997	0.993	0.996	0.997
31014	1.102	1.044	1.010	1.006	1.003	1.001
A16	1.095	1.039	1.009	1.006	1.003	1.004

TABLE 3. MEASUREMENT UNCERTAINTIES FOR MEASUREMENTS PERFORMED USING A 60012 DIODE (*expressed as 1σ*)

Source of uncertainty	Field size (mm)		
	5	7.5	60
Detector reproducibility	0.03%	0.03%	0.03%
Aperture reproducibility	0.39%	0.26%	na
Positioning accuracy	1.09%	0.75%	na
Total uncertainty	1.16%	0.79%	0.03%

4. DISCUSSION

The correction factors (Tables 1 and 2) are substantial for the smallest fields, at over 2.5% at 5 mm field size for every detector studied. Diode corrections are <1, and air filled microchamber corrections are >1, which is consistent with the results for fixed collimators and the previous CyberKnife linac design [3] . In comparison with this previous work, the IRIS collimator factors are generally within 1.0% of those calculated for the corresponding fixed collimator field size, which indicates that differences between the two linac

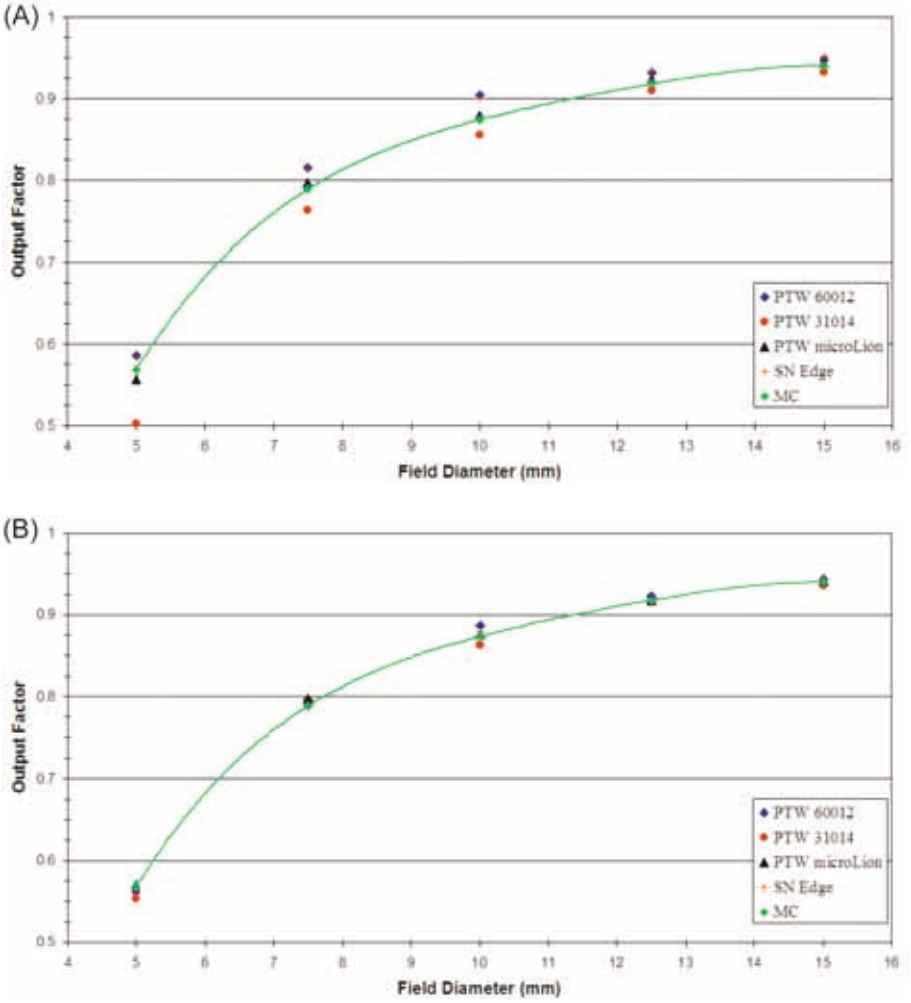

FIG. 4. Comparison of IRIS collimator output factors measured with multiple detectors and calculated by MC simulation. A 4th order polynomial is fitted to the MC data for illustration only. Output factors are shown (A) before application of correction factors and (B) after application of the correction factors given in Table 2.

designs and the iris vs. fixed collimator design have little impact on detector response. This is particularly interesting for the smallest field sizes, where the IRIS collimator output factors themselves are substantially lower than the equivalent fixed collimators (e.g. 0.57 versus 0.71 at 5 mm for IRIS and fixed, respectively [7]).

In comparison with MC calculated output factors, the diode measurements overestimated and the air filled microchambers underestimated (Fig. 4(A)). This trend is consistent with multiple previous results and is discussed in more detail elsewhere (e.g. Ref. [6]). The liquid filled microchamber measurements were consistently between the diode and air filled chamber results, and closest to the MC calculated output factor before corrections were applied. In this respect, the liquid filled chamber is closest to an ideal detector found in this study. However, there are disadvantages to this detector including relatively high cost (including the additional power supply) and the lack of long term stability data for this relatively new design. It should be recalled that the microLion measurements in this study were made at ±400 V, rather than the manufacturer recommended ±800 V, and further measurements will be required to verify the detector performance at ±800 V. The residual differences between measured output factors after correction are determined mainly by the unceratinty in positioning the dosimeter at the centre of the field and by the variation in aperture setting between measurements, as shown in Table 3. (These results are specific to a diode detector design, with an ion chamber the uncertainties might be different.) The physical aperture reproducibility achieved with the IRIS collimator is ≤0.1 mm [7]. Ideally, multiple measurements should be averaged with the aperture resized between measurements in order to obtain an output factor estimate for each mean aperture setting as specified in the vendor commissioning instructions; however, that was not done in this study. Further measurements incorporating this method would improve the accuracy of the results presented in Fig. 4.

A question raised by this study is whether small field output factors generated directly by MC simulation should be used rather than corrected measurements in order to avoid the complex measurement procedure and resulting uncertainties. This approach requires the use of a standard MC output factor data set to be applied to multiple systems, such as that calculated in this study. However, variations in accelerator settings (e.g. electron beam focusing and steering currents) can modify the electron beam properties in the MC model. In this study, MC calculated output factors were significantly more sensitive to these variations than MC calculated correction factors. For example, the variation in MC output factor at 5 mm field size between 1.9 mm FWHM and 2.2 mm FWHM was 9% compared with a maximum variation of just 0.6% in correction factors (Table 1), which reduces to an insignificant variation for diode detectors. For this reason, the use of corrected measurements should allow a more accurate assessment of the small field output factors on any specific treatment unit than is possible using standard MC output factors, although very careful measurement technique is required particularly to align the detector with the beam centre.

In conclusion, the correction factor magnitude (Table 2) and the improvement after correction factors are applied in both the inter-detector

agreement, and measurement agreement with MC output factors (Fig. 4) support the recommendation to apply correction factors for output factor commissioning and QA. The correction factor data set presented here can be used to apply this method to the IRIS collimator on the CyberKnife System.

ACKNOWLEDGEMENTS

The authors gratefully acknowledge the assistance of Mu Young Lee, A. Purwar and M. Nikolic of Accuray Inc., with the experimental measurements. The authors are also grateful to PTW-Frieburg for the loan of the microLion detector. This work was funded by a research grant from Accuray Inc.

REFERENCES

[1] ALFONSO, R., et al., A new formalism for reference dosimetry of small and nonstandard fields, Med. Phys. **35** (2008) 5179–5186.

[2] KILBY, W., et al., The CyberKnife Robotic Radiosurgery System in 2010, Technol. Cancer Res. Treat. **9** (2010) 433–452

[3] FRANCESCON, P., et al., Total scatter factors of small beams: a multidetector and Monte Carlo study, Med Phys **35** (2008) 504–513.

[4] FRANCESCON, P., et al., Application of a Monte Carlo-based method for total scatter factors of small beams to new solid state micro-detectors, J. Appl. Clin. Med. Phys. **10** (2009) 147–152.

[5] FRANCESCON, P., et al., Erratum: Total scatter factors of small beams: A multidetector and Monte Carlo study, Med Phys 35, (2008) 504–513, Med. Phys. **37** (2010) 947.

[6] PANTELIS, E., et al., On the implementation of a recently proposed dosimetric formalism to a robotic radiosurgery system, Med. Phys. **37** (2010) 2369–2379.

[7] ECHNER, G.G., et al., The design, physical properties and clinical utility of an iris collimator for robotic radiosurgery, Phys. Med. Biol. **54** (2009) 5359–5380.

CONCEPTUAL IMPROVEMENTS AND LIMITATIONS IN NON-STANDARD BEAM REFERENCE DOSIMETRY

H. BOUCHARD*,** I. KAWRAKOW***,[1], J.-F. CARRIER*,**, J. SEUNTJENS[+]

* Département de Physique, Université de Montréal, Montréal, Québec

** Département de Radio-Oncologie, Centre Hospitalier de l'Université de Montréal, Montréal, Québec

*** National Research Council of Canada, Ottawa, Ontario

[+] Medical Physics Unit, Montreal General Hospital, McGill University, Montreal, Québec

Canada

Abstract

During the past decade, advances in technology have considerably transformed radiation therapy treatment techniques. New treatment modalities improve target dose conformity compared to conventional methods, but increase the complexity of dosimetry procedures because deliveries are composed of treatment fields using a combination of small fields. The complexities of reference dosimetry of deliveries involving non-standard beams have triggered efforts by the IAEA and AAPM towards the development of a new protocol applicable to these beams. This paper summarizes three studies in the scope of the development of the new protocol. The first part of the paper concerns the fundamentals of non-standard beam dosimetry, developing theoretical aspects and summarizing a study of ionization chamber perturbation factors in modulated beams. Conceptual solutions are proposed and a theoretical expression of correction factors is obtained for ideal non-standard reference fields (PCSR). Limitations in the calculation of the correction factors are discussed. A second part of the paper discusses the improvement in k_Q experimental measurements in regard to direct absorbed dose to water measurements. Levels of uncertainty of the order of 0.3% are achieved with

[1] Present address: OCS Siemens AG, Hans-Bunte Strasse 10, 69123 Heidelberg, Germany.

radiochromic film and show great potential in non-standard beam dosimetry. A third aspect of the paper represents experimental uncertainties to also be considered. A method of evaluation of uncertainties induced by positioning errors is summarized. Results suggest that experimental uncertainties in non-standard beam can be higher than for standard conditions. This is an important issue to consider both during daily QA routine and reference dosimetry, and could be a limiting factor in the new generation of protocols.

1. INTRODUCTION

For the past 50 years, protocols have addressed the determination of absorbed dose in radiation beams using ionization chambers in specific conditions. These conditions, known as reference conditions, allow for accurate conversion of charge produced in the chamber volume by the ionizing radiation to absorbed dose to water. The accuracy of ionization chamber dose measurements has evolved considerably from general chamber independent approaches [1–9] to chamber-specific formalisms [10–12]. Using current absorbed dose to water based protocols [13, 14], an uncertainty level below 1% can be achieved on clinical reference dosimetry [15]. The current protocols consider measurement conditions where the quality-specific calibration coefficient is known, allowing to report absorbed dose to a point in water.

During the last decade, the use of novel non-standard beams, defined as beams involving small fields or modulated fields, became the delivery method of choice to improve target dose conformity as compared to conventional three-dimensional conformal radiation therapy (3-D CRT) techniques. As recent studies demonstrated the invalidity of absorbed dose to water based protocols [13,14] to non-standard beams [16,17], a new workgroup of the IAEA, endorsed by the AAPM, published a formalism [18] in preparation of a new protocol applicable to non-standard beams. The proposed method is a generalization of the absorbed dose to water approach to any beam quality and involves a series of beams, hence beam-specific chamber calibration coefficients ($N_{D,w}^{Q}$). The calibration of clinical beams is performed by applying a series of quality correction factors (k_{Q}) to the chamber standard lab calibration coefficient at

$$^{60}\mathrm{Co}\left(N_{D,w}^{^{60}\mathrm{Co}}\right)$$

The correction factors (k_{Q}) account for the change in beam quality from one given beam to another, and its effect on the chamber, generalizing the concept of quality conversion factor used in current protocols to non-standard beams.

Although applying correction factors to non-standard beam measurements is recommended in the upcoming protocol, conceptual problems in regard to non-standard conditions are yet to be resolved. The applicability of reporting absorbed dose to a point in water, as conceptually defined by the ICRU [19], needs to be questioned. A study of perturbation effects is necessary to understand the causes of non-unity correction factors and potentially provide solutions to minimize or simplify these corrections. This is particularly relevant since correction factor accuracy relies on Monte Carlo models, which can be sensitive to model parameters in Ref. [20].

In this regard, accurate measurements of k_Q factors for non-standard beams need to be performed in order to orient the development of the new protocol. Among several candidate detectors for direct absorbed dose to water measurements, radiochromic film is promising since perturbation effects and energy dependence are negligible in the megavoltage energy range [21]. In the measurement of non-standard beam k_Q factors, good reproducibility as well as adequate uncertainty estimation are essential, especially in the case where corrections are found below the 1% level. An extensive approach to radiochromic film dosimetry is needed in order to obtain a suitable procedure to non-standard beams.

Potential limitations in the accuracy of non-standard beam absorbed dose measurements also need to be addressed. Additional experimental uncertainties must be considered, notably due to set-up positioning errors, which can be critical in high fluence gradient measurements. Therefore, achievable accuracy in the new protocol is expected to be poorer than for standard conditions; this matter should be investigated in future developments. Complete evaluations of uncertainty are also important in order to perform sensitivity studies in the design of suitable non-standard reference fields in the lead up to the new protocol.

This paper provides a summary of methods used to clarify concepts in non-standard beam dosimetry and to identify limitations in accuracy. An understanding of the fundamental problem is provided in the theory section and a study of ionization chamber perturbation factors of modulated beams is provided in the summary. Solutions are proposed to improve measurement methods, and a simple theoretical expression of the correction factor is obtained for ideal plan class specific reference (PCSR) fields. To establish achievable levels of uncertainty in k_Q factors' experimental measurement, an extensive method of characterization and uncertainty analysis of radiochromic film is summarized A study of measurement uncertainties induced by positioning errors is summarized in order to address that matter in the future protocol development. Finally, potential conceptual improvements and limitations related to non-standard beam dosimetry are thoroughly discussed.

2. THEORY

2.1. Beam quality

In contemporary reference dosimetry of high energy X ray beams, measurement conditions are entirely constrained by the beam quality, which is representative of the electron fluence spectrum in water at the location of interest, as well as the geometry and composition of the detector. What essentially characterize the electron fluence in water are: (a) the beam energy spectrum, (b) the beam fluence in terms of diomension and geometry and (c) the measurement location. In conventional standard conditions, the location is chosen so that transient charged particle equilibrium (TCPE) is achieved in the volume of water displaced by the detector. For sufficiently large and flat beams, TCPE occurs beyond the depth of maximum dose and far enough from the edges of the beam so that the electron loss is compensated by electrons issued from interactions of the beam with the medium. Because of attenuation transported by electrons, charged particle equilibrium (CPE) is not perfectly achieved in the direction of the beam, which yields dose gradients in that direction. Although TCPE can be achieved for several beam energies and fluences, this condition does not entirely define the beam quality. While beam energy affects the energy of secondary electrons, beam geometry can also affect quality since beam scattering in the collimator and the phantom influence the electron energy spectrum.

Non-standard beam quality differs from standard conditions since the beam fluence is modulated or field size is smaller than the reference field. The fluence of small fields does not necessarily cover a sufficiently large area to achieve lateral equilibrium in a volume surrounding the detector. For single modulated fields, TCPE is not achieved since beam fluence gradients cause lateral disequilibrium. However, composite modulated beams could achieve TCPE, or even CPE. Nonetheless, modulation produces a change in the energy spectrum due to interaction in the collimator and therefore beam quality could differ significantly from standard conditions.

2.2. Detector perturbation effects

Quality correction factors (k_Q) depend on the beam quality as well as the detector geometry and materials. The electron fluence crossing the detection volume differs from the one at the point of measurement in water without the detector in place. This difference depends on the sensitive volume geometry and is characterized by the replacement perturbation effect (or combined cavity and displacement effects) [11, 12]. This effect combines three distinctive, yet

correlated effects [22]: (i) the fluence perturbation, (ii) the density replacement and (iii) detector volume averaging.

The fluence perturbation effect quantifies the change in electron fluence due to the presence of a material of different nature from water, mainly with respect to its material differences, expressed through mass stopping and scattering powers. Historically, Fano's theorem [23] was used to state that under CPE condition, the electron fluence is independent of mass density. In this regard, the fluence perturbation effect intends to describe the change in electron energy spectrum produced by the physical properties of the material, without considering the effect of replacing water by a material of different density.

The density replacement effect quantifies the change in electron fluence due to a detection material of different mass density than water. The effect is non-trivial since CPE is not perfectly established in the cavity. The density heterogeneity of the detector volume in the water phantom produces lateral scattering and attenuation of electrons in the detector, which is not representative of what occurs in water. In practice, the conditions required by Fano for the cavity response to be independent of its mass density are not achievable.

Detector volume averaging is a perturbation that accounts for averaging of the electron fluence over the water volume displaced by the detector, in comparison to the fluence at the point of measurement. The density replacement effect and volume averaging are known in literature as a single effect, namely the gradient perturbation effect (or displacement effect) [11, 12], which depends on the beam energy and fluence as well as the geometry of the detector. The combination of the gradient with the fluence perturbation effect is defined as the overall replacement effect (or displacement effect) [11, 12].

The difference in absorption of energy by the detection material and water is quantified by the stopping power ratio water-to-detection-material, as described by Spencer-Attix cavity theory with Nahum track ends [24, 25].

The electron fluence crossing the detection volume also depends on the non-sensitive components of the detector. The electronic and structural components cause electron fluence perturbations due to interactions with the beam and secondary electrons. For ionization chambers, these are known in the literature as the wall and the central electrode effects [11,12] as well as the stem effect [26].

2.3. Quality correction factor

The relation between ionization chamber perturbation factors and quality conversion factors is as follows. For two given beams f_1 and f_2, with respective beam qualities Q_1 and Q_2, the correction factor from Q_1 to Q_2, noted

$$k_{Q_2,Q_1}^{f_2,f_1},$$

is expressed as the ratio of the product of perturbation factors for qualities Q_2 over Q_1, using AAPM notation [11, 22, 26]:

$$k_{Q_2,Q_1}^{f_2,f_1} = \left[\left(\frac{\bar{L}}{\rho} \right)_a^w P_{fl} P_\rho P_{vol} P_{wall} P_{cel} P_{stem} \right]_{Q_1}^{Q_2} \quad (1)$$

where

$$\left(\frac{\bar{L}}{\rho} \right)_a^w$$

is the stopping power ratio water to air, P_{fl} and P_ρ are respectively the fluence perturbation and density replacement factors, P_{vol} is the volume averaging factor, P_{wall} and P_{cel} are respectively the wall and central electrode perturbation factors, and P_{stem} is the chamber stem perturbation factor.

3. METHODS

3.1. Study of non-standard beam perturbation factors

A study of non-standard beam ionization chamber perturbation factors is summarized [22]. Ionization chamber response to static and dynamic IMRT deliveries is extensively modelled using the Monte Carlo package EGSnrc [27] and its user codes egs_chamber [28] and BEAMnrc [29, 30]. The Exradin A12 and A14 cylindrical ionization chambers (Standard Imaging, WI, USA), with respective sensitive volumes of 0.65 and 0.016 cm^3, are modelled in detail using the general purpose geometry package provided by the EGSnrc C++ class library egspp [31]. IMRT deliveries are simulated with a BEAMnrc model of a Varian Clinac 21EX 6 MV photon beam with Millennium 120 multileaf collimator (MLC). Chamber perturbation factors are calculated defining a series of scoring volumes similarly to previous studies [32, 33], as shown in Fig. 1. Fourteen fields presenting high dose gradients are used during calculations (see Fig. 2) to obtain significant overall correction factors [16]. Perturbation factors relative to standard conditions are computed and compared to demonstrate their relative contributions to the overall quality correction factor.

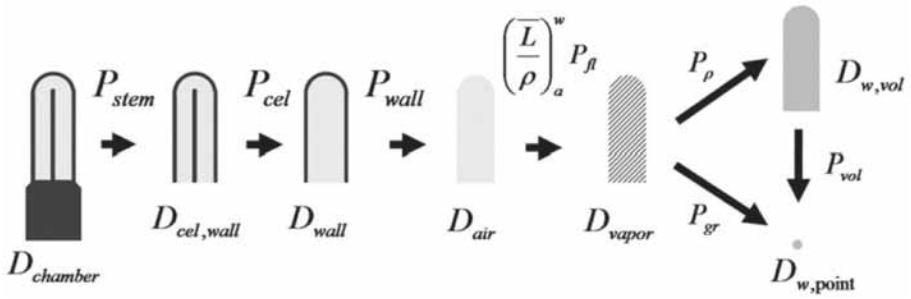

FIG. 1. Illustration of the series of cavity doses simulated to calculate the perturbation factors. (Courtesy of the American Association of Physicists in Medicine (see Ref. [22]).)

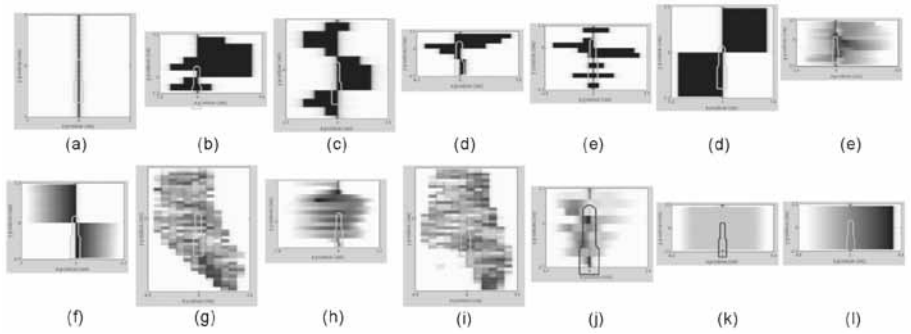

FIG. 2. Fluence maps of the irradiation fields used in the calculations as were used in Bouchard and Seuntjens study [16]. (Courtesy of the American Association of Physicists in Medicine (see Ref. [22]).)

3.2. Uncertainty in radiochromic film dosimetry for non-standard beams

Radiochromic film is studied as a candidate for direct relative absorbed dose to water measurements in non-standard beams. The summary of an exhaustive characterization and uncertainty analysis method applied to radiochromic film dosimetry is reported [34] in the scope of non-standard beam dosimetry. A complete account of the sources of uncertainties is considered in detail, and full variance analysis is performed, including statistical correlations of the obtained doses and improvement in film response to dose characterization. An extensive experimental protocol is developed in order to minimize uncertainties. Experimental criteria for achieving required levels of uncertainties are predicted using the method applied to EBT Gafchromic® film (ISP, NJ). Dose uncertainty levels are evaluated as a function of three criteria: (i) the number of

measurements needed to characterize the film response to dose, (ii) the dose delivered to the film and (iii) the number of measurement repetition to be averaged.

3.3. Additional uncertainties in non-standard beam dosimetry

Additional sources of uncertainty are investigated for ionization chamber non-standard beam dosimetry. The summary of a method to calculate uncertainties induced by positioning errors is described [35]. An implementation of original unbiased statistical estimators of dose uncertainty and k_Q uncertainty produced by setup positioning uncertainty is added to the egs_chamber [28] code. The method allows estimating these additional experimental uncertainties during reference dosimetry and is the only technique known to date in the literature that is suitable for non-standard beams. Models of the PTW (Freiburg, Germany) 60012 diode and the Exradin A12 chamber are used to numerically evaluate uncertainty produced by positioning uncertainty in non-standard beams. Examples of positioning error distributions are used to evaluate uncertainties on small beam output factor measurements using the diode. Six modulated fields are used (see Fig. 3) to assess the chamber response and k_Q factor uncertainties. In the examples shown, the positioning errors simulated account for translations of the detector as well as the machine isocenter position in each direction (x,y,z) of the phantom.

4. RESULTS

4.1. Study of non-standard beam perturbation factors

Results show that for both chamber models, the factor responsible for large deviations from unity for k_Q in non-standard beams is the gradient effect (see Fig. 4(a)), which is decomposed into two distinctive effects that share

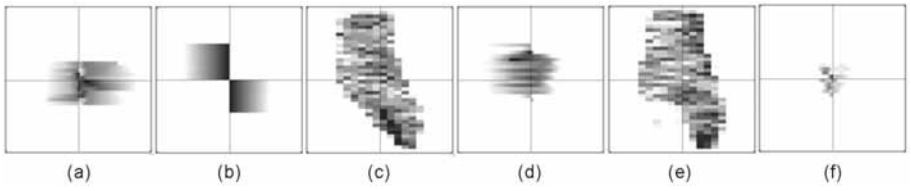

FIG. 3. Fluence maps of the IMRT beams used for non-standard output factor measurements simulation. Each map is shown within a 20 cm × 20 cm field centred at isocentre. (Courtesy of IOP Publishing (see Ref. [35]).)

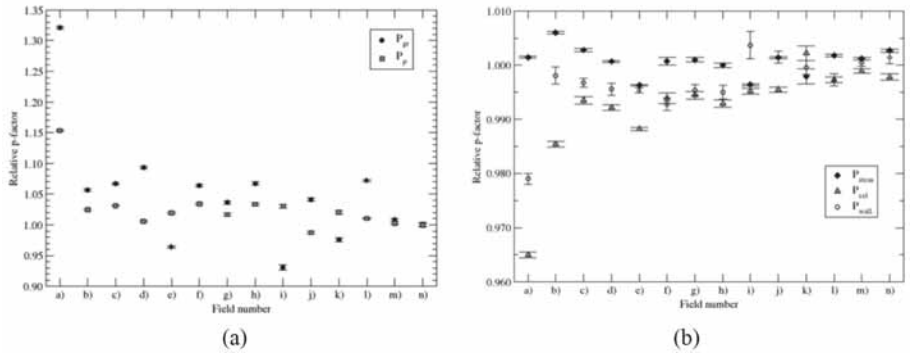

FIG. 4. Behaviour of perturbation factors of 14 non-standard beams relative to reference conditions: (a) the gradient perturbation effect (P_{gr}) and the density perturbation effect (P_{ρ}) for the Exradin A14 chamber and (b) the stem, central electrode and wall perturbation effects for the Exradin A12 chamber. (Courtesy of the American Association of Physicists in Medicine (see Ref. [22]).)

approximately half of the overall correction: volume averaging and the density replacement effect. It is shown that the other perturbation factors (P_{wall}, P_{cel} and P_{stem}) are within 1% of standard conditions for both ionization chambers studied (see Fig. 4(b)), except for one field (within 4%). Differences in stopping power ratios water-to-air and fluence perturbation factors are found to be insignificant, which is consistent with a previous publication [36].

4.2. Uncertainty in radiochromic film dosimetry for non-standard beams

Precision of radiochromic film dosimetry is improved as compared to previously reported studies [37, 38]. A strict experimental protocol is designed and an extensive method of characterization and uncertainty analysis is developed, including sensitometric curve-form criteria and variance analysis taking into account statistical correlations. One criterion that influences the uncertainties is the number of measurements necessary to characterize the film response to dose. By varying the number of characterization points between 5 and 35, it is demonstrated that at least 12 are necessary for a proper uncertainty evaluation (see Fig. 5(a)). The choice of dose delivered to the film is another criterion used to decrease the uncertainty. Applying the method to EBT film, a dose of 220 cGy is found to be ideal. A third criterion used to minimize the uncertainty is the number of measurement repetitions to be averaged. It is shown that levels of uncertainty of the order of 0.3% are achieved in relative dosimetry with EBT film (see Fig. 5(b)) when carefully following the defined experimental

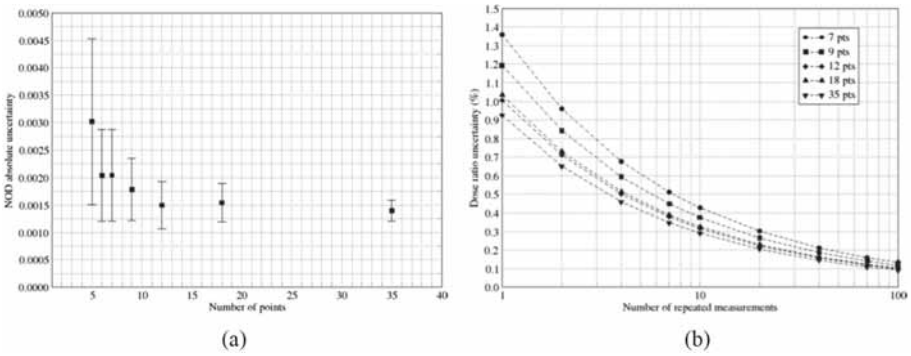

FIG. 5. Results of EBT film uncertainties as a function of experimental criteria: (a) estimated net optical density uncertainty as a function of number of points used to characterize the film response to dose and (b) dose ratio uncertainty calculation as a function of the number of measurement repetition for different numbers of points used to characterize the sensitometric curve. (Courtesy of the American Association of Physicists in Medicine (see Ref. [34]).)

protocol. This is feasible using 35 measurements to characterize the sensitometric curve, averaging ten repeated measurements and using doses of 220 cGy for each film. The adequacy of this uncertainty estimation was further confirmed by a recent study in comparison to other detectors in non-standard conditions [39].

4.3. Additional uncertainties in non-standard beam dosimetry

The construction of the Monte Carlo estimation method of dose uncertainty produced by positioning errors as well as its implementation in the egs chamber code has been successfully validated. Arbitrarily defining a positioning precision of ±0.6 mm (1σ) in each direction (*x*,*y*,*z*) for detector and isocenter and using truncated Gaussian distributions (2σ), uncertainties up to 4% and 38% on k_Q factors are reported using an Exradin A12 chamber in high dose gradients non-standard beams (see Table 1). These maximum values are obtained reporting dose to the volume of water displaced by the chamber and dose to the point of measurement respectively. For small beams down to 0.5 cm × 0.5 cm, uncertainties up to 3% on in-diode output factors are found using a PTW 60012 diode (see Fig. 6), assigning a positioning uncertainty of ±0.6 mm (1σ) in each direction for detector and isocenter and using uniform distributions.

TABLE 1. OUTPUT FACTOR AND NON-STANDARD BEAM QUALITY CONVERSION FACTORS OBTAINED FOR DYNAMIC IMRT BEAM SIMULATIONS WITH AN EXRADIN A12 CHAMBER PLACED AT 5 cm DEPTH IN A 30 cm × 30 cm × 30 cm PHANTOM USING AN SAD OF 100 cm

Field	Output factor in chamber	Output factor in water volume	Output factor at point in water	k_Q (water volume)	k_Q (at point in water)
(a)	0.3536(4) ± 0.005(1)	0.3687(2) ± 0.0039(3)	0.411(1) ± 0.022(3)	1.0428(0) ± 0.009(6)	1.1612(0) ± 0.063(9)
(b)	0.4505(5) ± 0.006(1)	0.4578(2) ± 0.0056(3)	0.433(1) ± 0.136(2)	1.0162(0) ± 0.00(2)	0.9601(0) ± 0.353(5)
(c)	0.2178(3) ± 0.0039(7)	0.2141(1) ± 0.0045(2)	0.1980(7) ± 0.041(1)	0.9827(0) ± 0.008(5)	0.9090(0) ± 0.242(6)
(d)	0.5118(4) ± 0.003(2)	0.5181(2) ± 0.0041(2)	0.518(1) ± 0.064(1)	1.0123(0) ± 0.000(4)	1.0115(0) ± 0.134(3)
(e)	0.2107(3) ± 0.0026(8)	0.2101(1) ± 0.0030(2)	0.1619(6) ± 0.0252(9)	0.9975(0) ± 0.00(1)	0.7685(0) ± 0.175(6)
(f)	0.1622(2) ± 0.0103(8)	0.1661(1) ± 0.0113(2)	0.284(1) ± 0.058(3)	1.0243(0) ± 0.038(9)	1.7538(1) ± 0.20(1)

Note: Uncertainties associated with reported values (i.e. separated by ±) are induced by positioning errors. The numbers in parenthesis correspond to the statistical simulation uncertainty on the last digit estimated with the sampling method. Dose is calculated in the chamber volume (column 2), in the volume of water displaced by the chamber sensitive volume (columns 3 and 5) and the point of in water placed at the centre of mass of the chamber sensitive volume (columns 4 and 6). (Courtesy of IOP Publishing (see Ref. [35].)

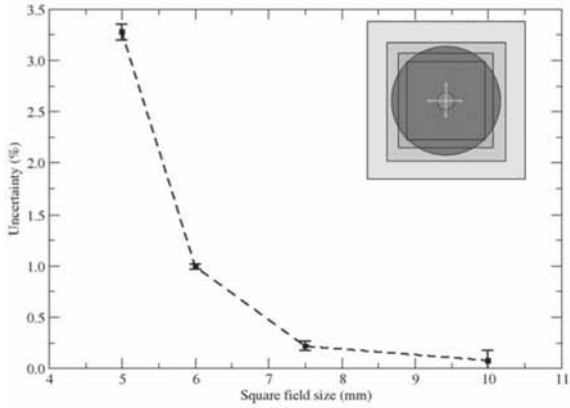

FIG. 6. Calculation results of detector output factors uncertainty induced by positioning errors in small beam measurements using a PTW 60012 diode model. The sketch in the upright corner shows a 'beam's eye view' of the diode placed in the fields, with the smallest circle to represent the sensitive volume of the diode and the large circle the whole volume. The cross illustrates the range of displacement of the detector in both directions perpendicular to the beam. (Courtesy of IOP Publishing (see Ref. [35].)

5. DISCUSSION AND CONCLUSION

5.1. The concept of point of measurement in non-standard beams

In standard conditions, the knowledge of the beam fluence and the dose gradient across the detector is used to report dose to a point in water. For such cases, the ionization chamber replacement effect is well known. In non-standard beam dosimetry, the replacement effect cannot be controlled as well as for standard conditions and is likely to differ from one beam to another. Detector volume is a limiting factor that might not be resolvable in the same way as in the past protocols. Presented results suggest that reporting dose in the volume of water displaced by the sensitive volume of the chamber, or the dose to the chamber cavity, instead of a point of measurement in water would diminish the magnitude of the correction factors. Adopting such a philosophy in a future protocol, the major remaining effect influencing the correction factors is the density replacement effect, which depends on the detector mass density and volume size as well as the dose gradients in the displaced volume.

5.2. Residual perturbation factors

Water-to-air stopping power ratios and fluence perturbation factors of modulated beams are kept reasonably within standard condition values. Non-sensitive components of the detector effects play a minor role in the corrections for non-standard beams. However, these effects on the electron energy spectrum remain difficult to predict, and the feasibility of their evaluation depends on the accuracy of correction factor calculations.

5.3. Dependence on Monte Carlo methods

Accuracy of non-standard beam dosimetry would rely on accurate Monte Carlo calculation techniques. In this case, one solution would be to adopt a direct chamber response calibration instead of reporting absorbed dose to water. This is relevant since absorbed dose to water calculation becomes arbitrary in the quality assurance procedure, since patient dose is the true quantity of interest. This philosophy would considerably simplify the formalism of the new protocol. Nonetheless, it is unclear how feasible it is to achieve a widespread implementation of accurate Monte Carlo methods in clinics.

5.4. Additional experimental uncertainties

Not only is the accuracy limited by correction factor calculation models, but also the experimental uncertainties can be significantly higher than for standard conditions. Results suggest possible limitations in the precision achieved in clinical non-standard beam measurements due to positioning errors. These uncertainties, mainly due to dose gradients, could be significantly reduced if the philosophy of reporting dose to the volume of the detector is adopted. Furthermore, the current limitation in precision of 0.3% in k_{Q} factor measurements sets an accuracy threshold. However, experimental methods could be improved in the future. Nonetheless, the issue of uncertainties should be addressed in future protocols in order to adjust quality assurance tolerances compared to current protocols.

ACKNOWLEDGEMENT

One of the authors (H. Bouchard) gratefully acknowledges support by the Natural Sciences and Engineering Research Council of Canada contract No. 344218.

REFERENCES

[1] HOSPITAL PHYSICISTS' ASSOCIATION, Code of Practice for X-ray measurements, Brit. J. Radiol. **33** 55 (1960).

[2] HOSPITAL PHYSICISTS' ASSOCIATION, A code of Practice for the Dosimetry of 2 to 8 MV X-ray and Caesium-137 and Cobalt-60 Gamma-ray Beams, Phys. Med. Biol. **9** 4 (1964).

[3] AMERICAN ASSOCIATION OF PHYSICISTS IN MEDICINE, Protocol for the Dosimetry of High Energy Electrons, Phys. Med. Biol. **11** 4 (1966).

[4] HOSPITAL PHYSICISTS' ASSOCIATION, A code of Practice for the Dosimetry of 2 to 35 MV X-ray and Caesium-137 and Cobalt-60 Gamma-ray Beams, Phys. Med. Biol. **14** 1 (1969).

[5] HOSPITAL PHYSICISTS' ASSOCIATION, A Practical Guide to Electron Dosimetry 5-35 MeV, Report Series no. 4, HPA, United Kingdom (1971).

[6] AMERICAN ASSOCIATION OF PHYSICISTS IN MEDICINE, Protocol for the Dosimetry of X- and Gamma Beams with Maximum Energies between 0.6 and 50 MeV, Phys. Med. Biol. **16** 3 (1971).

[7] NORDIC ASSOCIATION FOR CLINICAL PHYSICS, Procedures in Radiation Therapy Dosimetry with 5 to 50 MeV Electrons and Roentgen and Gamma Rays with Maximum Photon Energies between 1 and 50 MeV, Acta Radiol Ther. Phys. Biol. **2** 6 (1972).

[8] HOSPITAL PHYSICISTS' ASSOCIATION, Practical Guide to Electron Dosimetry Below 5 MeV for Radiotherapy Purposes, Report series no. 13, HPA, United Kingdom (1975).

[9] AMERICAN ASSOCIATION OF PHYSICISTS IN MEDICINE, Code of Practice for X-ray Therapy Linear Accelerators, Med. Phys. **2** 10 (1975).

[10] NORDIC ASSOCIATION FOR CLINICAL PHYSICS, Procedures in External Radiation Therapy Dosimetry with Electron and Photon Beams with Maximum Energies Between 1 and 50 MeV, Acta Radiol. Oncol. **19** (1980).

[11] AMERICAN ASSOCIATION OF PHYSICISTS IN MEDICINE TASK GROUP 21 RADIATION THERAPY COMMITTEE, A Protocol for the Determination of Absorbed Dose from High-Energy Photon and Electron Beams, Med. Phys. **10** 6 (1983).

[12] INTERNATIONAL ATOMIC ENERGY AGENCY, Absorbed Dose Determination in Photon and Electron Beams: An International Code of Practice, Technical Reports Series No. 277, IAEA, Vienna (1987).

[13] ALMOND. P.R., BIGGS, P.J., COURSEY, B.M., HANSON, W.F., HUQ, M.S., NATH, R., ROGERS, D.W.O., American Association of Physicists in Medicine's TG-51 protocol for clinical reference dosimetry of high-energy photon and electron beams, Med. Phys. **26** 9 (1999), 1847–1869.

[14] INTERNATIONAL ATOMIC ENERGY AGENCY, Absorbed Dose Determination in External Beam Radiotherapy: An International Code of Practice for Dosimetry Based on Standards of Absorbed Dose to Water, Technical Reports Series No. 398, IAEA, Vienna (2000).

[15] ROGERS, D.W.O., Fundamentals of Dosimetry Based on Absorbed-Dose Standards, Teletherapy Physics, Present and Future, AAPM (PALTA, J.R., MACKIE, T.R., Eds), Washington DC (1996).

[16] BOUCHARD, H., SEUNTJENS, J., Ionization chamber-based reference dosimetry of intensity modulated radiation beams, Med. Phys. **31** 9 (2004), 2454–5465.
[17] CAPOTE, R., SANCHEZ-DOBLADO, F., LEAL, A., LAGARES, J.I., ARRANS, R., HARTMANN, G.H., An EGSnrc Monte Carlo study of the microionization chamber for reference dosimetry of narrow irregular IMRT beamlets, Med. Phys. **31** 9 (2004), 2416–2422.
[18] ALFONSO, R., ANDREO, P., CAPOTE, R., HUQ, M.S., KILBY, W., KJALL, P., MACKIE, T.R., PALMANS, H., ROSSER, K., SEUNTJENS, J., ULLRICH, W., VATNITSKY, S., A new formalism for reference dosimetry of small and nonstandard fields, Med. Phys. **35** 11 (2008) 5179–5186.
[19] INTERNATIONAL COMMISSION ON RADIATION UNITS AND MEASUREMENTS, Report of the International Commission on Radiation Units and Measurements, National Bureau of Standards, Handbook No. 62, United States of America (1956).
[20] CROP, F., REYNAERT, N., PITTOMVILS, G., PAELINCK, L., DeWAGTER, C., VAKAET, L., THIERENS, H., The influence of small field sizes, penumbra, spot size and measurement depth on perturbation factors for microionization chambers, Phys. Med. Biol. **54** 9 (2009), 2951–2969.
[21] SUTHERLAND, J.G.H., ROGERS, D.W.O., Monte Carlo calculated absorbed-dose energy dependence of EBT and EBT2 film, Med. Phys. **37** 3 (2010) 1110.
[22] BOUCHARD, H., SEUNTJENS, J., CARRIER, J.-F., KAWRAKOW, I., Ionization chamber gradient effects in nonstandard beam configurations, Med. Phys. **36** 10 (2009), 4654–4663.
[23] FANO, U., Note on the Bragg-Gray cavity principle for measuring energy dissipation, Radiat. Res. **1** (1954), 237–240.
[24] SPENCER, L. V., ATTIX, F.H., A Theory of Cavity Ionization, Radiation Research, **3** 3 (1955).
[25] NAHUM, A.E., Water/Air Mass Stopping Power Ratios for Megavoltage Photons and Electrons Beams, Physics in Medicine and Biology, **23** 1 (1978) 24–38.
[26] BUCKLEY, L.A., ROGERS, D.W.O., Wall correction factors, P_{wall}, for thimble ionization chambers, Med. Phys. **33** 2 (2006) 455–464.
[27] KAWRAKOW, I., Accurate condensed history Monte Carlo simulation of electron transport. I. EGSnrc, the new EGS4 version, Med. Phys. **27** 3 (2000) 485-498.
[28] WULFF, J., ZINK, K., KAWRAKOW, I., Efficiency improvements for ion chamber calculations in high energy photon beams, Med. Phys. **35** 4 (2008) 1328–1336.
[29] ROGERS, D.W.O., FADDEGON, B.A., DING, G.X., MA, C.M., WE, J., MACKIE, T.R., BEAM: A Monte Carlo code to simulate radiotherapy treatment units, Med. Phys. **22** 5 (1995) 503–524.
[30] ROGERS, D.W.O., WALTERS, B., KAWRAKOW, I., BEAMnrc users manual, Report PIRS-509, IRS (NRC), Ottawa (2006).
[31] KAWRAKOW, I., MAINEGRA, E., TESSIER, F., WALTERS, B.R.B., The EGSnrc C++ class library, Report PIRS-898, IRS (NRC), Ottawa (2010).
[32] BUCKLEY, L.A., ROGERS, D.W.O., Wall correction factors, P_{wall}, for thimble ionization chambers, Med. Phys. **33** 2 (2006) 455–464.

[33] WULFF, J., HEVERHAGEN, J.T., ZINK, K., Monte-Carlo-based perturbation and beam quality correction factors for thimble ionization chambers in high-energy photon beams, Phys. Med. Biol. **53** 11 (2008) 2823–2836.

[34] BOUCHARD, H., LACROIX, F., BEAUDOIN, G., CARRIER, J.-F., KAWRAKOW, I., On the characterization and uncertainty analysis of radiochromic film dosimetry, Med. Phys. **36** 6 (2009), 1931–1946.

[35] BOUCHARD, H., SEUNTJENS, J., KAWRAKOW, I., A Monte Carlo method to evaluate the impact of positioning errors on detector response and quality correction factors in nonstandard beams, Phys. Med. Biol. **56** (2011) 2617–2634.

[36] SANCHEZ-DOBLADO, F., ANDREO, P., CAPOTE, R., LEAL, A., PERUCHA, M., ARRANS, R., NUNEZ, L., MAINEGRA, E., LAGARES, J.I., CARRASCO, E., Ionization chamber dosimetry of small photon fields: A Monte Carlo study on stopping-power ratios for radiosurgery and IMRT beams, Phys. Med. Biol. **48** 14 (2003) 2081–2099.

[37] DEVIC, S., SEUNTJENS, J., SHAM, E., PODGORSAK, E.B., SCHMIDTLEIN, C.R., KIROV, A.S., SOARES, C.G., Precise radiochromic film dosimetry using a flat-bed document scanner, Med. Phys. **32** (2005) 2245–2253.

[38] VAN BATTUM, L.J., HOFFMANS, D., PIERSMA, H., HEUKELOM, S., Accurate dosimetry with Gafchromic EBT film of a 6 MV photon beam in water: What level is achievable? Med. Phys. **35** (2008), 704–716.

[39] CHUNG, E., BOUCHARD, H., SEUNTJENS, J., Investigation of three radiation detectors for accurate measurement of absorbed dose in nonstandard fields, Med. Phys. **37** 6 (2010) 2402–2413.

CALORIMETRIC DETERMINATION OF k_Q FACTORS FOR NE2561 IONIZATION CHAMBERS IN 3 cm × 3 cm BEAMS OF 6 MV AND 10 MV PHOTONS

A. KRAUSS, R.-P. KAPSCH, M. ROUIJAA
Physikalisch-Technische Bundesanstalt, Braunschweig, Germany
Email: achim.krauss@ptb.de

Abstract

Within the framework of the iMERA-PLUS action of the European Metrology Research programme, k_Q factors for NE2561 ionization chambers have been measured in 3 cm × 3 cm beams of 6 MV and 10 MV photons using water calorimetry. This investigation demonstrates that the k_Q factors can be determined with standard uncertainties of less than 0.4%, and that compared to the k_Q factors in 10 cm × 10 cm reference fields, no dependence on the beam size can be found.

1. INTRODUCTION

The dosimetry of clinical photon beams is typically performed with ionization chambers, which are calibrated in a 10 cm × 10 cm ^{60}Co radiation field. To determine the absorbed dose to water, D_w, in megavoltage photon beams from a linear accelerator, beam quality dependent correction factors, k_Q are used. These k_Q factors can be determined either experimentally by using a standard for D_W at different beam qualities, Q, or, with larger uncertainties, they can be calculated on the basis of ionization chamber cavity theory. For reference conditions, i.e. for photon beams of 10 cm x 10 cm, k_Q factors for most of the commonly used ionization chambers can be found in various dosimetric measurement protocols like TRS-398 of the IAEA [1] or the German DIN 6800-2 [2]. However, recent developments in radiotherapy delivery techniques, such as IMRT, Tomotherapy or CyberKnife [3], have increased the use of small radiation fields. Furthermore, for some of these treatment units, the reference conditions specified in dosimetric protocols cannot be realized. The questions arise as to whether new concepts for dosimetry are required [4] and if the k_Q factors for reference fields are also valid for the dosimetry of small fields.

At the Physikalisch-Technische Bundesanstalt (PTB), a water calorimeter was used to determine the k_Q factors for ionization chambers of the type NE 2561

for photon beams of different sizes. In addition to previous measurements performed down to field sizes of 5 cm × 5 cm [5], this paper describes the investigation performed in 3 cm × 3 cm beams of 6 MV and 10 MV.

2. MATERIAL AND METHODS

2.1. Photon radiation fields

The linear accelerator used for the investigation is of the type Elekta Precise equipped with a multileaf collimator. The linac offers photon radiation fields of 6 MV, 10 MV and 15 MV, respectively, and the output dose rate at the isocentre can be varied between 0.2 Gy/min and 5 Gy/min by changing the pulse repetition frequency. The radiation field at a depth of 10 cm inside the water phantom of the calorimeter for a source-to-surface distance (SSD) of 116 cm was limited to 3 cm × 3 cm by using an external collimator made of 3 cm thick lead, which was mounted permanently in front of the radiation head. The setting of the multileaf collimator was fixed to a square opening of 3.2 cm. The gantry of the linac was locked for horizontal irradiations.

For the 6 MV and 10 MV photons, the lateral dose distributions of the 3 cm × 3 cm field inside the water phantom at a depth of 10 cm were measured by using both a diode of the type M60012 and a small ionization chamber of the type PTW31014. The latter was also used to determine the corresponding depth dose distributions. In both cases, a three-dimensional scanning device was used, which was adjusted to the central axis of irradiation. The central axis of irradiation is defined with the aid of an optical laser system, which is installed in the irradiation room and aligned to the beam axis of the gantry. The scanning device was used to move the detectors in steps of 1 mm either at different depths along the central axis of irradiation, or along the horizontal and vertical directions in a plane perpendicular to the central axis of irradiation. Fig. 1 shows the lateral dose distribution in vertical and horizontal directions for both radiation qualities; the maximum dose on the central axis has been normalized to 1. For all measured distributions, the widths with respect to the relative dose of half maximum amount to 30.2 mm. The uncertainty of the width is estimated to be about 0.40 mm from re-measuring the dose distributions several times during the course of the calorimetric measurements.

In this investigation, the specifier $TPR_{20,10}$ [1] was used to indicate the beam quality, Q. $TPR_{20,10}$ was determined for reference conditions, i.e. for a 10 cm × 10 cm field size, to be 0.683 for the 6 MV and 0.733 for the 10 MV photons, respectively.

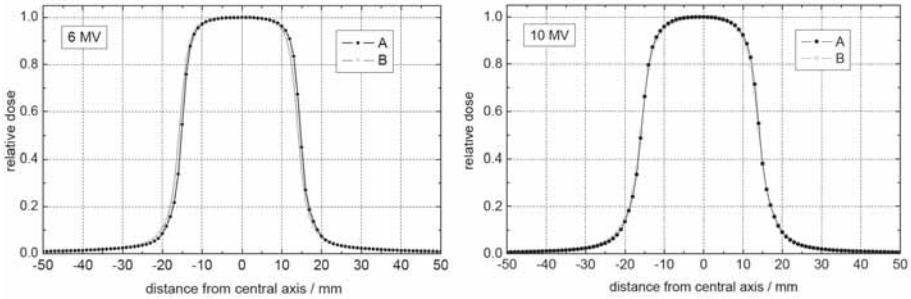

FIG. 1. Horizontal (A) and vertical (B) dose distributions of the 3 cm × 3 cm field for 6 MV (left) and 10 MV photons (right) measured with a PTW31014 chamber.

2.2. Set-up and operation of the water calorimeter

The technical details of the PTB water calorimeters which are operated at a water temperature of 4°C, have been described elsewhere [5,6]. The detector of the calorimeter is made of a thin-walled plane-parallel glass cylinder filled with high purity water saturated with hydrogen gas [6]. The glass cylinder has an outer diameter of 95 mm and an outside length of 41.4 mm. The thickness of the flat walls and the cylinder wall are 0.7 mm and 2.5 mm, respectively. Inside the cylinder, two temperature probes, made of conically shaped glass pipettes having a smallest outer diameter of about 0.5 mm, are mounted opposite each other and perpendicular to the cylinder axis. Each pipette contains a thermistor sensor 0.25 mm in diameter directly fused into the glass at the very end of the pipette. The temperature probes are adjusted in such a way that the thermistors are fixed at the measurement plane of the detector. The measurement plane of the detector is directed perpendicularly to the central axis of irradiation and is fixed at a water depth of 10 cm when the detector is mounted inside the water phantom of the calorimeter. The exact positions of the opposing thermistors with respect to the cylinder axis are determined with the help of an optical telescope to better than 0.1 mm. The detector's cylinder axis was found to coincide with the central axis of irradiation within less than 0.5 mm. During the experiments performed for the current investigation, three separate detectors with distances of the opposing thermistors from the cylinder axis ranging from –4.1 mm to +4.6 mm were applied.

During the measurements, the time evolution of the resistance of both thermistors of the calorimetric detector was determined separately using high stability digital multimeters (Agilent 3588A). Two of these multimeters were used within a 1.5 V dc powered voltage divider circuit for each thermistor, the

thermistor being one part of the voltage divider and the second part being a calibrated high precision resistor with a well-known resistance value. In this way, the resistance of the thermistor is given by the measured voltage ratio across the thermistor and the precision resistor times the resistance value of the precision resistor.

Typically, four consecutive measurements with drift periods of 130 s in between were performed for nominally 60 s and 120 s irradiation times before the calorimeter had to be re-conditioned due to the strong temperature gradients occurring during the irradiations. A total of nine separate calorimetric experiments were performed, and within each experiment, more than 100 measurements for each irradiation time were taken. For each irradiation, the separate measurement signals of both thermistors were analysed with the common procedure of performing linear fits over certain time intervals of the pre- and post-irradiation drift curves and extrapolating the fits to the mid-run position [6]. Time intervals of 110 s were applied for both the pre- and post-irradiation drift curves, with the fit interval for the post-irradiation drift curve starting 10 s after the end of an irradiation.

2.3. Calorimetric determination of D_W

The calorimetric determination of D_W requires the consideration of several correction factors or influence quantities. In Eq. (1), h designates the 'heat defect', the correction factor k_C accounts for the heat transport effects occurring during and after the irradiations, k_P indicates the perturbation correction necessary for the change of D_W due to the presence of the calorimetric detector, k_r corrects for the non-uniformity of the lateral dose distribution, dependent on the position of the thermistors, and k_T accounts for the effect due to the difference in the water temperature between the calorimetric measurements (4°C) and the ionization chamber calibrations (20°C).

$$D_w = \Delta T \cdot c_p \cdot (1 - h)^{-1} \cdot k_c \cdot k_p \cdot k_r \cdot k_T \quad (1)$$

The methods applied for the determination of the different correction factors are essentially the same as already described elsewhere [5] for the case of 10 cm × 10 cm fields. Table 1 summarizes the values of the different correction factors. However, in the case of 3 cm × 3 cm beam size, the influence of the heat transport occurring during and after the measurements is of major concern. To study the effects due to the heat transport experimentally, many sequences of four consecutive irradiations were performed for the 60 s and 120 s irradiation times with the three different calorimetric detectors. The expected differences between the mean values of the calorimetric results as a function of irradiation

numbers #1–#4 can be compared to the predictions of corresponding heat transport calculations. The heat transport calculations and the determination of the necessary heat conduction correction factors, k_C, for the different measurement conditions were performed on the basis of the finite-element method using the software package COMSOL 3.5. The calculations were performed for a full three-dimensional geometry model, taking into account the calorimetric detector including the temperature probes with the real positions of the thermistors as well as the measured lateral and depth-dose distributions of the 3 cm × 3 cm radiation fields.

Calculations were also made with two-dimensional geometry models considering the different heat transport effects separately. However, the superposition of the corresponding two-dimensional results, i.e. the separate correction factors, led to an agreement with the results of the full three-dimensional calculations within about 0.1%. Dependent on the irradiation time and the position of the thermistor, the calculated correction factors k_C for a single irradiation vary between 0.991 and 0.962. Figure 2 presents a comparison of the uncorrected results of calorimetric measurements and the results of the heat conduction calculations. The data shown are the mean values of the ratios of the first and the second irradiation of the four consecutive irradiations as a function of the position of the temperature sensor relative to the central axis of the field. These ratios are mainly affected by the superposition of the heat conduction effects of the consecutive irradiations. The calculated data are in good agreement with the experimental ones, which proves that the calculated correction factors k_C can be adequately used for the calorimetric determination of absorbed dose to water and, hence, for the determination of the k_Q factors for ionization chambers.

For each calorimetric experiment, separate values for D_W were determined from the measurements with each thermistor of the detector, applying the individual correction factors k_C and k_r. The observed relative difference between the results of the separate D_W determinations are generally less than 0.2% and can

TABLE 1. CORRECTION FACTORS USED FOR THE CALORIMETRIC DETERMINATION OF D_W (Eq. (1)) IN THE 3 cm × 3 cm PHOTON BEAMS

Energy	k_c [a]	k_p	k_r [b]	k_T
6 MV	0.9704–0.9854	1.0024	1.0003–1.0042	1.0007
10 MV	0.9775–0.9859	1.0019	1.0006–1.0089	1.0007

[a] Mean values for a series of four consecutive irradiations for different positions of the thermistor.

[b] Dependent on the position of the thermistor.

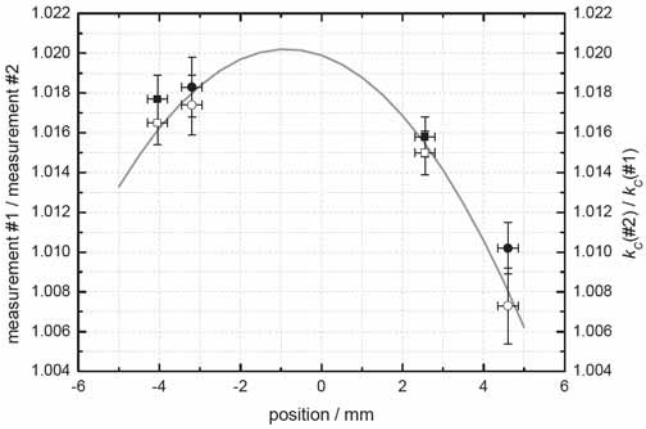

FIG. 2. For the case of 10 MV photons and for 120 s irradiation time, the solid line shows the ratio of the calculated heat conduction correction factors of the second and the first irradiation, $k_C(\#2)/k_C(\#1)$, as a function of the position relative to the central axis of irradiation. The ratios of the mean values of calorimetric results of the first and the second irradiation obtained from different experiments, together with their standard uncertainties, are also shown. The results obtained with different detectors are represented by different symbols.

be explained to be a purely statistical effect. Therefore, the mean value of both values was taken as the final result of a calorimetric experiment.

2.4. Calibration of NE2561 chambers and determination of k_Q factors

After each calorimetric experiment, ionization chambers of the type NE2561 (cavity volume: 0.33 cm^3) were mounted inside the water phantom of the calorimeter with the reference point positioned at a depth of 10 cm, i.e. at the same depth in water as the calorimetric detector was placed before. The ionization chambers were calibrated in both 3 cm × 3 cm high energy photon beams following the same procedures as described previously [5]. In order to achieve comparable calibration coefficients, the chamber measurements had to be corrected for the effect of the lateral non-uniformity of the radiation fields. This was done by integrating the measured lateral dose distribution over the cross-sectional area of the NE2561 ionization chamber perpendicular to the beam axis. In this way, a correction of 1.0016 ± 0.0005, to be applied to the reading of the chamber, was determined for both radiation qualities. From the calibration coefficient $N_{D,W,Q}$ of the chamber under test at radiation quality Q, the corresponding k_Q factor was determined by Eq. (2) using the known chamber calibration coefficient for ^{60}Co radiation:

$$k_Q = N_{D,w,Q}/N_{D,w,Co} \quad (2)$$

Prior to the measurements performed in the 3 cm x 3 cm beams, k_Q factors for the NE2561 chambers for 6 MV and 10 MV have also been determined in the 10 cm × 10 cm reference fields by use of the water calorimeter. Thus, the final results for this investigation for the NE2561 chamber can be presented as the ratios $k_Q(3 \times 3)/k_Q(10 \times 10)$, i.e. the ratio of k_Q factors in the 3 cm × 3 cm and in the reference field (10 cm × 10 cm), for both radiation qualities.

2.5. Characteristics of the monitor chamber

Throughout all the measurements, the photon radiation from the linac was monitored by means of a large area transmission ionization chamber, which was mounted in front of the linac's radiation head at a distance of about 40 mm behind the lead collimator, which was used for the limitation of the field size. The monitor chamber was developed at PTB and consists of two sensitive volumes of 4 cm diameter, which are placed directly after another. The monitor chamber has been proven to deliver a signal, which is proportional to the dose rate at the reference point in a water phantom, with a deviation well below 0.1% over a period of several hours [7]. However, measurements with the water calorimeter and the following calibrations of ionization chambers require the response of the monitor chamber to be stable over periods of more than a week. This was partly assured during the calorimetric measurements by determining the ratio of the readings of the monitor chamber and of an additional NE2571 chamber, which was placed behind the monitor twice a day. The ratio was stable within a standard deviation of about 0.1%. Nevertheless, it cannot be ruled out that the monitoring could be influenced by a systematic effect, so far unexplained. This is shown in the observation that if a calorimetric experiment including the ionization chamber calibrations is normalized either on the reading of the first or the second sensitive volume of the monitor chamber, the resulting k_Q factors can differ by up to 0.2%. Furthermore, the ratio of the readings of the first and the second sensitive volume of the monitor exhibits a slight dependency on the measured air temperature. This effect could lead to a systematic difference between the monitor chamber response between the time of the calorimetric measurements and the time of the ionization chamber calibrations, because the temperature of the monitor chamber could be influenced by the outer cooling housing of the water calorimeter during the 4°C operation. Further investigations are underway to understand these effects. An additional standard uncertainty of 0.15% has been considered for a possible change of the monitor response between the calorimetric measurements and the ionization chamber measurements.

3. RESULTS AND UNCERTAINTY BUDGET

A detailed analysis of the uncertainty budget for the determination of the k_Q factors in the 3 cm x 3 cm radiation fields shows that the main contributions stem from the uncertainties for the calculated heat conduction corrections k_C (0.18%), the correction k_r (0.10%), the stability of the monitor response (0.15%) and for the ionization chamber measurements (0.10%). The uncertainty of k_C can be separated into a contribution of 0.15% for the uncertainty of the heat transport calculations itself (e.g. for the geometry model, physical parameters, and an additional contribution of 0.10% taking into account the effect of a 0.5 mm uncertainty of the position of the thermistors in respect to the lateral dose distributions. Although the uncertainty for the heat defect h cancels out in principle in the experimental determination of a k_Q factor, a remaining contribution of 0.10% was considered for possible deviations of the response of the different calorimetric detectors applied during the experiments [5]. To give a resume, a relative combined standard uncertainty of less than 0.40% is achieved for a single k_Q determination in a 3 cm × 3 cm photon field.

The final results of the k_Q determination for the NE2561 chamber in the 3 cm × 3 cm radiation fields, presented as the ratios $k_Q(3 \times 3)/k_Q(10 \times 10)$, are given in Table 3 and in Fig. 3. The figure summarizes the data of different experiments and for different chambers of the type NE2561 for both radiation qualities. For the standard uncertainties of the single experiments, those uncertainty contributions which are common to all, like the uncertainty for $k_Q(10 \times 10)$, have been omitted. The mean of the $k_Q(3 \times 3)/k_Q(10 \times 10)$ values and their standard uncertainties were used to deduce the data given in Table 2. For the NE2561 ionization chamber with serial number #297, the corresponding k_Q factors and their standard uncertainties in the 10 cm × 10 cm reference fields are also presented in the table.

TABLE 2. RATIOS OF $k_Q(3 \times 3)/k_Q(10 \times 10)$
(i.e. the ratio of k_Q factors in the 3 cm × 3 cm and in the reference field (10 cm × 10 cm), together with their standard uncertainties for the NE2561 ionization chamber for 6 MV and 10 MV photons)

$TPR_{20/10}$ (10 cm × 10 cm)	k_Q (10 × 10)	$k_Q(3 \times 3)/k_Q(10 \times 10)$
0.683 (6 MV)	0.9934 ± 0.0029	0.9989 ± 0.0038
0.733 (10 MV)	0.9864 ± 0.0029	1.0034 ± 0.0037

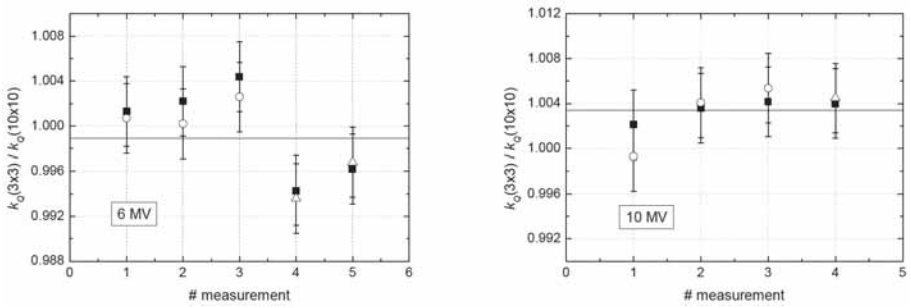

FIG. 3. Ratio of $k_Q(3 \times 3)/k_Q(10 \times 10)$ for different experiments in 6 MV (left) and 10 MV (right) radiation. The different symbols represent different chambers of the type NE2561, the solid line represents the mean value for $k_Q(3 \times 3)/k_Q(10 \times 10)$. The error bars indicate the standard uncertainties as they are valid for comparing the results of different experiments, i.e. uncertainty contributions which are common to all, like the uncertainty for $k_Q(10 \times 10)$, have been omitted.

4. CONCLUSION

This investigation demonstrates that water calorimetry can be applied to determine k_Q factors of ionization chambers also in high energy photon radiation with beam sizes down to 3 cm × 3 cm. A relative standard uncertainty of less than 0.4% is achievable for k_Q. However, within the standard uncertainties of this experimental method, no dependence of the k_Q factors on the size of the radiation fields was detected for NE2561 chambers in 6 MV and 10 MV beams. Further investigations on this issue will be performed over the total energy range available at PTB's accelerator facilities, i.e. between 4 MV and 25 MV.

ACKNOWLEDGEMENT

The research within this EURAMET joint research project leading to these results has received funding from the European Community's Seventh Framework Programme, ERA-NET Plus, under Grant Agreement No. 217257.

REFERENCES

[1] INTERNATIONAL ATOMIC ENERGY AGENCY, Absorbed Dose Determination in External Beam Radiotherapy: An International Code of Practice for Dosimetry Based on Standards of Absorbed Dose to Water, Technical Reports Series No. 398, IAEA, Vienna (2000).

[2] DEUTSCHES INSTITUT FÜR NORMUNG, Dosismessverfahren nach der Sondenmethode für Photonen- und Elektronenstrahlung, DIN 6800-2, Berlin (2007).

[3] BORTFELD, T., IMRT, A review and preview, Phys. Med. Biol. **51** (2006) R363–379.

[4] ALFONSO, R., et al., A new formalism for reference dosimetry of small and nonstandard fields, Med. Phys. **35** (11) (2008) 5179–5186.

[5] KRAUSS, A., KAPSCH, R.-P., Calorimetric determination of k_Q factors for NE2561 and NE2571 ionization chambers in 5 cm x 5 cm and 10 cm x 10 cm radiotherapy beams of 8 MV and 16 MV photons, Phys. Med. Biol. **52** (2007) 6243–6259 and Corrigendum: Phys. Med. Biol. **53** (2008) 1151–1152.

[6] KRAUSS, A., The PTB water calorimeter for the absolute determination of absorbed dose to water in ^{60}Co radiation, Metrologia **43** (2006) 259–272.

[7] KAPSCH R.-P., KRAUSS A., On the performance of monitor chambers to measure the output of medical linear accelerators for high-precision dosimetric investigations (World Congress on Medical Physics and Biomedical Engineering, Munich 2009) IFMBE Proceedings 25/I (2009) 85–88.

SMALL FIELD DOSIMETRIC MEASUREMENTS WITH TLD-100, ALANINE AND IONIZATION CHAMBERS: PRELIMINARY MEASUREMENTS

S. JUNELL*, L. DEWERD*, S. HUQ**, J. NOVOTNY, Jr.**, M. QUADER**, M.F. DESROSIERS***, G. BEDNARZ**

* Department of Medical Physics, University of Wisconsin, Madison, Wisconsin
Email: junell@wisc.edu

** University of Pittsburgh Cancer Institute, Pittsburgh, Pennsylvania

*** National Institute of Standards and Technology, Gaithersburg, Maryland

United States of America

Abstract

The new small and non-standard field dosimetry protocol introduced new reference field conditions for photon beam calibration. Preliminary measurements of beam quality correction factors corresponding to this formalism were performed for three different models of ionization chambers: a Farmer type ionization chamber, a thimble ionization chamber and a microchamber. Beam quality correction factor measurements were made in a cylindrical acrylic phantom and a water phantom using thermoluminescent dosimeters (TLDs) and alanine dosimeters to determine dose to water. The behaviour of the beam quality correction factor was observed as it transfers the calibration coefficient from the University of Wisconsin Accredited Dosimetry Calibration Laboratory ^{60}Co reference beam to the small field calibration conditions of the small field formalism. There was no statistically significant change in the beam quality correction factor for the ionization chambers in static and composite small fields compared to the TG-51 reference fields. Loss of lateral charged particle equlibrium was observed with the Farmer type ionization chamber. The beam quality correction factors for the ionization chambers as determined by the TLDs had an average standard deviation of ~1.5%, with an estimated relative combined standard uncertainty of ~3–4% (k = 1). The alanine absorbed dose to water measurements showed an average standard deviation of 5% and a discrepancy up to 4.9% from the American Association of Physicists in Medicine Task Group 51 (TG-51) [2] determined absorbed dose to water.

1. INTRODUCTION

1.1. Small field formalism

Codes of practice (CoPs) for 10 cm × 10 cm reference fields for photon beams are well established by the American Association of Physicists in Medicine (AAPM) TG-51 and the IAEA TRS-398 [2, 3]. However, no national or international guidelines exist for the calibration of small and non-standard photon fields. In a joint effort between the IAEA and the AAPM, a working group was formed to develop a CoP for reference dosimetry for small and non-standard fields. The working group has recently published a new formalism, which will be referred here as the 'proposed formalism' [1]. The proposed formalism introduces two calibration methods for performing reference dosimetry of small and non-standard fields. The first method involves small static field geometry, and the second involves composite field geometry. The small static field dosimetry method introduces the machine specific reference (MSR) field (f_{msr}) and its related beam quality correction factor

$$(k_{Q_{\text{msr}},Q}^{f_{\text{msr}},f_Q})$$

This f_{msr} is defined by a static beam at the user's facility. The f_{msr} was created for the calibration needs of stereotactic radiosurgery systems but can also be used for intensity modulated radiation therapy (IMRT) systems. The second method introduces the plan-class specific reference (PCSR) field (f_{pcsr}). The f_{pcsr} is a composite field composed of clinically relevant beams, which are similar to a treatment plan used for a patient [4]. The proposed formalism suggests that these new beam quality correction factors should be determined with Monte Carlo (MC) simulations or a dosimeter traceable to a primary standard of absorbed dose to water.

For the proposed formalism static field calibration, the absorbed dose to water

$$(D_{w,Q_{\text{msr}}}^{f_{\text{msr}}})$$

for a small field (f_{msr}) at the reference depth in water in a beam of quality Q_{msr} is given by Eq. 1:

$$D_{w,Q_{\text{msr}}}^{f_{\text{msr}}} = M_{Q_{\text{msr}}}^{f_{\text{msr}}} \cdot N_{D_w}^{Q_0} \cdot k_{Q,Q_0} \cdot k_{Q_{\text{msr}},Q}^{f_{\text{msr}},f_{\text{ref}}} \quad (1)$$

where

$M_{Q_{msr}}^{f_{msr}}$ is the reading of the ionization chamber in the MSR field corrected for pressure, temperature, ion recombination and polarity effects;

$N_{D_w}^{Q_0}$ is the absorbed dose to water calibration coefficient obtained from a ^{60}Co calibration at the national standards laboratory or an accredited dosimetry calibration laboratory (ADCL) for the reference beam quality (Q_0);

k_{Q,Q_0} is the beam quality correction factor, which corrects for differences between the reference beam quality in which the calibration coefficient was determined and the beam quality (Q) in the reference field (f_{ref}) used in conventional dosimetry CoPs;

$k_{Q_{msr},Q}^{f_{msr},f_Q}$ is a new factor which corrects for the differences between the conditions of field size, geometry, phantom material and beam quality of the conventional CoP reference field (f_{ref}) and the machine-specific reference field (f_{msr}). This factor,

$$k_{Q_{msr},Q}^{f_{msr},f_{ref}},$$

also accounts for the difference in ionization chamber responses between f_{ref} and f_{msr} and is defined as the ratio of dose (D) per unit reading (M) for f_{msr} and f_{ref} (Eq. 2).

$$k_{Q_{msr},Q}^{f_{msr},f_{ref}} = \frac{\left(D_{w,Q_{msr}}^{f_{msr}} / M_{Q_{msr}}^{f_{msr}}\right)}{\left(D_{w,Q}^{f_{ref}} / M_{Q}^{f_{ref}}\right)} \quad (2)$$

For the composite field calibration, the f_{msr} is replaced with the f_{pcsr} and Eqs 1 and 2 become Eqs 3 and 4, respectively.

$$D_{w,Q_{pcsr}}^{f_{pcsr}} = M_{Q_{pcsr}}^{f_{pcsr}} \cdot N_{D_w}^{Q_0} \cdot k_{Q,Q_0} \cdot k_{Q_{pcsr},Q}^{f_{pcsr},f_{ref}} \quad (3)$$

$$k_{Q_{pcsr},Q}^{f_{pcsr},f_{ref}} = \frac{\left(D_{w,Q_{pcsr}}^{f_{pcsr}} / M_{Q_{pcsr}}^{f_{pcsr}}\right)}{\left(D_{w,Q}^{f_{ref}} / M_{Q}^{f_{ref}}\right)} \quad (4)$$

1.2. Purpose

A preliminary investigation into the measurement component of the proposed formalism as it applies to IMRT fields was performed using multiple measurement techniques. Beam quality correction factors for ionization chambers were derived from TLD determined absorbed dose to water measurements to provide a basis for comparison with the secondary University of Wisconsin ADCL ^{60}Co standard. Figure 1 depicts the sequence of steps used in determining the beam quality correction factors, which transfer the calibration coefficient from the ADCL ^{60}Co standard conditions (step 1) to the proposed formalism's f_{pcsr} reference conditions (step 6). Table 2 lists the different calibration conditions used during each step of the beam quality correction factor measurements.

Beam quality correction factors were calculated for three different models of ionization chambers; a Farmer type ionization chamber (Exradin A19 — 0.65 cm^3 collecting volume), a thimble ionization chamber (Exradin A1SL — 0.057 cm^3 collecting volume), and a microchamber (Exradin A16 — 0.007 cm^3 collecting volume). All ionization chambers are manufactured by Standard Imaging Inc., (Middleton, WI).

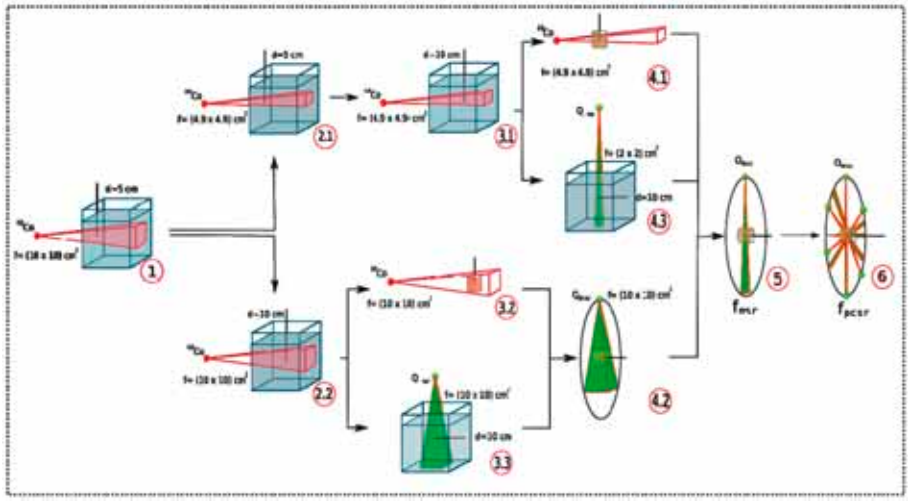

FIG. 1. Flowchart of ionization chamber calibration transfer from ^{60}Co reference field to PCSR field (f_{pcsr}). Table 2 lists the calibration conditions and results of each step.

2. METHODS

2.1. Measurements of beam quality correction factors

For this work, all beam quality correction factors were combined into a single quality correction factor,

$$k_{Q,Q_0}^{f_{\text{small fields}},f_0},$$

and are related, as shown in Eq. 5.

$$k_{Q,Q_0}^{f_{\text{small fields}},f_0} = k_{Q,Q_0} \cdot k_{Q_{\text{pcsr}},Q}^{f_{\text{pcsr}},f_Q} \quad \text{or} \quad k_{Q,Q_0}^{f_{\text{small fields}},f_0} = k_{Q,Q_0} \cdot k_{Q_{\text{msr}},Q}^{f_{\text{msr}},f_Q}$$

$$k_{Q,Q_0}^{f_{\text{small fields}},f_0} = k_{Q,Q_0} \cdot k_{Q_{\text{msr}},Q}^{f_{\text{msr}},f_Q} \tag{5}$$

Each

$$k_{Q,Q_0}^{f_{\text{small fields}},f_0}$$

was determined using Eq. 6; where beam quality Q_0 is for ^{60}Co and beam quality $Q_{\text{small fields}}$ corresponds to multiple linear particle accelerator (linac) 6 MV photon beam small field calibration conditions, including static and composite fields.

$$k_{Q,Q_0}^{f_{\text{small fields}},f_0} = \frac{(D_{w,Q_{\text{small fields}}}^{f_{\text{small fields}}} / M_{Q_{\text{small fields}}}^{f_{\text{small fields}}})}{(D_{w,Q_0}^{f_0} / M_{Q_0}^{f_0})} \tag{6}$$

the term $k_{Q,Q_0}^{f_{\text{small fields}},f_0}$

was determined for three different ionization chambers using both TLD and alanine to determine absorbed dose to water (D_w). TLD-100 chips (LiF:Mg,Ti) (Thermo Electron Corporation, Oakwood Village, OH) thermoluminescent dosimeters were provided by the University of Wisconsin Medical Radiation Research Center and alanine dosimeters were provided by the National Institute of Standards and Technology (NIST). The ^{60}Co measurements were performed in water using Virtual Water™ TLD holders (see Fig. 2) at a depth of 5 cm, an SSD of 95 cm, and a field size of (10 cm × 10 cm) (f_0). Ionization chamber and

FIG. 2. Virtual Water™ TLD holder with watertight O-ring. Five TLDs are positioned in a cross shape at the centre of the holder. Virtual Water™ alanine holders accommodate one pellet in the centre location.

TLD ($D_{w,Q_0}^{f_0}/M_{Q_0}^{f_0}$) measurements were performed with ^{60}Co at equal time intervals before and after they were exposed to the beam qualities, $Q_{\text{small fields}}$, from the linac. The average of the two ^{60}Co exposures were used to find the beam quality factor. Measurements of

$$k_{Q,Q_0}^{f_{\text{small fields}},f_0}$$

were made for multiple small field conditions including various static field sizes and a composite field representing a hypothetical head and neck case.

2.2. Dosimeter processing

The nominal dimensions of the TLDs were 3 mm × 3 mm × 1 mm (Fig. 3). A set of 380 TLD chips was annealed prior to each use to reset trap structures and reduce the intensity of peak two in the TLD glow curve. The annealing procedure consisted of a 400°C anneal for 80 min, 15 min cooling to room temperature on an aluminum plate, and an 80°C anneal for 24 h. TLDs were irradiated at least 12 h after annealing. The TLD chips were read using a Harshaw 5500 automatic reader at least 24 h after exposure. The time–temperature profile for the reader included a 50°C preheat, followed by a data collection region that used a 10°C/s temperature increase and a maximum temperature of 300°C. A chip calibration factor (CF) was determined for each TLD to account for the relative response to ^{60}Co irradiation. The CF is defined as the light output for each chip per median value of the TLD set when irradiated by ^{60}Co photons. CFs were determined before and after each experiment to ensure consistent response. All TLD

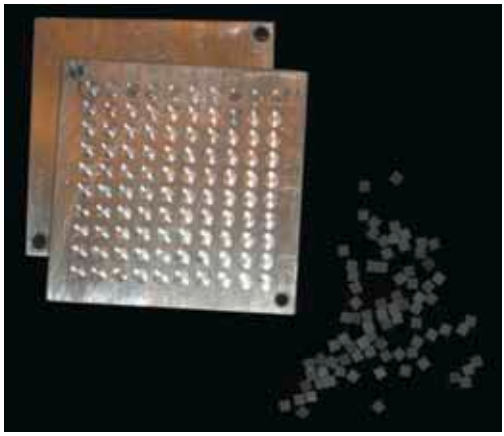

FIG. 3. LiF TLD-100 (LiF:Mg,Ti) thermoluminescent dosimeters and aluminum annealing tray.

measurements were corrected for relative response (CF), photomultiplier tube (PMT) non-linearity and background.

The alanine pellets obtained from NIST were sent back after beam quality conversion factor measurements and were read by NIST using electron paramagnetic resonance (EPR). A batch of eight cylindrical alanine pellets and three control pellets was provided by NIST for this work. Each pellet had a diameter of 5 mm and a height of 2.4 mm.

2.3. Measurements for calibration coefficient correction transfer

TLD and ionization chamber measurements in photon fields from a linac were made to track the beam quality correction factor from that of the standard NIST traceable ^{60}Co to that of the f_{msr} and f_{pcsr} as outlined in the proposed formalism (Fig. 1).

2.4. In-water measurements of beam quality correction factor of static small fields

Absorbed dose to water measurements for static small fields ranging from 1.6 cm × 1.6 cm to 10 cm × 10 cm were performed with an array of five TLDs or one alanine pellet held in a Virtual Water™ (Med-Cal, Verona, WI) holder (Fig. 2) in a water phantom at 10 cm depth. The Virtual Water™ holder had a watertight O-ring to prevent water from contacting the detectors. MC simulations show no statistical difference between the perturbation of a 6 MV beam or a ^{60}Co

beam in the Virtual Water™ holder versus liquid water. The Virtual Water™ holder was replaced with each ionization chamber and exposed at the same position of interest. Charge readings (M) in coulombs of each ionization chamber were completed using a Standard Imaging MAX 4000 electrometer and a water phantom in a 6 MV photon beam.

2.5. In phantom measurements of beam quality correction factor of static and composite fields

Static field and composite field measurements were performed in a specially developed cylindrical acrylic phantom (Standard Imaging Inc.) (Fig. 4). The cylindrical phantom has a diameter of 10 cm and a length of 10 cm. Exchangeable inserts are availible for positioning an array of TLDs, a single alanine pellet, a stack of three pieces of film, as well as each ionization chamber to ensure each dosimeter is positioned at the phantoms centre.

Measurements of the beam quality correction factor for a hypothetical composite small field treatment, as discussed in the proposed formalism, were performed. The composite field plan was created using the Pinnacle™ (Philips, Fitchburg, WI) treatment planning system and was designed to produce a uniform dose to a three dimensional volume sufficiently larger than the dimensions of the ionization chamber to eliminate partial volume measurement effects. The

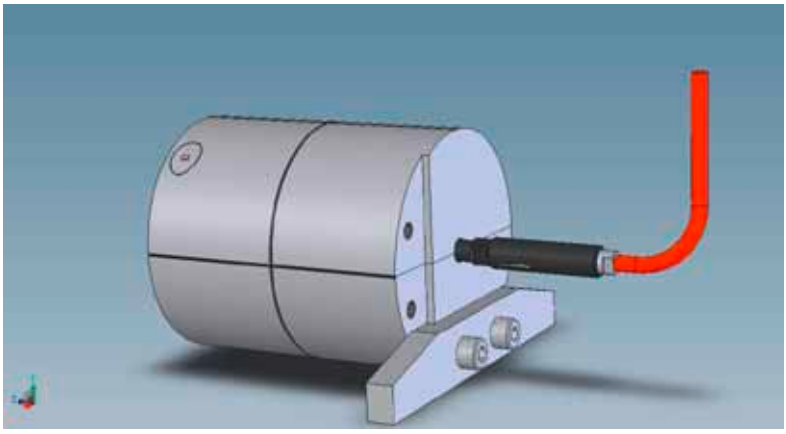

FIG. 4. Acrylic phantom with a diameter of 10 cm and a length of 10 cm used to measure beam quality correction factors. Inserts are available to accommodate a variety of detectors including TLDs, alanine, film, and ionization chambers (Standard Imaging, Inc., Middleton, WI).

treatment plan used in this work mimicked a typical head and neck treatment with one treatment volume and one organ at risk representing the spinal cord.

3. RESULTS

3.1. Measurements in water of static small fields

Figure 5(a)–(c) shows the results of the ionization chamber beam quality correction factors,

$$k_{Q,Q_0}^{f_{\text{small fields}},f_0}$$

and measurements for varying static field sizes, with TLDs used to determine absorbed dose to water. The Exradin A19 ionization chamber began exhibiting loss of lateral charged particle equilibrium at the 2.4 cm × 2.4 cm field size, which increased as the field size was further decreased (Fig. 5(a)). Both the Exradin A1SL and A16 ionization chambers displayed a statistically flat dependence with decreasing field size (Fig. 5(b) and (c), respectively). The k_{Q,Q_0} beam quality correction factor used in the standard TG-51 CoP was found to be within the first standard deviation for the majority of the TLD determined

$$k_{Q,Q_0}^{f_{\text{small fields}},f_0}$$

values. The k_{Q,Q_0} values for the ionization chambers in the 6 MV linac beam are: 0.997 for the Exradin A19 [2], 0.9946 for the Exradin A1SL, and 0.9959 for the Exradin A16 [5].

The results of the irradiations of the alanine pellets provided by NIST are shown in Table 1. The EPR determined alanine response showed a discrepancy of up to 4.9% between the measured and TG-51 determined delivered dose to water of 40 Gy, with the largest discrepancies observed for the 1.6 cm × 1.6 cm field.

3.2. Tracking the beam quality correction factor

Beam quality correction factor measurements for composite small field treatments were performed. Measurements were taken at multiple steps in the beam quality correction factor transfer process (Fig. 1). This chain starts at the standard ionization chamber absorbed dose to water calibration condition at 5 cm

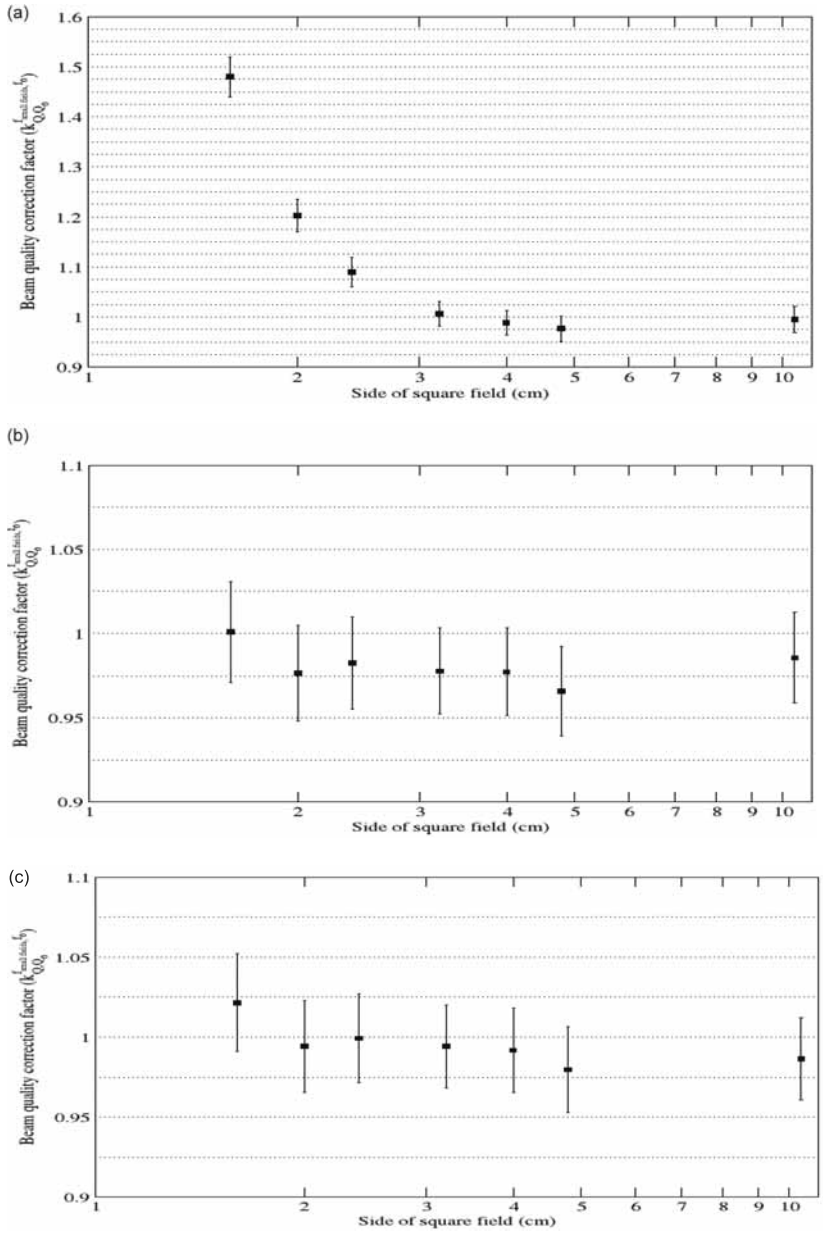

FIG. 5. The black markers are the TLD-determined small field beam quality correction factors for (a) Exradin A19 Farmer type ionization chamber (0.65 cm^3 collecting volume), (b) Exradin A1SL ionization chamber (0.057 cm^3 collecting volume), and (c) Exradin A16 ionization chamber (0.007 cm^3 collecting volume). Error bars correspond to the first standard deviation.

TABLE 1. STATIC FIELD ALANINE PELLET IRRADIATION RESULTS

Alanine pellet no.	Field size (cm)	Dose measured by NIST (Gy)	Difference from 40 Gy (%)
1	1.6 × 1.6	38.03	–4.9
2	1.6 × 1.6	38.51	–3.7
3	1.6 × 1.6	38.35	–4.1
4	3.2 × 3.2	39.23	–1.9
5	3.2 × 3.2	39.35	–1.6
6	4.8 × 4.8	39.37	–1.6

depth in water for a 10 cm × 10 cm ^{60}Co field, and ends with the ionization chamber in phantom in a f_{pcsr} field. Table 2 presents the results of the

$$k_{Q,Q_0}^{f_{\text{small fields}},f_0}$$

calculations for the various steps in the calibration coefficient transfer.

The beam quality correction factor remained close to unity under most of the calibration conditions. Variations may be attributed to beam hardening in the phantom or additional scatter from the phantom. The only statistically significant variation was for the A19 Farmer type ionization chamber in which the value spiked when field sizes of 2 cm × 2 cm on a 6 MV linac were measured. This is likely due to volume averaging effects and is similar to what was observed in the static field results for the 2.4 cm × 2.4 cm field. Despite the volume averaging effects, when the Farmer type ionization chamber was placed in the f_{pcsr}, the small field beam quality correction factor returned to unity within the one standard deviation of the conventional beam quality corrllection factor. Figure 6 graphically represent the beam quality correction factor for the three ionization chambers in each stage of the transfer process.

3.3. Uncertainty

The TLD-100 chips were found to have an average standard deviation of ~1.5%. The estimated relative combined standard uncertainty is ~3–4% (k = 1). Sources of uncertainty in the TLD measurements included TLD reproducibility, TLD positioning, PMT non-linearity correction, reader stability, linac stability, and ^{60}Co dose variations. The TLD reproducibility differs for each calibration

TABLE 2. MEASURED BEAM QUALITY CORRECTION FACTOR $k_{Q,Q_0}^{f_{\text{small fields}},f_0}$ FOR THE EXRADIN A19, A1SL AND A16 IONIZATION CHAMBERS

Calibration conditions					A16 (S/N XAA023126)		A1SL (S/N XW090634)		A19 (S/N XAQ090201)	
Sequential Step	Energy	Field size (cm^2)	SSD/depth (cm/cm)	Medium	$k_{Q,Q_0}^{f_{\text{small fields}},f_0}$	σ	$k_{Q,Q_0}^{f_{\text{small fields}},f_0}$	σ	$k_{Q,Q_0}^{f_{\text{small fields}},f_0}$	σ
1	^{60}Co	10 × 10	100/5	Water	1.00	0.016	1.00	0.016	1.00	0.016
2.1	^{60}Co	4.9 × 4.9	100/5	Water	1.00	0.026	0.994	0.026	0.998	0.026
2.2	^{60}Co	10 × 10	100/10	Water	0.992	0.021	0.984	0.021	1.00	0.021
3.2	^{60}Co	10 × 10	100/na	Phantom	1.01	0.018	0.996	0.018	1.00	0.018
3.3	^{60}Co	4.9 × 4.9	100/na	Phantom	1.03	0.011	0.997	0.010	1.01	0.010
4.1	^{60}Co	4.9 × 4.9	100/10	Water	0.989	0.010	1.00	0.010	0.989	0.010
3.3	6 MV	10 × 10	100/10	Water	0.997	0.018	0.995	0.018	1.00	0.018
4.2	6 MV	10 × 10	100/na	Phantom	1.02	0.022	1.02	0.021	1.02	0.021
4.3	6 MV	2 × 2	100/10	Water	1.02	0.017	1.00	0.016	1.30	0.021
5	6 MV	2 × 2	100/na	Phantom	1.03	0.026	1.01	0.026	1.30	0.033
6	6 MV	f_{pcsr}	100/na	Phantom	1.00	0.010	0.991	0.010	0.991	0.010

condition as it is the average of the standard deviation of the corrected readings of the TLDs irradiated in the 6 MV photon calibration condition and the corresponding ^{60}Co readings. Positioning was estimated to be within ±1 mm leading an estimated error of 0.2%. The alanine pellets were found to have an average standard deviation of ~5%. Uncertainty was not provided by NIST. For composite fields and single static fields, the precisions of TLDs and alanine remained constant.

4. CONCLUSIONS

Preliminary measurements were made to investigate the beam quality correction factor as it applies to the new proposed formalism for small and non-standard field beam calibration. The primary goal was to observe the behaviour of the beam quality correction factor as it transfers the calibration coefficients from the standard ADCL ^{60}Co beam to the small field calibration conditions defined in the proposed formalism. Within the statistical uncertainties of the dosimeters used, the beam quality correction factors were generally unity within the first standard deviation and all were unity within the second standard deviation, except for two of the conditions. For the A19 Farmer type ionization chamber, volume averaging effects in fields smaller than 2.4 cm × 2.4 cm resulted in a larger beam quality correction factor than observed in the other conditions. The TLD-100 chips were found to have an average standard deviation of ~1.5%, with an estimated combined relative standard uncertainty at ~3–4% (k = 1). The alanine absorbed dose to water measurements showed discrepancies of up to 4.9% from the TG-51 determined dose to water. Future beam quality correction factor studies will include TLD, film, and alanine absorbed dose to water measurement comparisons. The results of the beam quality correction factor measurements could also be used to benchmark future MC simulations of the beam quality correction factors. Ideally, this research will lead to an increased understanding of how the calibration coefficient from an ADCL can best be applied to the small field and non-standard field formalism.

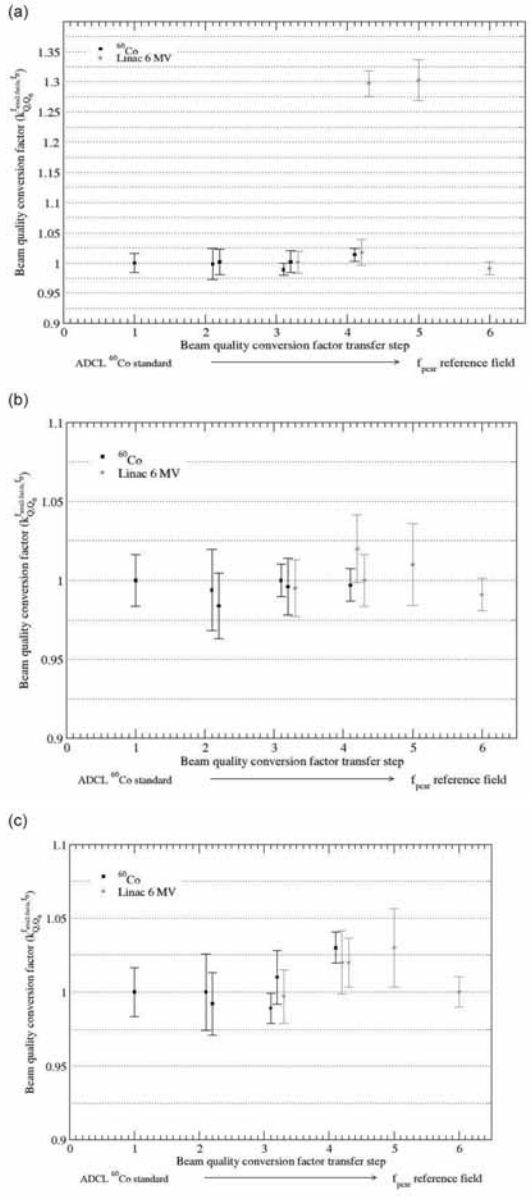

FIG. 6. Measured beam quality correction factor $k_{Q,Q_0}^{f_{\text{small fields}},f_0}$ *for the Exradin (a) A19, (b) A1SL, and (c) A16 ionization chambers. TLDs were used to determine absorbed dose to water for the beam quality correction factor. Calibration conditions for each transfer step are listed in Table 2 and displayed graphically in Fig. 1. All results are normalized to the standard ADCL* ^{60}*Co calibration conditions. Error bars correspond to the first standard deviation.*

ACKNOWLEDGEMENT

The authors would like to thank the customers of the University of Wisconsin ADCL, whose patronage helps fund continuing research.

REFERENCES

[1] ALFONSO, R., ANDREO, P., CAPOTE, R., HUQ, M.S., KILBY, W,. KJALL, P., MACKIE, T.R., PALMANS, H., ROSSER, K., SEUNTJENS, J., ULLRICH, W,. VATNITSKY, S., A new formalism for reference dosimetry of small and nonstandard fields, Med. Phys. **35** (2008) 5179–5186.

[2] ALMOND, P.R., BIGGS, P.J., COURSEY, B.M., HANSON, W.F., HUQ, M.S., NATH, R. and ROGERS, D.W.O. AAPM's TG-51 protocol for clinical reference dosimetry of high-energy photon and electron beams, Med. Phys. **26** (1999) 1847–1870.

[3] INTERNATIONAL ATOMIC ENERGY AGENCY, Absorbed Dose Determination in External Beam Radiotherapy: An International Code of Practice for Dosimetry Based on Standards of Absorbed Dose to Water, Technical Reports Series No. 398, IAEA, Vienna (2000).

[4] ROGERS, D., CYGLER, J., Clinical Dosimetry Measurements in Radiotherapy, Proceedings of the American Association of Physicists in Medicine Summer School (2009).

[5] McEWEN, M.R., Measurement of ionization chamber absorbed dose k_Q factors in megavoltage photon beams, Med. Phys. **37** (2010) 2179–2194.

EXPERIMENTAL EVALUATION OF REFERENCE DOSIMETRY FOR NON-STANDARD FIELDS IN AN APERTURE-BASED IMRT SYSTEM

R. ALFONSO-LAGUARDIA*, E. LARRINAGA-CORTINA*,
L. DE LA FUENTE**, I. SILVESTRE-PATALLO*

* Department of Radiotherapy, Institute of Oncology and Radiobiology

** Department of Neurosurgery, Institute of Neurology and Neurosurgery
Email: rodocub@yahoo.com

Havana, Cuba

Abstract

Absolute dose verification of intensity modulated radiation therapy (IMRT) plans is an important component of the patient specific quality assurance. This verification is made with ionization chambers, calibrated in standard conditions that usually differ notably from those encountered in IMRT. The IAEA/American Association of Physicists in Medicine initiative for extending the $N_{D,w}$ based dosimetry codes of practice (CoPs) to non-standard fields, is evaluated in the verification of head and neck IMRT plans delivered with a static, aperture-based inverse planning approach. A representative plan-class specific reference field for this kind of treatments was designed, and the corresponding dose factors and correction factors were determined, for three commonly employed ionization chambers, using gafchromic EBT2 films as suitable dose detector. Results showed that no further corrections, apart from those used in standard reference dosimetry CoPs, are required in our system for IMRT verification, due to two main reasons, namely, the rationality used for creating the beam segments and because the calculated dose is averaged over the volume of interest of the ionization chamber

1. INTRODUCTION

The use of intensity modulated radiation therapy (IMRT) has become commonplace, even in many developing countries. However, several studies have shown that IMRT treatments might not be as accurate as expected/desired [1]. The ionization chambers (ICs) are still the gold standard dosimeter for routine in-hospital calibration of clinical radiotherapy beams, but the most common dosimetry codes of practice (CoPs) used for these purposes, such as IAEA TRS-398 [2] and American Association of Physicists in Medicine (AAPM)

TG-51 [3], were not conceived for some frequent conditions met in IMRT delivery, where situations of high dose gradients, time–dose variance, and highly non-uniform beam distributions are encountered. The small-sized beamlets used in some composite IMRT beams put at risk the accuracy of both absolute and relative dose determination. This occurs essentially due to the nonequilibrium conditions created as a consequence of the secondary electron track lengths that are comparable to the treatment field finite size and the occlusion of the source size by the collimating system; this influences the electron fluence spectrum in the IC, hence affecting the cavity perturbation factor p_{cav}. On the other hand, the insertion of the IC into such fields usually perturbs the level of disequilibrium. This perturbation has been previously considered in some CoPs (p_{repl} in AAPM TG-21 [4] or p_{dis} in TRS-398 [2]), but depends not only on the detector geometry, but also on the medium in which the measurement is performed, as well as on the beam energy and field size [5].

This problem has been reported when verifying IMRT plans with standard dosimetry instruments and procedures, even with small volume ICs. Dong et al. [6] evaluated the discrepancies in the quality assurance (QA) of 751 clinical IMRT plans, showing that in 19% of the cases, the discrepancies between measurement and treatment planning were outside the ±2% band, ranging from –12.7 to +11.7%. Sanchez-Doblado et al. [7] studied the sources of uncertainties in IMRT absolute dosimetry verification, using several representative IMRT plans and different sized ICs, resulting in an increased relative uncertainty of 1–1.5%, provided that appropriate small-volume chambers are used; for some plans and ICs, up to 4% discrepancies were found between measurements and dose calculations by treatment planning systems (TPSs). National and international IMRT dosimetry intercomparison and audits have been also performed [8, 9], reflecting a non-insignificant occurrence of dose discrepancies above the established tolerance. These results suggested that the source of discrepancies might not be linked only to inaccuracies of the TPSs. A revision of the existing dosimetry CoPs is then required in order to address the complex situations encountered in composite beams as those used in IMRT treatments.

Bouchard and Seuntjens [10] examined reference dosimetry of IMRT fields using thimble (Farmer) type ICs, suggesting a method for correcting the IC absorbed dose calibration coefficient $N_{D,w,Q}$ using a correction factor that can be calculated by Monte Carlo or measured with appropriate dose detectors. They evaluated the correction factors for six static and nine dynamic IMRT fields, showing that for some of the single IMRT fields, the chamber correction factor can be very large (differing 10–60% from unity), especially for fields that have the potential to induce large effects of electron fluence disequilibrium within the chamber volume.

The IAEA and the AAPM have sponsored an international initiative for extending the $N_{D,w}$ based dosimetry CoPs to small and non-standard fields [11]. For conventional reference dosimetry of high energy photon beams (non-IMRT, 10 cm × 10 cm, at reference depth in the user's beam quality Q), the IAEA CoP [2] uses the well-known formalism:

$$D_{w,Q}^{f_{ref}} = M_{Q}^{f_{ref}} \cdot N_{D,w,Q_0} \cdot k_{Q,Q_0} \quad (1)$$

where

$M_{Q}^{f_{ref}}$ is the IC reading in the reference field at the actual user quality Q, corrected to the reference values of influence quantities, other than beam quality, for which the calibration factor is valid;

$N_{D,w,Qo}$ is the calibration coefficient in terms of absorbed dose to water of the user's IC, obtained from a standard dosimetry laboratory;

$k_{Q,Qo}$ is the correction factor for the effects of the difference between the reference beam quality Q_o and the actual user quality Q.

For composite fields such as those used in IMRT plans, the IAEA–AAPM initiative suggests an intermediate calibration condition, in which a plan-class specific reference field (f_{pcsr}) is created by a specific delivery sequence, similar to clinically delivered irradiation patterns. This field arrangement should be able to ensure a uniform dose distribution larger than the extent of the ICs used for patient specific QA, achieving charged particle equilibrium (CPE) in that volume. Under these conditions, the absorbed dose to water irradiated by a composite f_{pcsr}, at the reference depth in water, in a beam of quality Q_{pcsr}, in the absence of the IC, can be obtained with the conventional dosimetry formalism, adding a correction factor that accounts for the difference in IC responses between the conventional reference field f_{ref} (usually the 10 cm × 10 cm field) and the f_{pcsr}, as shown in Eq. 7 of Ref, [11], reproduced here:

$$D_{w,Q_{pcsr}}^{f_{pcsr}} = M_{Q_{pcsr}}^{f_{pcsr}} \cdot N_{D,w,Q_0} \cdot k_{Q,Q_0} \cdot k_{Q_{pcsr},Q}^{f_{pcsr},f_{ref}} \quad (2)$$

where

$$k_{Q_{pcsr},Q}^{f_{pcsr},f_{ref}}$$

accounts for the difference between the responses of an IC in the conditions of the fields f_{ref} and f_{pcsr}, and can be formulated combining Eqs (1) and (2), resulting in the following expression:

$$k_{Q_{pcsr},Q}^{f_{pcsr},f_{ref}} = \frac{D_{w,Q_{pcsr}}^{f_{pcsr}} / M_{Q_{pcsr}}^{f_{pcsr}}}{D_{w,Q}^{f_{ref}} / M_{Q}^{f_{ref}}} = \frac{D_{w,Q_{pcsr}}^{f_{pcsr}}}{D_{w,Q}^{f_{ref}}} \times \frac{M_{Q_{pcsr}}^{f_{pcsr}}}{M_{Q}^{f_{ref}}} \quad (3)$$

where

$$D_{w,Q_{pcsr}}^{f_{pcsr}} / D_{w,Q}^{f_{ref}}$$

is the dose factor, measurable with a suitable good dose detector, or computable with Monte Carlo techniques, and

$$M_{Q_{pcsr}}^{f_{pcsr}} / M_{Q}^{f_{ref}}$$

is the ratio of ion chamber readings, or chamber cavity dose factor, measured with the user's ICs.

The purposes of this study was to design a representative f_{pcsr} for head and neck (H&N) treatments with static aperture based IMRT, and to measure the corresponding correction factors

$$k_{Q_{pcsr},Q}^{f_{pcsr},f_{ref}}$$

for the ICs used in the clinic, in order to evaluate which of them are more suitable for patient specific QA.

2. MATERIALS AND METHODS

2.1. Definition of a plan class specific reference field

Several authors have already suggested different f_{pcsr} for their commonly used composite field arrangements. Bailat et al. [12] defined three helical f_{pcsr} in a cylindrical phantom delivered with a tomotherapy unit, and used alanine as reference dosimeter, determining experimentally the correction factors for three ICs, ranging within ±1.4%.

Chung et al. [13] established a candidate f_{pcsr} for a dynamic H&N IMRT delivery; they used a cylindrical phantom and three different reference instruments (diamond, liquid IC and radiochromic film). The correction factors for 5 ICs were assessed experimentally and by Monte Carlo calculation, differing from unity by no more than ±0.8%.

Rosser et al. [14] reported three f_{pcsr} implemented with dynamically evolving apertures achieved in an Elekta's volumetric modulated arc therapy

(VMAT) system; one of these VMAT fields is delivered in a slab phantom, while the other two are configured on a cylindrical phantom; the alanine was also employed as reference dosimeter. The correction factors were obtained experimentally for two ICs and one unshielded electron diode, resulting in values of up to 2.3% for the diode and 1.6% for one of the ICs.

IMRT treatments at the Department of Radiotherapy of the Institute of Oncology and Radiobiology (INOR) in Havana, Cuba, have been implemented with Elekta Precise® linear accelerators (linacs) and Elekta's PrecisePLAN® TPS. The linac allows static, 'step-and-shoot' IMRT treatments using 6 MV or 15 MV photons and a multileaf collimator (MLC) consisting of 40 pairs of leaves, each ensuring 1 cm width at the isocentre. The PrecisePLAN® TPS utilizes an aperture based inverse planning approach, which creates static apertures prior to calculating dose, using several rationales. The rationales used for developing these apertures are not limited to those automatically created by the TPS, since it may include user designed apertures.

For establishing a representative f_{pcsr}, a revision of actual H&N IMRT plans was done, combined with the recommended structure set of test I3 (mock H&N) in the AAPM TG-119 report [15], resulting in a averaged structure set, field arrangement and segment sequence. Two target volumes (PTV including neck nodules and boost PTV), and two organs at risk (spinal cord and parotids) were defined; their dimensions (length, width and height) were obtained averaging the corresponding values of the selected group of actual plans. The resulting structure set was delineated in the CT scans of a slab phantom, 30 cm × 30 cm × 11.5 cm, composed by water-equivalent plastic (RW3®, PTW, Freiburg). This is the same phantom used for routine IMRT patient specific QA, allowing point measurements both with ICs and film dosimeters. A beam arrangement consisting of nine fields at typical angles, averaged for the group of representative H&N plans, was applied to the structure set, as shown in Fig. 1(A). The TPS's inverse planning protocol with typical dose goals was employed to obtain the set of segments per beams, their shape and weights; segments were restricted to have more than two monitor units. The minimum equivalent field size of segments was allowed to reach 2 cm × 2 cm, which correspond to the smallest square field size used in the commissioning of the TPS. Owing to the shape of the used phantom, the beams of the hybrid plan calculated for patient specific QA are collapsed at 0^o gantry angle; hence, the corresponding f_{pcsr} was assessed for a collapsed beam delivery technique, with a measuring volume of interest (VOI) defined at low gradient dose region for this beam arrangement, 1 cm upstream of the isocentre, as shown in Fig. 1(B).

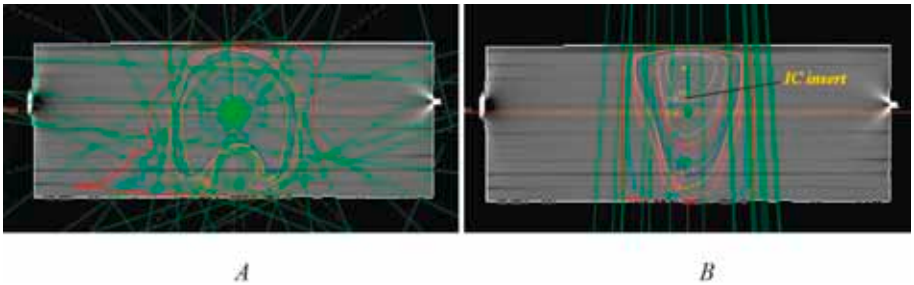

FIG. 1. Dose distributions in the slab phantom. A: Beam arrangement and dose distribution of averaged H&N IMRT plan. B: Dose distribution of collapsed beams, used to define the f_{pcsr} .

2.2. Measurement of correction factors $k_{Q_{pcsr},Q}^{f_{pcsr},f_{ref}}$

The correction factor

$$k_{Q_{pcsr},Q}^{f_{pcsr},f_{ref}}$$

might be obtained by a direct calibration of the user's IC, both in the conventional reference field and in the f_{pcsr}, against a primary standard or against another suitable dose detector, such as alanine, radiochromic film, or Fricke dosimetry, whose calibration ideally should be traceable to a primary standard of absorbed dose to water [11]. Using such a dose detector, one could obtain experimentally the dose factor defined in Eq. (3). As part of a coordinated research project of the IAEA, the Radiotherapy Department at INOR has received a limited amount of radiochromic film (Gafchromic® EBT2, International Special Products, Wayne, NJ). It was chosen as the suitable dose detector for obtaining the dose factor described in Eq. (3), due to its good energy response [16–18], which has been reported to show an energy independence within ±0.6% in the photon energy range of 100 keV to 18 MeV [19]. The authors of Ref. [20] introduce low perturbation, provide a wide dose range from 0.01 to 8 Gy, and some authors have referred to an adequate achievable precision for the purpose of absolute dosimetry [20, 21].

In order to calibrate the radiochromic film scanner system for absolute, accurate dose measurements, a procedure was established, based on the previous experience of other research groups [20, 22, 23].

Thirteen Gafchromic EBT2 film pieces of 1.5 cm × 2 cm were irradiated in a 6 MV photon beam from the Elekta Precise® linac, at a depth of 5 cm in the RW3® phantom. All the film pieces were irradiated at source–film distance of 100 cm with a 10 cm × 10 cm field, and the range of dose delivered varied from

0 to 500 cGy; a checkpoint of 100 cGy was repeated four times and intercalated between the other pieces, with the aim of verifying the constancy of the scanning device. The time between irradiation and reading of the EBT2 film pieces was 17 h. The film pieces were stored during this period in order to avoid exposure to ultraviolet light.

The authors used an Agfa DuoScan HiD desktop flatbed document scanner for the reading process with a maximum spatial resolution of 2000 × 1000 ppi. The scanning parameters were 48 bits RGB mode (16 bits per colour), a resolution of 150 ppi and with all the enhancement options turned off. Before beginning with the reading process, a pre-scan in transmission mode was made (because the scanner turns on in reflection mode by default) and the scanner was left to warm up for half an hour, with the transparent glass plate removed. The images were saved as TIFF. An opaque film was used to the determined zero-light transmitted intensity value I_{bckgd}, which characterizes the scanner's background signal.

An unirradiated film piece is scanned prior to each irradiated one in order to correct for the scanner warm-up. Since the value of optical density (OD) varied between one scan to another for the intercalated checkpoint film pieces, a calibration curve was generated with film pieces that were scanned at the same time (one film piece unirradiated, and seven film pieces irradiated), placing them all together at the centre of the scanning device in order to minimize the effect of the scanner's non-uniform horizontal response. Thus, each value of OD was compared to its corresponding average OD, which was obtained scanning three times the film piece for the same dose value. All the images were processed with the ImageJ software [24], with a region of interest (ROI) of 2 mm × 2 mm.

Using an in-house image application written in MatLab, the red component of the RGB image was extracted, since the absorption spectrum of the EBT2 has a maximum in the red region of the visible spectrum; a two dimensional Wiener filter (in 5 × 5 pixel regions) was also applied to each film image before averaging them, with the intention of decreasing the image noise caused by the imperfections in the film sample. We found that the mean pixel value over the ROI using the Wiener filter decreased and the correspond OD value was the same as the obtained without using the Wiener filter; however, it resulted in a reduced uncertainty of the mean pixel value over the ROI, from 0.72 to 0.33%.

Despite this rigorous process, the intrinsic reproducibility of measured dose was not completely satisfactory for the purpose of absolute dose measurement. This problem could originate from inhomogeneous film response, as was recently reported [25]. In order to reduce potential inaccuracies of the calibration curve, the dose delivered with the f_{ref} to the EBT2 film was tuned so that its planned value would lie as close as possible to that of dose administered with the f_{pcsr}, allowing us to use a very narrow portion of the calibration curve, where its

behaviour can be considered as linear. However, scanning simultaneously both the f_{ref} and the f_{pcsr} films, placed as close as possible to the flatbed centre, minimized uncertainties associated to the scanning process. The combined uncertainty of the dose measurements includes the contribution of the intrinsic reproducibility of the film (enhanced by using the Wiener filter and the tuning of the dose), the scanner reproducibility (enhanced by repeated scanning of film pieces) and the beam monitor/delivery system reproducibility.

Based on previous work of Devic et al. [20], the uncertainty of the net OD for the *i*th scanning of any irradiated film piece was calculated as follows:

$$\sigma^{i}_{netOD} = \frac{1}{\ln 10}\sqrt{\frac{(\sigma^{i}_{I_{un\exp}})^2 + (\sigma_{I_{bckg}})^2}{(I^{i}_{un\exp} - I_{bckg})^2} + \frac{(\sigma^{i}_{I_{\exp}})^2 + (\sigma_{I_{bckg}})^2}{(I^{i}_{\exp} - I_{bckg})^2}} \tag{4}$$

Where I_{unexp} and I_{exp} are the transmission scanning readings for the unexposed and exposed films, respectively, obtained in terms of averaged pixel value over the ROI.

Then, the resulting uncertainty of the averaged net OD over N multiple scanning of irradiated film pieces at the f_{ref} and the f_{pcsr} was obtained as follows:

$$\sigma_{netOD}(D_{ref} \text{ or } D_{pcsr}) = \sqrt{\frac{1}{\sum_{i}^{N}(1/(\sigma^{i}_{netOD})^2}} \tag{5}$$

3. RESULTS

Following this procedure, a combined uncertainty of 0.8% (1σ) was obtained for the dose calibration of the EBT2-scanner system. This allowed measuring the relative dose factor for the f_{pcsr} respect to the f_{ref} with acceptable dosimetric accuracy.

The cavity dose factors were measured for the proposed f_{pcsr}, with three different ICs, that potentially can be used for patient specific QA (Farmer type PTW 30013, semiflex PTW31010 and pinpoint PTW 31016). Consequently, the correction factors for these ICs were found out, using Eq. (3), resulting in the values shown in Table 1, and their relative uncertainty (1σ) was estimated to be 1.1–1.2%, depending on the type of chamber used, as shown in Table 2.

TABLE 1. $k_{Q_{pcsr},Q}^{f_{pcsr},f_{ref}}$ MEASURED CAVITY DOSE FACTORS AND CORRECTION FACTORS FOR THREE DIFFERENT ICs USED IN THE ROUTINE PATIENT SPECIFIC QA

	ICs		
	Farmer PTW 30013 (0.6 cm^3)	Semiflex PTW31010 (0.125 cm^3)	PinPoint PTW 31016 (0.016 cm^3)
Cavity dose factor	0.758 ± 0.003	0.760 ± 0.004	0.757 ± 0.005
$k_{Q_{pcsr},Q}^{f_{pcsr},f_{ref}}$	0.994 ± 0.012	0.991 ± 0.012	0.996 ± 0.012

TABLE 2. SOURCES OF UNCERTAINTIES OF THE DOSE FACTORS AND CORRECTION FACTORS $k_{Q_{pcsr},Q}^{f_{pcsr},f_{ref}}$

Source of uncertainty	Type A (%)	Type B (%)
Reference detector (EBT2)		
Reproducibility of dose measurements at the f_{pcsr}	0.8	—
Reproducibility of dose measurements at the f_{ref}	0.7	—
Overall dose factor uncertainty	1.06	
IC		
Reproducibility of IC readings at the f_{pcsr}		—
Farmer	0.2	
Semiflex	0.4	
PinPoint	0.5	
Reproducibility of IC readings at the f_{ref}		—
Farmer	0.2	
Semiflex	0.3	
PinPoint	0.3	
k_{pol}	—	0.1
k_s	—	0.1

TABLE 2. SOURCES OF UNCERTAINTIES OF THE DOSE FACTORS AND CORRECTION FACTORS $k_{Q_{pcsr},Q}^{f_{pcsr},f_{ref}}$ (cont.)

Source of uncertainty	Type A (%)	Type B (%)
Total uncertainty	0.3–0.6	0.14
Overall IC cavity dose factor uncertainty	0.33–0.61	
Overall $k_{Q_{pcsr},Q}^{f_{pcsr},f_{ref}}$	1.1–1.2	

4. DISCUSSION

The measured values of the correction factors were not significantly different from unity for the studied ICs. These results are in agreement with our routine IC based absolute dosimetry for IMRT patient specific QA, where the encountered discrepancies are usually within the established tolerances (±3%), in part attributable to TPS inaccuracies. This could be explained by the fact that the authors report the average dose calculated by the TPS in a VOI, which correspond to the sensitive volume of the IC, instead of in the centroid of the IC's VOI, and placing this VOI in a low gradient region. Even the VOI created in the TPS for the largest IC (Farmer type) is forced to lay within the low gradient region inside the f_{pcsr}, as shown in Fig. 2.

Furthermore, the correction factors

$$k_{Q_{pcsr},Q}^{f_{pcsr},f_{ref}}$$

will generally be close to unity under the condition that the addition and geometrical matching of fields in the homogeneous phantom compensates for the loss of CPE in the penumbrae of individual field segments [11]. This condition is reinforced in the proposed f_{pcsr} by the rationality used in this system for creating the segments; this essentially ensured low gradient effects, which are by far the main factor responsible for potentially large corrections in IC non-standard beam dosimetry [26].

The results of the

$$k_{Q_{pcsr},Q}^{f_{pcsr},f_{ref}}$$

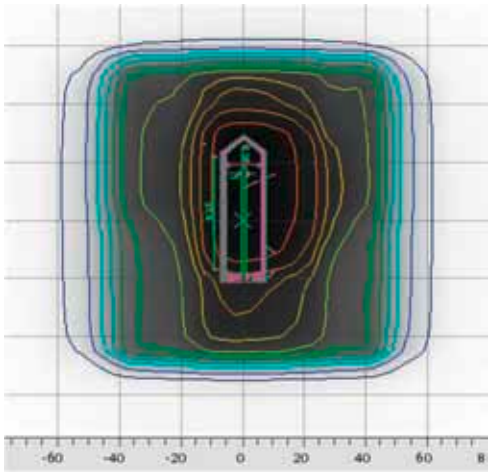

FIG. 2. Dose map and isodoses for the f_{pcsr} in the coronal plane of measurements. A schematic view of the Farmer type chamber is inserted for comparison purposes.

obtained in this study are consistent in some extent with the *C* factors reported by Sanchez-Doblado et al. in Ref. [7], for step-and-shoot IMRT delivery using similar ICs. A better consistency is observed with the results of Chung et al. in Ref. [13], for the collapsed delivery and similar ICs, even when they used a dynamic IMRT delivery with a beamlet based inverse planning approach.

5. CONCLUSIONS

This study supports the reliability of measurements with ICs in the absolute dose verification of our routine aperture based IMRT plans. According to recorded results, beam or phantom setup issues have been frequently identified as main causes of significant discrepancies between calculations and measurements. Sources of discrepancies related to TPS inaccuracies were previously evaluated through an exhaustive dosimetric commissioning of the system. Monte Carlo computation of the relative dose factor for the proposed f_{pcsr} is in progress.

REFERENCES

[1] DAS, I.J., CHENG, C., CHOPRA, K.L., MITRA, R.K., SRIVASTAVA, S.P., GLATSTEIN, E., Intensity-modulated radiation therapy dose prescription, recording, and delivery: Patterns of variability among institutions and treatment planning systems, J. Natl. Cancer Inst. **100** (2008) 300–307.

[2] INTERNATIONAL ATOMIC ENERGY AGENCY, Absorbed Dose Determination in External Beam Radiotherapy: An International Code of Practice Based on Standards of Absorbed Dose to Water, Technical Reports Series No. 398, IAEA, Vienna (2000).

[3] AMERICAN ASSOCIATION OF PHYSICISTS IN MEDICINE, AAPM's TG51 protocol for clinical reference dosimetry of high-energy photon and electron beams, Med. Phys. **26** (1999) 1847–1870.

[4] AMERICAN ASSOCIATION OF PHYSICISTS IN MEDICINE, Task Group-21, Radiation Therapy Committee, AAPM, A protocol for the determination of absorbed dose from high-energy photon and electron beams, Med. Phys. **10** (1983) 741–771.

[5] TESSIER, F., KAWRAKOW,I., Effective point of measurement of thimble ion chambers in megavoltage photon beams, Med. Phys. **37** 1 (2010).

[6] DONG, L., ANTOLAK, J., SALEHPOUR, M., FORSTER, K., O'NEILL, L., KENDALL, R., ROSEN, I., Patient-specific point dose measurement for IMRT monitor unit verification, Int. J. Radiat. Oncol., Biol., Phys. **56** (2003) 867–877.

[7] SÁNCHEZ-DOBLADO, F., HARTMANN, G., PENA, J., CAPOTE, R., PAIUSCO, M., RHEIN, B., LEAL, A., LAGARES, J.I., Uncertainty estimation in intensity-modulated radiotherapy absolute dosimetry verification, Int. J. Radiation Oncology Biol. Phys. **68** 1 (2007) 301–310.

[8] RADIOLOGICAL PHYSICS CENTER, REPORT TO THE AAPM THERAPY PHYSICS COMMITTEE, Report No. 123, 1 (2006).

[9] TOMSEJ, M., et al., Validation of IMRT treatments in head and neck cancer through a European multicentric dosimetric study. Radiother. Oncol. **76** S40, (2005).

[10] BOUCHARD, H., SEUNTJENS, J., Ionization chamber-based reference dosimetry of intensity modulated radiation beams, Med. Phys. **31** (9) (2004) 2454–2465.

[11] ALFONSO, R., ANDREO, P., CAPOTE, R., SAIFUL HUQ, M., KILBY, W., KJÄLL, P., MACKIE, T.R., PALMANS, H., ROSSER, K., SEUNTJENS, J., ULLRICH, W., VATNITSKY, S., A new formalism for reference dosimetry of small and nonstandard fields, Med. Phys. **35** 11 (2008) 5179–5186.

[12] BAILAT, C.J., BUCHILLIER, A., PACHOUD, M., MOECKLI, R., BOCHUDB, F.O., An absolute dose determination of helical tomotherapy accelerator, TomoTherapy High-Art II, Med. Phys. **36** 9 (2009).

[13] CHUNG, E., BOUCHARD, H., SEUNTJENS, J., Investigation of three radiation detectors for accurate measurement of absorbed dose in nonstandard fields, Med. Phys. **37** 6 (2010).

[14] ROSSER, K.E., BEDFORD, J.L., Application of a new dosimetry formalism to volumetric modulated arc therapy (VMAT), Phys. Med. Biol. **54** (2009) 7045–7061.

[15] EZZEL, G.A., et al., IMRT commissioning: Multiple institution planning and dosimetry comparisons, a report from AAPM Task Group 119, Medical Physics **36** 11 (2009) 5359–5373.

[16] CHIU-TSAO, S.T., HO, Y., SHANKAR, R., WANG, L., HARRISON, L.B., Energy dependence of response of new high sensitivity radiochromic films for megavoltage and kilovoltage radiation energies, Med. Phys. **32** (2005) 3350–3354.
[17] LINDSAY, P., RINK, A., RUSCHIN, M., JAFFRAY, D., Investigation of energy dependence of EBT and EBT-2 Gafchromic film, Med. Phys. **37** 2 (2010).
[18] ARJOMANDY, B., TAILOR, R., ANAND, A., SAHOO, N., GILLIN, M., PRADO, K., VICIC, M., Energy dependence and dose response of Gafchromic EBT2 film over a wide range of photon, electron and proton beam energies. Med. Phys. **37** (5) (2010).
[19] SUTHERLAND, J.G.H., ROGERS, D.W.O., Monte Carlo calculated absorbed-dose energy dependence of EBT and EBT2 film, Medical Physics, **37** 3 (2010).
[20] DEVIC, S., SEUNTJENS, J., SHAM, E., PODGORSAK, E.B., Precise radiochromic film dosimetry using a flat-bed document scanner, Med. Phys. **32** (2005) 2245–2253.
[21] VAN BATTUM, L.J., HOFFMANS, D., PIERSMA, H., HEUKELOM, S., Accurate dosimetry with GafChromic EBT film of a 6MV photon beam in water: what level is achievable? Med. Phys. **35** (2008) 704–716.
[22] SCHNEIDER, F., POLEDNIK, M., WOLFF, D., STEIL, V., DELANA, A., WENZ, F., MENEGOTTI, L., Optimization of the Gafchromic™ EBT protocol for IMRT QA, Med. Phys. **19** (2009) 29–37.
[23] FIANDRA, C., RICARDI, U., RAGONA, R., ANGLESIO, S., GIGLIOLI, F.R., CALAMIA, E., LUCIO, F., Clinical use of EBT model Gafchromic™ film in radiotherapy, Med. Phys. **33**, 11 (2006).
[24] ImageJ. Image Processing and Analysis in Java, http://rsb.info.nih.gov/ij
[25] HARTMANN, B., MARTIŠÍKOVÁ, M., JÄKEL, O., Technical Note: Homogeneity of Gafchromic® EBT2 film. Med. Phys. **37**, 4 (2010).
[26] BOUCHARD, H., SEUNTJENS, J., CARRIER, J., KAWRAKOW, I., Ionization chamber gradient effects in nonstandard beam configurations, Med. Phys. **36** (2009) 4654–4663.

ADVANCED DOSIMETRY TECHNIQUES FOR ACCURATE VERIFICATION OF NON-STANDARD BEAMS

E. CHUNG*, E. SOISSON*,**, H. BOUCHARD***,+, J. SEUNTJENS*

* Medical Physics Unit, McGill University
Email: eachung@medphys.mcgill.ca

** Department of Medical Physics, McGill University Health Centre

*** Département de Physique, Université de Montréal

+ Département de Radio-Oncologie, Centre Hospitalier de l'Université de Montréal

Montreal, Quebec, Canada

Abstract

The purpose of this work is to measure machine specific and plan-class specific correction factors applicable in reference dosimetry of non-standard fields. A cylindrical PMMA phantom filled with water was constructed at the center of which absorbed dose to water was measured. Two candidate plan-class specific reference (PCSR) fields were created; one for a linear accelerator (a Varian Clinac™ 6EX) and one for TomoTherapy® based dynamic head and neck IMRT delivery. Relative dose measurement for each PCSR field was carried out using Gafchromic® EBT films, a diamond detector, a guarded liquid-filled ionization chamber (GLIC-03) developed in-house and a PTW micro liquid ionization chamber. Based on the new dosimetry formalism, PCSR correction factors $k_{Q_{msr},Q}^{f_{msr},f_{ref}}$ were measured for five thimble air-filled ionization chambers: Exradin A12, NE2571, Exradin A1SL, Exradin A14 and PinPoint® 31006. For the linac based IMRT delivery, the correction factor was measured in both a fully rotated delivery and a delivery from a single gantry angle, termed a collapsed delivery. For the TomoTherapy® based IMRT delivery, the correction factor was measured only in a fully rotated delivery. For the linac based IMRT delivery, the correction factor for each ionization chamber in the fully rotated delivery was the same (0.996–0.999) within the measurement uncertainty, 0.3%. In the collapsed delivery, the correction factor was dependent on the ionization chamber type (0.992–1.005). For the TomoTherapy® based IMRT delivery, different determinations of the correction factor for the Farmer type chambers were within a 0.4% uncertainty for the different measurements, while there was more variability on the correction factor for smaller ionization chamber types, possibly due to positioning variability. Comparison of measured and expected PCSR

correction factors will aid in the determination of criteria for selecting PCSR fields, thereby paving the way for improved dosimetric accuracy of modern radiotherapy modalities.

1. INTRODUCTION

Modern radiotherapy has become more complicated in its quest to deliver a uniform dose to a defined target volume, while sparing normal structures near the target volume. The calibration and quality assurance of dose delivery also becomes more difficult because various radiotherapy techniques, such as intensity modulated radiation therapy (IMRT), volumetric modulated arc therapy (VMAT), tomotherapy, stereotactic radiosurgery, etc., usually use small fields or composite non-uniform fields. Conventional reference dosimetry protocols, e.g. AAPM TG-51 [1] and IAEA TRS-398 [2], are based on the absorbed dose to water calibration at reference fields, usually a 10 cm × 10 cm field. When these conventional dosimetry protocols are used for radiotherapy techniques using small or non-uniform fields, potentially large dosimetric errors can occur. Firstly, some radiotherapy machines cannot establish the reference 10 cm × 10 cm field. Second, measurements of dose in non-uniform fields are not standardized. Thirdly, reference conditions of non-uniform field deliveries are not defined in the conventional dosimetry protocols. To reduce the potential for errors in the calibration of small and non-uniform (non-standard) fields, new clinical dosimetry methods are required for accurate dose measurements in small and non-standard fields.

The purpose of this work is to determine (measured and calculated) the correction factors defined in the new dosimetry formalism [3]. These correction factors are involved in composite deliveries for air-filled ionization chambers. To this end, the authors created candidate machine specific reference (MSR) and plan-class specific reference (PCSR) fields for small and non-standard field deliveries. We follow the same methodology as published in a recent paper [4].

2. MATERIALS AND METHODS

2.1. Correction factors $k_{Q_{msr},Q}^{f_{msr},f_{ref}}$ and $k_{Q_{pcsr},Q}^{f_{pcsr},f_{ref}}$

An IAEA-AAPM international working group [3] published a new formalism for small and non-standard field dosimetry. They introduced new intermediate reference fields for small and non-standard fields, termed as MSR and PCSR fields, respectively. An MSR field is defined for radiotherapy modalities that cannot establish the 10 cm × 10 cm field. A PCSR field is

representative of a combined dynamic or step-and-shoot dose delivery, which, in total, provides a uniform dose to a simple target volume while maintaining beam modulation similar to clinical treatment fields. Correction factors are defined, which account for differences between conventional reference and small or non-standard field delivery conditions. An MSR correction factor $k_{Q_{msr},Q}^{f_{msr},f_{ref}}$ is defined as:

$$k_{Q_{msr},Q}^{f_{msr},f_{ref}} = \frac{D_{w,Q_{msr}}^{f_{msr}} \Big/ M_{Q_{msr}}^{f_{msr}}}{D_{w,Q}^{f_{ref}} \Big/ M_{Q}^{f_{ref}}} \quad (1)$$

where

$$D_{w,Q_{msr}}^{f_{msr}} \text{ and } D_{w,Q}^{f_{ref}}$$

are the absorbed dose to water in MSR and reference 10 cm × 10 cm fields, respectively, and

$$M_{Q_{msr}}^{f_{msr}} \text{ and } M_{Q}^{f_{ref}}$$

are the ionization chamber readings at the MSR and 10 cm × 10 cm reference fields, respectively. This correction factor was applied to a TomoTherapy® treatment system, which cannot establish the reference 10 cm × 10 cm field. In this work, the MSR field was defined as a 5 cm × 10 cm static field at a distance of 85 cm from the source. Similarly to the MSR correction factor, a PCSR correction factor $k_{Q_{pcsr},Q}^{f_{pcsr},f_{ref}}$ is expressed as below:

$$k_{Q_{pcsr},Q}^{f_{pcsr},f_{ref}} = \frac{D_{w,Q_{pcsr}}^{f_{pcsr}} \Big/ M_{Q_{pcsr}}^{f_{pcsr}}}{D_{w,Q}^{f_{ref}} \Big/ M_{Q}^{f_{ref}}} \quad (2)$$

where

$$D_{w,Q_{pcsr}}^{f_{pcsr}} \text{ and } M_{Q_{pcsr}}^{f_{pcsr}}$$

are the absorbed dose to water and ionization chamber reading, respectively, in a PCSR field. The ratios of dose (PCSR to ref., or MSR to ref.) were measured with energy independent detectors.

2.2. Dynamic head and neck IMRT deliveries

A cylindrical phantom made of a polymethyl methacrylate (PMMA) cylinder filled with water was constructed to mimic a head and neck case. At the center of the phantom, there was a cylindrical hole to insert a radiation detector or an air-filled ionization chamber with a custom-made PMMA sleeve. Two target volumes, PTV-HD (high dose) and PTV-ED (elective dose), and one organ at risk, a spinal cord, were virtually created inside the CT images of the cylindrical phantom using the Eclipse™ treatment planning system (Varian, Palo Alto, CA, USA). Then, two candidate PCSR fields were created for (i) linear accelerator (Varian Clinac™ 6 EX linear accelerator, Varian, Palo Alto, CA, USA) and TomoTherapy® (TomoTherapy Inc., Madison, WI, USA) based dynamic head and neck IMRT deliveries using the CORVUS® and TomoTherapy® inverse treatment planning systems, respectively. Each candidate PCSR field was optimized to deliver a uniform dose to the simple target volume, PTV-HD. The treatment planning system generated dose distributions inside the cylindrical phantom from these two candidate PCSR field deliveries are shown in Fig. 1. Table 1 summarizes the prescribed dose and dose statistics reported from the treatment planning systems for each candidate PCSR field.

2.3. Measurement of the correction factors

The absorbed dose to water in MSR or PCSR field normalized to that in a reference 10 cm × 10 cm field was measured using four radiation detectors: (i) Gafchromic® EBT films (International Specialty Products, Wayne, NJ, USA), a diamond detector (Central X-ray Radiological Institute, St. Petersburg), (ii) a guarded liquid-filled ionization chamber developed in-house (GLIC-03) [5]

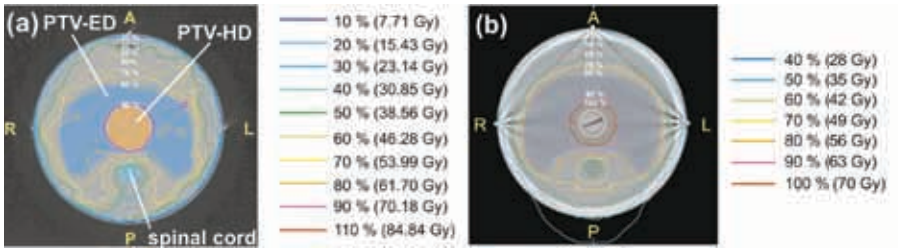

FIG. 1. Dose distribution in a water-filled cylindrical PMMA phantom from (a) linear accelerator and (b) TomoTherapy® based candidate PCSR fields for dynamic head and neck IMRT delivery. Two target volumes (PTV-HD and PTV-ED) and one organ at risk (a spinal cord) are also described.

TABLE 1. PRESCRIBED DOSE AND DOSE STATISTICS FOR THE TWO TARGET VOLUMES AND ORGAN AT RISK FROM THE TWO CANDIDATE PCSR FIELDS REPORTED BY CORVUS® AND TOMOTHERAPY® INVERSE TREATMENT PLANNING SYSTEMS

Volume	Size (cm^3)	Prescribed dose (Gy)	Linac based IMRT delivery		TomoTherapy® based IMRT delivery		
			Ave. (1σ) (Gy)	Dose uniformity(%) = (max.-min.)/ave.	DVH vol.(%)	Ave. (1σ) (Gy)	Dose uniformity(%) = (max.-min.)/ave.
PTV-HD	78.42	70	72.26 (1.16)	14.4	97	71.09 (0.45)	3.84
PTV-ED	585.22	56	64.44 (2.75)	32.9	97	59.78 (3.40)	26.1
spinal cord	21.00	25	20.26 (10.15)	206	50	26.55 (12.19)	154

for the linac based IMRT delivery, (iii) Gafchromic® EBT films and (iv) a PTW micro-liquid ion chamber 31018 (microLion, PTW, Freiburg, Germany) for the TomoTherapy® based IMRT delivery. The collecting region or volume of each radiation detector consists of a water or tissue-equivalent material. Before using them in the relative dose measurement, Gafchromic® EBT films were calibrated using the method described by Bouchard et al. [6]. For the other three detectors, the relative collection efficiency of each detector as a function of dose per pulse was measured or calculated to correct for the detector readings relatively between the PCSR, MSR and reference fields [4, 7].

MSR $k_{Q_{msr},Q}^{f_{msr},f_{ref}}$ and PCSR $k_{Q_{pcsr},Q}^{f_{pcsr},f_{ref}}$

correction factor measurements were carried out for five cylindrical air-filled ionization chambers: (i) Exradin Farmer type chamber model A12 (Standard Imaging, Madison, WI, USA), (ii) NE2571 Farmer type ionization chamber (Nuclear Enterprises, Fairfield, NJ), (iii) Exradin miniature Shonka Thimble chamber model A1SL (Standard Imaging, Madison, WI), (iv) Exradin Microchamber model A14 (Standard Imaging, Madison, WI) and (v) PinPoint® ionization chamber model 31006 (PTW, Freiburg, Germany). The Exradin A12 and NE2571 Farmer type chambers have a collecting volume of 0.6 cm^3 and 0.65 cm^3, respectively, while the other three chambers have a smaller collecting volume, 0.01–0.06 cm^3. In the candidate MSR and PCSR fields and the reference 10 cm × 10 cm field measurements, ion recombination P_{ion} and polarity P_{pol} correction factors for each chamber were measured using the two-voltage technique [1, 2] and the corrections taken into account in the measurement of the ratios of corrected charge. For the linac based IMRT delivery, the PCSR correction factor was measured both in a fully rotated delivery and a delivery from a single gantry angle, termed a ‘collapsed delivery’. For the TomoTherapy® based IMRT delivery, the PCSR correction factor was measured only in a fully rotated delivery. As the TomoTherapy® treatment system cannot establish the reference 10 cm × 10 cm field, the reference field measurement was carried out alternatively using the Varian 6 EX linear accelerator.

2.4. Calculation of the PCSR correction factor $k_{Q_{pcsr},Q}^{f_{pcsr},f_{ref}}$ in idealized conditions

Bouchard et al. [8] derived a simple relation of defining the correction factor in a study of ionization chamber responses to non-standard beams for the ideal PCSR field, where there is perfect dose uniformity (perfect CPE) and hence no gradient effect at the position of an ionization chamber. Under these conditions, the correction factor was shown to be equal to the reciprocal of the

gradient perturbation factor P_{gr} of an ionization chamber in the reference field. The gradient perturbation factor P_{gr} for each air-filled ionization chamber could be determined by two methods: (i) multiplying the dose gradient (0.4%/mm for a 6 MV photon beam at a reference depth) by the ionization chamber shift, which recently has been evaluated by Monte Carlo simulations by Tessier and Kawrakow [9] and (ii) using the empirical formula derived from extensive Monte Carlo simulations by Wang and Rogers [10].

3. RESULTS AND DISCUSSION

3.1. Uncertainty budget

The uncertainty budget in determining the correction factor measurements was investigated in this work. For the linac based IMRT delivery, the PCSR correction factor measurement uncertainty was presented in a recent article [4], which is 0.3% for each air-filled ionization chamber. Table 2 shows the uncertainty budget for the

MSR $k_{Q_{msr},Q}^{f_{msr},f_{ref}}$ and PCSR $k_{Q_{pcsr},Q}^{f_{pcsr},f_{ref}}$

correction factor measurements for TomoTherapy® based deliveries. The positioning uncertainty (type B) was not included. The estimated measurement uncertainty for the PCSR correction factor measurement, 0.29–0.41%, was greater than that for the MSR correction factor measurement, 0.25–0.27%. This was due to the dose rate fluctuation during the lengthy PCSR field measurement (246 s), and its effect was included in the uncertainty budget estimation. On the other hand, for the reference and MSR field measurement, as the irradiation could be finalized within 40 s, the dose rate fluctuation in these fields was very small and negligible.

3.2. MSR correction factor $k_{Q_{msr},Q}^{f_{msr},f_{ref}}$ measurement for the TomoTherapy static field

Figure 2 shows the measured MSR correction factors

$k_{Q_{msr},Q}^{f_{msr},f_{ref}}$

for the TomoTherapy® static 5 cm × 10 cm field. The correction factor measurement was carried out using (a) only the linear accelerator (Clinac™ 6 EX) and (b) the linear accelerator (10 cm × 10cm) and the TomoTherapy®

TABLE 2. UNCERTAINTY BUDGET ON THE DETERMINATION OF MSR $k_{Q_{msr},Q}^{f_{msr},f_{ref}}$ AND PCSR $k_{Q_{pcsr},Q}^{f_{pcsr},f_{ref}}$ CORRECTION FACTORS FOR EACH AIR-FILLED IONIZATION CHAMBER FOR TOMOTHERAPY® STATIC FIELD AND CANDIDATE PCSR FIELD DELIVERIES

Source of uncertainty		MSR correction factor $k_{Q_{msr},Q}^{f_{msr},f_{ref}}$		PCSR correction factor $k_{Q_{pcsr},Q}^{f_{pcsr},f_{ref}}$	
		Type A (%)	Type B (%)	Type A (%)	Type B (%)
Reference detector					
Reproducibility of detector readings in the non-standard fields (microLion)		0.04		0.12	
Reproducibility of detector readings in the reference field (microLion)		0.07		0.07	
Positioning of the detector					
Dose rate dependence			0.07		0.13
P_{pol}			0.05		0.08
Temperature and pressure					
Overall relative dose measurement for each individual reference detector	microLion	0.12		0.20	
	Gafchromic® EBT film	0.3 [Ref. 6]		0.3 [Ref. 6]	
Overall relative dose measurement for all reference detectors combined		0.23		0.25	
Air-filled ionization chamber					
Reproducibility of ionization chamber readings in the non-standard fields		0.03–0.07		0.08–0.19	

TABLE 2. UNCERTAINTY BUDGET ON THE DETERMINATION OF MSR $k_{Q_{msr},Q}^{f_{msr},f_{ref}}$ AND PCSR $k_{Q_{pcsr},Q}^{f_{pcsr},f_{ref}}$ CORRECTION FACTORS FOR EACH AIR-FILLED IONIZATION CHAMBER FOR TOMOTHERAPY® STATIC FIELD AND CANDIDATE PCSR FIELD DELIVERIES (cont.)

Source of uncertainty	MSR correction factor $k_{Q_{msr},Q}^{f_{msr},f_{ref}}$		PCSR correction factor $k_{Q_{pcsr},Q}^{f_{pcsr},f_{ref}}$	
	Type A (%)	Type B (%)	Type A (%)	Type B (%)
Reproducibility of ionization chamber readings in the reference field	0.02–0.05		0.02–0.05	
Positioning of the chamber				
P_{ion}		0.07–0.10		0.09–0.23
P_{pol}		0.03–0.05		0.06–0.12
Temperature and pressure		0.05		0.05
Total uncertainty	0.04–0.09	0.06–0.20	0.10–0.12	0.13–0.26
Overall relative chamber reading uncertainty	0.11–0.15		0.15–0.33	
Overall correction factor uncertainty	0.25–0.27		0.29–0.41	

(5 cm × 10 cm). An MSR field setup used in the linear accelerator measurement was the same as the TomoTherapy®. When using the linear accelerator only, the MSR correction factor is overestimated for all the chambers used in this work. This is because the dose profile from the static TomoTherapy® beam is not flat like the linear accelerator beam due to the absence of a flattening filter. Hence, linear accelerators with flattening filter cannot be used to emulate the MSR field of other radiotherapy modalities; instead, the machine itself has to be used. For the Exradin A12 and NE2571, the measured correction factors (0.997 ± 0.003 and 0.995 ± 0.003, respectively) agree very well with the calculated MSR correction factor in the literature, 0.997 ± 0.001 [11]. For the smaller ionization chambers, the correction factor was 0.4–1.0% lower than that for the Farmer type chambers.

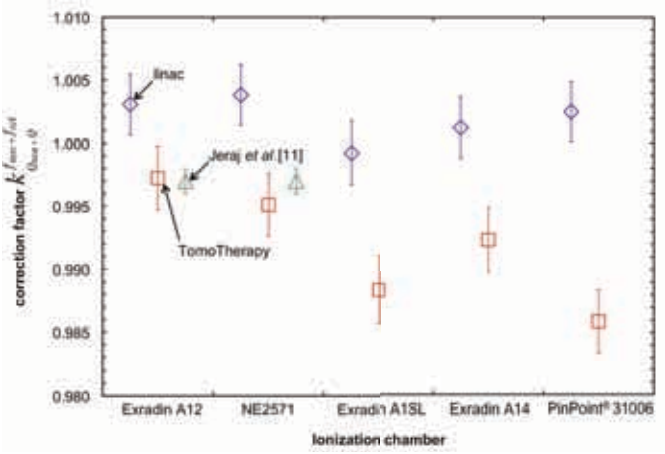

FIG. 2. Measured MSR correction factor $k_{Q_{msr},Q}^{f_{msr},f_{ref}}$ *of a TomoTherapy® static 5 cm × 10 cm field for each ionization chamber. The correction factors are obtained using (i) only the linear accelerator and (ii) the linear accelerator and TomoTherapy® machine. For Farmer type chambers, the calculated MSR correction factor (0.997 ± 0.001) by Jeraj et al. [11] is also presented.*

3.3. PCSR correction factor $k_{Q_{msr},Q}^{f_{msr},f_{ref}}$ measurement results for the two candidate PCSR fields

3.3.1. Linear accelerator based IMRT delivery

The measured PCSR correction factor

$$k_{Q_{pcsr},Q}^{f_{pcsr},f_{ref}}$$

of each air-filled ionization chamber for the linac based IMRT delivery is shown in Fig. 3. In the fully rotated delivery, the measured PCSR correction factor for each chamber is in a narrow range (0.996–0.999). However, the measured correction factor is systematically smaller than the calculated one for all the chambers, as shown in Fig. 3. As the theoretical values assume perfect CPE reconstitution in the dynamic field, the difference between the measured and calculated PCSR correction factors is likely due to residual dose non-uniformity in the region of interest, i.e. inside the PTV-HD. In the collapsed delivery, the measured correction factor shows chamber type dependence (0.992–1.005). In particular, for the smaller ionization chambers (Exradin A1SL, Exradin A14 and PinPoint® 31006), the correction factor is also dependent on the IMRT delivery

technique. This difference is due to systematic effects of gradients and measurement accuracy for the smaller ionization chambers. Details of the correction factor measurement results for the linacbased IMRT delivery have been published elsewhere [4].

3.3.2. TomoTherapy® based IMRT delivery

Figure 4 shows the PCSR correction factor measurement results for the TomoTherapy® based IMRT delivery obtain ed from two different measurements. For the Farmer type chambers, even though

$$k_{Q_{\mathrm{pcsr}},Q}^{f_{\mathrm{pcsr}},f_{\mathrm{ref}}}$$

is about 1% smaller than the calculated one in ideal conditions, the measured correction factor is the same within the measurement uncertainty for each chamber in different measurements. Similarly to the linac delivery, this result indicates that obtaining the full CPE condition may be impossible to achieve in composite non-standard field deliveries [12]. For the smaller ionization chambers, the correction factor for each chamber differs by up to 0.7% in different measurement sessions, possibly due to the influence of positioning uncertainties of the small air-filled ionization chambers in a not perfectly uniform

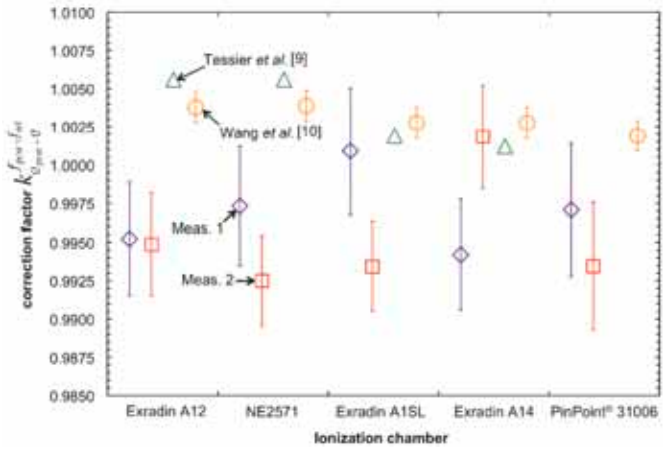

FIG. 3. Measured PCSR correction factor $k_{Q_{\mathrm{msr}},Q}^{f_{\mathrm{msr}},f_{\mathrm{ref}}}$ of the linac based IMRT delivery for each air-filled ionization chamber in fully rotated and collapsed deliveries. Calculated correction factors obtained from Tessier et al. [9] and Wang et al. [10] using Bouchard et al. [8] are also plotted for comparison. (Courtesy of the American Association of Physicists in Medicine (see Ref. [4]).)

composed field. This is shown in Fig. 4, where the measured correction factor agrees well with the calculated correction factors in one measurement, but it deviates from the calculated ones in another measurement session. For the Farmer type chambers, this positioning uncertainty effect was negligible due to the large collecting volume.

4. CONCLUSIONS

In this work, four independent dosimetry techniques were applied for measuring absorbed dose in small and non-standard fields, thereby determining correction factors for these fields based on the new dosimetry formalism [3]. Measurements of correction factors were carried out with a combined standard uncertainty of 0.4% (k = 1). For the two candidate PCSR fields, all measured PCSR correction factors did not differ from unity by more than ±1%. For the different Farmer type chambers, the measured PCSR correction factor for each chamber was the same within the measurement uncertainty and was almost independent of the IMRT delivery technique (fully rotated versus collapsed). On the other hand, the PCSR correction factor for the smaller air-filled ionization chambers was dependent on the IMRT delivery technique or varied by up to 0.7% in different measurement sessions. These results imply that Farmer type chambers may be more suitable for calibrating radiotherapy modalities carrying out composite non-standard field deliveries.

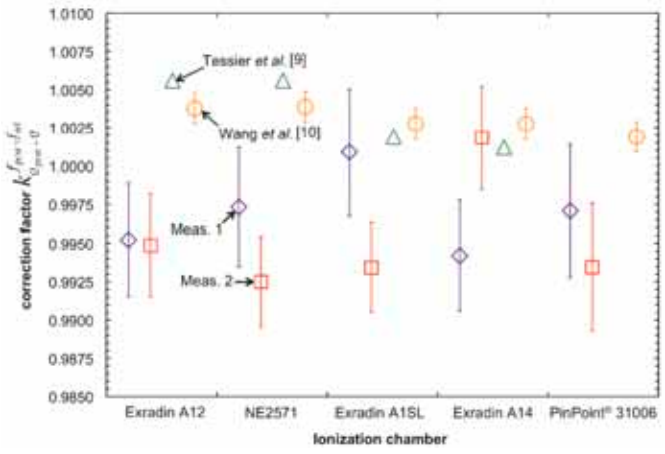

FIG. 4. Measured PCSR correction factor $k_{Q_{\text{pcsr}},Q}^{f_{\text{pcsr}},f_{\text{ref}}}$ *of the TomoTherapy® based IMRT delivery for each air-filled ionization chamber. Calculated correction factors for each chamber are the same as plotted in Fig. 3.*

Future work is to determine criteria for selecting plan-class specific reference fields for non-standard field dosimetry. These criteria may be based on the presumption that an acceptable PCSR field is constituted by the correction factor being close to unity to within a prescribed tolerance. This dictates a sensitivity analysis of the dependence of the correction factor on residual PCSR gradients. Once this is established, it will be possible to formulate recommendations on dosimetry techniques with the aim to improve dosimetric accuracy of radiotherapy techniques using non-standard fields present on virtually all modern dose delivery techniques.

ACKNOWLEDGEMENTS

We would like to thank to Dr. S. Vatnitsky for his guidance on the diamond detector. This work was supported in part by NSERC Grant No. RGPIN 298181. E. Chung is a recipient of a John McCrae Fellowship of the Faculty of Medicine at McGill University and a Research Institute of McGill University Health Centre studentship. H. Bouchard is a recipient of a NSERC doctoral scholarship.

REFERENCES

[1] ALMOND, P.R., et al., AAPM's TG-51 protocol for clinical reference dosimetry of high-energy photon and electron beams, Med. Phys. **26** (1999) 1847.

[2] INTERNATIONAL ATOMIC ENERGY AGENCY, Absorbed Dose Determination in External Beam Radiotherapy: An International Code of Practice for Dosimetry Based on Standards of Absorbed Dose to Water, Technical Reports Series No. 398, IAEA, Vienna (2000).

[3] ALFONSO, R., et al., A new formalism for reference dosimetry of small and nonstandard fields, Med. Phys. **35** (2008) 5179.

[4] CHUNG, E., et al., Investigation of three radiation detectors for accurate measurement of absorbed dose in nonstandard fields, Med. Phys. **37** (2010) 2404.

[5] STEWART, K.J., et al., Development of a guarded liquid ionization chamber for clinical dosimetry, Phys. Med. Biol. **52** (2007) 3089.

[6] BOUCHARD, B., et al., On the characterization and uncertainty analysis of radiochromic film dosimetry, Med. Phys. **36** (2009) 1931.

[7] CHUNG, E., et al., Comparison of characteristics of two liquid-filled ionization chambers, Med. Phys. **37** (2010) 3265.

[8] BOUCHARD, H., et al., Ionization chamber gradient effects in nonstandard beam configurations, Med. Phys. **36** (2009) 4654.

[9] TESSIER, F., et al., Effective point of measurement of thimble ion chambers in megavoltage photon beams, Med. Phys. **37** (2010) 96.

[10] WANG, L., et al., The replacement correction factors for cylindrical chambers in high-energy photon beams, Phys. Med. Biol. **54** (2009) 1609.
[11] JERAJ, R., et al., Dose calibration of nonconventional treatment systems applied to helical tomotherapy, Med. Phys. **32** (2005) 570.
[12] PALMANS, H., Small and composite field dosimetry: the problems and recent progress, Proceedings of IAEA International Symposium on Standards, Applications and Quality Assurance in Medical Radiation Dosimetry (2010).

APPLICATION OF A NEW FORMALISM FOR DOSE DETERMINATION IN TOMOTHERAPY HiArt

M.C. PRESSELLO*, C. DE ANGELIS**, R. RAUCO*, D. ARAGNO*, M. BETTI*, D. VISCOMI**, E. SANTINI*

* Department of Medical Physics,
Azienda Ospedaliera San Camillo Forlanini
Email: mpressello@scamilloforlanini.rm.it

** Department of Technology and Health, Istituto Superiore di Sanità

Rome, Italy

Abstract

The direct application of international Codes of Practice (CoPs) for absolute dose calibration of Tomotherapy HiArt (TTHA) is not possible because of the machine architecture that makes not feasible the recommended reference conditions. Many authors worked to determine correction factors for absorbed dose measurements in order to apply anyway the conventional protocols. Recently, IAEA-AAPM group proposed a new formalism for absolute dose calibration of small and non-standard fields. The authors faced an emerging topic associated to the newer technologies for radiation dose delivery, i.e. the fact that CoPs reference conditions for absolute dose determination (i.e. static, broad and uniform beam) are far from clinical dose delivery conditions (i.e. dynamic beams, superposition of a very large number of beamlets helicoidally delivered). The aim of this paper is to apply the new formalism for the absolute dose calibration with PTW30013 ionization chamber of TTHA static and composite reference beams. For static absolute dose calibration a machine specific reference field for TTHA was defined and a correction factor for ionization chamber reading was determined to take in account the difference in measurement geometry and beam quality between TTHA and the IAEA reference conditions at a conventional Linac. Alanine/EPR dosimetry system was used as reference system for correction factor determination. To perform measurements of absorbed dose to water in dynamic composite fields according the new formalism, a reference volume and a set of reference fields representative of clinical plans were defined. Correction factors for ion chamber response in such conditions were determined. Absolute dose values determined with alanine and with the IAEA new formalism were compared with those obtained applying the other methods proposed in literature to extend the use of CoPs to TTHA.

1. INTRODUCTION

Tomotherapy HiArt (TTHA) is a machine designed for image guided intensity modulated radiation therapy for cancer patients. TTHA radiation delivery modality is very complex, being a combination of rotation of the source, translation of the couch and fast binary movement of 64 pairs of leaves producing a very high number of beamlets (~10^7).

The application of international Codes of Practice (CoPs) for absolute dose determination for TTHA is a challenge because of the machine architecture that makes not feasible the recommended reference conditions. It cannot provide a 10 cm × 10 cm field and absolute dose determination in water is difficult because of the small diameter of the bore, forcing the user to perform absolute calibration in non-standard geometric conditions. Moreover, the lack of flattening filter leads changes in lateral profile of the photon fluence when compared to a conventional linear accelerator (linac) adversely affecting the homogeneity of the dose profile along the length of detector sensitive volume. In addition, energy spectrum modification in linacs without flattening filter has been demonstrated [1] to have an effect on the strength of relationship between beam quality indexes $TPR_{20,10}$ and %dd(10) and the beam quality correction factors k_{Q,Q_0} and k_Q for IAEA TRS-398 [2] and AAPM TG51 [3], respectively.

Some authors carried out Monte Carlo (MC) simulations to determine correction factors for limited number of ionization chambers in order to apply the conventional CoPs to TTHA for absorbed dose measurements [4, 5]. Some authors used those data for absolute dose determination [6], whereas other authors measured chambers correction factors by direct calibration against alanine dosimeters [7].

Recently, a new formalism for absolute dose determination in non-standard field was proposed by the IAEA–AAPM group [8]. It provides a comprehensive and effective extension of TRS-398 [2] for the dose determination in complex radiotherapy machines.

In this paper, the application of the new IAEA formalism to absolute dose determination with the PTW30013 ionization chamber (IC) for static and helical IMRT fields of TTHA is reported and compared to other methods proposed in literature.

Although some authors [9] are carrying out MC simulation to compute correction factors suggested by Alfonso et al. [8], to the authors' knowledge, a complete and systematic application of the new formalism at TTHA has not yet been addressed.

2. METHODS

2.1. Application of IAEA new formalism

According to the new formalism [8], a machine specific reference (MSR) field, f_{msr}, at the beam quality, Q_{msr}, was defined for TTHA and reported in Table 1. In such reference conditions, the absorbed dose, D_w, is given by [8]:

$$D_{w,Q_{msr}}^{f_{msr}} = M_{Q_{msr}}^{f_{msr}} \cdot N_{D,w,Q_0} \cdot k_{Q,Q_0} \cdot k_{Q_{msr},Q_{ref}}^{f_{msrt},f_{ref}} \quad (1)$$

where

M is the IC reading in TTHA specific reference conditions corrected for influence quantities;

$N_{D,w}$ is the IC calibration coefficient at the standards laboratory; and

k_{Q,Q_0} is the beam quality correction factor at TRS-398 compliant reference conditions.

The correction factor

$$k_{Q_{msr},Q_{ref}}^{f_{msrt},f_{ref}}$$

was determined for Farmer PTW30013 IC to account for the beam variations due to the non-conventional reference conditions at TTHA 6 MV photon beam with respect to a Primus Siemens linac 6 MV photon beam ($TPR_{20,10}$ = 0.674) at TRS-398 compliant reference conditions f_{ref}.

TABLE 1. CHARACTERISTICS OF f_{ref} AND f_{msr} FOR ABSOLUTE DOSE DETERMINATION AT LINAC AND TTHA, RESPECTIVELY

	Siemens Primus f_{ref}	TTHA f_{msr}
Field dimension	10 cm × 10 cm	5 cm ×10 cm
Source to surface distance (SSD)	90 cm	75 cm
Source to chamber distance (SCD)	100 cm	85 cm

The characteristics of the two reference conditions are summarized in Table 1. The term

$$k_{Q_{msr},Q_{ref}}^{f_{msr},f_{ref}}$$

as defined in Eq. (2) of Alfonso et al. paper [8], was determined with an experimental approach. Measurement was performed in a water phantom using alanine/EPR dosimetry system, operating at the Istituto Superiore di Sanità, Italian National Institute of Health and traceable to the Italian Primary Standards Dosimetry Laboratory (INMRI-ENEA), as the reference system [10].

The alanine dosimetry system shows suitable characteristics to the aim of this study. Among its features, it is water equivalent, weakly energy dependent (less than 0.6% respect to ^{60}Co) and dose rate independent, and it exhibitslinear behaviour with respect to dose. Moreover, EPR signal is stable with a not destructive the reading process. In addition, dosimeters can be made of small dimensions. In this work, in order to increase the signal to noise ratio, a dosimeter consists of a stack of 4 alanine pellets. Each pellet is 5 mm in diameter and 3 mm in height. All alanine irradiation were performed delivering dose of 10 Gy. The expanded uncertainty associated to absolute dose determination is 1% including the contribute coming from energy dependence.

The innovation of the new formalism consists in introducing a reference condition for composite beams dosimetry, closer to clinical actual delivery. This machine specific reference (MSR) condition has to be in some way intermediate between static broad beam and dynamic composite irradiation. Such a condition includes two new concepts. First, the dose must be measured in a geometrically simple reference volume (RV), extended respect to IC dimensions and with a high homogeneity in dose distribution (reference point is dismissed in composite beam). Then, the delivery modality must be representative of actual clinical treatment, i.e. it has to be a plan class specific reference field (PCSR).

Given a PCSR, dose to water is given by [8]:

$$D_{w,Q_{pcsr}}^{f_{pcsr}} = M_{Q_{pcsr}}^{f_{pcsr}} \cdot N_{D,w,Q_0} \cdot k_{Q,Q_0} \cdot k_{Q_{pcsr},Q_{ref}}^{f_{pcsr},f_{ref}} \quad (2)$$

where M, $N_{D,W}$ and k_{Q,Q_0} are defined in Eq. (1).

The correction factor

$$k_{Q_{pcsr},Q_{ref}}^{f_{pcrsr},f_{ref}}$$

takes into account for the variation in IC response in the composite delivery respect to the f_{ref} condition at linac.

Then, Eq. (9) in Alfonso et al. [8] allows to measure dose in a clinical treatment beam during patient quality assurance procedure, correcting IC response appropriately. This final application of new formalism is beyond the scope of this paper.

The PCSRs proposed in this paper are close to typical patient treatments and were generated varying field dimensions and pitches values (defined as the ratio of coach translation per rotation and field with), with a nearly constant value for the intensity modulation (MA, defined as the ratio of the maximum and the average leaves opening time). Their characteristics are summarized in Table 2. In the last column the dose delivered in a gantry rotation is also reported.

The proposed reference volume is the three dimensional expansion of the static machine specific reference field, a 5 cm × 10 cm × 5 cm parallelepiped. Planned dose distribution homogeneity across RV is better than 1% for all PCSRs. The

$$k_{Q_{pcsr},Q_{ref}}^{f_{pcrsr},f_{ref}}$$

values were determined for PTW30013 for all PCSRs, to investigate the influence of the various delivery parameters on chamber response. Correction factors were experimental determined with alanine according to Alfonso et al. recommendations [8].

A PTW Diamond detector was used to monitor beam stability during irradiations in static fields whereas elapsed monitor units were taken into account in helical irradiations. All measurements were repeated for at least 3 sessions.

Dose determination uncertainties were estimated according to GUM [11] and TRS-398 recommendations [2].

TABLE 2. GEOMETRICAL AND DOSIMETRIC CHARACTERISTICS OF PCSR

PCSR	Field width (cm)	Pitch value	MA	Dose per rotation (Gy)
1	1	0.430	2.3	5.32
2	2.5	0.287	2.1	5.00
3	5	0.215	1.9	4.97
4	5	0.287	2.1	4.94

2.2. Application of TRS-398 and TG51 through MC simulation based methods

Some authors [4, 5] proposed methods to apply TRS-398 and TG51 to dose determination for TTHA beams through correction factors determined with Monte Carlo simulation. The suggestion is to estimate beam quality indexes for CoPs reference conditions (i.e. $TPR_{20,10}$ and %dd(10) in f_{ref} conditions) starting from their experimental values obtained in machine specific reference conditions f_{msr}, in the following indicated as '$TPR_{20,10}$' and '%dd(10)'.

According to Jeray et al. [4], TRS-398 can be applied directly in f_{msr} conditions and absorbed dose to water, $D_{w,}$ is given by:

$$D_w = M \cdot k_{tot} \cdot N_{D,w} \tag{3}$$

where M and $N_{D,w}$ are defined in Eq. (1).

k_{tot} is the product of two terms, k_{mr} and k_Q, with k_{mr} calculated with Monte Carlo and is equal to 0.997.

It accounts for difference in set-up and geometry respect to IAEA reference conditions.

k_Q is the quality factor determined from TRS-398 tabulated values using as input the '$TPR_{20,10}$' value measured in f_{msr} and increased of about 2.5% [4].

To apply this method, '$TPR_{20,10}$' was measured in f_{msr} using two different phantoms, a flat solid water phantom (15 cm × 50 cm × 35 cm VitualWater™, Standard Imaging Inc.) and a 30 cm × 30 cm × 50 cm PTW water phantom.

For absolute dose determination with TG51 in TTHA beam, Thomas et al. [5] proposed a MC derived polynomial fit to determine %dd(10) from '%dd(10)' measured in f_{msr} conditions. Therefore, the percentage dose at 10 cm, '%dd(10)', was measured in water and %dd(10) determined. PTW 30013 chamber was identified by the manufacturer as the waterproof version of PTW30001 [4]; hence the TG51 CoP was applied for dose determination making this assumption.

Finally, an experiment was designed to irradiate the IC at 10 cm depth in water with a static field. Absolute dose value was determined applying TRS-398 and TG51 with the previous described MC based methods [4, 5]. Alfonso et al. [8] formalism was also applied thanks to the correction factor determined as described in Section 2.1. Results were compared with dose value measured directly with alanine dosimeters, which were also irradiated in that experiment.

3. RESULTS AND DISCUSSION

3.1. IAEA new formalism correction factors determination

Correction factor for PTW30013 in f_{msr}, determined according to the new formalism, with alanine as reference dosimeter, is summarized in Table 3.

According to the Xiong and Rogers MC study [1] the lack of linac flattening filter leads to an overestimation of $k_{q,q0}$ when $TPR_{20,10}$ is used as beam quality index. Therefore,

$$k_{Q_{msr},Q_{ref}}^{f_{msr},f_{ref}}$$

is expected to be less than unity differently than that determined in the present experiment. Our result could be explained taking into account the unflatness of transversal photon fluence profile along the length of detector sensitive volume causing volume averaging effects in charge collection.

In fact, the lowering of mean value of collected charge in f_{msr} condition leads to correction factor respect to f_{ref} condition at linac greater than unity, concealing the effect coming from the beam quality. This was proven by a multidetector study not reported in this paper and was observed by other authors in the application of the new formalism to Cyberknife [13].

Correction factors for the set of plan class specific reference fields are reported in Table 3. Uncertainties associated to correction factors determined in static and composite conditions are 1.5 % and 1.7%, respectively. Main contributes to uncertainties come from alanine reproducibility and dosimeters repositioning.

The

$$k_{Q_{pcsr},Q}^{f_{pcsr},f_{ref}}$$

for the different PCSR are all less than unity; PCSRs with the greater field width seems to have correction factors closer to unity regardless pitch values, so they

TABLE 3. NEW IAEA FORMALISM CORRECTION FACTORS FOR PTW30013 IC IN STATIC AND COMPOSITE REFERENCE FIELDS

$k_{Q_{msr},Q}^{f_{msr},f_{ref}}$	$k_{Q_{pcsr},Q}^{f_{pcsr},f_{ref}}$			
MSR	PCSR1	PCSR2	PCSR3	PCSR4
1.016	0.977	0.977	0.994	0.998

are good candidate for further steps of the implementation of the new formalism. PCSR3 and PCSR4 can be considered representative of clinical treatment plans with field with equal to 5 cm. It worth of note that this field width is typically used for medulloblastoma treatments that are only a little fraction of the overall patients treated with TTHA. On the other hand, PCSR2 is representative of a large number of treatments but it has a correction factor far from unity. It seems that a better understanding of the meaning of 'representativeness' is necessary. In the meantime, PCSR4 and PCSR5 will be used to carry on the application of the relative dosimetry route according the new formalism.

3.2. Absolute dose determination in TTHA static reference beam

The beam quality index '$TPR_{20,10}$' measured in f_{msr} in the solid water phantom resulted was equal to 0.613; in agreement (<0.2%) with other experimental values [6] determined in the same conditions. This confirms that the beam used in this paper can be considered representative of several TTHA machines.

'$TPR_{20,10}$' measured for f_{msr} also in water phantom resulted equal to 0.627, in agreement (<0.8%) with MC calculated [4] and analytically fitted [14] values. The difference with respect to solid water phantom measurement was of about 2% and it could be ascribed to different scatter conditions in the two experimental set-up, mainly due to the difference in phantoms dimensions as described in Section 2.2. Starting from '$TPR_{20,10}$' Jeraj et al. [4] method could then be applied to determine absolute dose with TRS-398.

The beam quality index, '%dd(10)', measured in water in f_{msr} conditions was 59.8%, in agreement (within 1%) with MC calculated value [4]. This value is within the range of applicability of the Thomas et al. polynomial fit [5] and therefore %dd(10) value was calculated and dose could be determined with TG51.

Alfonso et al. [8] formalism was also applied using the correction factor determined in this paper and reported in Table 3. Results are reported in Table 4 together with dose value measured directly with alanine dosimeters irradiated in the same experiment. For each method, percentage differences respect to alanine dose are reported in the last column.

As described in Section 2.2, the IC was irradiated at 10 cm depth in water with a static field. Absolute dose value was determined applying TRS-398 and TG51 with the previously described MC based methods, and the results are reported in Table 4.

Differences among data in Table 4 with respect to alanine are within experimental uncertainties, suggesting that the methods can be considered equivalent. Nevertheless, it should be pointed out that the 'recommendation' of

TABLE 4. ABSOLUTE DOSE DETERMINATION IN TTHA STATIC REFERENCE FIELD, f_{msr}

	Dose (Gy)	Percentage difference
TRS-398 expansion [4]	9.97	–1.8
TG51expansion [5]	10.01	–1.4
New IAEA formalism [8]	10.13	–0.2
Alanine	10.15	

measuring CoPs beam quality indexes in non reference conditions can lead to not univocal interpretations among users. For example, to apply Eq. (4), some authors [6] calculated $TPR_{20,10}$ directly from the '$TPR_{20,10}$' value measured in the flat solid water phantom, despitethe measured value being about 3% lower than the value determined in water in f_{msr}, both with the MC calculation [4] and with the experiment reported in this paper. Although such a difference in '$TPR_{20,10}$' leads to a difference of only about 0.5% in the estimated $k_{Q,Q0}$, it is clear that the standardization of the Alfonso et al. new formalism [8] is mandatory.

4. CONCLUSIONS

In this paper, the correction factors for Farmer PTW30013 IC for absolute dose determination in static and composite TTHA reference fields have been experimentally determined applying the Alfonso et al. formalism.

A set of a PCSR fields, representative of actual clinical treatments, was proposed, and a proper reference volume was defined with the aim to standardize composite fields dosimetry at TTHA.

The new IAEA formalism was eventually applied for absolute dose determination in a static beam irradiation, and the result was compared with those obtained using other CoPs extensions proposed in the literature and with alanine. Although differences among the obtained results are within experimental uncertainties, the application of the new formalism provides both a standardization of approach for dose determination at TTHA and a comprehensive and effective extension of TRS-398, which allows to overcome the problem relative to the appropriateness of $TPR_{20,10}$ as beam quality index in unflattened beams.

REFERENCES

[1] XIONG, G., ROGERS. D.W.O., Relationship between %dd10$_x$ and stopping-power ratios for flattening filter free accelerators: A Monte Carlo study Med. Phys. **35** (2008).

[2] INTERNATIONAL ATOMIC ENERGY AGENCY, Absorbed Dose Determination in External Beam Radiotherapy: An International Code of Practice for Dosimetry Based on Standards of Absorbed Dose to Water, Technical Reports Series No. 398, IAEA, Vienna (2000).

[3] ALMOND, P.R., BIGGS, P.J., COURSEY, B.M., HANSON, W.F., HUQ, M.S., NATH, R., ROGERS, D., W.AAPM's TG51 protocol for clinical reference dosimetry of high-energy photon and electron beams, Med. Phys. **26** (1999).

[4] JERAJ, R., MACKIE, T.R., BALOG, J., OLIVERA, G., Dose calibration of non-conventional treatment systems applied to helical Tomotherapy, Med. Phys. (2005).

[5] THOMAS, S., MACKENZIE, D., ROGERS, M., FALLONE, B.G., A Monte Carlo derived TG-51 equivalent calibration for helical Tomotherapy, Med. Phys. **32** (2005).

[6] BAILAT, C.J., BUCHILLIER, T., PACHOUD, M., MOECKLI, R., BOCHUD, F.O., An absolute dose determination of helical tomotherapy accelerator, TomoTherapy High-Art II Med. Phys. **36** (2009).

[7] DUANE, S., NICHOLAS, D., PALMANS, H., SCHAEKEN, B., SEPHTON, J., SHARPE, P., THOMAS, R., TOMSEJ, M., VERELLEN, D., VYNCKIER, S., Dosimetry audit for Tomotherapy using alanine/EPR, Med. Phys. **33** (2006).

[8] ALFONSO, R., ANDREO, P., CAPOTE, R., HUQ, M.S., KILBY, W., KJÄLL, P., MACKIE, T.R., PALMANS, H., ROSSER, K., SEUNTJENS, J., ULLRICH, W., VATNITSKY. S., A new formalism for reference dosimetry of small and nonstandard fields, Med. Phys. **35** (2008).

[9] STERPIN, E.S., MACKIE, T.R., LU, W., OLIVERA, G.H., VYNCKIER, S., Calculation of K Correction Factors with Monte Carlo Simulations in Tomotherapy Clinical Helical Deliveries for Future Ion Chamber Reference Dosimetry Protocols of Non-standard Beams, Int. J. R Onc Biol Phys **75**, 3 Suppl. (2009).

[10] ONORI, S., BORTOLIN, E., CALICCHIA, A., CAROSI, A., DE ANGELIS, C., GRANDE, S., Use of the commercial alanine and TL dosemeters for dosimetry intercomparisons among the Italian radiotherapy centres, Rad. Prot. Dosim. 120, 2006.

[11] BIPM, IEC, IFCC, ISO, IUPAC, IUPAP, OIML, Guide to expression of Uncertainty in Measurement, Geneva, International Organization for Standardization (1995).

[12] RAMESH, C., TAILOR, W.F., HANSON, N.W., IBBOTT, G.S., Consistency of absorbed dose to water measurements using 21 ion-chamber models following the AAPM TG51 and TG21 calibration protocols, Med. Phys. **33** (6) (2006).

[13] PANTELIS, E., MOUTSATSOS, A., ZOURARI, K., KILBY, W., ANTYPAS, C., PAPAGIANNIS, P., KARAISKOS, P., GEORGIOU, E., SAKELLIOU, L., On the implementation of a recently proposed dosimetric formalism to a robotic radiosurgery system Med. Phys. **37** (5) (2010).

[14] SAUER, O.A., Determination of the quality index Q for photon beams at arbitrary field sizes, Med. Phys. **36** (9) (2009).

CONCERNS IN FRANCE OVER THE DOSE DELIVERED TO THE PATIENTS IN STEREOTACTIC RADIATION THERAPY

S. DERREUMAUX
Institut de Radioprotection et de Sûreté Nucléaire, Fontenay-aux-Roses
Email: sylvie.derreumaux@irsn.fr

G. BOISSERIE
Groupe Hospitalier Pitié Salpêtrière, Paris

G. BRUNET
Centre René Gauducheau, Saint-Herblain

I. BUCHHEIT
Centre Alexis Vautrin, Vandoeuvre-les-Nancy

T. SARRAZIN
Centre Oscar Lambret, Lille

France

Abstract

Following the Toulouse accident, in which 145 patients treated by stereotactic radiation therapy were overexposed, the French authorities ordered in 2008 the creation of a national working group to establish a national protocol for the determination of the absorbed dose in very small photon beams. The WG made a national survey to know the current practices in the French centres regarding treatment delivery and beam commissioning. It also performed a comparison of the beam data measured in different centres but in similar irradiating conditions. The WG also began a campaign of measurements of the beam dosimetry data for different kinds of stereotactic systems delivering X ray beams (standard linear accelerators with additional mMLC, Novalis using m3 mMLC or additional circular collimators, CyberKnife). The results of the national survey and of the WG first measurements are presented here, confirming the need to improve rapidly the knowledge and the control of the dose delivered to the patients with small fields, especially the smallest ones (<10 mm).

1. INTRODUCTION

In 2006–2007, the Toulouse accident occurred that affected 145 patients treated by stereotactic radiation therapy (SRT) for head disease. The technical

expertise performed by the Institute of Radiation Protection and Nuclear Safety (IRSN) revealed that it was due to an error made during the commissioning of the installation of a Novalis system: the measurement of the total scatter factors (or output factors) for the beams defined by the BrainLAB m3 micro MLC had been made using an inappropriate detector (a Farmer type ionization chamber). This led to overdosage of all patients up to 200% [1, 2]. In addition, BrainLAB gave information that the values of the scatter factors measured by different users of the Novalis system varied from 0.4 to 0.68 for the beams collimated with the 4 mm diameter cone, which represents a spread greater than 50%.

Consequently, the French authorities asked the IRSN to set up a working group (WG), in collaboration with the French Society of Medical Physicists (SFPM) in order to establish a national protocol for the determination of the absorbed dose in very small photon beams.

2. NATIONAL SURVEY

The WG first conducted a national survey on the current practices in the French centres regarding treatment delivery and beam commissioning of the small beams used for stereotactic radiosurgery (SRS) or SRT. A questionnaire was sent to all the centres that are likely performing SRS/SRT. The questions were related to the techniques and the materials used to treat patients and to the materials and the procedures used for beam commissioning. Moreover, electronic files with the results of the beam data measurements were requested in order to evaluate the spread of the measured values. Fifteen out of the 23 recipient centres responded to the questionnaire and provided the WG with their beam data (voluntary participation).

2.1. Materials used in the French centres for small beams delivery and dosimetry

The devices used for the SRT/SRS treatments in the 15 participating centres are listed in Table 1. In 2008, the irradiation technique most commonly used in France for delivering stereotactic beams was a linear accelerator with the BrainLAB m3 micro MLC (mMLC), integrated (Novalis) or added to the machine (different models of the Varian Clinac family, Elekta SLi 25). Three centres had a CyberKnife and two centres had one or two Gamma Knife; two centres used circular collimators added to a linac. The survey also showed that the detector most commonly used for measurement of output factors of conventional linacs was, by far, the 0.015 cm^3 PTW PinPoint chamber (PTW 31006) (Table 2).

TABLE 1. DEVICES USED FOR SRS/SRT TREATMENTS IN THE 15 PARTICIPATING FRENCH CENTRES

	Conventional linac (including Novalis)				CyberKnife	Gamma Knife
Centre	Linac	Energy	mMLC	Circular collim.	6 MV	^{60}Co
1	BrainLAB Novalis	6 MV	BrainLAB m3 (integrated)	Yes	/	/
2	Varian Clinac 23 EX	6 MV	BrainLAB m3	/	Yes	/
3	Varian Clinac 2100 C	6 MV	BrainLAB m3	Yes	/	/
4	Varian Clinac 23 EX	6 MV	Millennium (integrated)	/	Yes	Yes
5	/	/	/	/	Yes	/
6	/	/	/	/	/	Yes (2)
7	Elekta Si 25	6 MV	BrainLAB m3	/	/	/
8	Varian Clinac 2100 C	6 MV	BrainLAB m3	/	/	/
9	Varian Clinac 2100 EX	6 MV	Millennium (integrated)	/	/	/
10	Elekta Synergy	6 MV	Beam modulator (integrated)	/	/	/
11	Varian Clinac 2100 CD	6 MV	BrainLAB m3	/	/	/
12	Varian Clinac 600 C/D	6 MV	BrainLAB m3	/	/	/
13	Varian Clinac 2100 C	25 MV	BrainLAB m3	/	/	/

TABLE 1. DEVICES USED FOR SRS/SRT TREATMENTS IN THE 15 PARTICIPATING FRENCH CENTRES (cont.)

	Conventional linac (including Novalis)				CyberKnife	Gamma Knife
Centre	Linac	Energy	mMLC	Circular collim.	6 MV	^{60}Co
14	Elekta SL	6 MV	Arancio DMLC	/	/	/
15	Varian Clinac 600 C/D	6 MV	BrainLAB m3	/	/	/

TABLE 2. DETECTORS USED IN THE 15 PARTICIPATING FRENCH CENTRES FOR THE MEASUREMENT OF OUTPUT FACTORS IN SMALL BEAMS

Irradiating device	Number of centres using 1, 2 or more different types of detectors			Number of centres using each type of detector					
				Ionization chamber			Other		
	1 detector	2 detectors	≥ 3 detectors	0.01 (cm^3)	0.015 (cm^3)	0.04 (cm^3)	Stereo. diode	Diamond	Film (silver)
Linac + mMLC	9	4	0	1	11	1	2	1	1
Linac + circ. collim.	1	0	1		2		1	1	1
CyberKnife	3	0	0				3		

For CyberKnife, the three centres used a stereotactic diode (PTW type P 60008). Few centres tried to measure the OF with more than one type of detector.

In fact, most physicists followed the instructions of the manufacturers regarding the choice of the detector while those instructions were not always optimal. For instance, for the measurement of the OF, BrainLAB recommended to use a medium-sized detector (PinPoint ionization chamber with a volume equal or smaller than 0.03 cm^3) for all field sizes Accuray recommended the use of the PTW 60008 diode for the Cyberknife.

A review of the international literature on the subject shows however that a Pinpoint chamber and a PTW 60008 diode respectively underestimates by about 10% and overestimates by about 5% the measured dose in the smallest field sizes (~5 mm) [3–6]. None of the manufacturers encouraged physicists to use different kind of detectors in order to compare the results and to have a critical approach.

2.2. Comparison of the beam data measured in different centres

For similar irradiation conditions (6 MV RX; BrainLAB m3 microMLC; SSD = 1000 mm; z = 50 mm), the spread of the measured values of scatter factors was around 5–10% for field sizes equal or greater than 12 mm × 12 mm and around 30% for the smallest field (6 mm × 6 mm), in agreement with the international literature. The position of the mMLC leaves and of the jaws are the one corresponding to the 'diagonal' of the BrainLAB protocol WOI 10-26: 6 mm, 12 mm, 18 mm, 24 mm, 30 mm, 36 mm, 42 mm, 60 mm, 80 mm, 100 mm for the mMLC leaves and 6 mm, 12 mm, 18 mm, 42 mm, 42 mm, 42 mm, 42 mm, 60 mm, 80 mm, 100 mm for the jaws.

The measurement uncertainty is a combination of uncertainties due to the size and the composition of the detector, the orientation (parallel or perpendicular to the beam axis) and the centring of the detector, and the drift of the response. The spread of the OF values is also due to the differences between machines: different geometry of the collimating systems upstream the mMLC and different focal spot size [7, 8].

For precise dosimetry, the response and possible correction factor of the detectors in small beams has to be determined for each type of dosimeter and for each machine model, and maybe each individual machine. For instance, for identical measuring conditions (X ray 6 MV, mMLC type, SSD, depth, type and orientation of the detector), a discrepancy of about 15% is observed between the extreme values of the OF measured with the PTW 31006 pinpoint chamber for the 6 mm × 6 mm beam of different Varian clinac models. This can be explained by the experimental uncertainties (chamber centring), but maybe also by different machine models.

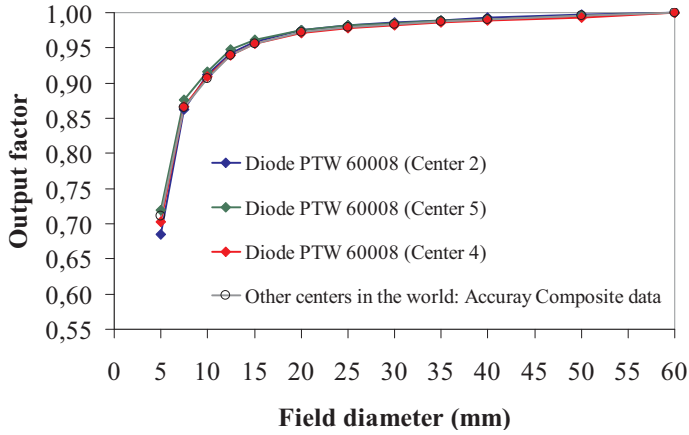

FIG. 1. Measurement of the OF for the CyberKnife in three centres (SDD = 800 mm, depth = 15 mm).

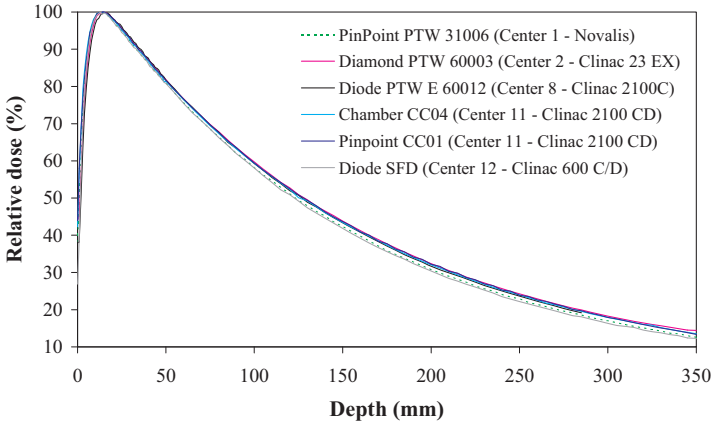

FIG. 2. Percentage depth doses for a 6 mm square field (6 MV) measured with different kinds of detectors for different linacs with the BrainLAB m3 mMLC (SSD = 1000 mm; depth = 50 mm).

For the CyberKnife: OF values from the three centres are very close, with maximum difference of about 5% in the smallest field of 5 mm diameter (Fig. 1). But this apparent excellent results are due to the fact that all of them use the same detector (PTW 60008 diode). So a possible systematic deviation due to the choice of the detector could not be detected [9].

The values of the percentage depth doses (PDD) with different types of detectors and for different linacs in five centres (6 MV X ray beams), for the smallest field size defined by the BrainLAB m3 mMLC (6 mm × 6 mm) reveals small discrepancies, with a maximum deviation of about 2% (Fig. 2).

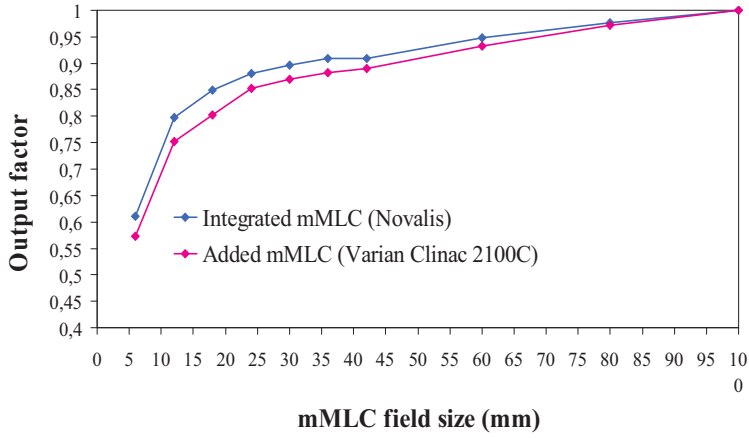

FIG. 3. Output factors measured with an SFD diode for the BrainLAB m3 mMLC integrated (Novalis) or added to the accelerator head (Varian Clinac 2100 C); 6 MV, SSD = 1000 mm; depth = 50 mm.

3. MEASUREMENTS PERFORMED BY THE WG

The WG began a campaign of measurements of the data needed to characterize the small beams for different kinds of stereotactic systems delivering X ray beams (standard linear accelerators with additional mMLC, Novalis using the m3 mMLC or additional circular collimators, CyberKnife). The aim of the campaign was to compare and analyse the response of commercial detectors that are usually used in the radiotherapy centres (different pinpoint chambers and stereotactic diodes) together with more particular but a priori more adapted detectors (various types of tissue equivalent solid state detectors).

The first results showed the strong impact of the collimation system upstream the mMLC: OF values measured with a SFD stereotactic diode are higher for all field sizes (up to about 5% for the beam sizes smaller than 20 mm) if the BrainLAB m3 mMLC is integrated in the head of the accelerator (Novalis) than if it is added to the head (Varian Clinac) (Fig. 3).

An expected small increase (of about 2%) of the OF values has also been observed for the BrainLAB m3 mMLC with the new PTW 31014 pinpoint chamber with an aluminium central electrode, as compared to the PTW 31006 chamber having a steel central electrode (Fig. 4). This can be explained by a slight over-response of the PTW 31006 chamber in the 100 mm × 100 mm reference field compared to its response in small fields, the reference field containing a higher scattered photon component [10].

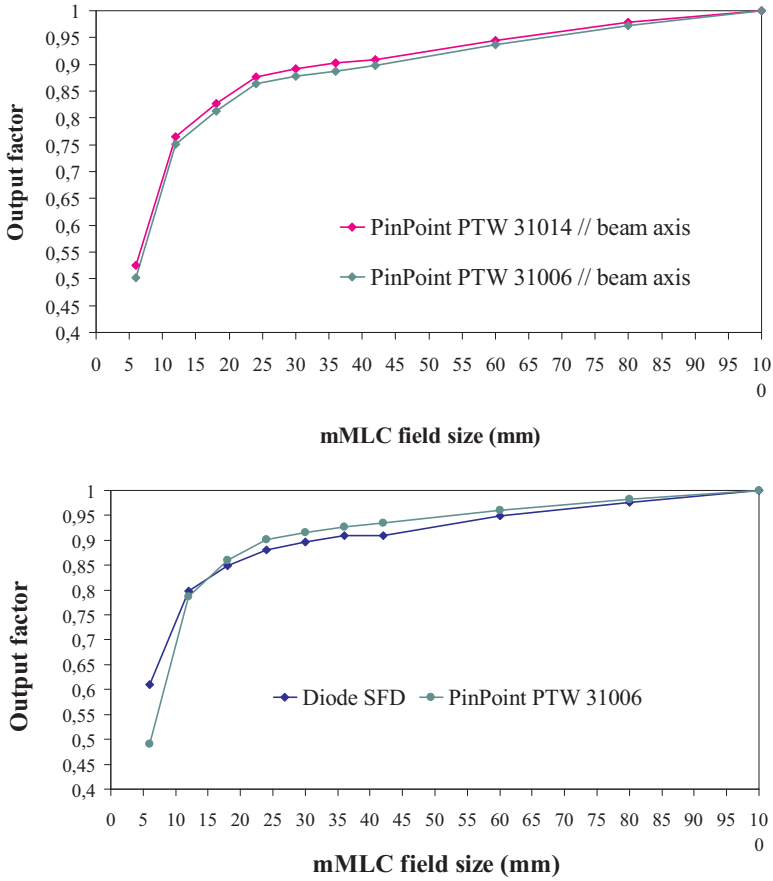

FIG. 4. Output factors measured for the BrainLAB m3 mMLC and 6 MV linacs, SSD = 1000 mm; depth = 50 mm. Top: measurements with a PTW 31006 and a PTW 31014 pinpoint chambers parallel to the beam axis and Varian 2100C linacs. Bottom: measurements with a stereotactic a SFD diode and a PTW 31006 PinPoint chamber on a Novalis.

Also, for the BrainLAB m3 mMLC and measurements performed on the same linac at a depth 50 mm, the SFD diode gives OF values smaller by about 2–3% than the one obtained with a PTW pinpoint chamber, for the beam sizes greater than 12 mm × 12 mm (Fig. 4). For the smallest beams, the SFD diode gives higher OF values due to volume effect of the pinpoint chamber. The particular behaviour of the SFD diode relative to other detectors (CC01 pinpoint chamber and a shielded diode) has already been observed by Ding, with the jaws position fixed to 98 mm × 98 mm [11]. It could be explained by an energy dependence of the SFD response (unshielded diode) and/or by an influence of the chamber (stem, handle).

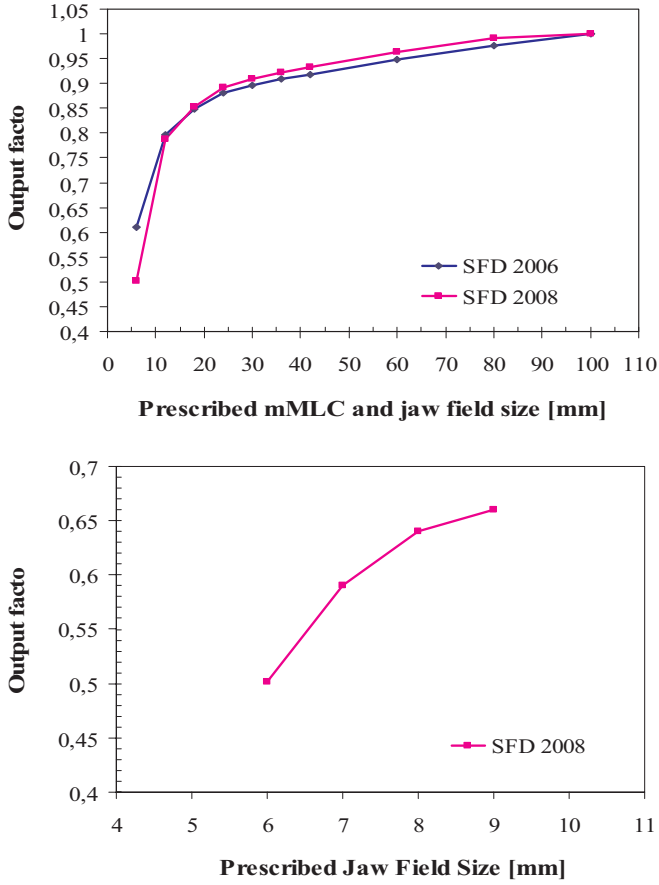

FIG. 5. Output factors measured with a stereotactic SFD diode in 2006 and in 2008, for the same Novalis system with BrainLAB m3 mMLC (6 MV, SSD = 1000 mm; depth = 50 mm). Top: The position of the mMLC leaves and of the jaws are the one corresponding to the 'diagonal' of the BrainLAB protocol WOI 10-26. Bottom: The position of the mMLC leaves is fixed to 6 mm × 6 mm, and the jaws are moved to define beam sizes of successively 6, 7, 8 and 9 mm (prescribed size).

An important observation was that using a mMLC, when the beam is collimated by aligned jaws and mMLC leaves (for instance, for a 6 mm × 6 mm square field delimited by the jaws and by the mMLC), additional important uncertainty on the OF values of the very small fields (< 10 mm) comes from the jaws 'aperture and centring. When comparing the OF measured with a SFD diode at the same Novalis installation in 2006 and in 2008, a large discrepancy of about 20% was discovered for the smallest field size (6 mm × 6 mm) (Fig. 5). It was found that the jaws were placed little inside the mMLC field and that the true

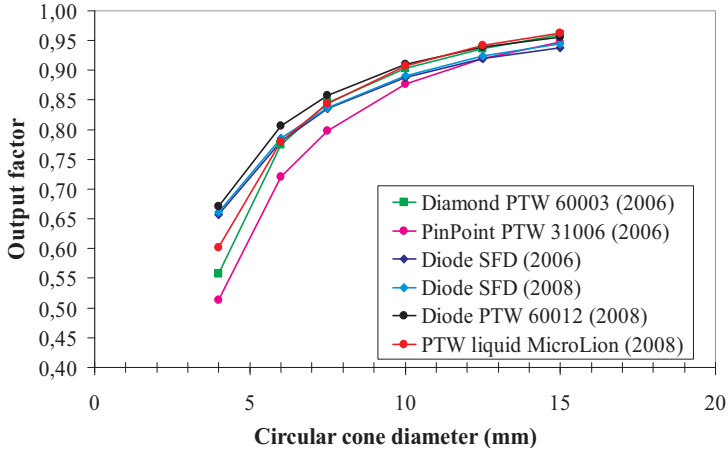

FIG. 6. Output factors measured with different commercial active detectors for a Novalis (6 MV) with added circular collimators, SDD = 1000 mm, depth = 14 mm, jaws aperture = 50 mm and m3 mMLC aperture = 100 mm (reference field: SSD = 1000 mm, depth = 14 mm, jaws aperture = 98 mm and m3 mMLC aperture = 100 mm).

field size was 4 mm in one direction and 5 mm in the other. When opening progressively the jaws 1 mm × 1 mm, the OF rapidly increased (Fig. 5), reaching a plateau a few millimetres further (results not shown).

Therefore, a ~1–2 mm uncertainty on jaws positioning can induce a very important change of the OF value for the smallest field sizes. It was determined that a systematic few millimetres withdrawal of the jaws outside the field defined by the leaves of the mMLC allows one to get free from the problem. For instance for a Novalis, the optimal withdrawal of the jaws is 2 mm and 5 mm in the directions perpendicular and parallel to the displacement of the leaves, respectively. A similar recommendation was inserted in the BrainLAB Physics Technical Reference Guide issued at the end of 2008.

Output factors measured with different commercial active detectors for a Novalis (6 MV) have also been compared in the case of additional collimation by circular cones. The irradiating conditions are quite different than the one for the mMLC, following the BrainLAB protocol WOI 09-10 (Fig. 6).

The OF obtained with the SFD diode are about 2% lower than those measured with the PTW 60012 diode. The fact that the PTW 60008 and 60012 diodes overestimate by a few per cents the OF in the smallest circular fields (<10 mm) of the CyberKnife [7, 12] suggests that the SFD diode better estimates the dose in the smallest fields than PTW diodes do in the case of measurements performed at the depth of maximum dose (depth = 14 mm).

It is interesting to note that the OF measured with the 'tissue-equivalent' PTW 60003 diamond detector and PTW MicroLion liquid chamber are in agreement with the PTW 60012 diode for the field sizes greater than 10 mm. For smaller beams, their responses fall, reaching values lower by more than 10% than those obtained with the diodes (SFD and PTW), for the smallest 4 mm diameter field. This is due to the volume effect: it is well known for the PTW natural diamond detector; for the PTW liquid chamber, the diameter of the active volume is also too large (2.5 mm) for the smallest field sizes.

Owing to the long time required to reach the initial goal of the WG measurement campaign and to the need for the WG to produce rapidly a report for the French authority, the WG ended its work providing provisory national recommendations on the dosimetry of small beams (see Section 5) [13]. One main recommendation was to continue the measurement campaign in order to improve the knowledge of the dose delivered in the smallest beams (size <10 mm). Today, this work is in progress through an IRSN R&D project in collaboration with the French centres that had participated in the WG. Results will be submitted for publication in the coming months, including measurements with solid state tissue-equivalent detectors and different SRT/SRS devices.

4. DOSE CALCULATION BY TREATMENT PLANNING SYSTEMS

Measurement uncertainties in small fields are not the sole problem for correct determination of the dose delivered to the patients in stereotactic radiotherapy. Indeed, one has also to take into account the uncertainties and errors due to the limits of usual algorithms, especially for calculation of the absorbed dose in highly heterogeneous medium in stereotactic body radiation therapy (SBRT).

Until 2008, all the algorithms in the systems dedicated to stereotactic radiotherapy were very simple and did not explicitly take into account the transport of secondary particles, so they presented limitations in situations with lack of electronic equilibrium like in the case of a highly heterogeneous medium. Today in France, these simple algorithms are still used. In the BrainLAB TPS, these are Pencil Beam algorithms for treatments with mMLC, with radiological path length corrected for tissue density inhomogeneities, and a global calculation using TMR and OAR for treatments with circular cones, with no correction for inhomogeneities. In the Accuray TPS for the CyberKnife, it is a Ray Tracing algorithm with effective correction for depth. In 2008, however, a Monte Carlo (MC) engine was implemented in the Accuray TPS [14] and in the BrainLAB TPS [15].

The implementation of MC engines for stereotactic treatments is very good news, but it is suprising that they arrived after the development of clinical use of SBRT (in particular, for lung treatments), because from a physical point of view, it was highly predictable that calculations with too simple algorithms would induce large errors for small fields in non-equilibrium conditions. Indeed, it has been shown that a possible large error in the calculated target dose (+10%) can occur using the Raytrace algorithm in case of lung heterogeneity (treatment with CyberKnife, 20 mm diameter beams) [14], and that the error increases when field size decreases [16]. In the same way, the use of the Pencil Beam algorithm for lung cancer patients can lead to an important underdose of the PTV, even in the case of large target volumes (maximum PTV width of 5 cm) with considerable dose heterogeneity within the PTV (treatment with Novalis) [15].

5. CONCLUSION AND MAIN RECOMMENDATIONS OF THE WG

The WG produced a report for the French authorities at the end of 2008 [13]. It concluded that it was impossible at that time to establish a national protocol for the determination of the absorbed dose in very small photon beams that would be applicable for all devices used in stereotactic radiotherapy. It underlined the necessity to reinforce research in the dosimetry of small beams, by supporting the development of a metrology standard for small fields (EURAMET project) and by continuing the measurement campaign on a variety of stereotactic installations and with high resolution tissue-equivalent detectors.

While waiting for the publication of an international or a national dosimetry protocol for small fields [17], the WG proposed a set of recommendations in order to diminish the uncertainties in the dose delivered to the patients. As far as beam commissioning is concerned, the main recommendations are:

— For the choice of the detectors to be used, the medical physicist should not apply the manufacturer's instructions without critical examination.
— More than one type of detector should be used, especially for the OF measurement.
— For the measurement of the OF, one should use a pinpoint ionization chamber for beam sizes (side or diameter) greater than 10 mm or greater or equal to 18 mm, respectively, when the axis of the chamber is placed parallel or perpendicular to the beam axis; for smaller fields, it is better to use a stereotactic diode such as the Scanditronix unshielded one.
— One should be very careful regarding the alignment of the jaws and of the mMLC leaves in the case of measurement in this configuration, especially for very small beams (<10 mm); for the treatment of patients with mMLC

devices, jaws position should be shifted slightly outside the mMLC leaves position (for treatment planning and beam delivery) in order to avoid uncertainties due to jaws aperture and centring.

— The physicist should verify the beam data by external audit or intercomparison with another centre, before treating the first patient.

Following the publication of the WG report, measures were taken in France to improve the knowledge and the control of the dose in small fields, including an IRSN R&D project in dosimetry in collaboration with French radiotherapy centres, and an official support of the development of a metrology standard for small fields at the LNHB laboratory in Saclay.

REFERENCES

[1] ETARD, C., L'accident de surexposition au Centre Hospitalier Universitaire de Toulouse, Rapport d'expertise n°1, Vérification des protocoles expérimentaux d'étalonnage des microfaisceaux avant et après correction du dysfonctionnement, Rapport IRSN/DRPH n°2007-04, IRSN, Fontenay-aux-Roses (2007).

[2] DERREUMAUX, S., et al., Lessons from recent accidents in radiation therapy in France, Radiat. Prot. Dosim. **131** 1 (2008) 130–135.

[3] C. McKERRACHER, C., THWAITES, D. I., Assessment of new small-field detectors against standard-field detectors for practical stereotactic beam data acquisition, Phys. Med. Biol. **44** (1999) 2143–2160.

[4] PAPPAS, E., et al., Relative output factor measurements of a 5 mm diameter radiosurgical photon beam using polymer gel dosimetry, Med. Phys. **32** 6 (2005) 1513–1520.

[5] LAUB, W. U., WONG, T., The volume effect of detectors in the dosimetry of small fields used in IMRT, Med. Phys. **30** 3 (2003) 341–347.

[6] HARYANTO, F., et al., Investigation of photon beam output factors for conformal radiation therapy — Monte Carlo simulations and measurements, Phys. Med. Biol. **47** (2002) N133–N143.

[7] FRANCESCON, et al., Total scatter factors of small beams: A multidetector and Monte Carlo study, Med. Phys. **35** 2 (2008) 504–513.

[8] SCOTT, A.J.D., et al., Monte Carlo modeling of small photon fields : Quantifying the impact of focal spot size on source occlusion and output factors, and exploring miniphantom design for small-field measurements, Med. Phys. **36** 7 (2009) 3132–3144.

[9] PANTELIS, E., et al., On the implementation of a recently proposed dosimetric formalism to a robotic radiosurgery system, Med. Phys. **37** (5) (2010) 2369–2379.

[10] MARTENS, C., et al., The value of the PinPoint ion chamber for characterization of small field segments used in intensity-modulated radiotherapy, Phys. Med. Biol. **45** (2000), 2519–2530.

[11] DING, G.X., et al., Commissioning stereotactic radiosurgery beams using both experimental and theoretical methods, Phys. Med. Biol. **51** (2006) 2549–2566.

[12] FRANCESCON, P., et al., Application of a Monte Carlo-based method for total scatter factors of small beams to new solid state micro-detectors, J. Appl. Clin. Med. Phys. **10** 1 (2009) 147–152.
[13] DERREUMAUX, S., et al., Mesure de la dose absorbée dans les faisceaux de photons de très petites dimensions utilisés en radiothérapie stéréotaxique, Rapport du groupe de travail IRSN/SFPM/SFRO, Rapport IRSN/DRPH/SER n°2008-18, IRSN, Fontenay-aux-Roses (2008).
[14] MA, C.-M., et al., Third McGill International Workshop, Journal of Physics: Conference Series 102, 2008.
[15] FRAGOSO, M., et al., Dosimetric verification and clinical evaluation of a new commercially available Monte Carlo-based dose algorithm for application in stereotactic body radiation therapy (SBRT) treatment planning, Phys. Med. Biol. **55** (2010) 4445–4464.
[16] WILCOX, E.E., DASKALOV, G.M., Accuracy of dose measurements and calculations within and beyond heterogeneous tissues for 6 MV photon fields smaller than 4 cm produced by Cyberknife, Med. Phys. **35** 6 (2008) 2259–2266.
[17] ALFONSO, R., et al., A new formalism for reference dosimetry of small and nonstandard fields, Med. Phys. **35** 11 (2008) 5179–5186.

CHAMBER QUALITY FACTORS FOR THE NACP-02 CHAMBER IN ^{60}Co BEAMS: COMPARISON OF EGSnrc AND PENELOPE MONTE CARLO SIMULATIONS

J. WULFF, K. ZINK
Institut für Medizinische Physik und Strahlenschutz,
University of Applied Sciences, Gießen, Germany
Email: joerg.wulff@tg.fh-giessen.de

Abstract

A new comparison of the values published for the chamber quality factor $f_{c,Q0}$ of a NACP-02 plane-parallel chamber in ^{60}Co, calculated with the Monte Carlo (MC) systems EGSnrc and PENELOPE, shows a difference of approximately 0.5%. The authors analyse possible reasons for this difference and recalculate the chamber quality factor with EGSnrc. Variations in the simulation transport parameters of EGSnrc result in changes smaller than the difference. An investigation of the most important uncertainties of cross-sectional data, considering variations in the mean excitation energy of stopping powers and in the total photon cross-sections, shows uncertainties comparable to the differences between the two codes for the chamber quality factor. Variations of the front wall thickness of the NACP-02 chamber, in the range of discrepancies with manufacturer data reported in the literature, result in significant changes in the calculated values. However, the difference in $f_{c,Q0}$ cannot be explained in terms of these modifications. Hence, although both codes have been demonstrated to yield artefact free ion chamber simulations, a convergence of results for this particular problem cannot be achieved. An uncertainty estimate which takes into account the 0.5% difference for the MC calculated chamber quality factors seems to be a reasonable assumption.

1. INTRODUCTION

Clinical dosimetry requires a beam quality correction factor k_Q (see, for example, Ref. [1]). An ion chamber and beam quality dependent factor $f_{c,Qo}$ (abbreviated chamber quality factor, see Ref. [2]) enters the determination of k_Q and equals the product of the stopping power ratio between water and air $s_{w,air}$ and the overall perturbation factor p of the employed ionization chamber in the reference beam (usually ^{60}Co).

There is a growing interest in the Monte Carlo (MC) aided calculation of ionization chamber perturbation factors, and there have been various studies presenting first results for electron and photon beams. There is a justified concern as to how reliable these results are. The advantage of MC based factors is, in

principle, a lower uncertainty compared to the 'classic' approaches, which make use of some approximations. MC codes exist, which allow the accurate calculation of ionization chamber cavity dose and corresponding perturbation correction factors. However, for the small magnitude of effects in the order of less than a percent only, various parameters influence the results, such as the geometry details of the ion chamber, transport parameter settings in the code, cross- sections and the accuracy of the MC code itself. Currently, two general purpose MC codes exist, which have been demonstrated to yield the correct ionization chamber cavity dose within 0.1% (normalized to own cross-sections) in photon/electron beams: EGSnrc [3, 4] and PENELOPE [5, 6]. Both have subsequently been used to calculate perturbation factors for clinical dosimetry.

Panettieri et al. [2] used the PENELOPE MC system to calculate $f_{c,Qo}$ = 1.1578(8) for the NACP-02 plane parallel ion chamber at a stated 0.6% total uncertainty, which was based on their statistical uncertainty (0.1–0.2%) combined with the relative estimated uncertainty for the stopping power ratio water to air $s_{w,air}$ given in IAEA TRS-398 [1]. The $f_{c,Qo}$ value was taken as a weighted mean for different types of ^{60}Co sources. They compared their results with the calculations by Mainegra-Hing et al. [7] based on the EGSnrc system and demonstrated an almost perfect agreement. Panettieri et al. calculated the $f_{c,Qo}$ value from the work of Mainegra-Hing et al. as $s_{wair} \times p_{wall}$, using stopping power data from TRS-398 (1.133), which yields $f_{c,Qo}$ = 1.156. If one takes the wall perturbation factor p_{wall} = 1.0204(8), and the stopping power ratio $s_{w,air}$ = 1.1332 of Ref. [7], and adds the proposed replacement correction $p_{repl} = p_{cav} \times p_{dis}$ = 1.0065(10) by Wang and Rogers [8] (also based on EGSnrc), a value of $f_{c,Qo}$ = 1.164(1) results. This corresponds to an approximate 0.5% difference between the two codes, which is unexpected since both codes are believed to yield the 'correct' answer. If one accepts the total uncertainty of 0.6%, both results would agree within this uncertainty. However, a more rigorous analysis of systematic (type B) uncertainties in these calculations seems appropriate.

Recently, Chin et al. have questioned the manufacturer's data on the NACP-02 chamber's entrance window mass thickness by tuning their EGSnrc MC model, leading to 140 mg/cm² instead of 104 mg/cm² used in all other studies [9]. In the light of the mentioned discrepancies and the proposed NACP-02 front wall thickness, $f_{c,Qo}$ was recalculated directly with EGSnrc and investigated the systematic uncertainties (type B uncertainties) as a possible explanation for the observed differences. In addition, the single perturbation factors p_{wall}, p_{repl} and the stopping power ratio $s_{w,air}$ underlying $f_{c,Qo}$ were re-calculated.

2. METHODS

2.1. Variations in the chamber quality factor

The egs_chamber code [10] of the EGSnrc system was used to calculate the chamber's cavity dose D_{ch}, for the NACP-02 chamber placed with the inner side of the front wall at 5 cm depth within a 30 cm × 30 cm × 30 cm water phantom. Dose to water D_w was calculated in a thin slab of water (0.2 mm thickness, 5 mm radius). Although Panettieri et al. used a much thinner slab, it was demonstrated in Ref. [8] that a variation in water slab thickness of less than 0.2 mm does not change the result of D_w for a ^{60}Co. The chamber quality factor $f_{c,Qo}$ was calculated as the dose ratio between D_w and D_{ch} with a combined statistical uncertainty of <0.1% (1σ). Default transport parameters of EGSnrc were used and cut-off/threshold energies were set to PCUT = AP = 1 keV and ECUT = AE = 521 keV. Various transport settings of EGSnrc were tested, including different cross-section databases, turning on/off various options and changed energy cut-offs.

Two different ^{60}Co spectra and a complete phase-space of a clinical cobalt treatment unit (ELDORADO 6) were used as radiation source. The phase-space was based on the recent work of Muir et al. [11], whereas the spectrum used was either based on this phase-space (default), or a spectrum, which is part of the EGSnrc distribution and based on a clinical treatment unit as well [12].

Due to the different data on the entrance wall thickness of the NACP chamber in literature, it is possible to determine $f_{c,Qo}$ as a function of entrance window mass thickness, either by changing the mass density or the thickness of the MYLAR (polyethyleneterephthalate) and carbon constituting it.

In a final step, the contribution of the mean excitation energy I to the total uncertainty of $f_{c,Qo}$ was estimated. This was accomplished by determining the sensitivity of $f_{c,Qo}$ to changes in the I-value of the different materials found in the chamber geometry. The sensitivity itself was calculated from a linear approximation for a reduced I-value of 50%. Using this sensitivity, the total uncertainty was estimated with:

$$u^2(f) = \sum_{i=1}^{N} \left(\frac{\partial f}{\partial x_i} \right)^2 u^2(x_i) \tag{1}$$

which assumes no correlation between the different contributions (i.e. covariances are assumed to be negligible).

In the above equation, the uncertainty $u(x_i)$ in the cross-sections of N materials is multiplied with the estimated sensitivity $\partial f/\partial x_i$ and yields the

contribution to the total uncertainty u of the result f. More details of this method can be found in Ref. [13]. In a similar manner, the contribution due to an assumed uncertainty in photon cross-sections was investigated.

2.2. Single perturbation factors

In addition to the chamber quality factor, the stopping power ratios between water and air $s_{w,air}$ and the two single perturbation factors that underlie $f_{c,Q0}$: p_{repl} and p_{wall} were calculated The wall perturbation factor p_{wall} was calculated as the dose ratio between the dose to the sensitive region of the bare air cavity and the chamber dose with the complete wall present. The replacement correction factor p_{repl} was calculated following the methodology of Ref. [8], i.e. as the dose ratio between the reference dose in water and dose to an air cavity filled with low density water ($\rho = \rho_{air} = 0.0012047$ g/cm³). The stopping power ratios between water and air ($\Delta = 10$ keV) were calculated with the EGSnrc user code SPRRZnrc.

3. RESULTS AND DISCUSSION

The chamber quality factor for the NACP-02 chamber with a wall thickness of 140 mg/cm² and all other parameters as mentioned in the previous section was calculated as $f_{c,Q0} = 1.1582(8)$.

3.1. Influence of ^{60}Co source and front wall thickness

The two different ^{60}Co spectra altered the calculated $f_{c,Q0}$ values by up to 0.17%. Using a complete phase-space instead of its spectrum did not influence the result beyond the statistical uncertainty of 0.1%. Hence, the information on direction and position of a particle within the phase-space is of no significant influence. This is in agreement with the findings of Panettieri et al. [2], who demonstrated an independence of their ^{60}Co source within 2σ for the NACP-02 chamber.

In Fig. 1 (left), the chamber quality factor $f_{c,Qo}$ is shown as a function of entrance wall mass thickness. Changing the density or thickness of the carbon layer led to similar results, whereas a changed Mylar thickness of up to 50% did not alter the chamber quality factor. The wall mass thickness of 104 mg/cm² results in a value close to the product of published values with EGSnrc, as mentioned in the introduction section above (1.164), but differs from the PENELOPE based value (1.158) by approximately 0.5%, where a density of 104 mg/cm² was also used.

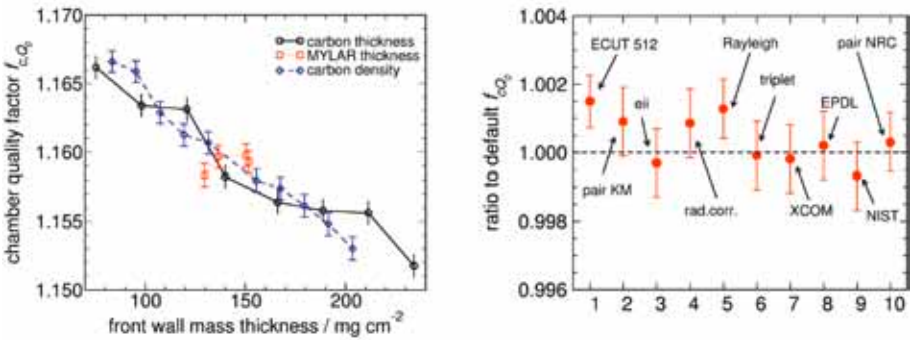

FIG. 1. (Left): Variation in the chamber quality factor as a function of the front wall mass thickness. (Right): Influence of transport parameter settings on the calculated chamber quality factor. The default settings correspond to unity. The error bar represents the 1σ statistical uncertainty.

3.2. Influence of transport parameters and cross-sections

The influence of changed transport parameters within the EGSnrc from defaults is shown in Fig. 1 (right). The reduction of the electron transport cut-off energy and production threshold respectively led to a deviation of ~0.15% ('ECUT512'). This is caused by the different energy-loss straggling for different particle production thresholds (AE). For the single dose values D_w and D_{ch}, the effect is up to 0.3%, but is cancelled to some degree, since it appears in both calculations. It must be noted that in the PENELOPE simulations of Panettieri et al. [2], an analogue collision-by-collision simulation was performed within the air of the ion chamber model and a cut-off energy of 0.1 keV for directly adjacent regions. The electron transport algorithm within EGSnrc uses a collision-by-collision simulation by default only within the distance of three mean free path lengths to media interfaces [4].

Turning on Rayleigh scattering resulted in an almost insignificant change of $f_{c,Qo}$ by 0.13% at a statistical uncertainty of 0.1% (1σ). All other variations in the transport parameter settings of EGSnrc did not alter the results beyond statistical uncertainties of ~0.1%. These parameter changes included turning on a more detailed angular sampling for pair-production events, explicit simulation of electron impact ionization, radiative corrections within Compton scattering events, and explicit simulation of triplet production within photon interactions. No change in the results beyond statistical uncertainties resulted for different total photon cross-section databases (XCOM and EPDL) instead of the EGSnrc default by Storm-Israel. Changing cross-sections for bremsstrahlung interactions from NIST databases and more accurate pair-production cross-sections instead of the

default by Bethe-Heitler did not change the chamber quality factor significantly. More details and references for the different transport options/cross-sections can be found in the EGSnrc documentation [3]. In summary, the EGSnrc calculations for this particular simulations for ^{60}Co are stable within <0.2% (1σ) for different transport options, cross-section databases and cut-off energies.

Table 1 summarizes the combined contribution due to uncertainties in the mean excitation energy entering into the stopping powers. These uncertainties sum up to ~0.6% using the estimated sensitivity and taking the quoted uncertainties for the *I*-values into account found in the ICRU37 report [14]. The influence of changing photon cross-section of all materials by a 1–2% led to insignificant changes in the $f_{c,Qo}$ value below the statistical uncertainty of <0.1%. The estimated total uncertainty here is comparable to the discrepancies between the PENELOPE and EGSnrc. However, both codes reproduce the stopping powers of the ICRU37 report with the default values of the excitation energies. Hence, the uncertainties in the *I*-value may actually not be the reason for the discrepancies.

3.3. Single perturbation factors

The wall perturbation factor p_{wall} for the chamber model with 140 mg/cm² front wall thickness was calculated as p_{wall} = 1.0165(9). A reduction of the front wall mass thickness to 107 mg/cm² (in terms of reduced graphite density) led to p_{wall} = 1.0206(9), which resembles the value of Mainegra-Hing et al. [7]. The replacement correction yielded p_{repl} = 1.0067(7), which is in perfect agreement with the calculations of Wang et al. [8]. The EGSnrc calculated value for the stopping power ratio between water and air was $s_{w.,air}$ = 1.1334(1). The product of all single factors yields $p_{wall} \times p_{repl} \times s_{w,air} = f_{c,Q0}$ = 1.1598(12), which corresponds to a ~0.14% deviation to the directly calculated chamber quality factor. Hence, although discussed in the past [15] within the statistical uncertainties, an assumed independence of single perturbation factors seems to be a reasonable approximation.

4. CONCLUSION

In the past, the PENELOPE and EGSnrc MC systems have been demonstrated to allow artefact-free ion chamber simulations due to their elaborate electron transport algorithms. Nevertheless, there is a difference of 0.5% between the results of the chamber quality factor $f_{c,Qo}$ of a NACP-02 plane parallel chamber. If one takes into account uncertainties in the chamber geometry and source model, uncertainties in the cross-sections and in the algorithms

TABLE 1. CALCULATED SENSITIVITY AND STANDARD UNCERTAINTY DUE TO VARIATIONS IN PHOTON CROSS-SECTIONS AND ELECTRON STOPPING POWERS

Parameter variation			Sensivity	Relative standard uncertainty	
x_i		Medium	$\lvert\partial(\Delta f_{c,Q0}/f_{c,Q0})/\partial x_i\rvert$	$u(x_i)/x_i$ /%	$\lvert\Delta f_{c,Q0}/f_{c,Q0}\rvert$/%
Percentage variation photon cross-sections	Photo effect		0.008	+/– 2	0.016
	Compton scattering		0.018	+/– 1	0.018
	Pair production		< 0.001	+/– 2	<0.001
Percentage change in mean excitation energy (I)		Mylar (78.7 eV)	0.006	+/– 2.3	0.014
		Carbon (78 eV)	0.094	+/– 6.1	0.574
		Air (58.7 eV)	0.182	+/– 1.3	0.236
		Polystyrene (68.7 eV)	0.044	+/– 2.7	0.117
		H_2O (75 eV)	0.018	+/– 2.7	0.047
				Total	0.63

Note: The standard uncertainties for the mean excitation energies were based on the estimated 68% confidence values given in the ICRU 37 report [14].

themselves, the difference between the two codes seems reasonable. If one accepts both calculated values to be equally probable an uncertainty of $u_B = (0.5\%/\sqrt{3})/2 = 0.14\%$ for the MC based chamber quality factor $f_{c,Qo}$ can be estimated.

Nevertheless, the total uncertainty is dominated by the cross-sections, i.e. the ionization energy I in electron stopping-powers. The 0.6% uncertainty calculated in this work is in good agreement with the estimations of Panettieri et al., who approximated the effect by the relative uncertainty of $s_{w,air}$ of 0.5% found in IAEA TRS-398, although it is actually dominated by the carbon within the chamber. Still, this is much lower than the combined standard uncertainty of 1.6% given in TRS-398 for the plane-parallel chambers entering the calculation of k_Q. Some of the uncertainties reported here even cancel out in the determination of k_Q. It was demonstrated, that a total, slightly energy dependent uncertainty of 0.2–0.4% can be addressed to the MC calculated k_Q of a NE2571 Farmer chamber in photon beams, when omitting uncertainties in the W/e value [13].

REFERENCES

[1] INTERNATIONAL ATOMIC ENERGY AGENCY, Absorbed Dose Determination in External Beam Radiotherapy: An International Code of Practice for Dosimetry Based on Standards of Absorbed Dose to Water, Technical Reports Series No. 398, IAEA, Vienna (2000).

[2] PANETTIERI, V., SEMPAU, J., ANDREO, P., Chamber quality factors in 60Co for three plane-parallel chambers: PENELOPE MC simulations, Phys. Med. Biol. **53** (2008) 5917–5926.

[3] KAWRAKOW, I., MAINEGRA-HING, E., ROGERS, D.W.O., TESSIER, F., WALTERS, B.R.B., The EGSnrc code system: Monte Carlo Simulation of Electron and Photon Transport, NRCC Report 701, NRC, Canada (2010).

[4] KAWRAKOW, I., Accurate condensed history Monte Carlo simulation of electron transport. II. Application to ion chamber response simulations, Med. Phys. **27** (2000) 499–513.

[5] SALVAT, F., FERNANDEZ-VEREA, J.M., SEMPAU, J., PENELOPE-2006: A Code System for Monte Carlo Simulation of Electron and Photon Transport, OECD Nuclear Energy Agency, France (2006).

[6] SEMPAU, J., ANDREO P., Configuration of the electron transport algorithm of PENELOPE to simulate ion chambers, Phys. Med. Biol. **51** (2006) 3533–3548.

[7] MAINEGRA-HING, E., KAWRAKOW, I., ROGERS, D.W.O., Calculations for plane-parallel ion chambers in 60Co beams using the EGSnrc MC code, Med. Phys. **30** (2003) 179–189.

[8] WANG, L.L.W., ROGERS, D.W.O., Calculation of the replacement correction factors for ion chambers in megavoltage beams by MC simulation, Med. Phys. **35** (2008) 1747–1755.

[9] CHIN, E., et al, Validation of a MC model of a NACP-02 plane-parallel ionization chamber model using electron backscatter experiments, Phys. Med. Biol. **53** (2008) N119–N126.
[10] WULFF, J., ZINK, K., KAWRAKOW, I., Efficiency improvements for ion chamber calculations for high energy photon beams, Med. Phys. **35** (2008) 1328–1336.
[11] MUIR, B., ROGERS, D.W.O., Co-60 phase-space files generated using BEAMnrc, CLRP-Report, CLRP-09-0: Canada (2009).
[12] ROGERS, D., EWART, G.M., BIELAJEW, A.F., VAN DYK, J., Calculation of electron contamination in a 60Co therapy beam, (Proc. Int. Symp. Dosimetry in Radiotherapy, Vienna, 1988), Vol. 1, IAEA, Vienna (1988) 303–312.
[13] WULFF, J., HEVERHAGEN, J.T., ZINK, K., KAWRAKOW, I., Investigation of systematic uncertainties in MC-calculated beam quality correction factors, Phys. Med. Biol. **55** (2010) 4481–4493.
[14] INTERNATIONAL COMMISSION ON RADIATION UNITS AND MEASUREMENTS, Stopping powers for electrons and positrons, Report 37, Washington DC (1984).
[15] SEMPAU, J., ANDREO, P., ALDANA, J., MAZURIER, J., SALVAT, F., Electron beam quality correction factors for plane-parallel ionization chambers: Monte Carlo calculations using the PENELOPE system, Phys. Med. Biol. **49** (2004) 4427–4444.

BEAM QUALITY CORRECTION FACTORS FOR PLANE-PARALLEL CHAMBERS IN PHOTON BEAMS

R.-P. KAPSCH
Physikalisch-Technische Bundesanstalt, Braunschweig
Email: Ralf-peter.kapsch@ptb.de

I. GOMOLA
IBA Dosimetry, Schwarzenbruck

Germany

Abstract

In order to examine the chamber-to-chamber variation of the beam quality correction factors for plane-parallel ionization chambers in high energy photon beams, these correction factors were determined for each of ten plane-parallel chambers of types IBA PPC05 and IBA PPC40, respectively. It was found that the variation of the individual beam quality correction factors was not larger than 0.7% for both chamber types and all beam qualities. From these results it is concluded that chamber type specific beam quality correction factors could be given for plane-parallel chambers in high energy photon beams, allowing for the application of the same formalism of absorbed dose measurements as with cylindrical chambers.

1. INTRODUCTION

Modern dosimetry protocols for external beam radiotherapy, such as IAEA TRS-398 [1], AAPM TG-51 [2] or the German protocol DIN 6800-2 [3] are based on the use of ionization chambers, which are calibrated in terms of absorbed dose to water in a ^{60}Co beam. The absorbed dose to water $D_{w,Q}$ in a high energy photon beam produced by a clinical accelerator is then obtained by:

$$D_{w,Q} = M_Q N_{D,w} k_Q \tag{1}$$

where

M_Q is the reading of the dosimeter in the photon beam of quality Q corrected for all influence quantities except the beam quality (e.g. mainly air density, ion recombination and polarity of chamber voltage);

$N_{D,w}$ is the calibration factor of the dosimeter in terms of absorbed dose to water obtained in a ^{60}Co reference beam; and

k_Q is the beam quality correction factor which corrects for the different response of the ionization chamber in the ^{60}Co reference beam and the actual photon beam of quality Q.

Under conditions in which the Bragg-Gray cavity theory is approximately valid this beam quality correction factor may be expressed as:

$$k_Q = \frac{(s_{w,\mathrm{air}})_Q}{(s_{w,\mathrm{air}})_{\mathrm{Co}}} \frac{(W_{\mathrm{air}})_Q}{(W_{\mathrm{air}})_{\mathrm{Co}}} \frac{p_Q}{p_{\mathrm{Co}}} \tag{2}$$

where

$s_{w,\mathrm{air}}$ is the stopping power ratio water to air;

W_{air} is the mean energy expended in air per ion pair formed; and

p is an overall perturbation factor, which depends on the design of the ionization chamber and which accounts for all deviations from an ideal Bragg-Gray detector [1].

For a number of cylindrical ionization chamber types, values of the correction factor k_Q are given in the dosimetry protocols. However, no k_Q values are given for plane-parallel chambers and consequently those chambers cannot be used for absorbed dose measurements in high energy photon beams using Eq. (1). The rationale for this[1] is that significant deviations of up to 4% between the perturbation factors[2] have been reported by different authors for chambers of the same design (mostly NACP type chambers) [5] , or even by the same author investigating different chambers of the same type [5]. Whereas some part of these discrepancies may be found in the application of different methods by different authors, it is known from the investigations by Mattson et al., [9], Andreo et al., [5], and Rogers [10] that some perturbation factors are very sensitive to minor differences in the construction of the chamber and the materials used

[1] See also the discussion in Section 8 of IAEA TRS-381 [4].

[2] Because the formalism of dose measurement changed in the past, in older publications usually no k_Q values can be found but rather perturbation factors.

(e.g. thickness and density of graphite coating). Hence, it is assumed that the observed variations of the perturbation factors are caused by small production tolerances of the chambers.

However, there is evidence from some recent studies that the variation of perturbation factors is much smaller for plane-parallel chambers of modern design (e.g. Roos, Markus and Advanced Markus type chambers) [11] possibly indicating an improvement in the manufacturing process of modern plane-parallel chambers yielding more uniform chambers with smaller production tolerances.

In this work, the chamber-to-chamber variation of the beam quality correction factor k_Q in high energy photon beams is investigated for two types of modern plane-parallel chambers, namely IBA PPC05 and IBA PPC40. Individual k_Q values were determined for ten chambers of each type (taken from different manufacturing batches) giving representative information on the typical spread of the k_Q values in high energy photon beams for these plane-parallel chamber types.

2. MATERIALS AND METHODS

Applying Eq. (1) to measurements using a cylindrical reference chamber and a plane-parallel chamber in the same photon beam of quality Q and assuming that both chambers are exposed to the same dose, the beam quality correction factor of the plane-parallel chamber k_Q^{pp} can be obtained from:

$$k_Q^{\mathrm{pp}} = \frac{M_Q^{\mathrm{ref}}\, N_{D,w}^{\mathrm{ref}}}{M_Q^{\mathrm{pp}}\, N_{D,w}^{\mathrm{pp}}}\, k_Q^{\mathrm{ref}} \tag{3}$$

where the superscripts ‘pp’ and ‘ref’ denote the plane-parallel chamber under test and the cylindrical chamber used as a reference, respectively. The corrected chamber readings in the photon beam M_Q^{pp} and M_Q^{ref} as well as the calibration coefficients

$$N_{D,w}^{\mathrm{pp}} \text{ and } N_{D,w}^{\mathrm{ref}}$$

can be obtained by measurements. The beam quality correction factor for the cylindrical reference chamber k_Q^{ref} can be taken from a dosimetry protocol or determined by a direct calibration of the reference chamber against a primary standard of absorbed dose to water (e.g. a water calorimeter). For the investigations presented here, k_Q^{ref} was taken from IAEA TRS-398 [1], providing

beam quality correction factors for the plane-parallel chambers k_Q^{pp}, which are consistent with the data base in IAEA TRS-398. It must be stressed here that the variation of the k_Q^{pp} values does not depend on the exact value used for the beam quality correction factor of the reference chamber, k_Q^{ref}, which is a constant (for a given beam quality), and does not contribute to the spread of the k_Q^{pp} values.

The plane-parallel chambers investigated in this study are ten chambers of type IBA PPC05 with serial numbers 83, 111, 156, 157, 158, 159, 160, 161, 474, 475, and ten chambers of type IBA PPC40 with serial numbers 342, 344, 507, 509, 510, 512, 808, 809, 810, 811. A cylindrical chamber of type NE2561 was used as the reference.

All chambers were calibrated in the ^{60}Co reference beam of the Physikalisch-Technische Bundesanstalt (PTB) in Braunschweig. All calibration factors $N_{D,w}$ are traceable to the German national standard for absorbed dose to water [15]. The polarity effect in the ^{60}Co beam was measured for each chamber. The relative standard deviations of the individual calibration factors obtained here are 3.3% for the PPC05 chambers and 3.9% for the PPC40 chambers, probably showing a larger variation of the sensitive volumes for IBA Roos type chambers than the variation found by Brass et al. [20] for Roos type chambers manufactured by PTW.

The readings M_Q of the plane-parallel and cylindrical chambers were obtained in the 4 MVX, 8 MVX and 25 MVX photon beams available at one of the Elekta Precise linacs of PTB. The beam quality specifiers of these beams are given in Table 1. All irradiations were performed in a 30 cm × 30 cm × 30 cm water phantom in a horizontal beam geometry with a field size of 10 cm × 10 cm at the source-to-surface distance (SSD) of 100 cm. The reference points of all ionization chambers were positioned at a depth of 10 cm in the phantom. The water equivalent thickness of the entrance window of the phantom was taken into account by scaling the physical thickness by the ratio of electron densities of the

TABLE 1. BEAM QUALITY SPECIFIERS OF THE PHOTON BEAMS USED IN THIS STUDY AND CORRESPONDING BEAM QUALITY CORRECTION FACTORS FOR THE NE2561 REFERENCE CHAMBER

Nominal accelerating voltage	Beam quality specifier $TPR_{20,10}$	Beam quality correction factor used for the reference chamber k_Q^{ref}
4 MV	0.638	0.996
8 MV	0.714	0.989
25 MV	0.799	0.969

Note: The k_Q^{ref} values were obtained by linear interpolation from Table 14 in IAEA TRS-398 [1].

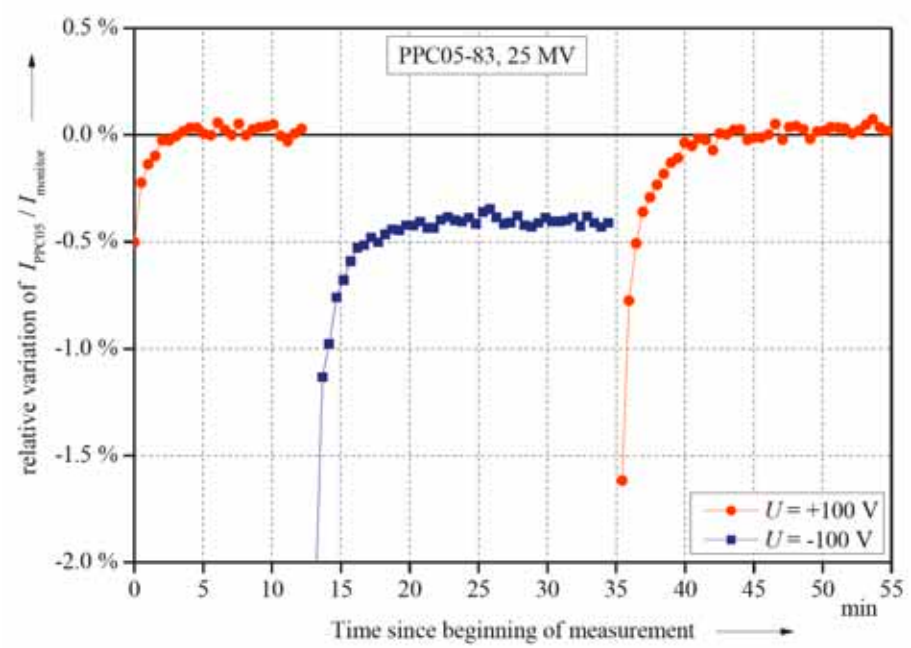

FIG. 1. Example of the time behaviour of the ionization current normalized to the monitor reading for a chamber of type PPC05 in the 25 MV photon beam. The polarity of the polarizing voltage was changed about 13 min and 35 min after the start of the irradiation.

different materials. For the NE2561 chamber, which is not waterproof, a PMMA sleeve was used for both the calibration and the measurements in the high energy photon beams.

The dose rate delivered by the linac was monitored using an external large area transmission chamber mounted on the shadow tray of the linac [16]. This monitor was used to normalize the ionization currents measured by the plane-parallel and cylindrical chambers.

Measurements using the cylindrical reference chamber were performed at the beginning and end of a set of measurements with the plane-parallel chambers to check the stability of the output of the linac during the measurements.

During an irradiation of an ionization chamber, the ionization current and the monitor signal were measured continuously until a stable state of the normalized ionization current was reached; this stable signal was then measured for about 10 min. Afterwards, the polarity of the polarizing voltage was changed from positive to negative, and the (normalized) ionization current was measured again. Finally, the polarizing voltage was switched back to positive, and it was checked to ensure that the signal obtained was the same as at the beginning of the measurement (see Fig. 1).

From the regions with stable signals, the mean values of the normalized ionization currents for positive and negative polarity of the chamber voltage were determined, and the correction for polarity was calculated. The variation of this correction factor for different chambers of the same type was found to be very small. For all chambers of type PPC05, the polarity correction was less than 0.33% in all beams; the relative standard deviation of the individual polarity correction factors (for each beam) was less than 0.08%. For the chambers of the type PPC40, the polarity correction was less than 0.1% in all beams; the relative standard deviation of the individual correction factors was less than 0.03%. A correction for ion recombination was applied to the ionization current using the data and procedures given by Bruggmoser et al. [17]. Finally, the k_Q^{pp} values for each plane-parallel chamber were calculated according to Eq. (3); the values k_Q^{ref} used for the reference chamber are shown in Table 1.

3. RESULTS

3.1. k_Q factors

The k_Q factors obtained for all chambers investigated here are shown in Figs 2 and 3. The error bars shown on the data do not include the uncertainty of the beam quality correction factor k_Q^{ref} for the reference chamber; they only denote the uncertainty attributed to the fraction term in Eq. (3), which characterizes the variation of the individual k_Q^{pp} values (see Section 3.2).

3.2. Estimation of uncertainty

The uncertainty budget for the experimentally determined k_Q^{pp} values is given in Table 2. It was established in line with the guidelines given by the International Organization for Standardization [18] or the IAEA [10]. Equation (3) was taken as the model equation and the following sources of uncertainty were taken into account:

(a) The uncertainty of the ratio of calibration factors

$$N_{D,w}^{ref}/N_{D,w}^{pp}.$$

Calibration factors of all chambers were traceable to the same primary standard for absorbed dose to water; therefore, the uncertainty of the primary standard cancels out in the ratio of calibration factors. The

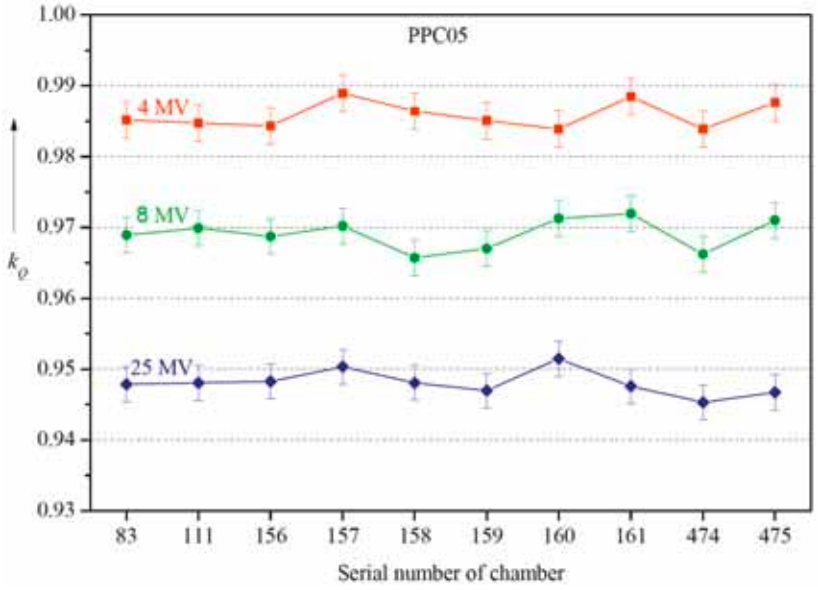

FIG. 2. Experimentally determined k_Q factors for the plane-parallel chambers of type PPC05.

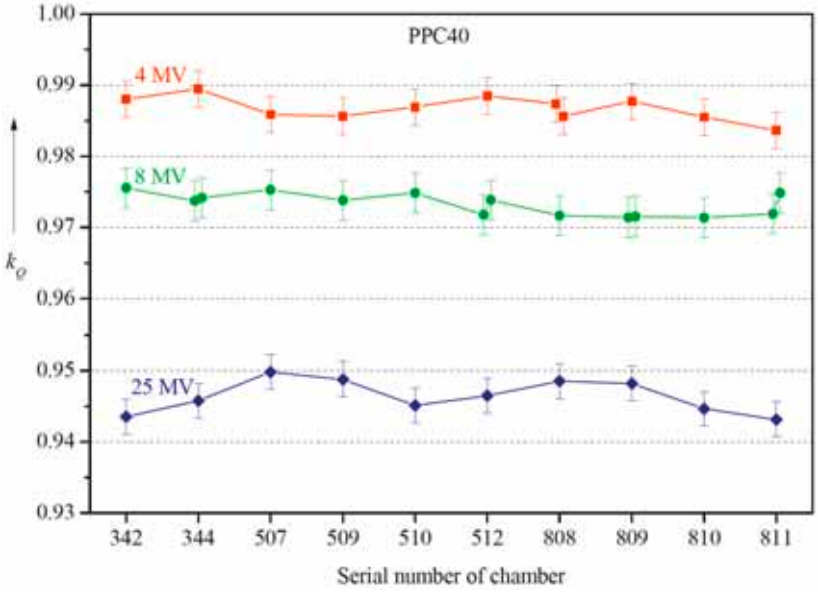

FIG. 3. Experimentally determined k_Q factors for the plane-parallel chambers of type PPC40. Some of the measurements were repeated after a few days in order to check the reproducibility of the results.

remaining uncertainty contributions due to positioning, electrometer calibration, leakage current, correction for air density, humidity, recombination and polarity are estimated to give a total relative standard uncertainty of 0.15% for the calibration of one ionization chamber. Because these uncertainty contributions can be assumed to be uncorrelated for the calibration of two chambers, a relative standard uncertainty of 0.21% is obtained for the ratio of calibration factors.

(b) The uncertainty of the ratio of the corrected chamber readings $M_Q^{\text{ref}}/M_Q^{\text{pp}}$. For the reference chamber a change of the normalized ionization current of not more than 0.3% over one day was observed (rectangular distribution with limits ±0.15%). This uncertainty includes all random influences related to the measurement (i.e. unnoticed changes of the linac beam output, changes of the air density, noise in the electrometer, drifts of the monitor signal, etc.). Variation of the normalized ionization current calculated from the readings of plane-parallel chambers was found to be less than 0.1% during a measurement[3] (rectangular distribution with limits ±0.05%). Additional uncertainty components, originated from positioning of the chamber, correction for ion recombination [17] and polarity were considered separately (see Table 2). All correlated uncertainty contributions (e.g. calibration of the electrometer, thermometer or barometer) cancel out here because the same devices were used for all measurements.

(c) The uncertainty of the k_Q^{ref} value is 1.0%, taken from IAEA TRS-398 [1]. It must be noted here that this uncertainty component is only of interest for the absolute values of the correction factor k_Q^{pp}. As long as only the (relative) variation of the individual k_Q^{pp} factors of the plane-parallel chambers is considered, this uncertainty can be neglected because k_Q^{ref} is the same for all chambers and does not contribute to the spread of the k_Q^{pp} values.

Following the rules of combining uncertainty components [18], a relative standard uncertainty of the k_Q^{pp} values of $u(k_Q^{\text{pp}}) = 1.04\%$ is obtained. Neglecting the uncertainty of the beam quality correction factor of the reference chamber k_Q^{ref}, an uncertainty of $u(k_Q^{\text{pp}}/k_Q^{\text{ref}}) = 0.26\%$ is obtained, which has to be taken into account when the spread of the beam quality correction factors is examined. This uncertainty is shown as error bars in Figs 2 and 3.

[3] Clearly, this is only valid after the signal reached a stable state (see Fig. 1).

TABLE 2. UNCERTAINTY BUDGET FOR THE DETERMINATION OF BEAM QUALITY CORRECTION FACTORS k_Q^{pp} FOR PLANE-PARALLEL CHAMBERS

Component of uncertainty	Relative expanded uncertainty	Expansion factor	Relative standard uncertainty
Calibration factor of the reference chamber $N_{D,w}^{ref}$			
Uncertainty, except the part dedicated to the primary standard	0.15%	1	0.150%
Calibration factor of the plane-parallel chamber $N_{D,w}^{pp}$			
Uncertainty, except the part dedicated to the primary standard	0.15%	1	0.150%
Normalized reading of the reference chamber M_Q^{ref}			
Variation of the normalized ionization current over one day	0.15%	1.73	0.087%
Positioning in phantom	0.05%	1.73	0.029%
Polarity correction	0.05%	1.73	0.029%
Ion recombination	0.10%	1.73	0.058%
Normalized reading of the plane-parallel chamber M_Q^{pp}			
Variation of the normalized ionization current during the measurement	0.05%	1.73	0.029%
Positioning in phantom	0.05%	1.73	0.029%
Polarity correction	0.05%	1.73	0.029%
Ion recombination	0.10%	1.73	0.058%
Relative combined uncertainty $u(k_Q^{pp}/k_Q^{ref})$:			**0.26%**
Beam quality correction factor k_Q^{ref}	1.0	1	1.0
Relative combined uncertainty $u(k_Q^{pp})$:			**1.04%**

4. DISCUSSION

The aim of this study was to investigate the chamber-to-chamber variation of beam quality correction factors for plane-parallel chambers of types PPC05 and PPC40 in high energy photon beams. The relative span (difference between maximum and minimum value divided by the mean value) and the relative standard deviation of the k_Q^{pp} values obtained in this study are shown in Table 3.

The variation of the individual k_Q^{pp} values for both chamber types is not larger than 0.7% for all beam qualities, and no significant difference between the PPC05 and PPC40 chambers could be observed. This result agrees very well with the results reported by McEwen at al. [12], who found a variation of ±0.4% for the k_Q^{pp} values of four NACP- and three Roos type chambers (the latter being very similar to the PPC40 investigated here).

In view of the relative standard uncertainty $u(k_Q^{pp}/k_Q^{ref})$ = 0.26% (see Table 2), which is slightly larger than the relative standard deviation of the k_Q^{pp} values observed here (see Table 3), no significant chamber-to-chamber variation of the experimentally obtained beam quality correction factors can be deduced. From these results, the authors conclude that for certain types of modern plane-parallel chambers, type-specific k_Q^{pp} values can be used for the determination of absorbed dose to water in high energy photon beams using the same formalism as for cylindrical chambers (Eq. (1)).

The relative standard uncertainty for the (absolute) values of the correction factors k_Q^{pp}, which is $u(k_Q^{pp})$ = 1.04% (see Table 2), is only 0.04% larger than the uncertainty given in IAEA TRS-398 [1] for the beam quality correction factors of cylindrical chambers in high energy photon beams. This slightly increased uncertainty should be appropriate for most routine dosimetric measurements. Of course, here it is not recommended to replace cylindrical chambers by plane-parallel chambers for the dosimetry in high energy photon beams, but it might be beneficial in some circumstances to use a chamber of a different type for an independent check of the dose measurement (for instance, should there be any

TABLE 3. RELATIVE SPAN AND STANDARD DEVIATION OF THE k_Q^{pp} VALUES OBTAINED IN THIS STUDY

Chamber	Relative span			Relative standard deviation		
type	4 MVX	8 MVX	25 MVX	4 MVX	8 MVX	25 MVX
PPC05	0.51%	0.64%	0.65%	0.19%	0.22%	0.18%
PPC40	0.59%	0.43%	0.70%	0.17%	0.16%	0.25%

doubt concerning the proper functioning of the cylindrical chamber) or to convert some measurements usually done with plane-parallel chambers (e.g. depth ionization curves) to absorbed dose to water measurements.

REFERENCES

[1] INTERNATIONAL ATOMIC ENERGY AGENCY, Absorbed Dose Determination in External Beam Radiotherapy: An International Code of Practice for Dosimetry Based on Standards of Absorbed Dose to Water, Technical Reports Series No. 398, IAEA, Vienna (2000).

[2] ALMOND, P.R., BIGGS, P.J., COURSEY, B.M., HANSON, W.F., SAIFUL HUQ, M., NATH, R., ROGERS, D.W.O., AAPM's TG-51 protocol for clinical reference dosimetry of high energy photon and electron beams, Med. Phys. **26** (1999) 1847–1870.

[3] DEUTSCHES INSTITUT FÜR NORMUNG, DIN 6800-2. Dosismessverfahren nach der Sondenmethode für Photonen- und Elektronenstrahlung — Teil 2: Dosimetrie hochenergetischer Photonen- und Elektronenstrahlung mit Ionisationskammern, Deutsche Norm, DIN, Berlin (2008).

[4] INTERNATIONAL ATOMIC ENERGY AGENCY, The Use of Plane Parallel Ionization Chambers in High Energy Electron and Photon Beams: An International Code of Practice for Dosimetry, Technical Reports Series No. 381, IAEA, Vienna (1997).

[5] ANDREO, P., RODRIGUES, L.N., LINDBORG, L., KRAEPELIEN, T., On the calibration of plane-parallel ionization chambers for electron beam dosimetry, Phys. Med. Biol. **37** (1992) 1147–1165

[6] LAITANO, R.F., GUERRA, A.S., PIMPINELLA, M., NYSTRÖM, H., KARLSSON, M., SVENSSON, H., Correction factors for calibration of plane-parallel ionization chambers with a ^{60}Co gamma-ray beam, Phys. Med. Biol. **38** (1993) 39–54

[7] KOSUNEN, A., JÄRVINEN, H., SIPILÄ, P., "Optimum calibration of NACP type plane parallel ionization chambers for absorbed dose determination in low energy electron beams", Measurement Assurance in Dosimetry (Proc. Symp. Vienna, 1993), IAEA, Vienna (1994) 505–513.

[8] WITTKÄMPER, F.W., AALBERS, A.H.L., MIJNHEER, B.J., Experimental determination of wall correction factors part II: NACP and Markus plane-parallel ionization chambers, Phys. Med. Biol. **37** (1992) 995–1004.

[9] MATTSSON, L.O., JOHANSSON, K.-A., SVENSSON, H., Calibration and use of plane-parallel ionization chambers for the determination of absorbed dose in electron beams, Acta Radiol. Oncol. **20** (1981) 385–399.

[10] ROGERS, D.W.O., Calibration of parallel-plate chambers: Resolution of several problems by using Monte Carlo calculations, Med. Phys. **19** (1992) 889–899.

[11] PALM, Å., CZAP, L., ANDREO, P., MATTSSON, O., Performance analysis and determination of the p_{wall} correction factor for ^{60}Co γ-ray beams for Wellhöfer Roos type plane-parallel chambers, Phys. Med. Biol. **47** (2002) 631–640.

[12] McEWEN, M.R., DUANE, S., THOMAS, R., "Absorbed dose calibration factors for parallel-plate chambers in high energy photon beams", Standards and Codes of Practice in Medical Radiation Dosimetry (Proc. Symp. Vienna, 2002), IAEA , Vienna (2003) 335–341.

[13] CHRIST, G., DOHM, O.S., BRUGGMOSER, G., SCHÜLE, E., The use of plane-parallel chambers in electron dosimetry without any cross-calibration, Phys. Med. Biol. **47** (2002) N121–N126.

[14] KAPSCH, R.-P., BRUGGMOSER, G., CHRIST, G., DOHM, O.S., HARTMANN, G.H., SCHÜLE, E., Experimental determination of p_{Co} perturbation factors for plane-parallel chambers, Phys. Med. Biol. **52** (2007) 7167–7181.

[15] KRAUSS, A., The PTB water calorimeter for the absolute determination of absorbed dose to water in ^{60}Co radiation, Metrologia **43** (2006) 259–272.

[16] KAPSCH, R.-P., KRAUSS, A., On the performance of monitor chambers to measure the output of medical linear accelerators for high-precision dosimetric investigations, World Congress on Medical Physics and Biomedical Engineering (IFMBE Proc. 25/I, 2009), Springer, Heidelberg (2009) 85–88.

[17] BRUGGMOSER, G., SAUM, R., SCHMACHTENBERG, A., SCHMID, F., SCHÜLE, E., Determination of the recombination correction factor k_S for some specific plane-parallel and cylindrical ionization chambers in pulsed photon and electron beams, Phys. Med. Biol. **52** (2007) N35–N50.

[18] INTERNATIONAL ORGANIZATION FOR STANDARDIZATION, Guide to the expression of uncertainty in measurements, ISO, Geneva (1995).

[19] INTERNATIONAL ATOMIC ENERGY AGENCY, Measurement Uncertainty: A Practical Guide for Secondary Standards Dosimetry Laboratories, IAEA-TECDOC-1585, IAEA, Vienna (2008).

[20] BASS, G., THOMAS, R., PEARCE, J., The calibration of parallel plate electron ionization chambers at NPL for use with the IPEM 2003 code of practice: summary data, Phys. Med. Biol. **54** (2009) N115–N124.

SECONDARY ELECTRON PERTURBATIONS IN FARMER TYPE ION CHAMBERS FOR CLINICAL PROTON BEAMS

H. PALMANS
National Physical Laboratory, Teddington,
United Kingdom
Email: hugo.palmans@npl.co.uk

Abstract

Monte Carlo calculations of wall and central electrode perturbation correction factors for Farmer type chambers with graphite and A150 walls and graphite and aluminium central electrodes in proton beams due to secondary electrons are performed using EGSnrc Monte Carlo simulations. The wall correction factors exponentially saturate at high energies at about 1.004 for an A150 wall and about 0.985 for a graphite wall. The central electrode correction is unity for a graphite central electrode and saturates exponentially at 0.998 for a 1 mm diameter aluminium central electrode. Experimental data from the literature are in agreement within the standard uncertainties. The calculated data result in an overall perturbation correction factor for a Farmer type chamber with a graphite wall and a central electrode of 0.9965 in high energy clinical proton beams.

1. INTRODUCTION

Dosimetry of proton therapy has reached a reasonable level of consistency with the introduction of absorbed dose based protocols in IAEA TRS-398 [1] and ICRU Report 78 [2]. Both recommendations have adopted the assumption from earlier protocols [3–6] that ion chamber perturbation factors in proton beams are unity for all ionization chamber types.

The overall perturbation factor, p_Q, can be decomposed in the product of four contributions: p_{dis} accounting for the displacement effect when the reference point of the ionization chamber is taken to be at the chamber centre instead of at the effective point of measurement, p_{cav} correcting for the difference of the charged particle fluence in the cavity and at the effective point of measurement in water in the absence of the cavity, p_{wall} correcting the response for the non-water equivalence of the chamber wall and any waterproofing material and p_{cel} correcting the response for the presence of the central electrode.

p_{dis} is mainly a gradient effect and has been extensively studied by experiment, Monte Carlo simulations and analytical model calculations [7–10]. Monte Carlo simulations indicate that p_{cav} is within 0.1% from unity if

Spencer-Attix stopping power ratios with an electron cut-off energy of 10 keV are used [7].

Concerning p_{wall}, some experiments have indicated a difference in response of up to 2% between ion chambers with a graphite wall and those with an A150 tissue equivalent wall [11, 12]. Another carefully designed experiment demonstrated that Farmer type chambers with graphite and A150 walls exhibit on average a difference in response of 0.5% [13]. Monte Carlo simulations [14] showed that secondary electrons are responsible for this effect but the uncertainty of those simulations was rather large due to limitations in available computation time and, of more relevance, they were performed with EGS4 using a pre-release version of PRESTA-II.

Regarding the central electrode perturbation, an experiment in a 170 MeV proton beam found a value of $p_{cel} = 0.997 \pm 0.004$ for a Farmer type chamber with an aluminium central electrode in a high energy proton beam [11]. In another experiment in a beam with an energy of 75 MeV, a value of 1.000 ± 0.002 was found for the same ionization chamber configuration [13]. No Monte Carlo simulations of the central electrode effect have been reported. It is worth to note that in high energy electron beams, the presently accepted value of the aluminium central electrode perturbation factor is 0.998 [1].

In this paper, new calculations of p_{wall} and p_{cel} are presented for Farmer type chambers using EGSnrc Monte Carlo simulations [15]. Graphite and A150 tissue equivalent plastic were considered as wall materials and graphite and aluminium and graphite as central electrode materials.

2. METHOD

The modelled geometry is shown in Fig. 1 and consists of an air cylinder with length 24 mm, diameter 6.4 mm surrounded by a wall with a thickness of 0.38 mm, i.e. dimensions close to that of a Farmer type chamber, immersed in water. Both graphite and A150 as wall material were modelled. The central electrode was modelled as a 1 mm diameter and 20 mm long cylinder of graphite or aluminium at the centre of the cavity protruding from its base.

The proton beam was considered mono-energetic, mono-directional (incident perpendicular to the axis of symmetry of the chamber model) and without any loss of energy over the geometry. In practice, except at low energies, there is a small energy loss over the dimensions of this chamber model so this approximation is only justified if the variation of perturbation factors with proton energy is slow, which can be verified retrospectively.

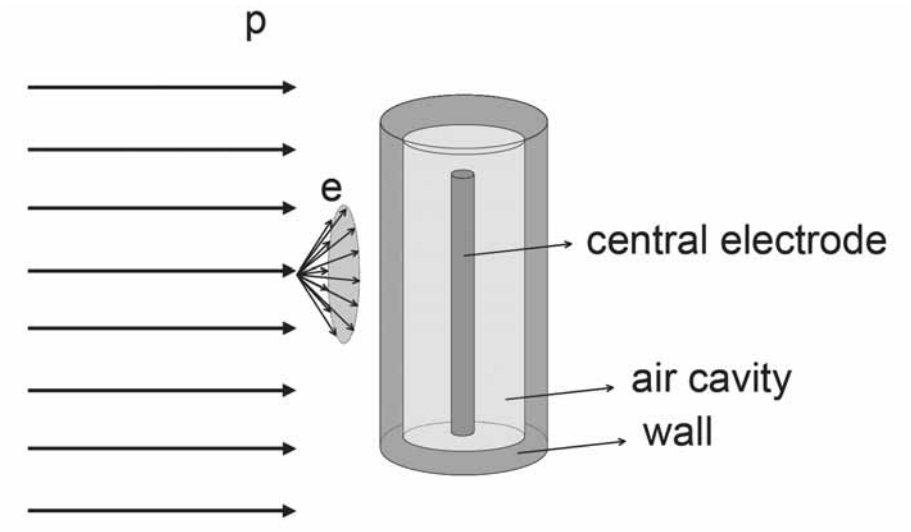

FIG. 1. Schematic drawing of the geometry used in the Monte Carlo simulations.

Electron recoil spectra in the cavity, central electrode, wall and surrounding water were calculated from the Bhabha cross-section [16] and the number of cross-section centres derived from the electron density in each medium. Isotropic emission of electrons was considered as well as an energy-angle relationship described by the Bethe ridge [17], which can be considered as two extremes. Electron transport through the geometry was simulated using DOSRZnrc [18]. The internal emission of electrons from different components (wall, air cavity, central electrode, water surrounding the chamber) was simulated separately so that they could be added with appropriate weights based on the electron density and volume of each component. In order to simulate a non-isotropic internal emitter, the DOSRZnrc user code had to be modified. The default transport and boundary crossing settings of DOSRZnrc were used and the cut-off energy for electron transport was 1 keV. The number of particle histories depended on the source region and varied between 10^9 and 10^{11} per simulation. These were chosen in view of the contributions of the different source regions to the final uncertainty. All contributions by electrons to the dose in the cavity were normalized per one electron set in motion within the cavity. The number of electrons for normalization of dose contributions from electrons set in motion in other regions was then the ratio of the number of atomic electrons in that region and in the cavity. Dose to air in the cavity, $D_{\text{air,cav}}$, for a broad proton field was evaluated as:

$$D_{\mathrm{air,cav}} = \Phi_{\mathrm{p}} \cdot \left(\frac{S^{\Delta}}{\rho} \right)_{\mathrm{air}} + \Phi_{\mathrm{p}} \cdot N_{\mathrm{A}} \cdot \left(\frac{Z}{A} \right)_{\mathrm{air}} \cdot \left[\int_{\Delta=1\mathrm{keV}}^{W_{\max}} \sigma_{W,\mathrm{Bahbha}} \cdot dW \right] \cdot E_{\mathrm{e,dep,MC}} \tag{1}$$

Where Φ_{p} is the (mono-energetic) proton fluence, $(S^{\Delta}/\rho)_{\mathrm{air}}$ the restricted mass stopping power at the energy of the protons, N_{A} Avogadro's number, $(Z/A)_{\mathrm{air}}$ the average ratio of atomic number and atomic weight of the medium, $W_{\max}$ the maximum energy that can be transferred to a secondary electron by the protons, $\sigma_{W,\mathrm{Bhabha}}$ the Bhabha cross-section differential in energy (the integral thus being the total cross-section for emission of an electron) and $E_{\mathrm{e,dep,MC}}$ the sum of all Monte Carlo calculated contributions to the dose in the cavity by electrons weighted, as explained before, per electron set in motion in the cavity.

The wall perturbation correction factors were then obtained as the ratio of $D_{\mathrm{air,cav}}$ calculated by expression (1) for the chamber geometry with the wall set to water and for the chamber geometry with the wall set to the actual wall material. Obviously, the proton fluence drops out in this ratio.

Central electrode perturbation correction factors were obtained as the ratio of $D_{\mathrm{air,cav}}$ calculated by expression (1) for the chamber geometry without the central electrode present and for the chamber geometry with central electrode present.

3. RESULTS

The calculated wall perturbation correction factors as a function of energy are shown in Fig. 2. For both wall materials, the correction factors exponentially saturate at high energies; for A150, around 1.004; and for a graphite wall, around 0.985.

In Fig. 3, the ratios of wall perturbation correction factors for the A150 and the graphite walled Farmer chamber are shown as a function of energy. This can be compared with experimental data obtained in a 75 MeV beam (55 MeV effective proton energy as derived from the residual range) reported in Ref. [13]. Each of the experimental data points has an uncertainty of about 0.2%, which is not shown on the graph for clarity. The most striking results of these datasets are those depicted with a large hollow square and triangle since they were obtained for an in-house made Farmer with an A150 wall with exactly the same dimensions as the graphite wall of a commercial NE2571 Farmer type chamber.

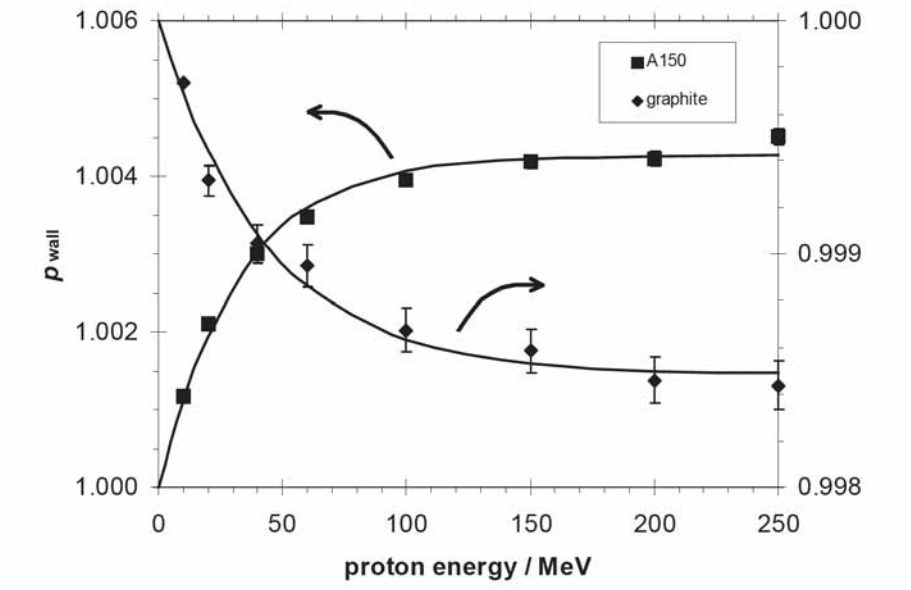

FIG. 2. Wall perturbation factor as a function of proton energy for a Farmer type chamber with graphite and A150 wall. The full lines are exponentials fitted to the data.

This configuration thus most closely matches the geometry simulated in the Monte Carlo calculations. The other data points were obtained for a NE2581 chamber which has more features differing from the NE2571, such as the wall thickness and the central electrode diameter. All the experimental data points, as well as the average, are in good agreement with the calculated data considering the experimental uncertainty.

In Fig. 4, the calculated central electrode perturbation correction factors as a function of energy are shown. Again, the correction factors exponentially saturate at high energies. For a graphite central electrode, the perturbation is negligible at all energies, while for an aluminium central electrode, it saturates at 0.998, identical to the value for high energy electron beams.

The ratios of the central electrode correction factors for the aluminium and graphite electrode are shown in Fig. 5. Here, the data can be compared with those obtained in Refs [11] and [13]. Again, there is a good agreement between experimental and simulated data, although the experimental uncertainties do not allow resolution of the small corrections.

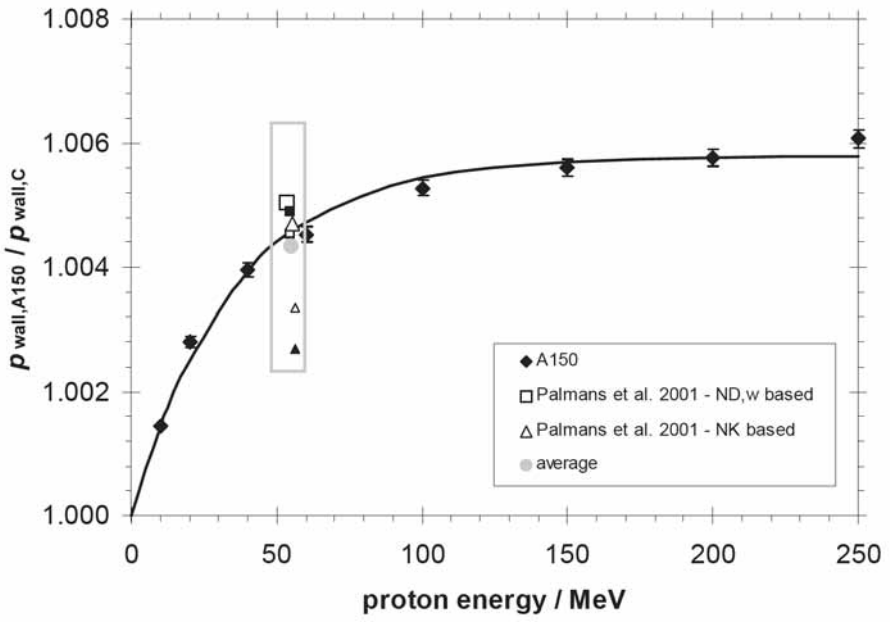

FIG. 3. Ratio of wall perturbation factors as a function of proton energy for a Farmer type chamber with a graphite and A150 wall. The full line is the ratio of the full lines in Fig. 2. The square and triangles are experimental data from Ref. [13]; the large hollow square and triangle symbols are for the same geometry, while the small hollow square and triangle are for the NE2581 in comparison with a NE2571 and the full square and triangle for the NE2581 in comparison with graphite wall and electrode The hollow grey circle is an average of the four data points and the grey rectangle an indication of the 0.2% experimental standard uncertainty.

4. CONCLUSIONS

Improved Monte Carlo calculations of wall and central electrode perturbation correction factors are presented for Farmer type chambers with graphite and A150 as wall materials and graphite, and aluminium central electrodes due to secondary electron effects in proton beams. The correction factors exponentially saturate at high energies at about 1.004 for an A150 wall and about 0.985 for a graphite wall. The ratios of wall perturbation factors for those two materials are in good agreement with experimental data. Monte Carlo simulation of the central electrode correction factor result in values that saturate exponentially at 0.998, the same value as for high energy electron beams. Also these values agree well with experimental data. The overall perturbation of a

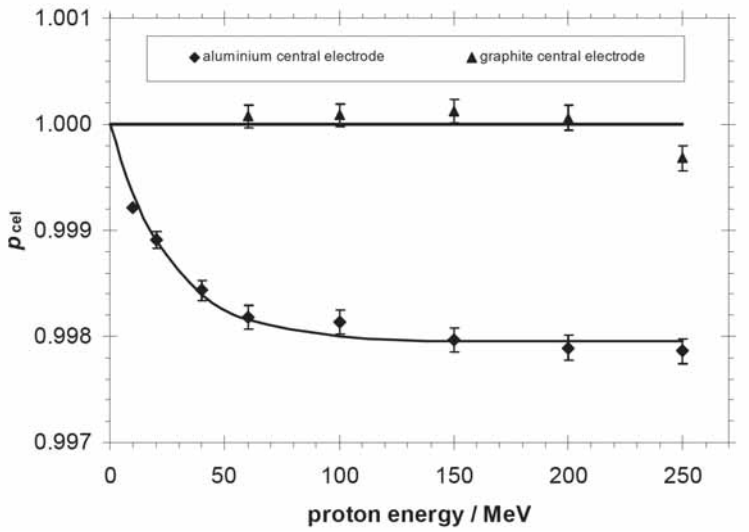

FIG. 4. Central electrode perturbation correction factor as a function of proton energy for a graphite and an aluminium electrode of 1 mm diameter and 20 mm length in a Farmer type chamber. The full lines are exponentials fitted to the data.

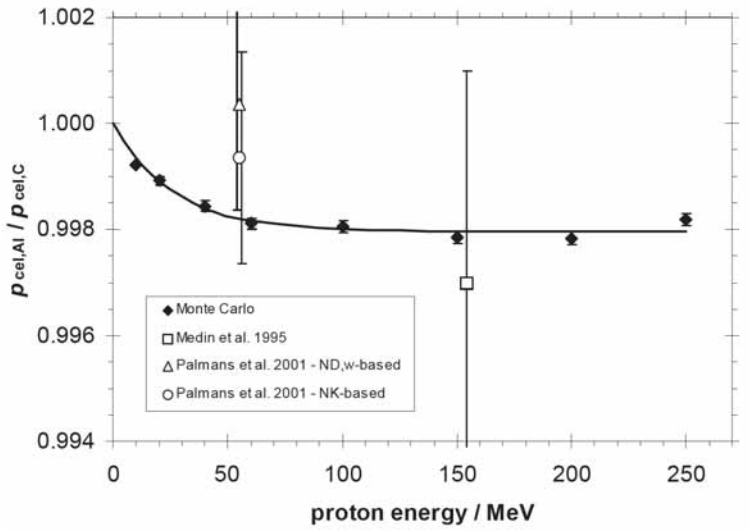

FIG. 5. Ratio of central electrode perturbation correction factors as a function of energy for a graphite and an aluminium electrode of 1 mm diameter and 20 mm length in a Farmer type chamber. The full line is the ratio of the full lines in Fig. 4. The hollow symbols are experimental data from Refs [11] and [13].

Farmer type chamber with graphite wall and aluminium central electrode derived from the simulations is thus $p_Q = p_{wall} \cdot p_{cel} = 0.9965$.

Future work will extend this to other chamber types frequently used in proton dosimetry, such as the Far West IC18 chamber, PMMA walled chambers and plane-parallel chambers, and the results will be compared with cavity theory models for which tuning parameters can be optimized by Monte Carlo simulations.

REFERENCES

[1] INTERNATIONAL ATOMIC ENERGY AGENCY, Absorbed Dose Determination in External Beam Radiotherapy: An International Code of Practice for Dosimetry Based on Standards of Absorbed Dose to Water, Technical Report Series 398, IAEA, Vienna (2000).

[2] ICRU, Prescribing, Recording, and Reporting Proton-Beam Therapy, International Commission on Radiation Units and Measurements Report 78, ICRU, Bethesda MD, USA (2008).

[3] AAPM, Protocol for heavy charged-particle therapy beam dosimetry: a report of Task group 20 Radiation Therapy Committee, American Association of Physicists in Medicine Report 16, American Institute of Physics, New York, NY (1986).

[4] VYNCKIER, S., BONNETT, D.E., JONES, D.T.L., Code of practice for clinical proton dosimetry, Radiother. Oncol. **20** (1991) 53–63.

[5] VYNCKIER, S., BONNETT, D.E., JONES, D.T.L., Supplement to the code of practice for clinical proton dosimetry, Radiother. Oncol. **32** (1994) 174–179.

[6] ICRU, Clinical proton dosimetry Part I: Beam production, beam delivery and measurement of absorbed dose, International Commission on Radiation Units and Measurements Report 59, ICRU, Bethesda MD, USA (1998).

[7] PALMANS, H., VERHAEGEN, F., "Calculation of perturbation correction factors for ionization chambers in clinical proton beams using proton-electron Monte Carlo simulations and analytical model calculations" Recent Developments in Accurate Radiation Dosimetry (SEUNTJENS, J.P., MOBIT, P.N., Ed.), Medical Physics Publishing, Madison WI, USA (2002) 229–245.

[8] PALMANS, H., VERHAEGEN, F., Monte Carlo study of fluence perturbation effects on cavity dose response in clinical proton beams, Phys. Med. Biol. **43** (1998) 65–89.

[9] PALMANS, H., Analytical models for the determination of the effective water depth of an ionization chamber in a proton beam and extension for application in the Bragg peak, NPL Report DQL-RD-002, National Physical Laboratory, Teddington, UK (2006).

[10] PALMANS, H., Perturbation factors for cylindrical ionization chambers in proton beams. Part I: corrections for gradients, Phys. Med. Biol. 51 (2006) 3483–501.

[11] MEDIN, J., ANDREO, P., GRUSELL, E., MATTSSON, O., MONTELIUS, A., ROOS, M., Ionization chamber dosimetry of proton beams using cylindrical and plane parallel chambers. Nw versus NK ion chamber calibrations, Phys. Med. Biol. **40** (1995) 1161–76.

[12] PALMANS, H., SEUNTJENS, J., VERHAEGEN, F., DENIS, J.-M., VYNCKIER, S., THIERENS, H., Water calorimetry and ionization chamber dosimetry in an 85-MeV clinical proton beam, Med. Phys. **23**: (1996) 643–50.

[13] PALMANS, H., VERHAEGEN, F., DENIS, J.-M., VYNCKIER, S., THIERENS, H., Experimental pwall and pcel correction factors for ionization chambers in low energy clinical proton beams, Phys. Med. Biol. **46** (2001), 1187–204.

[14] VERHAEGEN, F., PALMANS, H., A systematic Monte Carlo study of secondary electron fluence perturbation in clinical proton beams (70-250 MeV) for cylindrical and spherical ion chambers, Med. Phys. **28** (2001) 2088–95.

[15] KAWRAKOW, I., MAINEGRA-HING, E., ROGERS, D.W.O., TESSIER, F., WALTERS, B.R.B., The EGSnrc Code System: Monte Carlo Simulation of Electron and Photon Transport, National Research Council, Ottawa, Canada (2010).

[16] BHABHA, H.J., On the penetrating component of cosmic radiation, Proc. R. Soc. London A164 (1938) 257–294.

[17] INOKUTI, M., Inelastic collisions of fast charged particles with atoms and molecules — the Bethe theory revisited, Rev. Mod. Phys. **43** (1971) 297–347.

[18] ROGERS, D.W.O., KAWRAKOW, I., SEUNTJENS, J.P., WALTERS, B.R.B., MAINEGRA-HING, E., NRC User Codes for EGSnrc, NRCC Report PIRS-702(revB), National Research Council, Ottawa, Canada (2010).

TESTING THE ACCURACY OF ELECTRON TRANSPORT IN THE MONTE CARLO CODE FLUKA FOR CALCULATION OF IONIZATION CHAMBER WALL PERTURBATION FACTORS

M. KLINGEBIEL, M. KUNZ, S. COLBUS, K. ZINK, J. WULFF
Institut für Medizinische Physik und Strahlenschutz,
Gießen, Germany
Email: mandy.klingebiel@tg.fh-giessen.de

Abstract

The aim of this study was to investigate the Monte Carlo (MC) code FLUKA, regarding its ability to accurately simulate electron transport at density inhomogeneities and in ionization chamber geometries. In order to evaluate the accuracy of FLUKA's electron transport algorithm and the implementation of the condensed history technique, a Fano test was used. This test allows the comparison of calculated and theoretically expected results. The ratio of the two results is ideally equal to unity, and a deviation usually indicates artifacts in the treatment of density interfaces. As a more practical problem, wall perturbation factors p_{wall} of a plane parallel chamber in electron beams were calculated and compared with results based on the EGSnrc MC code. Additionally, the impact of wall material and thickness on calculated cavity dose was investigated for two different thimble chambers irradiated by ^{60}Co. The correct choice of parameters within FLUKA's electron transport algorithm ensured passing the Fano test within ~0.7% and a good agreement for practical examples within 0.4% compared to results of the EGSnrc MC code. The latter is known to allow an artifact free simulation of ionization chamber response in photon and electron beams. Based on these results, the electron transport accuracy within the FLUKA code can generally be regarded as much better than 1% for typical ionization chamber dosimetry problems.

1. INTRODUCTION

Within a Monte Carlo (MC) code, charged particle transport is usually simulated with the use of the condensed history technique (CHT). The CHT summarizes many charged particle interactions in one single step, sampled from an appropriate multiple scattering distribution. This is necessary since the time requirements for the simulation of every single elastic and inelastic collision would not be feasible. The artificial steps are limited by a maximum allowed energy loss, length or scattering angle and by media interfaces. Difficulties appear, especially at these interfaces of different materials or densities, and can

lead to artifacts [1]. Artifacts generally depend on the parameters chosen in the transport algorithm and are particularly evident in the simulation of air filled ionization chambers. Hence, a reliable MC based investigation of ionization chambers in medical physics problems depends on the accuracy of the implemented CHT.

Modern MC codes such as PENELOPE [2] and EGSnrc [3] are known to allow an artifact-free simulation (within 0.1% normalized to own cross-sections) of ionization chamber response in photon and electron beams, mainly due to special handling of media interfaces. Subsequently, they have been used for the investigation of ionization chamber dosimetry in photon and electron beams. The Fano test, explained below, is usually employed to test the accuracy of the electron transport and the implemented CHT.

The FLUKA [4] MC code allows the simulation of multiple particles and is generally suitable for an investigation of ionization chamber dosimetry within heavy ion beams. It incorporates a CHT for electrons and heavier charged particles. However, to the authors' knowledge, no Fano test has yet been performed for the FLUKA MC code. Hence, the aim of this work was the evaluation of FLUKA for calculation of ionization chamber response in photon/electron beams based on the Fano test. Further, realistic ionization chamber geometries were simulated in order to calculate perturbation factors for a plane parallel chamber and the dose ratio between two thimble chambers of different wall materials.

2. METHODS

2.1. Electron transport in FLUKA

Like other general purpose codes, FLUKA employs a CHT for the simulation of charged particles. In the following, only electrons are considered, although many aspects apply to other charged particles as well. Single elastic and inelastic interactions of charged particles are grouped into artificial multiple Coulomb scattering (MCS) steps. In the implemented CH class II technique, the length of such a step is limited by various constraints. The simulation of discrete events, often called catastrophic events, in which secondary particles are generated above a predefined threshold (EMFCUT/PROD-CUT), causes a truncation of the MCS step. Furthermore, a maximum allowed energy loss per MCS step (EMFFIX) is provided by the user, as well as a physical length restriction given in centimeters (STEPSIZE). Following the FLUKA documentation [4], the maximum step size should not be larger than one third of the geometry's minimum dimension in order to allow the multiple scattering to

work in optimal conditions. Considering the maximum allowed energy loss, the documentation recommends EMFFIX not to exceed 5–10% for dosimetry problems and in thin-slab geometries.

FLUKA uses a hybrid solution for treatment of media interfaces. During the charged particle's approach to a boundary, the length of MCS steps is progressively shortened until becoming comparable to the minimum allowed length of the underlying MCS theory by Molière (20–30 elementary scatterings) [5–8]. In order to avoid an accumulation of MCS steps at the interface itself, FLUKA employs a 'one step back algorithm' [7]. When a boundary is crossed during MCS transport, a single step length is sampled and randomly divided into two fractions. The fraction before the boundary is used for the calculation of the last scattering centre. At this estimated point the Molière deflection is applied, and the particle is transported in one (or more) single scatterings across the boundary. The user can choose the number of single scatterings. The single scattering in FLUKA itself is based on the Rutherford formula with atomic screening, by choice with nuclear finite size and spin-relativistic corrections. This single scattering can further replace the MCS based on the Molière theory, whenever this theory's validity conditions for the current step are not satisfied, i.e. the steps become too short to fulfill the requirements of multiple scattering. This occurs when steps are truncated by the restrictions mentioned above.

All the following MC based calculations were performed with the FLUKA code (version: 2008.3b.1) [4].

2.2. The Fano cavity test

To assess the accuracy of the electron transport in FLUKA a Fano test was implemented [2, 3]. This test can be employed to compare a calculated result for a typical ionization chamber cavity setup with a theoretically expected result. The ratio of these two values ideally equals unity. A difference from unity usually indicates artifacts in the treatment of interfaces. The advantage of this test is that it is independent of any cross-section uncertainties that are generally present in every MC simulation. Thus, the test can be understood as an impartial experiment, focusing on the implemented electron transport algorithm.

In order to perform the Fano test, the authors followed the methods of Sempau and Andreo [2]. The basic idea was to create a situation where the Fano theorem holds: under charged particle equilibrium (CPE), the influence of charged particles is independent of the local density as long as the cross sections are independent of the density. In a MC simulation a geometry can be constructed with same wall and cavity material but differing density. Furthermore, full CPE can be realized and the ratio Q between the calculated and the expected energy deposition in the cavity can be determined, which must be unity for an artifact

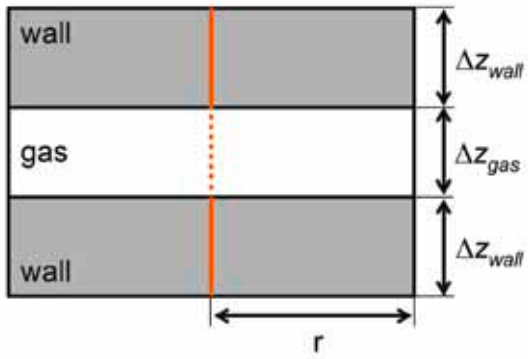

FIG. 1. Sectional view of the simulation set-up for the Fano cavity test. A gas filled cavity with thickness Δz_{gas} is surrounded by a solid wall of the same material with high density. The radius r of the cylindrical setup is larger than the range of electrons in the cavity gas. The thickness of the wall Δz_{wall} is chosen to be larger than the electrons' maximum range within the wall material. A line source is placed in the central axis and emits monoenergetic electrons. The volumetric source strength is proportional to the local mass density.

free simulation. In this case, the inhomogeneity was represented by an ionization chamber, constructed as a cylinder with a 2 mm cavity and walls of graphite, but differing density (Fig. 1).

According to Sempau and Andreo [2], using a line source that emits monoenergetic electrons with energy E_0 proportional to the local mass density the quantity Q follows:

$$Q = \frac{\Delta E}{N E_0}\left(1 + \frac{2\rho_{wall}\Delta z_{wall}}{\rho_{gas}\Delta z_{gas}}\right) \tag{1}$$

In the above equation, $\Delta E/N$ is the scored energy per primary particle with energy E_0, ρ is the mass density and Δz is the thickness of wall and cavity, respectively. The wall was made thicker than the maximum range of electrons. The difference of density between wall and cavity was a factor 1000, which resembles the situation in a real ionization chamber at normal air pressure. The ratio Q was determined for initial kinetic energy of electrons of 0.5 MeV, 1 MeV, 10 MeV and 20 MeV.

2.3. Calculation of the wall perturbation factor p_{wall} of a Roos type chamber

As a more practical application, a model of a Roos plane parallel chamber was implemented, which was placed at reference depth in a water phantom and

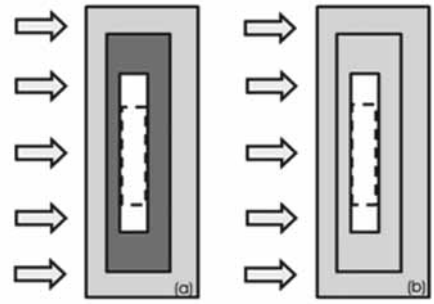

FIG. 2. Sectional view of the simulation geometries for the calculation of the wall perturbation factor. (a) shows the Roos chamber with chamber wall. The white volume indicates the air volume including the guard ring, whereby the dashed lines display the position of the active air volume. The chamber is surrounded by water (light grey). In (b), the chamber wall is replaced by water. In both cases, the monoenergetic electron beam comes from the left (referring to Ref. [10]).

irradiated by electrons. The wall perturbation factors p_{wall} were calculated for monoenergetic electrons of 6, 7, 8, 9 and 14 MeV. Two independent simulations using the geometries as shown in Fig. 2 were performed and the energy deposition within the sensitive volume of the air cavity was calculated. For the first simulation (Fig. 2, (a)), the chamber model was constructed as specified by the manufacturer [9], while the chamber wall in the second simulation was completely replaced by water (Fig. 2, (b)). The ratio of the latter and the former calculated value yields the perturbation factor p_{wall} by definition.

In addition to the default settings in FLUKA, the electron transport parameters were refined. The maximum step size of electrons was fixed to one third of the minimum dimension of each region. This resulted in step sizes between 0.06 and 0.003 cm. Transport cut-offs of 10 keV (kinetic energy) for electrons and 1 keV for photons were applied for all materials. The maximum energy loss in each CH step for all materials was set at 5% of the initial energy. Single scattering was activated for transport at interfaces and for steps considered too short, and two single steps for boundary crossing were chosen.

The results were compared to the values in Ref. [10] based on EGSnrc.

2.4. Different wall thicknesses and materials of thimble chambers

Following the work of Buckley et al. [11], the cavity dose was the calculated for thimble chambers of different wall material and thickness. The walls of the chambers were modelled to consist of aluminium and graphite, respectively. The figure of merit was the calculated dose ratio D_{Al}/D_{Gr} in a ^{60}Co

beam for the two chambers and was compared to the results in Ref. [11] based on EGSnrc.

The geometric details of the simulation setup were constructed as given in Ref. [11]. The thimble wall thicknesses were 0.35 and 0.09 mm for the graphite and aluminium chambers respectively, resulting in identical outer dimensions for both. As the chambers were placed free in air, the total wall thicknesses were taken as 0.5 g/cm^2 in order to achieve electronic equilibrium. The wall inside the aluminium thimble was coated with a dag layer (87.48% C, 3% H and 9.52% O) varying from 1–9 mg/cm^2. The additional thin dag layer between the cavity and the aluminium wall can be understood as a particular difficulty for the electron transport algorithm. The electron transport parameters were equal to those in the previous section. In the original work of Buckley et al. [11], different excitation energies (*I*-value) within the electron stopping powers of graphite were tested and the results were compared to a corresponding measurement. It was demonstrated that the results depend on the *I*-value. However, the *I*-value was not altered and the default values were used for the materials, which are based on the ICRU Report 37 [12].

3. RESULTS

3.1. The Fano cavity test

As mentioned, the Fano test yields the ratio between the calculated and expected result and can be employed to test the quality of the electron transport algorithm within a MC code. Independent of the energy, the quantity Q (see Eq. 1) should equal unity.

A simulation using the general FLUKA defaults without adjustments of the maximum step size and energy loss, and no special treatment of boundaries led to $Q = 1.0852 +/- 0.0005$ for the 1 MeV electron energy. Hence, the result is wrong by up to 8–9% when no special care of the electron transport parameters is taken.

In the case where the cavity and wall share the same density, Q equals unity within the statistical uncertainty for the graphite chamber and aluminum, respectively (result not shown). This demonstrates that the artifacts are clearly caused by the varying density between wall and cavity. Further, it validates the correct implementation of the Fano test, since for a homogeneous simulation geometry, no artifact (i.e. a deviation of Q from unity) must be observed.

Figure 3 shows the quantity Q as a function of energy, when single scattering is turned on at boundaries and for steps that are too short for restrictions of the geometrical step length and maximum energy loss. Generally, there is a non-constant deviation from the correct result. When varying the energy

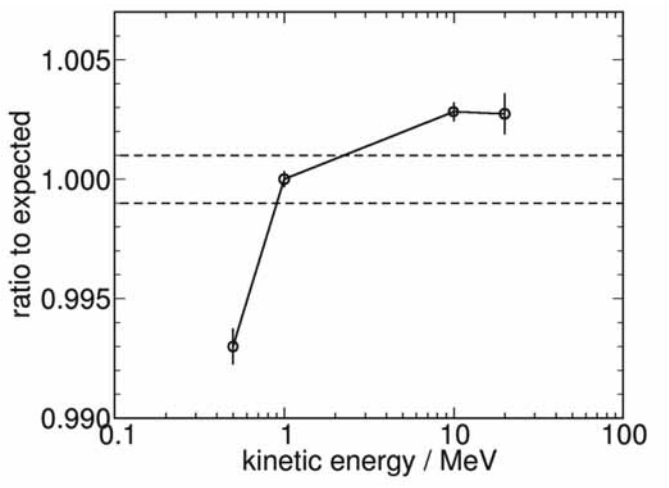

FIG. 3. Ratio of calculated to expected result (quantity Q in Eq.1) as a function of kinetic energy of the emitted monoenergetic electrons. The broken line represents a 0.1% level of agreement.

of the emitted electrons, the quantity Q changes by ~0.7% at most. The electron transport algorithm obviously fails to reproduce the correct answer differently. At lower energies, the calculated result is lower than the expected, and at higher energies, vice versa.

3.2. Calculation of the wall perturbation factor p_{wall} of a Roos type chamber

Figure 4 shows the wall perturbation factors p_{wall} for the Roos plane parallel chamber calculated with FLUKA in comparison to the values taken from Ref. [10], which were calculated with EGSnrc. As investigated in Ref. [10] p_{wall}, shows an energy dependent behaviour and decrease with increasing quality specifier R_{50} and exceeds unity. A significant deviation between the both codes is observable only for the lowest and highest energies used here (6 MeV/14 MeV). However, there is no clear trend of these discrepancies, and the results generally agree within the 2σ statistical uncertainties. The largest deviation amounts to ~0.4% for the lowest energy with a corresponding statistical uncertainty in the results of ~0.2%. It is worth noting that the calculation times for FLUKA were longer roughly by a factor 100.

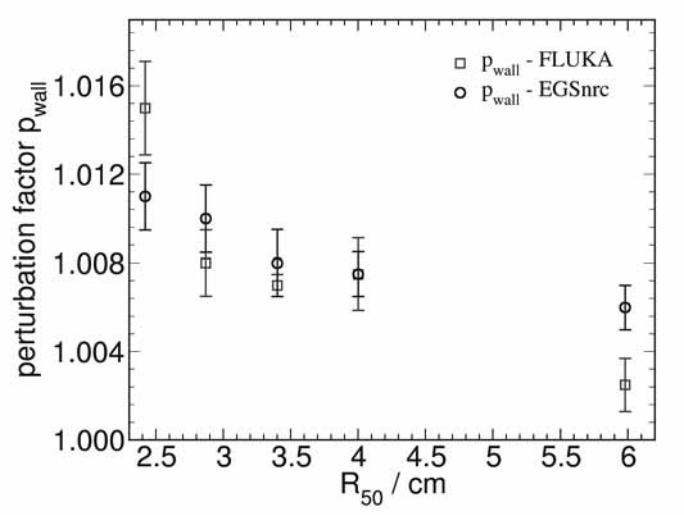

FIG. 4. Calculated wall perturbation factors p_{wall} for the Roos chamber as a function of the beam quality specifier R_{50} for various monoenergetic electron beams, calculated with FLUKA and EGSnrc [10]. Error bars indicate the statistical uncertainties (1σ), which are at most ~0.2% for both codes.

3.3. Different wall thicknesses and materials of thimble chambers

Figure 5 shows the calculated cavity dose ratio D_{Al}/D_{Gr} for two thimble chambers in a ^{60}Co beam as a function of the dag layer thickness. A dag layer of zero corresponds to a pure aluminium wall chamber. As can be seen, the dose ratio D_{Al}/D_{Gr} decreases with increasing dag layer thickness. There is a very good agreement between the two codes within statistical uncertainties. The maximum deviation between both codes is within ~0.5%, and again, no clear trend is observable.

4. DISCUSSION AND CONCLUSION

The aim of this work was the investigation of the FLUKA MC code regarding its ability to accurately calculate ionization chamber cavity dose and perturbation factors. In a first step, a general Fano test for a graphite cavity was implemented. It turned out that the test was fulfilled within a maximum deviation of ~0.7% in the energy range of 0.7–20 MeV. It was crucial to limit the CHT steps by defining a maximum energy loss and step size, and turning single scattering on

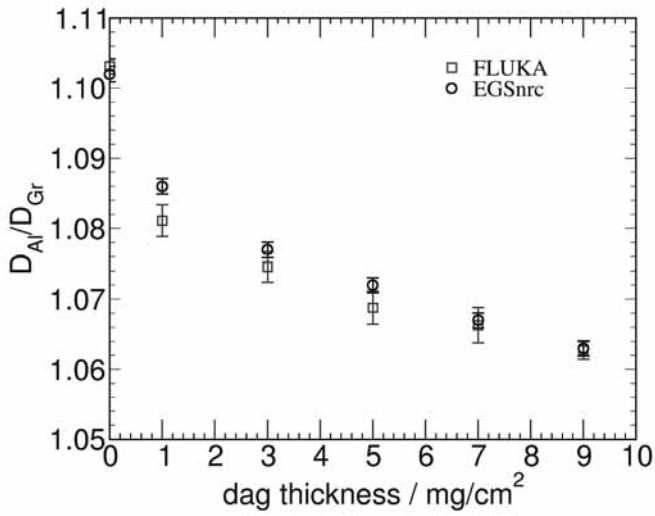

FIG. 5. Ratio D_{Al}/D_{Gr} as a function of the dag layer thickness. Error bars indicate 1σ statistical uncertainties (~0.1% for EGSnrc and ~0.2% for the FLUKA results).

for boundary crossings; otherwise significant artifacts of up to 8% resulted. This can be attributed to the fact that without special care, the approximated straight CH step parallel to an interface cannot accurately represent the true curved path of an electron, which might cross the boundary and take a considerably different path in the low density cavity compared to the wall (see Ref. [1]). No clear trend of the deviations in the Fano test was observable, although the deviations were slightly larger at lower energies. This might be caused by the much more curved trajectories of the low energy electrons, which make an interface artifact more likely if the boundary is not sensed correctly by the algorithm.

The calculation of the wall perturbation factor p_{wall} for the Roos chamber showed good agreement compared to results of EGSnrc, except at low and the highest energy. As another practical example, the dose ratio between two thimble chambers of different wall thicknesses and materials was calculated. The deviations between results of FLUKA and EGSnrc were generally within 0.4%. It must be noted that deviations between FLUKA and EGSnrc cannot be completely explained in terms of the different CHT in electron transport. There still might be some differences in cross-sections and models for the coupled transport of photons. However, as the results of the Fano test indicate, the main reason for deviations will be the electron transport accuracy of FLUKA.

In conclusion, the electron transport algorithm within the FLUKA MC code resulting in being capable of simulating ionization chamber dosimetry problems

in a comparable accuracy (<1%) as EGSnrc. However, the computing times for FLUKA exceeded that of EGSnrc by at least one order of magnitude.

It is doubtful that FLUKA is currently an alternative to EGSnrc or PENELOPE for pure electron transport problems since these codes are generally more reliable and much faster; however, they do not provide any hadron or heavy ion transport. There is a recent interest in particle therapy calculations. Only a few studies on correction factors have been performed yet in which a complete ionization chamber model was simulated. For example, Palmans [13] used a modified version of the PTRAN code [14] to calculate gradient effects in cylindrical chambers, and Kirby et al. [15] used FLUKA to calculate beam quality correction factors for plane-parallel chambers. The quality of these calculated corrections are influenced to some degree by the accuracy of the implemented charged particle transport algorithms, which is similar for electrons and heavier charged particles. Hence, future investigations will therefore focus on similar investigations for protons and heavy ions, the strength of FLUKA.

REFERENCES

[1] BIELAJEW, A.F., ROGERS, D.W.O., NAHUM, A.E., Monte Carlo Calculation of ionization chamber response to Co60-resolution of anomalies associated with interfaces, Phys. Med. Biol. **30** (1985), 419–427.

[2] SEMPAU, J., ANDREO, P., Configuration of the electron transport algorithm of PENELOPE to simulate ionization chambers, Phys. Med. Biol. **51** (14), (2006), 3533–3548.

[3] KAWRAKOW, I., Accurate condensed history Monte Carlo simulation of electron transport. I. EGSnrc the new EGS4 version. Med Phys. **27** (2000) 485–498.

[4] FASSÒ, A., FERRARI, A., RANFT, J., SALA, P., FLUKA: A multi-particle transport code, CERN-2005-10, INFN/TC-05/11, SLAC-R-773 (2005).

[5] FASSÒ, A., FERRARI, A., SALA, P.R.,, Electron-Photon Transport in FLUKA: Status, in 'Advanced Monte Carlo for Radiation Physics, Particle Transport Simulation and Application(Proc. of the Monte Carlo 2000 Meeting, Lisbon) (2000) 159–164

[6] AARNIO, P.A., FASSÒ, A., MÖHRING, H.J., RANFT, J., SALA, P.R., STEVENSON, G.R., ZAZULA, J.M., Electron-photon transport: always so good as we think? Experience with FLUKA (P. DRAGOVITSCH, P. LINN, S., BURBANK, M., Eds) (Proc. Int. Conference on Monte Carlo Simulation in High Energy and Nuclear Physics, 1994) (1994) 100–110.

[7] FASSÒ, A., FERRARI, A., SALA, P.R., An update about FLUKA, in G. Stevenson, ed., Proc. 2nd Workshop on Simulating Accelerator Radiation Environments (SARE 2), CERN, Geneva, CERN Report (1995) 158–170.

[8] FERRARI, A., SALA, P., GUARALDI, R., PADOANI, F., 'An improved multiple scattering model for charged particle transport', Nuc. Instr. and Meth. **B71** (1992) 412–426.

[9] PTW, Freiburg: Produktkatalog Ionizing Radiation Detectors 2009/2010 (2008).

[10] ZINK, K., WULFF, J., Monte Carlo calculation of beam quality factors kQ for electron dosimetry with a parallel-plate Roos chamber, Phys. Med. Biol. **53** (2008) 1595–1607.
[11] BUCKLEY, L.A., et al., An EGSnrc investigation of cavity theory for ionization chambers measuring air kerma: Med. Phys. **30** (6) (2003).
[12] ICRU, Stopping powers for electrons and positrons, ICRU Report 37, Washington DC (1984).
[13] PALMANS, H., Perturbation factors for cylindrical ionization chambers in proton beams. Part I: corrections for gradients, Phys. Med. Biol. **51**(14) (2006) 3483–3501.
[14] BERGER, M., Proton Monte Carlo transport program PTRAN (NISTIR 5113), National Institute for Standards and Technology (Gaithersburg, MS: NIST) (1993).
[15] KIRBY, D., GREEN, S., PALMANS, H., HUGTENBURG, R., WOJNECKI, C., PARKER, D., 'LET dependence of GafChromic films and ionization chamber in low-energy proton dosimety', Phys. Med. Biol. **55(**2) (2010) 417–433.

CONTRIBUTIONS OF THE DIFFERENT ION CHAMBER WALLS TO WALL PERTURBATION IN CLINICAL ELECTRON BEAMS: A MONTE CARLO STUDY OF THE NACP-02 PARALLEL-PLATE CHAMBER

K. ZINK
University Hospital Marburg, Department for Radiotherapy, Marburg
Email: klemens.zink@med.uni-marburg.de

J. WULFF
University of Applied Sciences Giessen, Institute for Medical Physics and Radiation Protection, Giessen

Germany

Abstract

Parallel-plate ionization chambers are widely used in clinical electron dosimetry. They are designed to minimize perturbations due to the presence of the chamber walls and the air-filled cavity. Therefore, the wall correction factor p_{wall} is assumed to be unity in all current dosimetry protocols and to be independent of electron initial energy and depth. Experimental and Monte Carlo (MC) data showed that this assumption is not valid for the NACP chamber. This perturbation is blamed on the quite massive graphite back wall of the chamber, resulting in a backscatter deficiency. Since the chamber is known to be 'well guarded', it is commonly assumed that the influence of the chamber's side wall is negligible. This paper presents detailed MC simulations for the NACP-02 chamber regarding the influence of the different chamber walls on the wall perturbation correction. The calculations are performed for a wide range of electron energies. The results unambiguously show that the side wall contributes up to one third to the wall perturbation correction. As expected, this contribution decreases with increasing electron energy. Variations of the guard ring width show that even a width of 17 mm is not wide enough to avoid a noticeable influence of the side wall. The contributions of the side and back wall on p_{wall} linearly increase with depth while the contributions from the entrance window exhibit a more complex depth dependence.

1. INTRODUCTION

All present dosimetry protocols recommend to use parallel-plate ionization chambers in clinical electron dosimetry [1–4]. They are designed to minimize

perturbations due to the presence of the chamber walls and the air-filled cavity. Therefore the wall correction factor p_{wall} is assumed to be unity whatever the initial electron energy and depth.

Previous experimental investigations (see Ref. [5]) have already given considerable evidence that the perturbations are not negligible. The back wall has been identified as a source of fluence perturbation, since the electrons that are backscattered from and through the rear wall make a significant contribution to the dose within the active volume of the chamber. The influence of different backscattering materials behind the cavity of parallel-plate chambers was experimentally investigated by Hunt et al. [6] and Klevenhagen [7]. According to these authors, the electron backscattering is proportional to the atomic number of the medium and inversely proportional to the electron energy. The rear wall of the NACP chamber is quite massive (thickness: 5.6 mm) and made of graphite. It has a higher density than water and an atomic number (Z) of 6, which is about 10% smaller than the effective atomic number of water [7]. Therefore, it is assumed that the measured wall perturbation correction of the NACP chamber may be ascribed to the backscatter deficiency of the back wall.

Several years ago, McEwen [18] reinvestigated the backscattering of different parallel-plate chambers in clinical electron beams and determined the wall perturbation correction due to the rear wall of the NACP chamber experimentally with high accuracy. The comparison with wall perturbation corrections of the whole chamber resulting from Monte Carlo (MC) simulations [8, 9] displayed a significant difference in the range of about 0.5% for the whole energy range of clinical electron beams included in his study (R_{50} = 1.2–6.6 cm). McEwen concluded that this difference may be due to the contributions of the front and side wall of the NACP chamber to the total wall perturbation correction. The side wall was always assumed to, but does not contribute to p_{wall}, since the NACP chamber was considered ‘well-guarded’.

MC simulations were performed for the NACP chamber in clinical electron beams focusing on the contribution of the different chamber walls to the global wall perturbation correction p_{wall}.

2. METHOD AND MATERIAL

2.1. Background theory

The dosimetry of high-energy photon and electron beams with ionization chambers is based on Spencer-Attix cavity theory [10, 11] according to which the dose-to-water D_w is related to the dose in an ideal air-filled cavity D_{cav} by the restricted stopping-power ratio $s_{w;a}$ between water and air. Owing to the chamber

walls and the cavity, the electron fluence in the cavity is not the same as in the ideal case. Therefore, a perturbation correction p is necessary, resulting in the following relationship between D_w and the averaged absorbed dose D_{det} within the active volume of the detector positioned at the depth z:

$$D_w(z) = p \cdot s_{w,a}^{\Delta} \cdot \bar{D}_{\mathrm{det}}(z) \tag{1}$$

The chamber's reference point, which is for parallel-plate chambers assumed to be the centre of the front face of the air cavity, is positioned at the depth of measurement z. The IAEA TRS-398 Code of Practice [1] as well as the IPEM protocol [3] and the German protocol DIN 6800-2 [4] interpret the depth of measurement z within the phantom as the water equivalent depth, i.e. the non-water equivalence of the ionization chamber entrance window must be accounted for by shifting the chamber by an amount Δz. This positioning should ensure that the mean electron energy within the chamber is the same as in the undisturbed water phantom. The American protocol TG-51 [2] neglects this shift in case of reference dosimetry.

The general assumption in perturbation theory is that the overall correction factor p may be factorized. For a parallel-plate chamber, this factorization is given as:

$$D_w = p_{wall}\, p_{cav} s_{w,a} \bar{D}_{\mathrm{det}} = \frac{\bar{D}_{cav}}{\bar{D}_{\mathrm{det}}} \frac{D_w}{\bar{D}_{cav} s_{w,a}} s_{w,a} \bar{D}_{\mathrm{det}} \tag{2}$$

The perturbation correction $p_{wall} = \bar{D}_{cav} / \bar{D}_{\mathrm{det}}$ corrects the response of the ionization chamber for fluence perturbations due to the chamber walls and p_{cav} for effects related to the air cavity itself. Within Eq. (2) $\bar{D}_{cav}$ is the dose in the air cavity of the chamber with walls entirely made of water.

2.2. MC simulations

All quantities given in Eq. (2) may be derived from MC simulations. In the present study, the authors used the EGSnrc MC user code CAVITY [12]. This code provides the dose values within user defined geometries. The principle simulation geometry is given in Fig. 1. The NACP chamber was modelled in detail according to available information from the manufacturer and in the literature [13]. Essential geometrical data and material compositions are summarized in Table 1, a picture of the modelled chamber is given in Fig. 2. To calculate the dose within the bare cavity, all chamber walls were replaced by

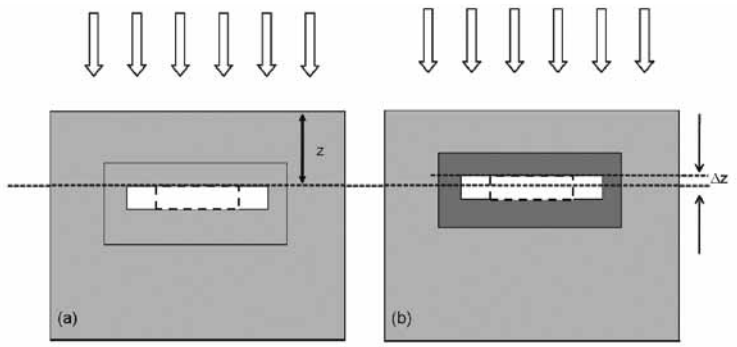

FIG. 1. Schematic diagram of the simulation geometries. The dose and fluence are scored inside the active volume of the air cavity, limited by the grey line. The complete air cavity, including the region defined by the guard ring of the parallel-plate chamber, is shown in white. The surrounding of the air cavity in (a) consists entirely of water (dose D_{cav}*). To calculate the dose* D_{det} *within the NACP chamber a detailed chamber model was placed into the water phantom (b). The chamber was positioned with its reference point in the water equivalent depth* z *[1] in a water phantom, i.e. to account for the non-water equivalence of the ionization chamber entrance window, the NACP chamber was shifted by* Δz *= -0.058 cm toward the focus. The electron beam is coming from the top.*

TABLE 1. GEOMETRICAL DATA AND MATERIAL COMPOSITIONS OF THE MODELLED NACP-02 CHAMBER

Entrance window	Entrance window thickness		Rear wall	Side wall
	d in mm	$d \times \rho_e$ in mg/cm^2		
0.17 mm mylar, ρ = 1.38 g/cm^3 0.53 mm graphite, ρ = 2.26g/cm^3	0.7	142	5.6 mm graphite, ρ = 1.75 g/cm 1.2 mm rexolite, ρ = 1.06 g/cm^3	7 mm rexolite ρ = 1.06 g/cm^3

Note: The diameter of the active volume is 10 mm, the height, 2 mm. The guard ring width is 3 mm. To account for the non-water equivalence of the entrance window in terms of electron density [4], the chamber must be shifted by Δz = –0.58 mm towards the focus [14].

water. To distinguish between the different contributions to the wall perturbation correction of the entrance window, the side and the back walls, successive simulations were performed replacing the different chamber walls by water. Moreover, the contributions of the side wall were investigated in detail by varying the guard ring width.

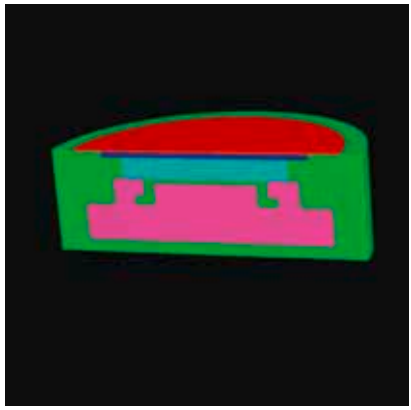

FIG. 2. NACP-02 chamber modelled with the EGSnrc C++ class library [15]. The different colours represent the different materials: red: mylar, dark blue: graphite (ρ = 2.26 g/cm^3), light blue: air, pink: graphite (ρ = 1.75 g/cm^3), green: rexolite (ρ = 1.06 g/cm^3).

TABLE 2. ELECTRON SPECTRA AND REFERENCE CONDITIONS USED FOR THE SIMULATIONS IN THIS WORK

Accelerator	E_{nom} (MeV)	R_{50} (g/cm^2)	z_{ref} (g/cm^2)
Varian Clinac	6	2.63	1.48
	9	4.00	2.30
	12	5.18	3.01
	15	6.50	3.80
	18	7.72	4.53
Siemens KD	6	2.31	1.29
	11	4.21	2.43
	21	8.30	4.88

Note: The spectra are taken from Ding and Rogers [16].

The chamber was positioned in a water phantom (30 cm × 30 cm × 30 cm) and irradiated with a divergent beam of electrons of 10 cm × 10 cm at the focus–surface distance 100 cm. Electron source spectra from different clinical accelerators were taken from literature (see Table (2) [16]) to cover the whole range of clinical applications. The transport cutoff energies were set to AE = ECUT = 521 keV and AP = PCUT = 10 keV. To get a satisfying statistical uncertainty, the number of primary electron histories in every simulations is around 10^9. To improve the efficiency, photon splitting is turned on, with a splitting factor of 40. Furthermore, the 'Russian Roulette' option of CAVITY for electrons that cannot reach the cavity is used with a survival probability of 1/10.

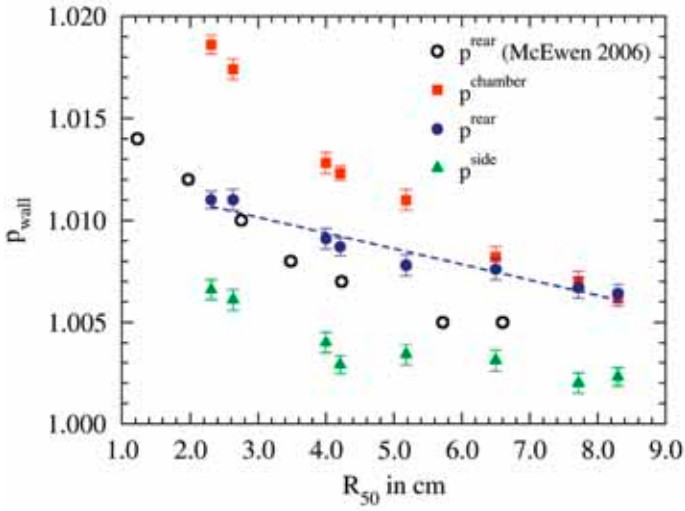

FIG. 3. Contributions of the different chamber walls of the NACP-02 parallel-plate chamber to the wall perturbation correction p_{wall} at the reference depth z_{ref} as a function of the electron beam specifier R_{50}. The index at the figure labels indicate, which part of the chamber wall is present during simulation. The error bars indicate the standard uncertainty arising from random effects. The open circles represent the experimental data for the rear wall taken from [18].

3. RESULTS

Figure 3 shows the calculated wall perturbation correction for the whole chamber ($p^{chamber}$) and the contributions from the rear (p^{rear}) and side (p^{side}) walls as a function of the electron beam specifier R_{50}. The upper index indicates, which chamber wall is present during simulation, i.e. for the calculation of p^{side} only the side wall of the NACP-02 chamber is present, the front and back walls are replaced by water. The overall wall perturbation correction deviates from unity, the recommended value in all dosimetry protocols, and displays a strong energy dependence, as already published by other authors for the NACP chamber [8]. The deviation from unity is about 2% for the lowest electron energy and about 0.6% for the largest energy included in this study. Comparable data were recently published for the Roos parallel-plate chamber [17].

The contribution to p_{wall} due to the side wall of guarded parallel-plate chambers is commonly assumed to be negligible. According to the authors' data, this assumption is not valid. For the NACP chamber this contribution is between 0.7% for low electron energies and about 0.2% for high electron energies (Fig. 3).

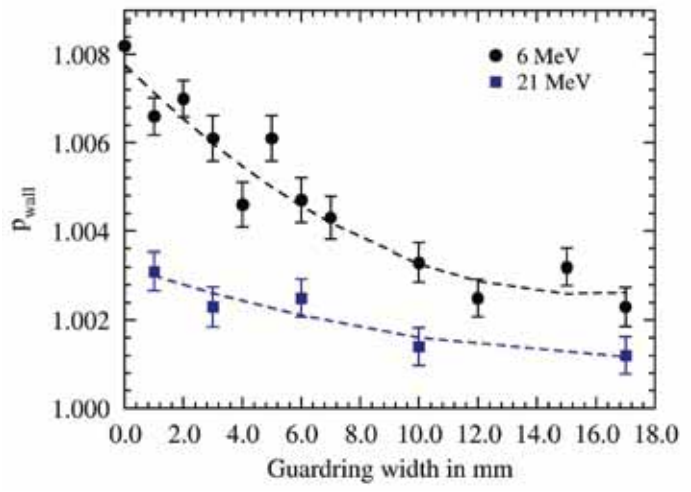

FIG. 4. Contributions to the wall perturbation correction p_{wall} due to the side wall of the NACP chamber at the reference depth z_{ref} as a function of the guard ring width for two electron energies. The guard ring width of the real chamber is 3 mm. The dashed lines are quadratic fits. The error bars indicate the standard uncertainty arising from random effects.

The contributions from the rear wall calculated in this study are in good agreement with the experimental data from McEwen et al. [18], which are also shown in Fig. 3.

The non-negligible contribution of the side wall to the overall wall perturbation correction obviously demonstrates that the guard ring is not wide enough to avoid scatter contributions from the side wall. To determine the necessary width of the guard ring for the NACP chamber to be 'well guarded', the width was varied in successive simulations in the range from 0 to 17 mm. During these simulations, the front and rear walls were replaced by water. These simulations were performed for the lowest and highest energies. The results are shown in Fig. 4. As expected, p^{side} decreases with increasing guard ring width but even for a width of 17 mm the resulting perturbation correction is larger than unity, even for the highest electron energy.

Figure 5 shows the depth dependence of the contributions from different chamber walls to the wall perturbation correction. The calculations were only performed with the lowest electron energy since the influence of different wall materials is the largest for this energy. The data points for the side wall (p^{side}) in Fig. 5 are calculated from two different simulations. In the first simulation, the rear and side walls are present ($p^{rear\&side}$), i.e. the front wall is replaced by water; in the second simulation, only the rear wall is present (p^{rear}). From these data, p^{side} was calculated as the ratio: $p^{side} = p^{rear\&side}/p^{rear}$, i.e. it was assumed that the wall

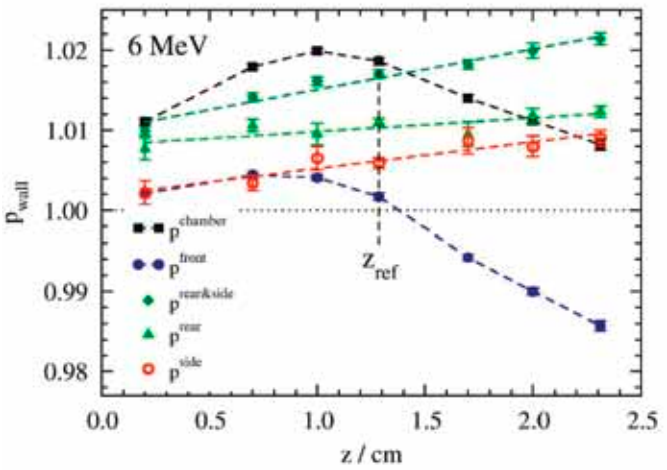

FIG. 5. Contributions of the different chamber walls to the perturbation correction p_{wall} as a function of depth for the primary electron spectrum Siemens KD 6 MeV (R_{50} = 2.31 cm). The non-water equivalence of the entrance window is accounted for, i.e. the chamber is positioned with its reference point in the water equivalent depth z. To perform this, the chamber is shifted by Δz = -0.058 cm toward the focus, except of course when the entrance window is replaced by water. The data for p^{side} are not a result of a simulation, but are calculated from the contributions of the side and back walls put together and from the contributions of the back wall alone (see text). The straight lines are linear regressions. The error bars indicate the standard uncertainty arising from random effects.

perturbation correction may be factorized. As can be seen in Fig. 5, there is a linear increase of the perturbation corrections for the rear and side wall with depth. This may be expected, as lectron energy decreases with depth and the backscatter deficiency of the wall materials is inversely proportional to the electron energy, as mentioned above. The depth dependence of p_{wall} due to the entrance window is somewhat unexpected. Up to the reference depth the correction p^{front} is larger than unity and decreases with increasing depth to values lower than unity. This depth dependence also appears in the overall wall correction p_{wall}.

4. DISCUSSION AND CONCLUSION

The goal of this study was the detailed investigation of the wall perturbation correction of a parallel-plate NACP-02 chamber in clinical electron beams. In accordance with previous studies[8]an energy and depth dependent wall perturbation correction p_{wall} deviating from unity up to 2% was established. Since

the chamber is considered as ‘well guarded’, the influence of the chamber's side wall is commonly assumed to be negligible. These MC simulations clearly show that this assumption is invalid. According to our simulations the side wall contributes up to 30% to the overall wall perturbation correction. This contribution is largest for low electron energies and thus increases with the depth of measurement within the water phantom. This result is in good agreement with experimental data recently published by McEwen et al. [18].

A wall perturbation correction larger than unity implies that the electron fluence within the cavity is smaller if the chamber's rear wall is present compared to the configuration where there is only water. This may be due to a backscatter deficiency as a result of the material of the rear wall. The scattering power of a medium is proportional to the number of electrons seen by the incoming electrons. Therefore, it is proportional to the effective Z and proportional to the density of the medium. Regarding the energy dependence, the scattering power is inversely proportional to the energy of the incoming electrons. As the rear wall of the NACP chamber is quite massive (see Table 1) and consists of graphite with Z = 6, which is about 10% smaller than the effective atomic number of water, backscatter deficiency could be an explanation for the wall perturbation larger than unity [7]. On the other hand, the density of the graphite rear wall is much higher than the density of water and therefore the lack of backscattering in the cavity may be also due to the higher scattering in graphite of electrons coming back from water and unable then to reach the cavity. To distinguish both effects, detailed simulations varying the thickness and the density of the wall materials would be necessary.

The side wall of the NACP chamber is made of rexolite with an effective atomic number Z = 5.35 and its thickness is comparable to the rear wall. In principle, similar arguments used for the back wall could also hold for the side wall: either less electrons entering the active volume of the cavity through the side wall (‘obliquity effect’ [19]) and/or backscattering deficiency due to the material of the chamber side wall.

The expansion of the guard ring width reduces the scatter contribution from the side wall. However, even a width of 17 mm, which is more than three times the radius of the active chamber volume, cannot completely neglect the contribution of the side wall to the wall perturbation correction. A similar result was recently published by Wang and Roger [20]. From their MC data, they concluded that even a guard ring width of 10 mm may not be enough to avoid scatter contributions from the side wall.

The effect of the entrance window on the wall correction factor is somewhat unexpected. At larger depth ($z > z_{ref}$) the presence of the entrance window results in an excess of electron fluence within the air cavity of the chamber resulting in a wall perturbation lower than unity. A similar result for the NACP chamber was

recently obtained by Chin et al. [21]. A reason for the complex depth dependence of p_{wall} shown in Fig. 5 may be the positioning of the chamber (assumed point of measurement). In the authors' calculations, the NACP chamber is positioned with its reference point at the water equivalent depth z, as recommended by the majority of present dosimetry protocols [1] . In a previous study concerning a parallel-plate Roos chamber [14], the authors demonstrated the strong influence of the positioning of parallel-plate chambers on the resulting wall perturbation correction for depth larger than z_{ref}. One result of this study was that the calculation of the water equivalent depth of the entrance window thickness according to the electron densities of the entrance window materials and the positioning of the chamber according to that rule is resulting in a minimized depth and energy dependence of p_{wall}. This rule was applied here for the NACP chamber (see Table 1). The chamber positioning in the work of Chin et al. was similar. The results in Fig. 5 suggest the conclusion, that the effective point of measurement for parallel-plate chambers is not constant with depth. Possibly, calculations of the fluence spectra within the chamber and within the bare cavity (spectral resolved contributions to p_{wall}) as proposed in Ref. [14] can help to explain the residual depth dependence of the wall perturbation due to the entrance window.

In conclusion, this study demonstrates that the scatter properties within a simple parallel-plate NACP chamber are much more complex than commonly assumed.

ACKNOWLEDGEMENTS

The authors would like to thank D. Jany from IMPS for maintaining the IMPS computer cluster. The work was supported by the Federal Ministry of Education and Research, Germany (BMBF — Grant 1751X07).

REFERENCES

[1] INTERNATIONAL ATOMIC ENERGY AGENCY, Absorbed Dose Determination in External Beam Radiotherapy: An International Code of Practice for Dosimetry Based on Standards of Absorbed Dose to Water, Technical Reports Series No. 398, IAEA, Vienna (2000).

[2] ALMOND, P.R., et al., AAPM's TG-51 protocol for clinical reference dosimetry of high-energy photon and electron beams, Med Phys, **26** 9 (1999) 1847.

[3] THWAITES, D.I., et al., The IPEM code of practice for electron dosimetry for 380 radiotherapy beams of initial energy from 4 to 25 MeV based on an absorbed dose to water calibration, Phys Med Biol, **48** 18 (2003) 2929.

[4] DIN6800-2. Procedures of dosimetry with probe-type detectors for photon and electron radiation – Part 2: Ionization chamber dosimetry of high energy photon and electron radiation, Technical report, Normenausschuss Radiologie (NAR) im DIN (2008).
[5] NILSSON, B., et al., Wall effects in plane-parallel ionization chambers, Phys Med Biol, **41** 4 (1996) 609.
[6] HUNT, M.A., et al., Electron backscatter corrections for parallel-plate chambers, Med Phys, **15** 1(1988) 96.
[7] KLEVENHAGEN, S.C., Implication of electron backscattering for electron dosimetry, Phys Med. Biol, **36** (1991) 1013.
[8] VERHAEGEN, F., et al., Perturbation correction factors for the NACP-02 plane-parallel ionization chamber in water in high-energy electron beams, Phys Med Biol, **51** 5 (2006) 1221.
[9] BUCKLEY, L.A., et al., Wall correction factors, Pwall, for parallel-plate ionization chambers. Med Phys, **33** 6 (2006) 1788.
[10] SPENCER, L.V., et al., A theory of cavity ionization, Radiat. Res. **3** 3 (1955) 239.
[11] SPENCER, L.V., et al., A cavity ionization theory including the effects of energetic secondary electrons, Radiology **64** 1(1955) 113.
[12] KAWRAKOW, I., et al., The EGSnrc code system: Monte Carlo simulation of electron and photon transport. National Research Council of Canada, Report PIRS-701 (2001).
[13] CHIN, E., et al., Validation of a Monte Carlo model of a NACP-02 plane-parallel ionization chamber model using electron backscatter experiment,. Phys Med Biol **53** 8 (2008) N119.
[14] ZINK, K., et al., Positioning of a plane-parallel ionization chamber in clinical electron beams and the impact on perturbation factors. Phys Med Biol **54** 8 (2009) 2421.
[15] KAWRAKOW, I., et al., The EGSnrc C++ class library (rev. A). National Research Council of Canada, Report PIRS-898 (2009).
[16] DING, G.X., et al., Calculation of stopping-power ratios using realistic clinical electron beams. Med Phys, **22** 5 (1995) 489.
[17] ZINK, K., et al., Monte Carlo calculations of beam quality correction factors kQ for electron dosimetry with a parallel-plate Roos chamber, Phys. Med. Biol. **53** (2008) 1595.
[18] McEWEN, M., et al., An empirical method for the determination of wall perturbation factors for parallel-plate chambers in high-energy electron beam, Phys. Med. Biol, **51** 20 (2006) 5167.
[19] HARDER, D., Einfluss der Vielfachstreuung von Elektronen auf die Ionisation in gasgefüllten Hohlräumen, Biophysik **5** (1968) 157.
[20] WANG, L.L.W., et al., Study of the effective point of measurement for ion chambers in electron beams by Monte Carlo simulation, Med Phys, **36** 6 (2009) 2034**.**
[21] CHIN, E., Analysis of dose perturbation factors of a NACP-02 ionization chamber in clinical electron beams, Phys Med Biol, **54** 2 (2009) 307.

CONVERSION OF DOSE-TO-GRAPHITE TO DOSE-TO-WATER IN A CLINICAL PROTON BEAM

H. PALMANS*, L. AL-SULAITI**, P. ANDREO***, R.A.S. THOMAS*, D.R.S. SHIPLEY*, J. MARTINKOVI[+], A. KACPEREK[++]

* National Physical Laboatory, Teddington, United Kingdom
Email: hugo.palmans@npl.co.uk

** University of Surrey, Guildford, United Kingdom

*** University of Stockholm, Sweden

[+] Slovak Institute of Metrology, Bratislava, Slovakia

[++] Clatterbridge Centre for Oncology, Wirral, United Kingdom

Abstract

Fluence correction factors for the conversion from dose to graphite in a graphite phantom to dose-to-water in a water phantom were obtained for 60 MeV mono-energetic, non-modulated protons by experiment, analytical calculations and Monte Carlo simulations using five different codes. All methods indicate that fluence correction factors are close to unity. Up to a depth of about 2.5 cm in water, an uncertainty of 0.3% could be assigned to the assumption that the fluence correction factor is unity for 60 MeV non-modulated protons.

1. INTRODUCTION

The feasibility of graphite calorimetry as a method for establishing a primary standard for absorbed dose to water in clinical proton beams has been demonstrated before [1], and a primary standard level portable graphite calorimeter for protons is under development at the National Physical Laboratory. The advantages of graphite calorimeters over water calorimeters are their higher sensitivity, compactness and portability. The disadvantage of graphite calorimetry is that a conversion is required from the measured quantity, absorbed dose to graphite, to the quantity of interest, absorbed dose to water. This constitutes the single largest uncertainty contribution on absorbed dose to water obtained from graphite calorimetry [2]. The conversion procedure requires accurate values of

the water to graphite collision stopping power ratios and possibly fluence correction factors.

Secondary charged particles from non-elastic nuclear interactions contribute considerably to dose in low-Z media and tissues [3], but their influence on stopping power ratios is considered small [4]. Monte Carlo simulations in various low-Z materials, however, showed that the differences in shape of depth dose curves is mainly due to the differences in the non-elastic nuclear interaction cross-sections for different elements [5] and suggested the need of fluence correction factors when converting dose distributions from a non-water material to water. This was confirmed experimentally [6] and by Monte Carlo simulations [6].

In this work, the fluence correction factor in the conversion from dose to graphite to dose to water has been studied for non-modulated 60 MeV proton pencil beams by experiment, analytical calculations and Monte Carlo simulations.

2. METHODS

2.1. Experiment

The experiment was performed at the Clatterbridge Centre for Oncology (CCO) 60 MeV proton beam [10], collimated to a diameter of 4 mm. A Roos chamber positioned right downstream of the brass collimator served as beam monitor. Ionization measurements in graphite and water were performed with an NACP-02. The 10 mm diameter collecting electrode of this ionization chamber type ensured that all primary particles that are not removed from the beam in non-elastic nuclear interactions would cross its collecting volume. The setup is shown schematically in Fig. 1.

The thickness of the graphite plates was determined in terms of mass thickness, i.e. weight divided by area and the uniformity of the thickness across the area was verified. Ionization measurements as a function of depth were performed in graphite at a constant source to detector distance (SDD), while in water they were made with constant source to surface distance (SSD). The front surface of the water phantom was at the same (isocentric) position as the front surface of the ionization chamber in the graphite phantom. Given the lateral integration, the measurement at constant SSD in water should give the same depth dependence as a measurement with constant SDD. To verify this (and to derive a correction for any deviation from this assumption), depth ionization measurements in water were made at several SSDs in steps of 5 mm.

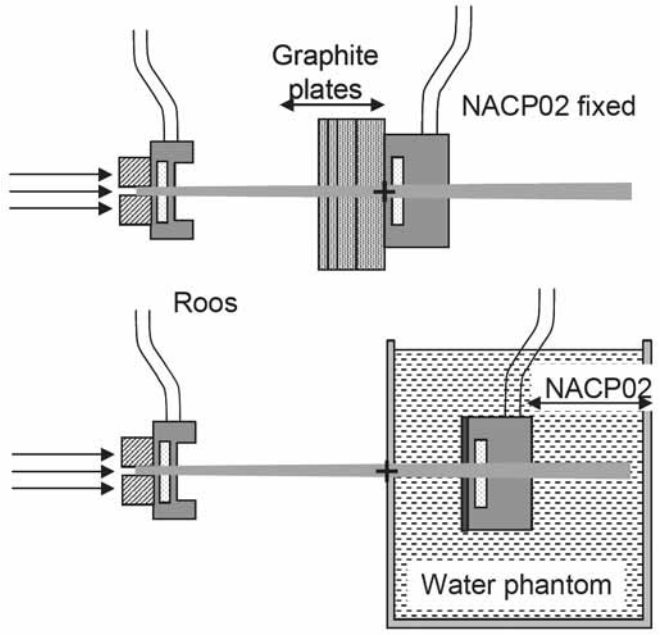

FIG. 1. Experimental set up for measurements in graphite (upper drawing) and for measurements in water (lower drawing). The isocentre position is indicated with a cross.

Ranges in water and graphite were estimated as depths $z_{80,w}$ and $z_{80,g}$ distal to the Bragg peak where the ionization drops to 80% of the maximum. A water equivalent depth, $z_{w\text{-}eq}$, was defined for any depth in graphite z_g as:

$$z_{w-eq} = z_g \cdot \frac{z_{80,w}}{z_{80,g}} \quad (1)$$

For each depth in graphite z_g, the ionization in water at $z_{w\text{-}eq}$ was evaluated by interpolation and the ratio of ionization in both phantoms was taken as an estimate of the fluence correction factor. For this to be correct, the main requirement is that the chamber perturbation is the same in both phantoms. This assumption needs verification, but is supported by the observation that secondary electrons contributing to the energy deposition in the air cavity but that do not originate in the cavity itself, are generated in a thin layer of less than 100 micron of wall material at the inner surface of the cavity [11].

2.2. Analytical calculations

Energy loss and attenuation of 60 MeV protons in water and graphite were calculated analytically in the continuous slowing-down approximation (CSDA) without considering angular scattering or energy straggling. This was done in slabs of 10 μm using stopping powers from ICRU Report 49 [12] for the energy loss and total non-elastic cross-sections from ICRU report 63 [13] for the attenuation, both evaluated at the entrance of each slab (for attenuation only loss of primary protons was considered neglecting the production of secondary particles in nuclear interactions). This slowing down process was repeated until the proton's kinetic energy dropped below zero. The depth where this happened was taken as an estimate of the CSDA range r_0. The obtained CSDA ranges where within the 10 μm resolution in agreement with those from ICRU Report 49. For a particular depth in graphite, z_g, the water-equivalent depth, $z_{w\text{-}eq}$, was calculated using the ratio of CSDA ranges in water and graphite, $r_{0,w}$ and $r_{0,g}$, respectively, as:

$$z_{w-eq} = z_g \cdot \frac{r_{0,w}}{r_{0,g}} \tag{2}$$

The fluence correction factor was obtained as the ratio of the number of surviving protons in water at depth $z_{w\text{-}eq}$ and number of protons in graphite at depth z_g.

2.3. Monte Carlo simulations

Monte Carlo simulations allow the most direct determination of the conversion factor or, alternatively, corrections to the simplified assumption that the charged particle fluence distributions at equivalent depths in both phantom materials are equal, i.e. $\Phi_{E,w,i} = \Phi_{E,g,i}$, for all energies, E, and all charged particle types, i. If this condition would be fulfilled, dose to graphite, $D_g(z_g)$, and dose to water at an equivalent depth, $D_w(z_{w\text{-}eq})$, are related by the water to graphite mass collision stopping power ratio for the total charged particle fluence distribution in graphite, $s_{w,g}(\Phi_g)$:

$$s_{w,g}(\Phi_g) = \frac{\sum_i \left[\int_0^{E_{\max,i}} \Phi_{E,g,i}(E) \cdot \left(\frac{S_{c,i}(E)}{\rho} \right)_w \cdot dE \right]}{\sum_i \left[\int_0^{E_{\max,i}} \Phi_{E,g,i}(E) \cdot \left(\frac{S_{c,i}(E)}{\rho} \right)_g \cdot dE \right]} \quad (3)$$

If the fluence distributions are not equal in both phantoms, a fluence correction factor needs to be introduced, and dose to water in water and dose to graphite in graphite at equivalent depths are related by:

$$D_w(z_{w-eq}) = D_g(z_g) \cdot s_{w,g}(\Phi_g) \cdot k_{fl} \quad (4)$$

With the fluence correction factor, k_{fl}, given by:

$$k_{fl} = \frac{\sum_i \left[\int_0^{E_{\max,i}} \Phi_{E,w,i}(E) \cdot \left(\frac{S_{c,i}(E)}{\rho} \right)_w \cdot dE \right]}{\sum_i \left[\int_0^{E_{\max,i}} \Phi_{E,g,i}(E) \cdot \left(\frac{S_{c,i}(E)}{\rho} \right)_w \cdot dE \right]} \quad (5)$$

This factor could be interpreted as the conversion of dose to water in the graphite phantom, to dose to water at an equivalent depth in the water phantom.

There are two ways of calculating k_{fl} using Monte Carlo simulations: (a) directly by using Eq. (5) with calculated fluence distributions, or (b) using Eq. (4) by calculating dose in both phantoms and calculating the stopping power ratio for the fluence distribution in graphite using Eq. (3). Some simplifications may be justified that need further investigation. In the first approach, if the contribution of secondary particles other than protons is negligible and proton spectra only differ in amplitude, then a simple calculation of the number of protons may suffice to determine the ratio in Eq. (5). The second approach only requires dealing with a stopping power ratio for one and the same spectrum. Given the small influence of secondary particles [4] and the narrow energy distribution of primary protons for most depths (except in the Bragg peak), stopping power ratios for mono-energetic protons may be sufficient.

Monte Carlo simulations where performed for 60 MeV mono-energetic, mono-directional protons incident perpendicularly on a slab phantom and scoring

laterally integrated proton fluence or dose. For every depth in graphite, a water equivalent depth was calculated according to Eq. (1).

2.3.1. McPTRAN.MEDIA

McPTRAN.MEDIA [14], derived from PTRAN [15], allows transport in media different than water (contrary to PTRAN itself) using ICRU Report 49 stopping powers [12] and ICRU Report 63 non-elastic nuclear interaction data [13]. The geometry consists of infinite slabs and energy loss per unit depth as well as proton fluence are scored at each plane separating slabs. 10^6 protons were simulated for each material. McPTRAN.MEDIA does not track secondary particles resulting from non-elastic nuclear interactions, but rather calculates their local energy deposits from production cross sections. This requires these contributions to be scaled separately from the electromagnetic interactions as explained in Refs. [2].

2.3.2. Geant4

Simulations were performed with Geant4 version 4.9.0 [16] based on the Hadrontherapy advanced example; 10^6 proton histories were simulated for each material. Various models for non-elastic nuclear interactions were used: precompound (PRECOMP), Bertini intranuclear cascade (QGSP+BERT) and binary intranuclear cascade (QGSP+BIC). For electromagnetic interactions, low energy models were used for all particles using the default ICRU Report 49 stopping power parameterization for protons. Production cut-offs for photons, electrons and positrons were set to a range of 0.005 mm. The phantom was a 100 mm diameter cylinder, and slab thicknesses were 0.05 mm for graphite and 0.07 mm for water.

2.3.3. MCNPX

MCNPX [17] simulations were performed with versions 2.4.0 and 2.5.0 in a cylindrical phantom with slabs of 0.1 mm thickness and a diameter of 40 mm. 10^6 proton histories were simulated. The nuclear cross sections were taken from the LA150H library. Physics model parameters for particle transport were: maximum energy 210 MeV, default cut-off energy 1 MeV, charged particle straggling and STOP LIGHT ION RECOIL (default). Tally 1 (F1: current integrated over cell surface) and tally 6 (F6: average energy deposition over cell) were used to score number of protons and energy loss as a function of depth.

2.3.4. FLUKA

Simulations were performed using FLUKA 2008.3c [18] in a cylindrical phantom of radius 50 mm and a thickness of 32 mm, and the total energy deposited in 0.1 mm thick slabs was determined using the USRBIN scoring option. In addition, 10^6 proton histories were simulated for each material. Physics settings suitable for hadrontherapy calculations (DEFAULTS card set to HADROTHE) were used together with new hadronic evaporation models and inclusion of heavy ion nuclear interactions. The particle transport threshold was 100 keV except for neutrons, which were transported down to thermal energies.

2.3.5. SHIELD-HIT

An updated version of SHIELD-HIT 08 [20] was used to simulate 10^6 protons of 60 MeV and their nuclear fragments down to 25 keV in water and graphite cylindrical phantoms of 200 mm diameter and 40 mm height, divided into slabs 0.1 mm thick. An improved track-length fluence estimator was used to determine fluence differential in energy for all particles in both media. Water stopping powers were those from the errata to ICRU Report 73 [21], based on an I-value of 78.0 eV, and the transport included Vavilov-Landau energy straggling and Molière multiple scattering.

3. RESULTS AND DISCUSSION

Figure 2 shows the measured ratio of NACP-02 readings in water in the constant SSD and constant SDD setups. The deviations from unity can possibly be explained by collimator scatter or secondary particles produced in the collimator which have a complex angular distribution [10]. The fit shown in Fig. 2 served as a correction for the depth ionization data in water.

Figure 3 shows fluence correction factors derived as ratios of ionization chamber readings in water (corrected with the curve of Fig. 2) and graphite at equivalent depths. The standard uncertainties shown combine statistical uncertainties on the ionization chamber readings and an uncertainty on assigning the dose value in water based on the uncertainty of graphite depth (typically 0.05%) and the depth dose gradient in water. From these experimental data, the fluence correction factor is found to be unity over the entire range within the experimental uncertainties.

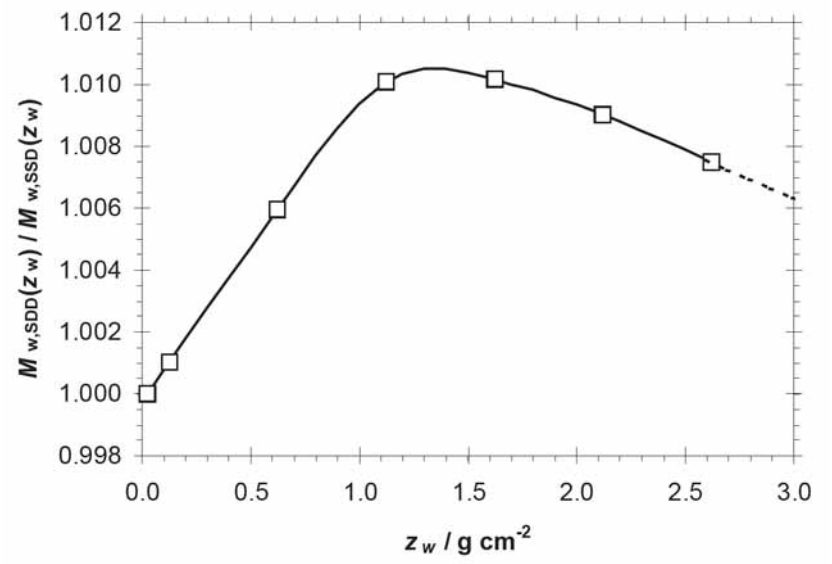

FIG. 2. Ratio of NACP-02 readings in the constant SSD and constant SDD set-ups. The full line represents a cubic spline through the data. The dashed line is a linear extrapolation at larger depths.

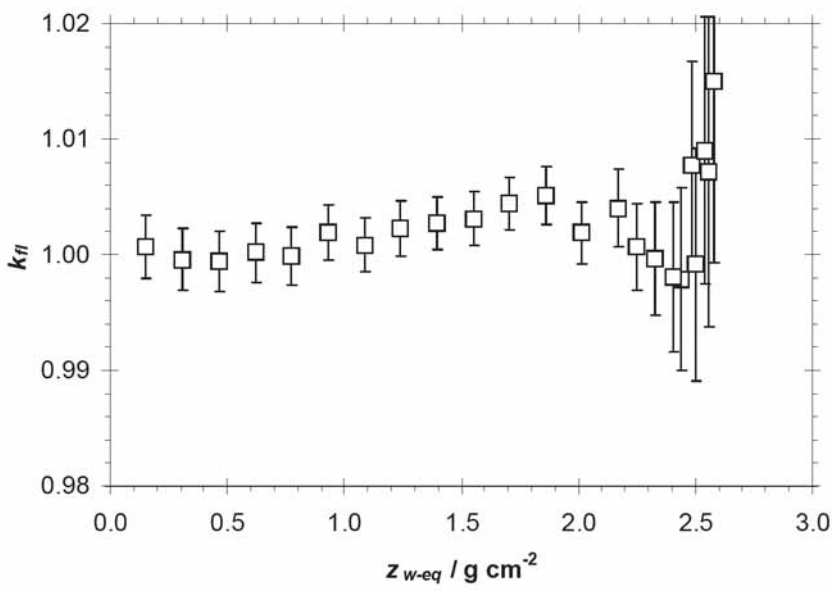

FIG. 3. Fluence correction factor as a function of depth derived as a ratio of NACP-02 ionization readings at equivalent depths in water and graphite.

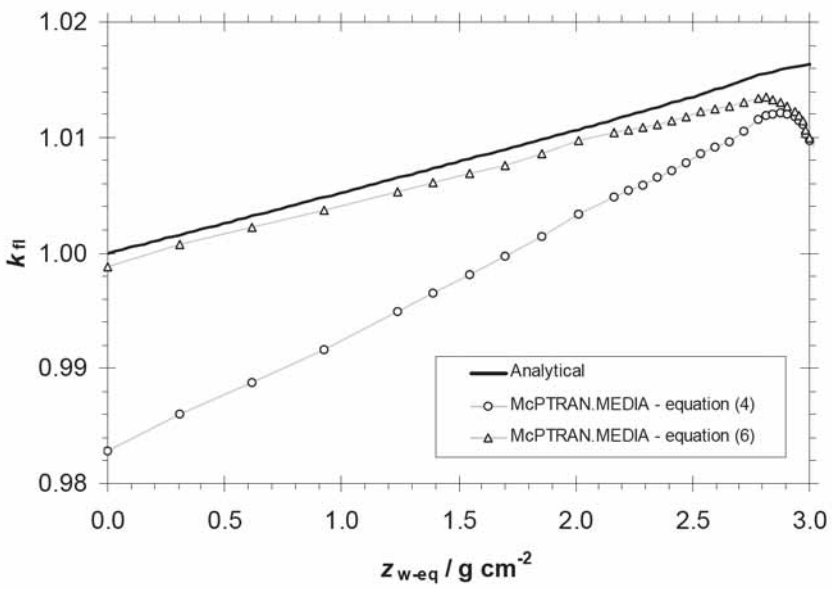

FIG. 4. Fluence correction factor as a function of depth obtained analytically and from McPTRAN.MEDIA Monte Carlo simulations using either Eq. (4) or the method converting local deposits from secondary particles separately. Type A uncertainties are too small to be shown.

Figure 4 shows the analytical calculation compared with the McPTRAN.MEDIA simulations using either Eq. (4) or the method converting local deposits from secondary particles separately. The good agreement of the latter method with the analytical result indicates that the separate conversion is required and that scattering and straggling (the main differences between the McPTRAN.MEDIA and analytical calculation) have a minor or negligible influence on the fluence correction.

Figure 5 shows the results from the MCNPX 2.4.0 and Geant4 simulations using stopping power ratios for mono-energetic protons (based on the residual range) to apply Eq. (4). Type-A uncertainties are about 0.1% for all depths shallower than the Bragg peak, which is reflected in the fluctuations, while on the distal edge they blow up rapidly. The Geant4 results show that differences between the three nuclear models are negligible. For the first half of the range, the fluence correction factor stays constant at unity, but beyond, increases more steeply than in the analytical result. The MCNPX 2.4.0 results show an increase of about 1% over the entire range. The fluence correction factor being different from unity at the surface may result from the fact that from all secondary particles being produced in non-elastic nuclear interactions, only secondary protons are

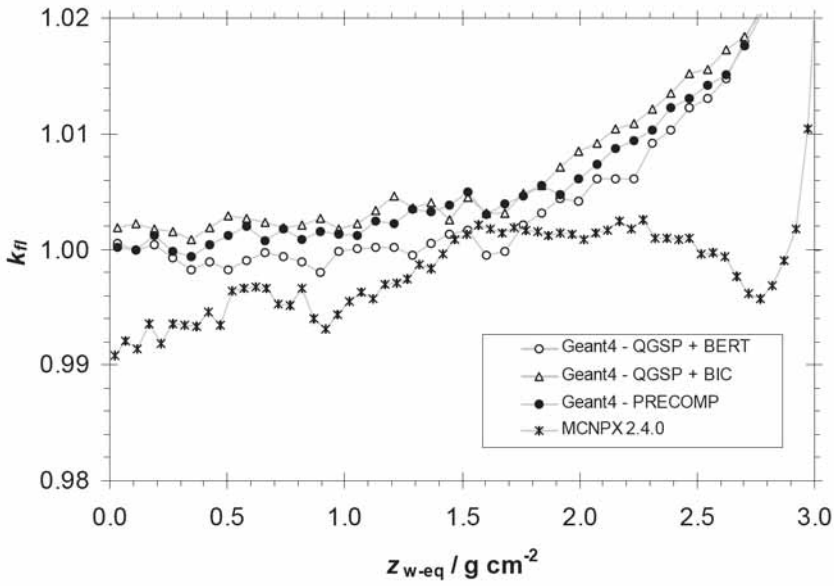

FIG. 5. Fluence correction factor as a function of depth obtained from MCNPX 2.4.0 and Geant4 Monte Carlo simulations using Eq. (4) and mono-energetic stopping power ratios.

transported. The local energy deposition of heavier particles may result in similar problems using Eq. (4), as discussed with respect to McPTRAN.MEDIA.

Figure 6 shows results obtained with SHIELD-HIT. The fluence correction factor calculated as a ratio of integrated proton fluences in water and graphite is within the same uncertainties as the one calculated directly with Eq. (5) applied to the entire proton spectrum, confirming that secondary protons have a negligible influence. When applying Eq. (5) to the entire charged particle spectrum, the fluence correction factor is not unity at the surface, which is currently not completely understood, but may be due to recoils with very short ranges. In general, the fluence correction factor obtained from SHIELD-HIT is increasing similarly to the analytical simulation but with a slightly smaller slope.

Figure 7 shows fluence correction factors calculated as a ratio of integrated proton fluences obtained with three Monte Carlo codes. There are some distinct differences but the corrections remain within 0.5% from unity over almost the entire range (up to the Bragg peak), confirming the results from the other Monte Carlo simulations and the experiment.

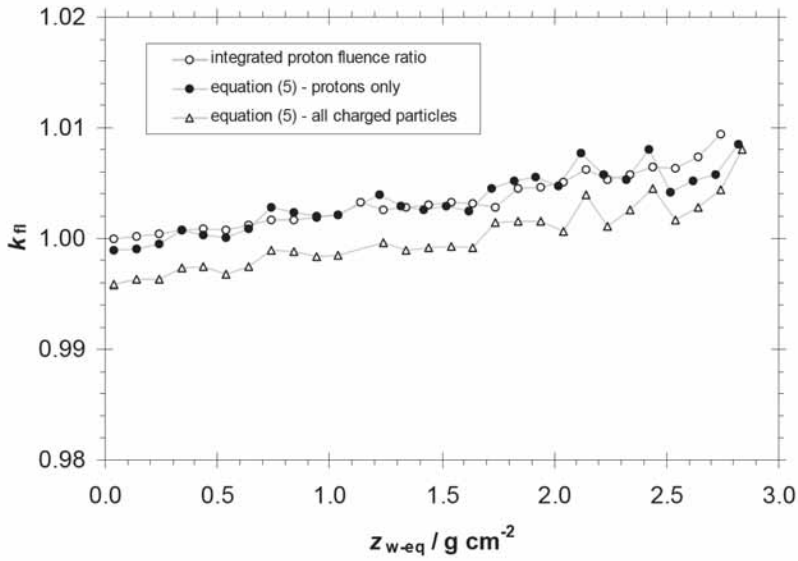

FIG. 6. Fluence correction factor as a function of depth obtained from SHIELD-HIT Monte Carlo simulations as a ratio of integrated proton fluences in water and graphite or from Eq. (5) applied to either the proton spectrum only or all charged particles.

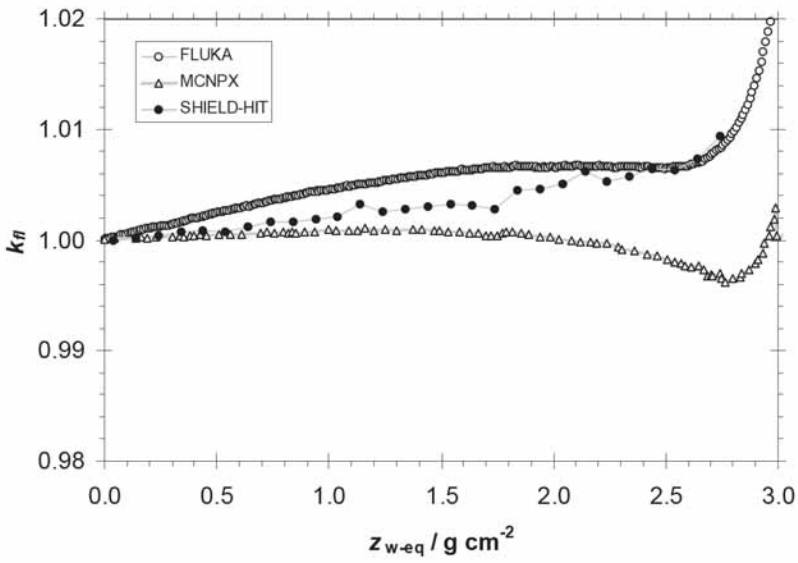

FIG. 7. Fluence correction factor as a function of depth obtained from FLUKA, MCNPX 2.5.0 and SHIELD-HIT Monte Carlo simulations as a ratio of integrated proton fluences in water and graphite.

4. CONCLUSIONS

Fluence correction factors to correct the conversion from dose-to-graphite in a graphite phantom to dose to water in a water phantom for 60 MeV non-modulated protons were obtained using experiment, analytical calculations and Monte Carlo simulations.

The fluence correction factors are in general close to unity, mostly within 0.5% and never deviating more than 2% at shallower depths than the Bragg peak. The approach used in the different Monte Carlo simulations was not uniform and the differences in results observed between the codes warrant a more in-depth and more systematic study.

From the observations in this study we suggest that $k_{fl} = 1.000 \pm 0.003$ (1SD) for a non-modulated 60 MeV proton beam.

ACKNOWLEDGEMENTS

The authors are grateful to the Douglas Cyclotron staff at CCO for their logistic support. The contributions of National Physical Laboratory staff are supported by the NMS AIR Metrology Program of the NMS Policy Unit of the UK Department of Business Innovation and Skills and by EC FP7 ERA-NET Plus, EC Grant Agreement No. 217257. Leena Al-Sulaiti is supported by the Ministry of Environment of Qatar.

REFERENCES

[1] PALMANS, H., THOMAS, R., SIMON, M., DUANE, S., KACPEREK, A., DUSAUTOY, A., VERHAEGEN, F., A small-body portable graphite calorimeter for dosimetry in low-energy clinical proton beams, Phys. Med. Biol. **49** (2004) 3737–3749.

[2] PALMANS, H., KACPEREK, A., JÄKEL, O., “Hadron dosimetry”, (Clinical Dosimetry Measurements in Radiotherapy (AAPM 2009 Summer School), |(ROGERS, D.W.O., CYGLER, J., Eds.) Medical Physics Publishing, Madison WI, USA (2009) 669–722

[3] PAGANETTI, H., Nuclear interactions in proton therapy: Dose and relative biological effect distributions originating from primary and secondary particles, Phys. Med. Biol. 47:747-764 (2002).

[4] MEDIN, J., ANDREO, P., Monte Carlo calculated stopping-power ratios, water/air, for clinical proton dosimetry (50–250 MeV), Phys. Med. Biol. **42** (1997) 89–105

[5] PALMANS, H., VERHAEGEN, F., Calculated depth dose distributions for proton beams in some low-Z materials, Phys. Med. Biol. **42** (1997) 1175–1183.

[6] PALMANS, H., SYMONS, J.E., DENIS, J.-M., DE KOCK, E.A., JONES, D.T., VYNCKIER, S., Fluence correction factors in plastic phantoms for clinical proton beams, Phys. Med. Biol. 47: (2002) 3055–3071.
[7] SCHNEIDER, U., PEMLER, P., BESSERER, J., DELLERT, M., MOOSBURGER, M., DE BOER, J., PEDRONI, E., BOEHRINGER, T., The water equivalence of solid materials used for dosimetry with small proton beams, Med. Phys. **29** (2002) 2946–2951.
[8] PALMANS, H., VERHAEGEN, F., Assigning non-elastic nuclear interaction cross sections to Hounsfield units for Monte Carlo treatment planning of proton beams, Phys. Med. Biol. **50** (2005) 991–1000
[9] PAGANETTI, H., Dose to water versus dose to medium in proton beam therapy, Phys. Med. Biol. 54: (2009) 4399–4421.
[10] KACPEREK, A., Proton therapy of eye tumours in the UK: a review of treatment at Clatterbridge, Appl. Radiat Isot. **67** (2009) 378–386.
[11] VERHAEGEN, F., PALMANS, H., A systematic Monte Carlo study of secondary electron fluence perturbation in clinical proton beams (70-250 MeV) for cylindrical and spherical ion chambers, Med. Phys. **28** (2001) 2088–2095.
[12] ICRU, Stopping powers and ranges for protons and alpha particles, International Commission on Radiation Units and Measurements Report 49, ICRU, Bethesda, MD (1993).
[13] ICRU, Nuclear data for neutron and proton radiotherapy and for radiation protection dose, International Commission on Radiation Units and Measurements Report 63, Bethesda, MD (2000).
[14] PALMANS, H., McPTRAN, R.Z.,"Monte Carlo codes for the simulation of proton beams and calculation of proton detector perturbation factors", The Monte Carlo Method; Versatility Unbounded in a Dynamic Computing World, American Nuclear Society, La Grange Park IL, USA (2005).
[15] BERGER, M.J., Proton Monte Carlo transport program PTRAN, National Institute for Standards and Technology Report NISTIR 5113, NIST, Gaithersburg MD, USA (1993).
[16] AGOSTINELLI, S., et al., GEANT4 – a simulation toolkit, Nucl. Instrum. Methods A **506** (2003) 250–303.
[17] PELOWITZ, D., MCNPX User's Manual, LANL Report LA-CP-05-369, Los Alamos National Laboratory, Los Alamos NM, USA (2005).
[18] FERRARI, A., SALA, P.R., FASSO, A., RANFT, J., FLUKA: A multi-particle transport code, CERN, Geneva (2005).
[19] BATTISTONI, G., MURARO, S., SALA, P.R., CERUTTI, F., FERRARI, A., ROESLER, S., FASSO A., RANFT, J., The FLUKA code: Description and benchmarking, (Proc. of the Hadronic Shower Simulation Workshop 2006, Fermilab 6–8 September 2006) (ALBROW, M., RAJA, R., Eds.), AIP Conference Proc. 896 (2007) 31–49.
[20] GUDOWSKA, I., SOBOLEVSKY, N., ANDREO, P., BELKIC, D., BRAHME, A., Ion beam transport in tissue-like media using the Monte Carlo code SHIELD-HIT, Phys. Med. Biol. **49** (2004) 1933–1958.
[21] SIGMUND, P., SCHINNER, A., PAUL, H., Errata and Addenda for ICRU Report 73, Stopping of Ions Heavier than Helium, Journal of the ICRU, Vol. 5, no. 1 (2005).

RECENT ADVANCES IN DOSIMETRY IN REFERENCE CONDITIONS FOR PROTON AND LIGHT-ION BEAMS

S. VATNITSKIY
MedAustron, Wiener Neustadt, Austria
Email: stanislav.vatnitsky@ebgmedaustron.at

P. ANDREO
Medical Radiation Physics, Stockholm University, Karolinska Institutet, Stockholm, Sweden

D.T.L. JONES
International Commission on Radiation Units and Measurements, Bethesda, Maryland, United States of America

Abstract

Radiotherapy with proton and light-ion beams is a rapidly expanding modality with more than 50 facilities expected to be operational by 2015. Uniformity of dose specification is a prerequisite for comparing clinical data from different institutions and for undertaking collaborative clinical trials. In recent years, considerable effort has been devoted to the development and improvement of the accuracy and reproducibility of reference dosimetry and the calibration of proton and light-ion beams taking account of the different beam-delivery techniques used for treatment. This paper reviews the developments in dosimetry under reference conditions of proton and light-ion beams that have taken place since IAEA International Symposium on Standards and Codes of Practice in Medical Radiation Dosimetry in 2002.

1. INTRODUCTION

There is continuously growing interest in the medical community throughout the world in establishing dedicated hospital based facilities employing proton and light-ion (heavier than protons) beams for radiotherapy. There are more than 30 such treatment facilities currently operational worldwide [1] and there are plans to open at least another 20 within the next five years. Treatment planning of high precision conformal therapy with ion beams requires accurate dosimetry and beam calibration in order to ensure delivery of the correct prescribed dose. Exchange of clinical experience and implementation of institutional and collaborative treatment protocols need to be based on consistent

and harmonized dosimetry procedures. This paper reviews the efforts to standardize the dosimetry of therapeutic proton and light-ion beams and summarizes the developments in dosimetry procedures in reference conditions that have taken place since the IAEA International Symposium on Standards and Codes of Practice in Medical Radiation Dosimetry in 2002. Since no national or international dosimetry standards for proton and light-ion beams have been established, major efforts have therefore been devoted to studies of the theoretical framework and practical guidelines for the use of ionization chamber dosimetry.

2. RECENT DEVELOPMENTS IN THE DOSIMETRY OF PROTON AND LIGHT-ION BEAMS

Currently, air-filled thimble ionization chambers with ^{60}Co calibration coefficients are recognized as the most practical and reliable reference instruments for proton and light-ion dosimetry. The following sections provide an overview of recent developments in absorbed dose determination in proton and light-ion beams with the emphasis on ionization chamber dosimetry.

2.1. ICRU Report 78 (2007)

ICRU 78 [2] recommended the adoption of a uniform dosimetry protocol for proton therapy. Both ICRU 59 [3] and IAEA TRS-398 [4] on proton dosimetry were considered in making the recommendations. Since calorimeters are absolute dosimeters they are the instruments of choice for determining reference absorbed dose in proton therapy beams; however, they are not suited for routine use, and the practical instruments are ionization chambers. Since there are no primary standards of proton beams, ionization chambers require calibration factors traceable to a primary standard ^{60}Co beam. Alternatively, they can be calibrated with a calorimeter in the user's proton beam. It is recommended in ICRU 78 [2] that TRS-398 [4] be adopted as the standard proton dosimetry protocol because it is very simple to use, harmonizes with other modalities' codes of practice (also given in TRS-398 [4]), which are being universally adopted, and has a more robust and rigorous formalism than ICRU 59 [3]. The energy required to produce an ion pair (w-value) in air is a significant factor and potentially the main source of uncertainty in ionometric proton dose determinations. The values used in the various protocols formulated in the past have differed significantly. Based on a comprehensive evaluation of published w-values [5], the adoption of a value of 34.2 J/C ± 0.4% was recommended in ICRU 78 [2]. This value is consistent with the value recommended in TRS-398 [4].

2.2. Basic data — *w*-values

Since calorimetry is the most direct way to determine absorbed dose to water (the reference material for dose specification), a comparison of the results of dose measurements using ionization chambers and calorimeters has always been considered a standard approach to determine *w*-values or beam quality correction factors k_Q. The results reported by Medin [6] who used a sealed water calorimeter in a 186 MeV proton scanning beam showed that k_Q values, determined for two NE2571 ionization chambers were 1.032 ± 0.013, which is in good agreement with the factor tabulated in TRS-398 [4] for this chamber type (1.039 ± 0.018). The present result has also been compared with a previously obtained result by Medin et al. [7] in a passively scattered proton beam having similar energy. This comparison yielded a 1.1% deviation, which is not significant considering the combined uncertainties of the two experimental determinations of k_Q. The dominating contribution to the combined uncertainty stems from the correction factor for ion recombination in the scanned proton beam (1%), and further studies are required in order to reduce this uncertainty and establish any possible differences in the k_Q value between these two proton beam delivery techniques. Palmans et al. [8] used a small-body portable graphite calorimeter for dosimetry in a low energy clinical proton beam. The *w*-values inferred from these measurements varied between 33.6 J/C and 34.9 J/C with standard uncertainties between 1.9% and 2.5%.

There is a paucity of recent data for heavier ion beams. A comparison performed by Brede et al. [9] in the clinical carbon-ion beams at the GSI Helmholtzzentrum für Schwerionenforschung confirmed the agreement between water calorimetry and ionization chamber dosimetry based on the recommended values of TRS 398 [4] within the standard uncertainty (k = 1) of 1.8% for calorimetry and of 3.0% for ionometry. Sakama et al. [10] deduced *w*-values for clinical carbon beams from measurements with a graphite calorimeter and ionization chamber. The mean *w*-value for the carbon beams was reported as 35.72 J/C with a standard uncertainty of 1.5%. This *w*-value is 3.5% higher than that estimated in TRS-398 [4] for heavy-ion beams; however, the result is based on stopping powers for carbon ions from ICRU 73 [11]. Following the data given in section 2.3, the results of Sakama et al. [10] may have to be re-evaluated. In any case there is a strong need for new experimental data for light ions to establish the *w*-values. Until new data are available, the value recommended in TRS-398 should be used in the dosimetry of light ion beams.

2.3. Basic data — stopping powers

Stopping power ratios are one of the major sources of uncertainty in the dosimetry of protons and heavier ions. While in the case of protons, TRS-398 [4] included accurate track-length fluence-weighted water to air stopping power ratios ($s_{w,air}$), for heavier ions this quantity was approximated by simple ratios of collision stopping powers, the basic data originating from rather inhomogeneous datasets. The emphasis in recent years on improving these dosimetry data, notably for carbon ions, is therefore well justified. Following the publication of a comprehensive new set of stopping powers for 16 ions ranging from lithium to argon (including carbon) in several elemental and compound materials in ICRU 73 [11], the work by Geithner et al. [12] introduced the use of Monte Carlo calculated track-length fluence for the calculation of carbon ion stopping power ratios that took account of all secondary particles generated. This work was complemented further by the calculations of Henkner et al. [13].

The investigations above emphasized the availability of mean excitation energy (I, used in the calculation of stopping powers) data for liquid water of around 80 eV, which differed from the 75 eV value recommended in ICRU 37 and 49 [14, 15]. The situation is further complicated by the fact that ICRU 73 [11] implicitly used an I_{water} value of 67.2 eV, which was questioned in an analysis by Paul et al. [16, 17] suggesting instead a value of (80.8 ± 2) eV. Shortly thereafter, referring to a previously published indirect experimental determination, Paul [18] concluded that the value of 75 eV used in ICRU 49 [15] agreed best with this experimental value. More recently, a study by Emfietzoglou et al. [19] using dielectric response functions yielded a I_{water} value of 77.8 eV. Other old and new values could be referred to, but for illustrative purposes only, a summary of the data presently available is shown in Fig. 1, where the range of variation of I_{water} is demonstrated. The resulting uncertainty of I_{water} jeopardizes not only the reference dosimetry of proton and carbon-ion radiotherapy beams, but also the spatial accuracy of clinical dose delivery related to the particle ranges in both water and human tissues [20].

Whereas an ongoing ICRU working group on key data for dosimetry will provide a final recommendation for I_{water} and other quantities of interest, an errata to ICRU 73 [11] has been released [21] recommending the use of a tentative value of 78.0 eV, adopted from an internal GSI report. The entire set of available data needs to be analysed and will probably result in a revision and a re-evaluation of all available stopping power ratios for electrons, protons and heavier ions. To a lesser extent, changes are also expected for $I_{graphite}$, following a recent analysis by Burns [22], who proposes a value of 82.5eV to replace the ICRU Report 37 [14] recommendation of 78.0 eV.

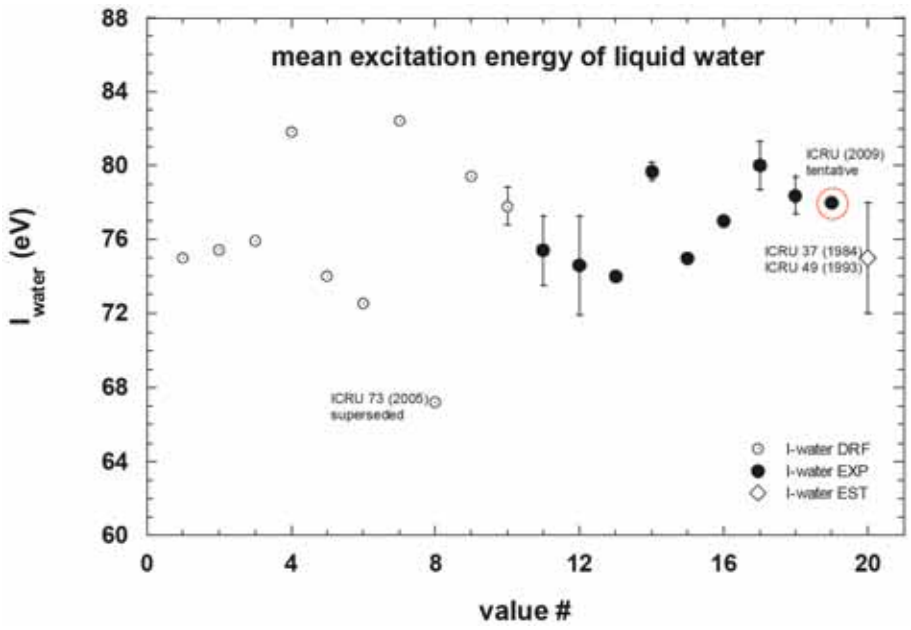

FIG. 1. Compilation of published data I_{water}, obtained using dielectric-response functions (open circles, left) and experimental data in heavy particle beams (solid circles, right). Within each group, the data are sorted chronologically from left to right. The classical ICRU estimated value (75 eV) [14, 15] is illustrated for comparison, as well as the recent 'tentative' value (circled).

2.4. Basic data — ion chamber perturbation factors

Owing to the lack of reliable data, it has been assumed to date that perturbations correction factors for ionization chambers are negligible both in proton and heavier ion dosimetry. Palmans and Verhaegen [23] developed analytical techniques for the evaluation of the wall correction factor p_{wall} in proton beams, verified with Monte Carlo calculations, showing that for most chambers in practical use the magnitude of the correction varied between 0.5% and 1%, reaching 1.5% in a few cases.

Although the corrections are small, the current high accuracy sought in light-ion beam dosimetry suggests that further investigations in the field are required to determine appropriate numerical values. In this context, new analytical models have been developed by Palmans [24] to evaluate gradient corrections of cylindrical chambers (the shift of the effective point of measurement), supported by Monte Carlo comparisons, showing that the

recommended correction of 0.75 r (r being the internal radius of the ionization chamber) given in TRS-398 [4] is not valid in many cases. Similar conclusions can be drawn for carbon ions, as discussed by Palmans et al. [25].

2.5. Recombination corrections

Ionization chamber measurements in proton and light-ion beams should be corrected for the recombination of ions and electrons within the air cavity as this reduces the amount of charge collected [2]. Most proton beams are considered to be of the continuous type [2], and initial recombination is largely independent of beam quality. ICRU 78 [2] endorses the recommendation of TRS-398 [4] that the two voltage method be used for recombination corrections for all clinical proton beams. The correction factor for protons k_s is given by:

$$k_s = \frac{\left(V_N/V_L\right)^2 - 1}{\left(V_N/V_L\right)^2 - \left(M_N/M_L\right)} \tag{1}$$

where the normalized readings of the dosimeter M_N and M_L are determined under the same irradiation conditions at the two voltages, the normal operating voltage V_N and a lower voltage V_L. Palmans et al. [26] found, however, that at dose rates of about 20 Gy/min, used clinically at some low energy proton eye-beam lines, the recombination correction factor can be overestimated by up to 2% if the expressions for pulsed beams are used as indicated in the worksheets of TRS-398 [4].

The treatment of recombination corrections for ionization chambers in delivery systems that use uniform beam scanning with energy stacking or small-diameter, high dose rate scanned beams are more complex than for systems that use passive beam delivery systems. The charge collection efficiency of ionization chambers for scanning systems should be determined by calibration against a dose-rate-independent device, such as a calorimeter or a Faraday cup (FC). If a dose rate independent device is not available, then the two voltage method can be used to determine the recombination correction factor:

$$k_S = a_0 + a_1\left(\frac{M_N}{M_L}\right) + a_2\left(\frac{M_N}{M_L}\right)^2 \tag{2}$$

where a_i are constants tabulated in TRS-398 [4]. The ratio V_N/V_L should ideally be equal to or larger than 3 (although TRS-398 provides data down to a factor 2), and V_N must not be too large in order to ensure that charge multiplication effects

do not contribute to the measured chamber signal. Farr et al. [27] used alanine dosimetry pellets and thermoluminiscence dosimeters with calibrations set to the US National Institute of Standards and Technology (NIST) as dose rate independent systems to verify the reference ionization chamber dose measurements in their uniform scanning/energy stacking beam delivery system. The use of the two voltage method to determine recombination corrections for fast uniform scanning may be considered appropriate as the doses determined with the ionization chamber agreed with the measurements made with the solid state dosimeters within the experimental uncertainties.

The two voltage method also appears to be applicable for the pulsed scanned beams used at the Paul Scherrer Institute [28]. However, its application for other types of pulsed scanned beams [29] requires special attention [30]. If the proton beam pulse duration is of intermediate length, and the pulse duration is of the same order of magnitude as the ion transit time in the ionization chamber, then the conditions pertaining to pulsed continuous beam irradiation are met and Eq. (1) should be used.

Correction factors for general recombination in ion beams heavier than protons should also be obtained with two voltage method [4]. When general recombination is negligible, initial recombination should be taken into account. However, the studies performed at available facilities [31] have indicated that the correction factor for initial recombination was consistent with unity within the uncertainties of the measurements. The carbon-ion beam at the GSI used a slow extraction mode (pulses of about 1 s duration); and an intensity-controlled raster beam scanning method that keeps the beam aimed at each spot for several milliseconds, which is far more than the average transit times of the ions in the Farmer type chamber. The general recombination corrections for typical Farmer type ionization chambers in this beam were found to be negligible [32]. However, if the formula for pulsed radiation were to be used, as suggested in TRS-398, a correction factor of about 1% for Farmer chambers would be expected.

3. FUTURE IMPROVEMENTS IN DOSIMETRY IN REFERENCE CONDITIONS

Future improvements in proton dosimetry would be focused on:

— Ion chamber specific factors and perturbation effects;
— Calculation of k_{Q,Q_0} beam quality correction factors, for new ionization chambers and experimental verification of calculated values.

Future improvements in light ion dosimetry would be focused on:

— Calculation of stopping power ratios;
— Calculation of k_{Q,Q_0} factors for new ionization chambers and experimental verification of calculated values;
— Experimental determination of the *w*-value for light ion beams.

The adoption of ICRU 78 and IAEA TRS-398 dosimetry recommendations for proton and heavier ion beam therapy facilities will allow consistency in the doses delivered to patients and will establish ion-beam ionization chamber dosimetry under reference conditions at a level of accuracy similar to that of high energy photon and electron beams.

REFERENCES

[1] PARTICLE THERAPY COOPERATIVE GROUP, http://ptcog.web.psi.ch/ptcentres.html
[2] INTERNATIONAL COMMISSION ON RADIATION UNITS AND MEASUREMENTS, Prescribing, Recording, and Reporting Proton-Beam Therapy, ICRU Report 78, JICRU 7,2 (Oxford University Press, Oxford, UK) (2007).
[3] INTERNATIONAL COMMISSION ON RADIATION UNITS AND MEASUREMENTS, Clinical Proton Dosimetry — Part I: Beam Production, Beam Delivery and Measurement of Absorbed Dose, ICRU Report 59 (ICRU, Bethesda, MD) (1998).
[4] INTERNATIONAL ATOMIC ENERGY AGENCY, Absorbed Dose Determination in External Beam Radiotherapy: An International Code of Practice for Dosimetry Based on Standards of Absorbed Dose to Water, Technical Reports Series No. 398, IAEA, Vienna (2000).
[5] JONES, D.T.L., The *w*-value in air for proton therapy beams. Radiat. Phys. Chem. **75** (2006) 541–550.
[6] MEDIN, J., Implementation of water calorimetry in a 180 MeV scanned pulsed proton beam including an experimental determination of k_Q for a Farmer chamber, Phys. Med. Biol. **55** (2010) 3287–3298.
[7] MEDIN, J., ROSS, C.K., KLASSEN, N.V., PALMANS, H., GRUSELL, E., GRINDBORG, J.-E., Experimental determination of beam quality factors, k_Q, for two types of Farmer chambers in a 10 MV photon and a 175 MeV proton beam, Phys. Med. Biol. **51** (2006) 1503–1521.
[8] PALMANS, H., THOMAS, R., SIMON, M., DUANE, S., KACPEREK, A., DUSAUTOY, A., VERHAEGEN, F., A small-body portable graphite calorimeter for dosimetry in low-energy clinical proton beams, Phys. Med. Biol. **49** (2004) 3737–3749.

[9] BREDE, H.J., GREIF, K.-D., HECKER, O., HEEG, P., HEESE, J., JONES, D.T.L., KLUGE, H., SCHARDT, D., Absorbed dose to water determination with ionization chamber dosimetry and calorimetry in collimated neutron, photon, proton and heavy ion radiation fields, Phys. Med. Biol. **51** (2006) 3667–3682.

[10] SAKAMA, M., KANAI, T., FUKUMURA, A., ABE, K., Evaluation of w values for carbon beams in air, using a graphite calorimeter, Phys. Med. Biol. **54** (2009) 1111–1130.

[11] INTERNATIONAL COMMISSION ON RADIATION UNITS AND MEASUREMENTS, Stopping of Ions Heavier than Helium, ICRU Report 73, JICRU **5**,1 (Oxford University Press, Oxford, UK) (2005).

[12] GEITHNER, O., ANDREO, P., SOBOLEVSKY, N., HARTMANN, G., JÄKEL, O., Calculation of stopping power ratios for carbon ion dosimetry, Phys. Med. Biol. **51** (2006) 2279–2292.

[13] HENKNER, K., BASSLER, N., SOBOLEVSKY, N., JÄKEL, O., Monte Carlo simulations on the water-to-air stopping power ratio for carbon ion dosimetry, Med. Phys. 36 (2009) 1230-1235.

[14] INTERNATIONAL COMMISSION ON RADIATION UNITS AND MEASUREMENTS, Stopping Powers for Electrons and Positrons, ICRU Report 37 (ICRU, Bethesda, MD, USA) (1984).

[15] INTERNATIONAL COMMISSION ON RADIATION UNITS AND MEASUREMENTS, Stopping Powers and Ranges for Protons and Alpha Particles, ICRU Report 49 (ICRU, Bethesda, MD, USA) (1993).

[16] PAUL, H., GEITHNER, O., JÄKEL, O., The influence of stopping powers upon dosimetry for radiation therapy with energetic ions, Adv. Quantum Chem. 52 (2007) 290–308.

[17] PAUL, H., GEITHNER, O., JÄKEL, O., The ratio of stopping powers of water and air for dosimetry applications in tumor therapy, Nucl. Instrum. Meth. Phys. Res. **B 256** (2007) 561–564.

[18] PAUL, H., The mean ionization potential of water, and its connection to the range of energetic carbon ions in water, Nucl. Instrum. Methods **B 255** (2007) 435–437.

[19] EMFIETZOGLOU, D., GARCIA-MOLINA, R., KYRIAKOU, I., ABRIL, I., NIKJOO, H., A dielectric response study of the electronic stopping power of liquid water for energetic protons and a new *I*-value for water, Phys. Med. Biol. **54** (2009) 3451–3472.

[20] ANDREO, P., On the clinical spatial resolution achievable with protons and heavier charged particle radiotherapy beams, Phys. Med. Biol. **54** (2009) N205–N215.

[21] SIGMUND, P., SCHINNER, A., PAUL, H., Errata and Addenda for ICRU Report 73, Stopping of Ions Heavier than Helium, Journal of the ICRU, Vol. 5, no. 1 (2005), http://www.icru.org/index.php?option=com_content&task=view&id=167I

[22] BURNS, D.T., A re-evaluation of the *I*-value for graphite based on an analysis of recent work on *W*, $s_{c,a}$ and cavity perturbation corrections, Metrologia **46** (2009) 585–590.

[23] PALMANS, H., VERHAEGEN, F., "Calculation of perturbation correction factors for ionization chambers in clinical proton beams using proton-electron Monte Carlo simulations and analytical model calculations", Recent Developments in Accurate Radiation Dosimetry (SEUNTJENS, J.P., MOBIT, P.N., Eds), Medical Physics Publishing, Madison, WI (2002) 229–245.

[24] PALMANS, H., Perturbation factors for cylindrical ionization chambers in proton beams. Part I: corrections for gradients, Phys. Med. Biol. **51** (2006) 3483–3501.

[25] PALMANS, H., KACPEREK, A., JÄKEL, O., "Hadron dosimetry", Clinical Dosimetry Measurements in Radiotherapy (Proc. AAPM Summer School, 2009) (ROGERS, W.O., CYGLER, J., Eds), Medical Physics Publishing, Madison, WI (2009) 669–722.

[26] PALMANS, H., THOMAS, R., KACPEREK, A., Ion recombination correction in the Clatterbridge Centre of Oncology clinical proton beam, Phys. Med. Biol. **51**(2006) 903–917.

[27] FARR, J.B., MASCIA, A.E., HIS, W.C., ALLGOWER, C. E., JESSEPH, F., SCHREUDER, A.N., WOLANSKI , M., NICHIPOROV, D.F., ANFEROV, V., Clinical characterization of a proton beam continuous uniform scanning system with dose layer stacking, Med. Phys. **35** (2008) 4945–4954.

[28] CORAY, A., et al.,"Dosimetry with the scanned proton beam on the Paul Scherrer Institute gantry", Standards and Codes of Practice in Medical Radiation Dosimetry (Proc. Int. Symp. Vienna, 2002), IAEA, Vienna (2002) 295–302.

[29] TILLY, N., GRUSELL, E., KIMSTRAND, P., LORIN, S., GAJEWSKI, K., PETTERSSON, M., BÄCKLUND, A., GLIMELIUS, B., Development and verification of the pulsed scanned proton beam at The Svedberg Laboratory in Uppsala Phys. Med. Biol. **52** (2007) 2741–2754.

[30] LORIN, S., GRUSELL, E., TILL, N., MEDIN, J., KIMSTRAND, P., GLIMELIUS, B., Reference dosimetry in a scanned pulsed proton beam using ionisation chambers and a Faraday cup, Phys. Med. Biol. **53** (2008) 3519–3529.

[31] JÄKEL, O., HARTMANN, G.H., KARGER, C.P., HEEG, P., VATNITSKY, S., A calibration procedure for beam monitors in a scanned beam of heavy charged particles, Med. Phys. **31** (2004) 1009–1013.

[32] JÄKEL, O., HARTMANN, G.H., HEEG, P., KARGER, C.P., "Dosimetry of 12C ion beams at the German Heavy Ion Therapy Facility: Comparison of the currently used approach and TRS-398", Standards and Codes of Practice in Medical Radiation Dosimetry (Proc. Int. Symp.Vienna, 2002), IAEA, Vienna (2002) 303–310.

COMPARISON OF CALIBRATION METHODS OF PLANE PARALLEL IONIZATION CHAMBERS FOR ELECTRON BEAM DOSIMETRY IN RADIOTHERAPY

I. JOKELAINEN, A. KOSUNEN
Radiation Metrology Laboratory,
Radiation and Nuclear Safety Authority (STUK),
Helsinki, Finland
Email: illka.jokelainen@stuk.fi

Abstract

The consistency of two alternative calibration methods of plane parallel (PP) ionization chambers for electron beam radiotherapy has been investigated. Cross-calibration in a linac electron beam and calibration in a ^{60}Co gamma beam with generic, type specific beam quality correction factors from the IAEA dosimetry protocol TRS-398 were studied for Roos (PTW and Wellhöfer) and for NACP-02 (Scanditronix) plane parallel ionization chambers. The ratios of the absorbed dose to water calibration coefficients of the two methods were 1.004 (SD 0.2%) for Roos PP chambers and 0.994 (SD 0.3%) for NACP-02 PP chambers. Results are expressed for a selected 8 MeV nominal electron beam energy and indicate +0.4% and –0.6% shifts in the measured absorbed doses in the electron beams due to change in the calibration method. From direct comparison of the two calibration methods, the experimental overall perturbation factors p_{Co}^{PP} for ^{60}Co gamma beam were determined for each type of the chambers. The experimental values of the overall perturbation factors were found to be 1.024 and 1.026 for the Roos chambers and NACP-02 chambers, respectively. For Roos type chambers, the p_{Co}^{PP} values deviate 1.4% from the data in IAEA TRS-398, but are consistent with reported results of several authors in 2001–2007. For NACP-02 type chambers, the determined p_{Co}^{PP} are consistent with the value used in IAEA TRS-398, and are within 1% of the results reported by other authors. Based on the results of this study, the calibration method of PP ionization chambers used for electron beam radiotherapy in Finland has changed from the cross-calibration approach to the calibration in a ^{60}Co gamma beam. The low chamber-to-chamber variation of p_{Co}^{PP} values of individual PP chambers of each type makes it possible to 'move' the calibrations back to the SSDL ^{60}Co gamma beam.

1. INTRODUCTION

IAEA dosimetry protocol TRS-398 [1] describes three optional methods for calibration of plane parallel (PP) ionization chambers for absorbed dose to water (ADW): (i) calibration at a series of electron beam qualities in a primary standards dosimetry laboratory (PSDL), (ii) calibration in a ^{60}Co gamma ray beam in an SSDL and (iii) cross-calibration in a high energy electron beam in a

clinic. Calibration in a ^{60}Co gamma ray beam implies use of generic beam quality factors for each type of the chamber. The primary method recommended is the third one. As the PSDL calibrations are not widely and locally available, the field PP chambers are usually calibrated either in a ^{60}Co gamma beam or by cross-calibration.

In Finland, since 1997, the cross-calibration of PP chambers in clinic beams has been performed by the secondary standards dosimetry laboratory (SSDL) of the Radiation and Nuclear Safety Authority (STUK). At that time, these calibrations were taken in use because of the high variation of wall correction factors $(p_{wall})_{Co}$ in a ^{60}Co gamma beam for NACP-E and CALCAM chambers, which forbids the use of the generic $(p_{wall})_{Co}$ [2].

However, the temperature stability, the setup accuracy and the stability of the calibration beam are difficult to achieve in clinical cross-calibrations, and since the Finnish hospitals have replaced the former PP chambers by Roos and NACP-02 type chambers, the possibility of returning the calibration procedure to the SSDL ^{60}Co gamma beam was investigated. The recent studies have also reported lower variation of $(p_{wall})_{Co}$ for Roos and NACP-02 type chambers [3–5]. A comparison was performed between cross-calibration and ^{60}Co calibration methods for 13 Roos (PTW and Welhöfer) and for 5 Scanditronix NACP-02 type PP chambers from the Finnish hospitals. A total of 22 cross-calibrations were carried out in a 16 MeV (range of 50% ionization $R_{50,ion}$ = 6.5 cm) linac electron beam and 54 calibrations in the ^{60}Co gamma beam at the SSDL of STUK.

The overall perturbation factor p_{Co}^{PP} for PP ionization chambers was determined experimentally by direct comparison of ADW in an electron beam by the two calibration methods. The values of the p_{Co}^{PP} were compared to the values given in TRS-398 [1] and more recent studies [2–8]. The chamber-to-chamber variation of the perturbation factor p_{Co}^{PP} for PP ionization chambers of Roos and NACP-02 types was determined to assure the use of generic, type specific p_{Co}^{PP} factors and calibration in a ^{60}Co gamma beam.

Conclusions on the measured ADW of electron beams when using the ^{60}Co gamma beam calibration together with the TRS-398 [1] or other data in respect to the existing cross-calibration method are drawn.

2. MATERIALS AND METHODS

The absorbed dose to water $D_{w,Q}$ in an electron beam of quality Q is obtained using an ionization chamber having an absorbed dose to water calibration coefficient $N_{Dw,Co}$ at ^{60}Co

$$D_w = M_Q N_{Dw,Co} k_{Q,Co} = M_Q N_{Dw,Co} \cdot \frac{(p_{wall}\, p_{cav}\, p_{cel}\, p_{dis})_Q}{(p_{wall}\, p_{cav}\, p_{cel}\, p_{dis})_{Co}} \cdot \frac{(s_{w,air})_Q}{(s_{w,air})_{Co}} \tag{1}$$

where

$k_{Q,Co}$ is a correction factor for calibration factor of the ionization chamber between ^{60}Co gamma beam quality and electron beam quality Q;
M_Q the ionization chamber reading, $(s_{w,air})_Q$ is water to air mass stopping power ratio;
p_{wall} corrects the effect for chamber wall;
p_{cav} corrects the effects of scatter of secondary electrons in air cavity;
p_{cel} is the distortion due to central electrode; and
p_{dis} is the displacement of a volume of water with the detector cavity in the phantom.

The perturbation factors can be presented as an overall perturbation factor, p_Q, which is a product of all the separate factors.

For PP chambers, the p_{dis} and p_{cel} are equal to unity in ^{60}Co gamma and electron beams because displacement correction is not needed and there is no central electrode. Since secondary electron equilibrium exists in the ^{60}Co gamma beam at the calibration depth and the chamber volume can be considered small, the p_{cav} is taken to be unity for both cylindrical and PP chambers. For PP chambers in ^{60}Co gamma beam, only p_{wall} is applied:

$$p_{Co}^{PP} = (p_{wall})_{Co}^{PP} \tag{2}$$

The effect of the chamber wall cannot be not measured separately from the other perturbation components. By comparing the cylindrical and PP chamber in an electron beam, the experimentally determined overall p_{Co}^{PP} includes all the perturbation components caused by the ionization chamber in the beam. It also summarizes the differences and effects of the calibration methods and data used.

Applying Eq. (1) to a cylindrical and PP chamber, and assuming that the dose measured with both chambers are equal; the value p_{Co}^{PP} can be derived from the Eq. (1):

$$p_{Co}^{PP} = \frac{M_Q^{PP} N_{Dw,Co}^{PP}}{M_Q^{cyl} N_{Dw,Co}^{cyl}} \cdot \frac{p_{Co}^{cyl}}{p_Q^{cyl}} \cdot p_Q^{PP} \tag{3}$$

where

p_{Co}^{PP} is the PP chamber type specific overall perturbation factor for ^{60}Co gamma beam;

M_Q^{PP} is the PP chamber reading for electron beam quality Q;

$N_{Dw,Co}^{PP}$ is the PP chamber calibration coefficient in ^{60}Co gamma beam;

M_Q^{cyl} is the cylindrical chamber reading for electron beam quality Q;

$N_{Dw,Co}^{cyl}$ is the cylindrical chamber calibration coefficient for ^{60}Co gamma beam;

p_{Co}^{cyl} is the cylindrical chamber type specific overall perturbation factor for ^{60}Co gamma beam;

p_Q^{cyl} is the cylindrical chamber type specific overall perturbation factor for electron beam quality Q;

p_Q^{PP} is the PP chamber type specific overall perturbation factor for electron beam quality Q.

The measurements were carried out at the SSDL of Radiation and Nuclear Safety Authority (STUK) and at the Docrates Radiotherapy Clinic (both in Helsinki, Finland) using Varian Linac iX accelerator.

Within a period of two months, a total of 13 PP chambers of Roos type (11 PTW34001, 2 Scanditronix-Wellhöfer PPC40) and 5 Scanditronix NACP-02 type chambers from Finnish hospitals and from STUK were calibrated in a ^{60}Co gamma beam and in a linear accelerator electron beam in the radiotherapy clinic. The calibrations were carried out in accordance with IAEA dosimetry protocol TRS-398 [1], and for calibrations in ^{60}Co gamma and electron beams, the quality factors (k_Q) from the TRS-398 [1] were applied.

For a comparison of the two calibration methods, the calibration coefficients $N_{Dw,Q}^{PP}$ are presented for an electron beam quality Q, a range of 50% ionization $R_{50,ion}$ = 3.5 cm and nominal energy of 8 MeV. The conversions of calibration coefficient were converted to this electron beam quality by k_Q factors from TRS-398 [1]. The formulations for the calibration coefficients are as follows:

For calibration in a ^{60}Co gamma beam:

$$N_{Dw,Q,Co}^{PP} = N_{Dw,Co}^{PP} \cdot k_{Q,Co}^{PP} = N_{Dw,Co}^{cyl} \cdot \frac{M_{Co}^{cyl}}{M_{Co}^{PP}} \cdot k_{Q,Co}^{PP} \quad (4)$$

For cross-calibration in electron beam quality, Q_{cross}:

$$N_{Dw,Q,Q_{cross}}^{PP} = N_{Dw,Q_{cross}}^{PP} \cdot k_{Q,Q_{cross}}^{PP} = N_{Dw,Co}^{cyl} \cdot k_{Q_{cross},Co}^{cyl} \cdot \frac{M_{Q_{cross}}^{cyl}}{M_{Q_{cross}}^{PP}} \cdot k_{Q,Q_{cross}}^{PP} \quad (5)$$

The experimental overall perturbation factors in ^{60}Co gamma beam p_{Co}^{PP} for PP chambers were determined by direct comparison of the ADW calibration coefficients for the two methods and for each individual chamber. The chamber type specific p_{Co}^{PP} were determined by averaging p_{Co}^{PP} values of the same chamber type. For both calibration methods, the reference dose was measured by cylindrical ionization chambers calibrated in ^{60}Co gamma beam at the SSDL of STUK traceable to BIPM. The NE2561 chamber with 1.0 mm thick PMMA waterproofing sleeve was used in ^{60}Co gamma beam and waterproof WH FC65-G chamber for cross-calibrations in clinic electron beam. All chamber readings were corrected for air density. In cross-calibrations in electron beam, the corrections for ion recombination were measured and applied. The measured recombination corrections were 0.7–1.3% and for 1.0% for PP chambers Roos and NACP-02 and 1.8% for the cylindrical WH FC65-G chamber. After positioning of the chamber the stabilization of the signal was checked before the reading was recorded. The data of the PP chamber window thickness for positioning the chambers effective point on the calibration depth were taken from TRS-398 [1] (Table 1). For positioning the cylindrical chambers, the diameter of chambers and waterproofing sleeve were measured (Table 1).

The determined p_{Co}^{PP} for PP chambers were compared to the data from TRS-398 [1] and other studies [2–8].

2.1. Calibration in a ^{60}Co gamma ray beam

A total of 54 calibrations of PP chambers were carried out at the SSDL of STUK in a 30 cm × 30 cm × 30 cm water phantom using the ^{60}Co gamma beam from Theratron AECL unit. The source-to-surface distance was 100 cm and the field size was 10 cm × 10 cm.

TABLE 1. DIMENSIONS OF IONIZATION CHAMBERS USED IN CALIBRATIONS

Chamber	Cavity radius r_{cyl}	Sleeve radius	Window thickness		Waterproof
	(mm)	(mm)	(mm)	(mg/cm^2)	
NE2561	3.7	5.4			No
WH FC65-G	3.5				Yes
PTW34001			1.0	118	Yes
WH PPC40			1.0	118	Yes
NACP-02			0.6	104	Yes

The reference point for cylindrical chambers is the centre of the air cavity, and for PP chambers it is the centre of the inner surface of the front window, and these were positioned at 5 cm depth in the water phantom. The substitution method was used in the calibrations: the SSDL reference chamber and the PP chamber were irradiated separately. The chamber readings were measured by laboratory Keithley 6517 electrometer. The dose rate in the ^{60}Co calibrations was 2 mGy/s.

2.2. Cross-calibrations in an electron beam

Twenty-two cross-calibrations were carried out in a 16 MeV electron beam. The measurements were taken in a 20 cm × 50 cm × 50 cm water phantom with the vertical beam geometry. In calibrations, the source-to-surface distance was 100 cm and the field size was 20 cm × 20 cm. For cylindrical chambers, the effective point was the half of the internal radius from the centre of the chamber air cavity towards to radiation focus. For PP chambers, the effective point was on the inner surface of the window at its centre. The reference depth z_{ref} in water in the electron beam was determined as:

$$z_{ref} = 0.6 \cdot (1.059 \cdot R_{50,ion} - 0.37\ \text{g/cm}^2) - 0.1\ \text{g/cm}^2 \quad (6)$$

where $R_{50,ion}$ is half-value depth determined from depth ionization distribution.

Calibration were made in three sessions, and for each session, the depth ionization curves were measured with a PP chamber in a 50 cm × 50 cm × 50 cm water phantom with a three-dimensional scanning system. For the 16 MeV electron beam, the measured $R_{50,ion}$ was 6.56 cm and the z_{ref} was 3.9 cm. The reference dose at z_{ref} was determined by SSDL cylindrical chamber before and after each PP chamber measurements. The dose rate in the cross-calibrations was 60 mGy/s.

The substitution method was used in electron beam cross-calibrations. The positioning of the cylindrical reference chamber and the PP chamber on the same reference depth was performed by high precision jig (Fig. 1). The precision jig consists of a frame fixed in the water phantom and a sled on the frame for changing the position of the chambers. Both types of chamber were fixed on the sled and were able to move to the in-beam position for measurement. The precision jig enables high repeatability for positioning of the cylindrical SSDL reference chamber and PP chamber's effective points on the same depth.

For every PP chamber cross-calibration, the reference dose was determined by measurements with SSDL cylindrical reference chamber before and after the measurements with PP chamber. The stability of the accelerator beam output while the calibration was monitored by two ionization chambers PTW31010 Semiflex located on the frame of the calibration jig on the ends of the radiation field at the same depth as the chamber on the beam. The signals of the reference

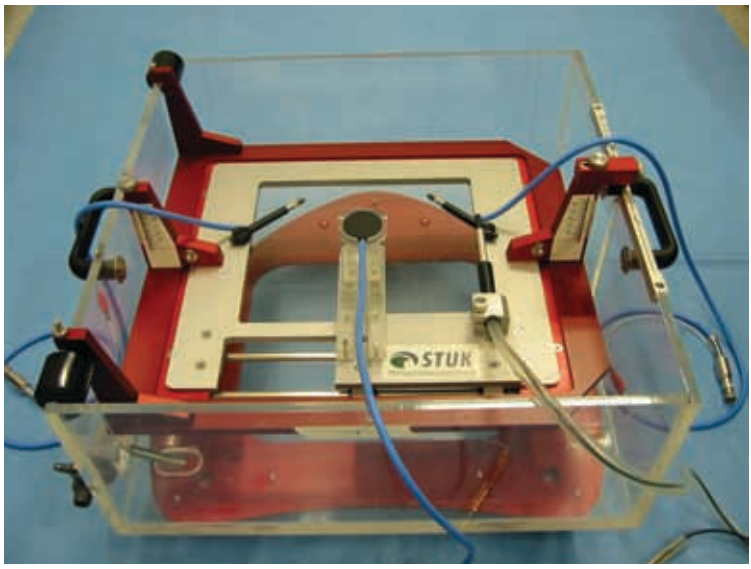

FIG. 1. High precision jig for cross-calibration of PP chambers in linear accelerator electron beam in the radiotherapy clinic.

cylindrical chamber, the PP chamber and the monitor chambers were monitored and evaluated graphically. As the readings of the reference cylindrical chamber and the PP chamber were not normalized to the monitor chamber readings, the acceptance level for accelerator beam output variation while the measurements by the PP chamber was 0.2%. The simultaneous reading measurements of the tree chamber (chamber in the beam and the two monitor chambers) were made by reference class PTW MULTIDOS electrometer.

3. RESULTS

3.1. Calibration of PP ionization chambers

The ratios

$$N_{Dw,Q,Co}^{PP} / N_{Dw,Q,Q_{cross}}^{PP}$$

for electron beam quality $R_{50,ion}$ = 3.5 cm and for all investigated chambers are shown in Fig. 2. The calibration coefficients were determined according to Eqs (4, 5).

For Roos type PP chambers, the mean value of the ratios of the calibration coefficients was 1.004, and for NACP-02 type chambers, 0.994. In the ^{60}Co gamma ray beam, an average standard deviation of 0.1% was determined for $N_{Dw,Co}^{PP}$ values of both chamber types in recalibrations of each individual

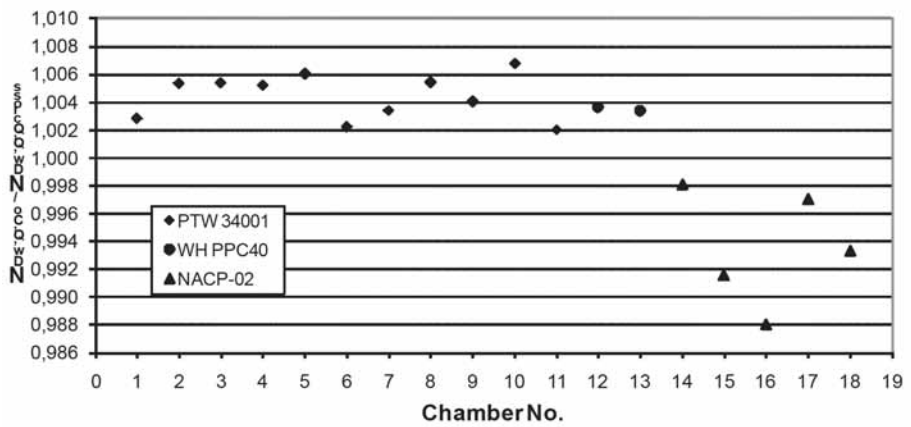

FIG. 2. Ratio of ADW calibration coefficients for electron beam ($R_{50,ion}$ = 3.5cm) derived from ^{60}Co calibration ($N_{Dw,Q,Co}^{PP}$) and from cross-calibration ($N_{Dw,Q,Q_{cross}}^{PP}$).

chamber. For two PTW 34001 and for two NACP-02 chambers, the calibrations were made twice and the difference in p_{Co}^{PPi} were 0.1% and 0.3%, respectively.

The determined individual perturbation factors for ^{60}Co gamma beam p_{Co}^{PP} are presented in Fig. 3. The mean value of p_{Co}^{PP} for PTW Roos PP chambers was 1.024 and for Wellhöfer Roos PP chambers, 1.026.

For all calibrated Roos PP chambers, the mean value of p_{Co}^{PP} was 1.024, with a standard deviation of 0.2%. For NACP PP chambers, the mean value of p_{Co}^{PP} was 1.026, with a standard deviation of 0.3%.

3.2. Uncertainties

Tables 2 and 3 summarize the uncertainty contributions to the experimentally determined perturbation correction p_{Co}^{PP} and calibration coefficients

$N_{Dw,Co}^{PP}$ and $N_{Dw,Q,Q_{cross}}^{PP}$.

The uncertainty analyses were divided into components of ADW calibration coefficients $N_{Dw,Co}$ corrected chamber readings M, k_Q factors and perturbation factors p_Q. Uncertainties were determined in accordance to the guidance TRS-398 [1]. In Tables 1 and 2, each source of uncertainties is expressed as a combination of type A and B uncertainties.

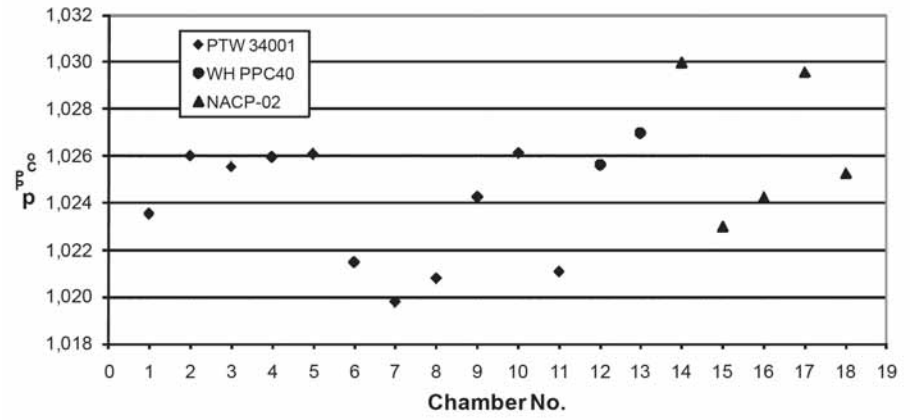

FIG. 2. Individual perturbation factors p_{Co}^{PP} in ^{60}Co gamma beam of PTW34001, WH PPC40 and NACP-02 PP chambers. The repeatability of the p_{Co}^{PP} determinations was 0.4%.

TABLE 2. RELATIVE STANDARD UNCERTAINTIES FOR QUANTITIES USED IN CALCULATIONS OF p_{Co}^{PP} FROM Eq. (3)

	Uncertainty (%)
$N_{Dw,Co}^{PP}/N_{Dw,Co}^{cyl}$	0.29
M_{Q}^{PP}/M_{Q}^{cyl}	0.25
$\frac{p_{Co}^{cyl}}{p_{Q}^{cyl}} p_{Q}^{PP}$	1.06
Combined (1σ) standard uncertainty	1.13

TABLE 3. RELATIVE STANDARD UNCERTAINTIES FOR QUANTITIES USED IN CALCULATIONS OF $N_{Dw,Q,Co}^{PP}$ AND $N_{Dw,Q,Q_{cross}}^{PP}$ FROM Eqs (4, 5)

	Uncertainty (%)	
	$N_{Dw,Q,Q_{cross}}^{PP}$	$N_{Dw,Q,Co}^{PP}$
$N_{Dw,Co}^{cyl}$	0.5	
$M_{Q_{cross}}^{cyl}/M_{Q_{cross}}^{PP}$	0.3	
$k_{Q_{cross},Co}^{cyl}$	1.2	
Combined (1σ) uncertainty of $N_{Dw,Q_{cross}}^{PP}$	**1.3**	
$k_{Q,Q_{cross}}^{PP}$	0.4	
$N_{Dw,Co}^{cyl,ref}$		0.4
$M_{Co}^{cyl,ref}/M_{Co}^{PP}$		0.2
Combined (1σ) uncertainty of $N_{Dw,Co}^{PP}$		**0.5**
$k_{Q,Co}^{PP}$		1.7
Combined (1σ) standard uncertainty	**1.4**	**1.8**

TABLE 4. THE PUBLISHED p_{Co}^{PP} VALUES FOR ROOS AND NACP-02 TYPE PLANE PARALLEL IONIZATION CHAMBERS

Reference	Roos	NACP-02
IAEA TRS-398 (2000)	1.010	1.025
Dohm et al. (2001)	1.024	
Palm et al. (2002)	1.018	
Christ et al. (2002)	1.024	
Stewart et al. (2002)		1.020
Palmans et al. (2003)		1.015
Kapsch et al. (2007)	1.020	
The present study	1.024	1.026

The uncertainty of $N_{Dw,Co}^{cyl}$ took into account the stability of the cylindrical reference chambers calibrated in the SSDL ^{60}Co gamma beam. The air density correction, the leakage current, the positioning of the chamber and recombination correction were included in the uncertainties of chamber readings *M*. For perturbation corrections p_Q and k_Q factors of cylindrical and PP chambers the uncertainty estimates were adapted from TRS-398 [1].

For electron beam PP chamber ADW calibration coefficients determined by ^{60}Co gamma calibration $N_{Dw,Q,Co}^{PP}$ and by electron cross-calibration

$$N_{Dw,Q,Q_{cross}}^{PP},$$

the k_Q factors are the dominant components of the uncertainty budgets. In TRS-398 [1], uncertainty estimation of $k_{Q,Co}^{PP}$, the highest component, is p_{wall} with a contribution of 1.5%, which is a higher value than that determined in this study for p_{Co}^{PP} (Table 2). In the published data of earlier investigations [3–8] reported in 2001–2007, the uncertainties of determined p_{Co}^{PP} values were near 1.0%.

4. DISCUSSION AND CONCLUSIONS

A summary of the published values of p_{Co}^{PP} for Roos and NACP-02 type PP chambers is presented in Table 4. For Roos chambers, the current p_{Co}^{PP} values are

consistent with the results reported in 2001–2007 in other studies [3–6], but deviates by 1.4% from the value presented in the IAEA dosimetry protocol TRS-398 [1]. For NACP-02 chambers, the p_{Co}^{PP} values of this work are consistent with those used in the IAEA dosimetry protocol TRS-398 [1] and are within 1% of the two published data of earlier investigations [7, 8]. The determined p_{Co}^{PP} values for Roos type PP chambers of two different manufacturers, PTW and Wellhöfer, are equal within the 0.2% standard deviation of all Roos type chambers, p_{Co}^{PP}.

In this type of experimental determination of p_{Co}^{PP}, the uncertainties of the perturbation coefficients for the cylindrical ionization chamber and for the PP chamber in the electron beam are dominant. The general consistency of the current results of p_{Co}^{PP} to those obtained by other authors emphasizes its general reliability.

Owing to a change in the calibration method of the PP chambers, from the electron beam cross-calibration to the ^{60}Co gamma beam calibration in the SSDL, and with the application of the IAEA TRS-398 [1] dosimetry protocol, a +0.4% change in the ADW calibration coefficients in an electron beam is expected for Roos (PTW and Wellhöfer) type PP chambers. For NACP-02 PP chambers, a -0.6% change is expected. The same changes occur in the measured absorbed doses in these electron beams. These results need to be seen in respect of a 0.2–0.3% level of standard deviation.

Based on the results of this study, the type of PP chambers used for electron beam dosimetry in radiotherapy in Finland can be calibrated with acceptable accuracy according to the ^{60}Co approach and using the methods and k_Q data of TRS-398 [1].

The results of this study for p_{Co}^{PP} are consistent with other recently published data [3–8]. The data used in the TRS-398 [1] are over ten years old (published in 2000). The results of this study, as well as those by other groups, emphasized the need for updating the k_Q data for PP chambers used for electron beam dosimetry in TRS-398 [1].

REFERENCES

[1] INTERNATIONAL ATOMIC ENERGY AGENCY, Absorbed Dose Determination in External Beam Radiotherapy: An International Code of Practice for Dosimetry Based on Standards of Absorbed Dose to Water, Technical Reports Series No. 398, IAEA, Vienna (2000).

[2] KOSUNEN, A., JÄRVINEN, H., SIPILÄ, P., “Optimum calibration of NACP type plane parallel ionization chambers for absorbed dose determination in low energy electron beams”, Measurement Assurance in Dositmetry (Proc. Int. Symp. Vienna, 1993), IAEA, Vienna (1994) 505–513.

[3] CHRIST, G., DOHM, O.S., BRUGGMOSER, G., SCHULE, E., The use of plane-parallel chambers in electron dosimetry without any cross-calibration, Phys. Med. Biol. **47** (2002) N121–N126.

[4] PALM, Å., CZAP, L., ANDREO, P., MATTSSON, O., Performance analysis and determination of the p_{wall} correction factor for ^{60}Co γ-ray beams for Wellhöfer Roos-type plane-parallel chambers, Phys. Med. Biol. **47** (2002) 631–40.

[5] KAPSCH, R.-P., BRUGGMOSER, G., CHRIST, G., DOHM, O.S., HARTMANN, G.H., SCHULE, E., Experimental determination of p_{Co} perturbation factors for plane-parallel chambers, Phys. Med. Biol. **52** (2007) 7167–81.

[6] DOHM O.S., CHRIST G., NUSSLIN F., Electron dosimetry based on the absorbed dose to water concept: A comparison of the AAPM TG-51 and DIN 6800-2 protocols, Med. Phys. **28** (2001) 2258–64.

[7] PALMANS, H., NAFAA, L., de PATOUL, N., DENIS, J.-M., TOMSEJ, M., VYNCKIER, S., A dosimetry study comparing NCS report-5, IAEA TRS-381, AAPM TG-51 and IAEA TRS-398 in three clinical electron beam energies, Phys. Med. Biol. **48** (2003) 1091–1107.

[8] STEWART, K., SEUNTJENS, J., Comparing calibration methods of electron beams using plane-parallel chambers with absorbed-dose to water based protocols, Med. Phys. **29** (2002) 284–9.

FERROUS AMMONIUM SULPHATE DOSIMETER CHEMICAL YIELD DETERMINATION FOR DOSE MEASUREMENT STANDARDIZATION IN HIGH ENERGY PHOTONS

O. MOUSSOUS, T. MEDJADJ
Centre de Recherche Nucléaire d'Alger
Email: ouiza_62@yahoo.fr

M. BENGUERBA
Faculté de Physique, Université des Sciences et de la Technologie Houari Boumediène

Algiers, Algeria

Abstract

The radiation chemical yield $G(Fe^{3+})$ of the ferrous ammonium sulphate (Fricke) dosimeter has been measured in high energy photon beams. The calibration of the dosimeters was performed at energies of ^{60}Co gamma radiation, 6 and 18 MV photons. The reference absorbed dose in a water phantom was measured at a reference depth using an ionization chamber calibrated in terms of absorbed dose to water. The Fricke solution was placed in Pyrex ampoules. The values of $G(Fe^{3+})$ thus obtained, for a solution with sodium chloride, are: 1.598 (±0.012), 1.597 (±0.020) and 1.603 (±0.020) μmol/J at ^{60}Co, 6 and 18 MV photon beams, respectively.

1. INTRODUCTION

High energy photon and electron beams are widely used in radiation therapy. The quantity of interest is the absorbed dose determined in a water phantom. In Algeria, the measurement of the output dose rates for medical accelerators is performed using ionization chambers calibrated in terms of absorbed dose to water in ^{60}Co gamma radiation according to the IAEA's TRS–398 Code of Practice [1]. Ionization chambers are recommended for beam calibration because they are accurate and precise, and provide instant readout. The composition of their materials, however, is different from that of water, which perturbs the particle fluence in the phantom and therefore many corrections factors are required for high energy beam dosimetry.

The Fricke dosimeter has advantages over an ionization chamber for high energy photon and electron dosimetry. Therefore it has been recommended as an alternative method for the determination of absorbed dose in water [2, 3]. Owing to its favourable characteristics such as high precision, dose rate independence, near water equivalence and energy independence, many national standards laboratories use Fricke dosimetry for absorbed dose standardization.

In photon and electron radiation fields [4, 5], the published values of the radiation chemical yield $G(Fe^{3+})$ of the Fricke dosimeter exhibit discrepancies notably due to differences in the characteristics of spectrophotometers and to the various techniques used in determination of the reference absorbed dose. The aim of this work is to determine the value of this radiation chemical yield in high energy photon beams in order to measure absorbed dose to water with good accuracy for such radiations based on the use of the ferrous sulphate dosimeter.

2. MATERIALS AND METHOD

2.1. Materials

All glassware was thoroughly rinsed with high purity water currently obtained at our laboratory using the arium®611 ultrapure water system (Sartorius, Germany). Tap water is prepurified by a distillation treatment, which removes more than 95% of contaminants, and by an electro deionization treatment, which further reduces the water ions content. After a final purification and filter process, the system provides water with a typical resistivity of about 18.2 MΩ at 25°C and total organic carbon less than 4 ppb.

The SSDL-CRNA Fricke dosimeter consists of a sealed glass ampoule filled with a Fricke aqueous solution. The Fricke solution was prepared from analytical reagent grade chemicals and high purity water. The solution components are: 0.4 mol/L H_2SO_4, 10^{-3} mol/L $Fe(NH_4)_2(SO_4)_2$,$6H_20$ (Mohr salt) and 10^{-3} mol/L NaCl. To improve the accuracy and sensitivity of the solution, the solution of sulphuric acid and water was pre-irradiated to about 10 Gy before adding the other chemicals [6, 7]. The dosimeter ampoules have the following dimensions: inner diameter 10.6 mm, height 31 mm (referred to the top surface of the liquid in the ampoule), and Pyrex wall thickness 0.5 mm. Hence, the volume of the dosimetric solution is about 2 cm^3. The ampoule shape was specifically designed to make it easier to fill and to seal the ampoule with the paraffin stopper without damaging the solution.

2.2. Irradiations

The irradiations with high energy photons were performed using the beam of a Varian Clinac 1800 linear accelerator. In the 6 MV beam, the dosimeters were placed in a water phantom with their geometrical center positioned at a reference depth of 5 g/cm^2, with a source-surface-distance (SSD) of 100 cm and a field size of 10 cm × 10 cm at the phantom surface. At 18 MV, a depth of 10 g/cm^2 was used.

The irradiations with ^{60}Co gamma radiation were performed using an Eldorado therapy unit, model 78. In this case, the dosimeters were placed in a water phantom with their geometrical centre positioned at a reference depth of 5 g/cm^2, with an SSD of 80 cm and a field size of 10 cm × 10 cm at the phantom surface.

Previous measurements with a calibrated ionization chamber established the absorbed dose rate to water at the reference depth in a water phantom of dimensions 30 cm^3 × 30 cm^3 × 30 cm^3, using the IAEA's TRS-398. These measurements were traceable to the BIPM primary standard of absorbed dose to water. According to this Code of Practice, the absorbed dose to water, D_W, is determined according to:

$$D_w^Q = M_{ref}^{corr} k_Q N_{D,w}^{^{60}Co} \quad (1)$$

where

M is the ionization chamber reading corrected for ion recombination, polarity, and to standard conditions of temperature and pressure;

$N_{D,w}^{^{60}Co}$ is the absorbed dose to water calibration coefficient of the reference chamber obtained from the standard laboratory in the reference beam quality, ^{60}Co γ radiation;

k_Q is the beam quality conversion factor, to take into account the differences in chamber response with beam quality.

At the time of calibration, the absorbed dose rate to water was about 0.5 ± 0.0025, 1 ± 0.011 and 1.8 ± 0.020 Gy/min, at ^{60}Co, 6 and 18 MV photon beams, respectively. Uncertainties were calculated in accordance with the International Organization for Standardization (ISO) Guide [8] and provided to a level of confidence of approximately 68% (using k = 1).

2.3. Dose and energy response

The dose and energy response of the prepared dosimeter were studied by irradiating the dosimeter with a range of doses from 5 Gy to 25 Gy at the

reference depth in water for ^{60}Co γ rays, 6 and 18 MV photon beams. The procedure was repeated five times to check the reproducibility of the dosimeter. The readings obtained are tabulated in Table 1. The dose response of the dosimeter was verified by plotting the measured optical density against the exposed dose, as shown in Fig. 1.

2.4. Spectrophotometric measurements

The absorbance readings of ferrous sulphate solution are carried out by a Varian Cary 100 UV-VIS spectrophotometer. Absorbance readings are made at a wavelength of 303 nm with a bandwidth of 1.5 nm, using a quartz microcell having a path length of 10 mm, and an optical window 4 mm wide and 20 mm high. After each absorbance reading the cell is cleaned with ultrapure water.

3. RESULTS AND DISCUSSION

3.1. Calibration curve

Figure 1 shows the absorbance of ferrous sulphate solution versus absorbed dose in the interval 5–25 Gy. This absorbed dose calibration curve is linear with a correlation coefficient R^2 equal to unity within 10^{-4} and the intercept of the resulting linear fit equal to zero within the uncertainty. The linear interval tested is consistent with the results cited in the literature and is adequate for radiotherapy purposes.

TABLE 1. REPRODUCIBILITY CHECK CARRIED OUT WITH THE FRICKE DOSIMETER

Dose (Gy)	^{60}Co		6 MV		18 MV	
	Mean[a]	SD[b] (%)	Mean	SD	Mean	SD
5	0.0179	0.58	0.0177	0.58	0.0187	0.60
10	0.0348	0.24	0.0347	0.24	0.0366	0.25
15	0.0537	0.33	0.0535	0.35	0.0542	0.33
25	0.0900	0.28	0.0901	0.30	0.0913	0.30

[a] Represent the mean value of five readings of ΔA.
[b] Experimental standard deviation of ΔA obtained using five dosimeters irradiated at the same dose.

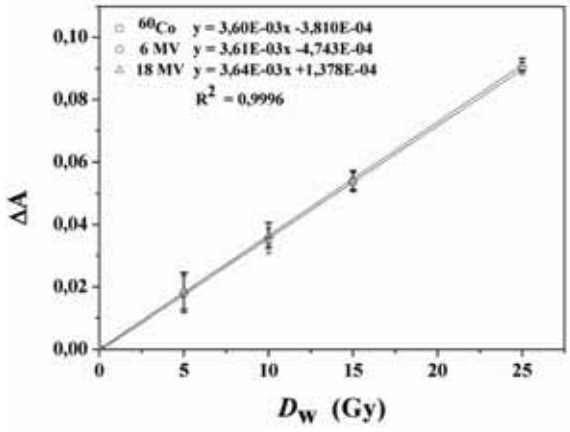

FIG. 1. Calibration curve for the Fricke dosimeter at ^{60}Co, 6 MV and 18 MV photons.

3.2. Precision (reproductibility)

Table 1 shows the results of the reproducibility check carried out with the Fricke solution prepared freshly for one day and irradiated at ^{60}Co, 6 MV, 18 MV photon beams. The standard deviation of the mean is found to be less than 0.6%. It was concluded that the prepared ferrous sulphate solution is reproducible, and its precision is not significantly dependent on the quality of radiation.

3.3. *G* value determination

$G(Fe^{3+})$ calculations were performed using the formula is that given in Ref. [9]

$$D_w = \frac{\Delta A}{G\,\varepsilon\,\rho\,l}\,f\,P_{wall} \Rightarrow G = \frac{\Delta A}{D_w\,\varepsilon\,\rho\,l}\,f\,P_{wall} \qquad (2)$$

where

D_w is the dose–to-water (Gy) as measured by the reference ionization chamber;

ΔA is the difference in absorbance between the irradiated and unirradiated ferrous sulphate solution. The absorbance readings are corrected for the influence of both the readout temperature, T_R, and the irradiation temperature, T_i [10]. The reference temperature is 25°C;

ε is the molar extinction coefficient (220.1 $mol^{-1} \cdot m^2$ determined in this work);
ρ is the density of the Fricke solution (1.024 g/cm^3);
l is the length of the light path of the cuvette (0.01 m);
G is the radiation yield of ferric ions;
f is the absorbed dose conversion factor which converts the dose to Fricke solution in a wall-less vessel to the dose to water (1.003 is the mean value taken from the Ref. [9]);
P_{wall} is a perturbation correction factor that accounts for the effect of the wall material of the Fricke vial.

In this work, the P_{wall} values are determined using the data obtained from Monte Carlo calculations for P_{wall} given in Ref. [9] for NPL vials, because these vials are similar to those used in our laboratory. To facilitate their use, these data have been fitted to a simple linear expression in terms of the tissue-phantom ratio, TPR_{10}^{20}:

$$P_{wall} = 1.02076 - 0.04002\ (TPR_{10}^{20}) \quad (3)$$

The values of TPR_{10}^{20} for radiation qualities investigated in this work are measured and are found to be 0.663, 0.784 and 0.573 for 6 MV, 18 MV and ^{60}Co, respectively. Substitution of these values into Eq. (3) yield P_{wall} values of 0.9942, 0.9894 and 0.9978, for 6 MV, 18 MV and ^{60}Co, respectively. Using the slope ($\Delta A/D_W$) of the line from Fig. 1 for each radiation quality, and the values of all parameters cited above, $G(Fe^{3+})$ is calculated using Eq. (2). The G values are found to be 1.598, 1.597 and 1.603 μmol/J at ^{60}Co, 6 and 18 MV photon beams, respectively.

3.4. Uncertainty analysis

Many factors affect the radiation yield $G(Fe^{3+})$, some of which have been identified and their effect evaluated in terms of uncertainties is analysed. The overall uncertainty is calculated according to the Ref. [8].

As can be seen in Table 2, the overall uncertainty over the $G(Fe^{3+})$ for ^{60}Co is 0.72% (1σ).

Estimated uncertainties over the $G(Fe^{3+})$ value for high energy X rays are evaluated following the same process as for ^{60}Co γ rays. Because of the additional uncertainty component due to the beam correction factor k_Q in Eq. (1), which is about 1% [1], the overall uncertainty for the value of $G(Fe^{3+})$ is 1.2%.

TABLE 2. UNCERTAINTY BUDGET FOR THE $G(Fe^{3+})$ OBTAINED AT A REFERENCE DEPTH IN WATER AT ^{60}Co

Source of uncertainties	Type A (%)	Type B (%)
1 Factors influencing the reference D_w		
$N_{D,w}$ calibration coefficient reported by IAEA[a]		0.49
Dosimeter reading[b]	0.01	
Constancy of the ionzation chamber[c]		0.10
Temperature: diff. between $T°$ inside cavity[d]		0.06
thermometer resolution		0.02
Pressure[e]		0.06
2 Factors influencing Fricke solution	0.2	
ΔA measurement[f]		0.20
T_{irr} correction[g]		0.20
T_{read} correction[h]		0.30
ε measurement[i]		0.10
ρ[j]		0.17
l[k]		0.05
f[l]		0.05
p_{wall}[m]		
Quadratic sum	0.20	0.69
Relative combined standard uncertainty	**0.72**	

[a] The value is given in the calibration certificate issued by IAEA dosimetry laboratory.

[b] For the reference measurements, a series of 20 readings is taken, and the standard deviation of the mean obtained is of the order 0.01%.

[c] Constancy of the secondary standard is obtained by evaluating the long-term stability of the secondary standard system.

[d] The standard deviation for the temperature reading is assumed to be 0.1°C. It is also assumed that the real temperature inside the chamber air cavity does not deviate by more than 0.3°C from the measured temperature Assuming a rectangular distribution, the uncertainty (taken as type B) is evaluated to be 0.02% and 0.06%.

[e] The pressure is measured with a classic barometer. When compared with a mercury absolute barometer, its readings are within ± 0.1%. Assuming a rectangular distribution, the type B relative uncertainty is 0.06%.

[f] Typical experimental standard deviation of the mean of ΔA obtained using five dosimeters irradiated at the same dose.

[g,h] The standard deviation for the temperature reading is assumed to be 0.1°C. Also assuming a rectangular distribution, the type B relative uncertainty is 0.2 for both corrections.

[i] The relative standard uncertainty over the determination of the molar extinction coefficient

[j] The density of the Fricke solution.

[k] The length of the light path of the cuvette is assumed to be within ±0.03 mm. Assuming a rectangular distribution, the type B relative uncertainty is 0.17%.

[l,m] The uncertainties on the calculated values of f and p_{wall} are around 0.05% taken from Ref. [9] and are reported as a type B uncertainty.

Values are assigned of 1.598 (± 0.012), 1.597 (± 0.020) and 1.603 (± 0.020) μmol/J at ^{60}Co, 6 and 18 MV photon beams, respectively. It should be noted that the results obtained are characterized by a low random uncertainty, resulting from a very good reproducibility of the ionometric and chemical measurements (with relative random uncertainties for the level of probability 68% equal to 0.01% and 0.2%, respectively).

The comparison of this result with the most recently published values (Klassen et al., 1999) seems to be delicate because since the determinations of $G(Fe^{3+})$ are based on spectrophotometric measurements at the same wavelength, the obtained values are directly function of values of the molar extinction coefficient $\varepsilon(Fe^{3+})$. Nevertheless, in order to remove all possibility of systematic errors on the values of this parameter, and to make the results more readily comparable with those from the literature, it is better to consider the values of the product $\varepsilon G(Fe^{3+})$. These values are calculated using Eq. (2) and are given in Table 3.

4. CONCLUSION

An experimental set-up and a measurement and data analysis procedure have been described, which allows to measure the value of $G(Fe^{3+})$ in the range of 5–25 Gy. From the authors' experience, for 5 Gy (lower limit) and above, a standard measurement reproducibility of ΔA within one day of 0.5% or better can be achieved with the measurement and analysis procedure presented. Moreover, as can be seen in Table III, the results obtained for the values of $\varepsilon G(Fe^{3+})$ agreed to within uncertainty with published values. Based on this result, the authors' Fricke dosimetry system is found to be suitable for carrying out the calibration and the determination of absorbed dose in water in high energy photon beams.

TABLE 3. COMPARISON OF VALUES OF $\varepsilon G(Fe^{3+})$ DETERMINED IN PHOTON BEAM

Reference	Radiation Quality	Method	ε (Fe^{3+}) (m^2/mol)	G (Fe^{3+}) (μmol/J)	εG (Fe^{3+}) (cm^2/J)
Klassen (1999)	^{60}Co	SEWC	217.4	1.613	3.506
Klassen (1999)	20 MV	SEWC	217.4	1.625	3.532
Present work	^{60}Co	Ion.ch	220.1	1.598	3.518
Present work	6 MV	Ion.ch	220.1	1.597	3.516
Present work	18 MV	Ion.ch	220.1	1.603	3.527

ACKNOWLEDGMENTS

Grateful acknowledgement is made to Dr. B. Hocini for allowing the authors to use their hospital's equipment. We would also like to thank the radiophysicists for their help in making the measurements.

REFERENCES

[1] INTERNATIONAL ATOMIC ENERGY AGENCY, Absorbed Dose Determination in External Beam Radiotherapy: An International Code of Practice for Dosimetry Based on Standards of Absorbed Dose to Water, Technical Reports Series No. 398, IAEA, Vienna (2000).

[2] AMERICAN ASSOCIATION OF PHYSICISTS IN MEDICINE, A Protocol for the Determination of Absorbed Dose from High-Energy Photon and Electron Beams, TG-21, Med . Phys. **10** (1983) 741–71.

[3] INTERNATIONAL COMMISSION ON RADIATION UNITS AND MEASUREMENTS, Radialion Dosimetry: Electron Beams with Energies Between 1 and 50 MeV, publication 35, Bethesda MD(1984a).

[4] SVENSSON, H., BRAHME, A., Acta Radiol. Ther. Phys. Biol. **18 (1979)** 326.

[5] COTTENS, E., et al., Proc. Symp. on Biomedical Dosimetry: physical (1980).

[6] DAVIES, J.V., LAW, J., Practical aspects of ferrous sulphate dosimetry, Phys. Med. Biol. **8** (1963) 91–6

[7] KLASSEN, N.V., et al., Fricke dosimetry: the difference between $G(Fe^{3+})$ for ^{60}Co-rays and high-energy x-rays Phys. Med. Biol. **44** (1999) 1609–1624.

[8] INTERNATIONAL ORGANIZATION FOR STANDARDIZATION, Guide to the Expression of Uncertainty in Measurement, 2nd ed. Geneva (1995).

[9] MA, C.-M., et al., Wall correction and absorbed-dose conversion factors for Fricke dosimetry: Monte Carlo calculations and measurements, Med. Phys. **20 (**1992) 283–92

[10] SHORT, K.R., The temperature dependence of $G(Fe^{3+})$ for the Fricke dosemeter, Phys. Med. Biol. 10 (1989) 1923–6.

REFERENCE DOSIMETRY AND COMPARISONS IN BRACHYTHERAPY

(Session 3)

Chairperson

J. VENSELAAR
European Society for Therapeutic Radiology and Oncology

Co-Chairperson

D. VAN DER MERWE
South Africa

NEW BRACHYTHERAPY STANDARDS PARADIGM SHIFT

M.P. TONI
Istituto Nazionale di Metrologia delle Radiazioni Ionizzanti,
ENEA, CR Casaccia, Rome, Italy
Email: mariapea.toni@enea.it

Abstract

The absorbed dose to water rate at short distances in water is the quantity of interest for dosimetry in radiotherapy, but no absorbed dose to water primary standards have been available to date for dosimetry of brachytherapy sources. Currently, the procedures to determine the absorbed dose imparted to the patient in brachytherapy treatments are based on measurements traceable to air kerma standards. These procedures are affected by an uncertainty that is larger than the limit recommended by the IAEA dosimetry protocol (IAEA TRS 398 (2000)). Based on this protocol, the goal for the uncertainty of the dose delivered to the target volume should be within 5% (at the level of one standard deviation) to assure the effectiveness of a radiotherapy treatment. The international protocols for the calibration of brachytherapy gamma ray sources are based on the reference air kerma rate or the air kerma strength. The absorbed dose to water, in water at the reference position around a brachytherapy source is then calculated by applying the formalism of the protocols based on a conversion constant, the dose rate constant Λ, specific for the characteristics and geometry of the brachytherapy source. The determination of this constant relies on Monte Carlo simulations and relative measurements performed with passive dosimeters, and therefore it is typically affected by large uncertainties, larger than 5% (at the level of one standard deviation). The conversion procedure needed for brachytherapy dosimetry is a source of additional uncertainty on the final value of the absorbed dose imparted to the patient. It is due to a lack of metrology standards that makes dosimetry of brachytherapy sources less accurate than dosimetry of external radiation beams produced by ^{60}Co sources and accelerators currently used in external beam radiotherapy. This paper reviews the current developments of absorbed dose to water primary standards for brachytherapy and the rationale for the choice of the measuring quantity in brachytherapy dosimetry. Once the new standards will be validated through comparison, an updated international protocol can be promoted for dosimetry in brachytherapy based on absorbed dose to water standards in place of the current air kerma standards. A gradual shift towards a more direct and accurate traceability chain of brachytherapy sources can be encouraged, according to the demand for a sounder metrology to minimize the final uncertainty in patient dose delivery.

1. INTRODUCTION

Over recent years, the availability of afterloading technology and the introduction of artificial radionuclides have increased the use of brachytherapy

(BT) in terms of the number of cancer patients treated by BT and in terms of typology of the clinical treatments. The increase in BT patients from 1997 to 2002 in the European area was about 10% [1]. About 10% of cancer patients who receive radiotherapy are treated by BT as the main treatment or as the boost treatment to increase the efficacy of the main treatment [1]. In particular, the availability of afterloading technology has increased the use of high dose rate (HDR) BT: during the reference year 2002, about 70% of BT treatments in Europe were performed using HDR sources such as ^{192}Ir [1]. Fractionated HDR BT treatments replaced some traditional low dose rate (LDR) BT treatments as in intracavitary BT for gynaecological tumour sites [2]. On the other hand, the interstitial BT with implanted low dose rate (LDR) sources — such as ^{125}I or ^{103}Pd seeds — has become an increasingly popular treatment for localized prostate cancer, allowing a cancer control comparable to the other techniques with better quality of life results. In the United States of America, the treatments of low and intermediate risk prostate cancer using LDR BT sources have increased from less than 5000 in 1995 to between 40 000 and 60 000 in 2002. This corresponds to about 30–40% of all eligible patients diagnosed annually in the USA for prostate cancer [2]. The increased clinical use of low energy photon-emitting BT sources led to the development of new source models: from the two seed models addressed in 1995 by the consensus dosimetry data sets published in the original international American Association of Physicists in Medicine (AAPM) Task Group 43 protocol [3] to the seven seed models in the 2004 protocol update [4, 5] and the 15 seed models in the 2007 protocol supplement [6].

The increasing use of high quality BT treatment calls for a more accurate dosimetry of the dose imparted to cancer patients, based on absorbed dose primary standards in order to optimize the final uncertainty in patient dose delivery. The absorbed dose rate to water in water, D_w, is the quantity of interest for dosimetry in radiotherapy, which includes either the dosimetry of external radiation beams, such as those produced by accelerators or ^{60}Co sources, or the dosimetry of BT sources. Patient dosimetry and algorithms for treatment planning dose calculation — in current radiotherapy treatments — are based on the quantity D_w. Moreover, the dose imparted to cancer patients must be known within a narrow band of uncertainty to avoid either damage to the healthy tissue resulting from exceeding international accepted tolerance levels or lack of tumor control due to a low dose delivered to the target volume. The goal for the uncertainty of the dose delivered to the target volume – taking into account the additional uncertainties in dose calculation algorithms – should be around 5% (at the level of one standard deviation), to assure the effectiveness of the radiotherapy treatment [7]. To achieve this goal and avoid undesirable additional uncertainties, a direct traceability chain is recommended starting on absorbed dose to water primary standards [7]. Absorbed dose primary standards are

currently operating for dosimetry of external radiation beams used in radiotherapy, but no absorbed dose primary standards have yet been made available to assure a direct traceability in dosimetry of the radioactive gamma ray sources used in current BT treatments. In this field of clinical treatment of cancer, the procedures to determine D_w are not directly based on absorbed dose standards, but rather on measurements traceable to air kerma standards. In fact, the recommended quantity for the calibration of BT gamma ray sources is the reference air kerma rate, $\dot{K}_R$, defined as the air kerma rate, at the reference distance of 1 m from the radioactive source, corrected for air attenuation and scattering [8]. The value of D_w around a BT source is currently calculated by a conversion procedure that applies the formalism of the international AAPM Task Group 43 protocol [3] and its updates [4–6]. This protocol is based on measurements of the air kerma strength, S_K, a quantity that is numerically equivalent to $\dot{K}_R$, at a distance of 1 m from the source. The value of S_K is converted to the value of the absorbed dose $D_{w,1\ cm}$ at a reference distance of 1 cm from the source located at the centre of a cubic water phantom with dimension of 30 cm. The value of the conversion factor — the dose rate constant Λ — is characteristic for the source and must be determined for each source model used clinically.

The determination of S_K is typically affected by an uncertainty within 1% (at the level of one standard deviation) [9–12]. The determinations of Λ are mainly the result of Monte Carlo calculations or a few relative measurements performed with passive dosimeters. Therefore, these factors are typically affected by an uncertainty of about 5% (at the level of one standard deviation) associated with the Monte Carlo determinations up about 10% (at the level of one standard deviation) associated with the experimental determinations [4, 10, 12]. Recent uncertainty estimates indicate a figure of 2.5% (at the level of one standard deviation) for the $D_{w,1\ cm}$ determination using the TG-43 protocol with a HDR BT source of ^{192}Ir [12]. This value can be regarded as a lower limit, as the uncertainty on $D_{w,1\ cm}$ is typically not less than 5% (at the level of one standard deviation) in BT dosimetry. The corresponding value is about 2% (at the level of one standard deviation) in dosimetry of external beams produced by clinical accelerators [7]. This situation makes BT dosimetry less accurate than dosimetry of clinical accelerators. Taking into account the additional uncertainties in algorithms for treatment planning dose, the procedures to determine the absorbed dose imparted to the patient in BT treatments are currently affected by an uncertainty up to 8% (at the level of one standard deviation). Deviations of 8% between administered and prescribed doses are expected to be clinically significant in the light of the above mentioned limit of 5% (at the level of one standard deviation) for the dose delivered to the target volume at clinical level. A significant part of this uncertainty is due to a lack of metrology, because the conversion procedure

needed for BT dosimetry is an additional source of uncertainty on the final value of the absorbed dose imparted to the patient.

Many national medical associations and scientific international organizations such as the European Society for Therapeutic Radiology and Oncology (ESTRO), Brachytherapy Subcommittee (AAPM-BTSC), the IAEA, the International Commission on Radiation Units and Measurement and the Bureau International des Poids et Mesures started research programmes in the field of BT and have encouraged the metrological community to develop absorbed dose standards for BT. Some relevant initiatives launched in recent years in response to this request are well advanced, as described in Section 2.

Based on the current developments of absorbed dose to water primary standards for BT, this paper reviews the rationale for the choice of the measuring quantity in BT dosimetry and encourages progress towards a paradigm shift for a more direct and accurate traceability chain of BT sources according to the demand for a more sound metrology, and for the optimization of radiation therapy dose delivery in BT.

2. THE PROJECT BRACHYTHERAPY WITHIN THE EUROPEAN METROLOGY RESEARCH PROGRAMME

According to the recommendation of national medical associations and scientific international organizations, several European national laboratories joined efforts aiming at establishing a more accurate metrological basis for the dosimetry of radioactive sources used for BT treatments in radiotherapy based on absorbed dose to water primary standards. In July 2008, the three-year Joint Research Project Brachytherapy was started within the European Association of National Metrology Institutes (EURAMET e.V.) with the support of the European Commission in the Seventh Framework Programme. The project responds to the need that the dose measurements in the clinical use of the radiation sources for BT be traceable to absorbed dose to water primary standards and that the uncertainty on the dose delivered to the target volume, at clinical level, be within 5% (at the level of one standard deviation) [13]. The European project group consists of the following European National Metrology Laboratories: Bundesamt für Eich- und Vermessungswesen (BEV, Physikalisch-technischer Prüfdienst, Vienna, Austria), Czech Metrology Institute, Inspectorate for Ionising Radiation (CMI, Prague, Czech Republic), Istituto Nazionale di Metrologia delle Radiazioni Ionizzanti (INMRI), Agenzia nazionale per le nuove tecnologie, l'energia e lo sviluppo economico sostenibile (ENEA, Roma, Italy), Instituto Tecnológico e Nuclear (ITN-LMRI, Sacavém, Portugal), Laboratoire National Henri Becquerel (LNE-LNHB, Gif-sur-Yvette, France), Van Swinden

Laboratorium (VSL, B.V., Delft, Netherlands), National Physical Laboratory (NPL, Teddington, United Kingdom), PTB (Physikalisch-Technische Bundesanstalt, Braunschweig, Germany), Swedish Radiation Safety Authority (SSM, Stockholm, Sweden) and the Radiation Metrology Laboratory (STUK, Radiation and Nuclear Safety Authority, Helsinki, Finland). Collaboration with regard to research activities was also formalized with PTW Freiburg (Germany), Linkoping University (Sweden) and IBA Dosimetry GmbH (Germany). A scientific collaboration has begun with the BRAPHYQS group of GEC-ESTRO as representative of the project end-users.

In particular, seven independent standard instruments have been developed within the project. Two distinct groups of standard instruments, described in Sections 3 and 4, based on different methods of measurement have been developed for the realization of $D_{w,1\ cm}$ close to LDR (^{125}I and ^{103}Pd seeds) and HDR (^{192}Ir) BT sources, respectively. The standards constructed within each group are different in measurement procedure and/or design, in order to highlight possible systematic errors and together give a more robust determination of $D_{w,1\ cm}$. Standard design are specific for measurements of absorbed dose to water at clinically relevant distances with photon-emitting BT sources. These new absorbed dose standards allow the determination of reference values for the absorbed dose to water at the reference distance of 1 cm LDR and HDR BT source which will be determined with a target value for the best relative measurement uncertainty on $D_{W,1\ cm}$ within 2% (at the level of one standard deviation).

Preliminary comparisons among the LDR and HDR standards were already started in July 2010, and results should be available by June 2011.

Once these new BT absorbed dose standards are validated by comparison, an updated calibration chain can be implemented, by calibration of the current well type ionization chambers (the ‘dose calibrators’) directly in terms of $D_{w,1\ cm}$ against the new standards.

3. ABSORBED DOSE TO WATER PRIMARY STANDARDS FOR PHOTON LDR BRACHYTHERAPY SOURCES

The standards developed within the project Brachytherapy for measurement with LDR BT sources are based on ionometry, this method being most sensitive to low intensity sources. Although only the water calorimetry allows the direct determination of the absorbed dose to water in a water phantom, this method is not applicable to the measurement of low intensity BT sources. Three independent designs of large angle ionization chambers have been developed by ENEA–INMRI (see Fig. 1), LNE-LNHB (see Fig. 2), and PTB (see Fig. 3). The

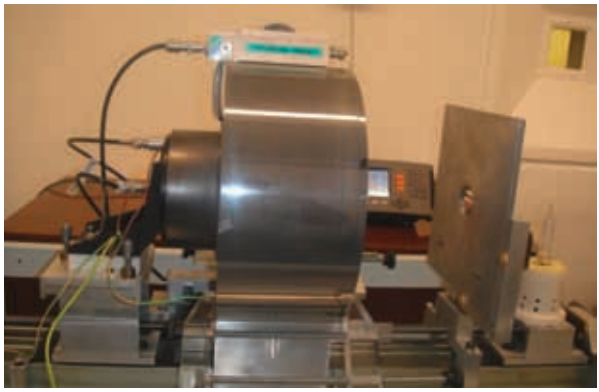

FIG. 1. The ENEA–INMRI standard for LDR BT sources based on a large angle and variable volume ionization chamber, in graphite phantom. The movable piston to vary chamber volume is shown on the left and the BT source positioned on the rotating source holder is shown on the right.

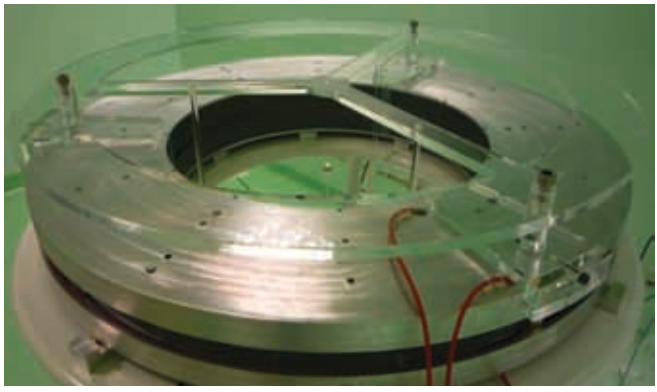

FIG. 2. The LNE-LNHB standard for LDR BT sources based on a free-in-air ring shaped ionization chamber with the 1 cm radius water equivalent spherical phantom placed in air in its centre and containing the LDR BT seed.

determination of $D_{w,1\ cm}$ is based on a two-step procedure. First, a measurement of water kerma in water equivalent or graphite phantom is obtained from measurements of the ionization current of the standard ionization chamber. Conversion factors, based on Monte Carlo simulations, are then applied to obtain the value of $D_{w,1\ cm}$.

The LDR BT standard constructed by the ENEA-INMRI is based on a large angle and variable volume ionization chamber in graphite phantom. The chamber consists of an extrapolation chamber operating in ‘wall-less air chamber’

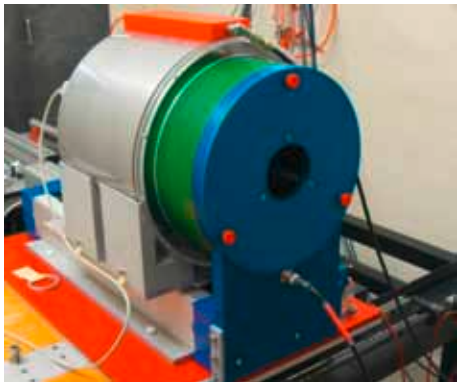

FIG. 3. The PTB standard for LDR BT sources based on a large air filled parallel plate extrapolation chamber with water equivalent walls.

conditions by measuring the increment of ionization current for increment of chamber volume at chamber depths greater than the range of the secondary electrons produced in the chamber front window. The instrument is designed to measure the air kerma in a graphite phantom at an in-air distance of 30 cm from the radioactive source and at a depth in graphite equivalent to 1 cm of water, corresponding to the thickness of the entrance window of the chamber. Correction factors calculated by Monte Carlo code PENELOPE account in particular for the conversions factors needed to determine $D_{w,1\ cm}$. Relevant details on the standard are given in Ref. [14].

The LDR BT standard developed by the LNE-LNHB is based on a free-in-air ring shaped ionization chamber and a 1 cm radius water equivalent spherical phantom placed in air at the centre of the ring and containing the LDR BT seed in its centre. The chamber has a torus shape with rectangular cross-section to account for the radial anysotropy of the BT source and to have a large signal-to-noise ratio. In the first step, the water kerma is measured at the surface of the spherical phantom placed in air, then correction factors provided by Monte Carlo simulations are applied to account for the contribution of additional scattered photons when water replaces air as the surrounding medium. Relevant details on the standard are given in Ref. [15].

The new PTB standard for LDR BT sources consists of a large air-filled parallel plate extrapolation chamber with water equivalent walls. The entrance and the back plate of the extrapolation chamber are made of a water equivalent material, and its thickness defines the measurement depth within the water phantom. For the determination of the absorbed dose rate to water, a new algorithm was developed, allowing the calculation of $D_{w,1\ cm}$ from air kerma

measurements by Monte Carlo simulations without the need of considering the electron transport. A prerequisite for the use of this algorithm is that the limits of the measurement volume are at least one CSDA range greater than the irradiated volume. Relevant details on the standard and some preliminary results are given in Ref. [16].

The radial anisotropy of the LDR BT sources was accounted for by the circular geometry for the LNE-LNHB ionization chamber (Fig. 2) and by rotating the source during measurements in the case of both the ENEA–INMRI (see details in Fig. 1) and the PTB large angle ionization chambers.

4. ABSORBED DOSE TO WATER PRIMARY STANDARDS FOR PHOTON HDR BRACHYTHERAPY SOURCES

The standards developed within the project Brachytherapy for the realization of D_w close to HDR BT sources are based on calorimetry, as this direct method is very well applicable to high intensity sources. They include four independent designs of calorimeters for the measurement of HDR ^{192}Ir sources.

Two existing water calorimeters were implemented by PTB and VSL for use with the BT source brought inside the calorimeter (see Figs 4 and 5). This method allows the direct determination of the absorbed dose to water in a water phantom. Relevant details on the PTB and VSL standards and some preliminary results are given in Refs [17] and [18], respectively.

Two specially shaped graphite calorimeters have been developed by ENEA–INMRI and NPL, respectively. The procedures for the conversion from

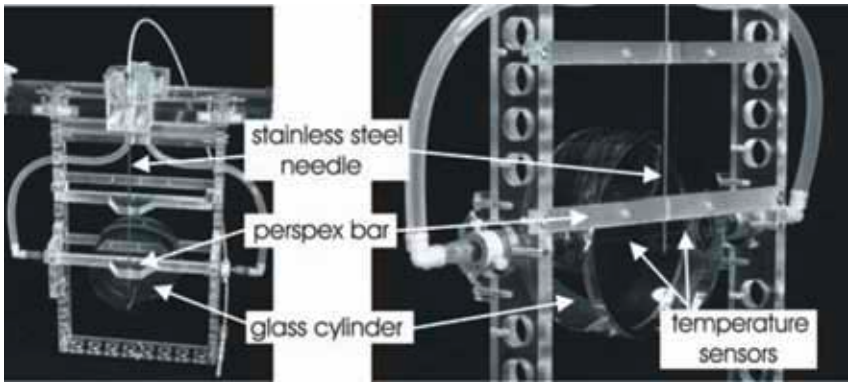

FIG. 4. Details of the PTB standard for HDR BT sources based on water calorimeter: calorimetric detector with additional bars to fix the stainless steel needle at both sides of the detector.

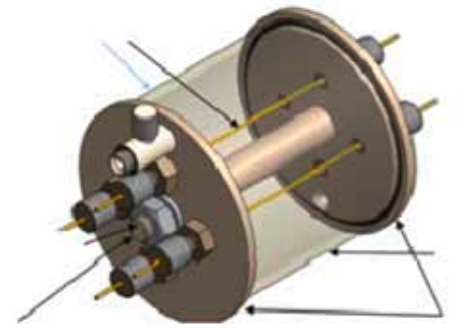

FIG. 5. Detail of the VSL standard for HDR BT sources based on water calorimeter: design of the high purity cell with an aluminium cylinder as heat sink, and four radially distributed thermistors to reduce the variations in dose related to variation in positioning.

the absorbed dose rate to graphite to the absorbed dose rate to water are well known and the use of in-graphite calorimetry associated with the in-water calorimetry increases the robustness of the system of standards.

The ENEA–INMRI calorimeter was designed to operate both in quasi-adiabatic and in isothermal mode. The dimensions of the calorimeter components (three body design) were derived from both Monte Carlo simulations (EGSnrc) and heat transfer simulations (COMSOL Multiphysics). The calorimeter will consist of a 25 mm diameter annular core, 2 mm thick and 5 mm high, surrounded by a jacket and a medium (graphite disc). The three components are surrounded by a PMMA vacuum housing and the disc shaped calorimeter (see Fig. 6) is inserted in a large graphite phantom. NTC thermistors, 0.3 mm in diameter, are embedded in the core and in the jacket to be operated either as sensors or as heaters. Relevant details on the standard are given in Ref. [14].

The NPL developed a prototype graphite calorimeter that allows the measurement of the absorbed dose to graphite at a reference distance of 2.5 cm from the HDR ^{192}Ir source. This quantity is converted to the quantity of interest, absorbed dose to water at 1 cm along the transverse axis of the source. The annular core of the calorimeter is 2 mm thick, 5 mm high and has a mean radius of 25 mm. For the operation in isothermal mode, eight small thermistors (four sensors and four heaters) are embedded in the graphite core (Fig. 7).

The graphite ring is separated from the surrounding cylindrical graphite phantom (20 cm diameter, 14 cm height) by a 1 mm vacuum gap. The vacuum gap is needed to minimize the heat transfer from the core (point of measurement) to the environment and to control for the self-heating of the radioactive source. A vacuum can surrounds the graphite assembly and the BT source will be inserted into the graphite phantom through an aluminium tube. Both the gamma spectrum

FIG. 6. The ENEA–INMRI graphite calorimeter (13 cm diameter, 11 cm height). The calorimeter is inserted in a larger graphite phantom (20 cm diameter, 20 cm height, not shown) to ensure full backscattering conditions for ^{192}Ir radiation at the core position.

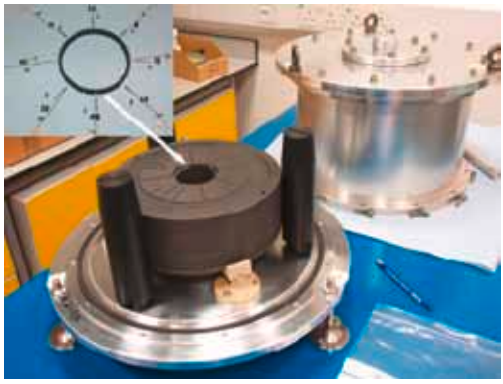

FIG. 7. Details of the NPL standard for HDR BT sources based on graphite calorimeter: Top left: ring-shaped graphite core with heating and sensing thermistors. The white arrow indicates the position of the graphite core in the calorimeter.

and the beta spectrum of the ^{192}Ir source were considered in the Monte Carlo simulations. Relevant details on the standard are given in Ref. [19].

An additional and interesting standard for direct measurements of absorbed dose to water with HDR ^{192}I BT sources has been realized by Sarfehnia and Seuntjens, as described in Ref. [20], which provides relevant details and preliminary results. This standard is based on a 4°C stagnant water calorimetry The estimated overall uncertainty on this standard is 1.90% (at the level of one standard deviation).

5. RATIONALE FOR A PARADIGM SHIFT

No absorbed dose primary standards are currently used to calibrate BT sources, and the conversion procedure needed for BT dosimetry is a source of additional uncertainty on the final value of the absorbed dose imparted to the patient. This situation was due to a lack of metrology: no absorbed dose primary standards have yet been made available to assure a direct traceability in dosimetry of BT sources. The development of standards for the realization of the absorbed dose to water due to BT sources and their validation are the first steps towards an implemented traceability chain starting on direct measurements of absorbed dose to water and lend support to change the quantity used at present to calibrate BT sources. The advantage of using the same quantity — the absorbed dose to water — and experimental conditions as the end user for calibration of radiotherapy dosimeters were already stressed in Refs [7] and [21]. The various steps between the calibration of BT sources in terms of the quantity reference air kerma or air kerma strength at the standard dosimetry laboratory and the determination of D_w at hospitals using dosimetry protocols introduce undesirable uncertainties in the measurement of D_w. The starting point of the calibration already involves a considerable additional uncertainty arising from the conversion procedure needed to obtain D_w from measurements of $\dot{K}_R$ or S_K. This contribution from the first step in BT dosimetry chain does not yet comply with the demand of accuracy to minimize the final uncertainty in patient dose delivery. Moreover, as pointed out also in Ref. [12], there is a significant added value in calibrating sources directly in terms of D_w. In fact, direct absorbed dose to water calibrations are less sensitive to the details of the source geometry.

After the validation by comparison of the D_w standards described in Sections 3 and 4, a more direct traceability chain for BT sources based on these new standards can be established with a reduced uncertainty for BT dosimetry. The new BT standards of D_w can be transferred to secondary standard dosimetry laboratories (SSDL) through calibration of reference dosimeters directly against the standards. There is no need to change the SSDL reference dosimeters, the current well type ionization chambers can be calibrated directly in terms of D_w instead of in terms of K_R. Finally, the dissemination process reaches the end users through calibration of hospital dosimeters carried out at the SSDL directly in terms of D_w.

In this way, the BT dosimetry system will be coherent with the dosimetry system of the other radiotherapy beams based on absorbed dose to water. Moreover, an extension of the international protocols for dosimetry in BT can be promoted, based on absorbed dose standards.

6. CONCLUSIONS

This work describes progress towards a more accurate traceability chain for photon-emitting BT sources based on direct measurements of absorbed dose to water. In particular, the activities undertaken within the European joint research project Brachytherapy are described. A number of absorbed dose to water primary standards have been developed for direct calibration of LDR (^{125}I and ^{104}Pd) and HDR (^{192}Ir) BT sources. These standards will be commissioned shortly, after their validation by comparison. The developments of BT absorbed dose standards and their validation represent concrete progress towards a more direct and accurate traceability chain of BT sources according to the demand for low uncertainty to minimize the final uncertainty in patient dose delivery. Moreover, an extension of the international protocol for dosimetry in BT can be promoted, based on absorbed dose standards. In this way, the BT dosimetry system will be coherent with the dosimetry system of the other radiotherapy beams based on absorbed dose to water.

ACKNOWLEDGEMENTS

The research within the EURAMET joint research project Brachytherapy receives funding from the European Community's Seventh Framework Programme, ERA-NET Plus, under the iMERA-Plus Project – Grant Agreement No. 217257.

The author would like to thank the partners of the Brachytherapy project for their support to this contribution and in particular: I. Aubineau-Lanièce (CEA, LIST, Laboratoire National Henri Becquerel, France), T. Sander (National Physical Laboratory, United Kingdom), H.J. Selbach (Physikalisch-Technische Bundesanstalt, Germany), J. de Pooter (Van Swinden Laboratorium B.V., Netherlands).

REFERENCES

[1] GUEDEA, F., et al., Overview of brachytherapy resources in Europe: A survey of patterns of care study for brachytherapy in Europe, Radiother Oncol **78** (2007) 50.

[2] THOMADSEN, B.R., et al., Anniversary Paper: Past and current issues, and trends in brachytherapy physics, Med. Phys. **37** (2008) 4708–4723.

[3] NATH, R., et al., Dosimetry of interstitial brachytherapy sources: Recommendations of the AAPM Radiation therapy Committee Task Group No.43. American Association of Physicists in Medicine. Med. Phys. **22** (1995) 209–234.

[4] RIVARD, M.J., et al., Update of AAPM Task Group No. 43 Report: A revised AAPM protocol for brachytherapy dose calculations, Med. Phys. 31 (2004) 633–674.
[5] RIVARD, M.J., et al., Update of AAPM Task Group No. 43 Report: A revised AAPM protocol for brachytherapy dose calculations, Med. Phys. 31 (2004) 3532–3533 (erratum)
[6] RIVARD, M.J., et al., Supplement to the 2004 update of AAPM Task Group No. 43 Report, Med. Phys. **34** (2007) 2187–2205.
[7] INTERNATIONAL ATOMIC ENERGY AGENCY, Absorbed Dose Determination in External Beam Radiotherapy: An International Code of Practice for Dosimetry Based on Standards of Absorbed Dose to Water, Technical Reports Series No. 398, IAEA, Vienna (2000).
[8] THE INTERNATIONAL COMMISSION ON RADIATION UNITS AND MEASUREMENTS, Dose and volume specification for reporting interstitial therapy, ICRU Report No. 58 (1997).
[9] INTERNATIONAL ATOMIC ENERGY AGENCY, Calibration of Photons and Beta Ray Sources Used in Brachytherapy, IAEA-TECDOC-1274, IAEA, Vienna (2002).
[10] SOARES, C.G., et al., Primary standards and dosimetry protocols for brachytherapy sources, Metrologia **46** (2009) S80–S98.
[11] BIDMEAD, A.M., et al., The IPEM code of practice for determination of the reference air kerma rate for HDR ^{192}Ir brachytherapy sources based on the NPL air kerma standard, Phys. Med. Biol. **55** (2010) 3145–3159.
[12] SARFEHNIA, A., et al., Direct measurement of absorbed dose to water in HDR ^{192}Ir brachytherapy: water calorimetry, ionization chamber, Gafchromic film, and TG-43, Med. Phys. **37** (2010) 1924–1932.
[13] TONI, M.P., et al., A Joint Research Project to improve the accuracy in dosimetry of brachytherapy treatments, in the framework of the European Metrology Research Programme, 11th World Congress on Medical Physics and Biomedical Engineering, 7–12 September Munich, Germany (2009),.
[14] BOVI, M., et al., "La riferibilità nelle misure di dose assorbita dal paziente nei trattamenti di brachiterapia" (Atti del VI° Congresso "Metrologia & Qualità", Torino, 7–9 April (2009).
[15] AUBINEAU-LANIÈCE, I., et al., Absorbed dose reference for LDR brachytherapy — the LNE-LNHB approach. XIV Congrès International de Metrologie, Paris, June 2009), Collège Francais De Metrologie (2009).
[16] SCHNEIDER, T., et al., A new device for the measurement of the absorbed dose to water for low energy x-ray sources used in brachytherapy. 11th World Congress on Medical Physics and Biomedical Engineering, 7–12 September, Munich, Germany (2009).
[17] BAMBYNEK, M., et al., Calorimetric determination of absorbed dose to water for a ^{192}Ir HDR brachytherapy source in near-field geometry. 11th World Congress on Medical Physics and Biomedical Engineering, 7–12 September (2009), Munich, Germany.
[18] DE POOTER, J.A., et al., Effective reduction of uncertainty for water calorimetry of HDR sources, presentation at ESTRO annual meeting (2009), Maastricht.
[19] SANDER, T., et al., "Design and principles of a graphite calorimeter for brachytherapy", these Proceedings, Vol. 1.

[20] SARFEHNIA, A., et al., Developments of a water calorimetry-based standard for absorbed dose to water in HDR ^{192}Ir brachytherapy, Med. Phys. **37** (2010) 1914–1923.
[21] REICH, H., Choice of the Measuring Quantity for Therapy-level Dosemeters. Phys. Med. Biol. **24** 5 (1979) 895–900.

FROM REFERENCE AIR KERMA RATE TO NOMINAL ABSORBED DOSE RATE TO WATER: PARADIGM SHIFT IN PHOTON BRACHYTHERAPY

U. QUAST[a], T.W. KAULICH[b], A. AHNESJÖ[c], J.T. ÁLVAREZ-ROMERO[d], D. DONNARIEX[e], F. HENSLEY[f], L. MAIGNE[g], D.C. MEDICH[h], F. MOURTADA[i], A.S. PRADHAN[j], M.J. RIVARD[k], C.G. SOARES[l], G.A. ZAKARIA[m]

[a] Ex-Essen University Hospital, Essen, Germany
Email: ulrich.quast@uni-essen.de
[b] Department of Radiation Oncology, University Hospital Tübingen, Tübingen, Germany
[c] Department of Oncology, Uppsala University, Uppsala, Sweden
[d] ININ, SSDL Ionizing Radiation Metrology Department, Mexico City, Mexico
[e] Centre Jean Perrin, Unité de Physique Médicale, Clermont-Ferrand, France
[f] Department of Radiation Oncology, University Hospital, Heidelberg, Germany
[g] Clermont Université, Clermont-Ferrand, France
[h] Radiation Laboratory, University of Massachussetts, Lowell, Massachussetts, United States of America
[i] Department of Radiation Physics, University of Texas, Houston, Texas, United States of America
[j] Health, Safety, Environment Group, Bhabha Atomic Research Centre, Mumbai, India
[k] Deptartment of Radiation Oncology, Tufts University School of Medicine, Boston, Massachussetts, United States of America
[l] National Institute of Standards and Technology, Gaithersburg, Maryland, United States of America
[m] Department of Medical Radiation, Gummersbach Hospital, University of Cologne, Gummersbach, Germany

Abstract

In brachytherapy (BT), photon radiation sources are presently calibrated in terms of the reference air kerma rate $\dot{K}_\delta$ (or air kerma strength S_K). By direct source calibration in terms of $\dot{D}_{w,1}$, the nominal absorbed dose rate to water at the TG-43U1 reference position at 1 cm in water and with the ability to measure distributions of this quantity, the accuracy of clinical BT-dosimetry should increase due to decreased calibration uncertainties compared to present methods. Several $\dot{D}_{w,1}$ primary standards are under development for high energy, high dose rate and low energy, low dose rate sources. To provide worldwide traceability and guidance for clinical medical physicists, an ISO standardization project, Clinical Dosimetry — Photon Radiation Sources Used in Brachytherapy, is considered, in continuation of ISO 21439 (2009) for beta sources. Clear terms and definitions are fundamental. Reclassification of BT-photon radiation qualities is also needed, introducing a range of medium energy photons with mean energies between 40 keV and 150 keV. Radionuclide BT-sources and electronic X ray BT-sources, BT-detectors and BT-phantoms should be characterized by sets of reference data, through which the clinical medical physicist could critically evaluate the data supplied by the manufacturer, prior to clinical application. Plastic scintillators have the potential for transfer standards of high accuracy and for verification measurements of BT-source output in phantoms. Based on and extending the AAPM TG-43U1 formalism, this planned ISO-standard will provide guidance for clinical BT-dosimetry in terms of absorbed dose to water and for estimating the uncertainties.

1. INTRODUCTION

Photon brachytherapy (BT) is applied successfully for about 10% of all cancer patients requiring radiation therapy [1]. Following a general principle of clinical dosimetry, radiation sources for radiation therapy should be calibrated under physical conditions as close as possible to the clinical conditions. This is fulfilled for all radiation sources but photon BT-sources. Thus, also photon BT-sources should be calibrated in their vicinity and in terms of absorbed dose to water, D_w [2]. At present, D_w primary standards are under development in several countries [3–5] . This paradigm shift from the reference air kerma rate calibration to the nominal absorbed dose rate to water calibration, requires international traceability to the new primary standards and guidance for the clinical medical physicists, worldwide. Based on and extending the AAPM TG-43U1 formalism [6] and complimentary algorithms [7], an ISO standardization project on Clinical Dosimetry — Photon Radiation Sources Used in Brachytherapy, should best fulfil these tasks [8], in continuation of ISO 21439 for beta radiation sources [9]. In order to find consensus and support, the basic ideas of the planned ISO project have been presented at the 52nd Annual AAPM Meeting (Philadelphia, July 2010) [10], discussed in the AAPM BTSC (Bachytherapy Subcommittee) meeting and submitted to Medical Physics for publication as a Vision 20/20 article [8].

2. PLANNED NEW ISO STANDARDIZATION PROJECT

2.1. Scope

This planned ISO standard will specify methods for the determination of distributions of the absorbed dose to water D_w and its uncertainty required prior to the application of BT. The standard will cover the photon energy range from 5 keV (typical cut-off energy) to 1.5 MeV and absorbed dose rates between 0.001 Gy/min and >10 Gy/min. The BT-photon radiation qualities will be reclassified: low energy photons with mean energies $E_{avg} < 35$ keV, medium energy photons of 35 keV $\leq E_{avg} \leq 140$ keV, and high energy photons of $E_{avg} > 150$ keV; reflecting the rapid variation in the energy dependence of the mass energy absorption coefficient relative to water. In the future, BT-sources and BT-detectors should be calibrated in terms of the nominal absorbed dose rate to water at 1 cm in water, as $\dot{D}_{w,1}$ primary standards become available in the next few years. The methods of calibration and clinical dosimetry should also be extended to include electronic X ray BT-sources. Sources, detectors and phantoms in brachytherapy should be characterized by sets of reference data, including Monte Carlo (MC) simulation based primary and scatter separated dose data, and by their calibration data. For standardized procedures in clinical dosimetry, the reader is referred to the literature, e.g. reports of AAPM and ESTRO; thus, details of quality assurance and treatment planning will be outside the scope of this work, as are electrical, safety and radiation protection issues.

2.2. Contents: Clinical dosimetry — photon radiation sources for brachytherapy

The following list of contents of the required ISO standards is proposed:

(1) Scope
(2) Normative and informative references
(3) Terms and definitions
(4) Photon sources for brachytherapy and source characterization
(5) Calibration in terms of absorbed dose to water and traceability
(6) Dosimetry measurements
(7) Dose calculation
(8) Clinical dosimetry
(9) Uncertainty analysis

2.3. Terms and definitions

Clear terms and definitions are fundamental, examples of proposed concepts are:

Nominal absorbed dose rate to water
$\dot{D}_{w,1}$ mean absorbed dose rate to water around a circle in the transverse plane through the calibration reference point p_{ref} at r_0 = 1 cm at the date and time of calibration and under reference conditions

Low energy
⟨for brachytherapy⟩ radiation parameter for photon-emitting radiation sources with mean energies E_{avg} below 35 keV.
Note: AAPM TG 43 defines 50 keV as the boundary energy between low and high energy BT-photons.

Medium energy
⟨for brachytherapy⟩ radiation quality parameter for photon emitting radiation sources with mean energies E_{avg} between 35 keV and 140 keV.

High energy
⟨for brachytherapy⟩ radiation quality parameter for photon emitting radiation sources with mean energies E_{avg} above 140 keV.

Special transfer standard
Type of transfer standard restricted to special calibration conditions, yielding a quantity related to the average absorbed dose rate to water for a certain type (model) of radiation source.

2.4. Photon sources for brachytherapy and source characterization

In the intermediate, e.g. medium photon energy range (proposed boundary energies: 35–140 keV), rapid changes occur in the energy dependence of the mass energy absorption coefficients, μ_{en}/ρ, relative to water, different for diverse materials, causing dramatic variations with energy in the response of dosimetry detectors [8–11]. Thus, a reclassification of photon radiation qualities is proposed (see Table 1), allowing for more differentiated and energy specific recommendations than the present AAPM classification with only two groups of radiation qualities, below and above 50 keV [5].

TABLE 1. PROPOSED RECLASSIFICATION OF BRACHYTHERAPY PHOTON RADIATION QUALITIES[a]

Radiation quality	E_{avg} (keV)	Examples of BT-photon sources
Low energy	<35	^{125}I (LDR[b]), ^{103}Pd (LDR), ^{131}Cs (LDR), electronic X rays (HDR[c])
Medium energy	35–140	^{169}Yb (HDR), ^{170}Tm (HDR)
High energy	>140	^{192}Ir (LDR, HDR, PDR[d]), ^{137}Cs (LDR, HDR), ^{60}Co (HDR, PDR)

[a] The appropriate boundary energies have to be decided by the ISO WG.
[b] LDR: low dose rate.
[c] HDR: high dose rate.
[d] PDR: 'pulsed' high dose rate.

Many photon radiation sources have been applied: radionuclides emitting high energy gamma radiation (at high dose rates, HDR; at 'pulsed' high doserates, PDR; or at low dose rates, LDR) and radionuclides emitting low energy characteristic X rays (at LDR) (see Table 1). Recently, radionuclide BT-sources emitting medium energy photons (at HDR), and dedicated electronic X ray BT-sources (low energy at HDR) have been developed. The number of commercially available types of source has increased substantially in the last decades especially those with LE and LDR characteristics. The source reference data, specific to a source model and the source calibration data, specific to an individual photon source, must be determined and stated by the manufacturer and checked by the clinical medical physicist prior to clinical application [5, 12].

MC simulation is ideal to characterize photon radiation sources by their dose distribution patterns in a homogenous water medium [13]. Recently, very helpful and comprehensive databases have been established by Rogers and Taylor [14] and by Ballester and Pérez-Calatayud [15], providing the source parameter data required for the AAPM TG-43U1 formalism to characterize commercially available brachytherapy photon sources.

2.5. Calibration in terms of absorbed dose to water and traceability

Presently, calibrations of photon BT-sources are performed in terms of the reference air kerma rate $\dot{K}_\delta$ or air kerma strength S_K ($S_K = \dot{K}_\delta(d) \cdot d^2$, the product of $\dot{K}_\delta$, due to photons of energies greater than δ, and the square of the distance d). Usually, the absorbed dose rate to water at 1 cm distance along the orthogonal

bisector of the source`s long axis must be calculated with the AAPM TG-43 formalism

$$\dot{D}_{w,1} = S_K \cdot \Lambda \cdot \prod_i f_i , \quad (1)$$

where Λ is the dose rate constant and f_i are other dosimetric functions [6]. However, with the goal of reducing the uncertainty in clinical dosimetry of photon brachytherapy in the future, the quantity nominal absorbed dose rate to water at 1 cm in water $\left(\dot{D}_{w,1}\right)$ should be the calibration measure for all photon radiation BT-sources. Several $\dot{D}_{w,1}$ primary standards are under development for high energy, HDR and low energy, LDR BT-photon sources (see, for example, Refs [3–5]. Thus, in the future, transfer standards can be used as an intermediary to establish traceability to stated references, usually national or international measurement standards. They should be calibrated in terms of $\dot{D}_{w,1}$ through an unbroken chain of comparisons, all with stated uncertainties (and for continuity also in terms of $\dot{K}_\delta$ or S_K). This should be performed at a national metrology institute, e.g. NIST, PTB, NPL or at an accredited secondary standards dosimetry laboratory (SSDL).

An ideal transfer standard should enable the direct and absolute measurement of absorbed dose to water, if calibrated together with all required components: detector, calibration phantom, test source and required accessories, e.g. source holder inserts and source guides. The calibration phantom of an ideal transfer standard must be a water phantom, providing high positioning precision and sufficient backscatter for the calibration of BT-sources and detectors.

Special transfer standards [8] can be applied as a restricted type of transfer standard for special calibration, yielding a quantity related to the average absorbed dose rate to water for a certain type of radiation source and under specific calibration conditions [9]. For some transfer standards, a specially designed water equivalent phantom can be utilized.

For photon brachytherapy, presently three types of dosimeter arrangements can be considered for the dissemination of the new reference quantity, $\dot{D}_{w,1}$ [8]:

— Transfer standard:
  • Plastic scintillator dosimeters with precision calibration water phantom.
— Special transfer standards:
  • Well-type ionization chamber dosimeters;
  • Detector–phantom arrangements (utilizing ionization chambers, thermoluminescent detectors, or plastic scintillator dosimeters).

2.6. Dosimetry measurements

To permit the measurement of the absorbed dose to water with sufficiently small uncertainties, dosimetry detectors should have clearly defined properties, e.g. the effective point of measurement. For each type of dosimetry detector used in photon brachytherapy, the detector's reference data and calibration data must be determined and stated by the manufacturer. This must be considered by the clinical medical physicist for each type of BT-photon radiation field, and may be for each position and orientation of the dosimetry detector probe. The recommended reference medium is water.

For solid dosimetry phantoms, the complete set of phantom RD has to be determined and stated by the manufacturer and considered by the clinical medical physicist for each radiation quality applied.

For the dosimetry of photon radiation used in brachytherapy, many dosimetry detectors have been tested or applied [8]. TLDs and radiochromic films are widely used for the measurement of distributions of absorbed dose to water in the vicinity of photon radiation BT-sources. Both are not real-time reading methods, however, but require further processing to obtain the measured signal.

The plastic scintillation detector with high spatial ($\leq\pm 0.3$ mm) and high temporal resolution ($\leq\pm 0.05$ s for HDR photons) [8–11] has the potential for the direct and fast measurement of distributions of absorbed dose to water in water in high dose gradient fields in the vicinity of high energy (HDR, PDR and LDR), as well as of low energy, LDR (and HDR) photon radiation BT-sources.

2.7. Dose calculation

Reviews of limitations of AAPM TG-43U1 and dose calculation methods for brachytherapy, especially MC simulation based methods, are given in Refs [7] and [16].

MC simulation based dose calculations should be reported with all the necessary information provided to others active in the field to be able to reproduce the work performed, and to use the data in treatment planning algorithms [8, 9], particular attention should be given to the uncertainty of each function or constant determined.

2.8. Clinical dosimetry

There is a growing need for high precision, high resolution, direct reading and fast verification measurements of 3D-D_w and 4D-D_w distributions. The following source documents can be consulted for the performance of acceptance

tests for all types of radiation sources, dosimetry detectors and software used in clinical dosimetry of photon brachytherapy: existing documents [8–12] such as AAPM, ESTRO, ICRU, IAEA, IEC, and ISO reports or documents prepared by national associations, such as DIN, DGMP, NCS; an widely accepted teaching books, e.g. Refs [17] and [18]. Thus, details of quality assurance and treatment planning of photon brachytherapy will be outside the scope of this planned ISO standard.

2.9. Uncertainty analysis

The fundamental idea is that the proposed ISO standard will provide a more accurate methodology than the TG-43 formalism for the calculation and measurement of $\dot{D}_w$ dose distributions [7], taking advantage of the future availability of $\dot{D}_{w,1}$ primary standards with acceptable uncertainties, $u < 2.0\%$ ($k = 1$) at primary level [2], and yielding a combined uncertainty of the dose delivered to the target volume, $u_c \leq 5\%$ ($k = 1$) [2].

3. CONCLUSION: THE NEED FOR THE INTERNATIONAL STANDARDS ORGANIZATIONS NEW WORK ITEM PROPOSAL

As soon as $\dot{D}_{w,1}$ primary standards are available for source calibration, the planned ISO standard should provide traceability and guidance to the clinical medical physicists, worldwide. Thus, this ISO standardization project Clinical Dosimetry — Photon Radiation Sources Used in Brachytherapy should be launched as soon as possible and within ISO TC 85/SC 2/ WG 22 [1]. An ISO New Work Item Proposal and a Working Draft have been prepared, with proposed terms and definitions, lists of required properties and recommended sets of reference data and calibration data for BT-photon sources, BT-dosimetry detectors, BT-transfer standards and BT-dosimetry phantoms.

ACKNOWLEDGEMENTS

The authors express their thanks to the members of the AAPM BTSC, especially to L. Beaulieu, S.-T. Chiu-Tsao, L.A. DeWerd, M. Mitch, R. Nath, J. Perez-Calatayud, D.W.O. Rogers, B. Thomadsen, J. Williamson and to many others for discussions and encouragement.

REFERENCES

[1] BOYLE, P., LEVIN, B. (Eds), World Cancer Report 2008, International Agency for Research on Cancer, IARC, WHO (2008).

[2] QUAST, U., BÖHM, J., KAULICH, T.W., "The need for international standardization in clinical beta dosimetry for brachytherapy", Standards and Codes of Practice in Medical Radiation Dosimetry (Proc. Int. Symp. Vienna, 2002), Vol. 2, IAEA, Vienna (2003) 111–119.

[3] BOVI, M., et al., "Traceability to absorbed-dose-to-water primary standards in dosimetry of brachytherapy sources used for radiotherapy", Fundamental and Applied Metrology (Proc. XIXth World Congress, IMEKO, Lisbon, 2009) 1674–1679.

[4] TONI, M.P., et al., "A joint research project to improve the accuracy in dosimetry of brachytherapy treatments in the frame of the European Metrology Research Programme" (Proc. IFMBE 25/I) (2009) 421–424.

[5] SARFEHNIA, A., SEUNTJENS, J., Development of a water calorimetry-based standard for absorbed dose to water in HDR ^{192}Ir brachytherapy, Med. Phys. **37** (2010) 1914–1923.

[6] RIVARD, M.J., et al., AAPM Report 85, Update of AAPM TG-43 Report: A revised AAPM protocol for brachytherapy dose calculations, AAPM TG Brachytherapy SC, Med. Phys. **31** (2004) 633–674.

[7] RIVARD, M.J., et al., The evolution of brachytherapy treatment planning, Med. Phys. **36** (2009) 2136-2153.

[8] QUAST, U., et al., Clinical dosimetry of photon sources used in brachytherapy: Need for calibration in terms of absorbed dose to water and for international standardization, based on and extending the AAPM TG-43U1 formalism, Med. Phys. (2010).

[9] INTERNATIONAL ORGANIZATION FOR STANDARDIZATION, Clinical dosimetry — Beta radiation sources for brachytherapy, ISO 21439, ISO, Geneva (2009).

[10] QUAST, U., et al., Clinical dosimetry of photon sources used in brachytherapy: Need for ISO standardization, based on and extending the AAPM TG-43U1 formalism by calibration in terms of absorbed dose to water, abstract SU-GG-T-278, Med. Phys. **37** 6 (2010) 3249.

[11] FLÜHS, D., et al., Direct reading measurement of absorbed dose with plastic scintillators – The general concept and applications to ophthalmic plaque dosimetry, Med. Phys. **23** (1996) 427–434.

[12] BUTLER, W.M., et al., AAPM Report 98, Report of the AAPM LEB SC WG: Third-party brachytherapy source calibrations and physicist responsibilities, Med. Phys. **35** (2008) 3860–3865.

[13] RUSSEL, K.R., AHNESJÖ, A., Dose calculation in brachytherapy for a ^{192}Ir source using a primary and scatter dose separation technique, Phys. Med. Biol. **41** (1996) 1007–1024.

[14] TAYLOR, R.E.P., ROGERS, D.W.O., An EGSnrc Monte Carlo-calculated database of TG-43 parameters, Med. Phys. **35** (2008) 4228–4241.

[15] BALLESTER, F., PEREZ-CALATAYUD, J., Brachytherapy Dosimetric Parameters (2008), http://www.uv.es/braphyqs/index2.htm

[16] RIVARD, M.J., BEAULIEU, L., MOURTADA, F., Enhancement to commissioning techniques and quality assurance of brachytherapy treatment planning systems that use model-based calculation algorithms, Med. Phys. **37** (2010) 2645–2658.
[17] THOMADSEN, B.R., et al. (Eds), The physics of brachytherapy, 2nd ed., AAPM Monographs Series **31,** Medical Physics Publishing, Inc., Madison, WI (2005).
[18] BALTAS, D., et al., Physics of modern brachytherapy for oncology, Taylor and Francis, New York, London (2007).

ON THE QUALITY CONTROL OF LOW ENERGY PHOTON BRACHYTHERAPY SOURCES: CURRENT PRACTICE IN BELGIUM AND THE NETHERLANDS

A. AALBERS*, M. DE BRABANDERE**, C. KOEDOODER***, M. MOERLAND[+], B. THISSEN[++], A. VAN'T RIET[+++], A. RIJNDERS[§], B. SCHAEKEN[§§], S. VYNCKIER[§§§]

* Van Swinden Laboratorium,
Delft, Netherlands
Email: taalbers@xs4all.nl

** Katholieke Universiteit Leuven,
Leuven, Belgium

*** Academisch Medisch Centrum,
Amsterdam, Netherlands

[+] Universitair Medisch Centrum Utrecht,
Utrecht, Netherlands

[++] Centre Hospitalier Universitaire,
Liège, Belgium

[+++] Deventer Ziekenhuis,
Deventer, Netherlands

[§] Europa Ziekenhuizen,
Brussels, Belgium

[§§] NuTeC, XIOS Hogeschool Limburg,
Diepenbeek, Belgium

[§§§] Cliniques Universitaire St. Luc,
Brussels, Belgium

Abstract

Treatment planning for permanent implant prostate brachytherapy requires accurate knowledge of the source strength of the radioactive sources. In Belgium and The Netherlands, this technique is applied using low energy photon (LEP) emitting sources of the radionuclide ^{125}I. As a part of a working programme of a subcommittee of the Netherlands Commission on Radiation Dosimetry (NCS), quality assurance aspects of source strength determination by local medical physicists and vendors of seeds have been investigated. Two well type ionization chamber devices with single seed holders were used by an NCS visiting team to measure the source strength of ^{125}I seeds during on-site visits at 24 hospitals in Belgium and The Netherlands. The measured source strength was compared with the manufacturer's stated value, and when available, to in-house measurements of the local physicist. Most of the measurement equipment available in hospitals for the quality control of LEP sources is not traceably calibrated. Independent source strength verification in terms of air kerma strength for single seeds is not routinely performed in most Belgian and Dutch hospitals. The deviation of the air kerma values measured for single seeds by the NCS team in participating hospitals from the manufacturer's stated value were within 3% for the source types Oncura 6711 and IBt Intersource 1251L. For a few seeds, larger deviations, but still within 5% were observed. Air kerma verification of single seeds in a hospital with calibrated equipment is feasible with a relative expanded uncertainty ($k = 2$) of about 3.5%.

1. INTRODUCTION

Over the last decade, a strong increase in the number of patients treated with permanent implant prostate therapy and in the number of institutions applying this technique have been observed in Belgium and the Netherlands. Radioactive low energy photon (LEP) emitting sources of ^{125}I are applied in this brachytherapy treatment modality. An independent and periodic verification of the source strength of clinically applied LEP sources in Belgian and Dutch radiotherapy institutes is not common practice and is even lacking in many hospitals. Therefore, data on the agreement between the source strength as stated by the manufacturer and actually measured values are rarely available.

These developments stimulated the Netherlands Commission on Radiation Dosimetry (NCS) in 2004 to establish a working group in order to study the clinical and the dosimetry aspects related to the use of LEP sources. The goal of this working group is to publish guidelines and recommendations on quality control (QC) with respect to the use of these sources.

To gain insight into the current clinical practice, a questionnaire was sent to Belgian and Dutch institutions. The questions were related to prostate implantation procedures and techniques, treatment planning software, source calibration and equipment. Based on these results, it was decided to develop a user test procedure for the treatment planning system and to perform an on-site

measurement programme to verify the source strength as measured by the local medical physicist and as stated by the manufacturer or vendors on their certificates of supplied batches of LEP sources. As the dosimetric properties of a source are highly dependent on the seed construction and its internal composition, measurement devices had to be calibrated for each specific source model that was used by the hospital. Owing to the low dose rate of LEP sources, usually well chambers are used in clinics for source strength measurements.

This paper reports the findings with respect to the determination of the source strength based on the response to the questionnaire and on the results of the on-site visits.

2. MATERIALS AND METHODS

To study the current practice of source strength verification by local medical physicists, an NCS visit team measured the source strength in all participating institutes with two commercially available measurement systems.

2.1. Measurement systems

The systems consisted of a PTW SourceCheck TM34051 device with a PTW Unidos T1001 electrometer and a Standard Imaging IVB1000 well type chamber connected to a PTW Unidos E electrometer.

Both instruments are specifically designed for source strength measurements of brachytherapy sources and have vent holes for maintaining the internal air at ambient atmospheric pressure. Each instrument was equipped with various adapters or inserts to accommodate commercially available seed types. The PTW Unidos electrometers are very sensitive, have a reading in charge or current, and a wide dynamic range, and are equipped with an interval time function. Ancillary equipment was available to measure the ambient air conditions of temperature, pressure and relative humidity on location.

Test measurements were performed to check the characteristics of the equipment, (e.g. background signal, leakage, stability of response, linearity) and to define measurement settings for single seed and strand measurements.

2.2. Calibration of QC equipment

The measurement devices and ancillary equipment for measuring ambient conditions were calibrated at the Dutch Standards Laboratory (VSL, Delft, Netherlands) with ^{125}I sources traceable to NIST (WAFAC standard) [1] and for one source type to PTB (GROVEX standard) [2]. The individual seeds were

provided by the vendors and after (primary) calibration in terms of air kerma strength ($\mu Gy \cdot m^2 \cdot h^{-1}$) transferred to VSL, Delft. At VSL, calibration coefficients for all involved source types were determined by measuring the seeds in the Standard Imaging IVB 1000 and the PTW SourceCheck devices, and in the secondary standard well chamber facility at VSL, respectively. The latter facility was used for reference purposes during the on-site measurement campaign. For all source types used in Belgium and the Netherlands at the time of the on-site audit campaign, calibration coefficients were determined directly traceable to NIST or PTB, respectively. The measurement devices were calibrated together with their respective electrometers; therefore, no separate calibration coefficient for the electrical calibration of the electrometers was required. It should be noted that for every seed type and the various measurement devices, the geometric conditions, the position of the seed in the sensitive area (or well) of the detector and the applied insert/adapter were kept the same during calibration and the on-site measurement.

2.3. On-site measurements of the NCS team

During the calibration measurements as well as for the on-site measurements performed by the NCS team, the following conditions were applied. All seeds were measured twice by reversing the orientation of the seed in the insert (‘up’ and ‘down’ orientation) in order to compensate for the polar anisotropy of the emitted photon radiation. At least five to six charge readings were taken during a measurement cycle and each charge reading was collected during 60 s. Charge readings were corrected for background, temperature and pressure. No correction for recombination loss was applied. The averaged charge reading of a measurement cycle was also corrected for decay, when appropriate. On-site measurements of seeds were performed on the same ranges of the electrometers as used during the calibration measurements at VSL, Delft.

The long term stability of the dosimetry systems was monitored with radioactive check sources, a ^{226}Ra source and a $^{90}Sr/Y$ source for the Standard Imaging IVB1000 well chamber and the PTW SourceCheck device, respectively.

At the time of the on-site visits, most Belgian and Dutch institutions used sources from Oncura model 6711 or IBt Intersource model 125IL. These sources were supplied as single seeds, in strands or in Mick cartridges. In three hospitals, different source types were applied: seeds from Bard model STM 1251, Bebig model 125.S17 and Isotron Selectseed model 130.002.

3. RESULTS AND DISCUSSION

3.1. Survey

Thirty-four institutions completed the questionnaire: 22 institutes in Belgium and 12 institutes in the Netherlands. In about 40% of institutes that responded to the survey, the local medical physicist did not perform any routine verification measurements on LEP sources purchased for clinical application. In the remaining 60%, most medical physicists performed only a consistency check, which was based on an averaged source strength value obtained from data supplied by the manufacturer for a number of purchased batches over a period of time. From these averaged data, a conversion factor was derived and then applied to the dial settings of the measurement equipment of the institution. In these measurements, the source strength data was usually expressed in the unit mCi. Owing to the lack of calibrated equipment only a few local medical physicists in Belgium and The Netherlands were able to perform verification measurements in terms of the quantity air kerma (rate) or air kerma strength.

In Table 1, an overview is given of the measurement equipment available for QC measurements in the participating institutes. In total, six out of the 34 institutes have no specific measurement device available to verify the source strength of LEP sources. Eleven instruments are designed as radionuclide calibrators for nuclear medicine and measure in units of activity. Only the Standard Imaging HDR1000 and IVB1000 chambers and the PTW SourceCheck are specifically designed for brachytherapy applications. Note that one institute uses two different measurement devices, which are both listed in Table 1.

Three measurement devices listed in Table 1 had a traceable calibration obtained from an ADCL (University of Wisconsin), four other devices were calibrated by the manufacturer. These latter factory based calibrations are not considered traceable to national or international standards.

3.2. On-site visits

The results of the air kerma strength measurements performed by the NCS visiting team during the on-site visits were analysed per seed type. On average, two to four seeds were measured in each institute by the NCS team. The seeds were selected at random from batches of single seeds or strands, purchased for patient treatments. For the IBt Intersource 1251L and Oncura 6711 seed types, the results were grouped and presented per measurement device in a histogram as the ratio of the values stated by the manufacturer and the corresponding measured values by the NCS visiting team. The data in terms of (nominal) air kerma

TABLE 1. MEASUREMENT EQUIPMENT IN USE FOR QC OF LEP BRACHYTHERAPY SOURCES BY RADIOTHERAPY INSTITUTES IN BELGIUM AND THE NETHERLANDS

	BE	NL	TOT
None	5	1	6
PTW SourceCheck	9	1	10
SI (HDR1000/IVB1000)	4	4	8
NA 34-070	3	3	6
Capintec (CRC-10/CRC-15R)	2	1	3
Veenstra VDC-303	—	1	1
Sun Nuclear 100840	—	1	1

strength from the manufacturer were taken from the certificates issued with the purchased sources.

The histograms present the ratio of the manufacturer/supplier stated value of the source strength over the measured air kerma value of the NCS team. In Fig. 1, the results are given for Oncura 6711/rapid strand sources measured with the Standard Imaging IVB1000 (Fig. 1, left) and the PTW SourceCheck (Fig.1, right) equipment, respectively. In total, 46 individual seeds were measured with both instruments.

The lowest ratio measured with the IVB1000 is 0.959 and the highest ratio is 1.046. For the PTW SourceCheck these values are 0.943 and 1.045, respectively.

For the IBt seeds, 51 seeds were measured with the Standard Imaging IVB1000 device, and 47 seeds with the PTW SourceCheck. The results for IBt sources are presented in Fig. 2 for the IVB1000 (Fig. 2, left) and for the SourceCheck (Fig. 2, right).

The lowest ratio measured with the IVB1000 is 0.951 and the highest ratio is 1.031. For the PTW SourceCheck, the values are 0.965 and 1.047, respectively.

The differences between the measured values (NCS) and the manufacturer's stated values are within 3% for the large majority of the seeds. With respect to the Oncura 6711 seeds, three out of 46 seeds show deviations in the range of 3–5% for the IVB1000 well chamber, and six out 46 seeds for the PTW SourceCheck.

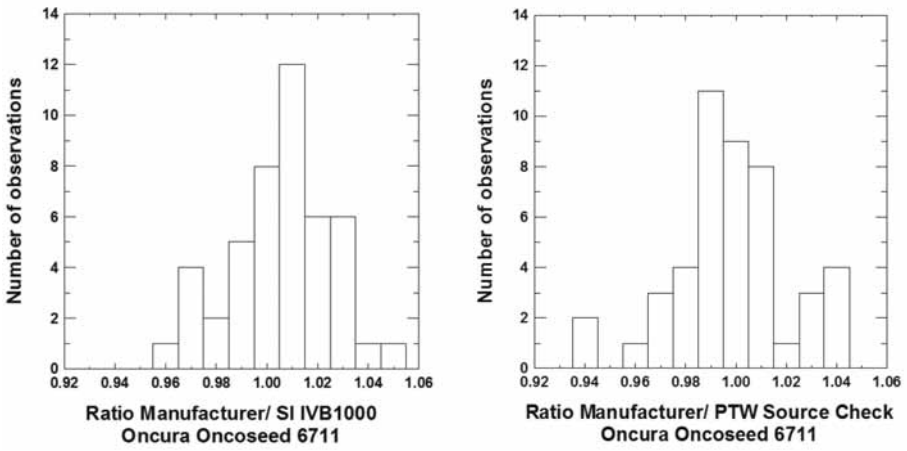

FIG. 1. Oncura seeds: ratio of air kerma strength values stated by the manufacturer and as measured by the NCS visiting team with the IVB1000 well chamber (left) and PTW SourceCheck (right), respectively.

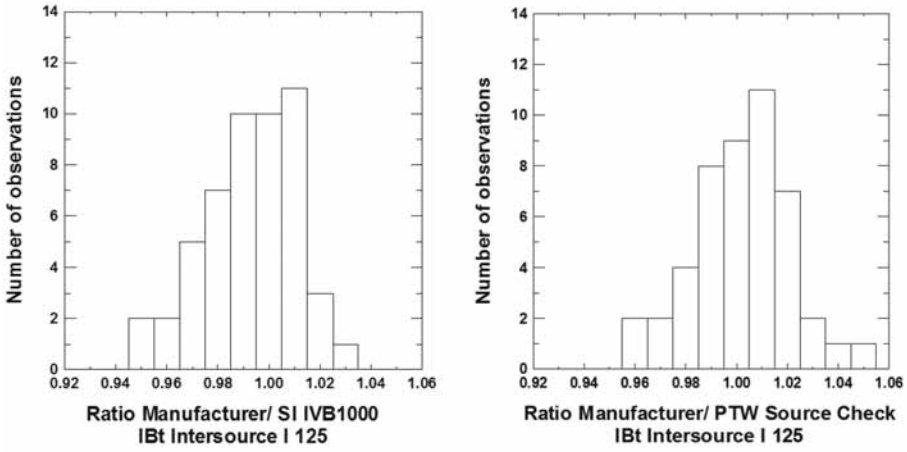

FIG. 2. IBt seeds: ratio of air kerma strength values stated by the manufacturer and as measured by the NCS visiting team with the IVB1000 well chamber (left) and PTW SourceCheck (right), respectively.

For the PTW SourceCheck, one out of 46 shows a discrepancy of 6%. A similar observation can be made for the IBt seeds. For the IVB1000 device, two out of 51 seeds show a deviation of more than 3%, but not larger than 5%. For the PTW SourceCheck, four out of 47 seeds exceed a deviation of 3%, but these deviations are no larger than 5%.

Also, for the Bard, Bebig and Isotron source types (see Section 2.3), the NCS team measured two to three individual sources. Air kerma strength values show differences up to 5% with values stated by the manufacturer. Only for the Bebig seeds were differences found of up to about 8%. However, the samples measured for these source types during the on-site visits were too small to draw general conclusions.

Based on the description of air kerma strength data stated on the certificates of manufacturers, it was often not clear how the source strength was derived, and methods might vary among manufacturers. Some manufacturers averaged over a number of single seeds or strands others assigned a median value. Moreover, certificates lacked sufficient information on bin sizes and on the uncertainty assigned to source strength data. However, the uncertainty was estimated in the air kerma strength measurements performed by the NCS visit teams. For all measured source types, the relative expanded uncertainty ($k = 2$) was within a range of 1.9–3.4%. It should be noted that most source types were directly calibrated at NIST, but one source type was directly calibrated at PTB. A relative expanded uncertainty of about 3% was assigned to the air kerma rate determination at PTB [3]. The reproducibility of the current measurements performed by the NCS team during the on-site visits was in the range of 0.1–0.2% ($k = 1$) for the IVB1000 device and in the range of 0.2–0.4% ($k = 1$) for the PTW SourceCheck. However, for the latter device, values to about 1% for the reproducibility in the current measurement were occasionally observed.

During the on-site visits in five institutes, the local medical physicist performed in-house measurements, which could be reported in terms of air kerma rate (or in kerma strength) and were obtained with traceable calibrated equipment or with factory calibrated equipment. In these five institutes, either IBt or Oncura source types were available. For these situations, two single seeds or two full strands were measured by the local medical physicist and the NCS team. The air kerma strength values from the in-house measurement were compared with measured values from the NCS team. Deviations were within 5%; on one occasion only, a deviation to about 6% was observed.

4. CONCLUSIONS

The results of the survey revealed that the vast majority of Belgian and Dutch medical physicists do not perform an independent source strength verification of LEP sources used for clinical brachytherapy application. In general, the measurement equipment available in hospitals has no traceable calibration. Until recently, all source strength measurements were relying on one primary standard (NIST). The development of primary standards in Germany,

France and other countries in Europe will foster the dissemination of the quantity air kerma to (secondary) calibration laboratories. However, it should be noted that currently no calibration services for LEP brachytherapy sources are operated in Belgium and the Netherlands.

From the experience of the NCS visiting team, it seems feasible that an independent air kerma strength verification of an individual seed in a clinical environment may be performed with a relative expanded uncertainty of about 3.5% at maximum. Traceable calibrated equipment is a prerequisite.

Finally, the NCS subcommission will publish a report with guidelines and recommendations on QC with respect to source strength verification and dose calculation of LEP sources. The recommendations published in this NCS report will be based on the work reported in this paper.

ACKNOWLEDGEMENTS

The authors wish to thank the providers of equipment and sources mentioned in this paper and are indebted to M. Mitch (NIST) and H.-J. Selbach (PTB) for performing primary calibrations on the single seeds used in this study.

REFERENCES

[1] SELTZER, S.M., LAMPERTI, P.J., LOEVINGER, R., MITCH, M.G., WEAVER, J.T., COURSEY, B.M., New national air-kerma-strength standards for ^{125}I and ^{103}Pd brachytherapy seeds, J. Res. Natl. Inst. Stand. Technol. **108** (2003) 337–357.

[2] SELBACH, H.J., KRAMER, H.M., CULBERSON, W.S., Realization of reference air kerma rate for low-energy photon sources, Metrologia **46** (2008) 422–428.

[3] SELBACH, H.J., Personal communication (2007).

INTERNAL CLINICAL ACCEPTANCE TEST OF THE DOSE RATE OF $^{106}Ru/^{106}Rh$ OPHTHALMIC APPLICATORS

T.W. KAULICH, M. BAMBERG
University Hospital for Radiation Oncology, Tübingen, Germany
Email: theodor.kaulich@med.uni-tuebingen.de

Abstract

Episcleral brachytherapy using $^{106}Ru/^{106}Rh$ ophthalmic applicators is a proven method of therapy for uveal melanomas, sparing the globe and in many cases, conserving vision. In its certificates, Bebig, the manufacturer of the product, indicates a dose rate for the $^{106}Ru/^{106}Rh$ ophthalmic applicators which ensures traceability to the NIST standard (12/2001). Since the introduction of the NIST calibration, the quality of the calibration provided by Bebig to the clinical user has been examined for 45 ophthalmic applicators with a plastic scintillator measurement system. Of these, 20 ophthalmic applicators had a dose rate at the dose specification reference point that exceeded the dose rate stated in the manufacturer's certificate by up to 23%.

1. INTRODUCTION

Ocular melanoma, the most frequent primary eye cancer in adults with an incidence of about six cases in 10^6, affects the iris, ciliary body and choroid. The traditional method of treatment has been enucleation. This method, however, entails cosmetic problems and causes loss of binocular vision. Methods of radiation therapy, including brachytherapy with various radioactive sources (e.g. ^{125}I, $^{106}Ru/^{106}Rh$, ^{60}Co, $^{90}Sr/^{90}Y$, ^{192}Ir, ^{103}Pd) and external beam therapy with protons or photons, constitute an attractive alternative because they preserve the eye and thereby the facial features.

For the last 40 years, episcleral brachytherapy using $^{106}Ru/^{106}Rh$ ophthalmic applicators has been a very reliable method of therapy for uveal melanomas, having the advantage of sparing the globe and in many cases even conserving the vision [1–3]. In episcleral brachytherapy, a radioactive $^{106}Ru/^{106}Rh$ ophthalmic applicator (Bebig Co., Berlin, Germany) is temporarily fixed on the surface of the bulbus oculi, whereby the intraocular tumour gets irradiated protractedly through the sclera (Fig. 1) [4, 5]. $^{106}Ru/^{106}Rh$ ophthalmic applicators are primarily beta sources, i.e. they generate a local dose escalation both in the vessels supplying the tumour and in the tumour itself, while simultaneously sparing the risk structures because they have a very steep dose gradient (Fig. 2) [4, 5].

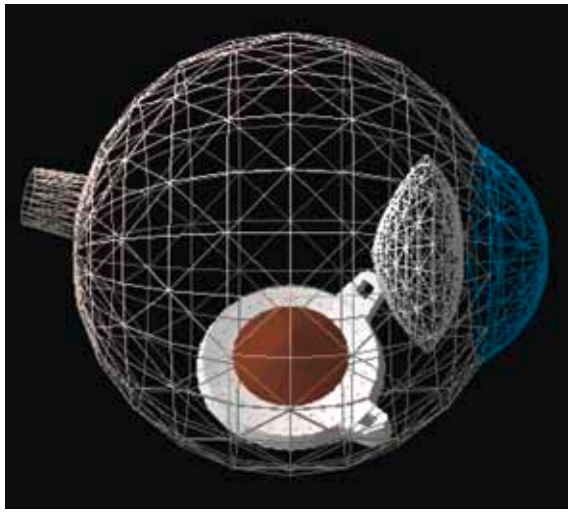

FIG. 1. Computer simulation of an ocular tumour therapy with $^{106}Ru/^{106}Rh$ ophthalmic applicator.

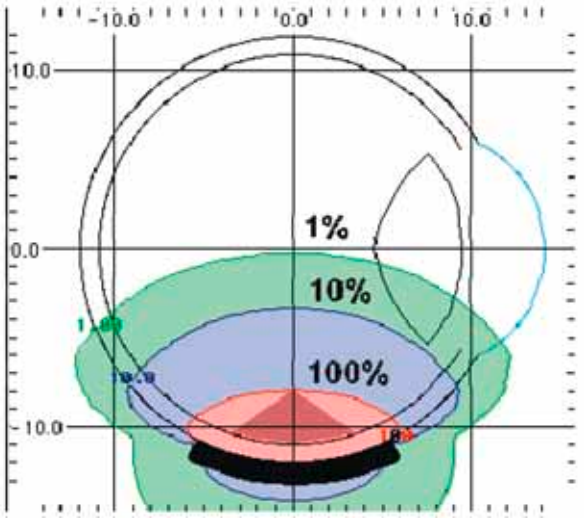

FIG. 2. Example of a dose distribution of a $^{106}Ru/^{106}Rh$ ophthalmic applicator in the eye (scale in mm).

In its source strength certificates, Bebig, the manufacturer of the ophthalmic applicators, indicates a dose rate for the $^{106}Ru/^{106}Rh$ ophthalmic applicators at a dose specification reference point [6] which ensures traceability to the NIST standard (12/2001). Since the introduction of the NIST calibration,

the ‘quality’ of the calibration passed on by Bebig to the user has been examined for 45 ophthalmic applicators.

2. MATERIALS AND METHODS

$^{106}Ru/^{106}Rh$ is a parent–daughter beta emitter that has a spectrum with a maximum energy of 3.54 MeV, a mean energy of 1.41 MeV emitted by ^{106}Rh, and half-lives of 373.59 d and 29.8 s [7].

The $^{106}Ru/^{106}Rh$ is encapsulated within pure silver sheets with a total thickness of only 1 mm. All plaques are spherically shaped with a radius of 12–14 mm and have special eyelets to be sutured to the sclera. The radiation window on the concave side is a 0.1 mm silver foil. For different applications (uveal, choroidal, ciliary body and iris melanomas, retinoblastoma and tumours close to the optical nerve), there are 16 plaque types commercially available [8].

The dose specification point (the ‘reference point’ throughout this paper) is defined at a distance of 2 mm from the middle of the inner (concave) surface of the $^{106}Ru/^{106}Rh$ ophthalmic applicators [6]; the manufacturer measured the dose rate with a scintillation detector (diameter 1 mm, height 0.5 mm) in water. The nominal value of the absorbed dose rate to water for every plaque type at the reference point is 80 mGy/min (4.8 Gy/h) corresponding to approximately 120 mGy/min (7.2 Gy/h) on the surface. The prescribed dose in the tumour apex is 130 Gy, and the duration of the treatment takes up to eight days.

The manufacturer indicates for this dose rate at the reference point, a relative measurement uncertainty of ±20% within the 95% confidence interval (CI).

The plastic scintillator measurement system used by the authors consists of a 0.8 mm^3 polyvinyl-toluol plastic scintillator of the type NE 102A (Nuclear Enterprise Technology Ltd., Reading, UK), a photomultiplier and a high voltage unit. For the measurement of the current of the photomultiplier, a UNIDOS therapy dosimeter (PTW Co., Freiburg, Germany) was used, which was operated as an electrometer [9] (Fig. 3).

For the constancy check of the complete plastic scintillator measurement system, a radioactive check device containing ^{90}Sr has been used (type T48010, PTW Co., Freiburg, Germany).

The plastic scintillator was also positioned in water at the dose specification reference point at a distance of 2 mm from the middle of the inner surface of the applicators with a MP3S (PTW Co., Freiburg, Germany) three dimensional water phantom.

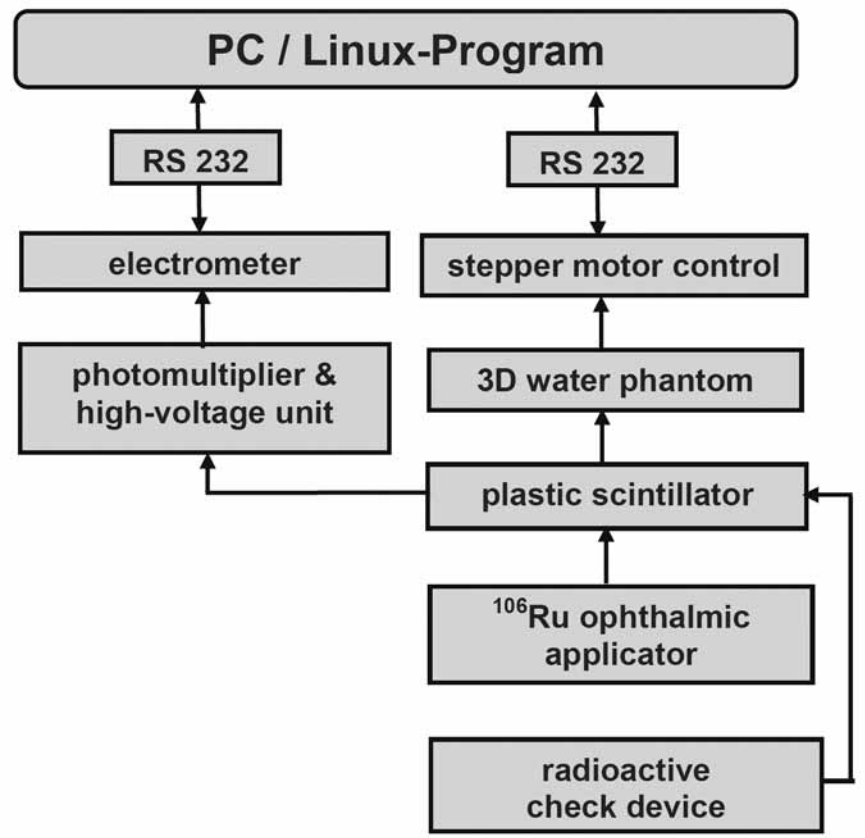

FIG. 3. Plastic scintillator measurement system.

3. RESULTS

To date, the users of $^{106}Ru/^{106}Rh$ ophthalmic applicators have not been able to measure the absorbed dose rate because a commercial secondary standard is not yet available. Therefore, the calibration of Bebig has been adopted, and the authors have been calibrating their scintillator measurement equipment using $^{106}Ru/^{106}Rh$ ophthalmic applicators.

For this purpose, the average of adopted calibration factors from 19 applicators was calculated. For the measurement equipment used by the authors, an average calibration factor of 38.0 Gy/μC ± 3.7% for the 95% CI was found for the 19 ophthalmic applicators in the internal clinical acceptance tests conducted between 2002 and 2004 (Fig. 4).

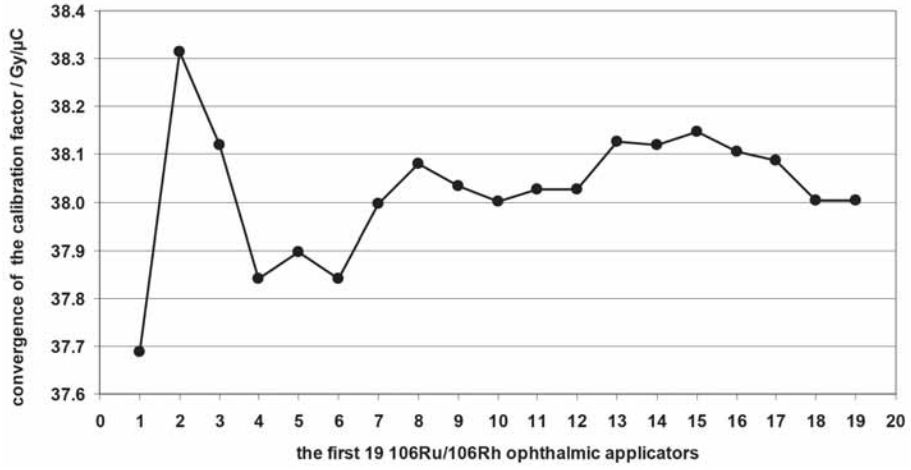

FIG. 4. Convergence of the calibration factor, adopted from Bebig.

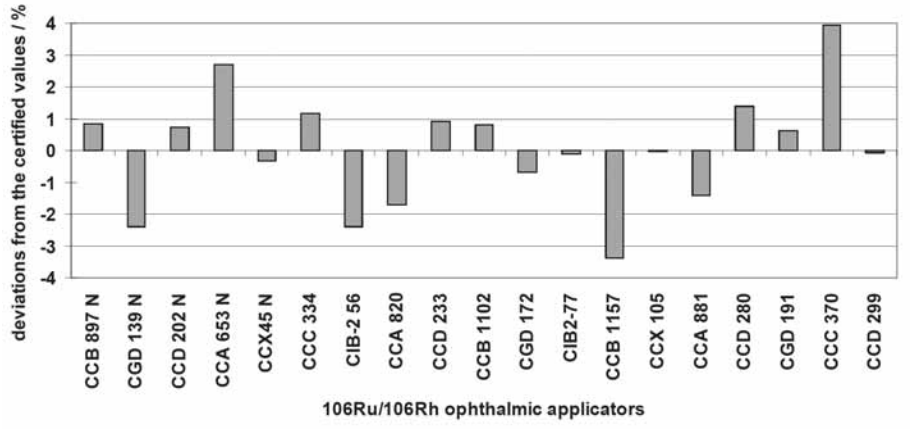

FIG. 5. Deviations from the certified values of 19 ophthalmic applicators from the calibration factor of 38.0 Gy/μC.

Fig. 5 shows the deviations from the certified values of the 19 ophthalmic applicators from the calibration factor of 38.0 Gy/μC. The relative measurement uncertainty for these 19 ophthalmic applicators for the 95% CI was ±3.7% (Fig. 5). Considering the steep dose gradient in Fig. 2, it can be derived from this small 95% CI that between 2002 and 2004, Bebig very efficiently passed on the NIST calibration to its customers. This calibration factor is still being used in the internal clinical acceptance tests for the ophthalmic applicators, as Bebig continues to ensure traceability of the dose rate values to the NIST standard.

Over the last six years, however, the internal clinical acceptance tests occasionally showed considerable deviations from the certified values.

In 2005, four ophthalmic applicators were purchased whose dose rates at the reference point were in the mean of 19.9% higher (from 17.9% to 22.6%) than the dose rate stated in the manufacturer's certificate. The standard deviation was ±2.1%.The manufacturer was informed and re-assessed its dose rate values. This examination identified an error in the manufacturer's measurement installation which was subsequently corrected.

In 2006 and 2007, the internal clinical acceptance tests did not reveal any particular deviations. Six applicators had a mean deviation of –1% from the calibration factor of 38.0 Gy/μC. The standard deviation was only ±0.8%.

In 2008 and 2009, 16 ophthalmic applicators were purchased that had a dose rate at the reference point that exceeded the dose rate stated in the manufacturer's certificate in the mean by 12.3%. The standard deviation was ±2.4% (Fig. 6). Again, the manufacturer was informed, but has not yet made an official statement. Bebig, however, informed the authors in a private communication that NIST had been asked to carry out a renewed calibration in 2009.

4. CONCLUSIONS

Based on the experiences derived from acceptance tests of $^{106}Ru/^{106}Rh$ ophthalmic applicators over the last few years, users should examine the dose rate at the reference point to verify the calibration provided by the manufacturer in an

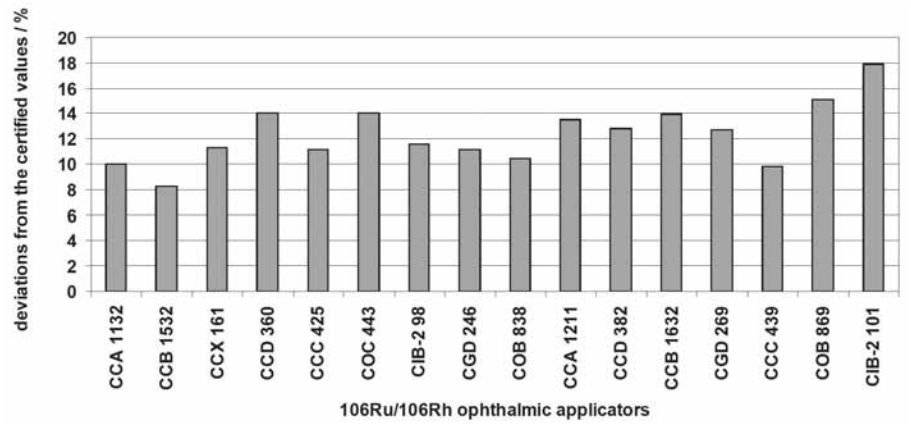

FIG. 6. Deviations from the certified values for 16 ophthalmic applicators in 2008 and 2009.

internal clinical test. For the clinical measurement of the dose rate of $^{106}Ru/^{106}Rh$ ophthalmic applicators, however, the user needs commercially available measurement equipment whose calibration is traceable to a metrological institute. Since commercial measurement equipment is not obtainable, the dose rate at the dose specification reference point for $^{106}Ru/^{106}Rh$ ophthalmic applicators cannot be measured directly by the user.

NIST primary standards for beta particle brachytherapy sources rely on extrapolation chamber measurements, and uncertainties were very high in 2001. In 2001, NIST issues an uncertainty of ±15% to their calibration measurements. Since 2003, the use of the new divergence corrections resulted in a significant (approximately a factor two) lowering in the NIST uncertainty in absorbed dose calibrations of beta brachytherapy sources [10]. It is hoped that a required $^{106}Ru/^{106}Rh$ calibration can be disseminated with the reduced absolute dose calibration uncertainty in the short term to SSDLs and then onto end-users.

ACKNOWLEDGEMENTS

The authors have to express their thanks to Prof. U. Quast (ex-Essen University Hospital, Essen, Germany) and Prof. G. Christ (University Hospital for Radiation Oncology, Medical Physics, Tübingen, Germany) for discussions and encouragement.

REFERENCES

[1] LOMMATZSCH, P.K., Experiences in the treatment of malignant melanoma of the choroid with $^{106}Ru/^{106}Rh$ beta-ray applicators, Trans. Ophthalmol. Soc. UK **93** (1973) 119–32.

[2] LOMMATZSCH, P.K., WERSCHNIK, C., SCHUSTER, E., Long-term follow-up of $^{106}Ru/^{106}Rh$ brachytherapy for posterior uveal melanoma, Graefes Arch Clin Exp Ophthalmol **238** (2000) 129–37.

[3] BERGMAN, L., NILSSON, B., LUNDELL, G., LUNDELL, M., SEREGARD, S., Ruthenium brachytherapy for uveal melanoma, 1979-2003: survival and functional outcomes in the Swedish population,Ophthalmology, **112** (5) (2005) 834–40.

[4] Plaque Simulator by ASTRAHAN MA.

[5] ASTRAHAN, M.A., et al., An interactive treatment planning system for ophthalmic plaque radiotherapy, Radiation Oncology Biol. Phys. **18** (1990) 679-687.

[6] SOARES, C.G., (convener), ISO 21439, Clinical dosimetry — Beta radiation sources for brachytherapy, ISO, Geneva (2009).

[7] National Nuclear Data Center (2001).

[8] BEBIG, Factsheet_Ru-106_Ophthalmic_Plaques_Rev._05_eng.pdf

[9] KAULICH, T.W., ZURHEIDE, J., HAUG, T., NÜSSLIN, F., BAMBERG, M., Clinical quality assurance for ^{106}Ru ophthalmic plaques, Radiotherapy and Oncology **76** (2005) 86–92.

[10] SOARES, C.G., BERGSTROM, P.J., Jr., The divergence correction for extrapolation chambers measuring brachytherapy sources. Med. Phys. **30**(6) (2003) 1427.

CHARACTERIZATION OF A PARALLEL PLATE IONIZATION CHAMBER FOR THE QUALITY CONTROL OF CLINICAL APPLICATORS

P.L. ANTONIO, L.V.E. CALDAS
Instituto de Pesquisas Energéticas e Nucleares,
São Paulo, Brazil
Email: patrilan@ipen.br

Abstract

A parallel plate ionization chamber, developed at the Calibration Laboratory of IPEN (LCI), was utilized with the objective to verify the possibility of its application in the quality control programme of $^{90}Sr+^{90}Y$ clinical applicators at clinics and hospitals that perform betatherapy procedures. The characterization of this ionization chamber was realized using a reference clinical applicator. The results of this work showed that this kind of ionization chamber may be useful in quality control programmes of $^{90}Sr+^{90}Y$ sources, including the calibration procedures for these sources.

1. INTRODUCTION

Parallel plate ionization chambers are utilized in electron beam dosimetry because they have some advantages due to different geometries, applications and a simple construction. Parallel plate ionization chambers have been applied in the determination of absorbed doses for many years [1].

At the Calibration Laboratory of IPEN, several parallel plate ionization chambers have been developed [2–4]. A parallel plate ionization chamber developed by Souza et al. [3] was designed for utilization in high energy electron beam dosimetry.

The calibration of clinical applicators is recommended by protocols of calibration and dosimetry of sources used in brachytherapy [5, 6]. The extrapolation chambers are adequate instruments for the determination of absorbed dose rates for these kinds of sources [7, 8]. Some extrapolation chambers were developed at IPEN [9, 10], to calibrate dermatological (plane) and ophthalmic (curve) applicators of beta radiation. However, due to the relative complexity in their construction and utilization, they were not recommended for use in clinics and hospitals where $^{90}Sr+^{90}Y$ clinical applicators were used, but were more appropriate for use at calibration laboratories. In lieu of the parallel

plate chambers for the calibration of clinical applicators used at radiotherapy clinics, another recommended method is the use of thermoluminescent dosimeters.

At radiotherapy clinics, three main tests would be recommended for a quality control programme of clinical applicators, using a parallel plate ionization chamber ('homemade' or commercial): leakage current, reproducibility (for the ionization chamber) and measurements of the clinical applicator radiation beam, positioned at, for instance, three known different short distances from the chamber. An extrapolation of the chamber's response to null distance will allow the determination of the absorbed dose rate at its surface, using a calibration factor previously provided for the ionization chamber from a calibration laboratory.

The objective of this work was to characterize a homemade parallel plate ionization chamber to verify its potential application in a quality control programme and for the calibration of the $^{90}Sr+^{90}Y$ clinical applicators.

2. MATERIALS AND METHODS

Initially, the stability and linearity of the ionization chamber response were determined. For these tests, a $^{90}Sr+^{90}Y$ check source (33 MBq, 1994), PTW, model 8921, was positioned on a PMMA support.

In this work, a $^{90}Sr+^{90}Y$ clinical applicator (termed the NIST applicator), calibrated at the US primary standards dosimetry laboratory of the National Institute of Standards and Technology, was utilized in the characterization tests. Three other clinical applicators (A1, A2 and A3) were calibrated using the NIST applicator as a reference applicator. The A2 applicator did not have an original calibration certificate. The characteristics of the applicators are given in Table 1.

TABLE 1. CHARACTERISTICS OF THE $^{90}Sr+^{90}Y$ CLINICAL APPLICATORS TESTED IN THIS WORK

$^{90}Sr+^{90}Y$ applicator	Manufacturer and model	Nominal absorbed dose rate (Gy/s)	Calibrated by	Calibration date
NIST	Atlantic Research Corporation/B-1 S/N 233	0.40 ± 0.02	NIST	28.01.2003
A1	Amersham/SIQ 18	0.056 ± 0.011	Amersham	08.11.1968
A3	Amersham/SIQ 21	0.053[a]	Amersham	17.09.1986

[a] No uncertainty provided in its calibration certificate.

The measurements were performed with the objective to characterize a parallel plate ionization chamber. The chamber was made of acrylic and in a cylindrical geometry, with an entrance window of aluminized Mylar and collecting electrode of graphite. This chamber had a 25.4 mm diameter and a 17.25 mm thickness. The collecting electrode had a 6.0 mm diameter [3]. Figure 1 shows the schematic diagram of the parallel plate ionization chamber used in this work [3].

PMMA supports were developed to allow the reproducible positioning of the parallel plate ionization chamber (Fig. 2). A goniometer was also utilized (Fig. 3) for the measurements of the angular dependence of the chamber response.

The ionization currents were obtained using a UNIDOS E electrometer from PTW, Freiburg. The ionization current was always taken as the mean value of the ionization currents obtained for both polarities (in absolute values).

3. RESULTS

The ionization chamber was studied in relation to several characterization tests.

3.1. Leakage current without irradiation

The leakage current was measured during a time interval of 20 min, before and after an irradiation, and the maximum leakage value obtained in this work was 0.02%. According to the IEC [11], the recommended limit to the leakage

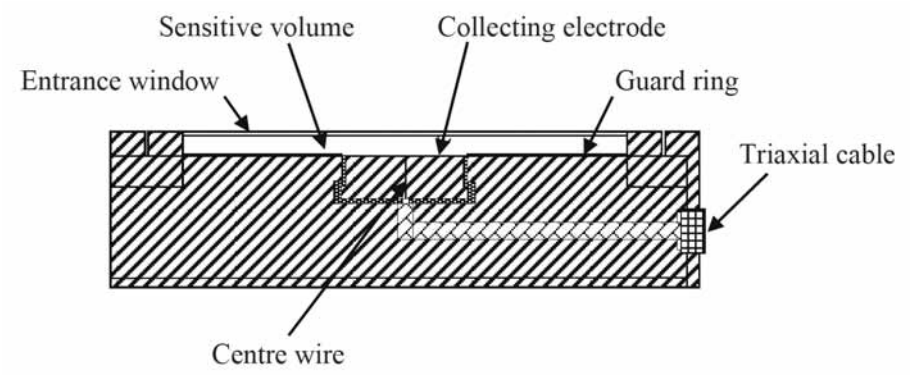

FIG. 1. Schematic diagram of the PMMA parallel plate ionization chamber, with a centre wire of Teflon [3].

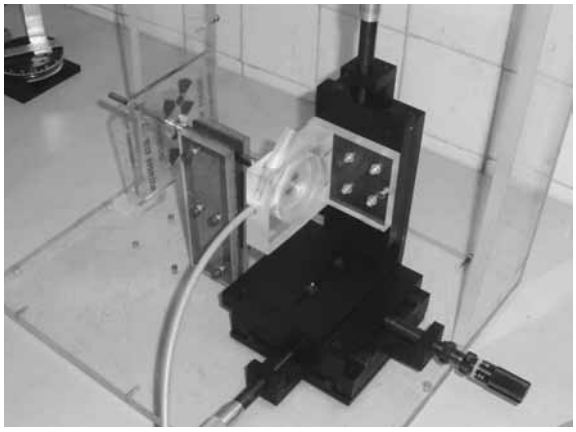

FIG. 2. Set-up utilized in the measurements with the parallel plate ionization chamber and the clinical applicators.

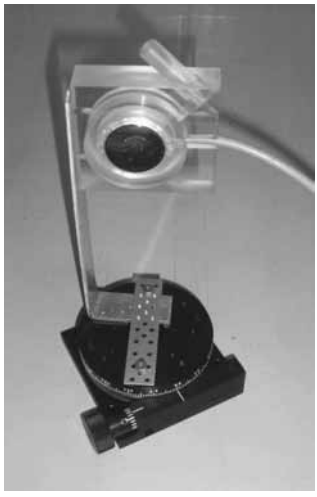

FIG. 3. Goniometer for the angular dependence test.

current test before irradiation is 0.5% of the highest value of the measurements. Therefore, the leakage current obtained in this work was within the recommended limit.

3.2. Stability tests

The chamber response was tested with respect to its stability (reproducibility tests). The reproducibility for the chamber was obtained from ten

readings of charge at each polarity (±300 V), during a time interval of 60 s. The highest variation coefficient obtained was 0.17% and according to the IEC recommendations [11], the acceptable limit to this stability test when a check source is utilized is 0.3%.

The reproducibility test was performed with successive repeatability tests. The maximum variation coefficient obtained was 0.44% (results shown in Fig. 4). The recommended limit in this case is 0.5% [11].

3.3. Linearity of response

The linearity of the parallel plate ionization chamber response was studied in relation to the collected charge as a function of the irradiation time. In the linearity test, the charge collecting time was in 30 s intervals, and the polarity voltage used was ±300 V. Linear behaviour was observed, with a correlation factor, r^2, of 1.00. For these measurements, a $^{90}Sr+^{90}Y$ check source was utilized. Figure 5 shows the results obtained for the linearity test.

3.4. Stabilization time

According to IEC international recommendations [11], the stabilization time of an ionization chamber response should be studied during two time periods, 15 min and 2 h, and the variation of response shall not exceed 0.5%. In order to verify the variation of the chamber response, the interval studied in this work ranged from 0.5 min to 2 h. The voltage used in this test was 300 V, in the

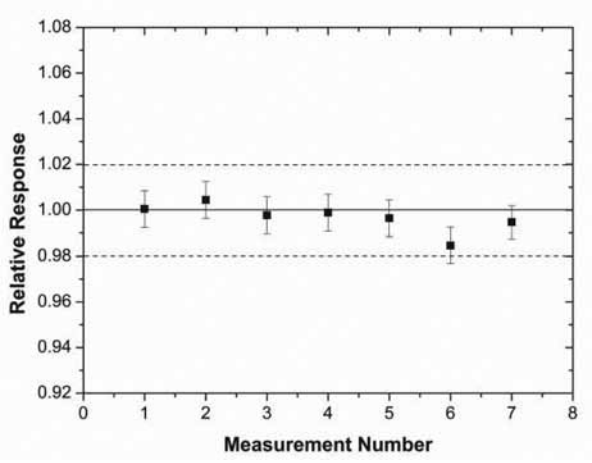

FIG. 4. Stability test of the parallel plate ionization chamber performed with a $^{90}Sr+^{90}Y$ check source.

positive and negative polarities, and the mean value of the ionization currents (in absolute values) was considered. After the voltage application, the maximum variation observed was 0.05% in 1 h for the positive polarity. Table 2 shows the results obtained for the determination of the stabilization time. The ionization currents were normalized to the measurement at 1 h after the application of the polarity voltage to ionization chamber.

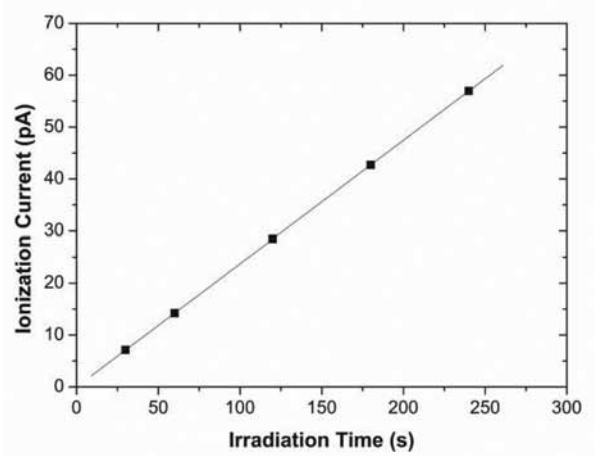

FIG. 5. Linearity of the ionization chamber response in function the irradiation time, using a $^{90}Sr+^{90}Y$ check source. The maximum standard deviation of all measurements was less than 0.5%.

TABLE 2. STABILIZATION TIME TEST FOR BOTH POLARITIES SHOWING THE MAXIMUM DEVIATION FOR THE STATED IRRADIATION TIME

Time (min)	Polarity	
	Positive	Negative
0.5	1.0030	1.0116
1	1.0475	1.0099
5	1.0022	0.9740
10	1.0018	1.0033
15	1.0014	0.9940
60	1.0000	1.0000
120	0.9980	0.9913

3.5. Saturation curve

The saturation curve was utilized for the determination of the optimum polarity voltage to be applied to the ionization chamber. A saturation curve (Fig. 6) was obtained varying the voltage from –300 V to +300 V, in steps of 50 V. A distance equal to 1.0 cm was utilized between the $^{90}Sr+^{90}Y$ NIST applicator and the ionization chamber, and the charge collection time was 30 s.

The mean value of the ionization current obtained was 48.99 pA (46.01 pA for the positive polarity and 51.98 pA for the negative polarity), and the maximum coefficient of variation obtained was 0.9%. These results indicated that the ionization chamber achieved saturation over the whole polarity voltage interval.

3.5.1. Polarity effect

The saturation curve data was used to determine two of the chamber's characteristics: polarity effect and ion collection efficiency.

The polarity effect was determined by comparing the collected charges in the same voltages of opposite signals. This effect was obtained by Eq. (1) [12].

$$k_{\text{pol}} = \frac{|Q_+| - |Q_-|}{|Q_+| + |Q_-|} \tag{1}$$

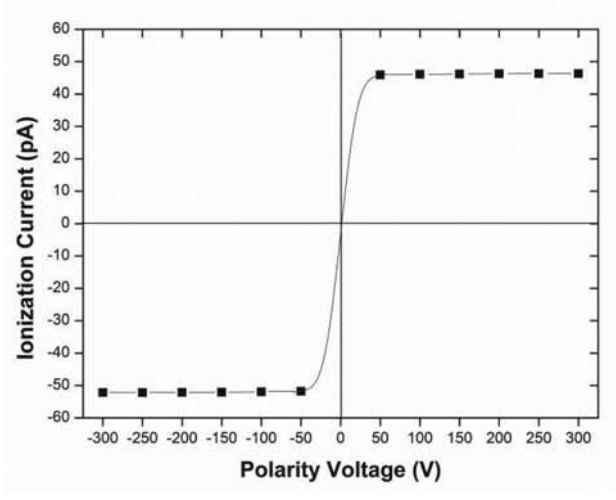

FIG. 6. Saturation curve for the parallel plate ionization chamber, using the NIST applicator. The maximum standard deviation of the measurements was less than 0.5%.

where

p is the polarity effect;
Q_+ is the collected charge of the ionization chamber with the positive polarity;
Q_- is the collected charge of the ionization chamber with the negative polarity.

For all pairs of polarity voltage tested during the saturation test, the maximum polarity effect was 6.02%, according to Table 3. Although this result is greater than the recommended value of 1% in Ref. [11], the value obtained in this work was considered acceptable, since these measurements were taken using the $^{90}Sr+^{90}Y$ beta radiation source. In this case, the effect becomes more pronounced because there is the presence of a different ionization current that is originated by the interaction between the beta radiation and the collecting electrode of the ionization chamber.

3.5.2. Ion collection efficiency

The ion collection efficiency was obtained taking into consideration the collected charges for both polarity voltages [13], according to the two voltage technique shown in Eq. (2):

$$k_s = \frac{\left(\frac{V_1}{V_2}\right)^2 - 1}{\left(\frac{V_1}{V_2}\right)^2 - \left(\frac{M_1}{M_2}\right)} \tag{2}$$

TABLE 3. VALUES OF POLARITY EFFECT OBTAINED DURING THE MEASUREMENTS FOR THE DIFFERENT VOLTAGES

Voltage (V)	Polarity		Value (%)
	Positive	Negative	
50	1239.6	1397.0	5.97
100	1245.0	1403.0	5.97
150	1247.0	1406.2	6.00
200	1249.0	1408.0	5.98
250	1250.0	1410.0	6.02
300	1251.8	1410.0	5.94

where

k_s is the value of ion collection efficiency;
V_1 is the greatest voltage value;
V_2 is the lowest voltage value;
M_1 is the collected charge at voltage V_1;
M_2 is the collected charge at voltage V_2.

The ion collection efficiency obtained in this work was better than 99.9% resulting in losses by ion recombination of less than 0.1%.

3.6. Angular dependence

The angular dependence test was performed to determine the ion chamber response as a function of the incident radiation at small angles away from a perpendicular beam to the surface of the parallel plate chamber. The objective of this study was to verify how small positioning errors influence the ionization chamber response. The chamber was moved around its central axis at angle intervals ranging between –16º to +16º, in steps of 4º. During the measurements, a distance of 4.0 cm was kept between the source and the chamber center. According to Ref. [11], the value obtained at each angle was not to differ from 0º by more than 3%. In this work, the average value obtained was 0.84 pA, and the maximum variation measured was 3%, as can be observed in Fig. 7.

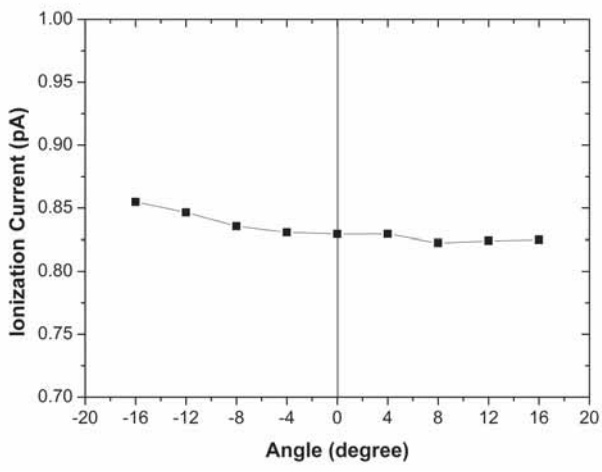

FIG. 7. Angular dependence test of the parallel plate ionization chamber exposed to the NIST clinical applicator. The maximum standard deviation of the measurements was less than 1.0%.

3.7. Variation of the response as a function of distance

Ionization measurements were taken in order to verify the chamber response in relation to the variation of the chamber-source distance.

The variation of the response was studied using the NIST applicator and at over a distance interval from 0 to 4.0 cm (Fig. 8). The charge collecting time was 60 s at each position.

This test was very useful for dosimetry of sources used in betatherapy. According to the IEC international recommendations [5, 6], the quantity recommended for the specification of beta radiation source calibrations is the absorbed dose rate in water, at a reference distance. For dermatological applicators, this distance is 1.0 mm; however, the dosimetry procedure at this distance is difficult because of the physical positioning. Therefore, these sources are usually calibrated at a null distance between source and detector [14].

The variation of the response as a function of the distance allows the determination of the difference in the measurements to distances of 0 and 1 mm. A decrease of 23% was observed when the source was 1.0 mm away of the source, in relation to null distance.

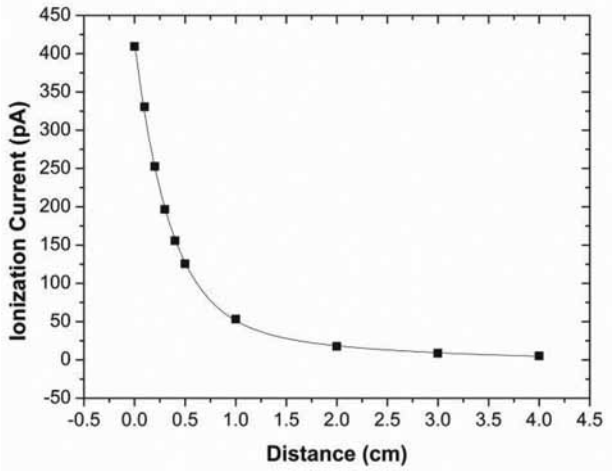

FIG. 8. Variation of the chamber response in function of the distance between NIST applicator and parallel plate ionization chamber. The maximum standard deviation of the experimental points was 1.3%, which is not indicated in the graph.

3.8. Determination of the absorbed dose rates for dermatological applicators

Three dermatological applicators were calibrated using the NIST applicator as the reference. A calibration factor was obtained for the ionization chamber in relation to the NIST applicator, taking the ratio between the absorbed dose rate of the NIST applicator (provided in its calibration certificate and corrected for radioactive decay), and the measured ionization.

Measurements were taken of the A1, A2 and A3 applicators, physically in contact with the detector (null distance), and a charge collecting time of 60 s. The original absorbed dose rate of each applicator was corrected for radioactive decay. Applying the calibration factor of the ionization chamber (for the NIST applicator) to the measurements of the A1, A2 and A3 applicators, their absorbed dose rates were determined at the null distance. The results obtained can be observed in Table 4.

The values obtained in this work were compared with the results showed in a previous study [15], in which the absorbed dose rates were determined using a mini-extrapolation chamber as a reference instrument. This extrapolation chamber was developed by Oliveira and Caldas [10].

Taking into consideration that the expanded uncertainty given in the NIST applicator calibration certificate is 12%, and that the uncertainties described in the manufacturer source certificates are equal to 20% in the case of dermatological applicators, the uncertainties and the differences obtained and shown in this work can be considered acceptable.

TABLE 4. ABSORBED DOSE RATES OBTAINED IN THIS WORK, AT THE NULL DISTANCE, USING THE NIST APPLICATOR AS REFERENCE

$^{90}Sr+^{90}Y$ applicator	Absorbed dose rate (Gy/s)	
	Previous study [15]	This work
A1	0.0195 ± 0.0040	0.0154 ± 0.0031
A2	0.0218 ± 0.0045	0.0169 ± 0.0034
A3	0.0297 ± 0.0060	0.0207 ± 0.0041

4. CONCLUSION

The results show that the parallel plate ionization chamber with a collecting electrode of graphite may be used with efficiency for the quality control programmes of clinical applicators

ACKNOWLEDGEMENTS

The authors are thankful to Fundação de Amparo à Pesquisa do Estado de São Paulo (FAPESP), Conselho Nacional de Desenvolvimento Científico e Tecnológico (CNPq), Coordenação de Aperfeiçoamento de Pessoal de Nível Superior (CAPES) and Ministério de Ciência e Tecnologia (MCT, Project INCT for Radiation Metrology in Medicine), Brazil, for partial financial support.

REFERENCES

[1] AMERICAN ASSOCIATION OF PHYSICISTS IN MEDICINE, A protocol for the determination of absorbed dose from high-energy photon and electron beams, Task Group 21, Radiation Therapy Committee, Med. Phys. **10** (1983) 741.

[2] ALBUQUERQUE, M.P.P, CALDAS, L.V.E., New ionization chambers for beta and X radiation, Nucl. Instrum. Met. A **280** (1989) 310.

[3] SOUZA, C.N., CALDAS, L.V.E., SIBATA, H., HO, A.K., SHIN, K.H., Two new parallel-plate ionization chambers for electron beam dosimetry, Radiat. Meas. **26** 1 (1996) 65.

[4] MAIA, A.F., CALDAS, L.V.E., A new extended-length parallel plate ionization chamber, Phys. Med. Biol. **50** (2005) 3837.

[5] INTERNATIONAL ATOMIC ENERGY AGENCY, Calibration of Photon and Beta Ray Sources Used in Brachytherapy, IAEA-TECDOC-1274, IAEA, Vienna (2002).

[6] INTERNATIONAL COMMISSION ON RADIATION UNITS AND MEASUREMENTS, Dosimetry of beta rays and low energy photons for brachytherapy with sealed sources, **4** 2 (ICRU Report No. 72) United Kingdom (2004).

[7] SOARES, C.G., Calibration of ophthalmic applicators at NIST: A revised approach, Med. Phys. **18** 4 (1991) 787.

[8] SO SOARES, C.G., Comparison of NIST and manufacturer calibrations of $^{90}Sr+^{90}Y$ ophthalmic applicators, Med. Phys. **22** 9 (1995) 1487.

[9] DIAS, S.K., CALDAS, P.L., Development of an extrapolation chamber for the calibration of beta-ray applicators, IEEE Transactions on Nuclear Science **45** 3 (1998) 1666.

[10] OLIVEIRA, M.L., CALDAS, L.V.E., A special mini-extrapolation chamber for calibration of $^{90}Sr+^{90}Y$ sources, Phys. Med. Biol. **50** (2005) 2929.

[11] INTERNATIONAL ELECTROTECHNICAL COMMISSION, Medical electrical equipment dosimeters with ionization chamber as used in radiotherapy, IEC 60731, Geneva (1997).

[12] RAMSEY, C.R., SPENCER, K.M., OLIVER, A.L., Ionization chamber, electrometer, linear accelerator, field size, and energy dependence of the polarity effect in electron dosimetry, Med. Phys. **26** 2 (1999) 214.

[13] INTERNATIONAL ATOMIC ENERGY AGENCY, Absorbed Dose Determination in External Beam Radiotherapy: An International Code of Practice for Dosimetry Based on Standards of Absorbed Dose to Water, Technical Reports Series No. 398, IAEA, Vienna (2000).

[14] SOARES, C.G., VYNCKIER, S., JÄRVINEN, H., CROSS, W.G., SIPILÄ, P., FLÜHS, D., SCHAEKEN, B., MOURTADA, F.A., BASS, G.A., WILLIAMS, T.T., Dosimetry of beta-ray ophthalmic applicators: Comparison of different measurement methods, Med. Phys. **28** 7 (2001) 1373.

[15] ANTONIO, P.L., OLIVEIRA, M.L., CALDAS, L.V.E., "Calibration of the $^{90}Sr+^{90}Y$ clinical applicators using a mini-extrapolation chamber as reference system", (XIV Medical Physics Brazilian Congress, São Paulo, Brazil, 8–12 October 2009) (in Portuguese).

IAEA
International Atomic Energy Agency

Where to order IAEA publications

In the following countries IAEA publications may be purchased from the sources listed below, or from major local booksellers. Payment may be made in local currency or with UNESCO coupons.

AUSTRALIA
DA Information Services, 648 Whitehorse Road, MITCHAM 3132
Telephone: +61 3 9210 7777 • Fax: +61 3 9210 7788
Email: service@dadirect.com.au • Web site: http://www.dadirect.com.au

BELGIUM
Jean de Lannoy, avenue du Roi 202, B-1190 Brussels
Telephone: +32 2 538 43 08 • Fax: +32 2 538 08 41
Email: jean.de.lannoy@infoboard.be • Web site: http://www.jean-de-lannoy.be

CANADA
Bernan Associates, 4501 Forbes Blvd, Suite 200, Lanham, MD 20706-4346, USA
Telephone: 1-800-865-3457 • Fax: 1-800-865-3450
Email: customercare@bernan.com • Web site: http://www.bernan.com

Renouf Publishing Company Ltd., 1-5369 Canotek Rd., Ottawa, Ontario, K1J 9J3
Telephone: +613 745 2665 • Fax: +613 745 7660
Email: order.dept@renoufbooks.com • Web site: http://www.renoufbooks.com

CHINA
IAEA Publications in Chinese: China Nuclear Energy Industry Corporation, Translation Section, P.O. Box 2103, Beijing

CZECH REPUBLIC
Suweco CZ, S.R.O., Klecakova 347, 180 21 Praha 9
Telephone: +420 26603 5364 • Fax: +420 28482 1646
Email: nakup@suweco.cz • Web site: http://www.suweco.cz

FINLAND
Akateeminen Kirjakauppa, PO BOX 128 (Keskuskatu 1), FIN-00101 Helsinki
Telephone: +358 9 121 41 • Fax: +358 9 121 4450
Email: akatilaus@akateeminen.com • Web site: http://www.akateeminen.com

FRANCE
Form-Edit, 5, rue Janssen, P.O. Box 25, F-75921 Paris Cedex 19
Telephone: +33 1 42 01 49 49 • Fax: +33 1 42 01 90 90
Email: formedit@formedit.fr • Web site: http://www. formedit.fr

Lavoisier SAS, 145 rue de Provigny, 94236 Cachan Cedex
Telephone: + 33 1 47 40 67 02 • Fax +33 1 47 40 67 02
Email: romuald.verrier@lavoisier.fr • Web site: http://www.lavoisier.fr

GERMANY
UNO-Verlag, Vertriebs- und Verlags GmbH, Am Hofgarten 10, D-53113 Bonn
Telephone: + 49 228 94 90 20 • Fax: +49 228 94 90 20 or +49 228 94 90 222
Email: bestellung@uno-verlag.de • Web site: http://www.uno-verlag.de

HUNGARY
Librotrade Ltd., Book Import, P.O. Box 126, H-1656 Budapest
Telephone: +36 1 257 7777 • Fax: +36 1 257 7472 • Email: books@librotrade.hu

INDIA
Allied Publishers Group, 1st Floor, Dubash House, 15, J. N. Heredia Marg, Ballard Estate, Mumbai 400 001,
Telephone: +91 22 22617926/27 • Fax: +91 22 22617928
Email: alliedpl@vsnl.com • Web site: http://www.alliedpublishers.com

Bookwell, 2/72, Nirankari Colony, Delhi 110009
Telephone: +91 11 23268786, +91 11 23257264 • Fax: +91 11 23281315
Email: bookwell@vsnl.net

ITALY
Libreria Scientifica Dott. Lucio di Biasio “AEIOU”, Via Coronelli 6, I-20146 Milan
Telephone: +39 02 48 95 45 52 or 48 95 45 62 • Fax: +39 02 48 95 45 48
Email: info@libreriaaeiou.eu • Website: www.libreriaaeiou.eu

JAPAN
Maruzen Company, Ltd., 13-6 Nihonbashi, 3 chome, Chuo-ku, Tokyo 103-0027
Telephone: +81 3 3275 8582 • Fax: +81 3 3275 9072
Email: journal@maruzen.co.jp • Web site: http://www.maruzen.co.jp

REPUBLIC OF KOREA
KINS Inc., Information Business Dept. Samho Bldg. 2nd Floor, 275-1 Yang Jae-dong SeoCho-G, Seoul 137-130
Telephone: +02 589 1740 • Fax: +02 589 1746 • Web site: http://www.kins.re.kr

NETHERLANDS
De Lindeboom Internationale Publicaties B.V., M.A. de Ruyterstraat 20A, NL-7482 BZ Haaksbergen
Telephone: +31 (0) 53 5740004 • Fax: +31 (0) 53 5729296
Email: books@delindeboom.com • Web site: http://www.delindeboom.com

Martinus Nijhoff International, Koraalrood 50, P.O. Box 1853, 2700 CZ Zoetermeer
Telephone: +31 793 684 400 • Fax: +31 793 615 698
Email: info@nijhoff.nl • Web site: http://www.nijhoff.nl

Swets and Zeitlinger b.v., P.O. Box 830, 2160 SZ Lisse
Telephone: +31 252 435 111 • Fax: +31 252 415 888
Email: infoho@swets.nl • Web site: http://www.swets.nl

NEW ZEALAND
DA Information Services, 648 Whitehorse Road, MITCHAM 3132, Australia
Telephone: +61 3 9210 7777 • Fax: +61 3 9210 7788
Email: service@dadirect.com.au • Web site: http://www.dadirect.com.au

SLOVENIA
Cankarjeva Zalozba d.d., Kopitarjeva 2, SI-1512 Ljubljana
Telephone: +386 1 432 31 44 • Fax: +386 1 230 14 35
Email: import.books@cankarjeva-z.si • Web site: http://www.cankarjeva-z.si/uvoz

SPAIN
Díaz de Santos, S.A., c/ Juan Bravo, 3A, E-28006 Madrid
Telephone: +34 91 781 94 80 • Fax: +34 91 575 55 63
Email: compras@diazdesantos.es, carmela@diazdesantos.es, barcelona@diazdesantos.es, julio@diazdesantos.es
Web site: http://www.diazdesantos.es

UNITED KINGDOM
The Stationery Office Ltd, International Sales Agency, PO Box 29, Norwich, NR3 1 GN
Telephone (orders): +44 870 600 5552 • (enquiries): +44 207 873 8372 • Fax: +44 207 873 8203
Email (orders): book.orders@tso.co.uk • (enquiries): book.enquiries@tso.co.uk • Web site: http://www.tso.co.uk

On-line orders
DELTA Int. Book Wholesalers Ltd., 39 Alexandra Road, Addlestone, Surrey, KT15 2PQ
Email: info@profbooks.com • Web site: http://www.profbooks.com

Books on the Environment
Earthprint Ltd., P.O. Box 119, Stevenage SG1 4TP
Telephone: +44 1438748111 • Fax: +44 1438748844
Email: orders@earthprint.com • Web site: http://www.earthprint.com

UNITED NATIONS
Dept. I004, Room DC2-0853, First Avenue at 46th Street, New York, N.Y. 10017, USA
(UN) Telephone: +800 253-9646 or +212 963-8302 • Fax: +212 963-3489
Email: publications@un.org • Web site: http://www.un.org

UNITED STATES OF AMERICA
Bernan Associates, 4501 Forbes Blvd., Suite 200, Lanham, MD 20706-4346
Telephone: 1-800-865-3457 • Fax: 1-800-865-3450
Email: customercare@bernan.com · Web site: http://www.bernan.com

Renouf Publishing Company Ltd., 812 Proctor Ave., Ogdensburg, NY, 13669
Telephone: +888 551 7470 (toll-free) • Fax: +888 568 8546 (toll-free)
Email: order.dept@renoufbooks.com • Web site: http://www.renoufbooks.com

Orders and requests for information may also be addressed directly to:

Marketing and Sales Unit, International Atomic Energy Agency
Vienna International Centre, PO Box 100, 1400 Vienna, Austria
Telephone: +43 1 2600 22529 (or 22530) • Fax: +43 1 2600 29302
Email: sales.publications@iaea.org • Web site: http://www.iaea.org/books

The use of properly calibrated dosimeters, together with approved codes of practice and peer reviewed quality assurance programmes, is essential for ensuring safe and effective diagnosis and treatment of patients with ionizing radiation. Owing to its dual role in disseminating radiation measurement standards and verifying the accuracy of dosimetry applied at the hospital level, the IAEA is well positioned to convene international meetings focused on dosimetry and relevant quality assurance programmes. The International Symposium on Standards, Applications and Quality Assurance in Medical Radiation Dosimetry (IDOS), which was held at the IAEA in Vienna on 9–12 November 2010, provided a unique opportunity to review advances in radiation dosimetry during the last decade, since the previous international symposium on the same topic was held in 2002. These proceedings present the conclusions reached at the end of the symposium as well as a refereed selection of papers that were given at the symposium. Emphasis was placed on dosimetry standards and implementation of dosimetry protocols in therapeutic and imaging applications of radiation in medicine. A key 'take home' message was that advances in technology for radiation therapy dose delivery require vigilance to ensure adequate quality control. In the future, advances in diagnostic capabilities may lead to better therapy planning. Certainly, the coupling between diagnostic information and therapy delivery is expected to strengthen. In this case, many challenges in dosimetry remain to be solved.

INTERNATIONAL ATOMIC ENERGY AGENCY
VIENNA
ISBN 978–92–0–116210–6
ISSN 0074–1884